US Army Corps of Engineers®

Performance Evaluation of the New Orleans and Southeast Louisiana Hurricane Protection System

Final Report of the Interagency Performance Evaluation Task Force

Volume IV – The Storm

26 March 2007

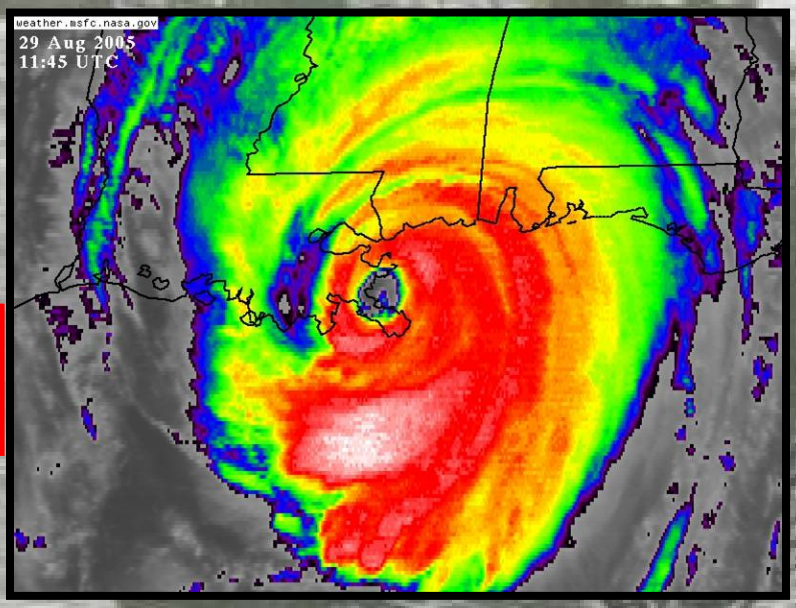

FINAL

Volume I – Executive Summary and Overview
Volume II – Geodetic Vertical and Water Level Datums
Volume III – The Hurricane Protection System
Volume IV – The Storm
Volume V – The Performance – Levees and Floodwalls
Volume VI – The Performance – Interior Drainage and Pumping
Volume VII – The Consequences
Volume VIII – Engineering and Operational Risk and Reliability Analysis
Volume IX – General Appendices

Volume IV
The Storm

Contents

Executive Summary

Hurricane Katrina produced unparalleled wave and storm surge conditions for the New Orleans vicinity. Hurricane Katrina was a very large Category 3 storm when it passed the New Orleans area on the morning of 29 August 2005. Twenty-four hours earlier this storm had been the largest Category 5 and most intense (in terms of central pressure) storm on record within the northern Gulf of Mexico. Due east of the Mississippi River delta, a deepwater National Oceanic and Atmospheric Administration (NOAA) buoy recorded the highest significant wave height (55 ft) ever measured in the Gulf of Mexico. The large size of Katrina throughout its history, combined with the extreme waves generated during its most intense phase, enabled this storm to produce the largest storm surges (reliable observations up to 28 ft) that have ever been observed within the Gulf of Mexico, as determined from analyses of historical records. As another example of Katrina's strength in terms of storm surge, the previous highest high-water mark (HWM) from Hurricane Camille was 24.6 ft; Camille is the only Category 5 storm to make landfall in the Gulf of Mexico over the interval that records have been kept (approximately 150 years). In the vicinity of Biloxi, MS, the surge produced by Camille was 15.8 ft, the highest surge that had ever been recorded at that location prior to Katrina. Katrina generated surges of 24 to 26 ft at Biloxi. In other words, Katrina (a Category 3 storm at landfall) generated substantially higher surges than Camille (a Category 5 storm at landfall) in the area where they both made a direct hit. Whereas the Saffir-Simpson scale is a good predictor of wind damage from hurricanes, it is not a particularly good predictor of the surge and wave generation potential for these storms. Hurricane Katrina had much greater wave and storm surge generation potential than the Standard Project Hurricane (SPH) storms used to design the hurricane protection system. In Louisiana, the east-facing protection levees of Orleans, St. Bernard, and Plaquemines Parishes bore the brunt of Katrina's storm surge, and coupled with energetic long-period wave conditions, the hurricane protection system was overwhelmed in many places.

This volume presents the regional hydrodynamic conditions (waves and water levels) created by Katrina. Local high-resolution hydrodynamic waves and water levels at the levees and floodwalls, as well as hydrostatic and hydrodynamic forces and loadings that the levees and floodwalls were subjected to during the storm, are also presented. In addition to maximum conditions, temporal variation of waves and water levels and loadings are of great interest, as are timing and phasing of different types of loadings and forces. All conditions were evaluated. A time line of inundation and notable project responses is presented, based on many eyewitness accounts and analyses of information and observations.

A combination of numerical model results and measured data was used to assess the regional-scale wave and water level conditions along the entire periphery of the hurricane protection system. The WAM and STWAVE wave models, and the ADCIRC storm surge model, all standard models used by the Corps of Engineers, were used to characterize the regional wave and storm surge climate produced by the hurricane. All models needed very high resolution to capture the complex geographical features of the system, and they were forced with high-accuracy, data-assimilated surface wind and atmospheric pressure fields. Computations were made on high-performance supercomputers.

In spite of the fact that Katrina exceeded the design storm, water levels and waves roughly corresponded to design conditions in some parts of the New Orleans area. In other parts of the hurricane protection system, waves and water levels significantly exceeded design conditions. Observed peak water levels at the entrances to canals along the south shore of Lake Pontchartrain were 10.8 to 11.8 ft, which were slightly less than or at the design peak water levels of 12.0 ft. In the Inner Harbor Navigation Canal (IHNC), north of the intersection of IHNC with the Gulf Intracoastal Waterway (GIWW)/Mississippi River Gulf Outlet (MRGO), there was a large gradient in observed peak water level, from 15 ft at the intersection to 11.8 ft at the IHNC entrance to Lake Pontchartrain. In this reach of canal, peak water levels were at, above, or below design levels, depending on location. Between this intersection and the IHNC Lock to the south, peak water levels exceeded the design water level of 13.5 ft by as much as 2 ft. Along the east/west-oriented GIWW/MRGO channel section, peak water levels exceeded the design value of 13.5 ft by approximately 2 ft. Along the MRGO adjacent to the St. Bernard Parish hurricane protection levee, peak water levels were 16 to18 ft, which exceeded design levels by as much as 5 ft. Along the east-facing hurricane protection levees in south Plaquemines Parish, peak water levels reached 20 ft, exceeding design levels by as much as 5.5 ft. All water levels cited in this volume are referenced to the North American Vertical Datum of 1988 (NAVD 88) 2004.65 datum. Appropriate adjustments have been made to design water levels to convert them to this datum.

Peak significant wave height along the south shore of Lake Pontchartrain reached at least 8.7 ft, exceeding design values by about 1.0 ft. Wave periods were about equal to design values. Along the levees adjacent to Lake Borgne, computed significant wave heights were consistent with or less than design values, but wave periods (15 to 16 sec) exceeded the design wave periods by a factor of 3. In south Plaquemines Parish maximum significant wave heights reached as high as 10 ft, and wave periods were 15 to 16 sec; design wave height conditions were exceeded by up to 4 ft, and design wave periods were exceeded by a factor of 2 to 3. Since both wave height and wave period influence the potential for wave runup and overtopping, the design wave height and period values should be reexamined for these east-facing levee systems, as well as the west-facing levees in Plaquemines Parish.

An analysis was performed to examine the influence of the MRGO channel on storm surge propagation into the New Orleans vicinity. The section of waterway where the GIWW and MRGO occupy the same channel allows Lake Pontchartrain and Lake Borgne to be hydraulically connected to each other via the IHNC. Storm surge experienced in the IHNC and the GIWW/MRGO section of waterway is influenced by storm surge conditions in both lakes due to this hydraulic connection. The long northwest/southeast-oriented section of the MRGO channel to the east of Paris Road bridge, which seems to be the section of canal that has raised much concern, has little influence on water levels in the IHNC and GIWW/MRGO for high storm surge events such as Hurricanes Betsy and Katrina. It has a more important role for low surges, less than 4 ft in amplitude, but still creates changes of less than 0.6 ft in some cases and less than 0.3 ft in most cases. The MRGO role in propagation of low-amplitude astronomical tide and influx of higher saline water into Lake Pontchartrain has been established; the low-amplitude tide propagates primarily through channels, of which the MRGO is one. However, during high storm surge conditions, when the wetlands become inundated, this reach of the MRGO becomes

much less important regarding storm surge propagation into the IHNC. A more detailed analysis is provided in the form of a white paper on the subject (Appendix 6).

As storm effects propagated onto the large flood protection levees and into the outfall and navigation canals, local wave and water level conditions exerted very large forces on the flood protection system. Detailed hydrodynamic and engineering models were nested inside the model domains used in the regional hydrodynamics to represent conditions in the vicinity of a range of engineering structures within the New Orleans area. As part of these calculations, forces on structures, overtopping rates, and fine-scale velocity fields were estimated for periods of interest. At this scale of estimation, accurate specification of these forces requires a combination of very careful detailed-scale hydrodynamic modeling and assimilation of all available observations. To obtain the most reliable representation possible for the outfall canals, a series of digital photographs at the northern ends of the 17th Street Canal and the IHNC, along with interpolations of these water levels at the London Avenue and Orleans Avenue Canals, were used as the final boundary conditions for detailed wave and water level simulations.

Fine-scale ADCIRC simulations showed that, in the absence of breaching or overtopping within the outfall canals, even for the case of high rates of pumping into these canals, histories of water levels in these canals would virtually mirror those at the entrances. However, this simple situation was not the case in the 17th Street and London Canals, where outflows via breaching had a significant effect on water levels throughout the canals. Debris on the north side of the Hammond Highway bridge near the entrance of the 17th Street Canal also appeared to have had a significant effect on water levels within this canal. The net effect of these factors is that estimated water levels within the 17th Street Canal are about 3 ft lower than water levels at the entrance to this canal after full breach formation. Since there was no major source of debris within the London Avenue Canal and since the breaches were smaller than the breach in the 17th Street Canal, the water levels were not reduced as much within this canal, with water level conditions about 2 ft lower than those at the entrance after full breach formation. A low section of levee in the Orleans Avenue Canal acted as a weir at its southern end; consequently, once water levels exceeded the weir height (about 8.3 to 9.8 ft), water levels within the canal sloped somewhat from north to south.

A physical model study was conducted for the northern portion of the 17th Street Canal in order to obtain objective estimates of wave decay in the entrance to this canal and the dissipative effects of the hurricane-proof bridges on waves propagating under these structures. Results from this model showed that most wave energy was removed by the combination of entrance losses and dissipation under these bridges. In the physical model wave heights of over 8 ft that were incident on the canal entrances at the peak of the storm were reduced to less than 1 ft in the vicinity of the breach site within the 17th Street Canal. COULWAVE (Boussinesq) model runs corroborated estimates of entrance loss effects and, once tuned to similar dissipation rates under bridges, showed that long-period wave energy also remained quite small over the length of the canal. Since neither the physical model nor COULWAVE includes the effects of local wind generation, STWAVE, modified to simulate the physical model's estimated bridge dissipation, was exercised to investigate the effects of local wind generation inside the canal; however, results from these runs indicate that wave heights remained under 1 to 1.5 ft in all areas of the canal. Simulations with COULWAVE and STWAVE show that wave conditions past the first

500 ft or so within both the London Avenue and Orleans Canals were also quite small, with wave heights remaining less than 1 to 1.5 ft throughout these canals during the storm.

Estimated forces on the canal floodwalls are provided. As a close approximation, these forces are similar to what would be expected if the water level at the wave crests were simply taken as the still-water level for force estimation. Maximum individual crest heights are estimated to be about 1 foot above the still-water levels in the vicinity of the breaches in the 17th Street and London Avenue Canals. Depending on the type of failure experienced by these floodwalls, contributions due to waves could be significant in causing gap formation in these locations.

Breaching within the IHNC occurred in locations near the junction of the GIWW/MRGO and IHNC and south of this junction. In this area, waves entering from the north from Lake Pontchartrain and from the east from the Gulf of Mexico are largely dissipated; however, during peak conditions for winds out of the east (around 0900 to 1100 UTC), wave heights of 4 ft or larger were generated within the GIWW/MRGO. These waves propagated into the IHNC and were diffracted and reflected from side to side within this canal. Estimated wave heights are in the 2- to 3-ft range for the area along the Lower Ninth Ward that may have breached early around 0930 to 1030 UTC. Later in the morning, around 1430 UTC, winds had rotated to where they were coming from the north, roughly aligned with the axis of the IHNC, and waves in the 2- to 3-ft range were generated near the southern end of the IHNC.

Similar to the approach used for the canals, observational data were assimilated into water levels along the large flood protection levees in St. Bernard Parish, New Orleans East, and Plaquemines Parish in order to ensure the maximum accuracy possible for calculations at the detailed scale. Mean water levels ranged from slightly below the levee crest to 2 or 3 ft above the levee crests in the St. Bernard Parish area facing northeast along the MRGO. Overtopping would have been extensive along the central portion of this section of levees, even without erosion/breaching; however, extensive erosion/breaching substantially increased the rate of discharge into this area. Results from COULWAVE show that combined wave and mean flow velocities were higher on the back faces of levees than on the front face of the levees (the part of the levee exposed to direct wave attack). This is consistent with observations of partially eroded levees in this area which show much greater erosion on levee back faces in many areas where there is no erosion on the levee front face.

Along New Orleans East Levees, the mean water level appears to have been very close to the levee crest elevation. These levees were exposed to wave overtopping for several hours on the morning of Katrina landfall; and significant erosion/breaching occurred. An interesting contrast was seen along the GIWW, where water levels were also near the crest of the levee but waves were propagating parallel to the crest of the levee rather than normal to it. In this case, even though the wave heights were similar to those along the exposed section of levees in New Orleans East, velocities on the back face of the GIWW Levee section were about 50 percent lower than those estimated for the exposed levee section. Levees along this GIWW section exhibited only minor erosion.

In Plaquemines Parish, the major levees and floodwalls were massively overtopped and many of these failed. Calculations with a Navier-Stokes model were used to show the

magnitudes and distribution of forces on the vertical walls. Wave and mean flow overtopping were extensive with jets of water propelled 6 to 12 ft beyond the crest of the floodwalls.

Participants

This report represents a combined effort by individuals from various governmental, private, and academic institutions. The following is a list of individuals that actively participated on this project during the period October 2005 through May 2006 and directly contributed to this report.

NAME	AGENCY	ROLE
Regional Hydrodynamics		
Bruce Ebersole	USACE/ERDC-CHL	Co-Lead, Regional Hydrodynamics
Joannes Westerink	University of Notre Dame	Co-Lead, Regional Hydrodynamics
Andrew Garcia	USACE/ERDC-CHL	High-water Marks/Hydrographs
Steve Maynord	USACE/ERDC-CHL	High-water Marks/Hydrographs
Kevin Knuuti	USACE/ERDC-CHL	High-water Marks/Hydrographs
Mary Claire Allison	USACE/ERDC-CHL	High-water Marks/Hydrographs
Brian Jarvinen	NOAA NWS (Retired)	High-water Marks/Hydrographs
Phil Turnipseed	USGS	High-water Marks/Hydrographs
Robert Mason	USGS	High-water Marks/Hydrographs
Van Wilson	USGS	High-water Marks/Hydrographs
Shabbar Saifee	DHS/FEMA	High-water Marks/Hydrographs
Lynn Mayo	URS (for DHS/FEMA)	High-water Marks/Hydrographs
Vincent Cardone	Oceanweather, Inc.	Winds/Pressures
Andrew Cox	Oceanweather, Inc.	Winds/Pressures
Brian Callahan	Oceanweather, Inc.	Winds/Pressures
Erin Harris	Oceanweather, Inc.	Winds/Pressures
Mark Powell	NOAA AOML HRD	Winds/Pressures
Shirley Murillo	NOAA AOML HRD	Winds/Pressures
Peter Dodge	NOAA AOML HRD	Winds/Pressures
John Gamache	NOAA AOML HRD	Winds/Pressures
Peter Black	NOAA AOML HRD	Winds/Pressures
Sonia Otero	University of Miami (NOAA CIMAS)	Winds/Pressures

Nick Carrasco	University of Miami (NOAA CIMAS)	Winds/Pressures
Bachir Annane	University of Miami (NOAA CIMAS)	Winds/Pressures
Russell St. Fleur	University of Miami (NOAA CIMAS)	Winds/Pressures
Eric Uhlhorn	University of Miami (NOAA CIMAS)	Winds/Pressures
Krystal Valde	University of Miami (NOAA CIMAS)	Winds/Pressures
Jane Smith	USACE/ERDC-CHL	Waves
Robert Jensen	USACE/ERDC-CHL	Waves
Barbara Tracy	USACE/ERDC-CHL	Waves
Jeff Hanson	USACE/ERDC-CHL	Waves
Ann Sherlock	USACE/ERDC-CHL	Waves
Hendrik Tolman	SAIC for NOAA NCEP	Waves
Shintaro Bunya	University of Notre Dame	Storm Surge
Casey Dietrich	University of Notre Dame	Storm Surge
Ethan Kubatko	University of Notre Dame	Storm Surge
Hans Westerink	University of Notre Dame	Storm Surge
Jay Grossman	University of Notre Dame	Storm Surge
John Atkinson	Ayres Associates	Storm Surge
Lyle Zevenbergen	Ayres Associates	Storm Surge
Dusty Robinson	Ayres Associates	Storm Surge
Anthony Alvarado	Ayres Associates	Storm Surge
Victor Parr	Consultant	Storm Surge
Mary Cialone	USACE/ERDC-CHL	Storm Surge
Michael Tubman	USACE/ERDC-CHL	Storm Surge
David Mark	USACE/ERDC-CHL	Storm Surge

Field Data Recovery and Timeline Analysis

Steve Maynord	USACE/ERDC-CHL	Field Data Recovery/Timeline
David Biedenharn	USACE/ERDC-CHL	Field Data Recovery/Timeline
Ron Heath	USACE/ERDC-CHL	Field Data Recovery/Timeline

David Abraham	USACE/ERDC-CHL	Field Data Recovery/Timeline
David Maggio	USACE/ERDC-CHL	Field Data Recovery/Timeline
Fred Pinkard	USACE/ERDC-CHL	Field Data Recovery/Timeline
Jim Leech	USACE/ERDC-CHL	Field Data Recovery/Timeline
Peggy Hoffman	USACE/ERDC-CHL	Field Data Recovery/Timeline
Steve Wilhelms	USACE/ERDC-CHL	Field Data Recovery/Timeline
Mario Sanchez	USACE/ERDC-CHL	Field Data Recovery/Timeline

Detailed Hydrodynamics

Don Resio	USACE/ERDC-CHL	Co-Lead Detailed Hydrodynamics
Bob Dean	University of Florida	Co-Lead Detailed Hydrodynamics
Pat Lynett	Texas A&M University	Boussinesq Model Applications
Bill Dally	Surfbreak Engineering Sciences Inc.	Data Analysis & Quality Control
Stan Boc	USACE/ERDC-CHL	Data Analysis & Quality Control
Ray Chapman	USACE/ERDC-CHL	ADCIRC Model Applications
Mary Cialone	USACE/ERDC-CHL	ADCIRC Model Applications
Jennifer Irish	USACE/ERDC-CHL	ADCIRC Model Applications
Nobu Kobayashi	University of Delaware	Basic Engineering Analysis
Jeff Melby	USACE/ERDC-CHL	Basic Engineering Analysis
Bill Seabergh	USACE/ERDC-CHL	Principal Investigator – Physical Model
Jane Smith	USACE/ERDC-CHL	STWAVE Grid Setup

Overview

Fundamental Questions that were Addressed

This volume of the report addresses the second of the five fundamental questions: **What were the storm surge and waves used as the basis for design, and how do these compare to the storm surge and waves generated by Hurricane Katrina?** Answers to these questions will be addressed in reverse order, characterization of wave and water level conditions experienced during Katrina, first, followed by comparison to design values. Knowledge of storm water levels and waves also is required to address the third fundamental question: **How did the floodwalls, levees, pumping stations, and drainage canals, individually and acting as an integrated**

system, perform in response to Hurricane Katrina, and why? This volume addresses the following issues, which are central to system performance: runup and overtopping, and the static and dynamic loadings to which the levees and floodwalls in New Orleans and Southeast Louisiana were subjected.

Description of Work

Work described in this volume is comprised of several key components, and those are listed here and described in more detail in subsequent sections and supporting appendices: 1) acquisition and analysis of measured data collected throughout the region (such as HWMs, water level hydrographs, wind speed and direction, and wave energy, height, period and direction), 2) development of surface wind and atmospheric pressure fields for Hurricane Katrina using sophisticated techniques developed by the National Oceanic and Atmospheric Administration (NOAA) Atlantic Oceanographic and Meteorological Laboratory (AOML) Hurricane Research Division (HRD) and Oceanweather, Inc. (OWI), which blend numerical meteorological model results with an extensive set of atmospheric measurements, 3) a regional wave and storm surge hindcast, which involves application of numerical wave and storm surge models developed by the Corps and one of its academic research partners (University of Notre Dame), 4) reconstruction of a timeline from eyewitness accounts and other information sources that describes how water levels and inundation evolved throughout the hurricane protection system during the storm, and 5) detailed, high-resolution hydrodynamic modeling (both laboratory scale modeling and numerical modeling) and data analyses to define wave and water level conditions and loadings in close proximity to the hurricane protection structures. The high-resolution hydrodynamics work utilized laboratory test facilities at the Corps' Engineer Research and Development Center (ERDC), and numerical models developed and applied by the Corps and its other academic partners (University of Florida, Texas A&M University, and University of Delaware).

Regional Wave and Storm Surge Modeling

Detailed, comprehensive, high-resolution coastal prediction models were set up for the Southeast Louisiana and southern Mississippi regions. Models employed were the standard models used by the Corps for coastal storm prediction (WAM and STWAVE wave models and the ADCIRC storm surge model). The models were then applied to predict time-varying water levels and wave conditions (heights, periods, directions, energy spectra) and peak values along levees and floodwalls fronting the various parishes, within main navigation channels, and at the entrances to the canals situated along the southern Lake Pontchartrain shoreline. The models were forced with surface wind and pressure fields of the highest accuracy produced by HRD and OWI. Computations were made on high-performance supercomputers located at the Department of Defense Major Shared Resource Center in Vicksburg, MS. HRD staff who participated in the development of hurricane wind fields stated that this was the most comprehensive analysis of a hurricane's surface wind fields that has ever been performed. Because so few wave measurements were available, other wave models that are commonly used in the coastal science and engineering community were applied to examine uncertainty in model-derived results (the WAVEWATCH III basin-scale wave model, done in concert with NOAA National Centers for

Environmental Prediction staff, and the SWAN nearshore wave model, done in consultation with Naval Research Laboratory staff). Those model-to-model-to-measurement results are included in this report.

Complimentary Roles for Modeling Results and Measurements

In the New Orleans metropolitan area, measurements and observations that captured the time variation of water levels, including the peak, were only available at a few locations. Most water level measurement devices failed prior to the peak of the storm. HWMs, which at best only capture peak values but provide no information on temporal variation of water level, were available at many locations. Many of the marks are of uncertain and questionable accuracy. Model-derived storm water level results were used to supplement HWM data and observed hydrographs, and were the only source of information in certain areas. In some areas where reliable HWMs were obtained, they were used to scale model-generated hydrographs to try to improve the accuracy of the estimated water level hydrograph. Wave measurements along the path of the storm were available at a few deepwater offshore locations in the Gulf of Mexico; but shallow-water wave measurements were only available at two nearly co-located locations in the primary impact zone, in Lake Pontchartrain (data from these sensors are of questionable accuracy near the storm peak). Because of the paucity of measured wave data, wave conditions throughout nearly the entire Southeast Louisiana region were estimated using numerical models. Measurements were used to assess the accuracy of and uncertainty in model results. Since model results were used in so many areas where measurements were not made or where gauges failed to capture the maximum conditions, considerable effort was expended to compare model results with measured data and assess model uncertainty.

Model Sensitivity Tests

A number of tests were done to examine sensitivity of model results to several key sources of uncertainty, particularly model input and representation of the physical system: 1) uncertainty in wind field estimates, which are so crucial to wave and storm surge model accuracy, and 2) uncertainty in timing of barrier island degradation and loss of wetland vegetation cover during the storm. Quality of model input and detail in representing the physical system are the two main factors that influence model accuracy. Sensitivity of model predictions of waves and water levels to these facets of uncertainty was assessed. The relative roles of tide and wave setup as contributors to peak water levels were also assessed.

Volume Outline

The flow of this volume is as follows. A brief, very general, overview of the formative processes behind hurricane waves and water levels is presented. The overview provides order of magnitude estimates for the various contributing factors to unusually high storm water levels in Southeast Louisiana for Hurricane Katrina. This is followed by a brief summary of the history of the storm, with a broad overview of how it evolved, in terms of intensity and track, and how the regional storm waves and water level conditions evolved in response to the storm's changing

intensity and path. Next, acquisition and analysis of HWMs and observed water level hydrograph data are described. This section includes a summary (details are provided in Appendix 1) of the detailed effort to reconstruct hydrographs from digital pictures taken during the storm at two key locations on the south shore of Lake Pontchartrain, where no recorded hydrographs were available. Following that, a summary of the regional wave and storm surge modeling is presented (this takes a broader, regional perspective). A comparison is made between measured and computed waves and water levels produced by Katrina, and computations and observations are compared to values that were used to design the different hurricane protection projects throughout the region. Next, the timeline of water level changes and inundation experienced during the storm is provided, which refers to some of the observed water level data. The timeline sets the stage for analyses of hydrodynamic conditions and loadings at the structures, as well as assessment of project performance that is covered in the next volume. Volume IV then summarizes the high-resolution hydrodynamic analysis done for critical sections of hurricane protection levees and floodwalls, and the key breach areas. The volume concludes with a discussion of findings and lessons learned from all work done to characterize the storm. The main text of this volume only provides a summary of work and key results. Considerably more detailed documentation is provided in technical appendices that are referenced throughout the volume.

Storm Water Levels and Waves – Formative Processes

Higher-than-normal water levels and wave conditions observed during hurricanes are created by a number of processes. Both waves and water level changes are primarily forced by the wind. It is important to note that the forces that generate waves and water levels are nonlinearly related to wind speed. Wave generation by wind occurs in both deep and shallow water. Other processes also can have significant influence on wave conditions in shallow water (refraction, shoaling, and energy dissipation, for example). Changes in water level due to wind occur primarily in shallow water because the effect of wind is inversely proportional to water depth.

When hurricanes enter the Gulf of Mexico, they begin to spawn shorter-period surface wind waves (generally waves with periods of up to 20 sec) in response to the wave generation source, which is constantly changing hurricane winds that rotate counterclockwise around the advancing storm center. The higher the wind speed the greater the energy contained in the wave field (i.e., higher significant wave heights) and the greater the wave period. Wave generation potential in storms is related to the surface wind stress (which is, in turn, related to the wind speed raised to the second power). The available fetch, or the distance over which winds blow, also strongly influences wave height and period conditions that are generated. Waves propagate outward in a radial pattern away from the storm, throughout the deep waters of the gulf, at speeds that are greater than the forward speed of the storm itself. Waves can propagate long distances within the gulf. The short-period wind waves cause the water surface to rise and fall locally with periodicities on the order of 20 sec or less.

During their growth and transformation from deep water to shallow water, wave height and direction can change as they begin to be influenced by the bottom topography. The highest significant wave height that can exist locally in shallow water is about 0.6 to 0.65 times the local

water depth (higher individual waves can exist locally). This depth limitation on wave energy (limit to the significant wave height) has been observed in many prior studies of irregular wave transformation and breaking during severe storms. When waves propagate into an area in which the significant wave height reaches this fraction of the water depth, significant wave breaking is induced. When waves break, the change in momentum results in a thrust or force on the water column, which acts to raise the local water level (a process called wave setup). The magnitude of the wave setup contribution to storm water level was computed to be as much as 2.5 ft away from the levees for Katrina and up to another 2 ft at the levees, with magnitude depending on location. Waves in shallow water also act to continually raise and lower the local water surface with a frequency that corresponds to the wave period. The increase in elevation, above the mean (or still) water level, associated with a wave crest is roughly equal to half the significant wave height (wave height being approximately the vertical distance from wave trough to wave crest). When waves reflect off vertical walls, local heights at the wall are increased; and when waves break and run up a smooth levee slope, the additional elevation above the mean or still-water level reached by the wave uprush can be as much as 2 to 3 times the incident significant wave height. Wave runup is a function of wave height, wave period, levee slope, and roughness of the levee surface.

Winds also change the water level, a process called storm surge generation. Storm surge is defined here as the abnormally high still-water levels attributable to the presence of the storm itself. The water level experienced during a storm is dictated not only by the storm surge but also by the astronomical tidal variations that normally occur without the presence of a storm, but which also occur along with a storm. The word “still” to describe the water level is used rather loosely here, but it is intended to differentiate between the slower rise and fall of the water surface due to the storm surge/tide that occurs over time scales of hours and the changes in water surface that occur at much higher frequencies associated with the continuous up and down water surface motion due to wave action which occurs over time scales of seconds and tens of seconds.

Primary contributors to storm water levels, in order of descending importance for Southeast Louisiana are: wind; geographic/topographic controls; breaking wind waves; within the Mississippi River between its confining levees, the river discharge; atmospheric pressure; astronomical tide; and precipitation. Wind and geographic/topographic controls are generally more important than all the other factors; and for severe hurricanes impacting Southeast Louisiana, these two factors exceed the combined effects of all the other factors. The contribution of breaking waves to storm surge was significant for Katrina. This process, called wave setup, was described above. The other primary contributors to storm water levels are discussed below.

Winds exert a shear stress on the water surface that pushes the water. Wind is most effective in contributing to the development of storm surge in shallow water. The shallower the water the more effect wind of a constant speed can have in developing storm surge. Like waves, the storm surge generation potential of a storm is related to the surface shear stress. In the case of surge generation, the shear stress that creates it is related to the wind speed raised to the second or third power, a highly nonlinear relationship. Broad, shallow continental shelf regions are the most effective areas for generating storm surge. As winds push water, water moves until it encounters a coastal land mass or other obstruction where it then begins to accumulate. Indentations,

irregularities, and pockets along the U.S. coast, which are key topographic controls, are particularly prone to catching water pushed toward and into these geographic features by the wind. The Mississippi River delta is a coastal land feature that acts to catch water being pushed toward it along the Mississippi and Alabama continental shelves. Since winds in hurricanes rotate in the counterclockwise direction, hurricanes in the northern Gulf of Mexico tend to create winds that blow from the east in the northern gulf. These winds from the east act to push water toward Southeast Louisiana, toward the Mississippi River delta. As storm surge grows and inundates the wetlands of Southeast Louisiana, the Mississippi River Levees themselves become a topographic control, acting in the same manner as the delta because the levees extend nearly its entire length. Along the Southeast Louisiana coast, for Katrina, the storm surge contribution due to wind and geographic/topographic controls exceeded 15 ft in places, and along the Mississippi coast it exceeded 20 ft in places. This component of the water level can vary greatly with location.

Mississippi River discharge can influence the storm surge within the river, which is confined by levees. The effect can be on the order of feet depending on the magnitude of the discharge. Discharge can be higher earlier in the hurricane season (early summer) and lower in the later parts of the season, and the discharge will influence the storm-induced water levels within the river. The storm surge wave can propagate great distances up the Mississippi River, depending on the speed of the storm and its track, magnitude of storm surge at the river's mouth, wind speed and direction, and discharge from the upstream watershed.

Atmospheric pressure differences also affect local water level. Atmospheric pressure is the weight of air above the water surface. At the center of hurricanes, atmospheric pressure is much lower than pressure at the periphery of the storm. This means the weight of air pushing down on the water column is greater at the edges of the storm than it is at the storm's center. Consequently, a slight bulge, or increase, in the water surface occurs within the storm, and the magnitude of the bulge is greatest at the storm's center and decreases to near zero at the storm's periphery. The magnitude of this atmospheric pressure effect can be as much as 1 to 2 ft in the center of the bulge, for a severe hurricane.

Astronomical tide can have a positive or negative effect on the storm-induced water level. If the other contributors act to produce a peak storm surge that occurs at low tide, then the peak storm water level will be lessened; however, if the peak surge coincides with high astronomical tide the peak storm water level will be increased. For Southeast Louisiana, this effect is rather small because of the small astronomical tide range (ranging from about 0.5 ft in Lake Pontchartrain to about 1.5 ft in Breton Sound).

Precipitation can increase the storm-induced water level, either by falling directly on the local water bodies, or by falling on the adjacent watershed and then running off into the water bodies. The effect of direct precipitation can be as much as a 1-ft contribution to the peak storm surge, perhaps slightly more in the case of hurricanes with very high rainfall. Typically, some of the effect of direct precipitation will be felt after the storm surge peak is experienced; and often the effect of runoff from the adjacent watershed will be experienced after the peak storm water level has been experienced.

Hurricane Katrina Description and History

Storm Parameters and Track

The approximate storm track for Hurricane Katrina is shown in Figure 1. The term H*Wind is used throughout this report to refer to a real-time hurricane wind analysis system developed by HRD. The position of the storm center is shown with "X's", at particular days/times in late August 2005. All times are referenced to UTC (Coordinated Universal Time). Table 1 shows the latitude/longitude coordinates for the storm center, the minimum central pressure in the eye of the storm, and the maximum sustained surface wind speed (1-min sustained wind speed at 10-m elevation), radius to maximum winds, and the Saffir-Simpson hurricane intensity categorization (based on the sustained surface wind speed), every 3 hr between the times of 0000 UTC on 26 August and 0000 UTC on 30 August. The information displayed in Table 1 was produced by the HRD and OWI, as part of this investigation. The Saffir-Simpson scale, a hurricane intensity rating scale, assigns the following categories based on sustained wind speed ranges:

- Category 1: 64 to 82 knots
- Category 2: 83 to 95 knots
- Category 3: 96 to 113 knots
- Category 4: 114 to 135 knots
- Category 5: greater than 135 knots

The Saffir-Simpson scale, originally derived as a measure of potential hurricane damage, is based solely on the maximum hurricane wind speed observed anywhere within the storm. However, as described above, many other factors dictate the water level and wave climate produced by a particular hurricane, aside from the maximum wind speed. These factors include: coastline and continental shelf characteristics, storm track, central pressure, forward speed of the storm, spatial extent and variability of the surface wind fields, phasing with the astronomical tide, and precipitation. It is also important to note that hurricane intensity can vary considerably throughout the life of a hurricane (Katrina is an excellent example of this; see Table 1). The unusually high wave and water level conditions produced by a hurricane are dictated not only by hurricane characteristics at landfall but also, and importantly, by its characteristics along its path over open water especially as it approaches landfall.

Wind, Wave, Surge Evolution – the Big Picture

Katrina impacted Florida with hurricane intensity. Once the storm reemerged in the Gulf of Mexico after passing over the Florida peninsula, it strengthened quickly and again reached hurricane strength. The storm gradually intensified, and late on 26 August Katrina first became a Category 2 storm, with maximum sustained winds reaching 83 knots. During the day on 27 August, the storm tracked primarily westward at Category 2 strength, occasionally decreasing slightly in intensity. Knabb et al. (2005) provide a more detailed summary of Hurricane Katrina's evolution as a storm system.

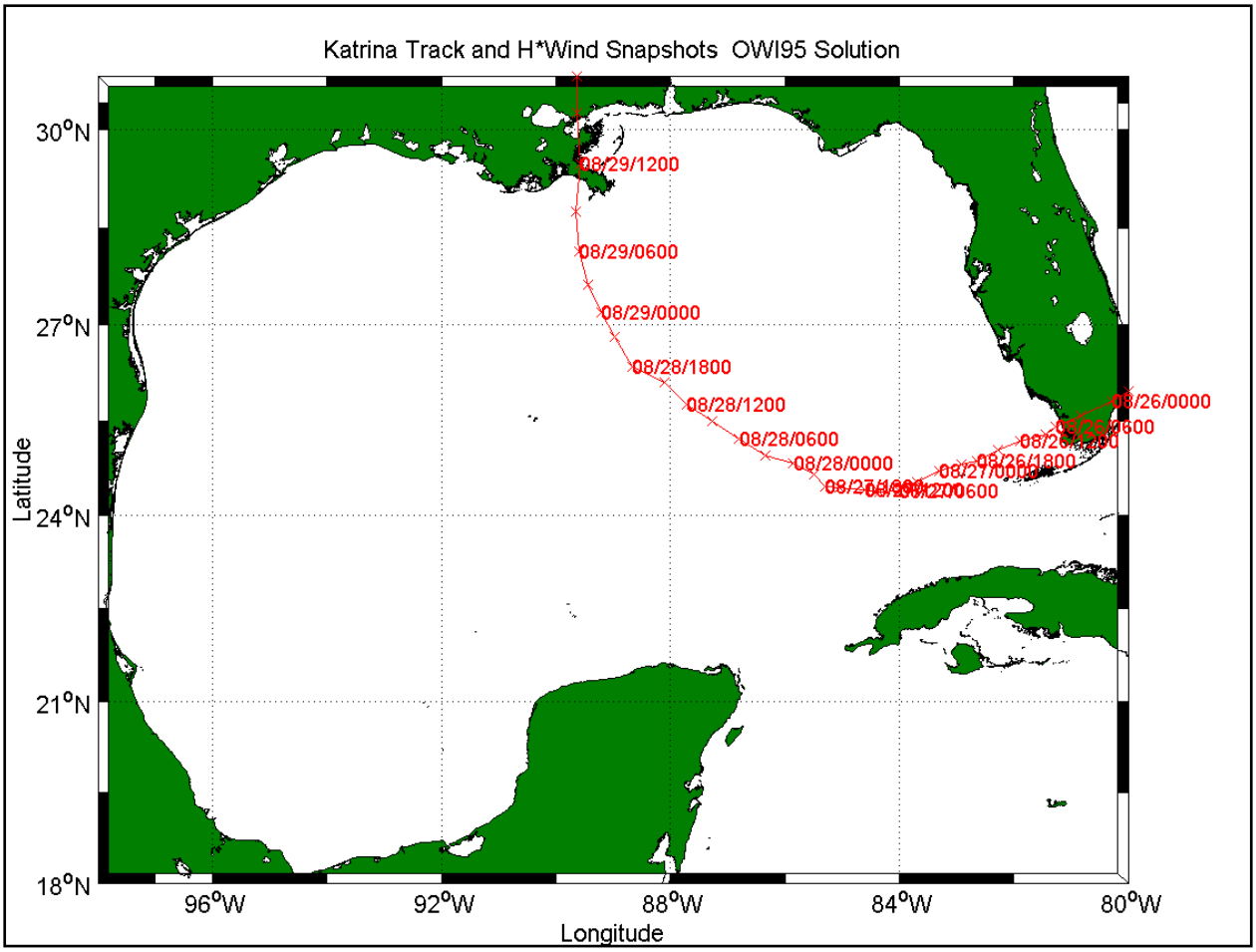

Figure 1. Hurricane Katrina track and times of H*Wind snapshots. [All times are referenced to UTC.]

Table 1
Hurricane Katrina Characteristics

Date/Time (UTC) (2005)	North Latitude (deg)	West Longitude (deg)	Central Pressure (mb)	Maximum Surface Wind Speed (knots)	Radius to Maximum Winds (nautical miles)	Saffir-Simpson Scale
26 Aug 0000	25.799	80.289	984	67	10	Category 1
26 Aug 0300	25.581	80.816	984	63	12	Tropical Storm
26 Aug 0600	25.402	81.227	987	69	13	Category 1
26 Aug 0900	25.291	81.436	983	72	12	Category 1
26 Aug 1200	25.174	81.890	979	75	10	Category 1
26 Aug 1500	25.035	82.282	971	75	12	Category 1
26 Aug 1800	24.854	82.650	969	82	13	Category 1
26 Aug 2100	24.817	82.906	965	83	13	Category 2
27 Aug 0000	24.708	83.309	959	82	18	Category 1
27 Aug 0300	24.529	83.684	954.5	87	7	Category 2
27 Aug 0600	24.389	83.995	950	90	7	Category 2
27 Aug 0900	24.373	84.336	945	93	6	Category 2
27 Aug 1200	24.400	84.600	942	81	7	Category 1
27 Aug 1500	24.438	85.040	942	86	23	Category 2
27 Aug 1800	24.459	85.300	948	87	23	Category 2
27 Aug 2100	24.645	85.484	945	87	23	Category 2
28 Aug 0000	24.833	85.846	941	95	28	Category 2
28 Aug 0300	24.958	86.331	939	97	19	Category 3
28 Aug 0600	25.217	86.797	935	113	16	Category 3
28 Aug 0900	25.500	87.277	915	128	16	Category 4
28 Aug 1200	25.747	87.721	908	139	14	Category 5
28 Aug 1500	26.100	88.100	907	139	16	Category 5
28 Aug 1800	26.347	88.661	902	138	18	Category 5
28 Aug 2100	26.807	88.968	903	134	15	Category 4
29 Aug 0000	27.198	89.212	904	124	14	Category 4
29 Aug 0300	27.624	89.435	908	115	18	Category 4
29 Aug 0600	28.132	89.590	910	108	18	Category 3
29 Aug 0900	28.751	89.649	917	99	31	Category 3
29 Aug 1200	29.479	89.575	923	102	36	Category 3
29 Aug 1500	30.255	89.626	932	97	20	Category 3
29 Aug 1800	31.043	89.640	948	84	16	Category 2
29 Aug 2100	31.754	89.314	954	75	25	Category 1
30 Aug 0000	32.729	89.042	963	51	18	Tropical Storm

At about 0000 UTC on 28 August the storm turned toward the northwest and experienced rapid intensification; it evolved from an upper Category 2 intensity storm to a Category 5 storm in only 12 hr, a very rapid rate. Katrina attained its peak intensity at around 1200 UTC on 28 August, when the maximum sustained surface wind speed reached 139 knots. The storm remained at Category 5 intensity, with the same maximum wind speed, for the next 6 hr as it tracked to the northwest. At 1800 UTC on 28 August, the storm was centered approximately

170 miles south-southeast of the Mississippi River mouth, headed to the northwest, and still at Category 5 strength.

Katrina was a very large storm, in terms of its spatial extent, during its migration through the gulf. From the time Katrina entered the gulf, winds along Southeast Louisiana began to blow from the east, and they remained steady from this direction from 0000 UTC on 26 August through 1800 UTC on 28 August (nearly 3 full days). During this time surface winds along Southeast Louisiana grew steadily in speed from 5 knots to between 30 and 35 knots. These winds pushed water to the west along the Alabama and Mississippi continental shelves toward the Mississippi River delta and began to inundate the coastal wetlands of Southeast Louisiana, east of the Mississippi River. By 1800 UTC on 28 August, when the storm was still 170 miles away, water levels in Lake Borgne had reached levels that were 3 ft above normal. In response to the high water level in Lake Borgne, Lake Pontchartrain began to fill and at this same time on 28 August, water levels in Lake Pontchartrain were about 1 ft above normal. At 1800 UTC on 28 August, significant wave heights east of the Mississippi River entrance had reached almost 20 ft in deep water and about 10 ft just north of the Chandeleur barrier islands. Peak wave periods were 12 sec at both locations.

During the next 6 hr, between 1800 UTC on 28 August and 0000 UTC on 29 August while the storm was tracking to the northwest, its intensity began to decrease; maximum sustained surface wind speeds decreased from 139 knots to 124 knots (Category 4 intensity). At about 0000 UTC on 29 August, the storm turned to the north; and as it tracked northward for the next 6 hr it continued to diminish in intensity. Maximum wind speed decreased to 108 knots (Category 3 intensity) by 0600 UTC on 29 August. During the 12 hr between 1800 UTC on 28 August and 0600 UTC on 29 August, water levels in Lake Borgne (at Paris Road bridge over the GIWW/MRGO) continued to rise, reaching levels that were 5.5 ft above normal. These levels were high enough to completely inundate much of the wetland system east of the Mississippi River Levees. Water levels along the southern shoreline of Lake Pontchartrain rose by another 2 ft to levels that were nearly 3 ft above normal. By 0600 UTC on 29 August, significant wave heights had reached almost 35 ft at a location due east of the southern tip of the Mississippi River delta, in deep water. Just north of the Chandeleur Islands, wave heights had reached 17 ft. Peak wave periods were nearly 15 sec at both locations. The wave gauge just north of the Chandeleur Islands (a NOAA National Data Buoy Center buoy) failed shortly after this time.

At around 0600 UTC on 29 August (about 1:00 a.m. CDT on 29 August), about 5 hr out from landfall in Louisiana, the rate of rise of both water level and wave height increased considerably in Southeast Louisiana. Katrina made landfall near Buras, LA, at around 1100 UTC (6:00 a.m. CDT) on 29 August. At landfall, the maximum sustained surface wind speed was approximately 100 knots (Category 3 strength). The storm retained its large spatial extent, even as it weakened prior to and after landfall. At approximately 1445 UTC (9:45 a.m. CDT) on 29 August, the storm again crossed the coast near the Mississippi/Louisiana border. The maximum sustained surface wind speed at final landfall was estimated to be 97 knots. Katrina continued to weaken, and was at Category 2 strength by 1800 UTC 29 August at which time it had moved well inland.

During the 12-hr period prior to Katrina making its final landfall, despite its decreasing intensity, the storm pushed a considerable volume of water against the Mississippi River delta

and the east-facing levees along the Mississippi River, and in the "pocket" formed by the delta and the Mississippi coast. The storm then pushed that volume of water northward with hurricane strength winds toward the Mississippi coast and into Lakes Borgne and Pontchartrain as the storm tracked to the north. Locally, hurricane force winds from east and east-northeast in advance of the storm center also pushed water against the east-facing levees and floodwalls of the hurricane protection system in Plaquemines, St. Bernard, and Orleans Parishes. The increased water levels in Breton Sound and Lake Borgne allowed considerable wave energy that was generated in the gulf to propagate over and through gaps between the barrier islands, across the inundated wetlands, to the hurricane protection system in Plaquemines, St. Bernard, and Orleans Parishes. Local wave generation also occurred in these inundated areas.

High water levels in Lake Borgne acted to drive water into Lake Pontchartrain (because of the water level difference between the two lakes). In addition to this filling action, locally high winds in Lake Pontchartrain acted to tilt the water surface in the lake, raising the water surface on the downwind side and lowering the water surface on the upwind side of the lake. These same winds created high wave conditions on the downwind side of the lake. Winds blew counter-clockwise about the hurricane's eye, and the storm tracked to the east of Lake Pontchartrain. So as the storm made landfall in Louisiana, tracked north, made final landfall again, and then continued north into Mississippi, wind direction in Lake Pontchartrain changed steadily (winds first from the east, then northeast, then from the north, then northwest, and finally from the west). In response to this changing wind direction, the region of maximum storm surge and high waves translated along the southern half of the lake, moving from west to east.

Throughout the system, the very high water levels and wave energy levels created by Hurricane Katrina exposed the hurricane protection system to considerable hydrodynamic forces. This section provides a general overview of how the wave and water level conditions evolved during the storm. Appendix 5 contains a very detailed discussion of the physics of storm surge wave propagation through the region. The focus for the rest of this volume is characterizing, in much more detail, the water level and wave conditions along the periphery of the hurricane protection system. Forces and loadings on the system created by those conditions are also discussed in more detail. The hydrodynamic conditions created by Katrina are then compared to the conditions which the projects were designed to withstand, from both regional and local, high-resolution hydrodynamic perspectives.

High-Water Marks and Hydrographs

Introduction

The Interagency Performance Evaluation Task Force (IPET) study used a combination of measured data and model-simulated data to characterize the time varying water level conditions. Measured data fell into two categories: HWM measurements which capture peak water levels (with some uncertainty); and hydrographs, which capture the water level as a function of time (with more certainty). An extensive post-storm effort was undertaken to identify and survey HWMs following passage of the storm. While certain HWMs capture the peak water levels well, they contain no information about the temporal variation of water level. HWMs also have their

own inherent issues of quality, uncertainty whether they in fact do reflect a peak condition, and whether or not water surface motions due to short wind waves or other factors are reflected in a HWM.

Measured hydrographs are the most reliable source of data for capturing both the temporal variation and the maximum water level, and they were used to define conditions wherever possible. Water level fluctuations were measured with instrumentation during the build-up stage of the storm at a number of sites throughout the study region; however, few instruments operated throughout the storm. Most of them failed prior to the peak. Consequently, there are little measured data that capture peak conditions. In a few cases, photographs and other visual observations were utilized to provide information about the temporal variation of water level to supplement the recorded hydrographs. These constructed hydrographs proved to be extremely valuable for characterizing conditions along the south shore of Lake Pontchartrain.

High-Water Mark Acquisition and Analysis

The passage of hurricanes often results in short-period wind waves on top of the much longer-period storm surge that creates significant entrainment of various types of debris including vegetation, seeds, dirt, man-made trash, and dislodged building material. Depending on local conditions, the entrained debris will deposit on or adhere to some surfaces once the peak water level has been reached and water levels begin to fall. The deposited debris leaves what is referred to as a HWM and the mark is used to quantify the magnitude of peak water level. The highest quality marks for estimating storm still-water levels are those that have little or no wave effect (i.e., no influence of wave crests or wave runup). Some HWMs are collected where significant wave effects are present, but that effect is noted. In this analysis, the focus was on use of HWMs as indicators of storm water level, without the effects of water level fluctuations due to wave crest or wave runup effects. Some of the marks do provide useful information on the extent of wave runup.

Acquisition of HWMs following Katrina was performed by three federal agencies, United States Geological Survey (USGS), U.S. Army Corps of Engineers (USACE), and Federal Emergency Management Agency (FEMA) (or a FEMA contractor), and the State of Louisiana through the Louisiana State University (LSU). All four entities shared the data. Marks identified by USACE, FEMA, and LSU were also recovered by each respective agency. Most of the marks identified by USGS were recovered by FEMA (or a FEMA contractor). A selected subset of approximately 50 marks identified by USGS was also recovered by USGS field crews to confirm elevations provided by FEMA contractors.

All HWMs were reviewed and assigned a reliability rating. The reliability of each HWM is assessed as “Excellent,” “Good,” “Fair/Poor,” or “Unknown” if there was no information provided regarding the type of mark or setting in which it was acquired. There is no standard method for determining HWM reliability. Moreover, assignment of reliability values to HWMs is not a totally objective process, but by its nature involves both objective and subjective elements. Discussion by the IPET team assigning the reliability values led to a consensus that the mark should reflect, as closely as possible, the stable (“still”) or mean, storm water level. That is, the physical setting where the mark was located should approximate a tide gauge stilling-well

type environment. The basis for this consensus is that storm surge models do not explicitly include wave crest or runup effects, and one of the important uses of the HWM data is validation and verification of surge model simulations.

Approximately 790 HWMs were identified and recovered by the four previously identified agencies in Louisiana and Mississippi following Katrina's passage, excluding marks identified and recovered within the New Orleans levee system. Of these 790 marks, approximately 95 marks (about 12 percent) were recovered from the interior of structures and are considered to be the most reliable measures of the storm water level. The remaining 695 HWMs are debris lines (wrack lines), or on the exterior of structures where they could include wave or wind-blown water effects. It should be emphasized that the exterior HWMs are not less valid measures of inundation, just that they are not as accurate indicators of what is generally defined as storm water level.

The area of Southeast Louisiana, including the New Orleans metropolitan area, is known to be subsiding. To provide the best vertical datum reference for leveling marks in Louisiana, the National Geodetic Survey (NGS) was consulted. The NGS staff recommended a time-dependent datum designated NAVD88 (2004.65) be used. The use of NAVD88 (2004.65) resulted in vertical adjustment of network monumentation in this geographic area of between 0.4 and 0.7 ft. Adjustment of the vertical datum used for Mississippi HWMs was considered not required at this time, so all HWMs in Mississippi are referenced to NAVD88 vertical datum.

Figure 2 is an example image of an HWM presentation, which includes the HWM identifier and water surface elevation. The shape of the HWM identifier indicates the HWM reliability. Superposition of the mark on a photographic image aids in assessment and interpretation of HWMs in light of their geographic setting. The setting in which an HWM was collected is important in assessing the physical processes that might be reflected in a mark.

These HWM images were produced for the areas shown in Figures 3 and 4, which show locations of all the individual images that were created.

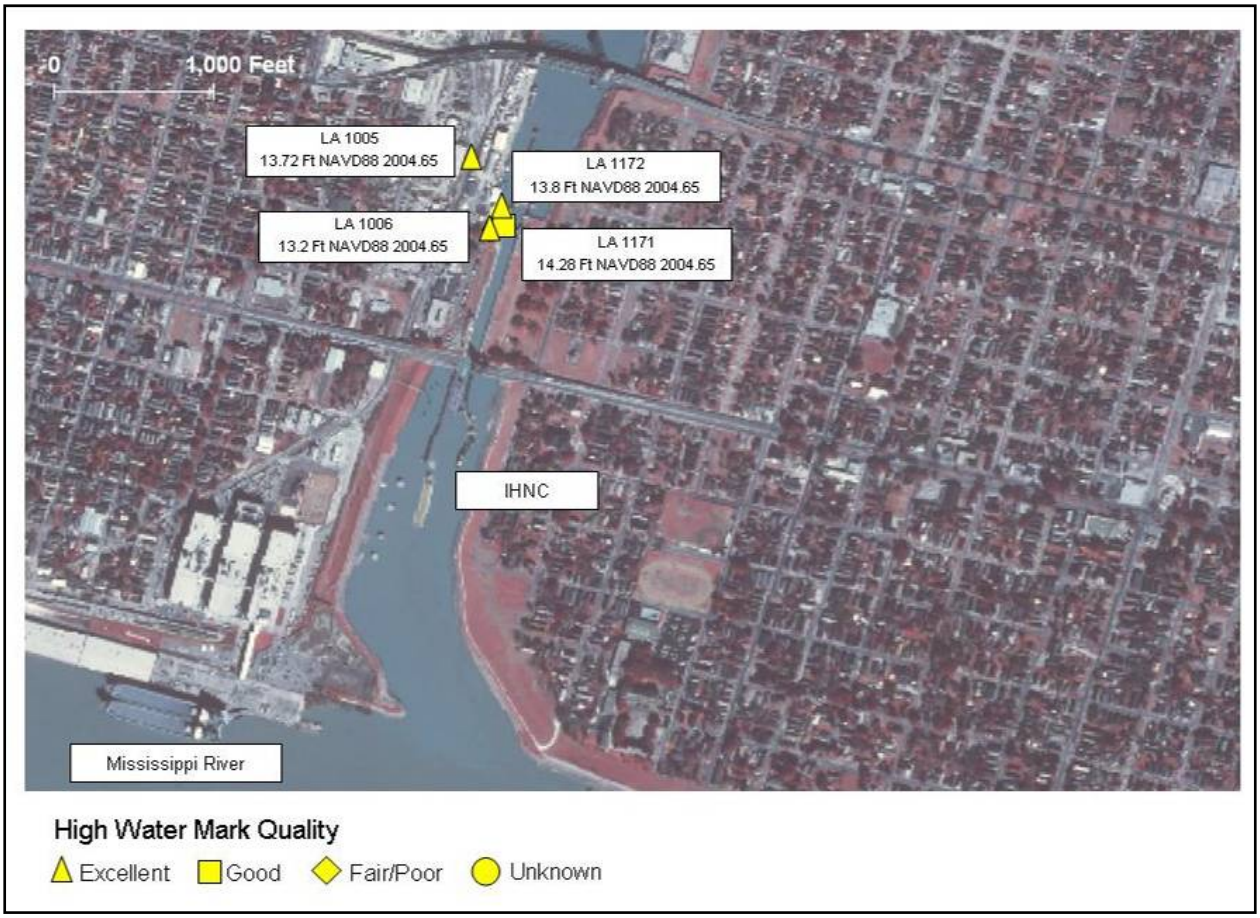

Figure 2. Sample image of the Inner Harbor Navigation Canal and Lock vicinity showing locations of HWMs and water elevation for each mark.

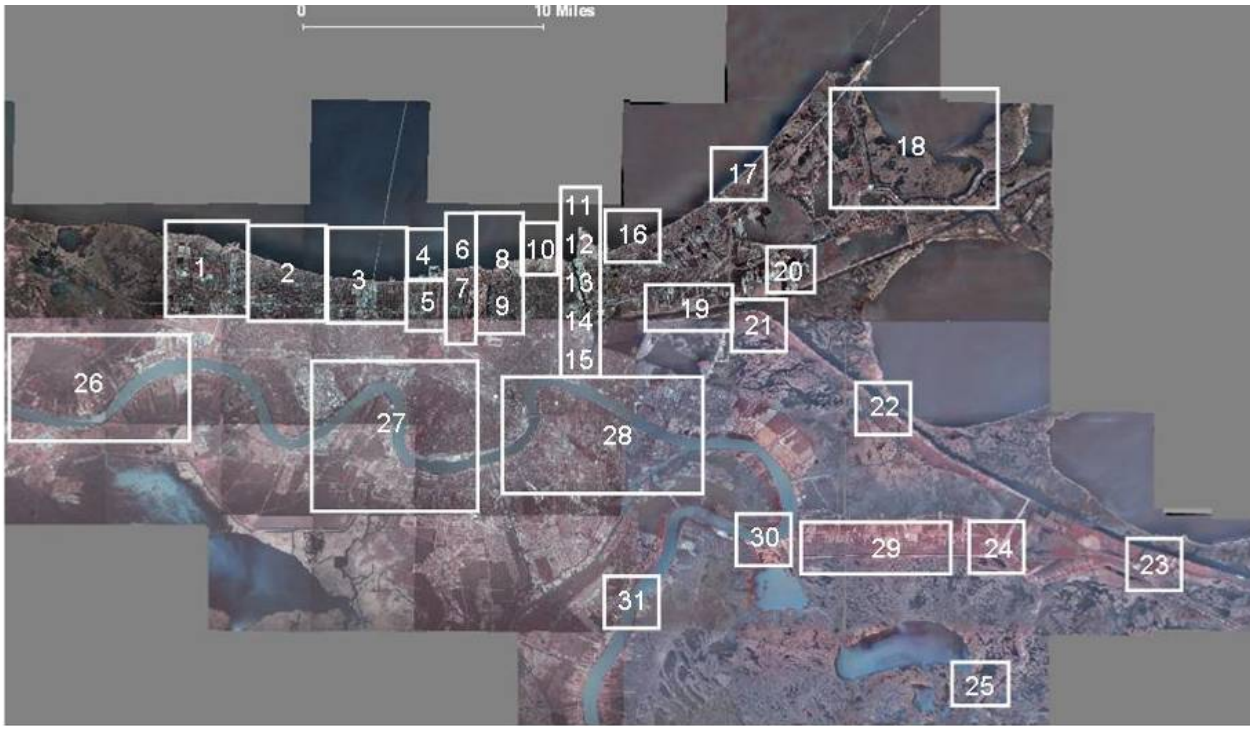

Figure 3. Index map for northern set of HWM images.

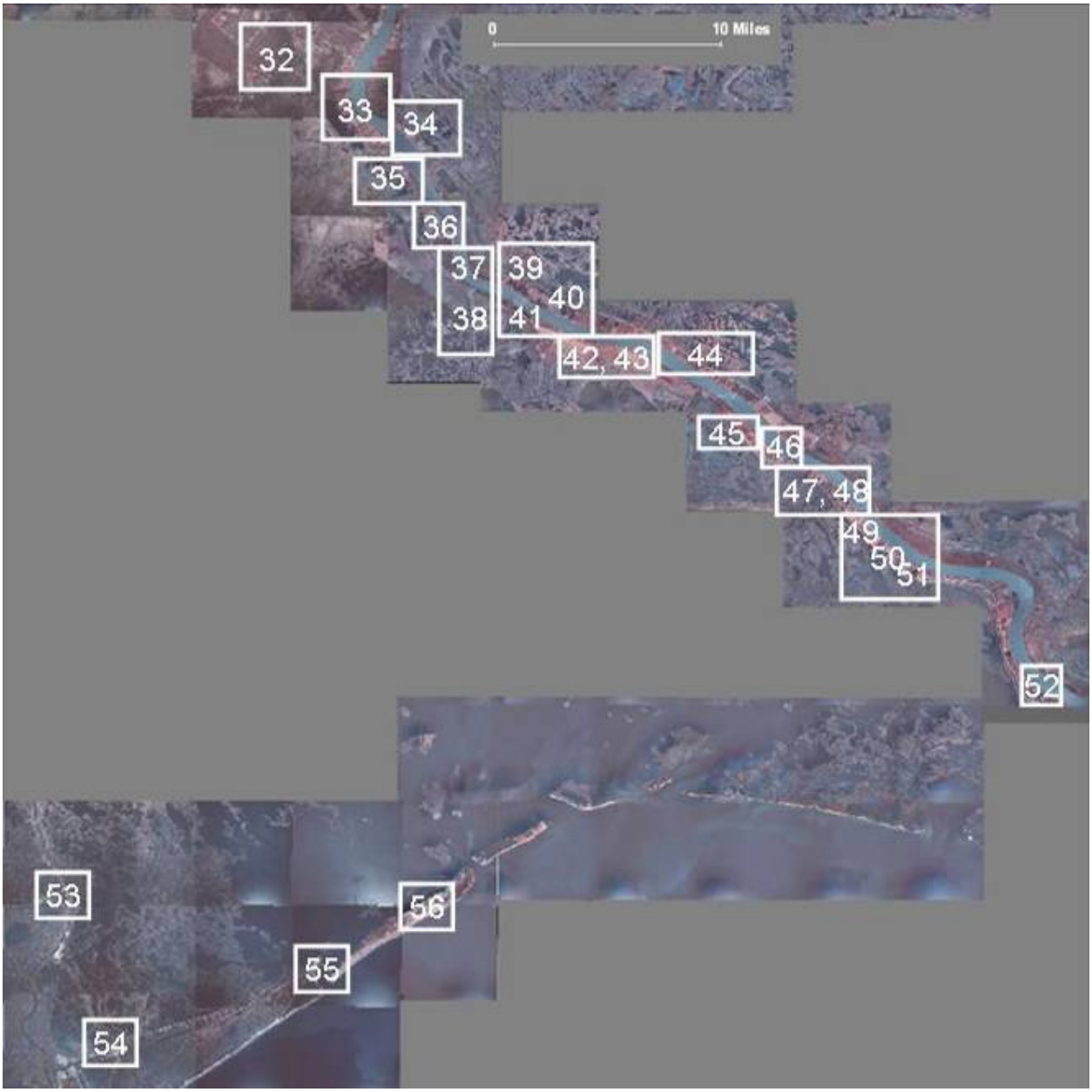

Figure 4. Index map for southern set of HWM images.

The images were only produced for HWMs collected in Southeast Louisiana, and for the most part, only HWMs in unprotected areas are shown in these images. All images and the index maps are provided in Appendix 1 that accompanies this volume.

All HWMs that were acquired as part of this investigation are provided in a spreadsheet at the end of Appendix 1. The spreadsheet includes all HWMs collected in Louisiana and Mississippi, in both unprotected and protected areas. Generally, there are a number of HWMs in protected areas of Orleans, St. Bernard, and Plaquemines Parishes. There are fewer HWMs in the unprotected areas of eastern St. Bernard, Orleans and particularly southern Plaquemines Parishes. Analysis and presentation of HWMs presented in this volume focus on those marks that

reflect water level conditions along the outer perimeter of the hurricane protection system, for use in analyses of the regional water level conditions.

Additional information is also provided later in this volume that compares estimates of water level maxima to the maximum water level conditions considered in the design of the hurricane protection projects. The results presented there reflect our present best estimates of water level maxima using HWMs where excellent marks exist, maxima from measured hydrographs, or maxima determined from model results in the many locations where no measured data are available.

Water Level Hydrograph Acquisition and Analysis

Hydrograph data, as defined here, differ from HWM data in that time and magnitude are known for water level data whereas only magnitude is known for HWM data. The hydrograph data come from various sources including gauge data, staff readings, and surveys of physically identifiable objects in time-tagged digital pictures. In the usual (and strict) sense of usage, the term "hydrograph" refers to water level data from a calibrated staff or instrument recorded either manually or automatically. Because the time sequence of events is of paramount importance for the post-Katrina project performance studies, every available technique has been used to depict as accurately as possible the rise, peak, and fall of storm water levels. All hydrograph data from identified conventional gauges or calibrated staffs in the affected area have been reviewed. Unfortunately, most gauges malfunctioned or did not survive, and therefore they did not record the peak water level of Katrina. Moreover, there were no gauges at the entrances to the 17th Street, Orleans, and London Avenue Canals, the GIWW, or the IHNC except at the IHNC Lock which is located at the southern end of the IHNC. The hydrograph from the IHNC Lock was derived from staff gauge readings made by a member of the lock operation staff.

Time-tagged digital images from the Lake Pontchartrain - New Orleans lakefront were taken by several individuals who remained in buildings or on vessels during Katrina's passage. Using these images (which contained physically identifiable reference marks), logs of observations, and nearby HWMs, hydrographs were constructed for the 17th Street Canal entrance, the New Orleans Lakefront Airport, and the IHNC Lock. The constructed hydrographs were crucial pieces of information for characterizing the time variation of water level along the south shore of Lake Pontchartrain during the peak of the storm. Recorded and constructed hydrographs are presented in the following sections. Note that all elevations are presented in the time-dependent vertical datum NAVD88 (2004.65), and all subsequent discussion will refer to elevations relative to this vertical datum.

Observed Water Levels in Lake Pontchartrain

High-Water Marks at 17th Street Canal Entrance

Figure 5 shows HWMs that were acquired at the entrance to the 17th Street Canal. This particular site had a very high density of excellent marks. The harbor shown at the top of the image was the harbor where digital photos were taken and used to construct a water level

hydrograph. Analysis of the highest quality marks resulted in a best estimate for the peak water level at the canal entrance of 10.8 ft NAVD88 (2004.65). It is interesting to note that there was a 1.7-ft range reflected in the set of excellent marks, and a standard deviation of +/- 0.5 ft about the best estimate of 10.8 ft.

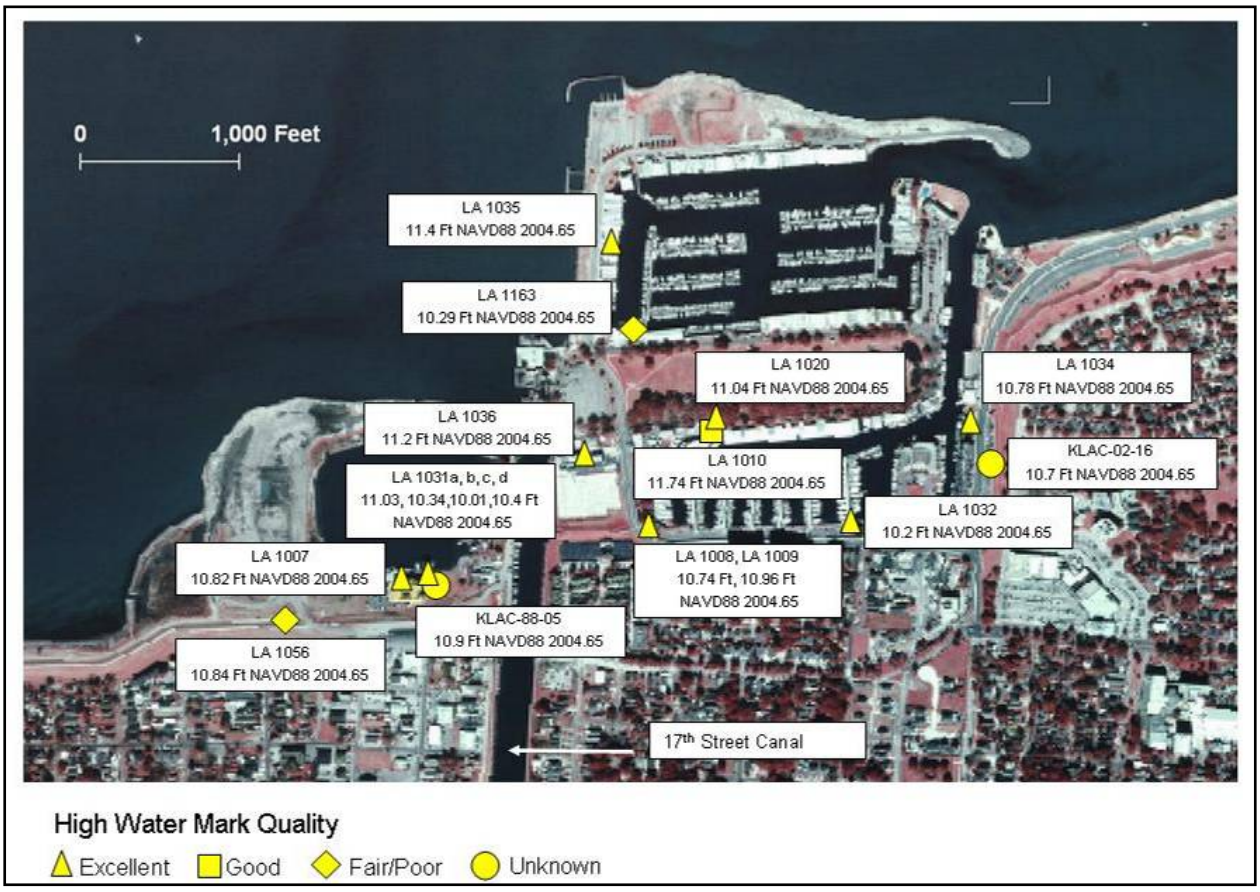

Figure 5. 17th Street Canal entrance showing locations of HWMs and water elevation for each mark.

High-Water Marks at Orleans Avenue Canal Entrance

Figure 6 shows HWMs collected at the entrance to Orleans Avenue Canal. Several of the marks along the lakefront appear to reflect the influence of wave runup on the levees and are not reliable indictors of the peak still-water level. One very reliable mark along the lakefront east of the entrance showed an elevation of 11.8 ft NAVD88 (2004.65), and a less reliable mark inside the canal (a debris line), which probably does not reflect much wave action, shows an elevation 10.8 ft. These marks are consistent with those from the 17th Street Canal entrance. In light of the trend in peak water level variation along the south shore of Lake Pontchartrain, a gradual increase from west to east, and storm surge model results that show a similar trend, the peak water level conditions at Orleans Avenue Canal entrance should not greatly differ from those at the entrance to 17th Street Canal.

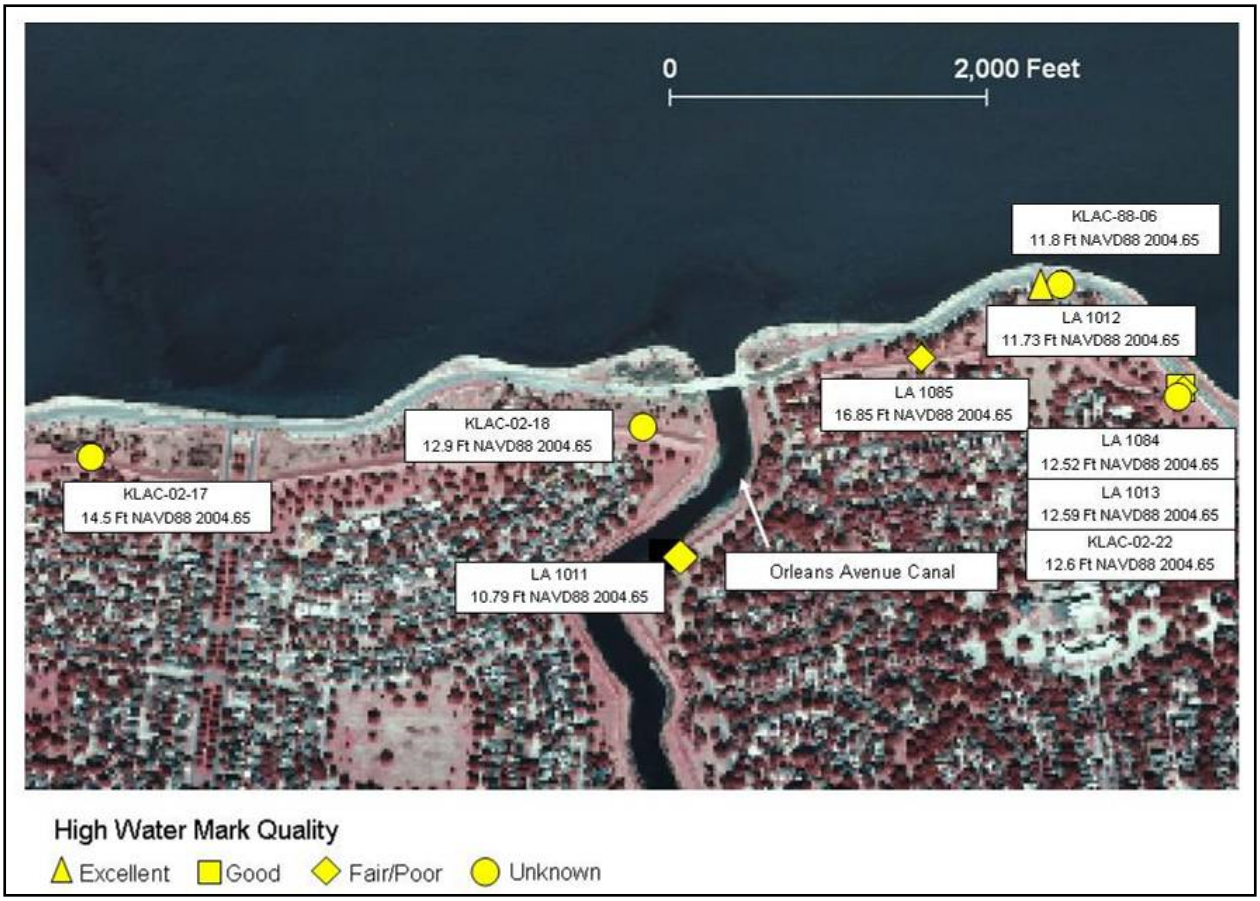

Figure 6. Orleans Avenue Canal entrance showing locations of HWMs and water elevation for each mark.

High-Water Marks at London Avenue Canal Entrance

Figure 7 shows HWMs at the entrance to London Avenue Canal. Many marks were acquired; however, none were rated as either excellent or good (reliable) measures of the peak still-water level. Taken as a group, the most reliable of the marks within the more protected confines of the canal suggest peak elevations in the range from 10.0 to 11.2 ft. These peak values are consistent with marks from the 17th Street and Orleans Avenue Canal entrances. Several higher marks along the exposed portions of levees seem to reflect the influence of wave runup.

High-Water Marks at Lake Pontchartrain Entrance to the IHNC

Figures 8 and 9 show images to the west and east, respectively, of the Pontchartrain entrance to the IHNC. There are several reliable marks at this location, which are consistent with each other and show a range of peak water levels of 11.7 to 12.1 ft. Lakefront Airport is also the location where a hydrograph was constructed from a series of digital photos. Data used to construct the hydrograph are consistent with these HWMs. The best estimate for peak water level at this location is 11.8 ft NAVD88 (2004.65), and it is based on numerous very reliable HWMs.

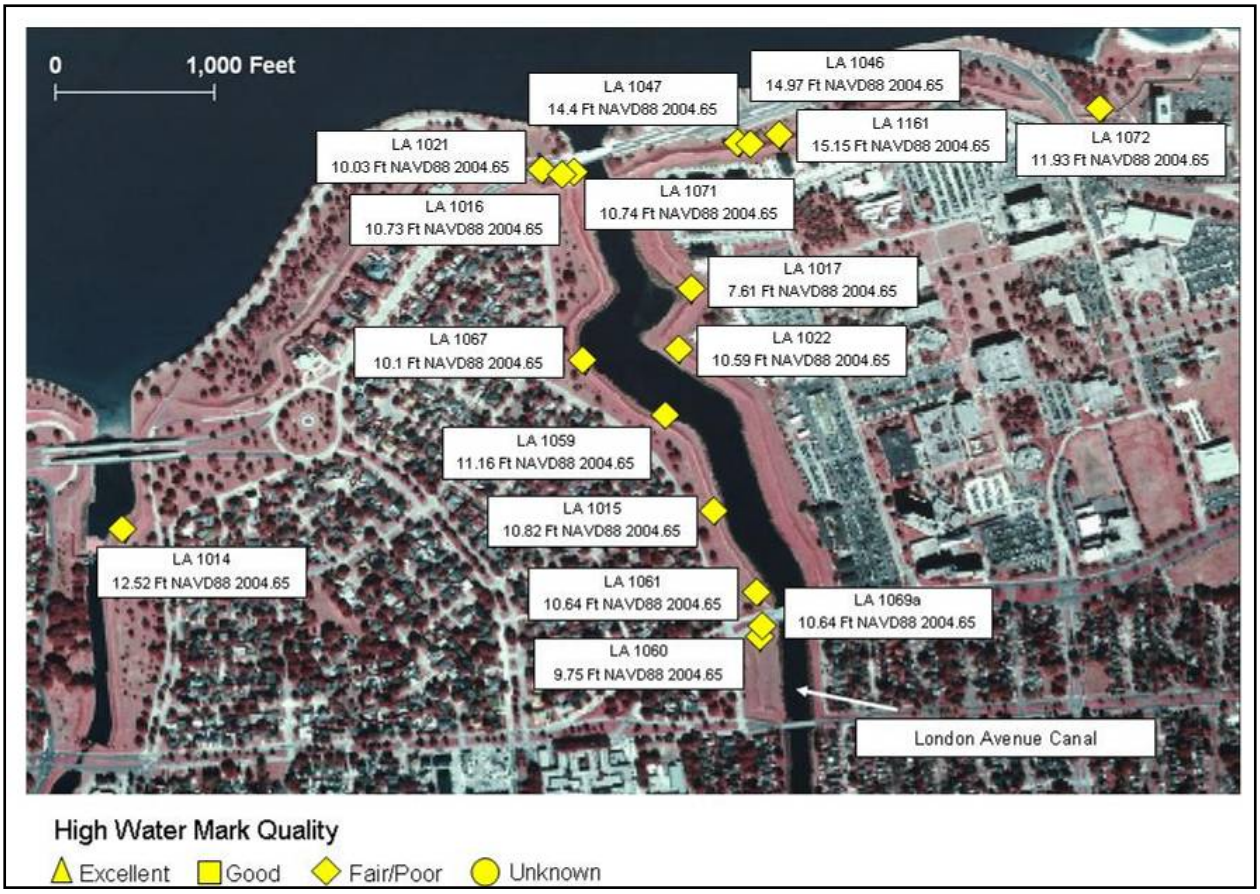

Figure 7. London Avenue Canal entrance showing locations of HWMs and water elevation for each mark.

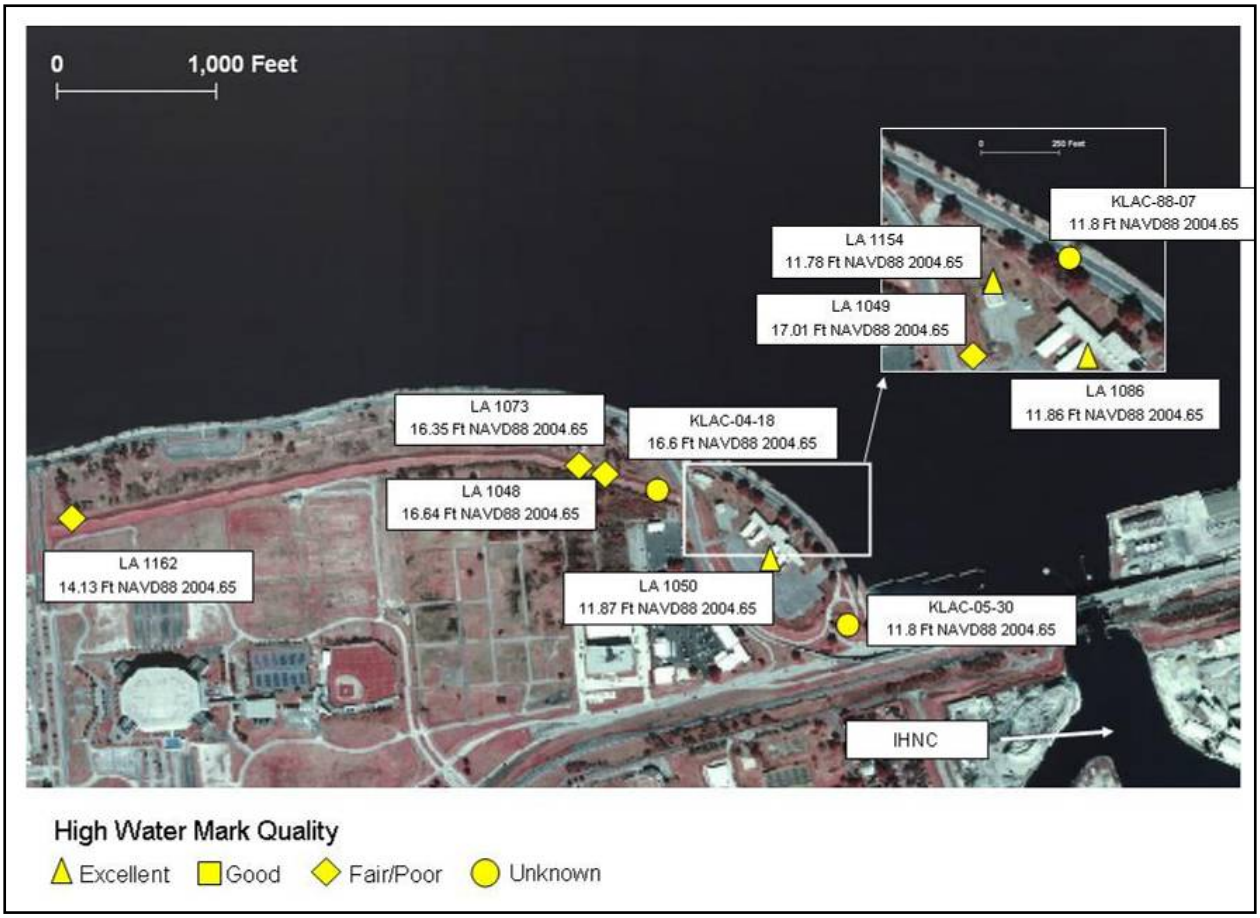

Figure 8. Lake Pontchartrain entrance to the IHNC, west side, showing locations of HWMs and water elevation for each mark.

Figure 9. Lake Pontchartrain entrance to IHNC, Lakefront Airport, showing locations of HWMs and water elevation for each mark.

Lake Pontchartrain Hydrographs

Figure 10 shows a map of various locations in Lake Pontchartrain where measured hydrographs were acquired or where hydrographs were constructed from digital photos. Figure 11 shows a plot of five hydrographs recorded at gauge sites and the two constructed hydrographs (at the entrance to 17th Street Canal and at the New Orleans Lakefront Airport). A very detailed description of procedures used to construct the two hydrographs and all photos used in the analysis are provided in Appendix 1. Each hydrograph in Figure 11 is also labeled with a relative location in Lake Pontchartrain, west, central, or east.

The constructed hydrographs at the 17th Street Canal and the Lakefront Airport and the gauge hydrographs at Southshore Marina, Little Irish Bayou, Pass Manchac, and Bayou Labranch were all established directly to NAVD88 (2004.65) via surveying. For the purposes of this work, the Midlake Gauge was adjusted to NAVD88 (2004.65) by matching the average of the Pass Manchac and Bayou Labranch gauge hydrographs before the storm.

Along the south shore of Lake Pontchartrain, a much more rapid rate of water level rise began at about 0600 UTC (1:00 a.m. CDT) on 29 August. At this time, water level along the

south shore began to increase from a level of about 3 ft NAVD88 (2004.65) and rose to a peak level of about 11 to 12 ft NAVD88 (2004.65) roughly 8 hr later (an average rate of rise of approximately 1 ft/hr). The peak water level, based on the reconstructed hydrographs from the 17th Street Canal entrance and Lakefront Airport, was observed along the south shore of the Lake sometime between 1400 and 1500 UTC (9:00 a.m. and 10:00 a.m. CDT) on 29 August.

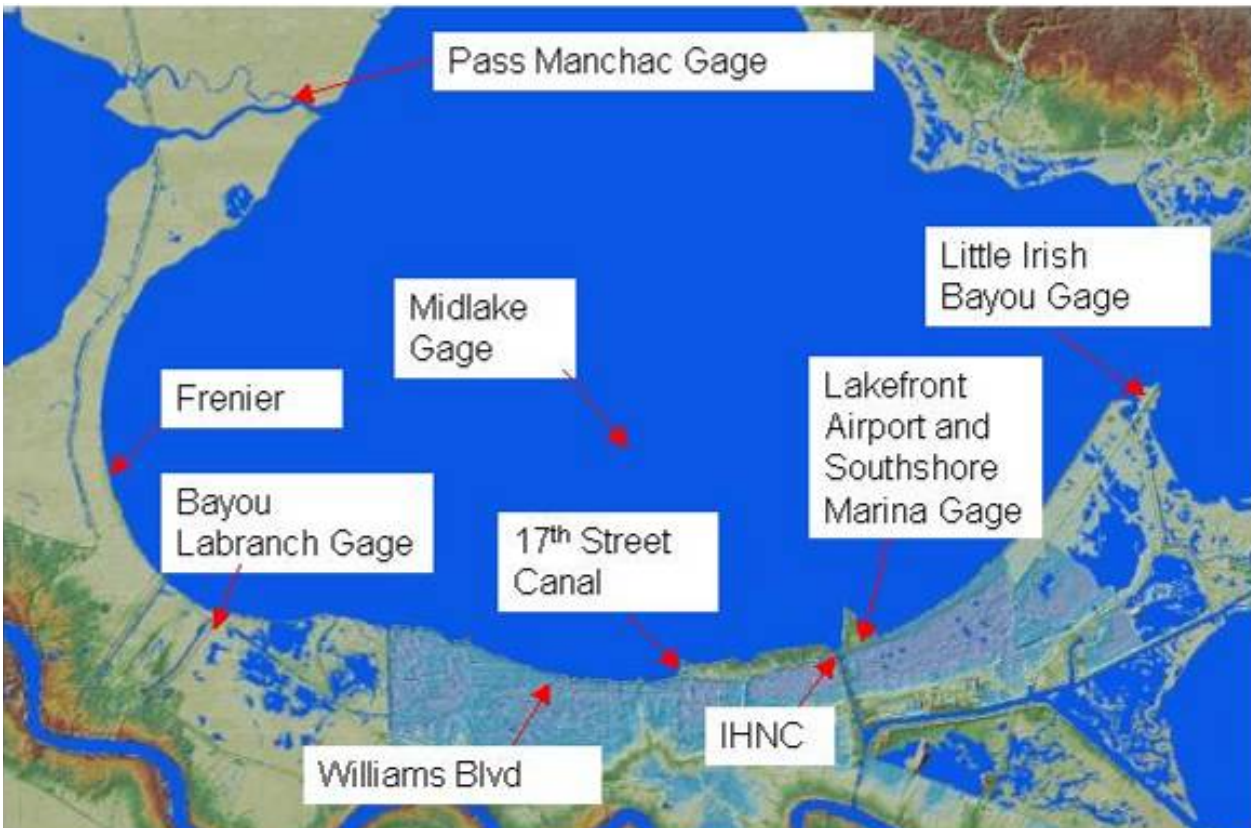

Figure 10. Lake Pontchartrain hydrograph locations.

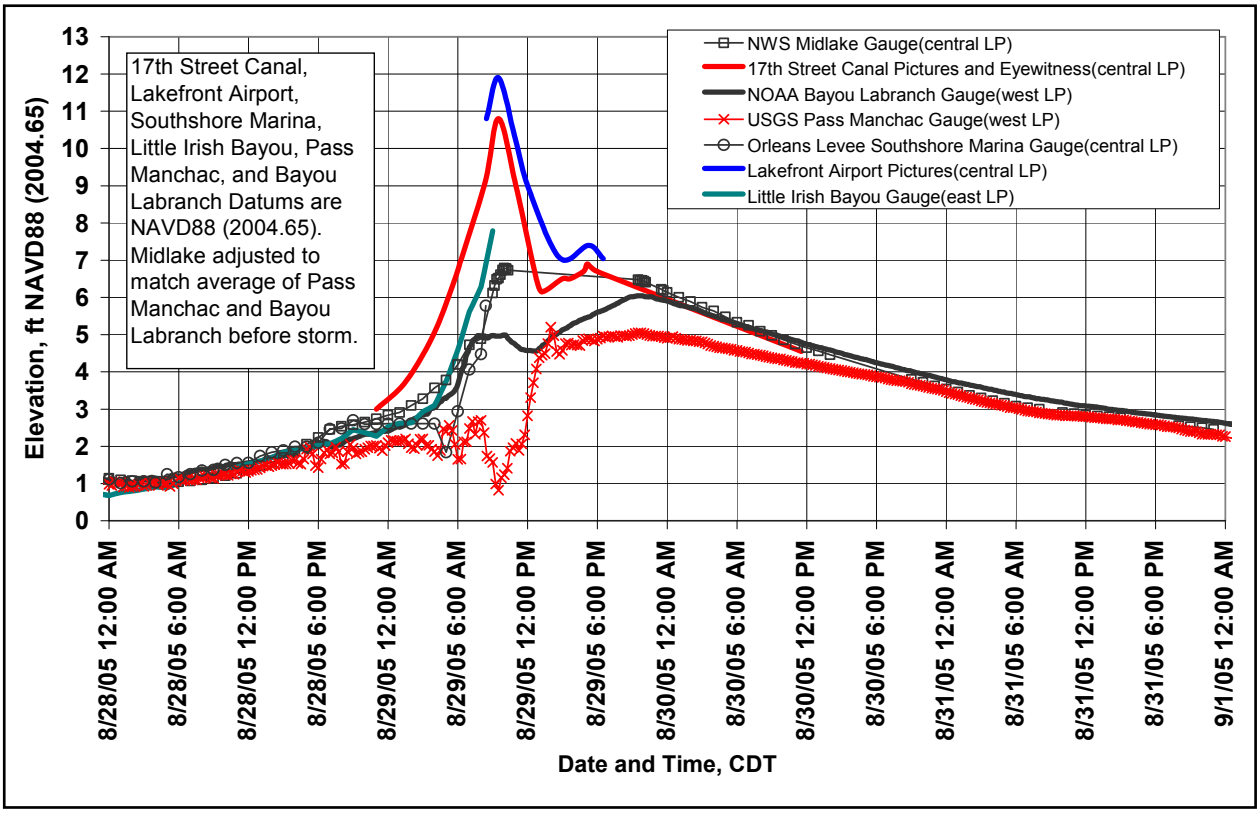

Figure 11. Gauge hydrographs and constructed hydrographs on Lake Pontchartrain [Note time axis is referenced to CDT not UTC. To convert from CDT to UTC, subtract 5 hours.).

Lake Pontchartrain South Shore - Alongshore Variation in Peak Water Level

Figure 12 shows a plot of HWMs along the south shore of Lake Pontchartrain. The marks are separated into three categories: USACE marks inside buildings, USACE levee debris marks, and FEMA wrack or debris line marks, with the last two categories being essentially the same type of mark in terms of reliability. The plot also shows a best estimate of the alongshore variation of peak storm water level based on the highest quality HWMs. The figure clearly shows the wide range of variability associated with less-reliable HWMs (debris lines and wrack lines), relative to the trend that is apparent based on the marks that are considered to be the most reliable indicators of the maximum storm still water level.

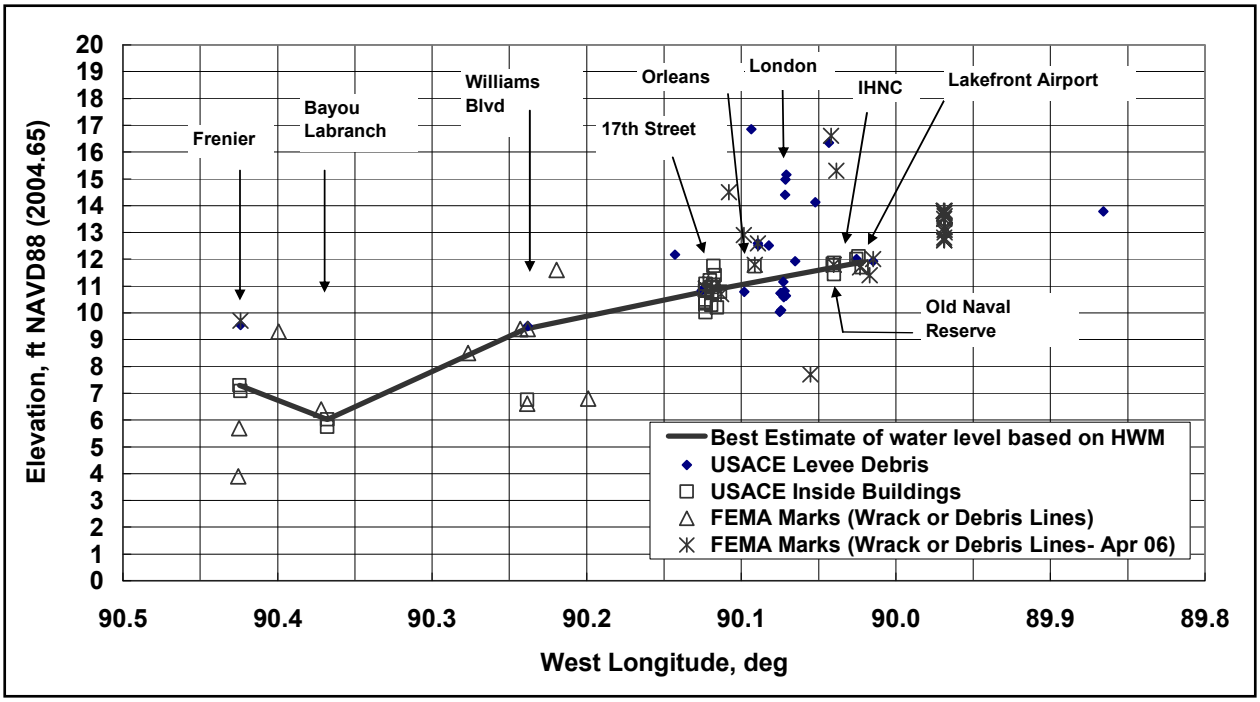

Figure 12. Variation of peak water level along south shore of Lake Pontchartrain based on high-water marks.

With the exception of the Williams Boulevard location, the best-estimate line is based on USACE marks inside buildings that were rated as having excellent reliability. At Williams Boulevard, there is a restroom on the lakefront that has all the characteristics of an excellent stilling well. The elevation of the mark (6.5 ft) in this restroom is much lower than the levee debris found by both the USACE and the FEMA teams. The 6.5 ft elevation is consistent with the elevations from Hurricane Rita. Any marks on Figure 12 less than about 7.5 ft and to the east of Bayou Labranch could reflect Hurricane Rita rather than Hurricane Katrina. The levee debris is accepted at this location because the foreshore slope between the levee debris and the lake is extremely flat and long that would have resulted in minor wave action at the location where the levee debris was deposited.

Using the best estimate peak HWM curve, the peak water level at the entrance to the four canals along the south shore of Lake Pontchartrain were assigned the following values: 1) 10.8 ft at 17th Street Canal entrance, 2) 11.1 ft at Orleans Avenue Canal entrance, 3) 11.4 ft at London Avenue Canal entrance, and 4) 11.8 ft at the entrance to the IHNC. Using these peak water levels at the canal entrances along with the constructed hydrographs at 17th Street Canal and the Lakefront Airport, hydrographs were interpolated for Orleans Avenue Canal, London Avenue Canal, and the IHNC entrances as shown in Figure 13. These constructed hydrographs were the best available information for characterizing the water level hydrographs at the entrances to each of the canals, and they were used to define the time variation of water level during Hurricane Katrina at these locations. The peak water levels occurred sometime between 1400 and 1500 UTC (9:00 a.m. and 10:00 a.m. CDT) on 29 August, but were defined to occur at 1430 UTC (9:30 a.m. CDT).

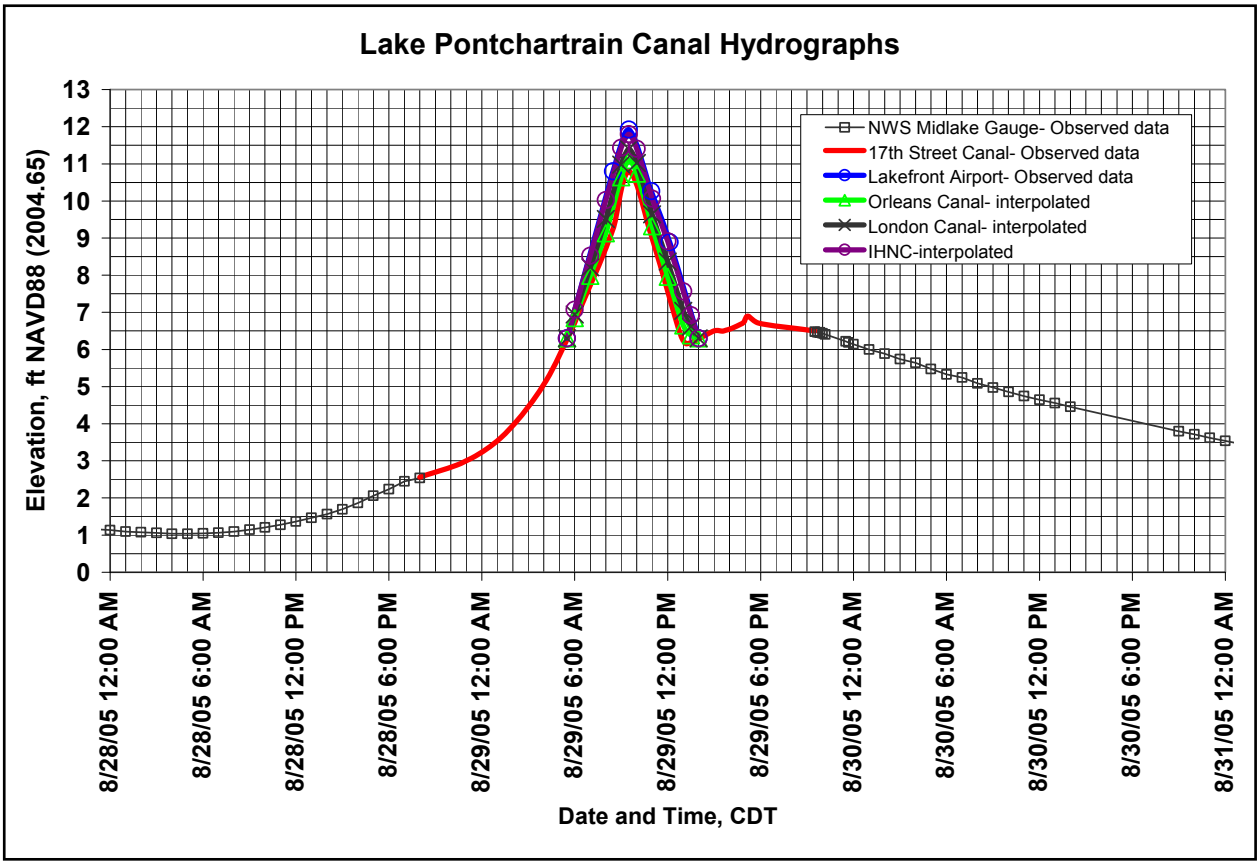

Figure 13. Constructed and interpolated hydrographs at canal entrances. [Note time axis is referenced to CDT not UTC. To convert from CDT to UTC, subtract 5 hours.]

Observed Water Levels along the IHNC

This section summarizes HWMs and hydrographs from self-recording gauges, staff gauges, and digital pictures along the IHNC. The variation of peak water level along the IHNC from HWMs is also presented. Figure 14 shows a plot of data from two self-recording gauges at I-10 on the IHNC, a self-recording gauge at Paris Road (I-510) on the GIWW/MRGO, staff gauge readings at the IHNC Lock, and water levels derived from digital pictures taken at the IHNC Lock.

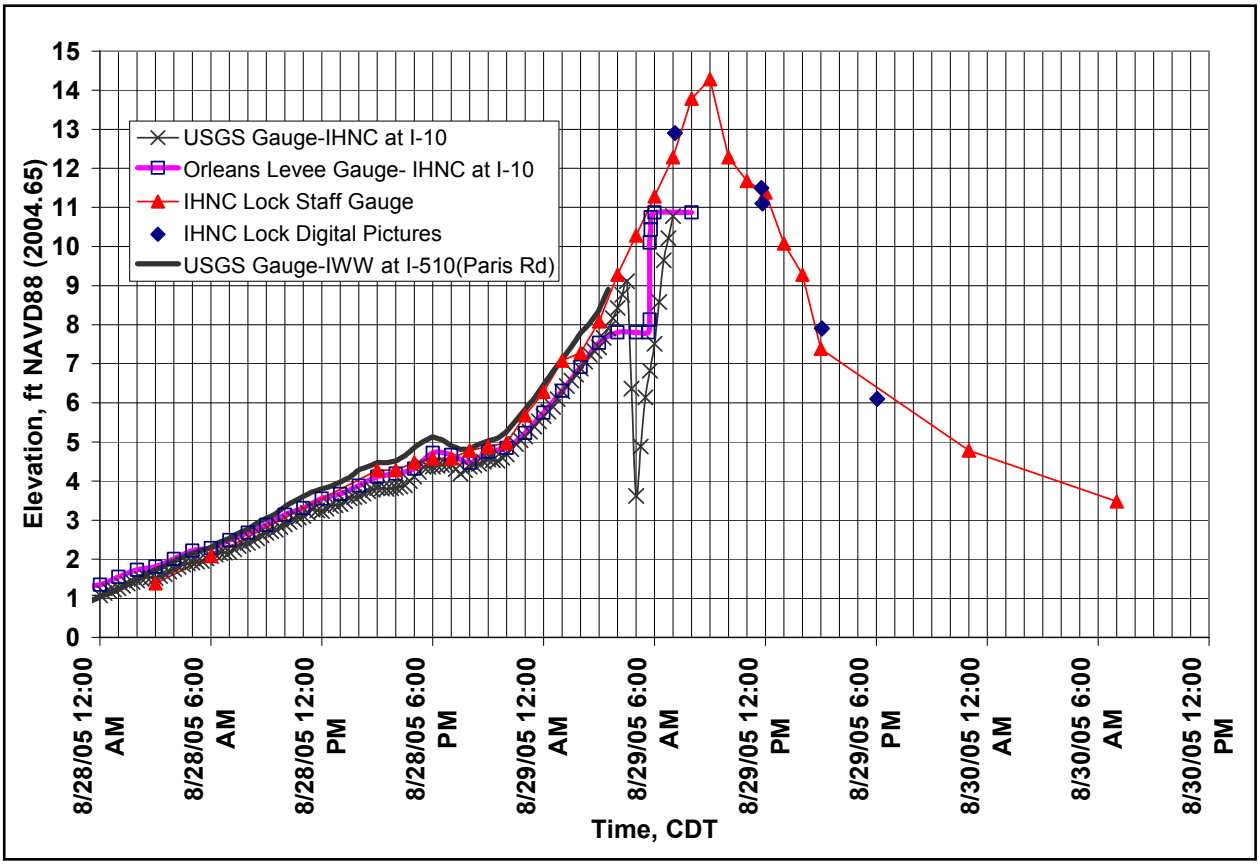

Figure 14. Hydrographs on the IHNC and GIWW. [Note time axis is referenced to CDT not UTC. To convert from CDT to UTC, subtract 5 hours.]

During passage of Hurricane Katrina, water levels were recorded by an operator from the staff gauge at the IHNC Lock. The operator stated that each hour, on the hour, he would read the high and low and record an average value. Based on the recorded readings and the operator's statements, the gauge was being read to the nearest 0.1 ft for elevations below about 12.5 ft and the nearest 0.5 ft while the stage was approaching the peak and wave action was significant. The staff gauge was surveyed by the IPET datum team and the 15-ft mark was found to be equal to an elevation of 14.3 ft NAVD88 (2004.65). All IHNC staff gauge readings were reduced by 0.7 ft to convert to NAVD88 (2004.65). The hydrograph established from these staff gauge readings was the only hydrograph that captured the peak water level condition in the IHNC and GIWW. Digital pictures also were taken by one of the IHNC Lock personnel, and water levels were derived from the photos following the same procedures used to construct hydrographs for Lake Pontchartrain. See Appendix 1 for more details.

The rate of water level rise at the IHNC Lock significantly increased, beginning at about 0400 UTC on 29 August (11:00 p.m. CDT on 28 August) when the water level was about 5 ft NAVD88 (2004.65). Peak water level at the IHNC Lock was observed at approximately 1400 UTC (9:00 a.m. CDT) on 29 August, when the maximum hourly elevation was recorded, but the actual peak may have occurred a little earlier. Between 0400 and 1400 UTC on 29 August, the water level rose approximately 9 ft, an average rate of 1 ft/hr.

HWMs that were rated excellent in terms of reliability were also collected in the vicinity of the lock. However, in light of the perceived reliability of the operator who read the staff gauge, the reading of 14.3 ft NAVD88 (2004.65) is considered the best estimate of the peak high water at this location. HWMs acquired nearby ranged from 13.2 to 13.8 ft (see Figure 2).

As shown in Figure 14, the USGS gauge at I-10 on the IHNC experienced a 5-ft drop in stage at about 0930 UTC (4:30 a.m. CDT) on 29 August when the stage was about 9.5 ft. At first, this drop was interpreted to mean that a breach on the IHNC occurred at this time, but most people doubted that the water level dropped 5 ft. A PVC pipe holding the USGS gauge has a top elevation of about 9 ft on the staff gauge. The electronic cable holding the USGS pressure transducer inside the PVC pipe is exposed above the top of the pipe. One possible explanation of the 5-ft drop is that the high velocities through the railroad/I-10 bridge opening in the floodwall which did breach, along with debris, snagged the cable and pulled the transducer up out of the pipe giving it an apparent drop in water level. The Orleans Levee District (OLD) gauge, which is located beside the USGS gauge, is a float gauge that did not experience this magnitude of drop in water level but did experience identical 7.8 ft readings at 0900, 1000, and 1040 UTC (4:00 a.m., 5:00 a.m., and 5:40 a.m.CDT) followed by a rapid rise in 8 min to about 10.9 ft. The 10.9-ft reading is in agreement with the IHNC Lock readings. The pattern of constant readings followed by a rapid rise is consistent with a float gauge that became stuck. Because the OLD and USGS gauges are located within 10 ft of each other, the difference in water levels between the two gauges raises concerns about readings on both gauges after about 0930 UTC (4:30 a.m. CDT).

The peak water level variation along the IHNC is complicated by railroad bridges that were in the down position and had relatively low chord elevations. Low chord elevation on a bridge refers to the lowest elevation at which the bridge structure begins to block the flow area. The low chord elevations for bridges on the IHNC are as follows:

- Railroad bridge at Lakeshore Drive- elevation 2.4 ft
- Railroad bridge at I-10- elevation 3.5 ft
- Railroad bridge at Florida Avenue- elevation 4.1 ft

Peak water levels are also complicated by the presence of the Port of New Orleans (PONO) floodwall that was never finished and does not tie into the USACE protection on the north end of the PONO. In addition, some or all of the floodgates on the PONO were either not closed or only partially closed during Katrina. Personnel of the OLD stated that these floodgates are generally not closed because of the lack of completion of the PONO floodwall on the north end.

Figures 15, 16, and 17 show HWMs and layout of the USACE hurricane protection along the west side of the IHNC. Figure 16 shows the layout of the PONO floodwall. In Figures 15 and 16, at the railroad south of I-10 on the west side, is the floodwall opening that was sandbagged prior to Katrina and failed sometime during Katrina (the breach referenced above). HWM LA 1054 at 13.0 ft is close to this opening and may have been affected by the sandbag failure. The other marks in this area of 14.2 to 14.4 ft are believed to better represent water levels immediately south of the railroad bridge, which is just south of the I-10 bridge.

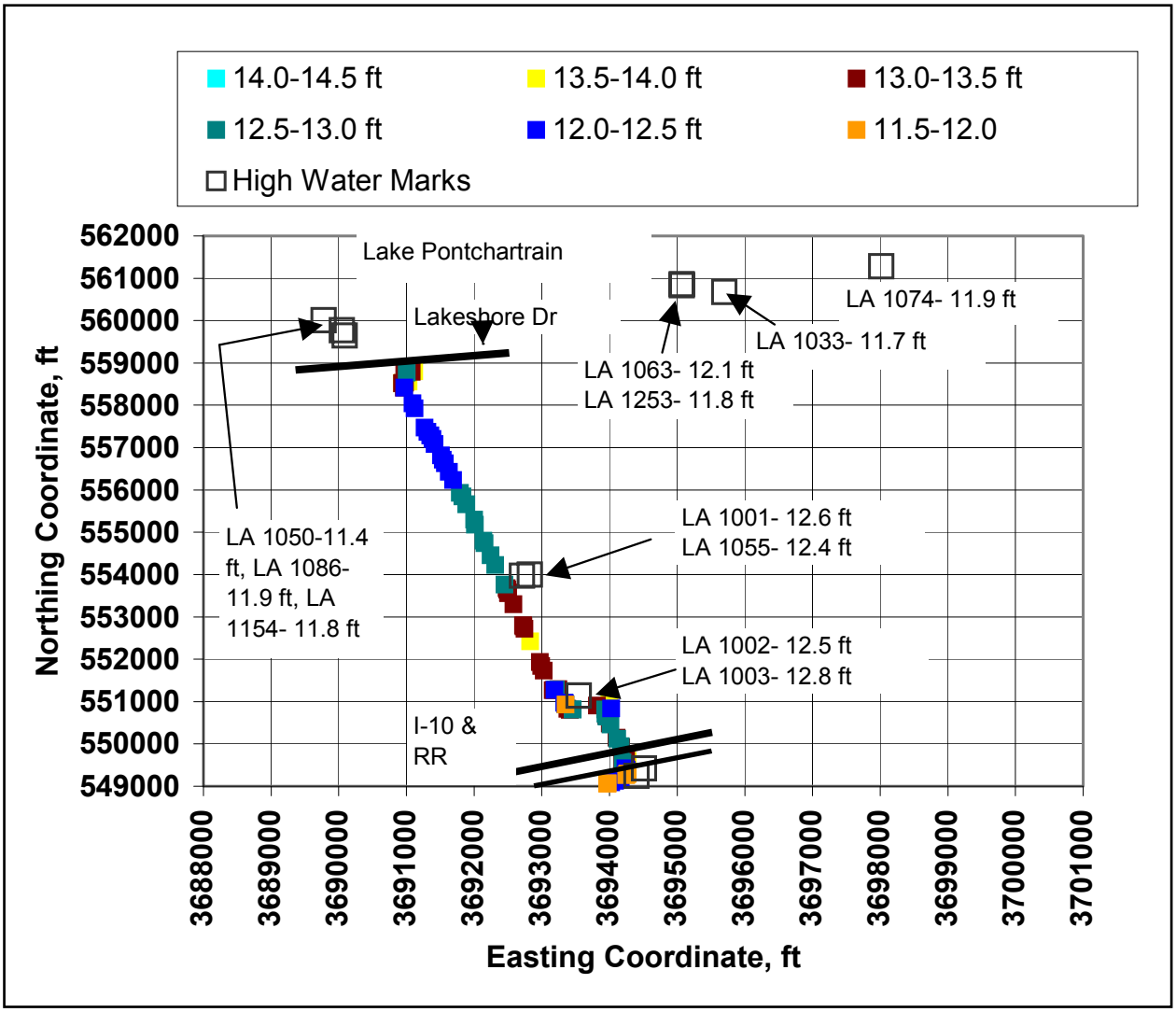

Figure 15. Floodwall layout, wall elevations, and high-water marks along the west side of IHNC, Lake Pontchartrain to I-10.

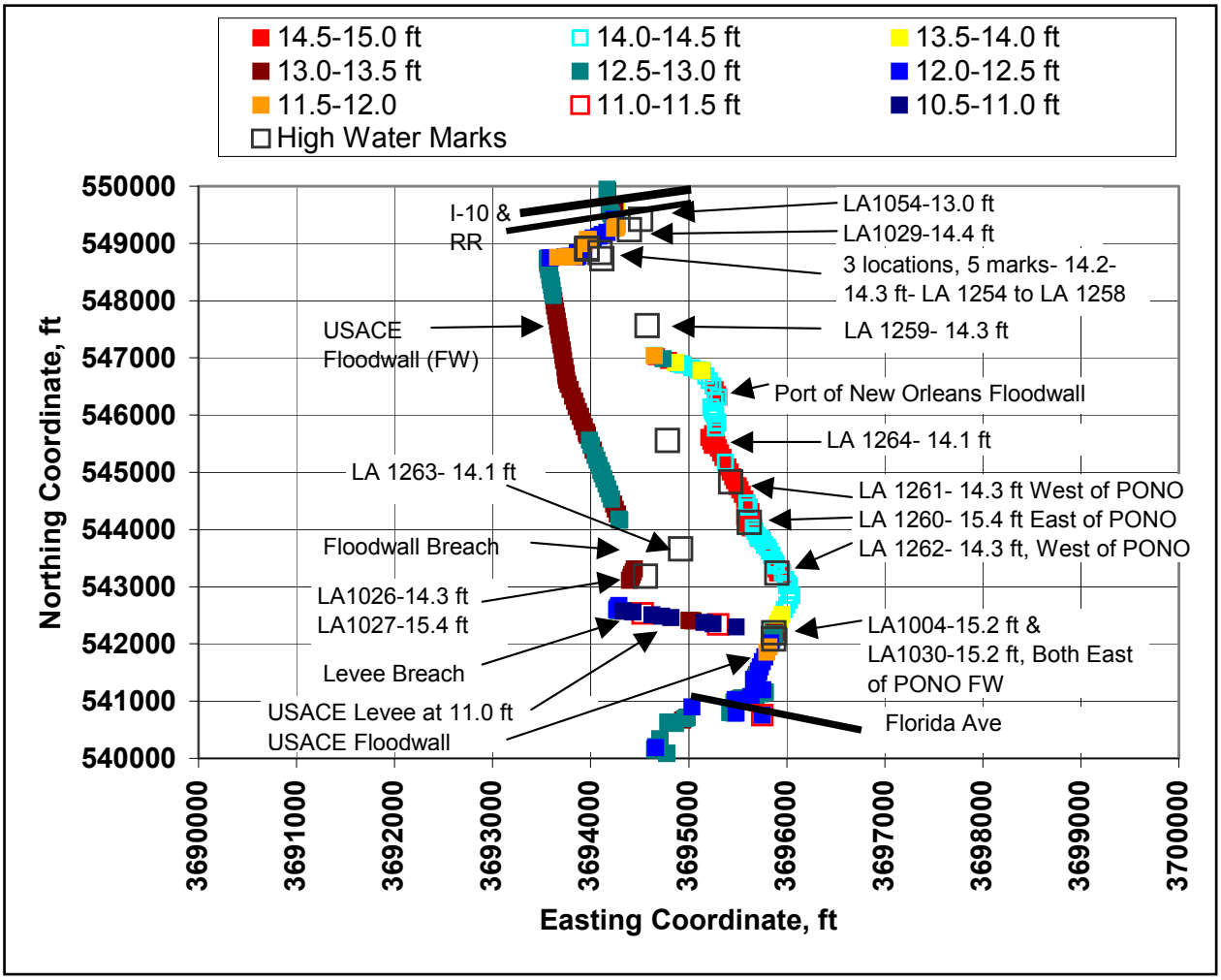

Figure 16. Floodwall layout, wall elevations, and high-water marks along the IHNC, I-10 to Florida Avenue railroad bridge.

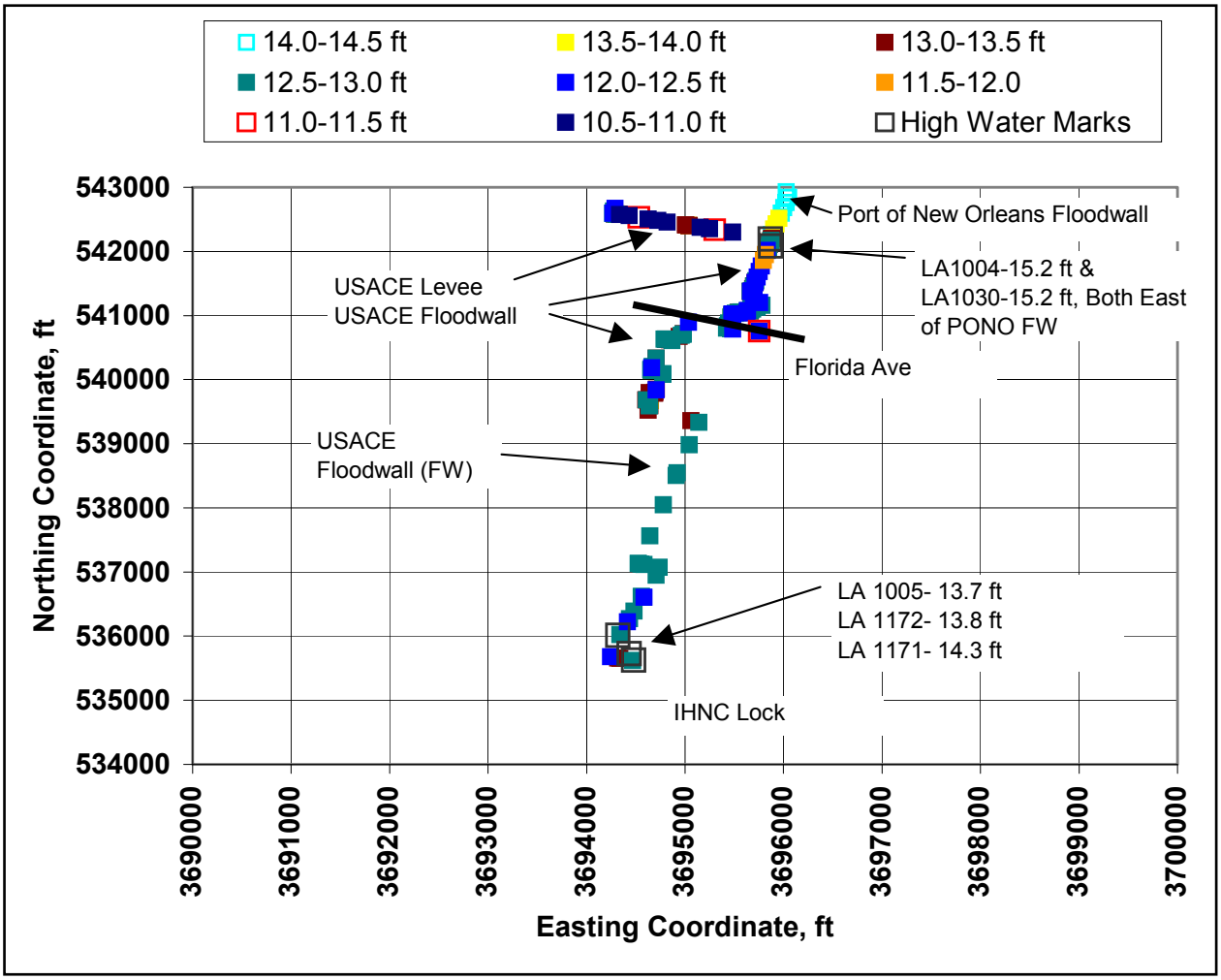

Figure 17. Floodwall layout, wall elevations, and high-water marks along the west side of IHNC, Florida Avenue railroad bridge to IHNC Lock.

HWMs on the north side of the railroad bridge (12.5 and 12.8 ft) show about a 1.5-ft drop in water level across the bridge. The large difference in elevation on either side of the railroad bridge might be due to head loss across the bridge. The railroad bridge was in the down position during Katrina. Photographic evidence on the ground showed vegetation laid down indicating high velocity in a northerly direction through the I-10/railroad area of the IHNC.

In Figure 16, HWMs acquired east of the PONO floodwall show peaks of 15.2 ft at several locations. At the junction of the IHNC and MRGO, a HWM of 15.4 ft was recorded. HWMs on the west side of the PONO generally show values that are approximately 1 ft lower, peaks of 14.2 to 14.3 ft. The difference in peak water level across the PONO floodwall is likely due to (1) the 1,600-ft-long east-west earth levee on the west side of the PONO that was at an elevation of about 11.0 ft and experienced overtopping and breaches, and (2) overtopping of the USACE floodwall all along the reach west of the PONO floodwall. Overtopping of the floodwalls and breaching may have created a local drawdown in water surface and reduced the peaks west of the PONO floodwall to values closer to 14 ft.

In Figure 17 on the south end of the floodwall, note that HWM data are only available at the IHNC Lock and at the south end of the PONO floodwall. The elevation drops from 15.2 ft at the south end of the PONO floodwall to about 14.3 ft at the lock based on the staff gauge or about 13.8 ft based on the HWMs. As stated above, this could have been the result of one or both of the breaches into the Lower Ninth Ward. Another possibility or a contributing factor could have been the head loss across the Florida Avenue railroad bridge that was also reported to be in the down position during the storm.

Figure 18 shows the variation of peak water level along the IHNC based on HWMs. Note the gradient in peak water level from the IHNC's Lake Pontchartrain entrance to the confluence of the IHNC with the GIWW/MRGO. The peak water level increases from 11.8 to 15.4 ft, a difference of nearly 4 ft over a rather short distance. As described below, the peak high water at Paris Road bridge on the GIWW/MRGO is 15.5 ft and the peak high water further to the east along the GIWW at Chef Menteur Pass is 15.7 ft. This high peak water level gradient within the northern section of the IHNC reflects the hydraulic connectivity present in the system between Lake Borgne, where the storm surge was much higher (15.5 ft or more), and Lake Pontchartrain, where the storm surge was lower (11.8 ft). The connectivity is created by the presence of the IHNC and GIWW/MRGO channels.

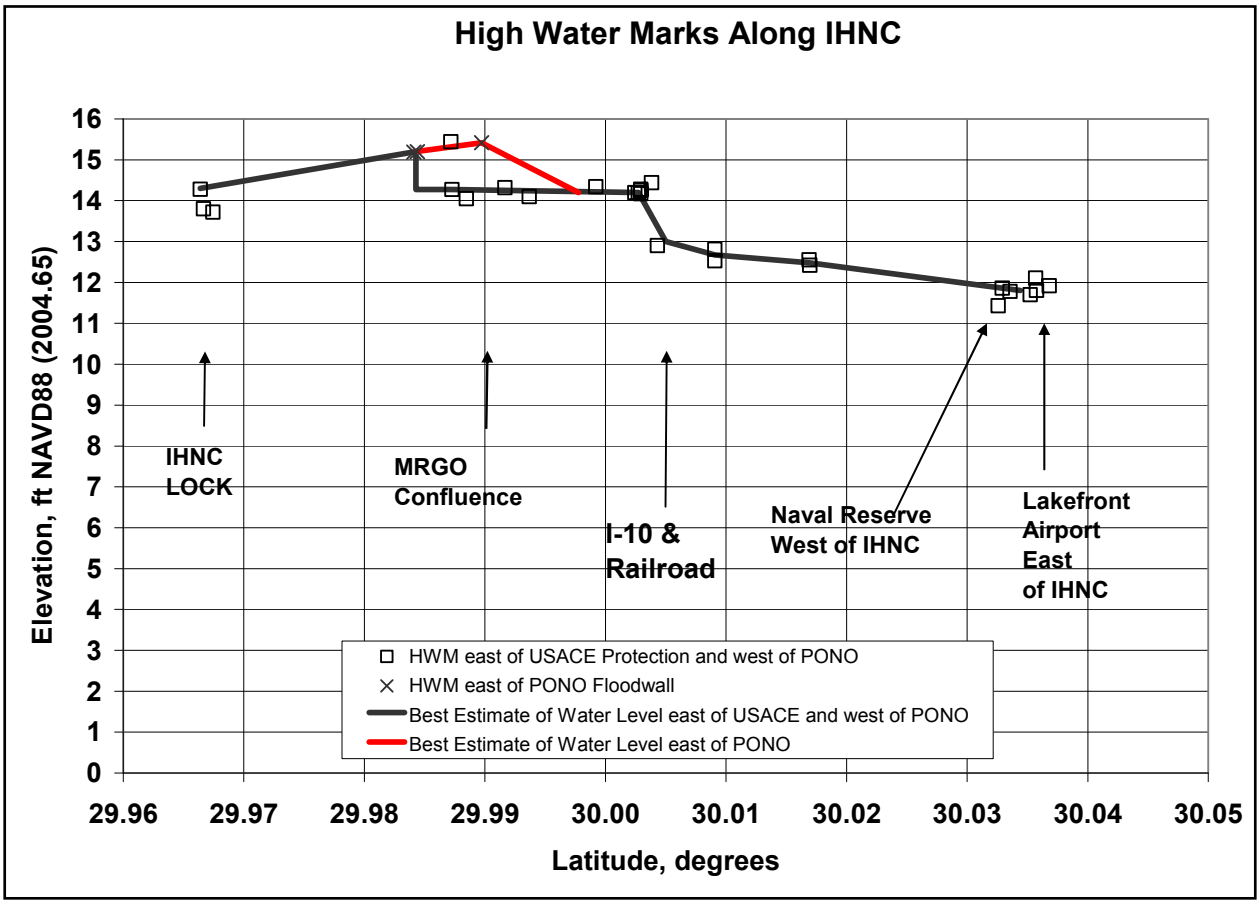

Figure 18. Variation of peak water level along IHNC based on high-water marks.

Observed Water Levels along the GIWW and MRGO

HWMs collected along the GIWW and the MRGO are described in the following paragraph. Marks are presented below, beginning at the IHNC, then moving east along the GIWW. The marks suggest a gradual increase in peak water level from about 15.2 to 15.4 ft NAVD88 (2004.65) at the confluence of the IHNC and GIWW/MRGO to a slightly higher value of about 15.5 ft where the MRGO and GIWW channels diverge. A little further to the east along the GIWW, adjacent to the Chef Menteur Pass, two excellent marks were collected in the interior of homes that had elevations of 15.7 and 15.8 ft NAVD88 (2004.65). These marks are consistent with the trend of gradually increasing peak water level from west to east along the GIWW. The marks that were rated either good or excellent in terms of reliability as indicators of storm water level are indicated with asterisks.

a. LA 1004* (elevation 15.2 ft) - Mark is debris line on interior wall of Crane Building at Maersk/Sealand located at the intersection of the IHNC and the GIWW/MRGO. Structure is located on the east side of the Port of New Orleans floodwall.

b. LA 1030* (elevation 15.2 ft) - Mark is debris line on interior wall of Crane Building at Maersk/Sealand located at the intersection of the IHNC and the GIWW/MRGO. Structure is located on the east side of the Port of New Orleans floodwall.

c. LA 1260* (elevation 15.4 ft) - Mark is debris line on interior wall of bathroom located at the intersection of the IHNC and the GIWW/MRGO. Structure is located on the east side of the Port of New Orleans floodwall.

d. LA 1039* (elevation 15.5 ft) - Mark is located at Boh Bros. construction site on the north side of the GIWW/MRGO about 2.4 miles west of the confluence of the GIWW and MRGO. The mark was a debris line on an interior wall of the elevated office building. On the initial visit, the highest mark found was at 14.5 ft, but it was a weak debris mark at 2.3 ft above the floor. On a subsequent visit, a better debris line was found at 3.3 ft above the floor giving an elevation of 15.5 ft.

e. LA 1053* (elevation 15.5 ft)- Mark is at the Entergy power plant that is on the north side of the GIWW/MRGO and about 0.7 mile west of the confluence of the GIWW and MRGO. The mark was inside a building that is at the water's edge of the MRGO. The mark was a debris line inside an electrical panel box.

f. LA 1093 (elevation 14.7 ft)- Mark is at the Entergy power plant that is on the north side of the GIWW/MRGO and about 0.7 mile west of the confluence of the GIWW and MRGO. Mark was debris on a chain-link fence.

g. LA1083* (elevation 15.7 ft) – Mark is from the interior of a home on the north side of the GIWW, adjacent to the Chef Menteur Pass.

h. LA1090* (elevation 15.8 ft) – Mark is from the interior of another house in on the north side of the GIWW, adjacent to the Chef Menteur Pass, in the same vicinity as the LA1083 mark.

HWMs collected along the MRGO are described in the following paragraph. Marks are presented beginning at a point where the GIWW and MRGO channels diverge and then moving to the southeast along the waterway. Marks referenced here end at Shell Beach. The marks that were rated either good or excellent in terms of reliability as indicators of storm water level are indicated with asterisks.

a. LA 1043 (elevation 18.2 ft)- Located 1.1 miles southeast of the GIWW/ MRGO junction at the Bayou Bienvenue structure. This mark is debris inside a radiator that is inside the gauge house (Figure 19). The doors to this gauge house were damaged by the storm surge and significant flow was passing through the gauge house. The large amount of flow through the gauge house and potential for wave effects within the gauge house may cause this mark to be high.

b. LA 1044 (elevation 18.5 ft)- Also at Bayou Bienvenue. The mark was debris on the upper handrail outside the gauge house in a setting that was exposed to wave activity.

c. LA 1045 (elevation 16.5 ft)- Also at Bayou Bienvenue. The mark was debris on the lower handrail outside the gauge house and in a setting that was exposed to wave activity.

d. LA 1040 (elevation 20.8 ft)- At Bayou Dupre Structure on MRGO about 7.5 miles southeast of the GIWW/MRGO junction. The mark was acquired inside a gauge house that was heavily damaged, and was small amount of debris in window frame. The mark is likely high as a measure of storm water level due to exposure to wave action inside the small gauge house.

e. LA 1041 (elevation 16.8 ft)- Also at Bayou Dupre. Debris on lower guardrail. Wave influence is likely.

f. LA 1042 (elevation 21.7 ft)- Also at Bayou Dupre. Debris on light standard on outside of gauge house, and likely high due to wave action.

g. LA 1155- This mark was not surveyed and was only accessible by boat since it was on channel marker No. 107 (Figure 20). The marker is about 13.8 miles southeast of the GIWW/MRGO junction and about 0.7 mile southeast of where the levee protection leaves the MRGO. The debris on this tower was measured at 19.6 ft above the water level on 17 October 2005. The Bayou Dupre gauge read about 1.8 ft on this same day giving an elevation of about 21.4 ft (relative to an uncertain datum). This exposed setting likely experienced considerable wave action. Water depth at the channel marker on the day of the inspection was about 12 ft.

h. LA 1087* (elevation 18.1 ft)- Well-defined debris line inside a bedroom of a home (Figure 21) at Shell Beach that is about 19 miles southeast of the GIWW/MRGO junction. HWM is 31 in. (2.6 ft) above second level floor.

i. LA 1088* (elevation 18.7 ft)- Well-defined debris line inside pantry of a different home at Shell Beach. Of the three marks at Shell Beach, this house is closest to the MRGO.

j. LA 1089* (elevation 17.1 ft)- Inside a business at Shell Beach. Of the three marks at Shell Beach, this business is farthest from the MRGO. There are two additional marks of unknown reliability near this same mark which are very consistent with the elevation of LA 1089 (KLA-USGS-94, elevation 16.9 ft, and KLAC-88-02, elevation 17.1 ft).

Figure 19. Bayou Bienvenue gauge house.

Figure 20. LA 1155 on MRGO. Debris on tower.

Figure 21. Home in Shell Beach containing high-water mark LA 1087 at 31 in. (2.6 ft) above second level floor.

Figure 22 shows a plot of the HWM data along the GIWW and the MRGO along with a best estimate line. The best estimate line ends at the Entergy plant because of uncertainty in the role of waves in the HWMs at Bayou Bienvenue and Bayou Dupre gate houses, the large wave component at channel marker No. 107, and the fact that Shell Beach is beyond the levee protection. Of all the marks southeast of the GIWW/MRGO junction, the marks at Shell Beach are the most reliable estimates of the peak still-water level.

Observed Water Levels in South Plaquemines Parish

Only two reliable HWMs were acquired in south Plaquemines Parish in unprotected areas. They were at the same location, the Empire Lock, along the Mississippi River. Elevations at LA1077 and LA1078 were 14.2 and 14.4 ft NAVD88 (2004.65), respectively (see photo 52 in Appendix 1). These were the southernmost HWMs that were collected. There were several other marks acquired at different locations along the Mississippi River in south Plaquemines Parish. All others were rated as having lower reliability, and they exhibited great variability. Some of the other higher marks were in the 15- to 17-ft range.

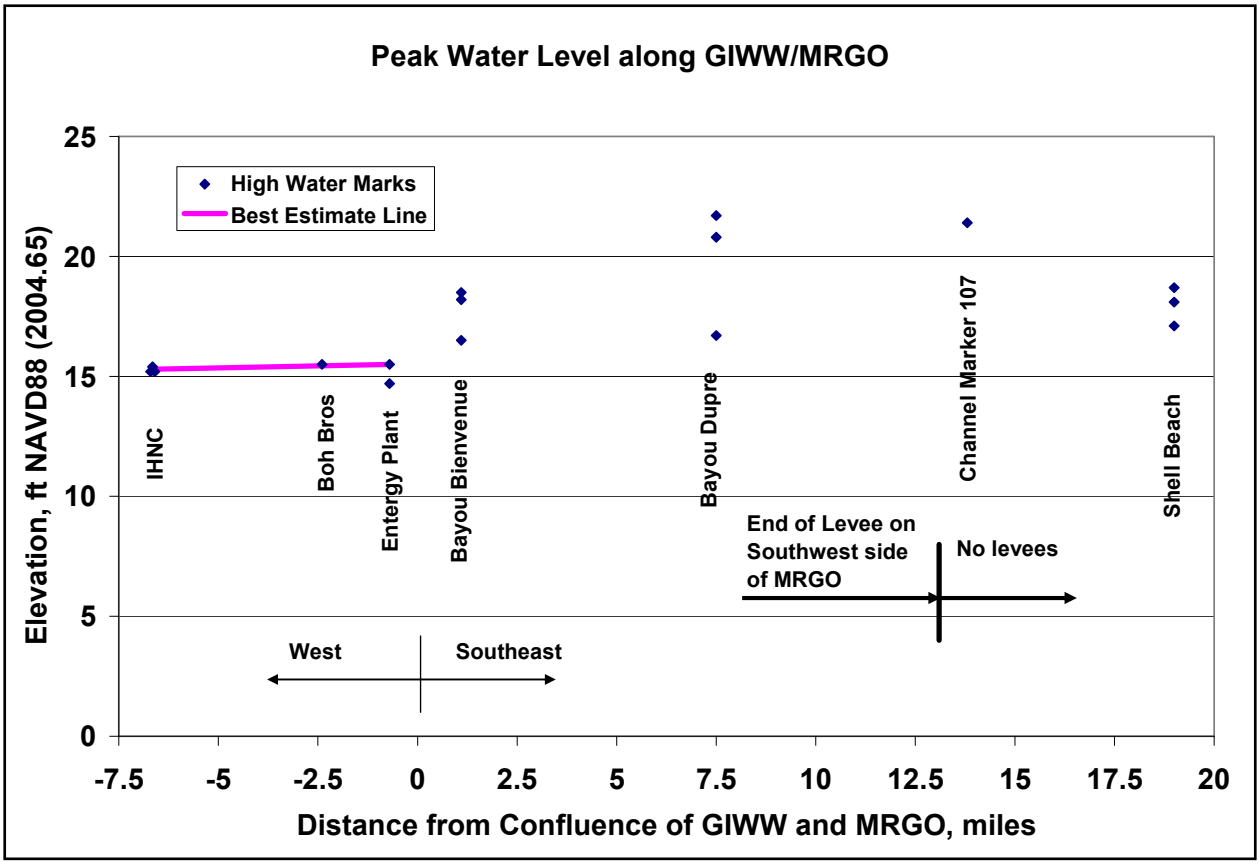

Figure 22. Peak water level along GIWW and MRGO based on high-water marks.

Additional Relevant Hydrographs

Figures 23 and 24 are hydrographs acquired by NOAA National Ocean Service stations 8761724 at Grand Isle, LA and 8760922 at Southwest Pass, LA. The instruments at these stations, which were outside of the high impact zone east of the Mississippi River, are among the few that functioned throughout Katrina's passage and recorded peak water levels. The Grand Isle station recorded a peak water level of 5.70 ft above mean lower low water (MLLW) at 0906 UTC on 29 August 2005. The Southwest Pass station recorded a peak water level of 7.61 ft above MLLW at 0930 UTC on 29 August 2005. The best information we have suggests that 0.0 ft MLLW is approximately equal to 0.0 ft NAVD88 (2004.65) at Grand Isle. The relationship at Southwest Pass is undetermined at this time. Note that predicted water levels shown in these two figures are predicted water level changes due to astronomical tide only.

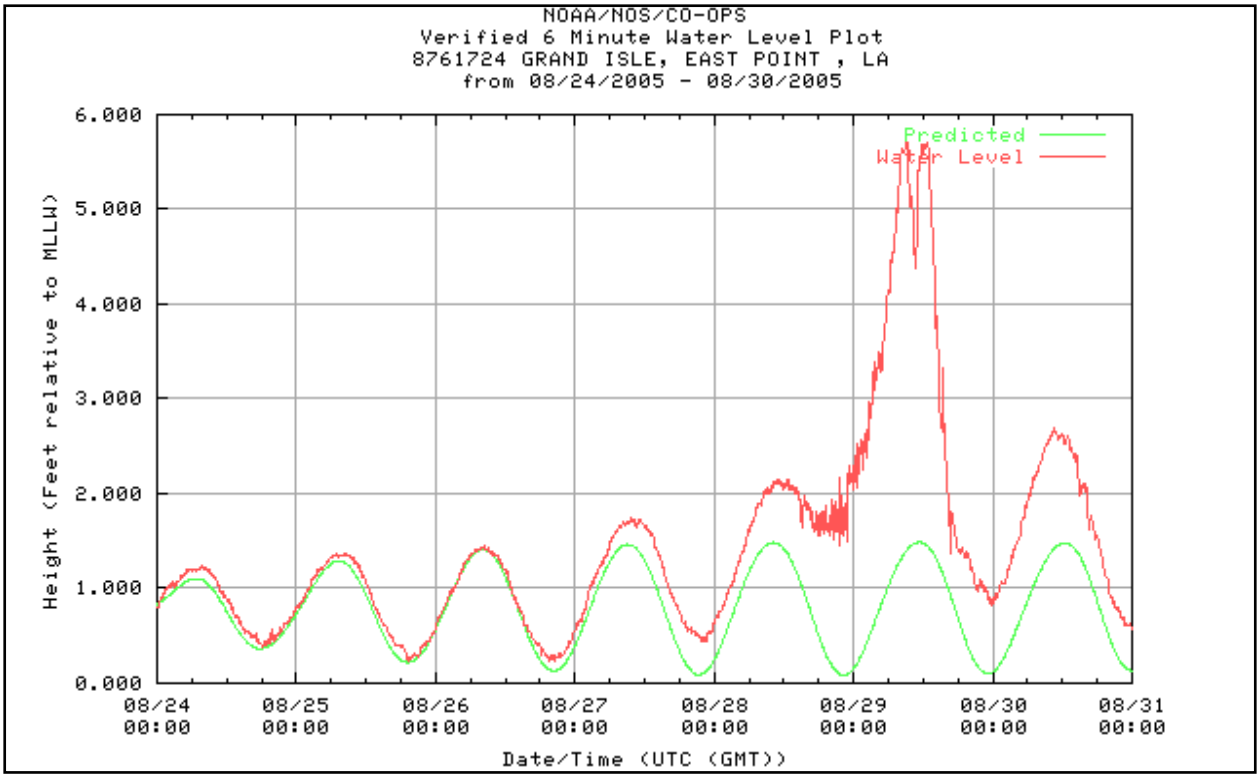

Figure 23. Hydrograph for NOAA National Ocean Service station at Grand Isle, LA.

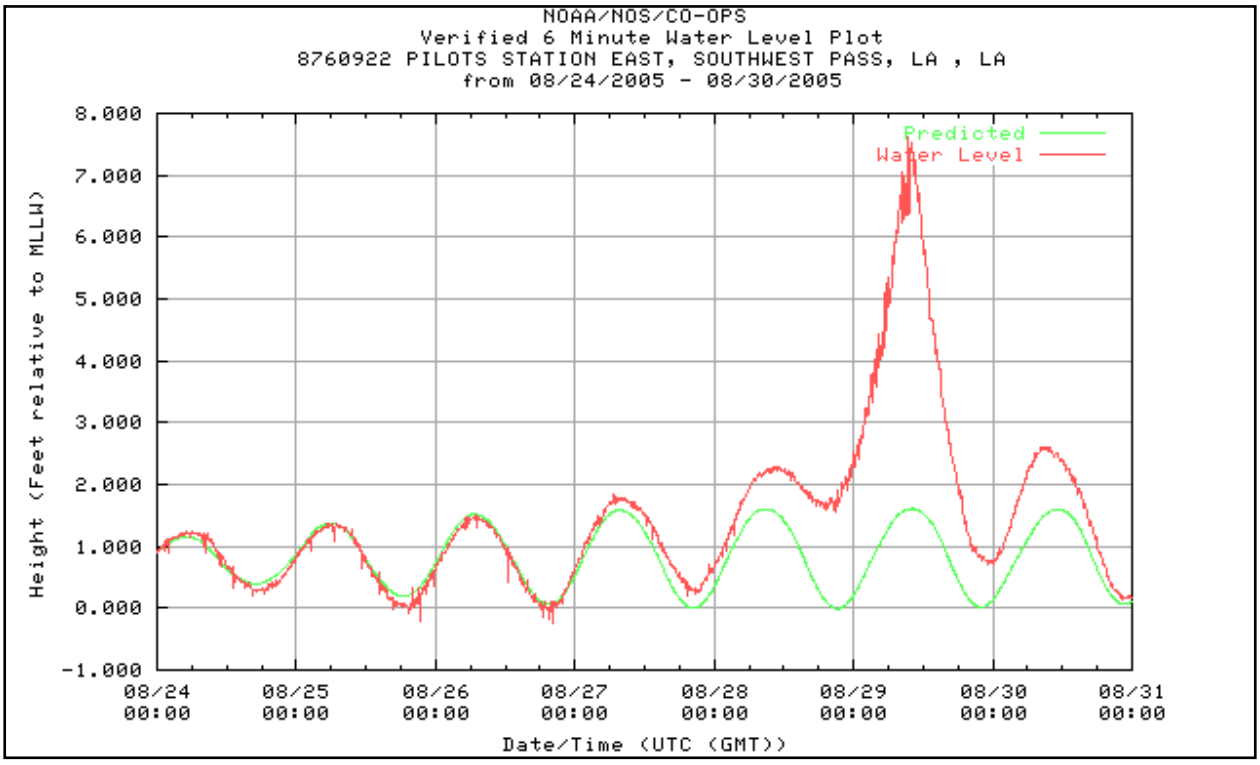

Figure 24. Hydrograph for NOAA National Ocean Service station at Southwest Pass, LA.

Winds and Atmospheric Pressures

Input to Hydrodynamic Models

Accurate regional-scale modeling of waves and storm surge is highly dependent on the accuracy of wind input to the models. Wind speed is the most important factor influencing the regional wave and storm surge climate, in addition to topographic features which influence wave and surge development and propagation. Surface wind shear stress, the primary forcing to both types of models for hurricane simulations, dictates the magnitude and frequency of wave energy and storm surge amplitude. Shear stress is nonlinearly related to wind speed (either a quadratic or cubic dependency depending on the formulation of the wind drag coefficient), so having accurate winds is crucial. Errors in input winds are amplified in a nonlinear manner.

The models applied in this study require wind and pressure fields for the entire modeling domain, which for this study was the entire Gulf of Mexico. Characterization of regional wave and water level conditions was required by several other study tasks, and needed early in the study process. Therefore, a spiral development approach was adopted to produce results quickly and then refine the results once other tasks had the information they needed to proceed. The need to produce results quickly dictated the approach that was taken.

For the storm surge modeling done early in the study, wind and atmospheric pressure fields were generated using a Planetary Boundary Layer (PBL) model (Cardone et al., 1994, Thompson and Cardone 1996). Coupled ADCIRC-PBL models were already in place as a result of prior work done for the U.S. Army Engineer District, New Orleans, so they were utilized while work on the "final" wind and pressure fields was underway. The PBL model employs a moving nested-grid approach (five levels or nests with increasingly higher resolution nearest the storm center) to compute spatially-varying wind and pressure fields as a function of time. For input, the PBL model requires information about the storm position (track), the maximum sustained surface wind speed and central pressure (the type of information shown in Table 1). These input data for the PBL model were obtained from NOAA. Radius-to-maximum-wind values are computed internally within the five-level model using the method presented in Jelesnianski and Taylor (1973). Radii-to-maximum-winds, which influence spatial variation of the wind field, were calculated as a function of central pressure and maximum sustained wind speed. For the final storm surge modeling, winds and pressure fields were derived using the procedure described below.

Development of the H*Wind/IOKA Wind Product and Pressure Fields

For all the gulf-scale and regional-scale wave modeling reflected in this report, wind fields produced by OWI were used, which include H*Wind snapshots developed by the HRD. This approach was taken because the method to link these wind inputs to Gulf-of-Mexico-scale and region-scale wave modeling had been previously developed as part of a National Ocean Partnership Program (NOPP) project, the linkage was readily adaptable for use in this investigation. This methodology for generating surface winds was adopted to provide input to all final storm surge and wave modeling. The H*Wind snapshots integrated into the preliminary

wind fields were primarily based on those created in real-time as part of the NOPP project effort, with some limited reanalysis. The final winds benefited from a much greater reanalysis effort; which according to HRD staff, was the most intensive analysis of hurricane surface winds that has ever been undertaken by that office.

H*Wind snapshots for the inner core of the hurricane are constructed using a method developed at HRD called the HRD Surface Wind Field Analysis System (Powell et al. 1998, *http://www.aoml.noaa.gov/hrd/Storm_pages/katrina2005/wind_realtime.html*) which utilizes measured meteorological data from a number of different types of sensors and data acquisition processes. All wind measurements are transformed to a standard 10-m reference elevation, averaging period (1-min sustained wind speed) and marine or land exposure, whichever is desired. The data are scrutinized for quality. The product of this man-machine mix is a wind streamline and isotach contour plot that is fixed (storm centered) in space and time. HRD produced a series of H*Wind analysis snapshots that comprise the duration of this storm. Of greatest interest for this study are the snapshots produced every 3 hr between 0000 UTC on 26 August and 1200 UTC on 30 August. They represent the best wind estimate for the target domain on which the snapshot is placed. The development of the full domain winds requires two procedures. First, snapshot H*Wind fields are repositioned to the storm track, and then a moving center interpolation algorithm is applied to preserve the characteristics of the tropical storm wind core in space and time.

The wave and surge modeling activities require complete wind field specification for the entire target domain; the H*Wind technique defined the wind conditions to within about 4 degrees of latitude around the storm, but peripheral winds are also needed. Accomplishing this task requires background estimates which are derived from the NOAA National Centers for Environmental Prediction/National Center for Atmospheric Research (NCEP/NCAR) Reanalysis Project (Kalany et al. 1996). The NCEP/NCAR winds are rigorously analyzed and rely on data assimilation methods using data not originally used in the NCEP operational forecast. A final step is to inject local marine data, adjusted to a consistent 10-m elevation and adjusted for neutral stability. This procedure uses an Interactive Objective Kinematic Analysis (IOKA) System (Cox et al. 1995, Cox and Cardone 2000) developed by OWI. OWI produced the final wind and pressure fields used in this study.

The pressure fields generated for the Katrina study are built from a single exponential pressure profile (see Holland, 1980, for example) which also reflects the central pressure estimates from the NOAA Tropical Prediction Center/National Hurricane Center. No synoptic-scale pressure inputs were considered. The pressure field snapshots, aligned to the storm track, are spatially and temporally interpolated in a similar fashion as done for the winds and placed on the identical fixed latitude/longitude grid. The track applied represents a linear 3-hr interpolation of the HRD analysis results for storm position.

All wind and pressure fields produced by OWI (*http://www.oceanweather.com*) were created for two domains, a Gulf-of-Mexico-scale domain (called the basin-scale domain) and a Louisiana/Mississippi regional domain. Specifics of the wind and pressure field domains are provided in Table 2. Winds and pressures are more highly resolved at the regional scale that at the basin scale. Wind and pressure fields were defined every 15 min. Surface winds from OWI

represent 30-min average wind speeds, and they are adjusted as needed for input to the wave and surge models (ensuring consistency with the wind stress formulations embedded in the models). A few results of the wind analysis are presented below. More detail about the process used to generate the wind and pressure fields and the quality of results are contained in Appendix 2.

Table 2
Wind and Pressure Field and Offshore Wave Model Domain Characterization

Domain	Longitude (deg)		Latitude (deg)		Res. (deg)	Duration	Wind Output Interval (min)
	West	East	South	North			
Basin	98 W	80 W	18 N	30.8 N	0.1	0000 UTC 26 August to 0000 UTC 31 August	15 (30-min avg winds)
Region	91 W	88 W	28.5 N	30.8 N	0.025	0000 UTC 28 August to 0000 UTC 30 August	15 (30-min avg winds)

Katrina Surface Wind Fields at Landfall

Figures 25 through 27 show the 1-min sustained surface wind field associated with the H*Wind snapshot at the following times on 29 August: 1) 0900 UTC, several hours prior to landfall, 2) 1200 UTC which is about an hour after landfall near Buras, LA, and 3) 1500 UTC slightly after landfall near the Mississippi/Louisiana coastal border. The white vectors in the figures indicate the general wind direction and they reflect the counterclockwise rotation of the winds about the storm center. Peak wind speeds are seen to the right of the storm center, at times shifted slightly toward the right front quadrant, which is typical for hurricanes. Maximum surface wind speeds throughout this time period are approximately 100 knots.

At 0900 UTC (Figure 25), much of the water surrounding coastal Southeast Louisiana is located within the right front quadrant of the storm, which means winds from the east and south-east directions in a counterclockwise rotating wind field. Wind speeds throughout the region are for the most part at hurricane strength (i.e., speeds in excess of 64 knots). The highest winds, those exceeding 95 knots, are located in two zones. One is just offshore of the Mississippi River delta where they blow from the south, and a second zone is over the delta itself where they blow from the southeast and east. Winds in Lake Borgne, which is due north of the storm center and directly in its path, are out of the east-northeast at speeds of 55 to 65 knots. Lake Pontchartrain is in the left-front quadrant of the storm, a little more distant from the eye of the storm, and winds there are from the north-northeast at 40 to 50 knots. Wind speeds in Lake Pontchartrain are lower because it is further away from the storm center.

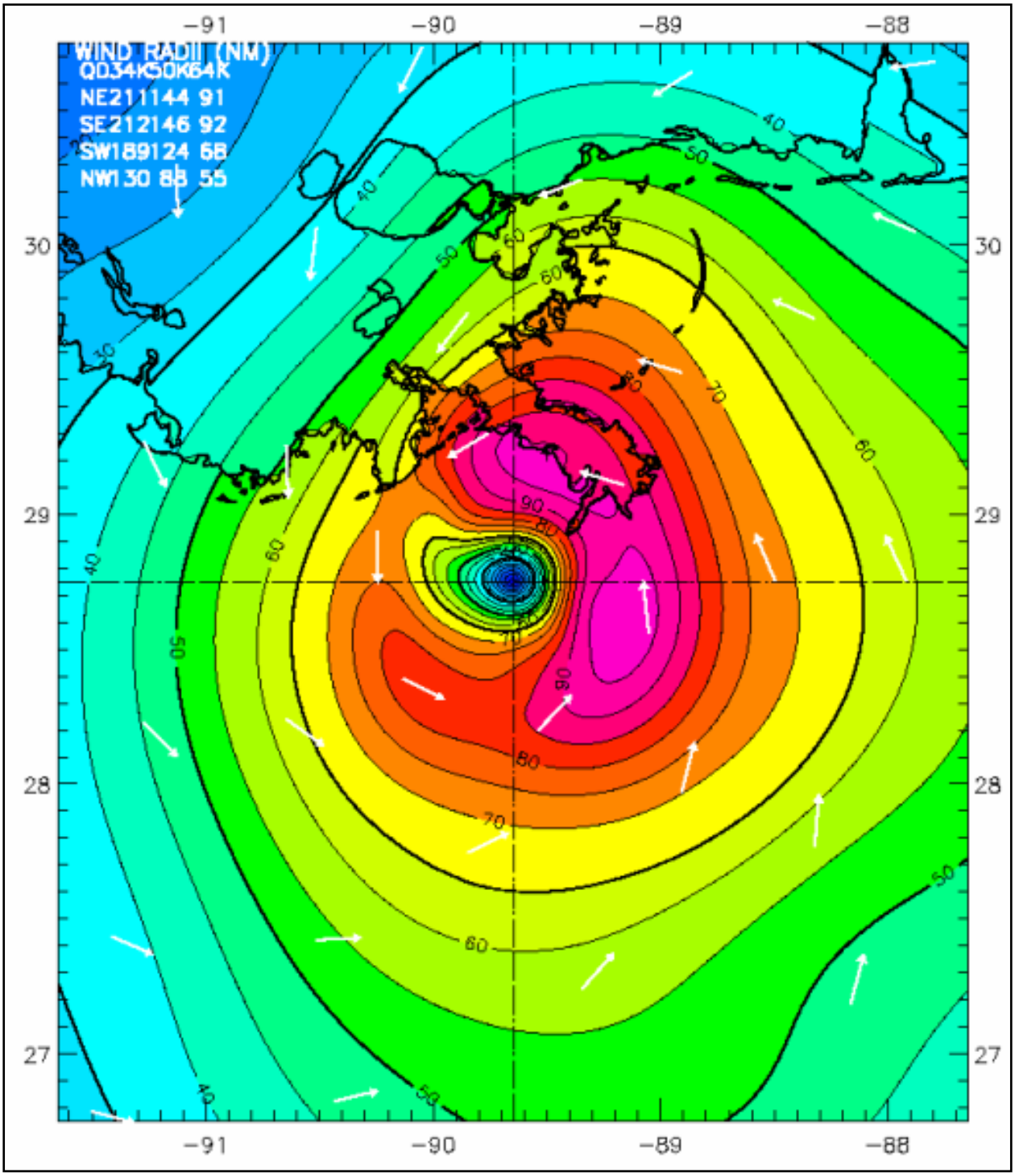

Figure 25. H*Wind snapshot for 0900 UTC on 29 August, just prior to landfall.

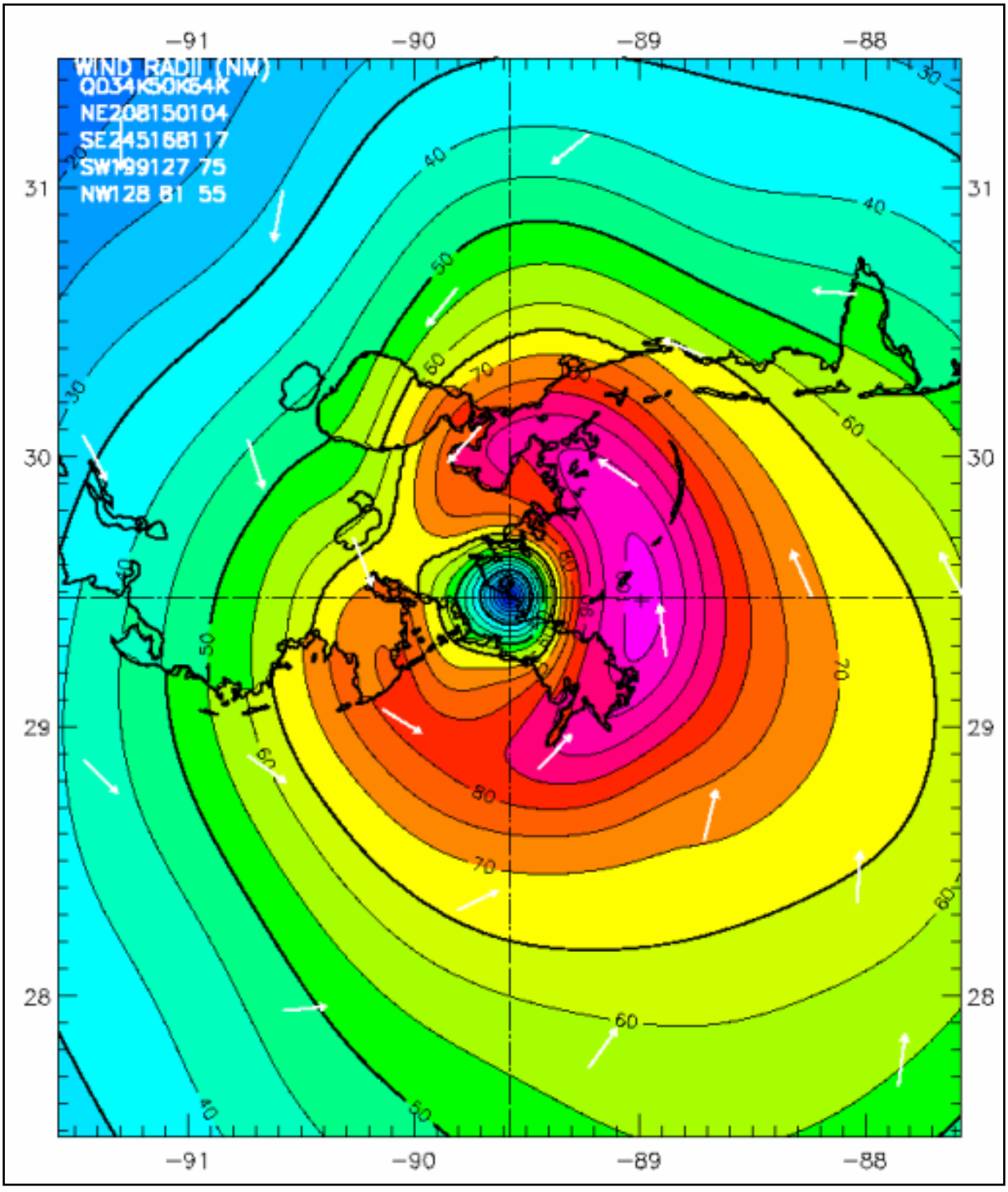

Figure 26. H*Wind snapshot for 1200 UTC on 29 August, just after landfall near Buras, LA.

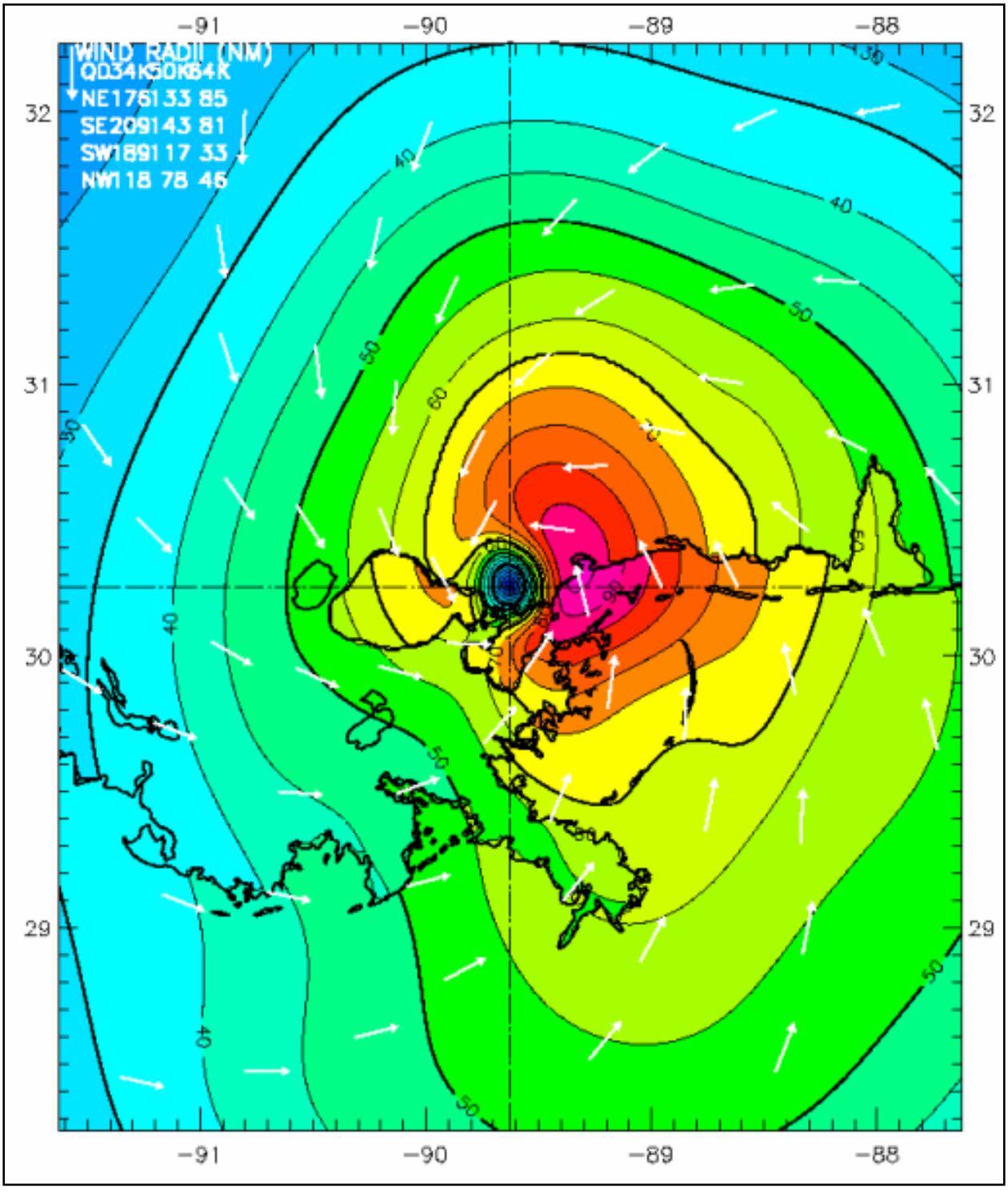

Figure 27. H*Wind snapshot for 1500 UTC on 29 August, near landfall at Mississippi/Louisiana border.

At 1200 UTC (Figure 26), just after the storm has made landfall, most of the coastal waters surrounding Southeast Louisiana waters are exposed to winds greater than 85 knots, a very large area of intense winds. The eye of the storm is in south Plaquemines Parish at this time, east of the Mississippi River. With the closeness of the storm center, the different water bodies of

Southeast Louisiana are being exposed to different and rapidly changing wind conditions. Winds in Breton Sound continue to blow from the south and southeast at speeds between 80 and 100 knots. Winds over Lake Borgne are now blowing from the northeast at speeds of approximately 90 knots. In Lake Pontchartrain, winds are shifting rapidly and are now from the north-northeast at speeds ranging from 55 to 80 knots depending on location within the lake (higher wind speeds on the east side of the lake).

At 1500 UTC (Figure 27), only 4 hr after landfall in Buras, the wind field pattern has completely changed in Southeast Louisiana. The storm center has moved through Southeast Louisiana and it is making landfall at the Mississippi/Louisiana coastal border. Breton Sound is now located in the rear right quadrant of the storm, and winds are now blowing out of the southwest and south, at speeds of 65 to 80 knots. In Lake Borgne, which is also in the rear quadrants, winds are blowing from the west and southwest at speeds of 65 to 75 knots. Winds in Lake Pontchartrain have continued to shift and now blow out of the northwest at speeds from 60 to 70 knots. That pattern will continue and winds will eventually blow from the west in the lake.

Comparison: H*Wind/IOKA Winds with Measurements

Figure 28 shows locations where wind measurements were available for the region encompassing Southeast Louisiana. The figure also shows the exact size of the regional, higher-resolution, domain for which H*Wind/IOKA wind fields were produced. Figures 29 through 32 show measured wind speed and direction at four locations (30-min sustained surface winds from the H*Wind/IOKA product), Southwest Pass to the Mississippi River, BURL1 (Figure 29), Buoy 42067 just north of the Chandeleur Islands, USM3M01 (Figure 30), Waveland, MS, WAVM6 (Figure 31), and Lake Pontchartrain Causeway, MDLL1 (Figure 32). All of these locations, except the Midlake site on the causeway in Lake Pontchartrain, are in positions that were east of the storm's path. Figures 29 through 32 also show the comparison between measured wind data and results from the H*Wind/IOKA wind product.

The H*Wind/IOKA winds show that for at least 4 to 5 days prior to landfall in Louisiana, winds were steadily out of the east and northeast and they gradually increased in speed during that time. This trend is confirmed by the measurements shown above and those shown in Appendix 2. As discussed previously, persistent winds blowing from east to west acted to push water from east to west along the Mississippi/Alabama continental shelf toward the Mississippi River delta and Southeast Louisiana. This regional-scale movement of water began to build the storm surge in Southeast Louisiana and flood low-lying wetlands well in advance of the storm's arrival, i.e. the core of the storm. Measurements at the Southwest Pass site and Buoy 42067 clearly show these steady winds from the east with gradually increasing wind speeds.

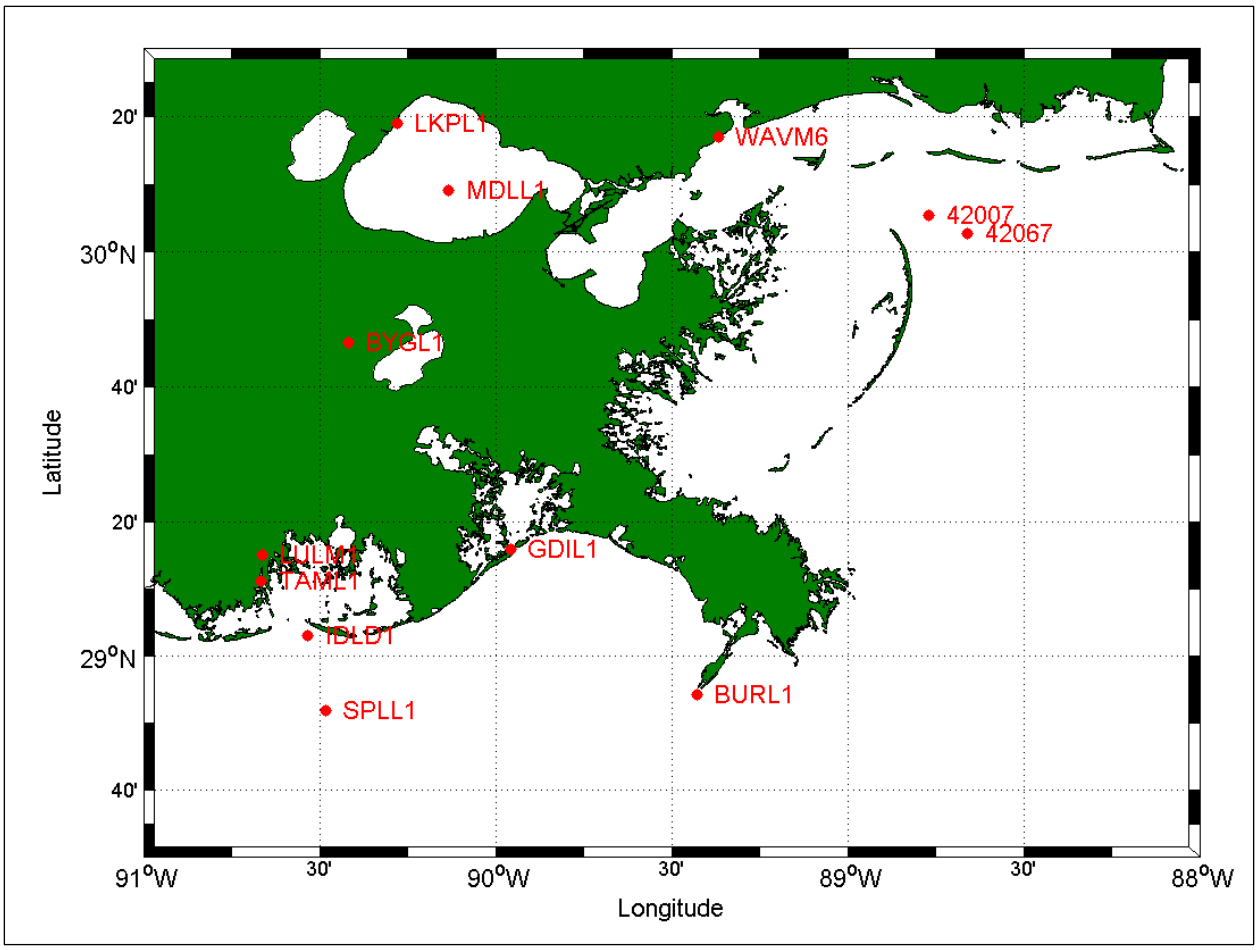

Figure 28. Wind measurement sites within the regional domain.

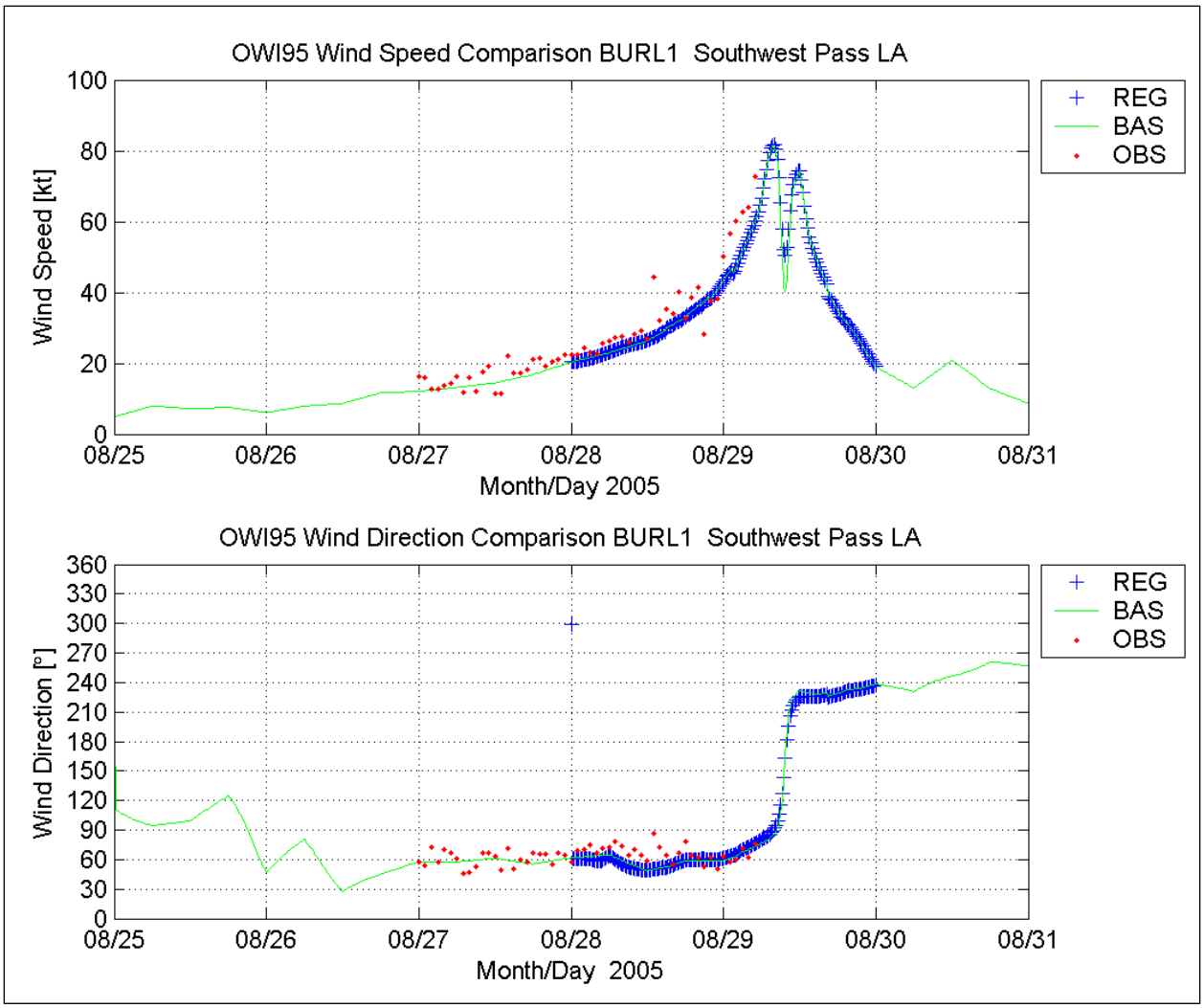

Figure 29. Comparison of wind speed (upper panel) and direction (bottom panel) at Southwest Pass, LA. [Time is referenced to UTC].

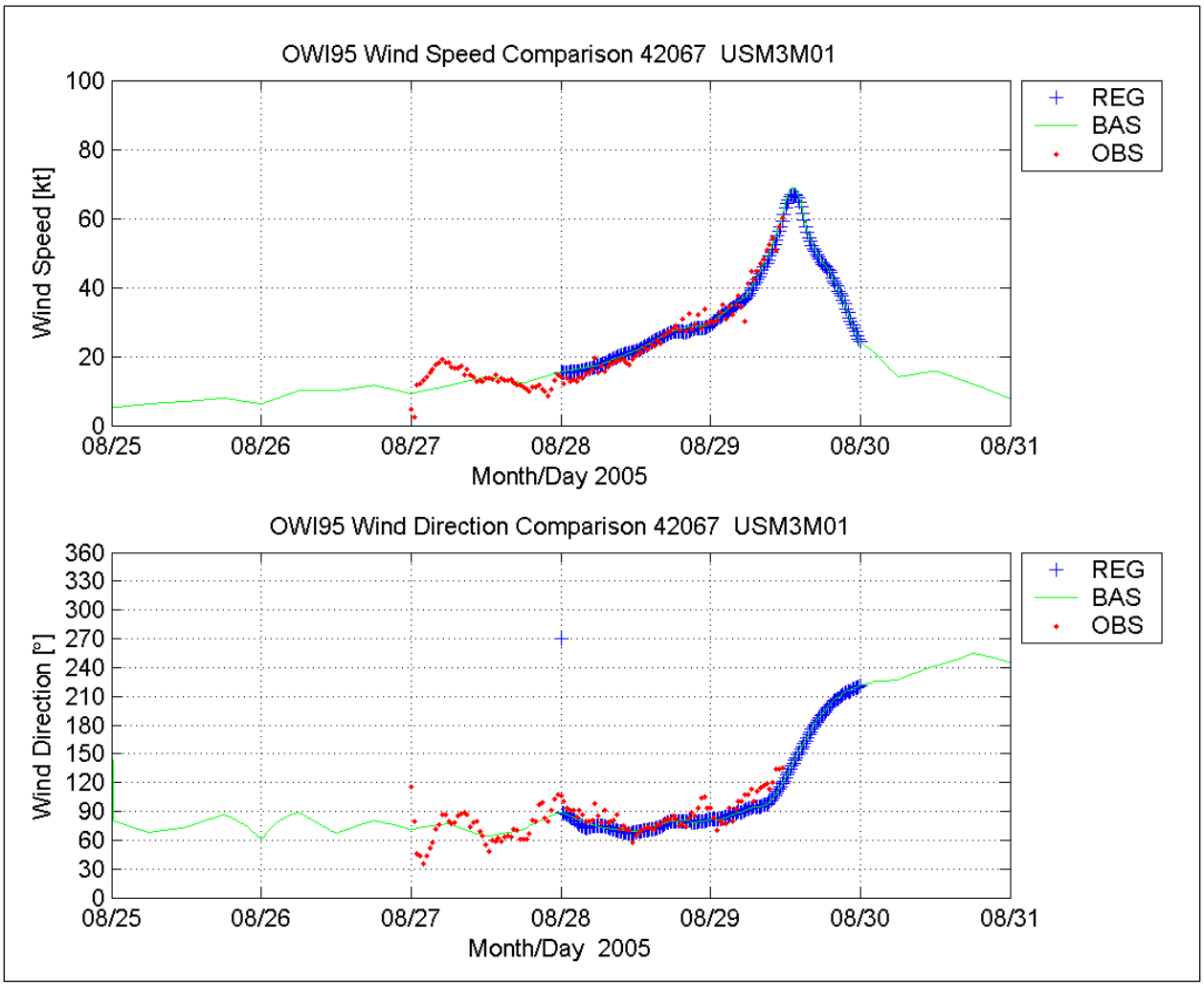

Figure 30. Comparison of wind speed (upper panel) and direction (bottom panel) at Buoy 42067. [Time is referenced to UTC].

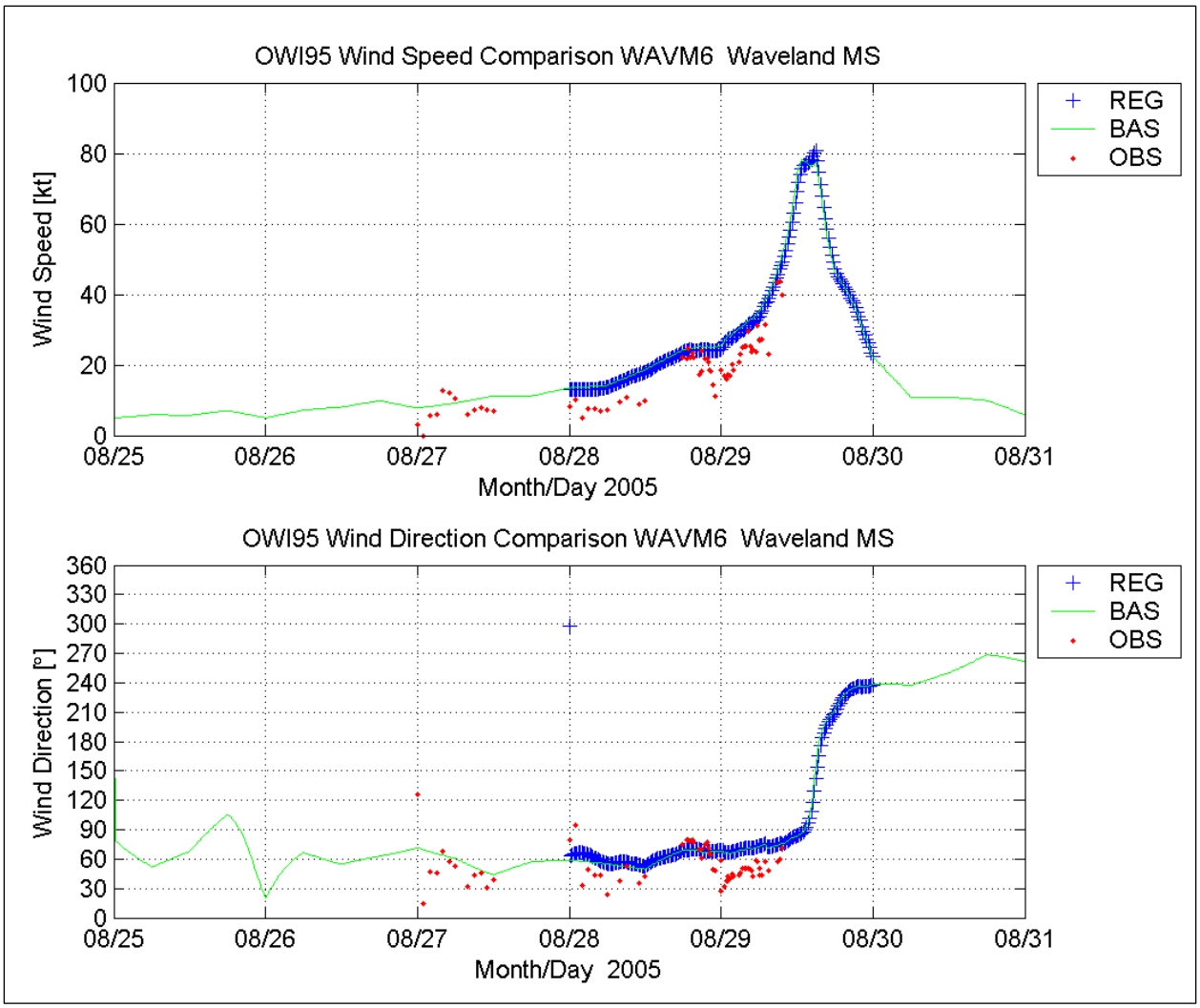

Figure 31. Comparison of wind speed (upper panel) and direction (bottom panel) at Waveland, MS. [Time is referenced to UTC].

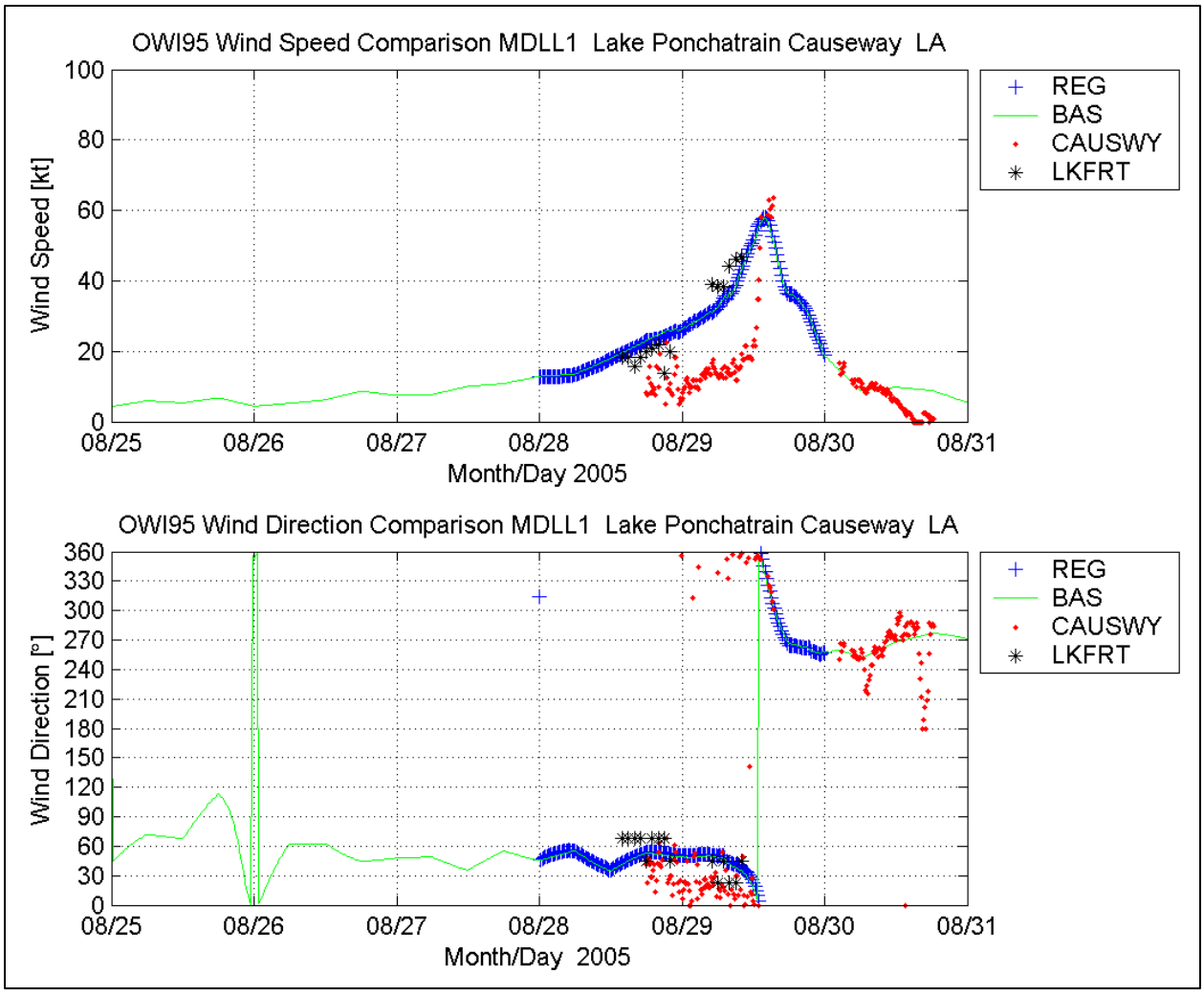

Figure 32. Comparison of wind speed (upper panel) and direction (bottom panel) at Midlake, Lake Pontchartrain, LA. [Time is referenced to UTC].

As the storm approached landfall, winds increased at a more rapid rate. Measurements at Southwest Pass show the intensification occurring at around 0000 UTC on 29 August. At Buoy 42067 it occurs later, at 0400 UTC; and at Waveland it occurs at about 0600 UTC. This trend is consistent with the northward track of the storm. As shown earlier in this volume, an increase in the rate of water level rise also occurs at about this same time. The timing of wind speed and water level increases are correlated. The H*Wind/IOKA wind product at Southwest Pass also shows the close proximity of the storm center to that site, as evidenced by the rapid rise of winds prior to arrival of the storm eye, a rapid decrease and then increase associated with passage of the eye, then gradual reduction in wind speed as the storm moved away toward the north (two peaks in the computed wind speed time series).

Wind speed measurements from the Midlake Lake Pontchartrain site on the causeway (Figure 32) show an unusually abrupt increase in wind speed. The rapid change was not seen in any other data that were acquired in the region, and data from Lakefront Airport (also shown in Figure 32) along the south shore of Lake Pontchartrain suggest a more gradual increase in wind

speed, so the data from the Midlake measurement site were considered to be suspect, likely due to the causeway obstructing the flow for wind directions from the north.

A considerable effort was made to maximize use of measured meteorological data in the process to create H*Wind snapshots as well as the IOKA process to develop the basin and regional-scale wind fields, because of the critical nature of winds in the wave and storm surge modeling. In many locations, particularly south Plaquemines Parish, model results are the only source of information for quantifying the temporal variation of wave and water level conditions along the periphery of the hurricane protection system. So it was very important to compare wind measurements and wind input to the models, and quantify accuracy of model input throughout the entire wave and storm surge generation area. Comparison of model results to measurements was given a high priority in all facets of the IPET wave and water level analysis. Figures 29 through 32 provide an indication of the accuracy of the H*Wind/IOKA wind field products. The greatest errors are in wind direction. Errors are smallest during the day just prior to landfall, when wind speeds rapidly increase in magnitude. Some small-scale wind features are not captured. However, overall trends and patterns are captured well and magnitudes are reasonably accurate. Comparisons between measured wind data and the H*Wind/IOKA wind product for the Southwest Pass and Waveland sites are indicative of results seen at other measurement sites.

Figure 33 shows additional locations throughout the Gulf of Mexico where wind measurements were compared to results from the H*Wind/IOKA product. These are sites where NOAA National Data Buoy Center buoys are located, and where both wind and wave data were recorded. The storm track is also shown in the figure. Wind speed data from several of these buoys nearest the storm track were compared to results from the basin-scale H*Wind/IOKA wind field product. Table 3 shows results from these comparisons, in terms of several statistical measures; mean, bias, absolute error, root-mean-square error (RMSE), scatter index which is related to RMSE/bias, correlation coefficients, and results from linear regression analyses (one that does not force the y-intercept to zero, “Corr (r)”, and one that does, denoted “Symm r”). Definitions for each of these error measures are given in Appendix 2.

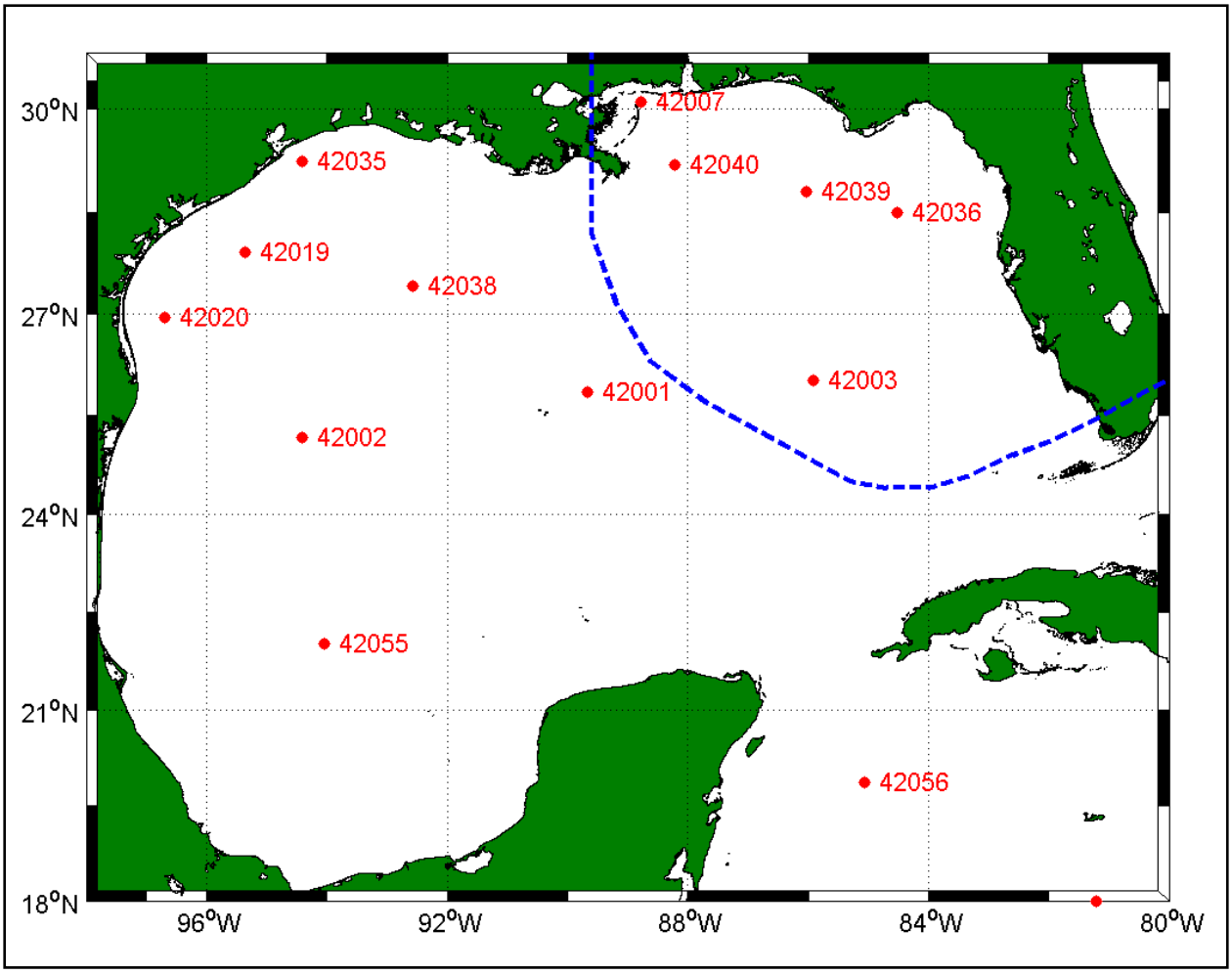

Figure 33. Locations of NOAA National Data Buoy Center buoys.

Table 3
Statistical Results: Basin-Scale Winds for Hurricane Katrina – All Wind Speeds in knots

Buoy ID	Mean Cond.		Bias	Abs. Err	RMS Error	Scat Indx	Linear Regression Estimators				No. Obs
	Meas	Model					Corr (r)	Symm r	Slope (a)	Intercp (b)	
42001	18.08	18.58	0.50	1.52	1.90	10	0.99	1.03	1.03	0.04	82
42003	22.97	21.81	-1.16	2.53	3.03	13	0.99	0.92	0.82	3.05	42
42007	15.92	15.49	-0.43	2.60	3.42	21	0.92	0.98	0.93	0.62	57
42036	21.36	21.01	-0.35	1.32	1.73	8	0.95	0.98	0.89	1.92	83
42038	12.97	13.41	0.44	1.94	2.35	18	0.95	1.01	0.90	1.71	82
42039	21.71	22.32	0.61	1.94	2.58	12	0.95	1.01	0.87	3.38	84
42040	20.74	21.62	0.87	2.06	2.72	13	0.98	1.01	0.93	2.27	84
42055	9.43	10.48	1.05	2.92	3.48	37	0.64	1.05	0.44	6.36	84

The statistical results for the wind estimates at eight offshore buoy locations (see Figure 33) show close agreement to the measurements. This is not surprising because IOKA uses all

available measurements in the final blending step. There does not appear to be any systematic bias in the H*Wind/IOKA wind product. Biases in the modeled winds range from -1.16 to +1.05 knots (Note that a negative bias is model under-estimation and a positive bias is an over-estimation). The absolute error is more or less a factor of two greater, 1.3 to 2.9 knots. The RMSE, a measure of the error variability, is slightly less than 3.5 knots demonstrating the high-degree of accuracy in the wind fields. The Scatter Index (SI) falls into a range that is consistent with that of research quality wind products (Cox et al. 1995). The correlation coefficient is no less than 0.92 in the area surrounding Katrina's path. Results from the linear regression analysis reflect the accuracy of the wind fields at these point source measurements, ranging from -8 to +5 percent.

Two offshore oil platforms, equipped with wind and wave measurement sensors, recorded peak winds during the time of Katrina. Maximum wind speeds measured at the two platforms were between the H*Wind/IOKA wind field estimates of 51.9 and 56.7 knots at the two locations.

The full set of wind comparisons (time series comparisons), utilizing data from each buoy and land measurement site, are provided in Appendices 3 and 2, respectively.

Performance of Wind Instrumentation

Note that most of the wind measurement sensors in the regional domain shown in Figure 28 near the path of the storm failed prior to the peak of the storm. Instruments at most sites in the immediate Southeast Louisiana vicinity failed to fully capture the wind speed and direction record during the storm. This was a recurring theme, for both wind and water level instrumentation in the high impact zone: failure of sensors to function or survive and capture conditions just prior to, during, and after the storm peak, i.e., the crucial part of the storm. The deeper-water buoys fared better because most were located at greater distances from the core of the storm. Instruments on Buoys 42007, 42067, and 42003 failed prior to the peak. There is great need for instruments that can reliably measure surface wind conditions, water levels, and nearshore wave conditions during the peaks of severe hurricanes.

Katrina versus SPH Storm Parameters

Volume III discussed the design hurricane for the Lake Pontchartrain, LA, and Vicinity hurricane protection system, and the Standard Project Hurricane (SPH). The hurricane parameters that defined the SPH were: central pressure of 27.6 in. of mercury (934 mb); radius-to-maximum-winds of 30 nautical miles; maximum wind speed of 100 mph (87 knots); and, a range of forward speeds, 5 to 11 knots.

Figure 34 shows the temporal variation of central pressure, maximum wind speed, and radius-to-maximum-winds for Katrina during the time the storm was in the Gulf of Mexico. Note the high degree of temporal variability in all three parameters. Values of the same parameters for the SPH, plotted as constant values, are also shown in the figure. The original SPH work only considered hurricane conditions at landfall. During the period of time between 0900 UTC on

28 August through 1500 UTC on 29 August (time of final landfall), the central pressure of Katrina was lower than the SPH value, and it was 32 mb lower at one point near the time when the storm reached peak intensity. In terms of central pressure, Katrina was much more severe than the SPH. The direct effect of central pressure on storm surge is not that great. However, the lower central pressure is an indicator of storm intensity, i.e. wind conditions. Figure 34 shows the high degree of correlation between central pressure and maximum wind speed.

During the time period from 0300 UTC on 27 August through 2100 UTC on 27 August the intensity of Katrina, as indicated by the maximum wind speed, hovered around the same intensity as the SPH (87 knots). From 0000 UTC on 28 August through the time of final landfall, maximum winds exceeded those of the SPH. At the height of the storm's intensity, the maximum wind speed for Katrina (139 knots) greatly exceeded that of the SPH, by 52 knots. At landfall, the maximum wind speed of Katrina (100 knots) exceeded the SPH value by 13 knots. Wind speed differences are most important. The role of wind speed in determining storm surge and wave energy levels, through its nonlinear relationship with surface wind shear stress, was discussed earlier.

The wave producing potential of a storm is related to the wind speed raised to the second power (the relationship between wind speed and surface shear stress). While the storm was in deeper water at its peak intensity, Katrina was actively spawning waves consistent with those of a Category 5 intensity storm; and the wave producing potential of Katrina was 250 percent of the potential for the SPH design storm. The wave energy created in deep water, even while the hurricane was located away from the coast, is extremely important in determining what takes place at the coastline. Waves will propagate from deep water to the coast and contribute to water level increases at the coast (storm surge) through the process of wave setup. They are also important because the magnitude of wave height and period in the storm-generated wave field directly influences nearshore wave conditions, which dictate wave runup and overtopping on levees and floodwalls. Waves are effectively generated by wind in deep water; however, winds are much less effective in generating storm surge in deep water.

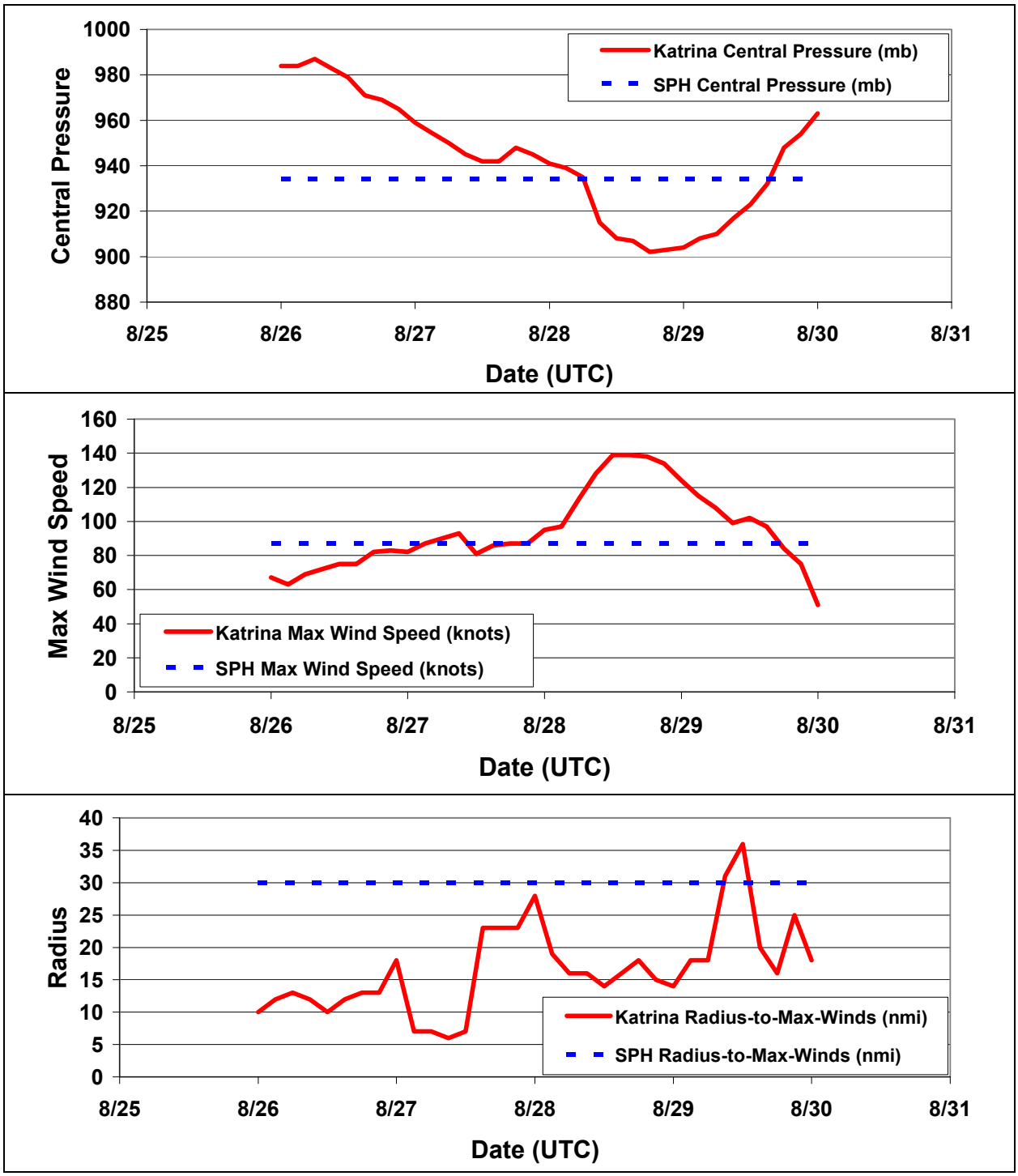

Figure 34. Comparison of Katrina and SPH storm parameters.

The storm surge producing potential of a storm is related to wind speed raised to the second or third power (the latter assuming the surface wind drag coefficient is a linear function of the wind speed). The cubic relationship is implicit in the storm surge modeling done as part of this IPET investigation. Just prior to and at landfall, Katrina's storm surge producing potential was 130 to 150 percent of that for the SPH storm intensity, depending on whether the quadratic or cubic dependency is assumed. That 15% difference in maximum wind speed near landfall translates into 30 to 50 percent more storm surge generating potential. Either case represents a significant increase.

The surge and wave potential of Katrina greatly exceeded that of the SPH throughout the time during which the storm had it greatest influence on conditions along Southeast Louisiana, even despite the significant decrease in Katrina's intensity during the 12-hr period prior to landfall. Katrina's large size and extreme intensity contributed to development of high water levels and wave conditions along Southeast Louisiana, even while the storm was some distance away from the coast. Results also suggest that the Saffir-Simpson scale is not a reliable indicator of the surge and wave producing potential of a hurricane. The scale does not adequately reflect the strongly nonlinear relationships between wind speed and storm size and surge or wave producing potential of a hurricane. The scale also neglects topographic controls, which for Southeast Louisiana is a crucial factor in storm surge generation.

A radius-to-maximum-winds value of 30 nautical miles was adopted for the SPH. Prior to landfall, values for Katrina were less than the SPH value. Values ranged from 6 to 28 nautical miles most of the time, except near landfall. From 0000 UTC on 28 August until just prior to landfall, the radius-to-maximum-winds varied within a fairly narrow range, between 14 and 20 nautical miles At landfall, the radius-to-maximum-winds of Katrina increased substantially, to values of 31 to 36 nautical miles, values roughly equal to the SPH value.

The forward speed of the SPH was allowed to vary in the original design studies, from 5 to 11 knots. During the 24-hr period between 0000 UTC on 28 August and 0000 UTC on 29 August, the forward speed of Katrina was about 10 knots. Between 0300 UTC on 29 August and 1200 UTC on 29 August, as the storm approached and made landfall in Southeast Louisiana, Katrina's average forward speed was about 13 knots. Assuming everything else about a hurricane is constant, a slower moving storm along the track of Katrina would be expected to produce a higher storm surge because winds have more time to push water into the region.

Regional Wave Modeling

Purpose and Approach

Wave modeling was done to characterize wave conditions just seaward of the hurricane protection system, throughout the entire study region. With one exception (two buoys located in close proximity at a single location in Lake Pontchartrain just north of the 17th Street Canal), no shallow-water wave measurements were available that captured wave conditions during the storm just seaward of the levees and floodwalls. Wave measurements were available at a few offshore sites, some of which survived the peak of the storm; but these sites are too far away

from the high impact zone and in much deeper water, and they can not be used to directly characterize conditions immediately adjacent to the hurricane protection system. The paucity of nearshore wave data highlights the need for shallow-water wave measurements that are collected during hurricanes, using instrumentation that can withstand, survive, and record during severe hurricanes and capture the peak conditions. In light of the limited amount of nearshore wave measurements, wave modeling was employed to provide the required information, at the resolution needed, for the very large study area.

Wave modeling was done using a nested approach, with three levels of nesting: 1) basin-scale modeling for the entire Gulf of Mexico; 2) regional-scale modeling at higher resolution for a much smaller domain that encompassed Southeast Louisiana and part of the Mississippi coast, with more resolved wind field input, and 3) nearshore, shallow-water, local-scale modeling which was done at very high 200-m resolution. At each successive nest level, additional resolution was employed to maximize accuracy (resolution is directly related to accuracy) and to treat the important physical processes such as depth effects as accurately as was computationally feasible. Wave boundary conditions for modeling done in each successively refined domain were derived from modeling done at the next coarser domain. The effects of storm surge on water depth were only addressed in the nearshore, shallow-water wave modeling.

The key output product from the most refined nearshore wave modeling work was information to characterize the temporal variation of significant wave height, peak spectral wave period, and mean wave direction computed using the full energy spectrum, along the entire periphery of the hurricane protection system that was considered in this study. Maximum wave conditions were also of great interest, and local maxima were compared to the design wave conditions and to the limited set of wave measurements that was available. Comparisons to design wave conditions are presented in a later section. Frequency-direction energy spectra were computed and saved at locations where the high-resolution hydrodynamic analysis required the information.

Every effort was made to compare model predictions with measured wave data for the purpose of assessing model accuracy, assess uncertainty in model results, and provide a level of confidence in model-derived results. Comparisons were made using measurements from several sources: 1) two small buoys (nearly co-located) that were deployed in Lake Pontchartrain just prior to the storm by the U.S. Army Corps of Engineers, New Orleans District, functioned during the storm, and were recovered after the storm, 2) a number of large NOAA NDBC buoys that are located in deeper water (see Figure 35 for buoy locations), and 3) satellite-mounted altimeter. Standard Corps wave prediction models were applied to simulate wave conditions during Katrina; however, other frequently used models were also applied to aid in assessing uncertainty in model results.

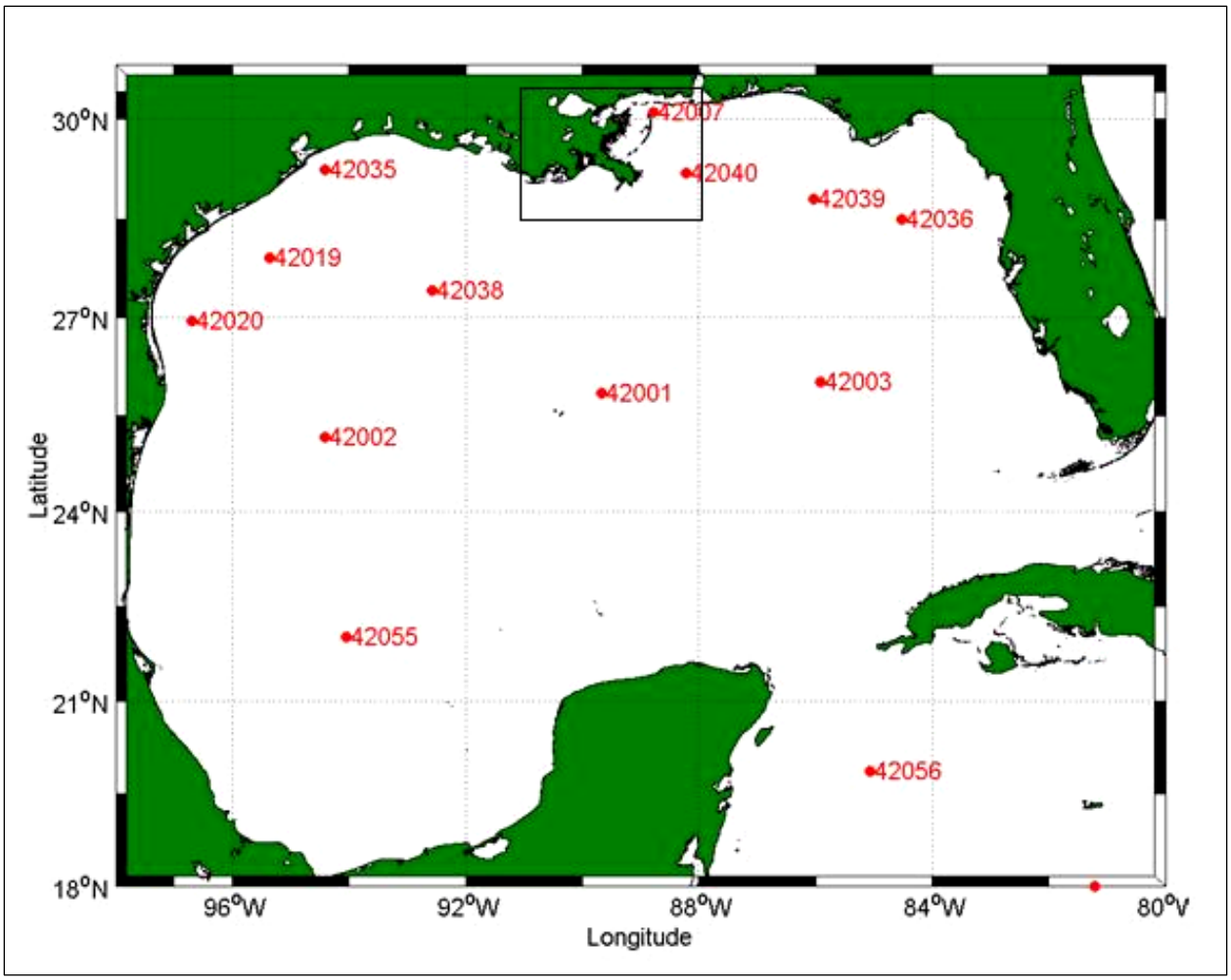

Figure 35. Offshore and regional wave modeling domains and location of NOAA NDBC buoys.

Simulation of Offshore Waves

WAM Results

Offshore wave-modeling was done using two models, WAM Cycle 4.5 (Komen et al. 1994) and WAVEWATCH III (Tolman 1998, 1999). The WAM model was selected to generate wave conditions for the "production" modeling, since it has been used during the past decade or so by the Corps for its detailed wave generation modeling (particularly for hurricanes) and it has undergone extensive critical evaluation for the 2003 through 2005 hurricane seasons as part of the NOPP project: Real-Time Forecasting System of Winds, Waves and Surge in Tropical Cyclones *http://www.hurricanewaves.org*. The WAM model was applied for basin- and regional-scale domains, the same ones defined in Table 2. Both domains correspond to those employed in development of wind and pressure fields. Figure 35 shows the basin-scale domain (entire gulf) and the regional domain (the black box in the figure that encompasses the Louisiana/Mississippi coastal region). The exact regional domain and the local bathymetry in this area are shown in more detail in Figure 36.

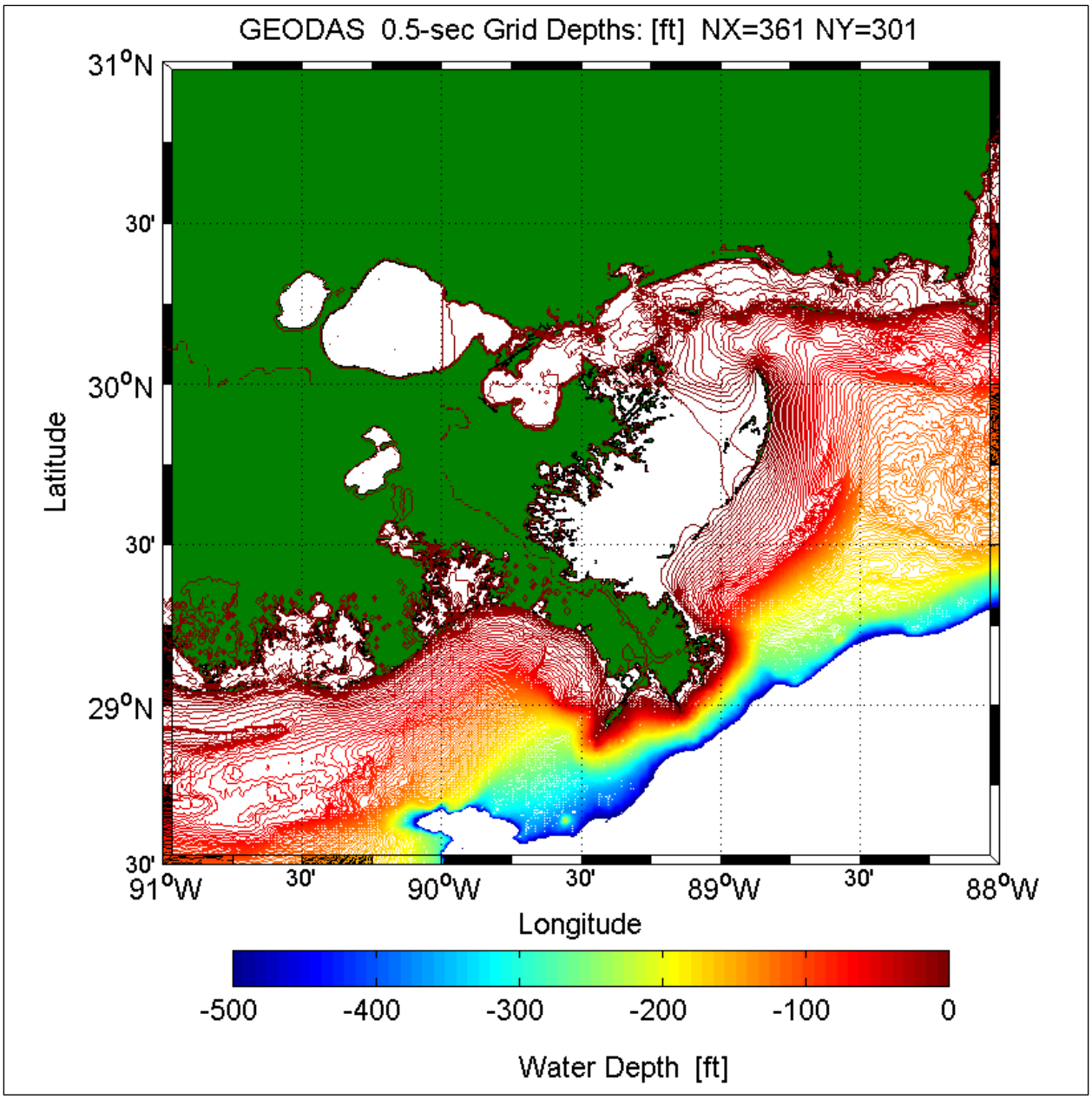

Figure 36. Regional wave modeling domain and bathymetry.

Figure 37 shows the maximum significant wave height field produced by Katrina throughout the Gulf of Mexico. The maximum significant wave height was computed to be 55 ft. The area in which the storm produced 20-ft or greater waves or higher is vast, encompassing most of the northern Gulf. The figure also illustrates the extreme wave climate produced by the storm as it rapidly intensified while still in deep water in the middle of the gulf. The region of extreme wave energy followed the path of the storm. Large significant wave heights were experienced along the Louisiana coast. Considerable wave energy was generated when the storm was in its most intense state further offshore in the gulf and waves radiated outward ahead of the storm. Those

waves propagated northward to Southeast Louisiana region despite the storm weakening just prior to landfall.

Figure 38 further illustrates the complexities of the wave field generated by Hurricane Katrina. The figure shows the maximum significant wave height computed at each point in the regional domain, at any time during the simulation. The regional-scale simulation starts on 0000 UTC 28 August and ends on 0000 UTC 30 August. The overall maximum significant wave height, 55 ft, occurs just south of the Mississippi River delta. These wave conditions are extreme. Shallow water effects of shoaling and, more importantly, refraction focus the offshore energy towards the Mississippi River delta. When waves break due to their arrival in shallow water, wave energy decreases. In areas dominated by depth-induced breaking, significant wave heights are generally on the order of 60 percent of the local water depth. For example, a sea state in which the significant wave height is about 40 ft would begin to experience considerable depth-limiting breaking in about 65 ft of water. This tendency is evident in the dramatic decrease in wave height along the Mississippi River delta. It is also apparent along the Southeast Louisiana barrier island chain where considerable energy dissipation takes place well seaward of the barrier islands due to depth-induced breaking. The pattern of wave height maxima follows the bathymetry pattern closely (compare Figures 38 and 36), an indication of depth limited breaking effects. Offshore, deeper-water wave conditions along the Southeast Louisiana coast are computed to be 35 ft in the northern areas, increasing to approximately 50 ft adjacent to the Mississippi River delta.

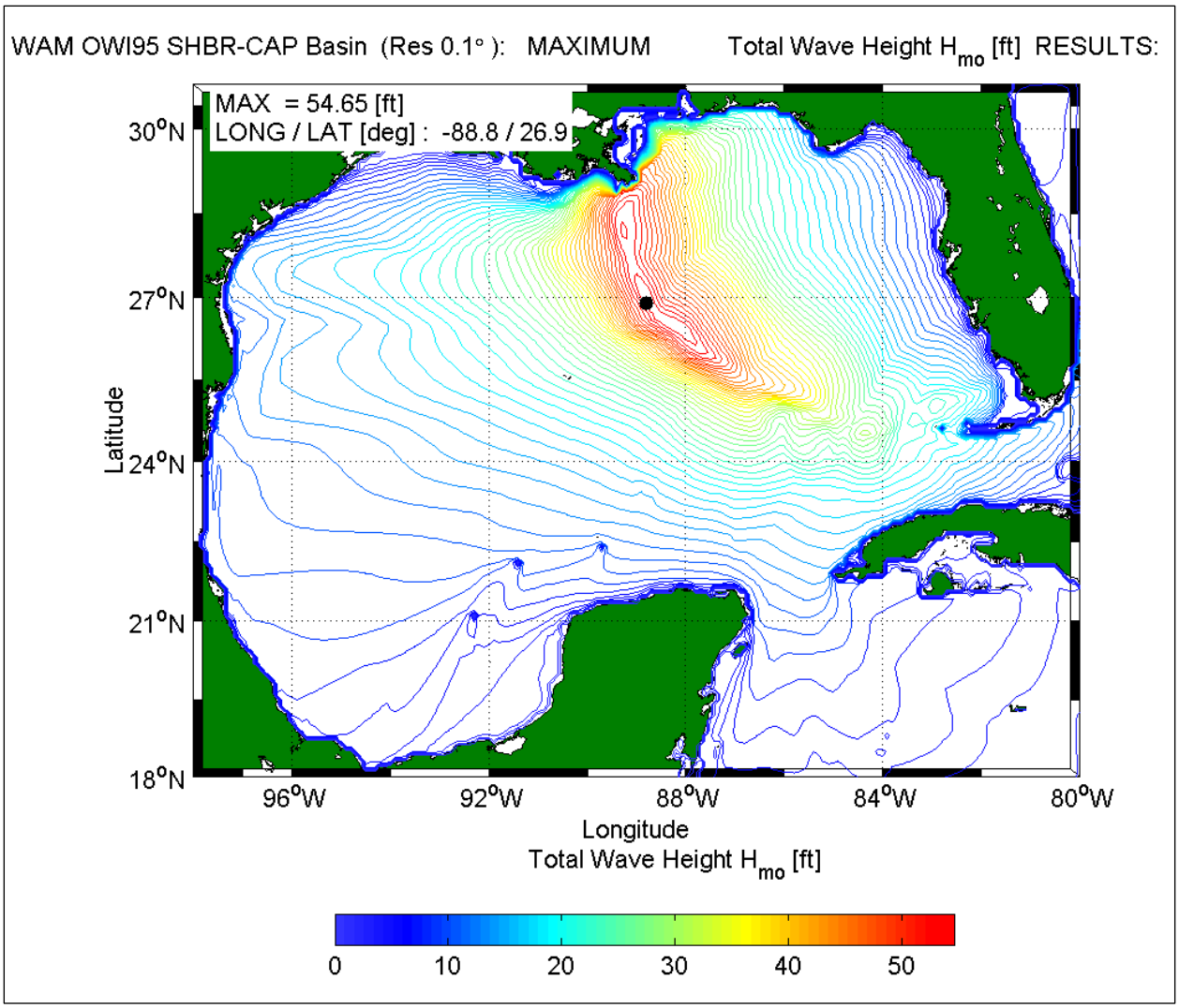

Figure 37. Color contour of the maximum wave height conditions in the basin domain.

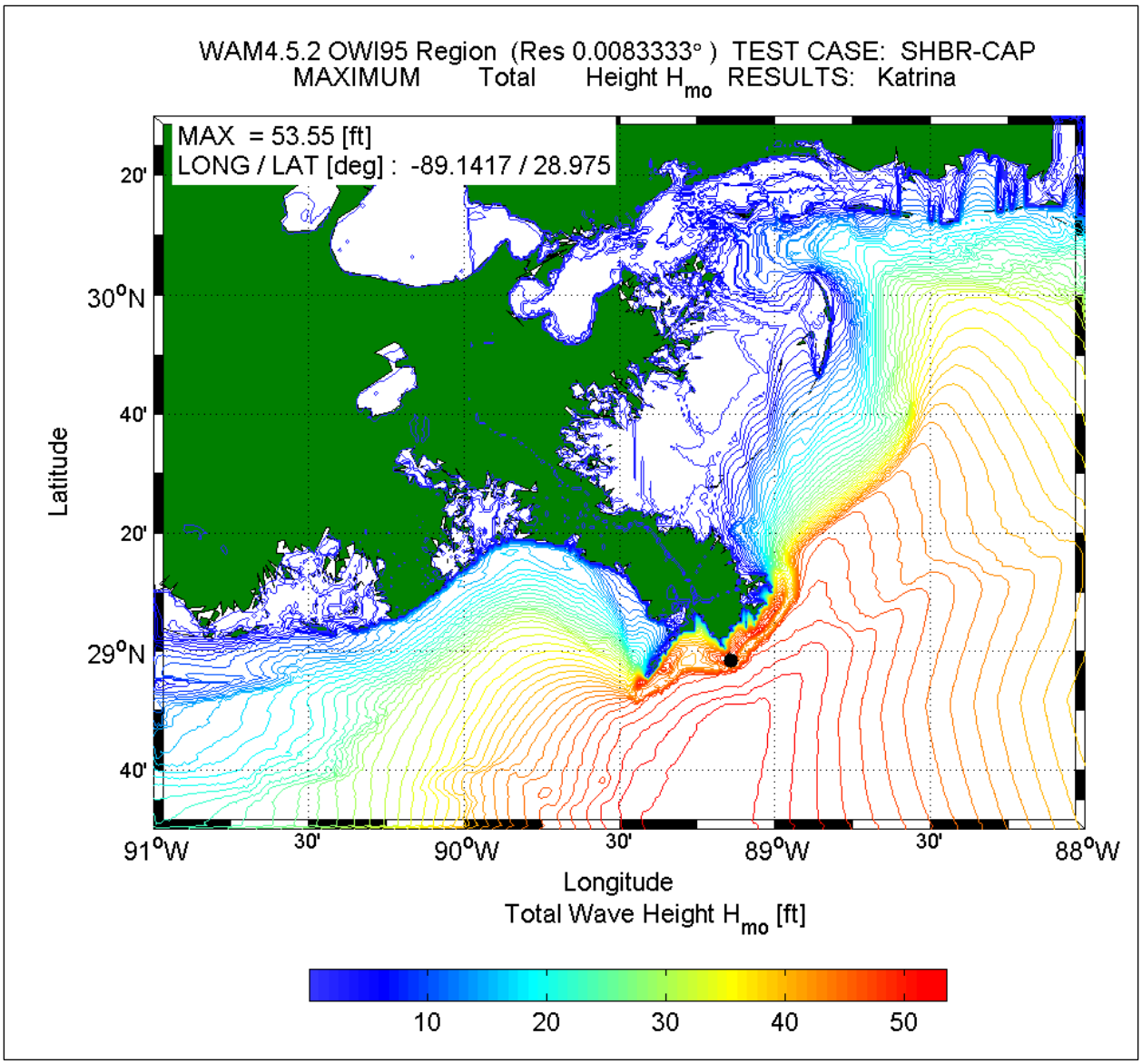

Figure 38. Color contour of the maximum wave height conditions in the region domain.

The WAM simulation assumes constant water depths, i.e., no changes due to storm surge. Therefore WAM results landward of the barrier islands indicated in Figure 38 will be lower compared to expected results when storm surge effects on water depth (increases) are considered. The nearshore wave modeling considers this effect.

The maximum mean wave period results for the regional WAM simulation are shown in Figure 39. This figure illustrates the long periods associated with the hurricane. Wave period is dominated by swells propagating into the region from the southeast, having mean periods ranging from 12 sec to more than 15 sec. In the front right hand quadrant of Katrina, local wind seas also abound. To the west of the storm, the wave climate is dominated by longer-period swells, with a smaller wind sea component.

Comparison: WAM Results with Wave Measurements

Comparisons of wave model results with measurements were an important facet of the work. A few of those comparisons are presented below. A much more detailed description of the offshore wave modeling work, additional model-to-measurement comparisons, and much more information on the model-to-model comparisons are presented in Appendix 3.

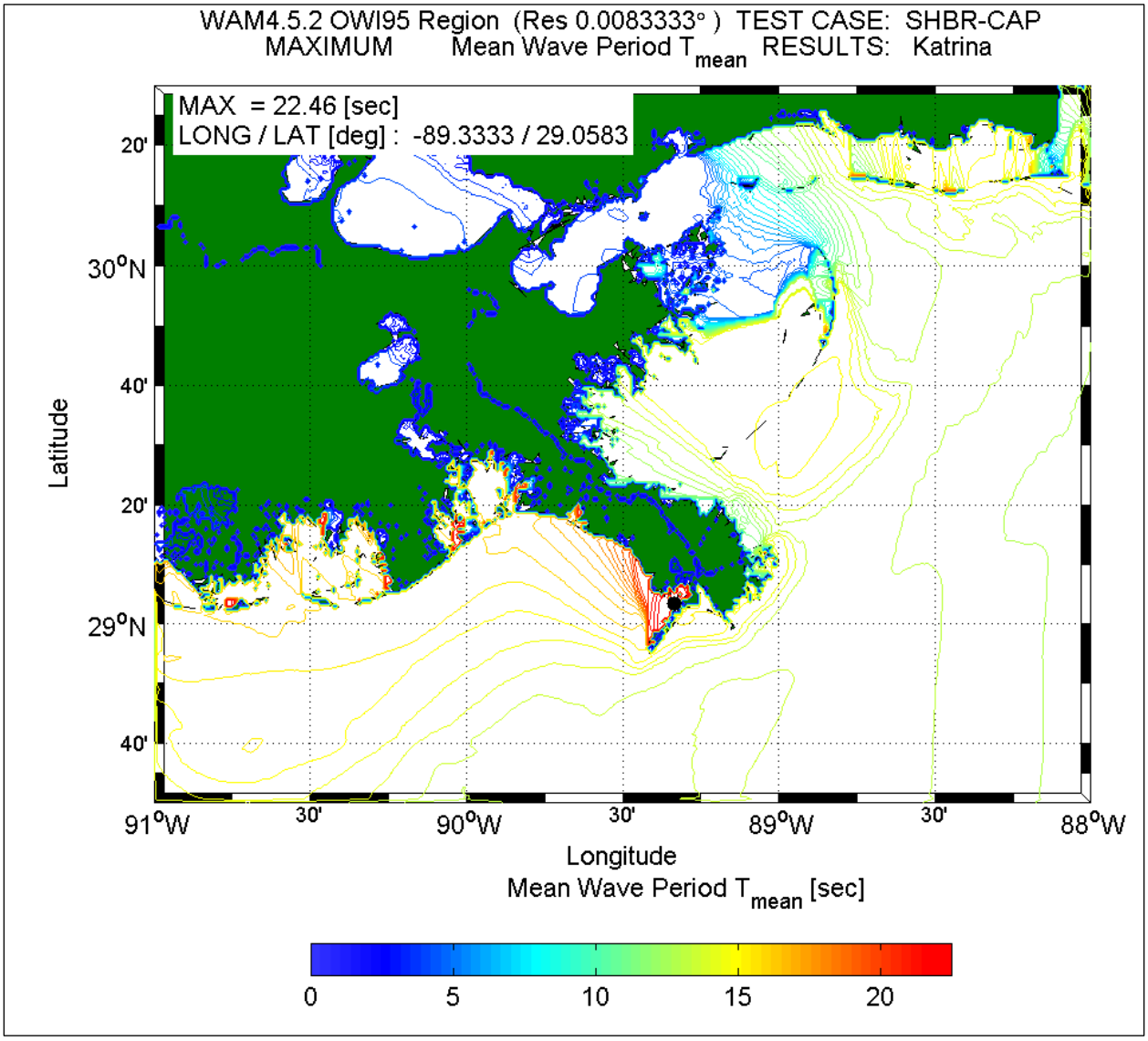

Figure 39. Color contour of the maximum mean wave period conditions in the region domain.

Comparisons of WAM results to measurements made at NOAA NDBC Buoys 42040 and 42007 are shown here. Of all the buoys for which data are available, these two are in locations that best reflect the offshore wave climate that Southeast Louisiana was subjected to during the storm. Buoy locations are shown in Figure 35. Comparisons for Buoy 42040 are shown in Figure 40 and comparisons for Buoy 42007 are shown in Figure 41. Each figure shows a

comparison for energy-based significant wave height, peak and mean spectral wave periods, mean wave direction, wind speed, and wind direction.

The maximum height measured at buoy 42040 is 55 ft. According to NOAA, this measured significant wave height is the highest value ever recorded in the Gulf of Mexico, and the reading matches the highest value ever recorded at one of their buoys. The following statement is made on the NOAA web site:

> "Station 42040, located at 29°11'03"N 88°12'48"W approximately 64 nautical miles south of Dauphin Island Alabama, reported a significant wave height of 16.91 meters (55 feet) at 1100 UTC, August 29, 2005. Station 42040 is a 3-meter diameter discus hull buoy deployed and operated by National Oceanographic and Atmospheric Administration's National Data Buoy Center (NDBC). Although 42040 does not measure maximum wave heights, the maximum wave height may be statistically approximated by 1.9 times the significant wave height (World Meteorological Organization, 1998), which would be 32.1 meters (105 feet). At the time of the report, Hurricane Katrina was approximately 73 nautical miles to the west of 42040 with maximum sustained winds of 145 miles per hour (Public Advisory 26A issued by the National Hurricane Center). In addition to the 55-foot report, 42040 reported seas 12 feet or greater for 47 consecutive hours.
>
> The 55-foot report surpasses the previous highest significant wave height reported by an NDBC buoy in the Gulf of Mexico of 15.96 meters (52 feet), also reported by 42040 during Hurricane Ivan in September 2004, and matches the previous highest significant wave height reported by an NDBC buoy of 16.91 meters reported by station 46003 (in the Northeast Pacific Ocean south of the Aleutian Islands) in January 1991." (*http://www.ndbc.noaa.gov/hurricanes/katrina/*)

The trend of increasing wave height with time mimics the pattern of wind speed increase. Southeast Louisiana experienced a severe wave climate for an extended period of time. Offshore wave heights exceeded 15 ft for a least a day prior to landfall. Measured peak wave periods show a marked increase later in the day on 27 August, two days prior to landfall, increasing from 7 sec to more than 10 sec. This change represents the arrival and predominance of longer period swells that are generated by the hurricane while it is well away from the coast. At the peak of the storm, peak spectral wave periods are between 13 and 15 sec. Wave direction shows a gradual shift as the storm approaches landfall. Several days out from landfall, waves are predominantly from the east; but as the storm approaches, waves shift to directions that are from the southeast.

The maximum computed significant wave height at this buoy location is about 42 ft, considerably less than the measured maximum. At this location, the greatest difference between peak measured and computed wave heights was observed. The maximum wave height computed for Katrina was 55 ft, but this value was computed much closer to the core of the storm. By comparison, Hurricane Camille wave model simulations reached approximately 47.2 ft as an absolute maximum (Jensen and Cardone 2005). Camille was a Category 5 intensity storm that produced the highest storm surge in recorded history, prior to Katrina.

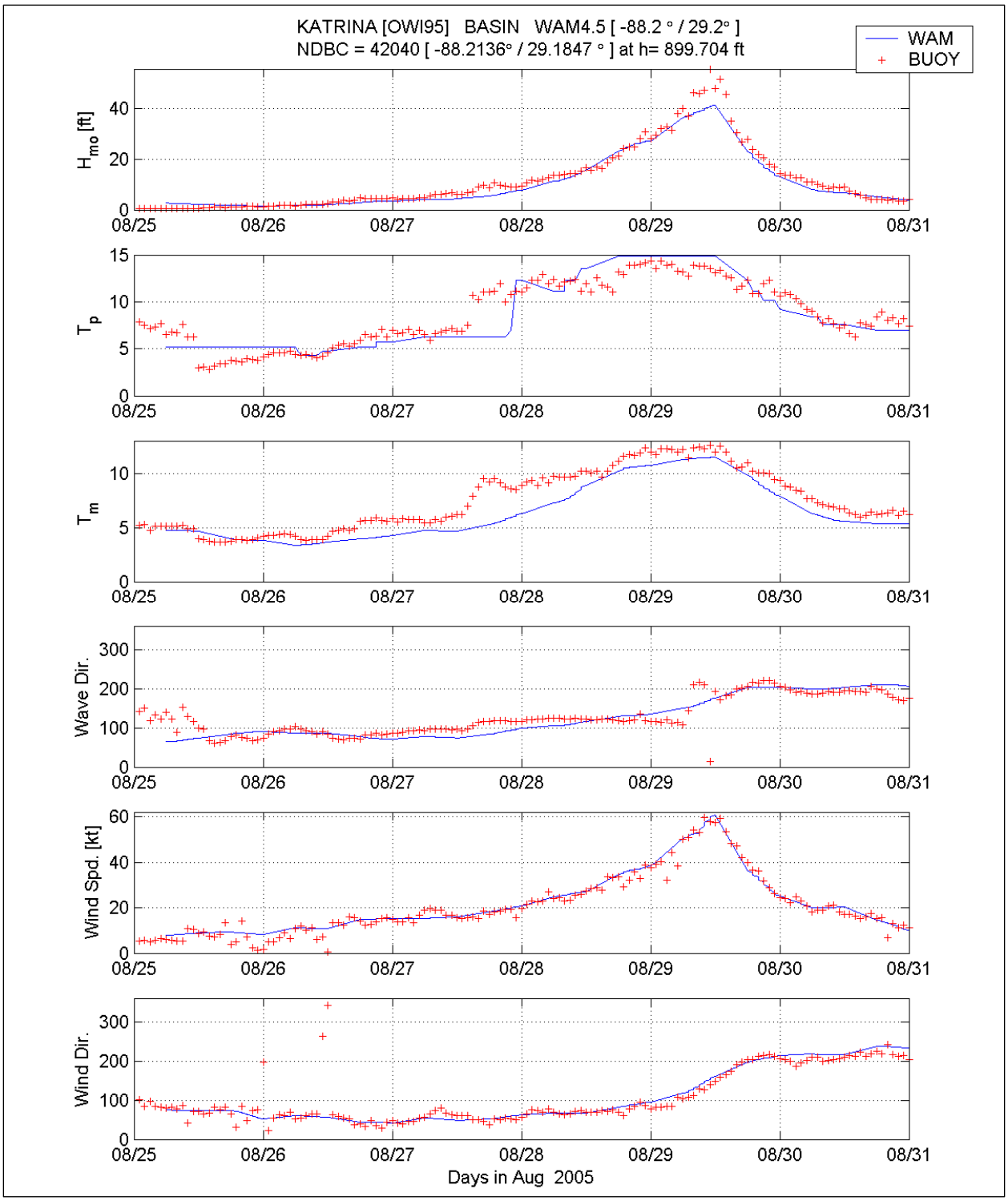

Figure 40. Comparison of WAM Cycle 4.5 basin-scale (blue line) to the measurements at NDBC 42040. [Time is referenced to UTC. Wave Direction is the angle of approach in degrees relative to true north.]

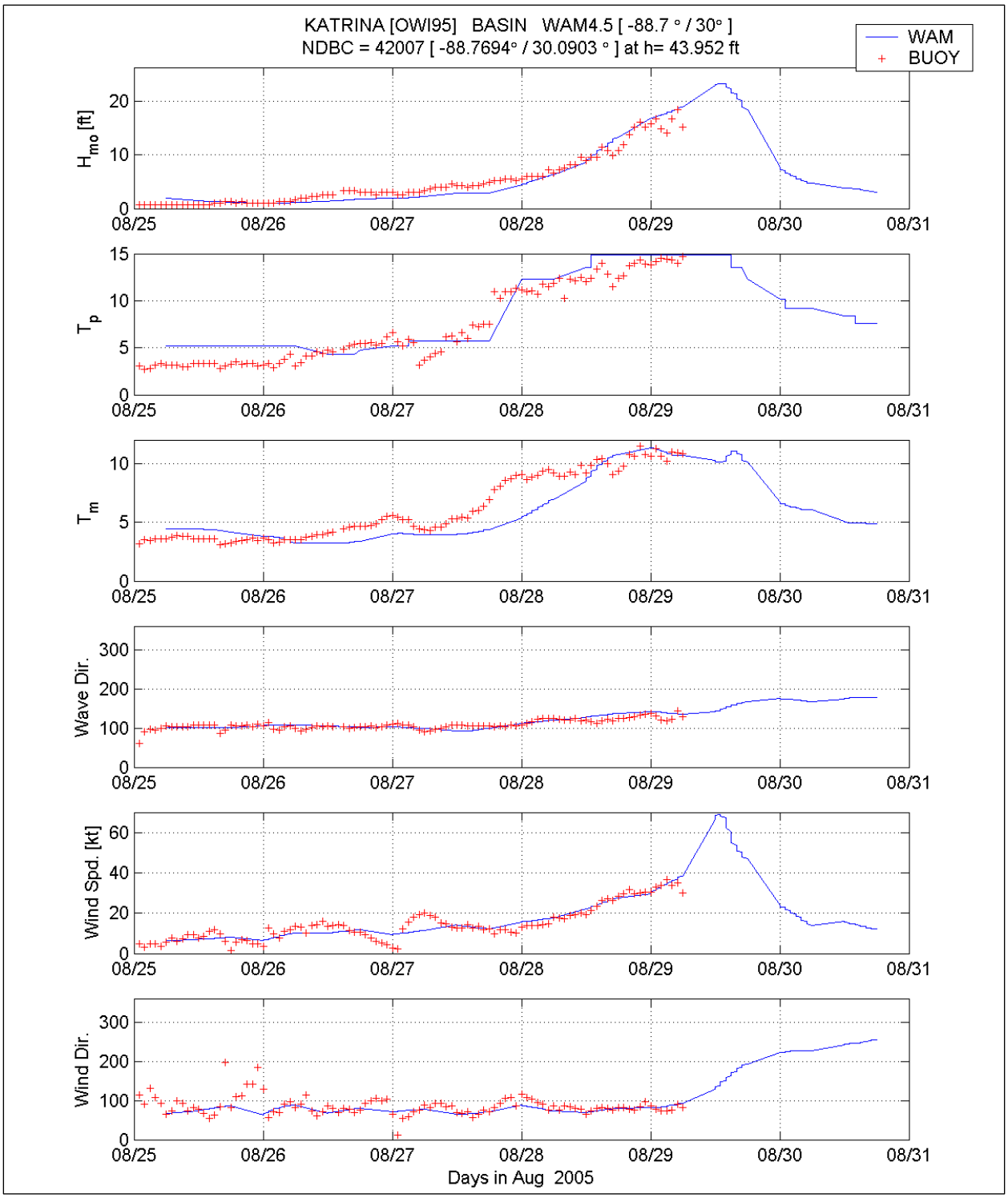

Figure 41. Comparison of WAM Cycle 4.5 basin-scale (blue line) to the measurements at NDBC 42007. [Time is referenced to UTC. Wave Direction is the angle of approach in degrees relative to true north.]

Leading up to the peak, agreement is close as it is immediately following the peak. Computed peak periods are 15 sec, consistent with the measured periods. The change in period, indicating the arrival of longer period swells, is simulated by the model; however, the timing of the shift is computed at a slightly later time. Computed wave directions agree reasonably well with measured wave directions.

Buoy 42007 is located just west of the northern tip of the Chandeleur Island chain in a water depth of 44 ft. Patterns in wave condition changes are similar to those at Buoy 42040. It is unfortunate, though, that this buoy did not survive Katrina; and as evidenced by the wave record, it failed well before the storm peak. The maximum wave height recorded at this buoy prior to failure was approximately 18 ft. During the growth stage of the storm, measurements indicate a methodical, slowly increasing wave height that is dominated by wind-seas (characterized by short periods on the order of 5 sec). On 1800 UTC 27 August there is a noticeable shift in peak wave period, an indication of the early arriving swell energy that reaches Southeast Louisiana well before (2 days) arrival of the intense core of the storm. The downshifting in frequency (or increasing Tp) continues, with the increase in wave energy until failure of the buoy. Approaching the time of failure, there is only a modest change in the vector mean wave direction, changing by at most 30 deg from about 100 to 130 degrees. This should not be surprising because to the south, west, and north there is considerable sheltering due to the influence of land features. Thus there is a very small window available to receive wave energy at this location. Waves are approaching from the east-southeast at the time the instrument failed.

Prior to 28 August, wave heights are underpredicted. After 28 August, model results agree reasonably well with measurements. The maximum computed significant wave height at this location is approximately 23 to 24 ft, with peak wave periods of 15 sec. Computed wave directions agree well with measured directions. It is clear that the hurricane has spawned energetic long-period swells which propagate into the region.

Two offshore oil platforms, equipped with wave measurement sensors, recorded peak significant wave heights and peak spectral periods. These measured values were compared to co-located WAM estimates corresponding to the platform measurements; WAM predictions were 33.3 and 38.6 ft with peak period estimates of 14.9 and 13.5 sec, respectively, for the two platform sites. Measured wave heights were similar to the upper value of predicted wave height; measured wave periods were 1 to 4 sec less than the predicted periods.

Wave predictions were also compared to results obtained from altimeters on board two satellites. Data from three separate satellite passes were analyzed. Wave height estimates from satellite-based altimeters provide a useful source of data over space but for selected time intervals. Use of both data sets (temporally varying point source measurements, and spatially varying measurements at discrete times) complement each other and better assess the capability of a wave model's performance in this complex meteorological situation. Wave height altimeter results were available from two sources: 1) Envisat (ENVSAT) operated by European Space Agency, and 2) Jason (JS1) operated jointly by NASA and French Space Agency CNES. Three distinct tracks, two from ENVSAT and one from JS1 are used here.

Figure 42 shows data for the satellite pass made closest to Southeast Louisiana, acquired by ENVSAT on 0400 UTC on 28 August, along with the predicted wave height field from the WAM model. The WAM wave heights are color contoured, and the colored symbols are the estimates from the various altimeter data sets. The altimeter estimates are spatially filtered, eliminated near the coast where estimates are contaminated, and any other spurious data are removed. Comparisons between WAM and data from all three satellite passes are shown in Figure 43, and exact times of the passes are given in the figure. The other two passes occur later in the storm but were made in the eastern gulf, well way from the core of the storm. As shown in Figure 42, the altimeter cannot accurately estimate wave heights though the core of Hurricane Katrina. However, the remainder of the Gulf of Mexico provides useful data to compare to the WAM results.

From Figure 43, it is very apparent WAM replicates the ENVSAT data until it reaches about the 27-ft wave height contour in the left front quadrant of Katrina. As the satellite passes out of the core, WAM again over-estimates wave heights on the order of 5 ft to, at most, 10 ft. Away from the core, WAM predictions are more accurate. Note that WAM estimates in the core of Katrina (not visible in the altimeter data) have been removed from the upper panel of Figure 43. Overall, the structure of the wave height field is reasonably well predicted by the WAM model for each of the three passes.

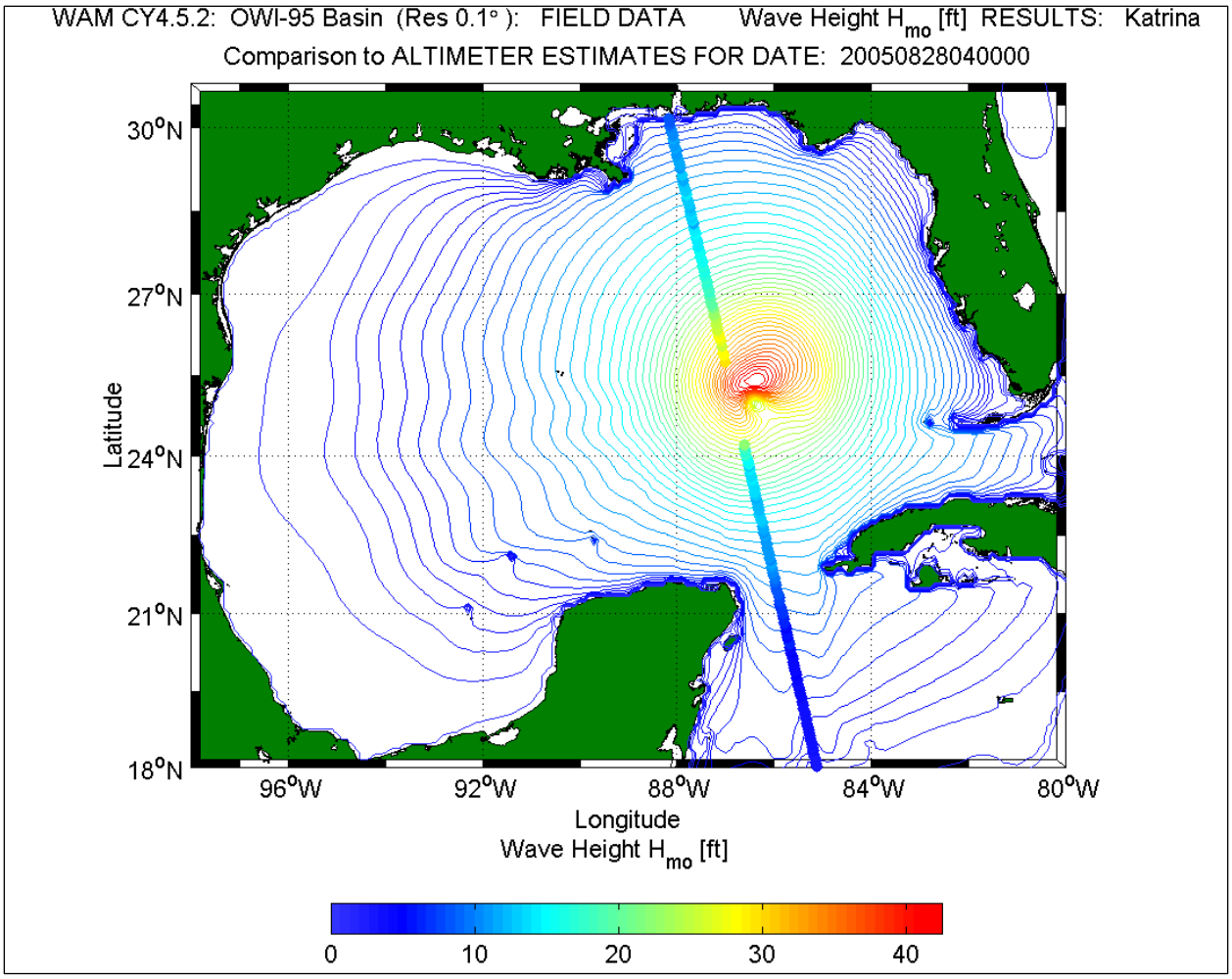

Figure 42. WAM wave height color contour overlaying ENVSAT altimeter wave height estimates at 0400 UTC 28 August 2005..

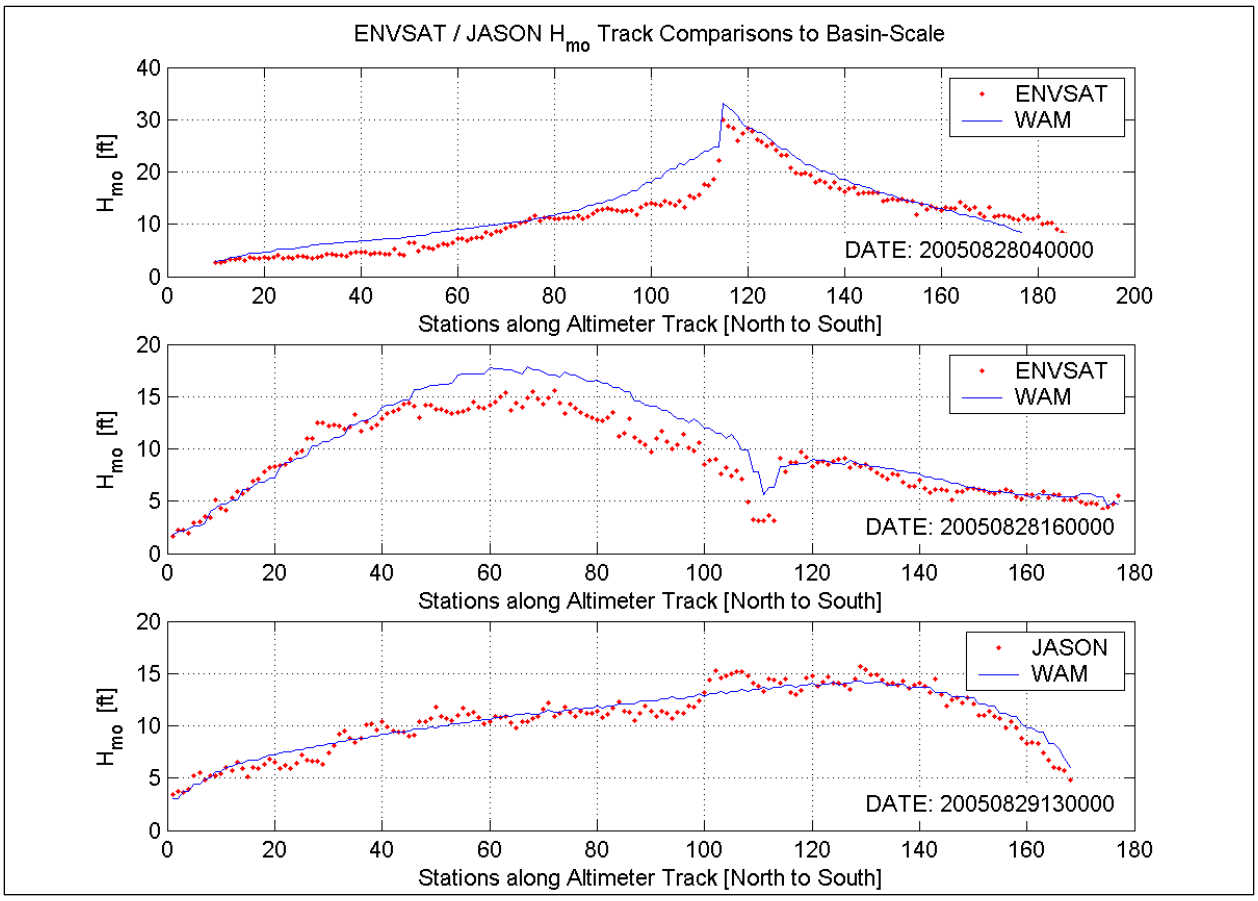

Figure 43. Comparison of WAM wave heights and estimates for the two ENVSAT passes and one Jason altimeter pass.

WAM – WAVEWATCH III Comparisons

The WAVEWATCH III model was also applied; it is another commonly used model for ocean-scale wave generation and it is the standard ocean-scale wave prediction model used by NOAA. A comparison of the two models is shown in a later section. Wind input for all wave modeling was done using the wind fields described previously based on the H*Wind/IOKA process.

Figure 44 shows results of comparisons between the WAM and WAVEWATCH III models, both run on the basin domain for several deepwater buoys that were closest to the path of Katrina. The variation of significant wave height with time is shown. Results are similar and mixed. One model is more accurate at one buoy, the other more accurate at another buoy. Overall, across all buoys WAM seems to slightly outperform WAVEWATCH III. This is confirmed in the statistical comparisons presented below.

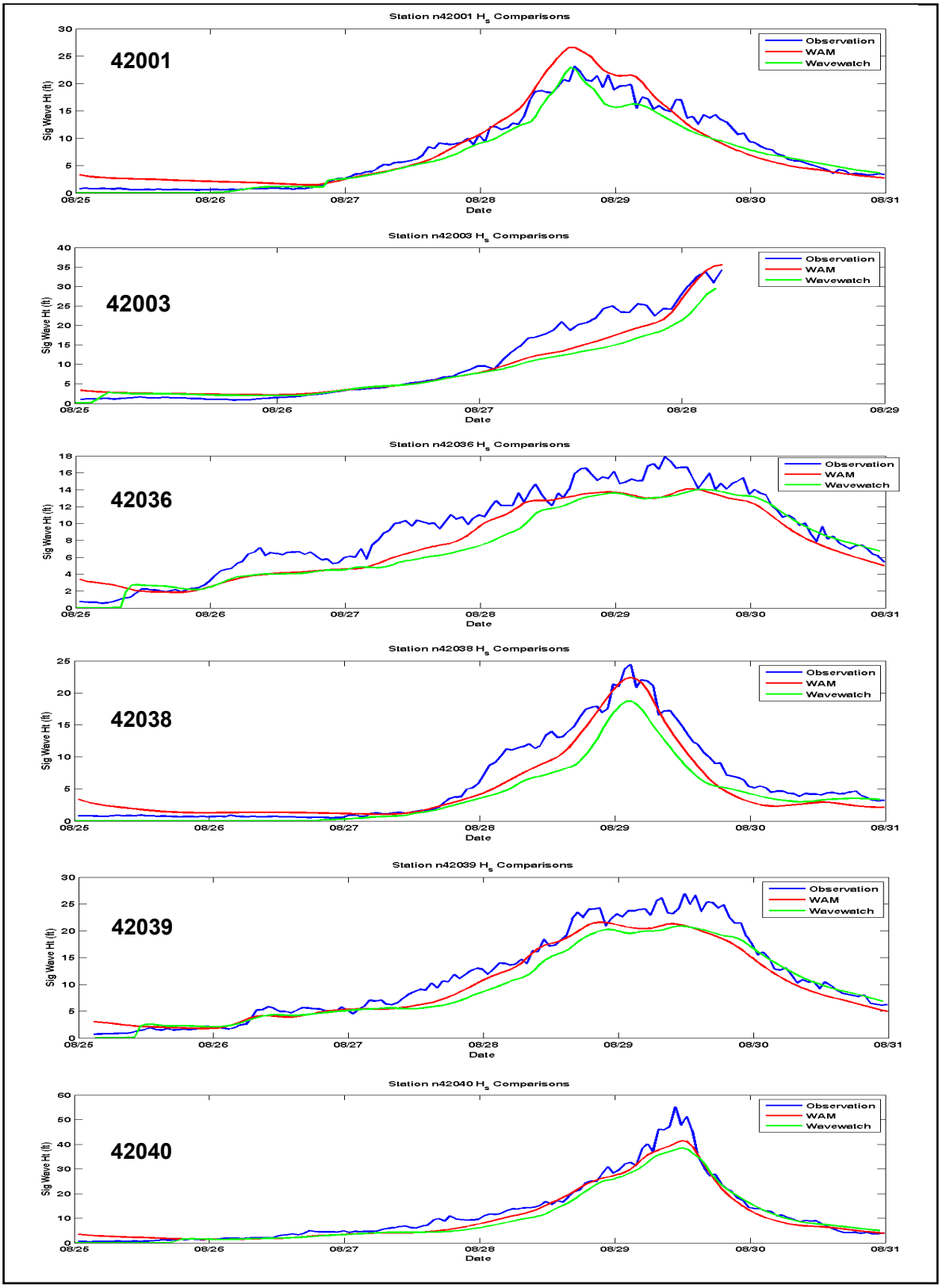

Figure 44. Comparison of significant wave heights (ft) as a funtion of time from observation stations (blue), WAM hindcast (red), and WAVEWATCH III hindcast (green). [Time is referenced to UTC]

The overall (across all stations) model performance scores for significant wave height and peak wave period appear in Tables 4 and 5, respectively. In each table, the results of the temporal correlations (TC) and the quantile-quantile (QQ) distributions are given for each wave system component, combined across all buoys. The time correlations examine agreement between time-paired observations; the QQ correlations examine agreement between cumulative frequency of occurrence distributions. The scores are derived for different components of the wave field, both wind sea and swell. The final combined scores provide a weighted performance across all wave system components.

Table 4
Wave Height Performance Summary

	Temporal Correlations		Quantile-Quantile	
Component	WAM	WW3	WAM	WW3
Wind sea	0.86	0.85	0.87	0.88
Young Swell	0.75	0.74	0.76	0.78
Mature Swell	0.85	0.72	0.87	0.73
Combined	0.83	0.80	0.84	0.82

Table 5
Wave Period Performance Summary

	Temporal Correlations		Quantile-Quantile	
Component	WAM	WW3	WAM	WW3
Wind sea	0.93	0.89	0.95	0.92
Young Swell	0.90	0.85	0.91	0.86
Mature Swell	0.93	0.87	0.95	0.89
Combined	0.92	0.88	0.94	0.90

Overall, the wave height performance scores are reasonably good for both models. The combined wave height and peak period scores for WAM show a 2 to 4 percent improvement over WAVEWATCH III for both TC and QQ statistical analyses. WAM and WAVEWATCH III wind sea heights depict only 1 percent difference, while WAM wind sea periods exhibit a 3 to 4 percent improvement over WAVEWATCH. Most significant for this study, however, are a 14 percent improvement in mature swell heights by WAM over WAVEWATCH III, and a corresponding 6 percent improvement in WAM mature swell wave periods. These large waves propagated away from Katrina as the hurricane moved north across the Gulf of Mexico.

Many more details regarding model-to-model comparisons are provided in Appendix 3.

Boundary Conditions for Nearshore Wave Modeling

The primary purpose of the offshore wave modeling task is to provide boundary condition information to the nearshore wave modeling effort (all nearshore domains). An example of the directional wave spectrum provided as a boundary condition to the nearshore wave modeling is shown in Figure 45. The spectrum reflects the directional distribution of the incident wave

energy as a function of wave frequency (frequency is inversely related to wave period). In Figure 45 the red vector indicates a mean wave direction, here showing waves approaching from the southeast. The colored area indicates the spectral region encompassing all wave frequencies and directions that are present in the sea state at this location. The red colors indicate the frequency-direction characteristics that contain the highest energy levels (the integrated energy-based significant wave height is almost 13 ft).

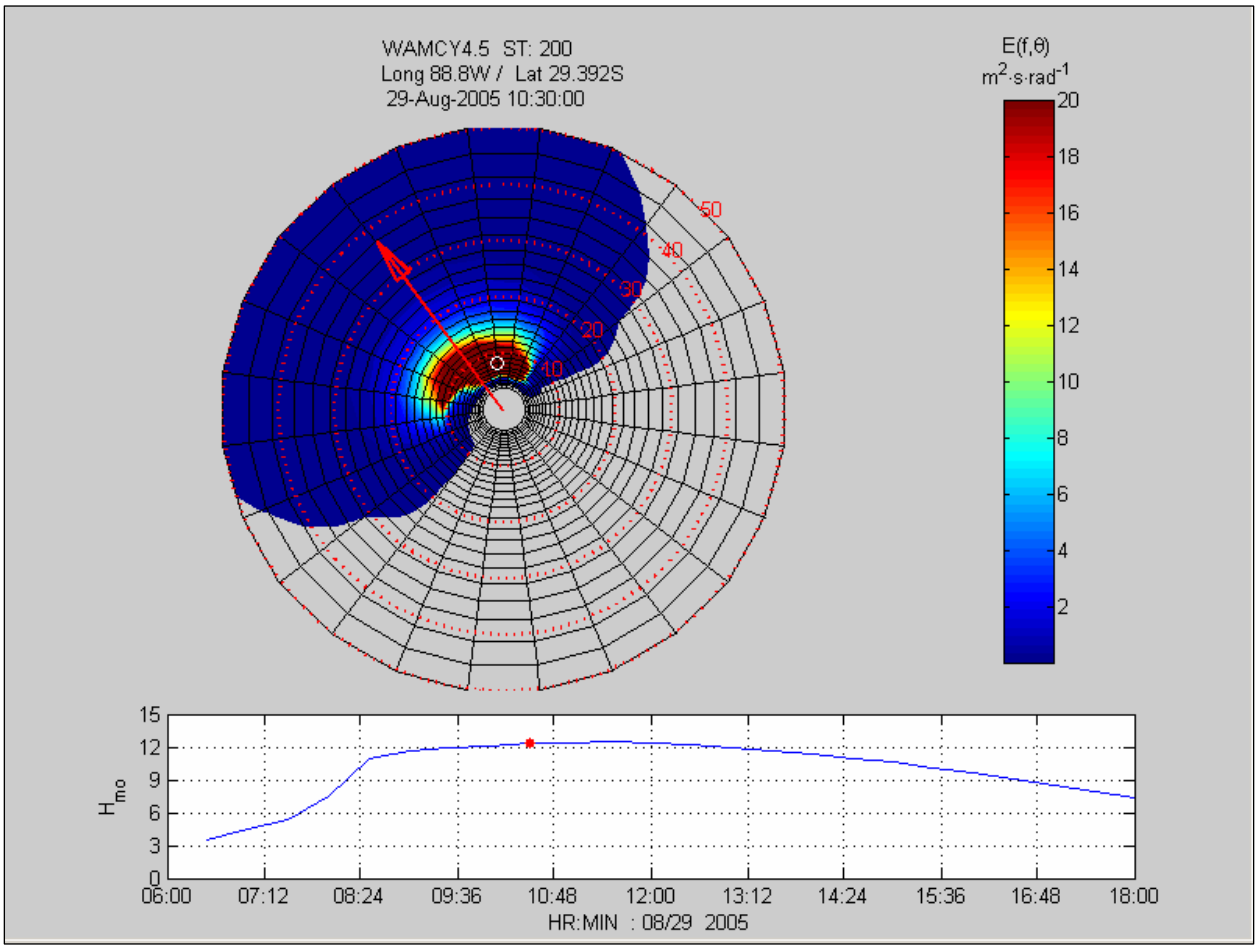

Figure 45. Example of the directional wave spectra color contoured in the upper panel and the significant wave height trace in the lower panel (note units are in CGS system). [Time is referenced to UTC]

Simulation of Nearshore Waves

Approach and Model Domains

Nearshore waves are required to calculate wave runup and overtopping on structures, the wave momentum (radiation stress) contribution to elevated water levels (wave setup), and wave forces on structures. The STWAVE model (Smith, Sherlock, and Resio 2001) was adopted for the nearshore wave transformation modeling; it is the standard model used by the Corps of

Engineers to simulate nearshore wave transformation. All "production" runs and results presented in this report were made with STWAVE.

STWAVE was applied on four grids for the southern Louisiana area: Lake Pontchartrain, Louisiana Southeast, Louisiana South, and Mississippi/Alabama (see Figure 46). The input for each grid includes the bathymetry (interpolated from the ADCIRC model domain), water surface elevation fields (interpolated from ADCIRC fields), and wind (interpolated from the ADCIRC wind fields, which apply land effects to the H*Wind/IOKA marine wind fields). The wind applied in STWAVE is spatially variable for all domains. STWAVE was run at 30-min intervals from 0030 UTC on 28 August 2005 to 0000 UTC on 30 August 2005.

The first grid covers Lake Pontchartrain at a resolution of 656 ft (200 m). Earlier runs were made at finer resolution 164 ft (50 m) by 328 ft (100 m), but the results were essentially the same, so the more efficient coarse grid was used for these simulations. The domain is approximately 25.8 by 41.9 miles (41.6 by 67.4 km). Lake Pontchartrain was run with the full-plane STWAVE to include generation and transformation along the entire lake shoreline. The grid parameters are given in Table 6. Figure 47 shows the bathymetry for the Lake Pontchartrain grid relative to NAVD 88 (2004.65). Brown areas in the bathymetry plots indicate land areas at 0 ft or higher elevation.

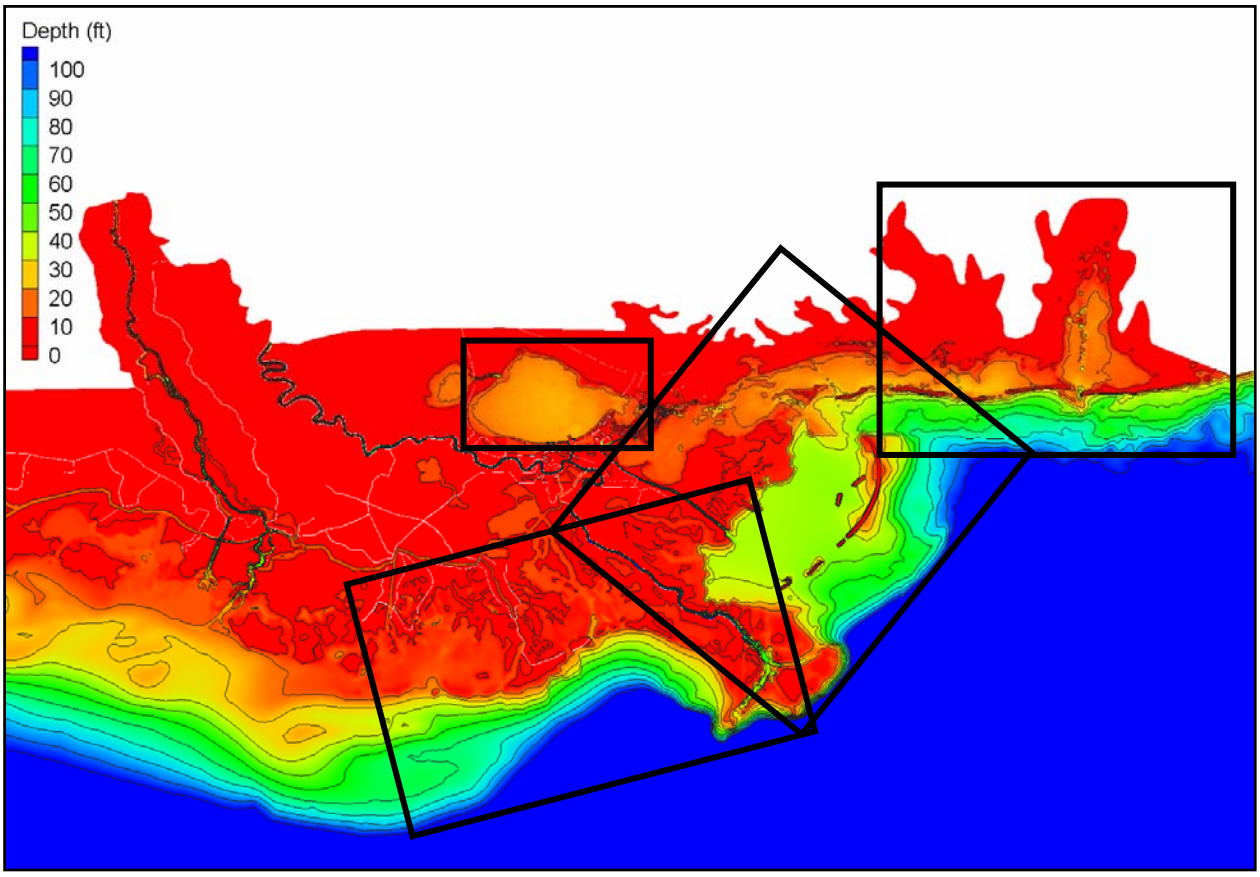

Figure 46. STWAVE modeling domains.

Table 6
STWAVE Grid Specifications

Grid	State Plane	X origin, ft	Y origin, ft	Δx, ft	Δx, ft	Orient Deg	X cells	Y cells
Lake Pontchartrain	LA South	3563779.5	690485.6	656	656	270	208	337
Louisiana Southeast	LA Offshore	4294586.6	1639491.5	656	656	141	683	744
Louisiana South	LA Offshore	3997126.0	1264895.0	656	656	108	664	839
Mississippi/ Alabama	LA Offshore	4463976.4	1653950.1	656	656	90	563	605

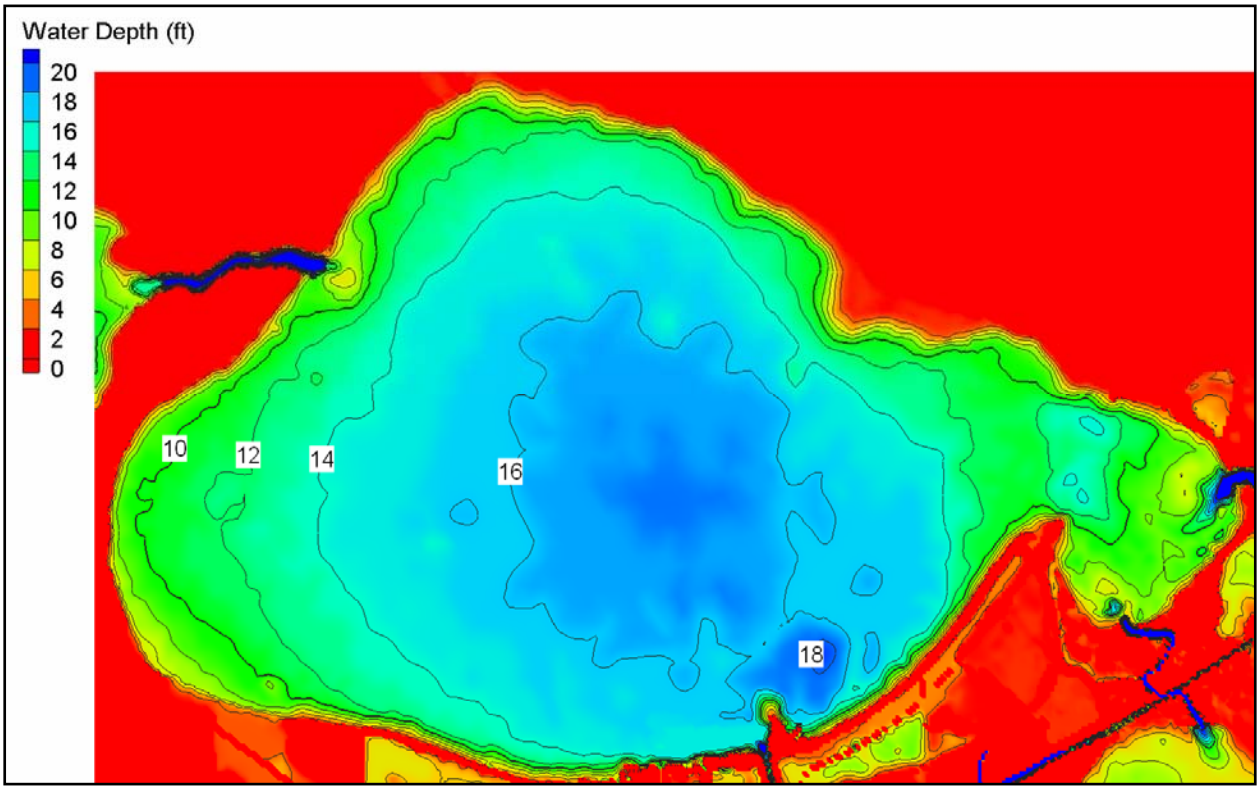

Figure 47. Lake Pontchartrain bathymetry grid (elevations in feet NAVD88).

The second, third, and fourth grids cover the coastal area east, southeast, and south of New Orleans at a resolution of 656 ft (200 m). The domain for the Louisiana southeast grid is approximately 84.9 by 92.4 miles (136.6 by 148.8 km) and extends from Mississippi Sound in the northeast to the Mississippi River in the southwest. The domain for the Louisiana south grid is approximately 82.5 by 104.2 miles (132.8 by 167.8 km) and extends from the Mississippi River in the east to the Atchafalaya River in the west. The domain for the Mississippi and Alabama coasts was added to simulate the wave momentum fluxes that increase the surge in Mississippi Sound and Lake Pontchartrain. The Mississippi/Alabama domain is approximately 70.0 by 75.2 miles (112.6 by 121.0 km) and extends from east of Mobile Bay to Biloxi, MS. These three grids were run with the half-plane STWAVE for computational efficiency. The grid parameters are given in Table 6. Figures 48 to 50 show the bathymetry for the Louisiana southeast, Louisiana south, and Mississippi/Alabama grids, respectively. These simulations were

forced with both the local winds and waves interpolated on the offshore boundary from the regional WAM model.

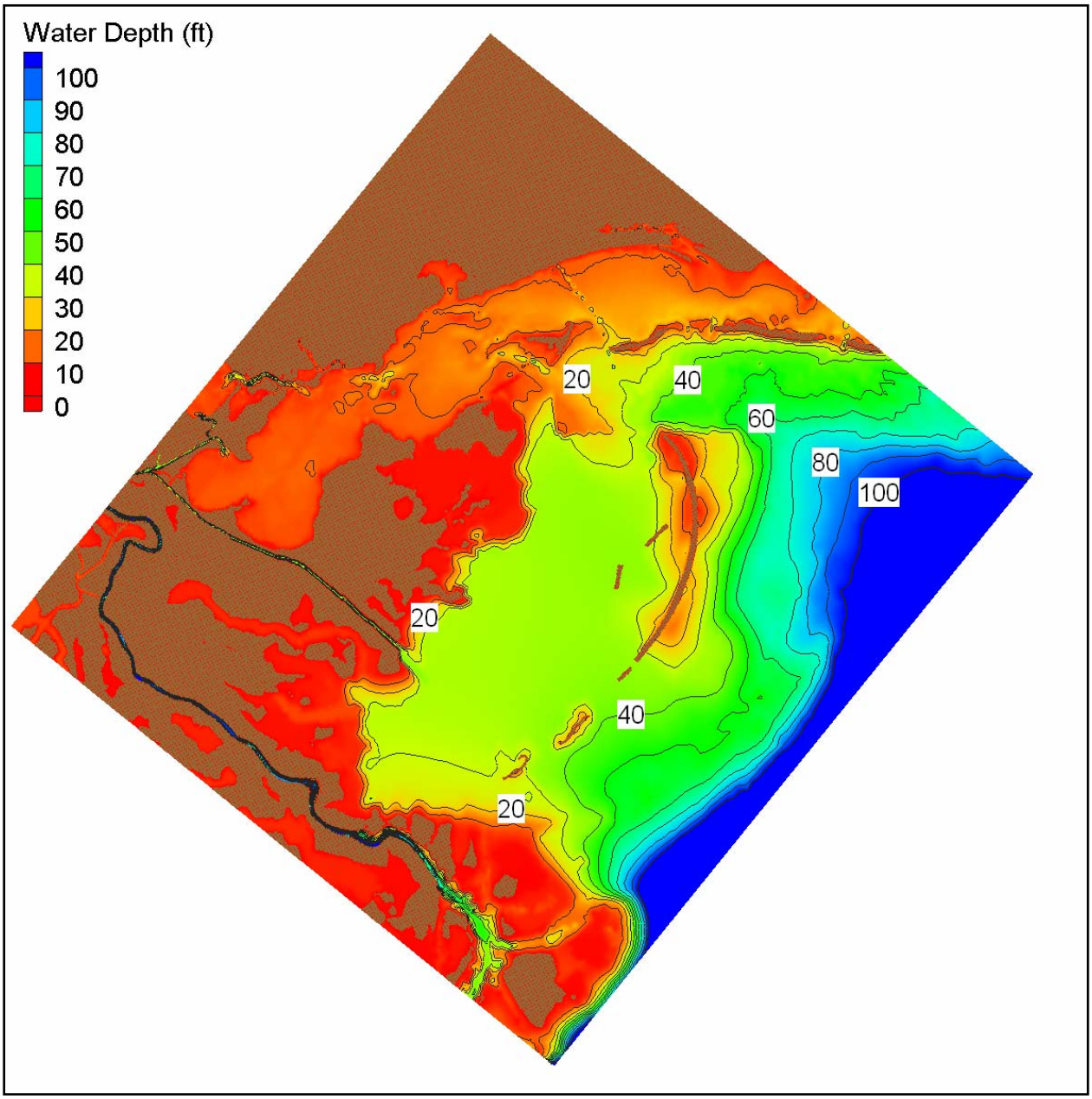

Figure 48. Louisiana southeast bathymetry grid (elevations in feet NAVD88).

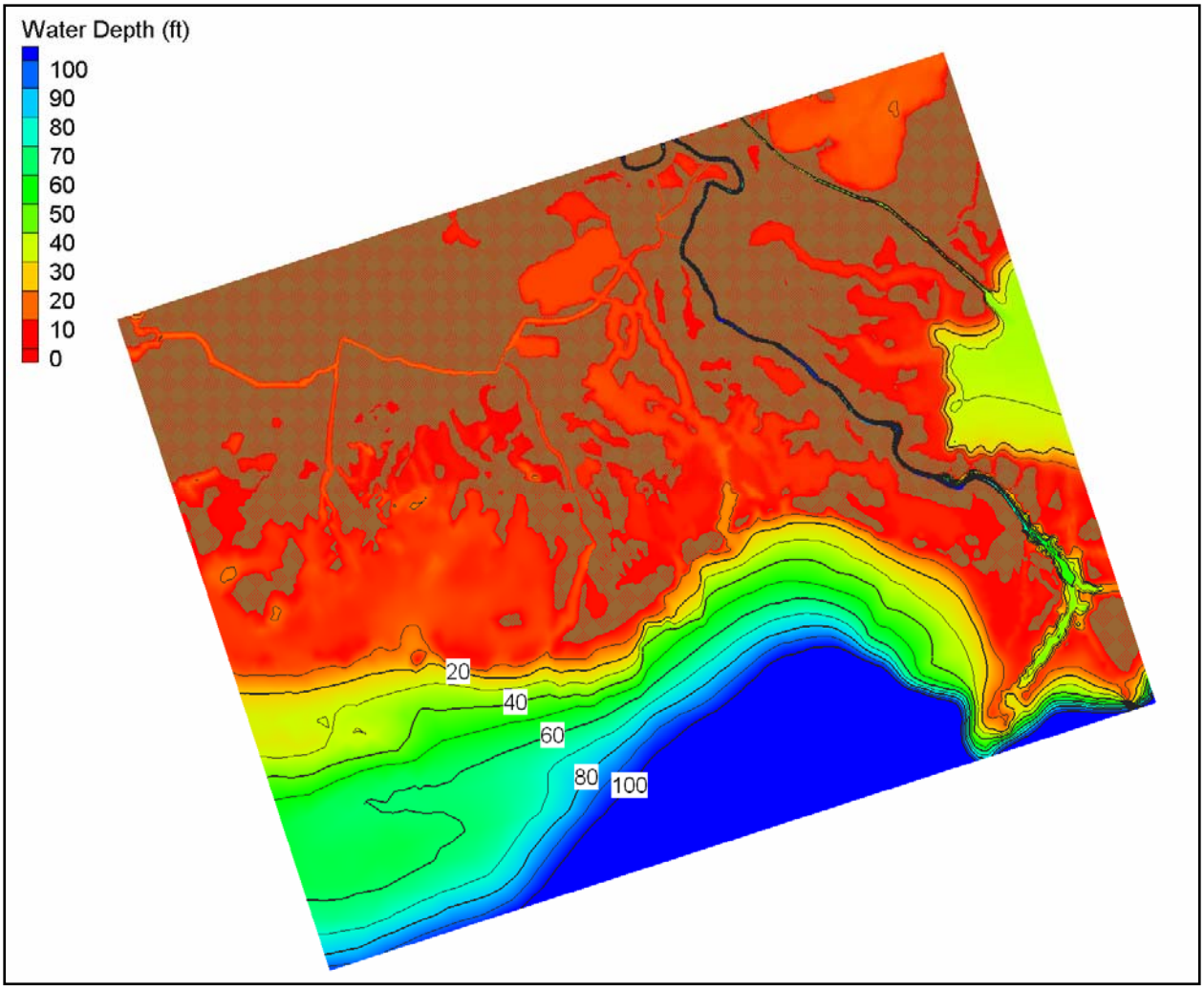

Figure 49. Louisiana south bathymetry grid (elevations in feet NAVD88).

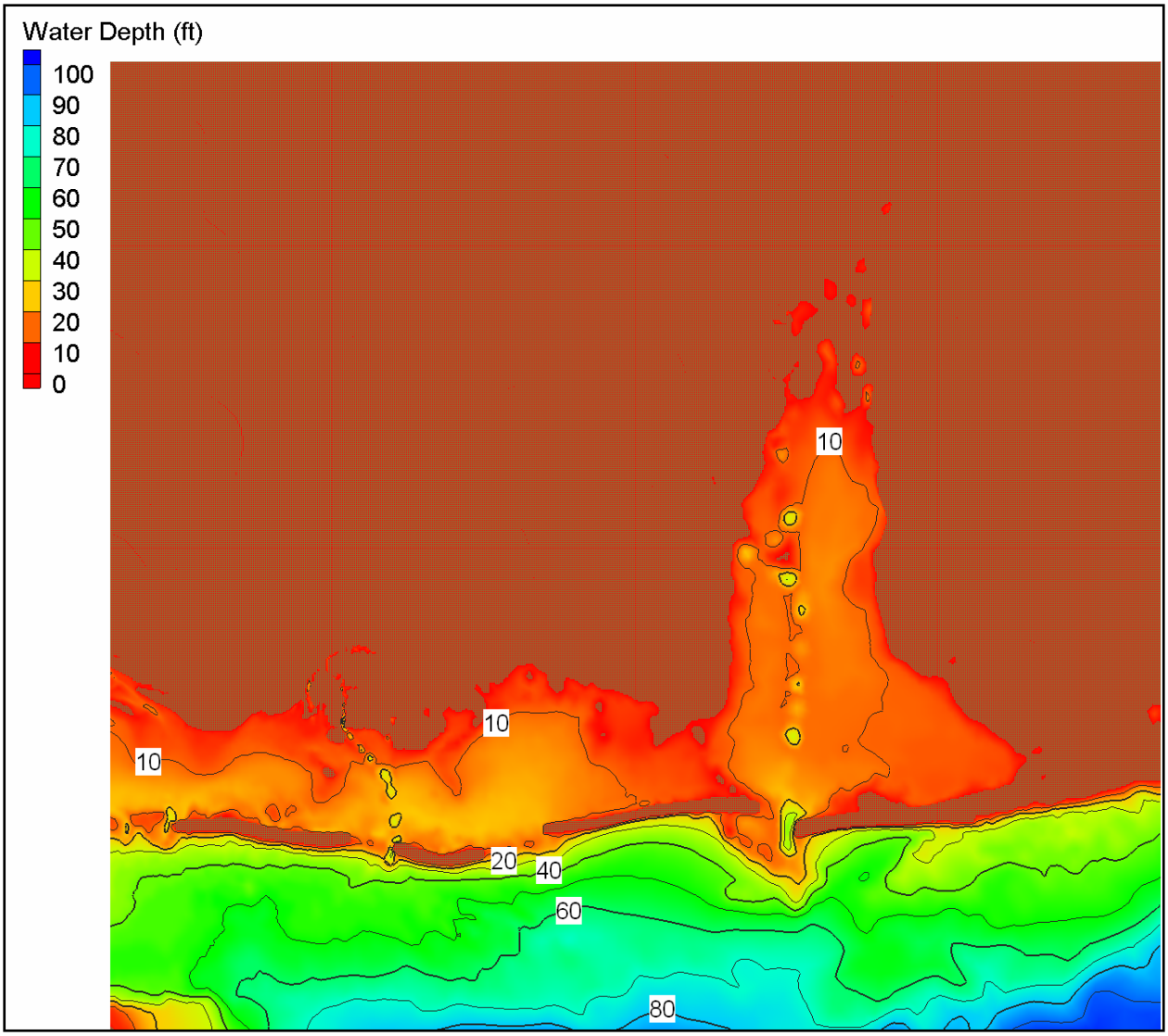

Figure 50. Mississippi/Alabama bathymetry grid (elevations in feet NAVD88).

STWAVE Results

Lake Pontchartrain. The peak wave conditions on the south shore of Lake Pontchartrain occur at approximately 1330-1430 UTC on 29 August 2005. Figure 51 shows a snapshot of wave height and wave direction at 1430 UTC. The wind speed is approximately 60 knots (30 m/sec) from the north to northwest. The maximum significant wave height is 8.7 ft with a peak wave period of 7 sec. Figure 52 shows the maximum significant wave height for the entire simulation period for each grid cell within the domain, along with the mean wave direction that corresponds to the maximum wave height. Figure 53 shows the peak wave period corresponding to the maximum wave height for each cell. The maximum wave heights range from 8.0 to 8.7 ft on the New Orleans lakefront and the associated peak periods are 6.5 to 7.5 sec.

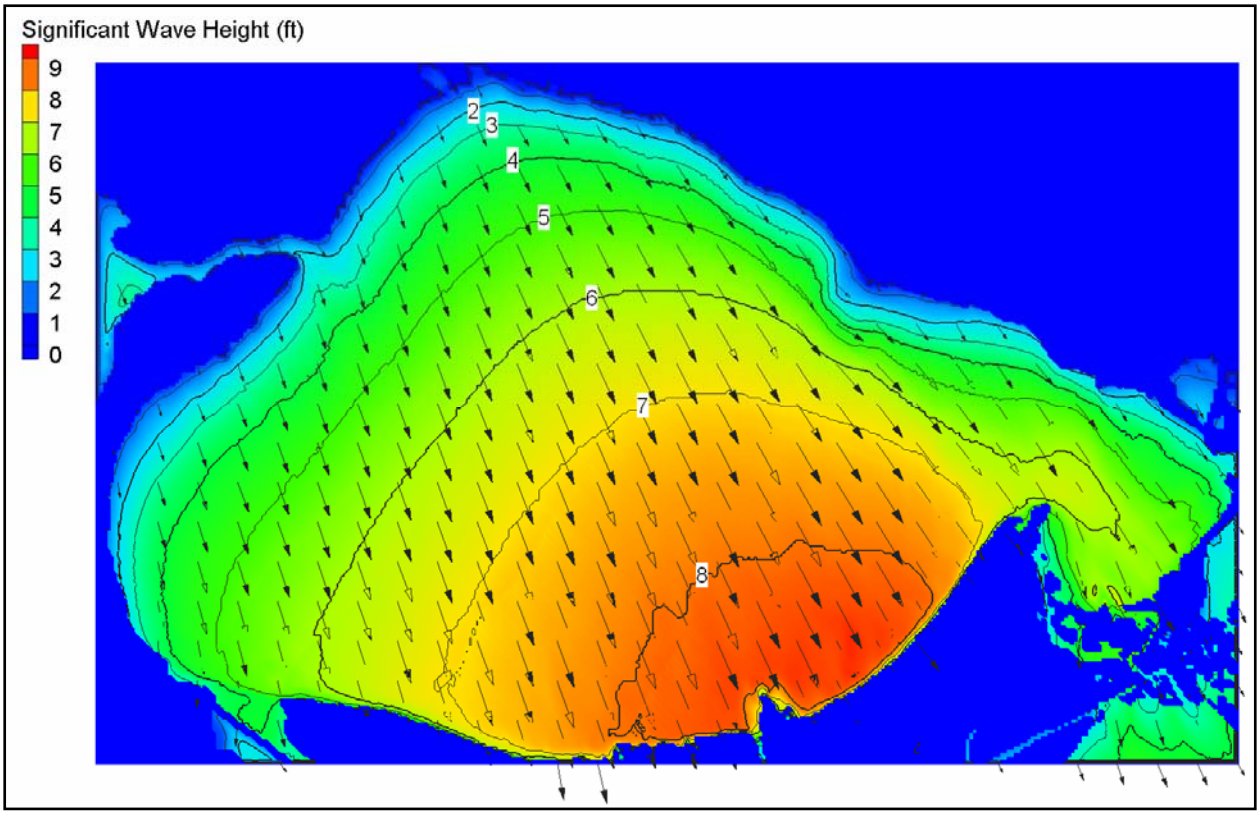

Figure 51. Lake Pontchartrain modeled significant wave height and mean wave direction for 1430 UTC on 29 August 2005 (wave heights in feet).

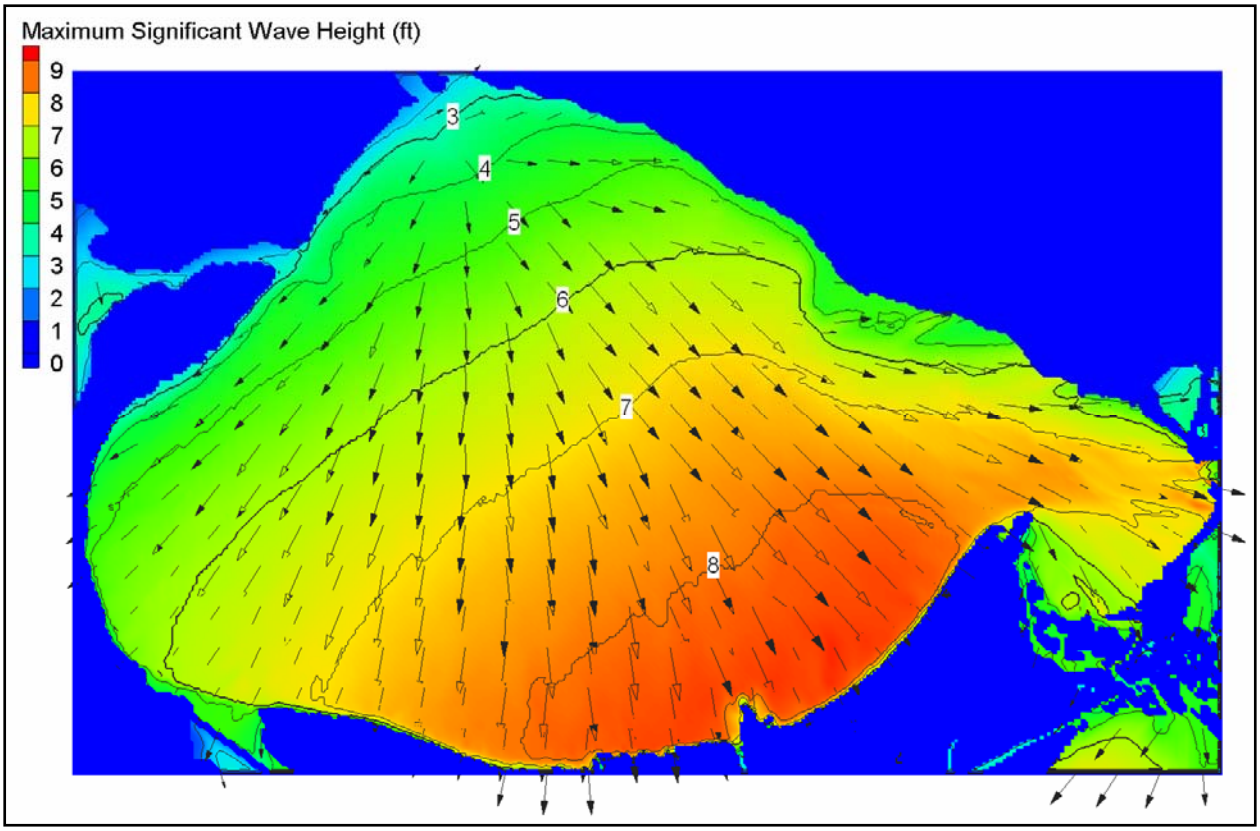

Figure 52. Lake Pontchartrain maximum modeled significant wave height and corresponding mean wave direction (wave heights in feet).

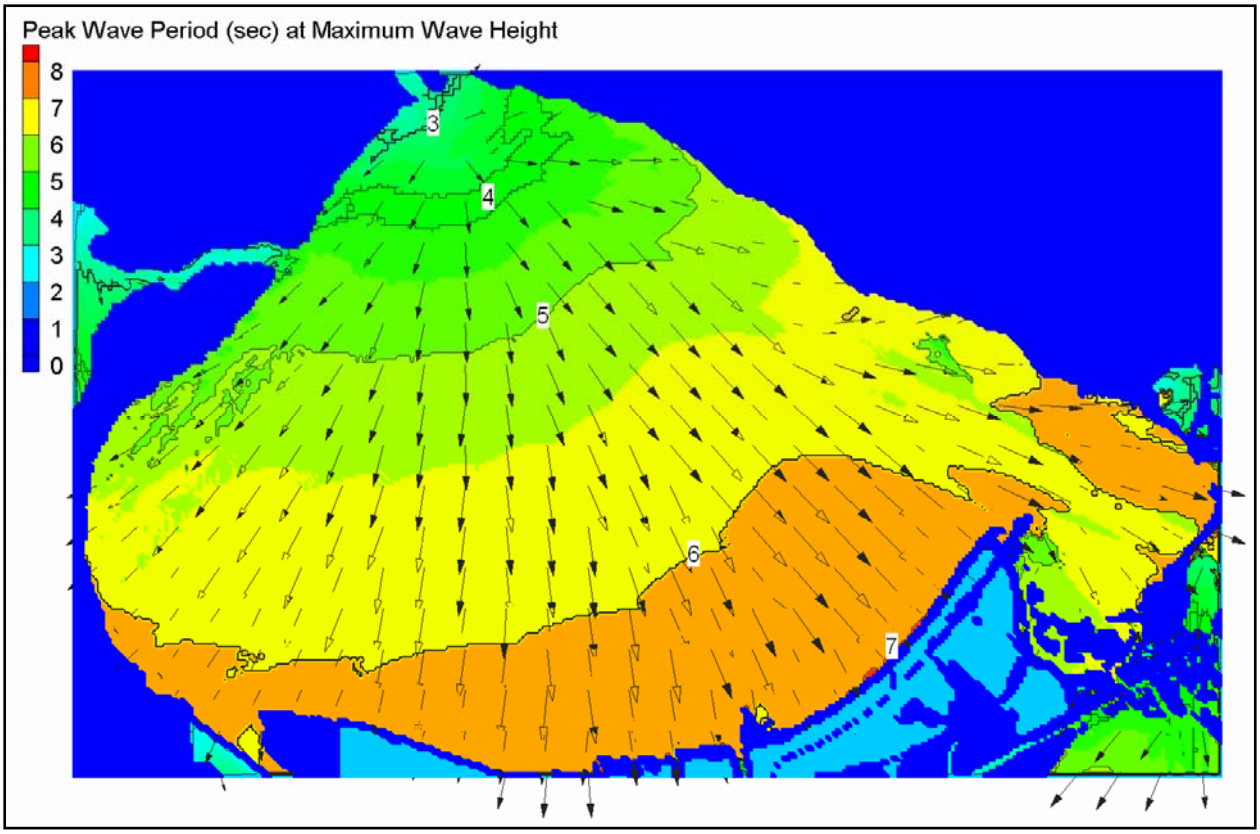

Figure 53. Lake Pontchartrain modeled peak wave period and mean wave direction corresponding to the maximum significant wave height (periods in seconds)

Figure 54 shows the variation of significant wave height, peak period, and mean wave direction at a site along the southern shoreline of Lake Pontchartrain, in the vicinity of the entrance to Orleans Avenue Canal. These results are quite similar to conditions computed at entrances to the other canals. In the early stages of the storm just before landfall, winds are out of the northeast and waves approach from the same direction (45 deg). As the storm approaches, winds increase in speed and both wave height and wave period steadily increase. As the storm makes landfall and its center moves northward, winds begin to shift blowing from the northeast then from the north (0 deg). Winds are blowing out of the north at the time peak wave conditions are generated along the south shoreline of the lake. Local wave generation within the lake tracks closely with the local wind speed and wind direction. Peak wave heights are about 8.4 ft and peak periods are 6.7 sec. As the storm passes and moves into Mississippi, winds continue to shift, finally blowing from the northwest. Wave heights and periods decrease rapidly following passage of the storm.

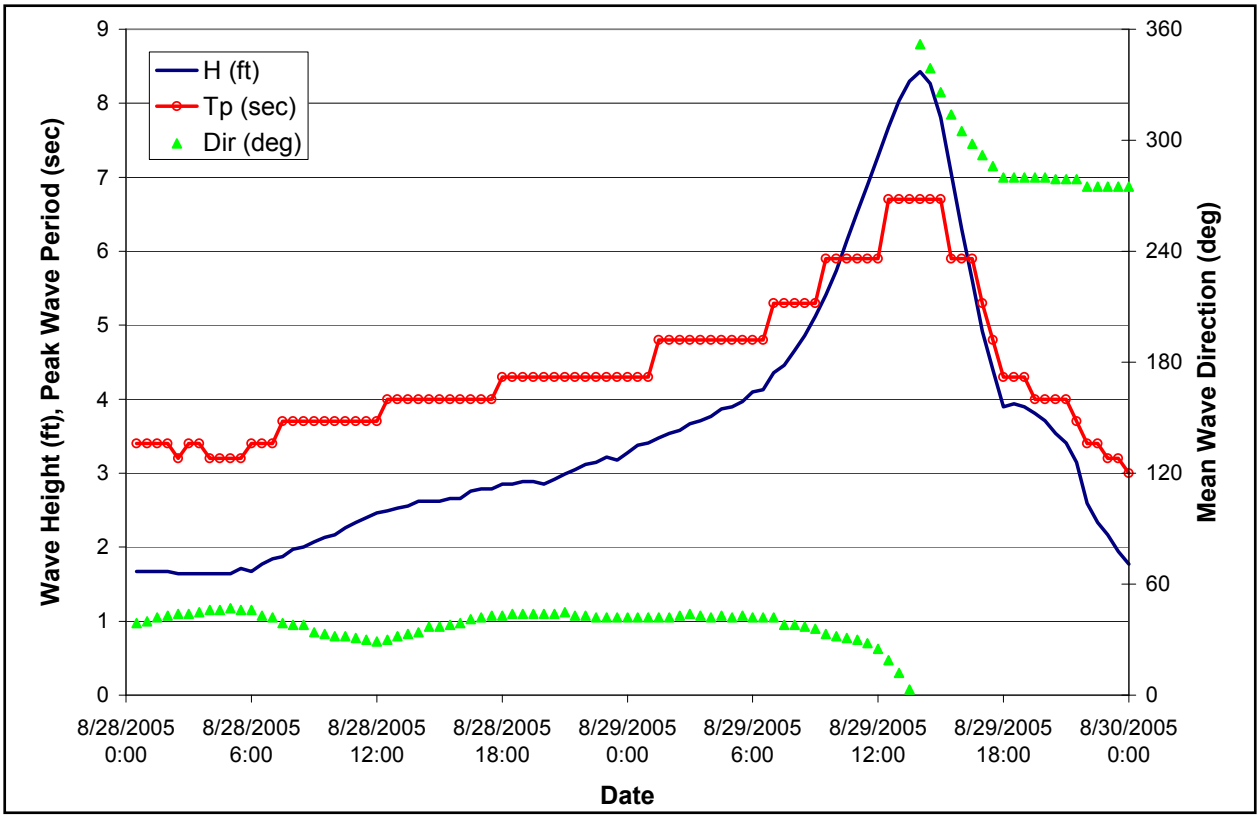

Figure 54. Temporal variation of significant wave height, peak period, and mean wave direction along the south shore of Lake Pontchartrain. [Time is referenced to UTC]

Comparison with Measurements. Three small wave buoys were deployed in Lake Pontchartrain on 27 August 2005 to capture wave conditions in Hurricane Katrina. Two of those gauges were recovered and provide valuable comparison data. The deployment locations were 30 deg 2.053 min North, 90 deg 7.358 min West for Gauge 22 and 30 deg 1.989 min North, 90 deg 7.932 min West for Gauge 23. Gauge 22 was directly north of the 17th Street Canal entrance and Gauge 23 was west of Gauge 22. Both gauges were in approximately 13 ft (4 m) water depth. The sampling records were a relatively short 8.5 min, so there is a lot of scatter in the data. Also, at the peak of the storm, the wave heights drop from approximately 8 ft to 5 ft, indicating that the buoys were not functioning properly at that time (they may have experienced excessive tilt due to the wind or been submerged or overturned). Figures 55 and 56 show comparisons of significant wave height and peak period, respectively, for the buoy locations. The blue lines are the measurements with the spectra averaged over three records (25.5 min), and the red line is the modeled parameters (30-min average). The STWAVE results are essentially the same for the two gauge sites. The modeled wave heights are an average of 1.04 ft (0.32 m) lower than the measurements in the growth stage of the storm (0000-1200 UTC 29 August 2005) and 0.26 ft (0.08 m) lower than the measurements in the decaying stage of the storm (1530-2400 UTC 29 August 2005). Comparisons at the storm peak are not meaningful. The modeled peak periods are consistent with the measurements, but 1.6 sec shorter in the decaying stage of the storm.

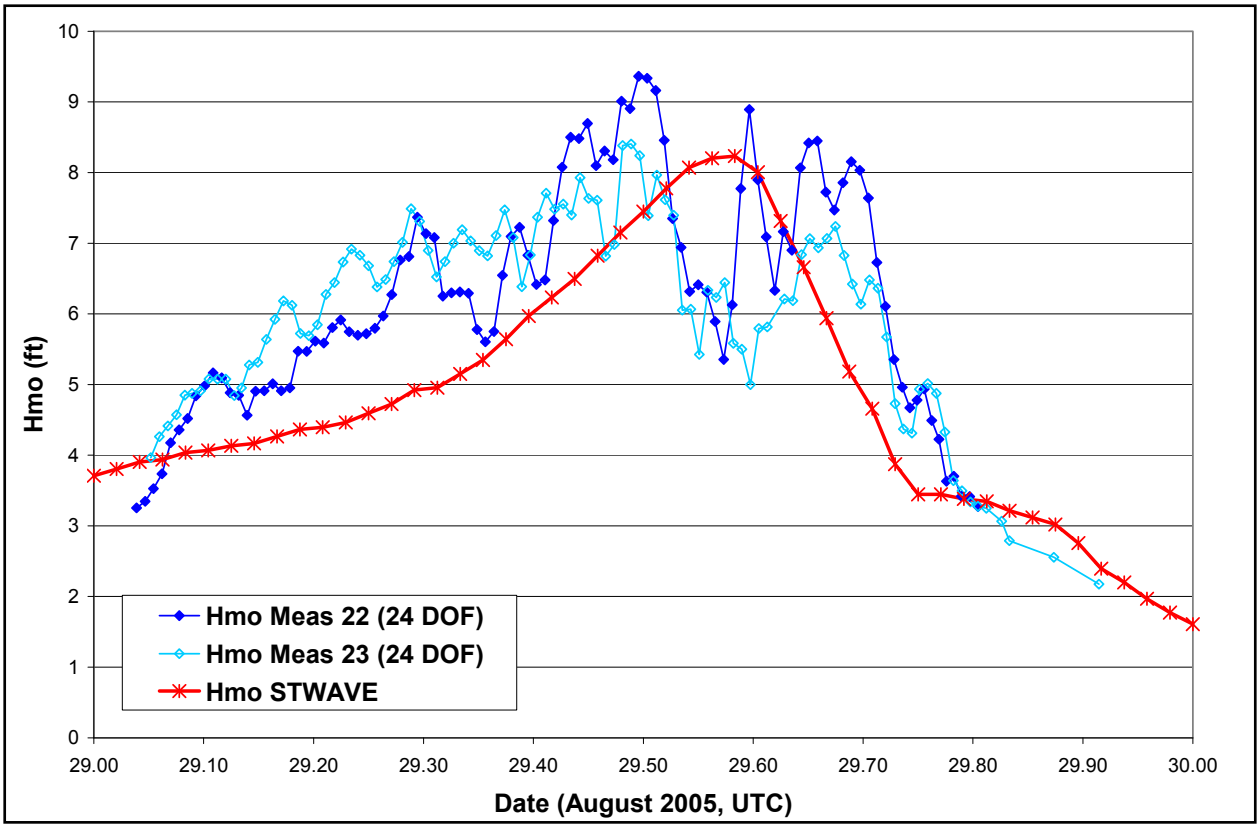

Figure 55. Lake Pontchartrain measured and modeled significant wave height.

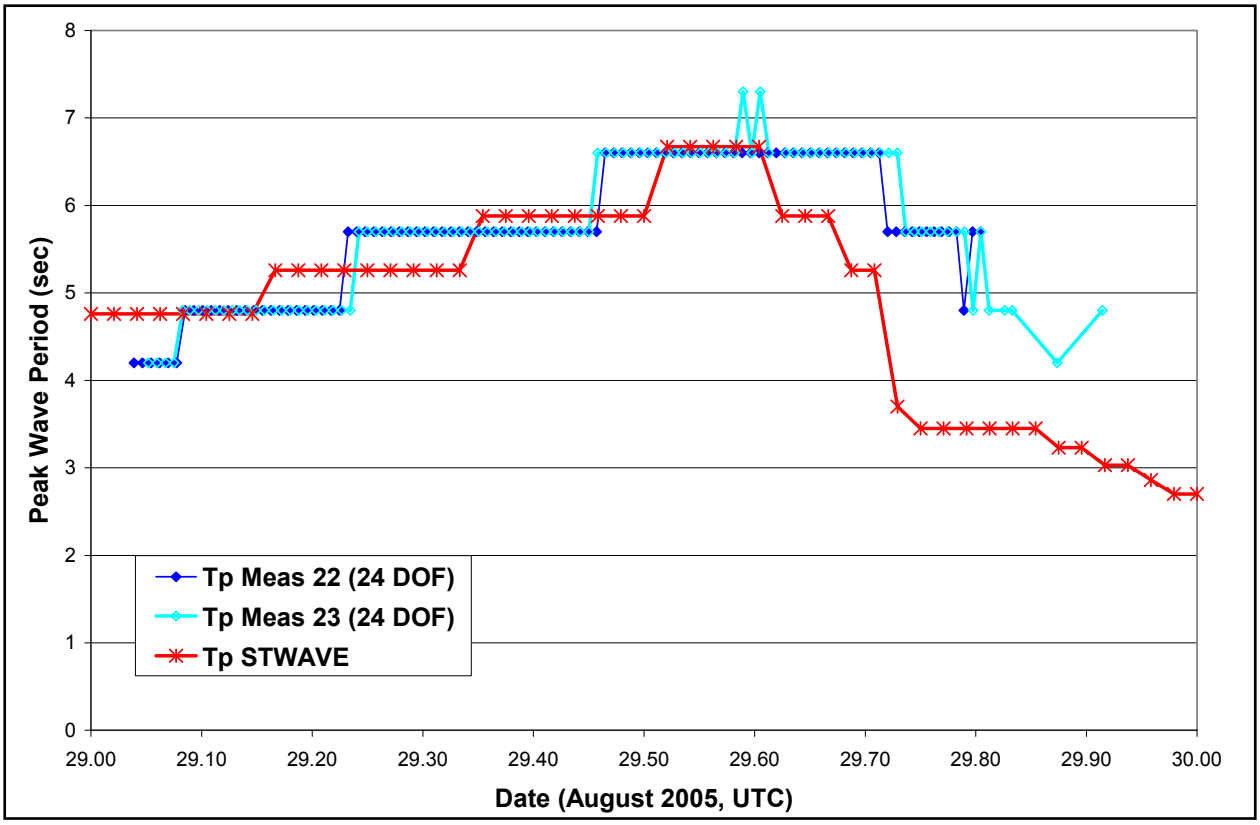

Figure 56. Lake Pontchartrain measured and modeled peak wave period.

Louisiana Southeast. The peak wave conditions on the southeast grid occur between approximately 1000 and 1500 UTC on 29 August 2005. The highest waves along the Mississippi River Levees occur around 1000-1200 UTC and along the Lake Borgne Levees around 1400-1500 UTC. Figure 57 shows a snapshot of wave heights and direction at 1200 UTC. Figures 58 and 59 show the maximum wave height and corresponding wave direction, and wave period for the entire simulation period for each grid cell within the domain. The maximum wave heights range from 4 to 10 ft along the hurricane protection system levees and the associated periods are 7 to 16 sec. The longer wave periods originate from wave energy traveling between and over the islands from the Gulf of Mexico. Figure 59 shows only the periods corresponding to the maximum wave height. Peak period along the levees can change appreciably as the offshore wave direction varies, allowing swell to propagate through the island gaps. Larger wave heights occur in lower Plaquemines Parish (6 to 10 ft) and smaller heights in upper Plaquemines and St. Bernard Parishes (4 to 6 ft). The peak periods are relatively large (up to 16 sec) because of wave penetration through and over the barrier islands.

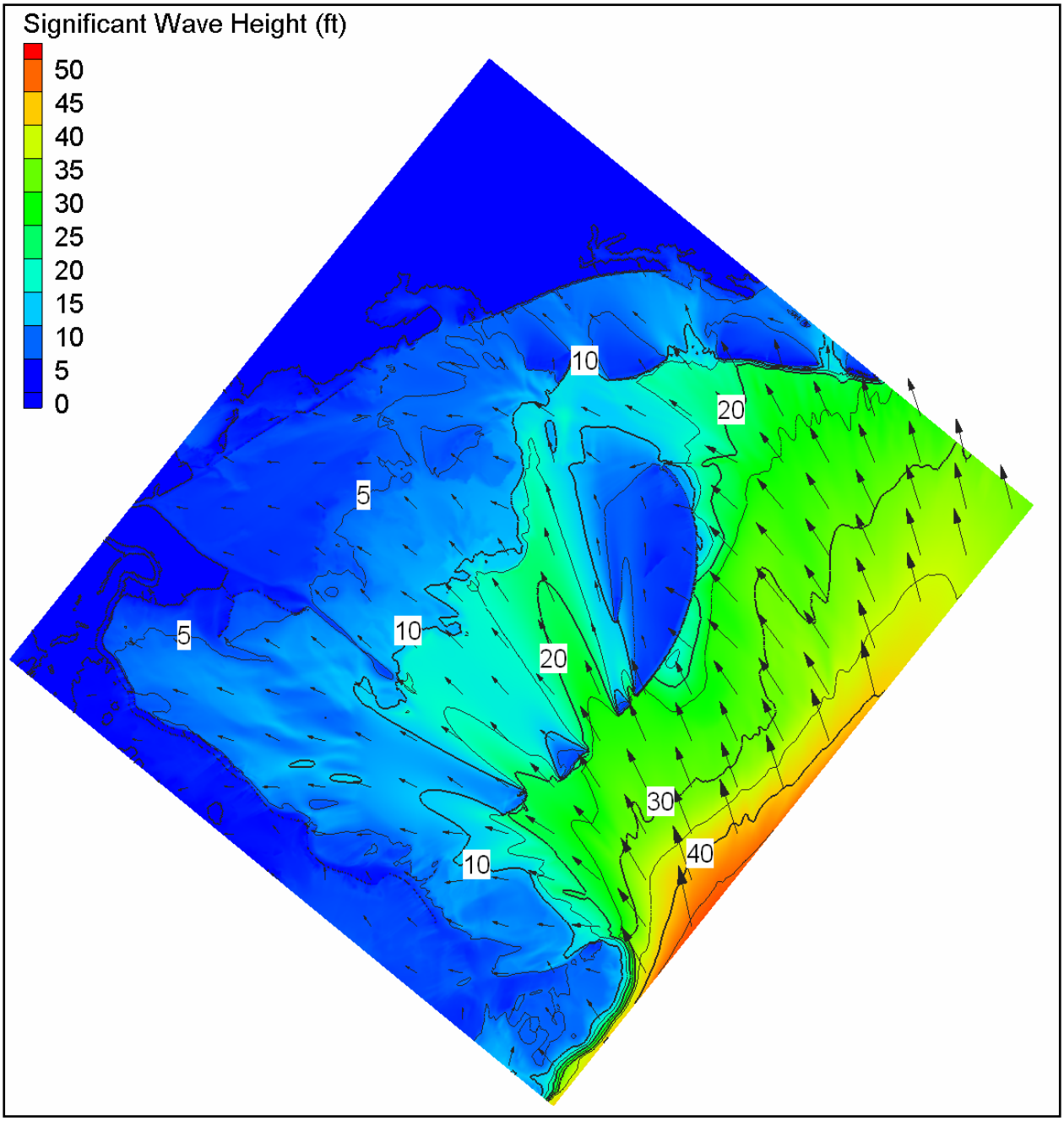

Figure 57. Southeast Louisiana modeled significant wave height and mean wave direction for 1200 UTC on 29 August 2005 (wave heights in feet).

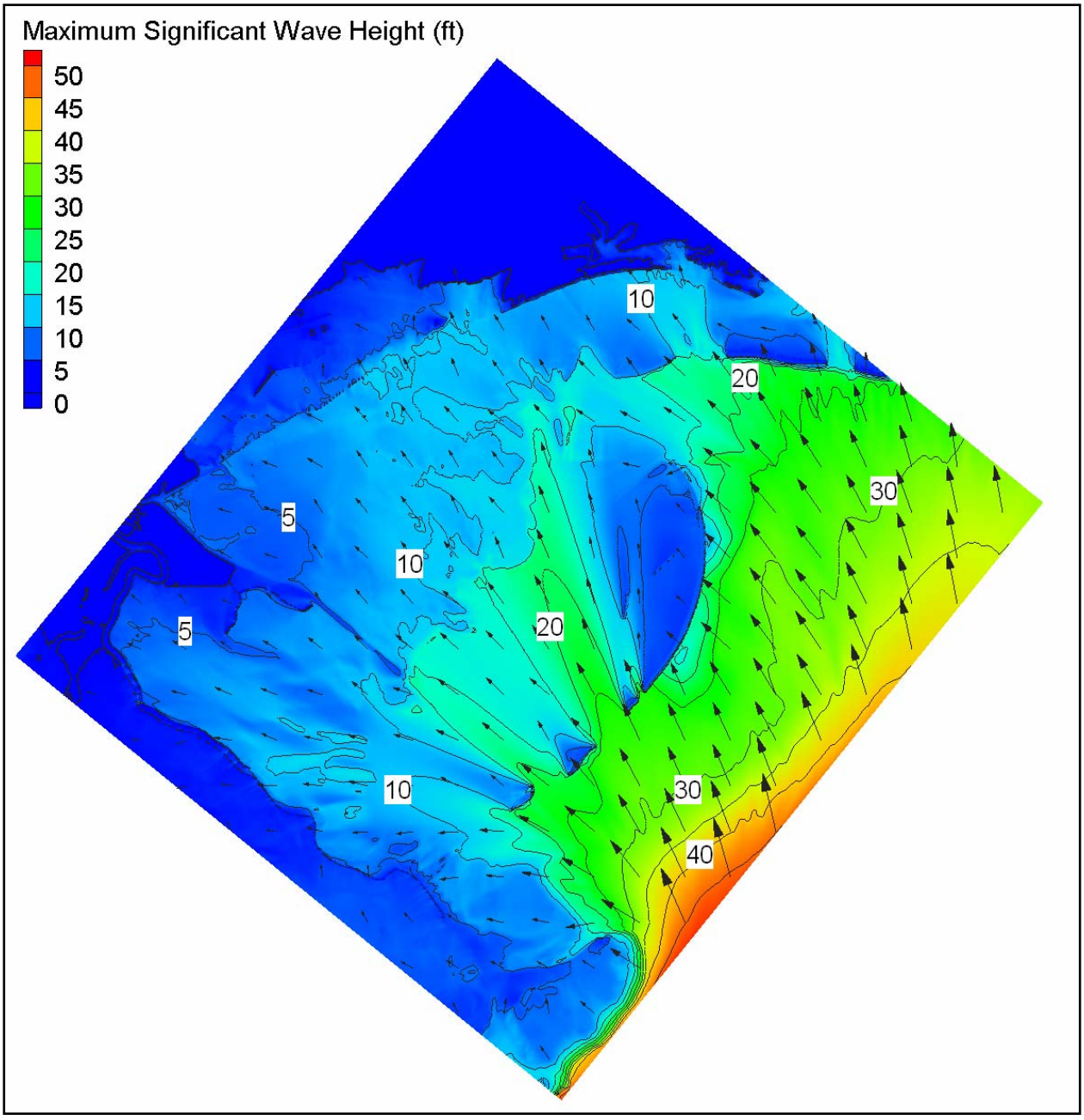

Figure 58. Southeast Louisiana maximum modeled significant wave height and corresponding mean wave direction (wave heights in feet).

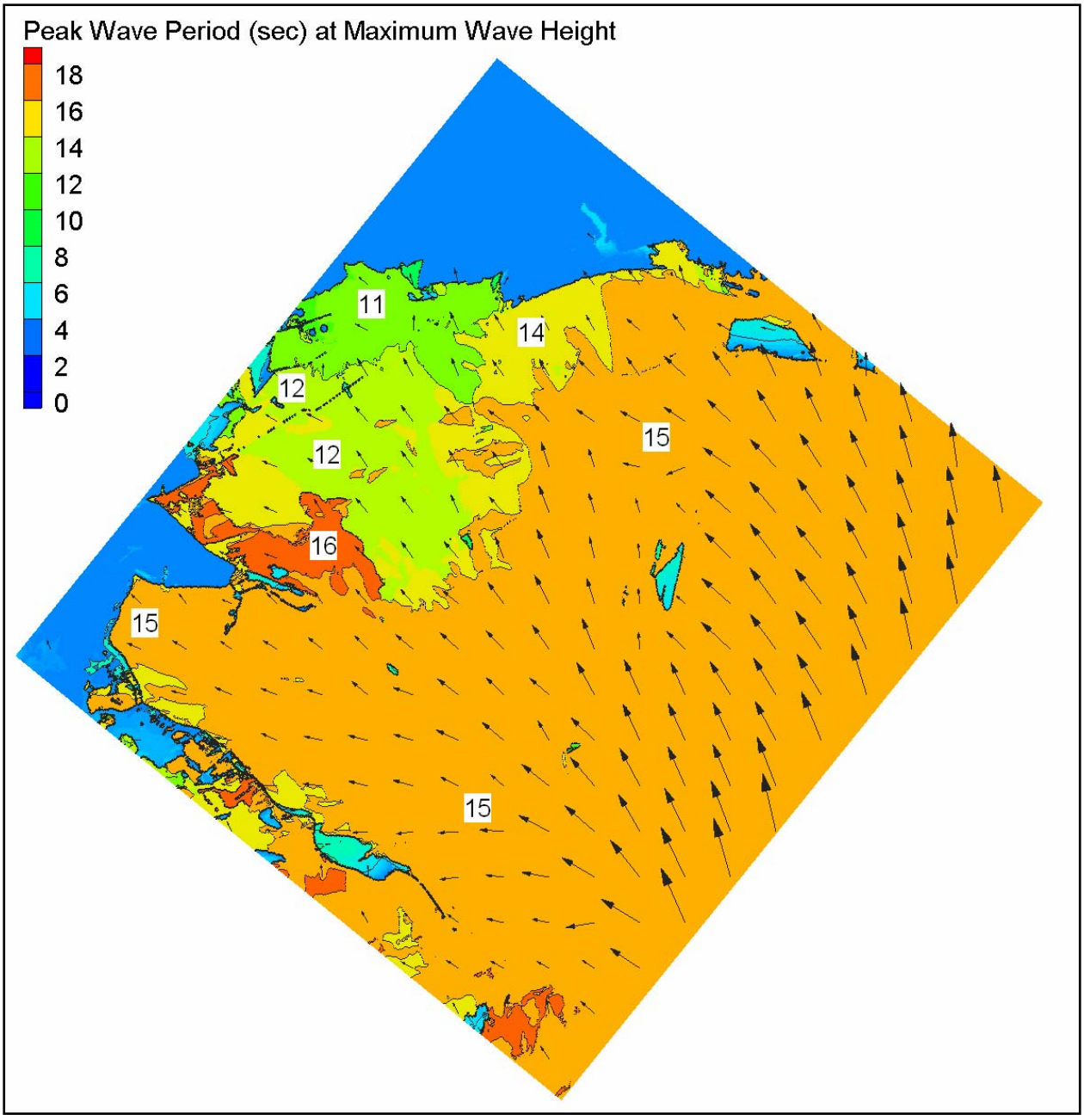

Figure 59. Southeast Louisiana modeled peak wave period and mean wave direction corresponding to the maximum significant wave height (periods in seconds).

Figure 60 shows the variation of significant wave height, peak period, and mean wave direction at a location near Bayou Bienvenue, along the hurricane protection levee adjacent to the MRGO. These results are similar to those at other locations along the same levee. In the early stages of the storm wave heights are quite low, on the order of 1 to 1.5 ft, and periods range between 4 and 6 sec. These periods are typical of locally generated wind sea conditions. Waves approach from the southeast (direction of 135 deg). As the hurricane makes landfall, wave energy begins to increase, as does the wave period as larger swells from the gulf arrive at the levee. The peak significant wave height reaches 5.7 ft, and the peak period reaches 16 sec. Wave

direction remains constant out of the southeast the entire time. As the storm passes wave heights decrease rapidly; peak wave periods also decrease somewhat, to 10 sec.

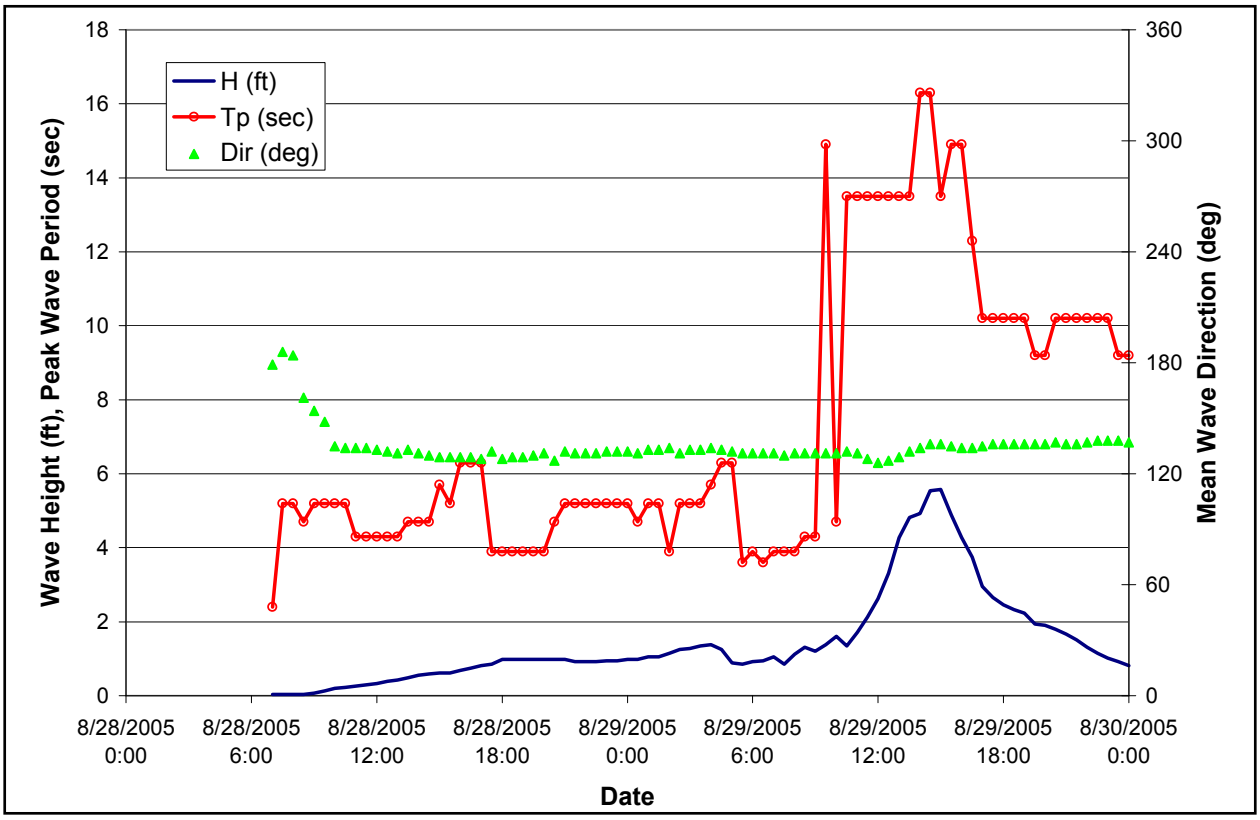

Figure 60. Temporal variation of significant wave height, peak period, and mean wave direction along the MRGO at Bayou Bienvenue. [Time is referenced to UTC].

Figure 61 shows the variation of significant wave height, peak period, and mean wave direction at a location in south Plaquemines Parish, adjacent to the east-facing levee at Tropical Bend. Prior to the storm's arrival, wave heights are low, ranging between 0.5 and 1 ft, and the temporal variation in wave height reflects the influence of the changing tide level. Periods increase rapidly from 4 to 15 sec with the arrival of long period swells from the east well before the storm makes landfall. Locally generated waves and longer period swells approach from the east and northeast. Refraction and sheltering cause the waves from the gulf to approach from the east. Fluctuations in peak wave period and direction indicate sea state components at a range of frequencies and directions. With the arrival of the core of the storm, wave heights increase rapidly, peaking at 9.7 ft. Wave periods remain steady at 15 sec. As the storm passes, wave heights and wave periods decrease rapidly, at about the same rates as they grew with the approach of the storm.

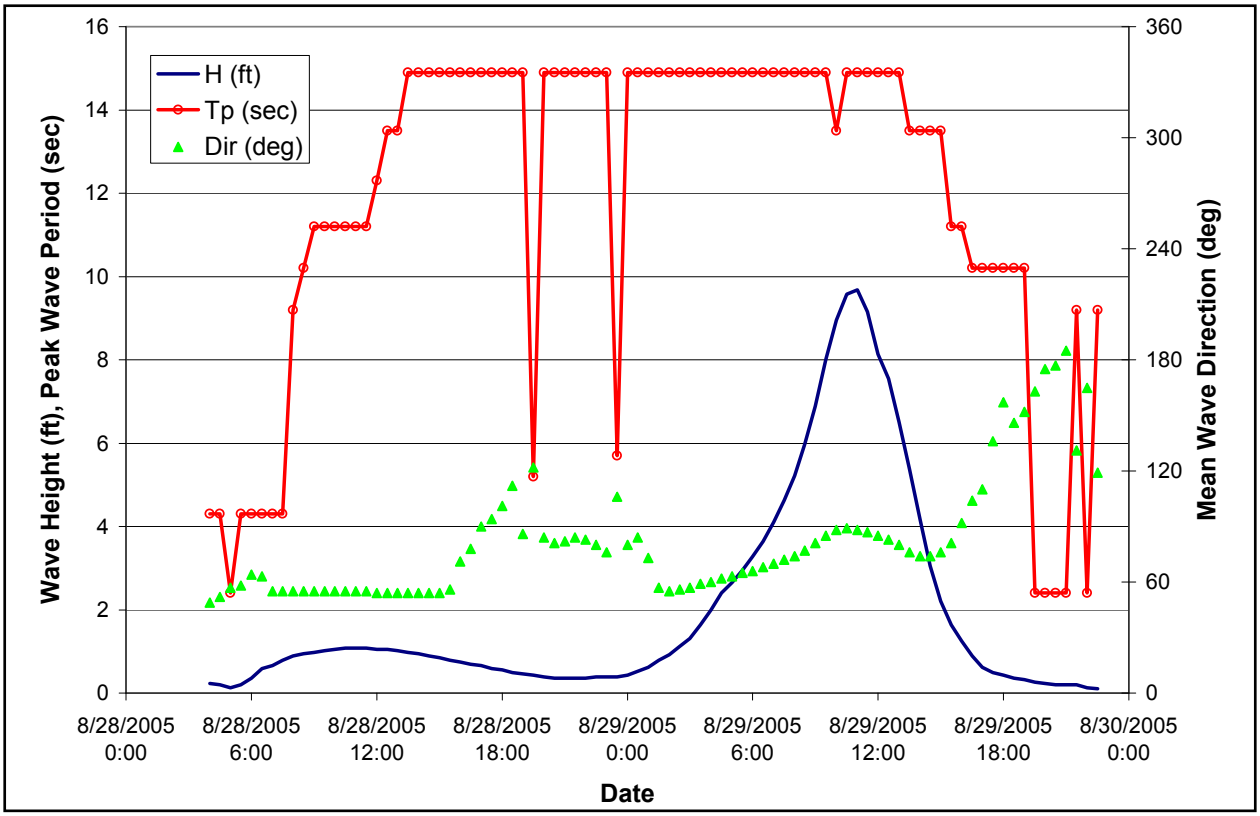

Figure 61. Temporal variation of significant wave height, peak period, and mean wave direction along the east-facing levee near Tropical Bend in south Plaquemines Parish. [Time is referenced to UTC].

Louisiana South. The peak wave conditions on the south grid occur between 0800 and 1030 UTC on 29 August 2005. Surge elevation on this grid is generally less than the southeast Louisiana grid, so the wave penetration over the marsh is less severe. Figure 62 shows a snapshot of wave height and direction at 0800 UTC. Figures 63 and 64 show the maximum wave height, wave direction, and corresponding wave period for the entire simulation period for each grid cell within the domain. The maximum wave heights at the barrier islands are approximately 10 to 14 ft (depth limited) and associated periods are 15 to 16 sec. Wave heights were significantly lower along the Mississippi River and hurricane protection levees. The barrier islands dissipated much of the wave energy arriving from the Gulf of Mexico and they help protect the interior shorelines. The waves "wrap" around the Mississippi River delta and approach from the southwest with peak periods of 10 sec. Wave heights along the west-facing levees are greatest at the southern reaches of the levee system, and they decrease to the north. These simulations were made with pre-Katrina bathymetry, so as barriers eroded, this protection may be overstated. The local winds were not important on this grid because the winds generally blow along the shore or offshore in the area.

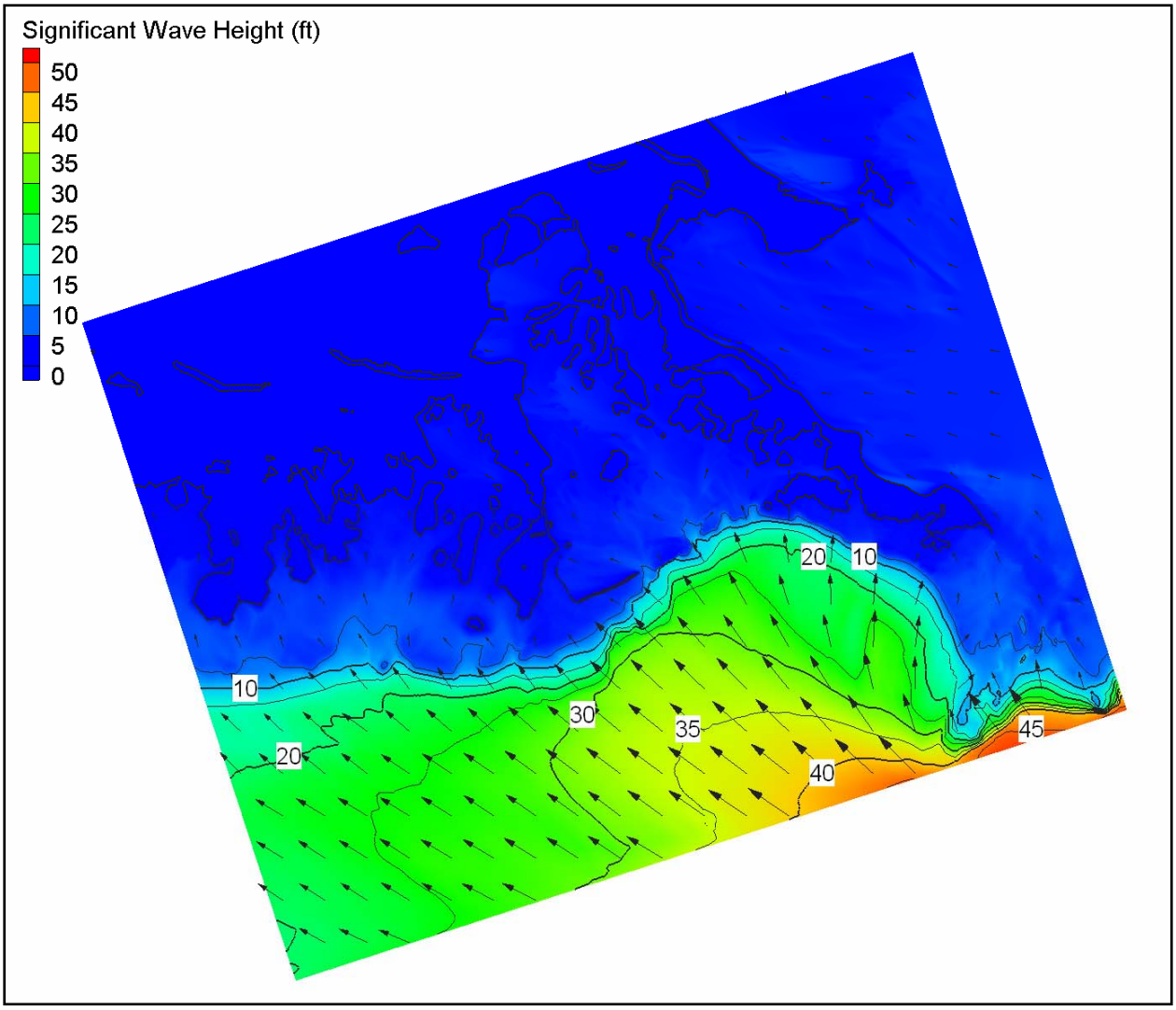

Figure 62. South Louisiana modeled significant wave height and mean wave direction for 0800 UTC on 29 August 2005 (wave heights in feet).

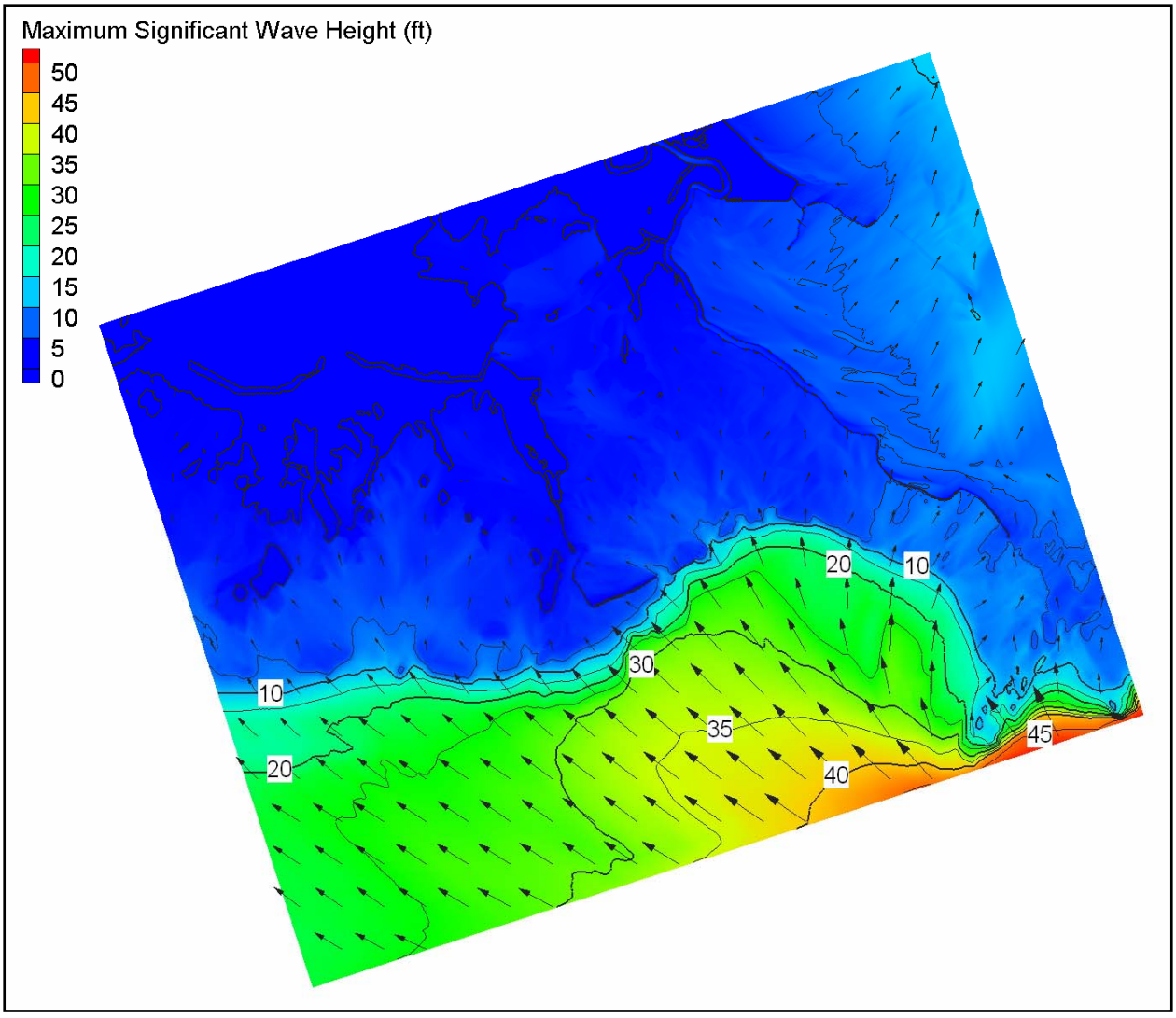

Figure 63. South Louisiana maximum modeled significant wave height and corresponding mean wave direction (wave heights in feet).

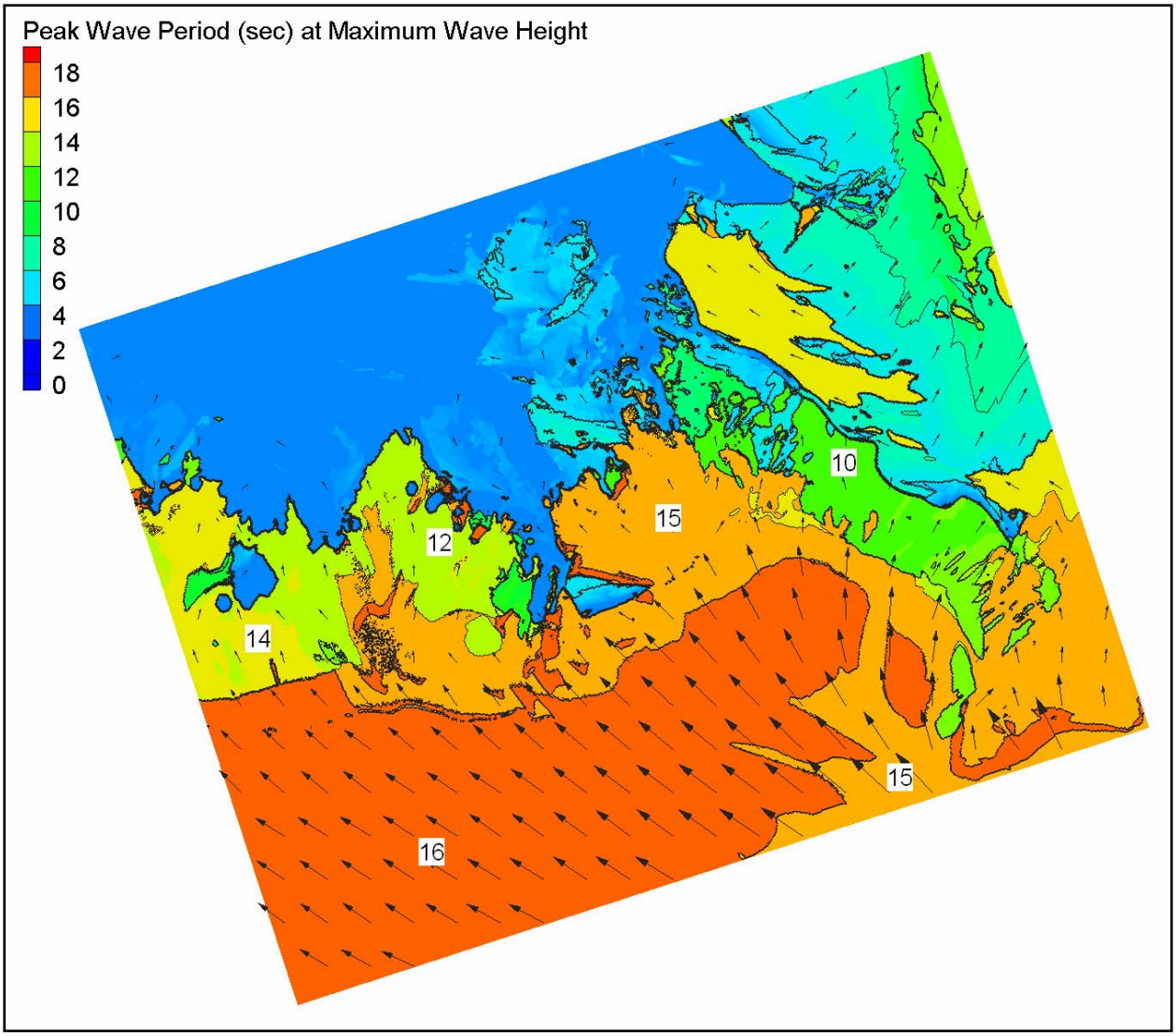

Figure 64. South Louisiana modeled peak wave period and mean wave direction corresponding to the maximum significant wave height (periods in seconds).

Mississippi/Alabama. The peak wave conditions occur around 1430 UTC on 29 August 2005, near the time of the hurricane landfall in Mississippi. Figure 65 shows a snapshot of wave height and direction at 1430 UTC. Figures 66 and 67 show the maximum wave height and corresponding wave period for the entire simulation period for each grid cell within the domain. The maximum wave heights at the barrier islands are approximately 20 ft (depth limited) and associated periods are 15 sec. The barrier islands dissipated much of the wave energy arriving from the Gulf of Mexico and help protect the interior shorelines. These simulations were made with pre-Katrina bathymetry, so as barriers eroded, this protection may be overstated. Wave heights in Mississippi Sound and Mobile Bay generally range from 5 to 10 ft, but are 10 to 20 ft in the lee of the inlets on the Mississippi coast. Large wave periods (15 sec) penetrate to the interior shorelines. The wave dissipation on the Mississippi and Alabama barrier islands and nearshore regions generates wave setup within Mississippi Sound, which forces additional water into Lake Pontchartrain.

More details regarding the nearshore wave modeling work, including presentation of additional time series results and wave spectra at various locations around the periphery of the hurricane protection system, are presented in Appendix 4.

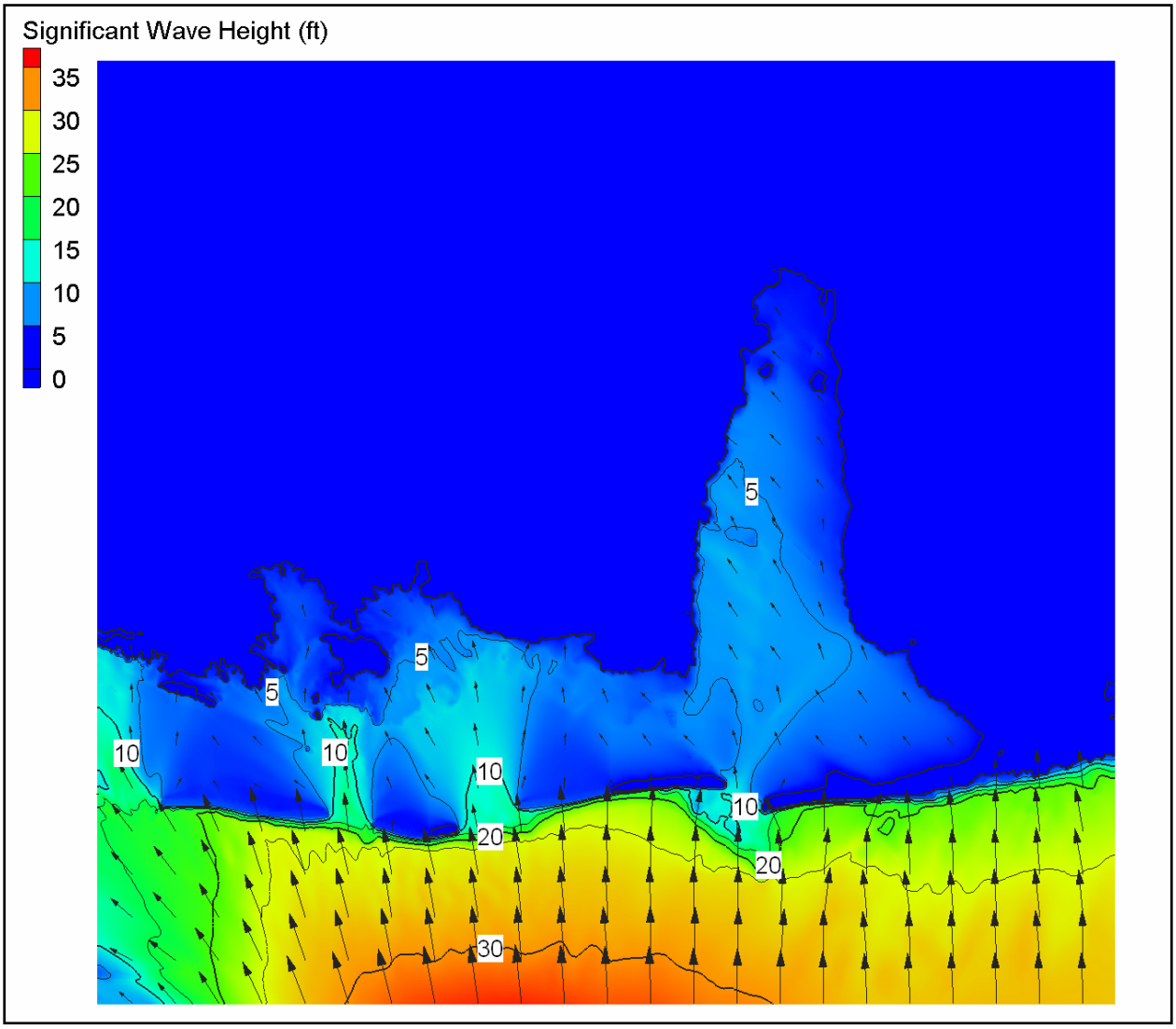

Figure 65. Mississippi/Alabama modeled significant wave height and mean wave direction for 1430 UTC on 29 August 2005 (wave heights in feet).

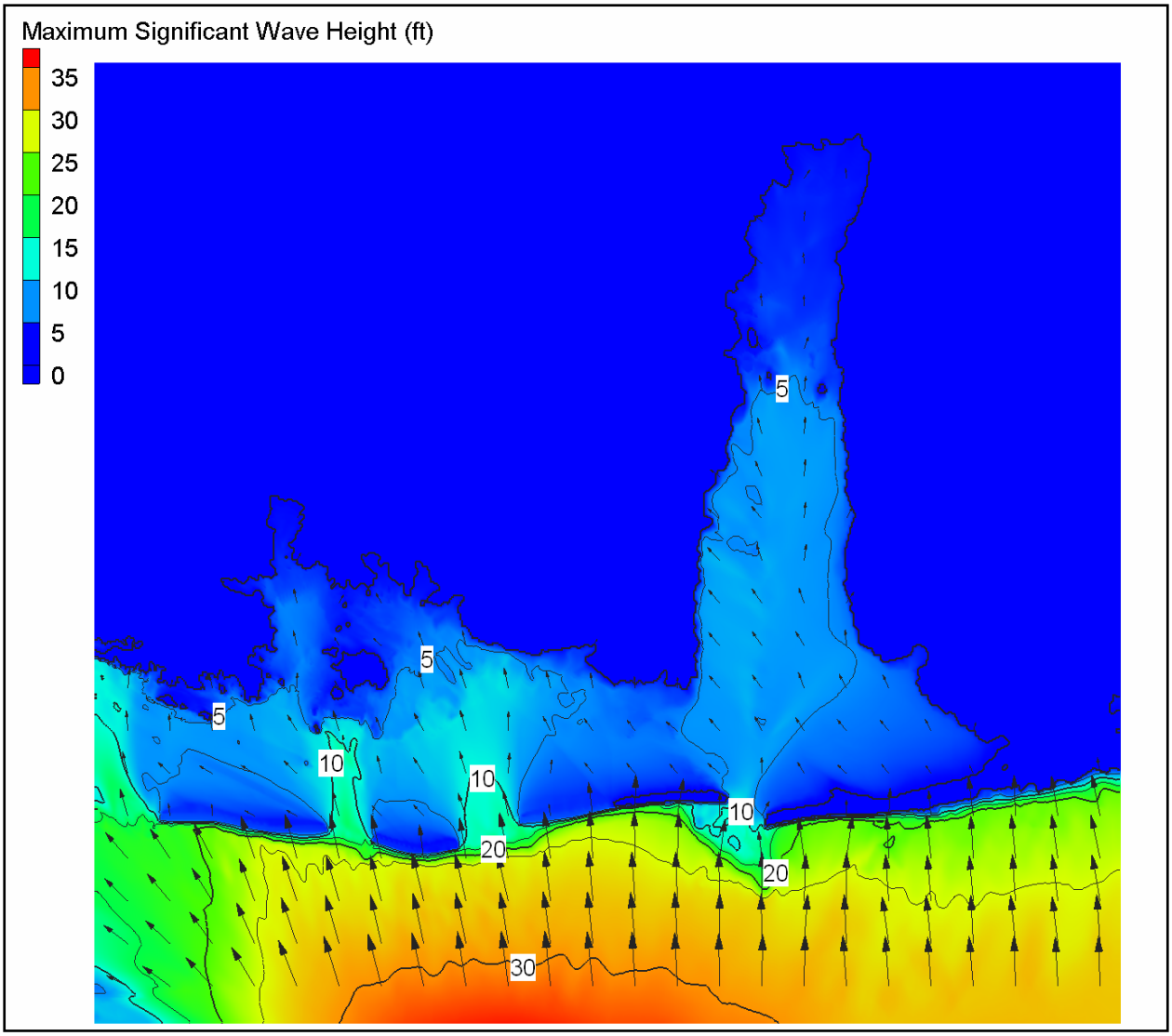

Figure 66. Mississippi/Alabama maximum modeled significant wave height and corresponding mean wave direction (wave heights in feet).

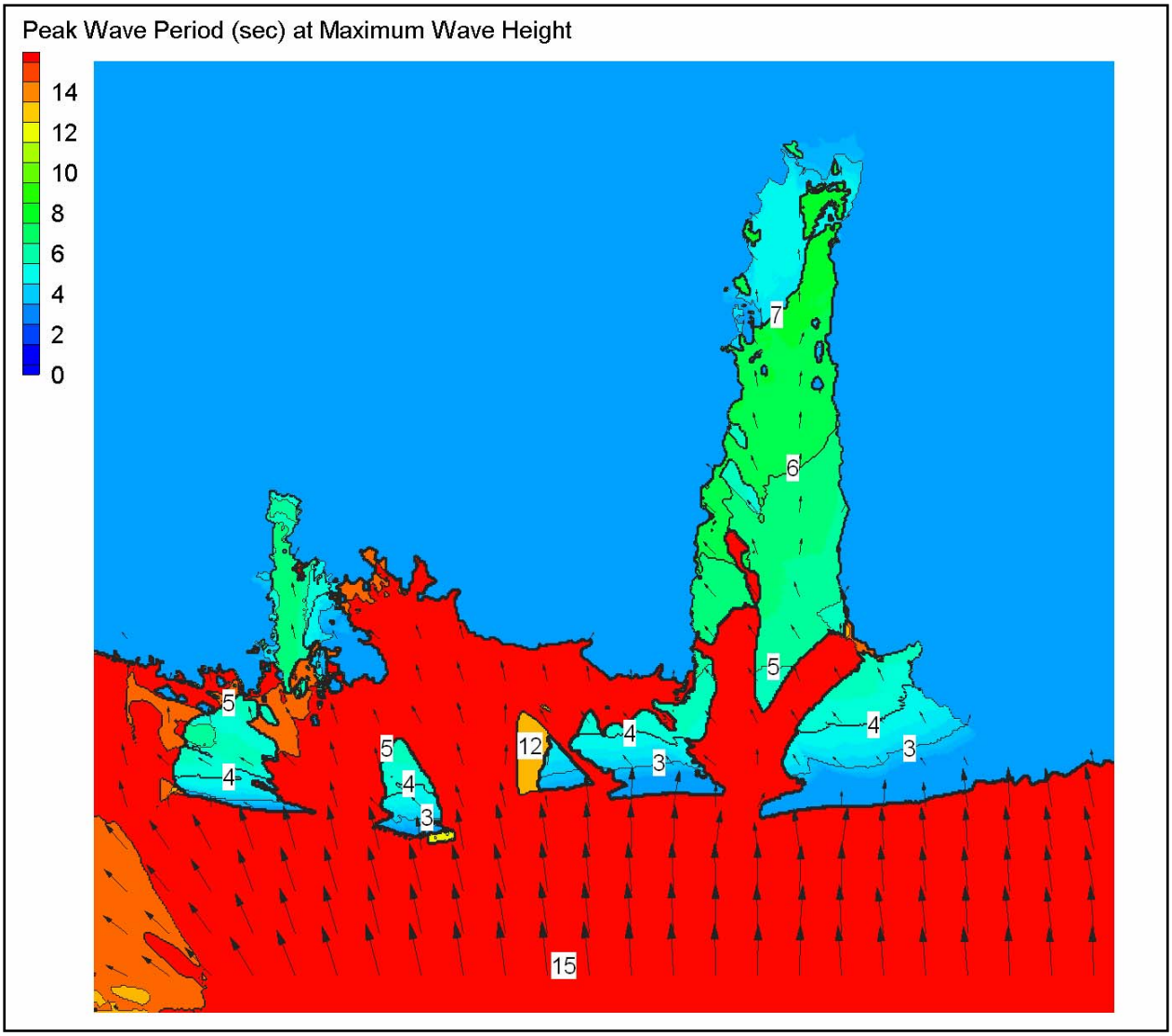

Figure 67. Mississippi/Alabama modeled peak wave period and corresponding mean wave direction (periods in seconds)

STWAVE – SWAN Comparisons

STWAVE is a steady-state wave model, which means that the waves reach equilibrium with the local forcing conditions (wind, surge, and boundary waves). Thus, the STWAVE modeling assumes that the winds and surge vary slowly enough for the waves to reach quasi steady state. For Hurricane Katrina, the winds are time varying and the grid domains are relatively large, so the time-dependent SWAN model (Booij, Ris, and Holthuijsen 1999; Booij et al. 2004) was used to evaluate the importance of time variation. Lake Pontchartrain was chosen for this test because the waves are all locally generated and time dependence is expected to have the greatest impact there. To test the time dependence, SWAN was run in time-dependent and steady-state modes from 0000 UTC 29 August 2005 to 0000 UTC 30 August 2005. The simulation was made using 1-min time steps for the time-dependent run and forcing the steady-state run to an accuracy of 99 percent with a maximum of 15 iterations (this is more stringent than the default). All other

SWAN model defaults were used. SWAN was run with the same spatially varying surge and wind as STWAVE.

Figures 68 and 69 show the SWAN and STWAVE results with the data measured in Lake Pontchartrain. The time-dependent and steady-state SWAN give essentially the same results through the peak of the storm, after a 3-hr model ramp-up from initial conditions. Thus, the steady-state solution is adequate for the simulations. STWAVE wave heights are 4 percent higher than SWAN at the peak of the storm and lower height on the building (11 percent) and waning (24 percent) legs of the storm. SWAN results are closer to the measurements on the building portion of the storm and STWAVE results are closer on the waning portion of the storm. The measurements are not reliable at the peak of the storm, when the wave heights are most critical. STWAVE peak periods are 8 percent longer than the SWAN peak periods through the peak of the storm and 23 percent shorter than SWAN periods after the storm peak. STWAVE shows better agreement with the wave period measurements through the storm peak, but both models are generally within 1 sec of each other.

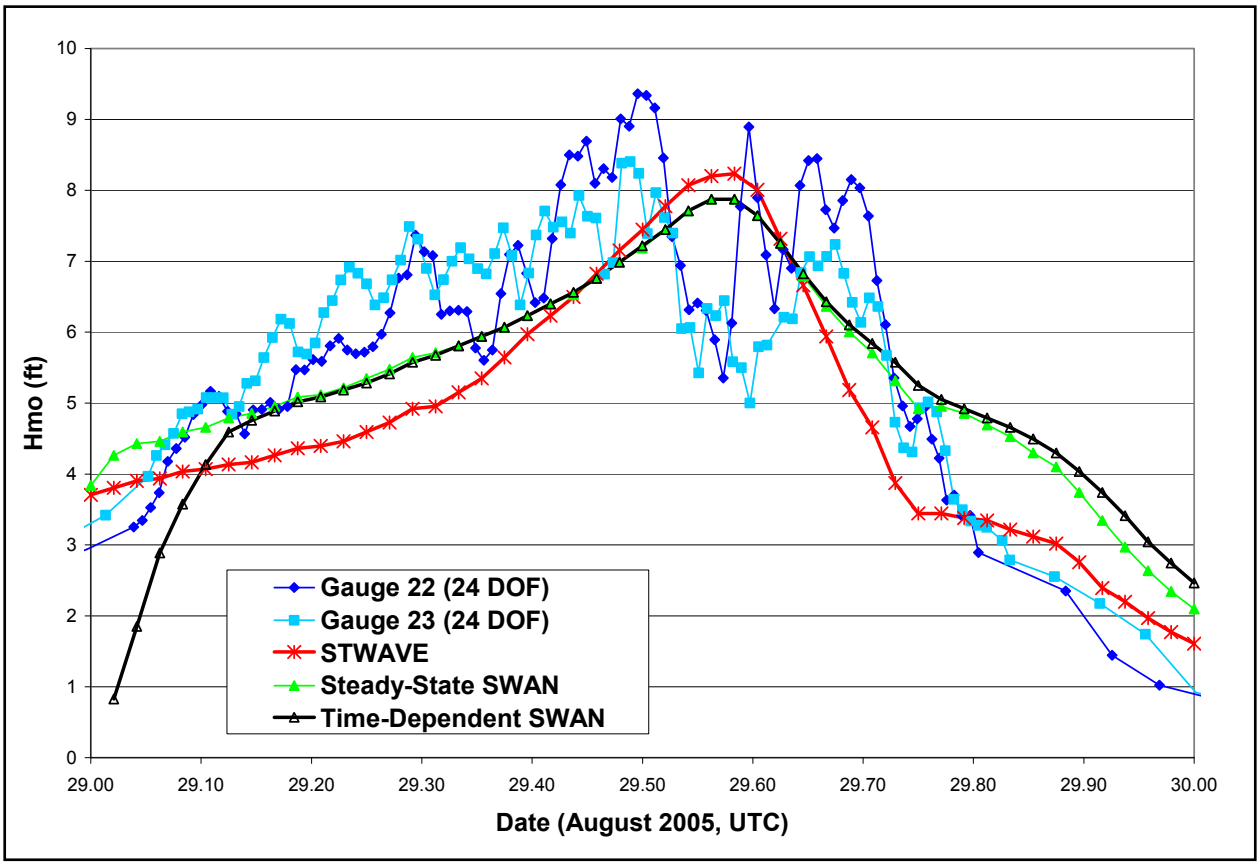

Figure 68. Time-dependent and steady-state SWAN and STWAVE modeled significant wave heights for Lake Pontchartrain and measured significant wave height.

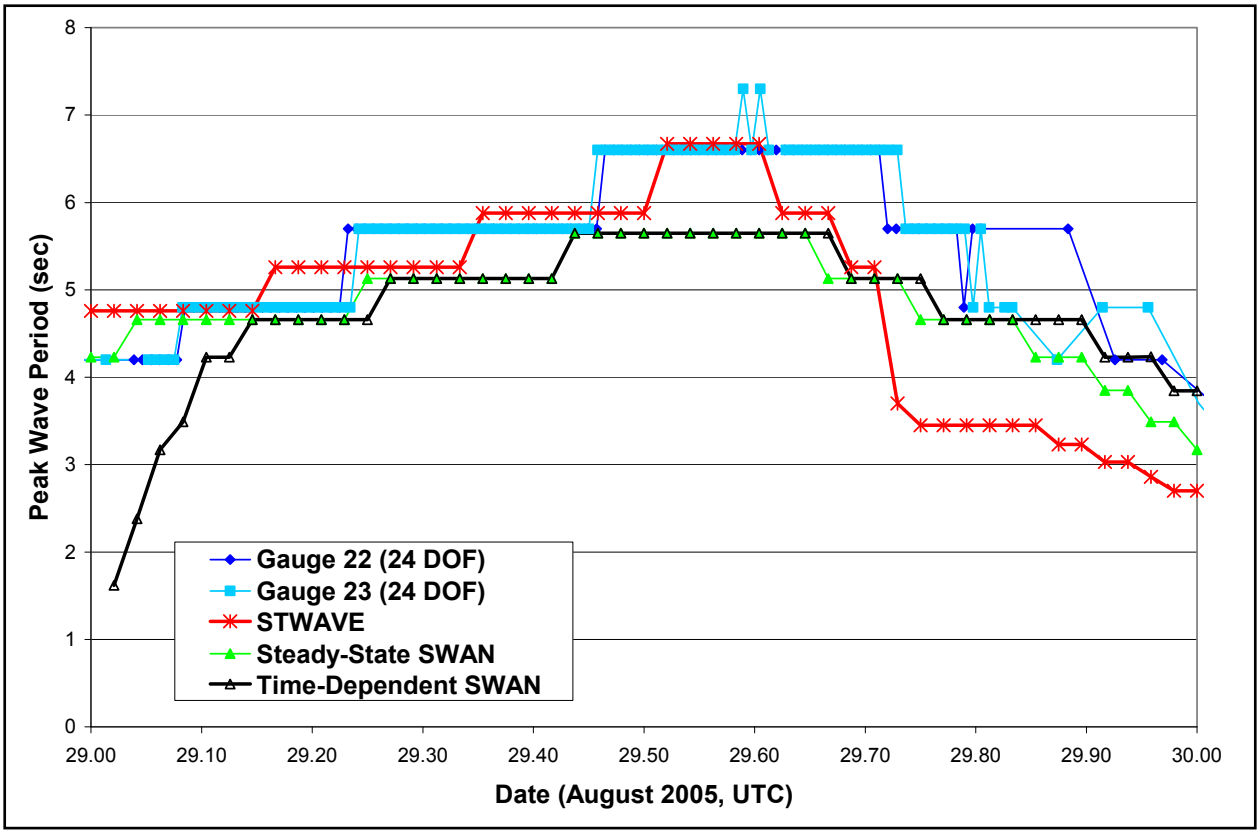

Figure 69. Time-dependent and steady-state SWAN and STWAVE modeled peak wave periods for Lake Pontchartrain and measured peak periods.

Regional Storm Surge Modeling

Purpose and Approach

A combination of measurements and numerical modeling using the ADCIRC model was used to develop information with which to characterize the temporal variation of water level and local water level maxima associated with Hurricane Katrina. Development of the ADCIRC model of southeastern coastal Louisiana (Westerink et al. 2005, Feyen et al. 2005) has been underway for several years. All major contributors to water level are considered in the storm surge modeling: tide, wind and atmospheric pressure, wave setup due to breaking waves, and flow entering the Mississippi River at Baton Rouge and the Atchafalaya River at Simmesport. The term water level as used in this volume describes the more slowly varying water surface, variations that occur on the time scales typically associated with the astronomical tide or storm surge (time scales on the order of minutes to days). Variations in water level on these time scales are contrasted with the much more rapidly varying water surface associated with shorter-period wind wave action (oscillatory motions in which the water surface varies over time scales of seconds and tens of seconds). Wind waves are discussed in the previous sections.

Measured water level hydrographs are the most reliable source of data for capturing both the temporal variation in water level and the maximum values. Water level hydrographs were

measured during the build-up stage of the storm at a number of sites throughout the study region; however, few operated throughout the storm. Most gauges failed prior to the time of peak water level. Consequently, there is little measured data that capture both the temporal variation of water level prior to, during, and after the peak conditions and the maximum condition. In a few cases, photographs and other visual images were utilized to provide information about the temporal variation of water level.

An extensive post-storm effort was undertaken to identify and survey HWMs following passage of the storm. While certain HWMs capture the peak water levels well, they contain no information about the temporal variation of water level. HWMs also have their own inherent issues of quality, uncertainty whether they in fact do reflect a peak condition, and whether or not water surface motions due to short wind waves or other factors are reflected in a HWM.

Water level measurements are able to provide temporal variation and maxima information at only a subset of the locations of interest. Many of the HWMs are of questionable quality. Storm surge modeling was used to complement quality water level measurements where they existed and provide water level information in the many locations where measured data were not available or were of questionable quality. Hydrograph data and the highest quality HWMs also are used to evaluate the accuracy of the storm surge model. As is the case for the wave modeling, model-to-measurement comparisons provide valuable information for quantifying the uncertainty in model predictions.

In this brief summary, we describe application of the ADCIRC hydrodynamic model to hindcast the storm surge development and propagation during Hurricane Katrina. Over the past decade, extensive storm surge model development, application, and validation efforts have been made in Southeast Louisiana. This work has improved storm surge modeling capabilities within a physics-based framework that correctly accounts for and simulates the forcing and response processes (Westerink et al. 2005, Feyen et al. 2005). These efforts have taken advantage of the evolution of unstructured grid computational algorithms as well as massively parallel software and hardware.

TF01x2 Computational Model

The model domain/grid applied in the Katrina simulation is based on an extension of the S08 model (Westerink et al. 2005, Feyen et al. 2005). The S08 model incorporates the western North Atlantic Ocean, the Gulf of Mexico, and Caribbean Sea to allow for full dynamic coupling between oceans, continental shelves, and the coastal floodplain without necessitating that these complicated couplings be defined in the boundary conditions (see the work of Blain et al. 1994 and Blain et al. 1998). The S08 domain/grid has been extensively applied and validated in a number of hindcast studies. These hindcasts included air-sea interaction and forcing as well as tides. Wave-current interaction was not taken into account in these previous studies.

For the Katrina hindcast, the S08 model/domain was extended by adding resolution along the north shore of Lake Pontchartrain as well as the inlets and coastal floodplain (up to the 60-ft contour) along the Mississippi and Alabama coasts. Detail was added to resolve the anticipated surf zone around the periphery of Lake Pontchartrain and in shallow water along the wetlands of

Southeast Louisiana, Mississippi, and Alabama as well as in the vicinity of barrier islands. Barrier islands were fully incorporated into the hydrodynamic computation to allow for full coupling between the wave and hydrodynamic models. Minimum resolution of approximately 300 ft was added in these regions. Resolution of the barrier islands allowed for representation of wave transmission over and past the islands, wave breaking, and generation of nearshore currents and wave setup. Detail was added to improve the treatment of water exchanges between Lake Borgne and Lake Pontchartrain. Detail was also added along the south shore of Lake Pontchartrain to resolve features such as the various harbors and Lakefront Airport. The resulting TF01x2 model, shown in Figures 70 through 73, allows for a better representation of the physical system and, therefore, better representation of system response during the entire storm event. Appendix 5 provides more detailed information concerning development of the ADCIRC model grid mesh and specification of topographic/bathymetric elevations.

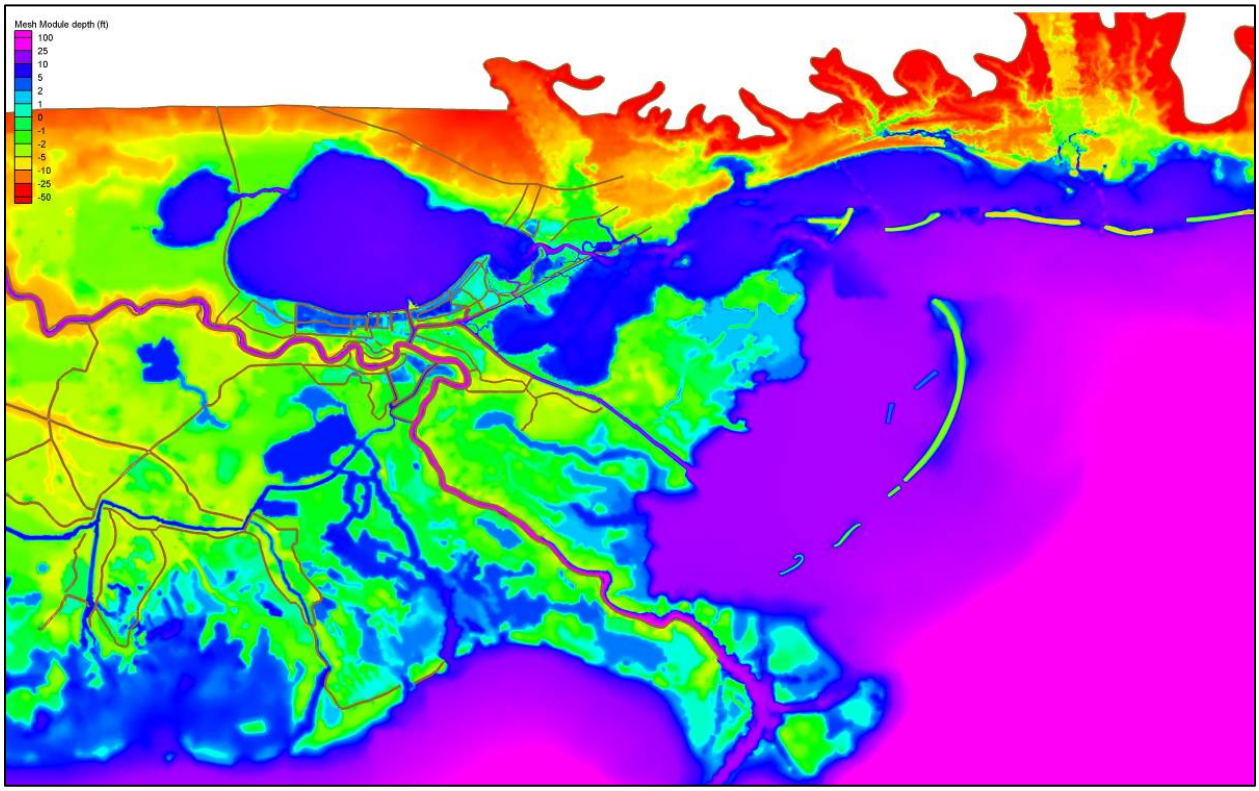

Figure 70. Bathymetry/topography used in the ADCIRC storm surge model (TF01x2 grid).

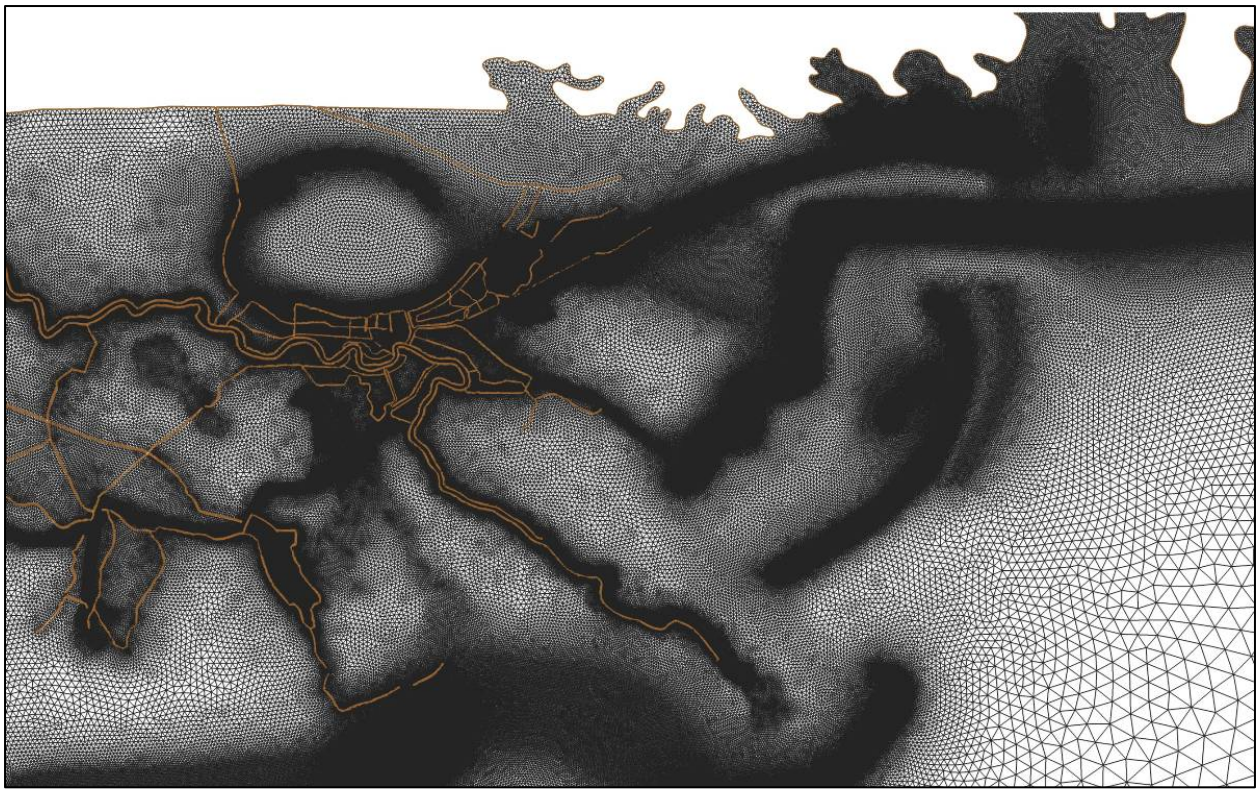

Figure 71. Grid resolution used in the ADCIRC storm surge model (TF01x2 grid).

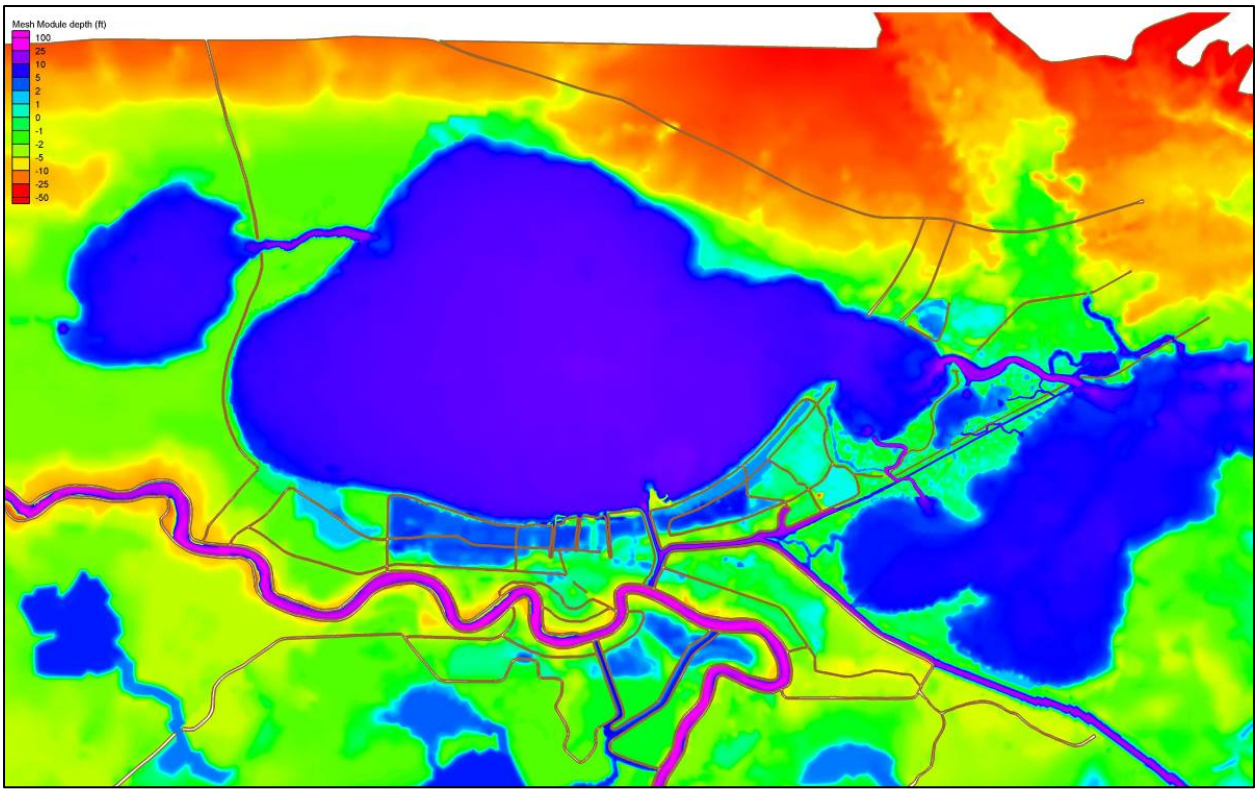

Figure 72. Bathymetry/topography used in the ADCIRC storm surge model (TF01x2 grid); Lake Pontchartrain vicinity.

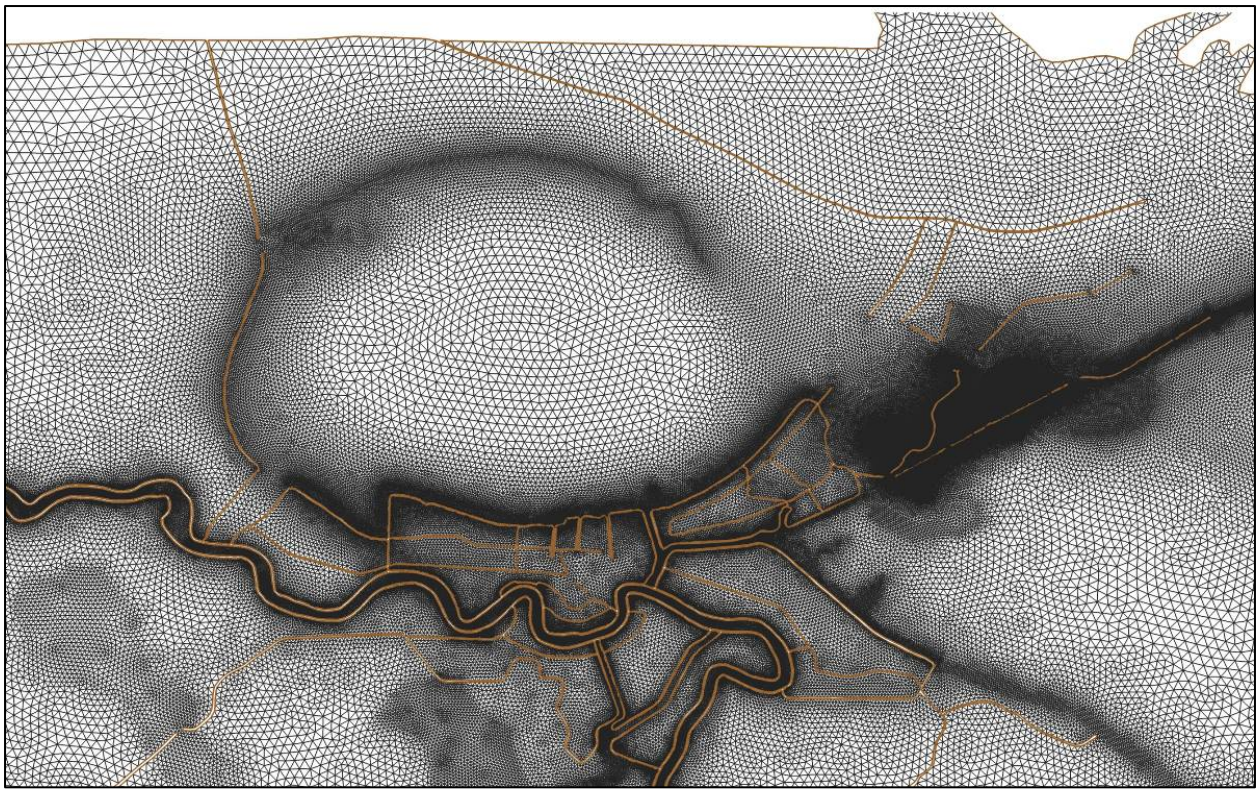

Figure 73. Grid resolution used in the ADCIRC storm surge model (TF01x2 grid); Lake Pontchartrain vicinity.

Storm Forcing and Other Details

Astronomical tides are applied as a forcing in the simulation. The K1, O1, M2, S2, and N2 tides were forced on the Atlantic open ocean boundary and with tidal potential functions throughout the domain to represent interior domain lateral gravitational forcing. The interior potential functions are particularly important in the resonant Gulf of Mexico. Nodal factors and equilibrium arguments were computed for both boundary and interior tidal forcing functions. Earth tidal potential reduction factors were applied to the interior tidal forcing functions. Radiation stress gradients from the four STWAVE models are included. The Mississippi and Atchafalaya Rivers are forced with steady flows of 220,000 and 67,000 ft^3/s, respectively. Steady flows are applied to work with the river radiation boundary conditions used in these rivers.

Steric effects due to the thermal expansion of surface ocean water during late summer are pronounced in the Gulf of Mexico. This expansion is approximately captured by the long term solar annual and semiannual (Sa and Ssa) harmonic constituents. Examination of the harmonic constants computed by NOAA for stations across Southeast Louisiana shows that the amplitude of the Sa and Ssa constituents is on average just over 0.52 ft. It is assumed that the hurricanes generally take place during the times when the expansion is at its largest in the late summer. Therefore, the initial water surface was raised an additional amount, a steric adjustment of 0.52 ft.

Marine wind and atmospheric pressure fields were generated using the procedures outlined in previous sections of this volume and in Appendix 2. The H*Wind/IOKA marine winds were applied as the wind forcing. To account for land roughness effects, marine winds were adjusted using directionally-dependent upwind roughness factors. Forested canopies are identified and it is assumed that negligible momentum transfer takes place through the canopy to any underlying water. The process to reduce winds in light of surface roughness accounts for inundation which reduces roughness elements. The H*Wind/IOKA wind fields were provided as 30-min average surface winds. Since the air-sea drag laws have been developed assuming 10-min averaged winds, conversion to 10-min averaged winds was implemented. Garratt's air-sea drag law was applied without limiting the maximum value of the surface drag coefficient.

Viscous hydrodynamic parameters were specified as a globally constant value for bottom friction and lateral viscosity using standard physically relevant values as were applied in previous S08 simulations. The bottom friction values used were the same ones used in previous tide and storm surge modeling done for the region using ADCIRC. No tuning or optimization was performed with respect to the selected values and, with the exception of the domain/grid enhancement, all model parameters were defined as in previous hindcasts.

Peak Water Level Maps

Figure 74 shows color-shaded contours of the maximum water level computed for the storm at each grid node of the ADCIRC model, in feet NAVD88 (2004.65), for the entire Louisiana and Mississippi coastal region. Figure 75 shows maximum water level contours for the metropolitan New Orleans vicinity. Peak water levels in Southeast Louisiana were computed to be about 20 ft along the east-facing Mississippi River and back levees that protect communities along the river in south Plaquemines Parish. The maximum water level occurs mid-way along the levee system and decreases to the north to a minimum peak value of less than 14 ft near English Turn. Adjacent to the levees along the MRGO, maximum computed water levels are 16 to 17 ft. The model predicts a low gradient in water level within the GIWW/MRGO, decreasing water levels from east to west, with a peak water level of about 14 ft at the confluence of the GIWW/MRGO and the IHNC. From this point south to the IHNC Lock, water levels are fairly constant, approximately 14 ft. From the confluence to the northern extent of the IHNC, a high water level gradient is computed, decreasing from a value of 14 ft at the confluence to approximately 9 ft in Lake Pontchartrain at Lakefront Airport. Along the south shore of Lake Pontchartrain, maximum levels were computed to range between 9 and 10 ft. Note that these computed peak water levels do not include the effects of wave setup or runup at the levee systems. They do include the contribution of wave setup that is generated away from the structures. The high-resolution hydrodynamic task of the IPET investigation examined the magnitude of wave setup and runup at the structures and found the contribution of wave setup at the structures to be 1.5 to 2 ft.

Along the coast of Mississippi, maximum water levels were computed to be as much as 29 ft. The large size of Katrina throughout its history, combined with the extreme waves generated during its most intense phase, enabled this storm to produce the largest storm surges that have ever been observed within the Gulf of Mexico (reliable HWM observations of up to 28 ft), as

determined from analyses of historical records. As an example of Katrina's strength in terms of storm surge, the previous highest HWM from Hurricane Camille was 24.6 ft, the only Category 5 storm to make landfall in the Gulf of Mexico over the interval that records have been kept (approximately 150 years). In the vicinity of Biloxi, MS, the surge produced by Camille was 15.8 ft, the highest surge that had ever been recorded at that location prior to Katrina. Katrina generated surges of 24 to 26 ft at Biloxi. In other words, Katrina (a Category 3 storm at landfall) storm generated substantially higher surges than Camille (a Category 5 storm at landfall) in the area where they both made a direct hit. Whereas the Saffir-Simpson scale is a good predictor of wind damage from hurricanes, it is not a particularly good predictor of the surge and wave generation potential for these storms. The following quotes about Camille's intensity are made by NOAA and the USACE:

> "A minimum pressure of 26.84 inches was reported in Bay St. Louis, Mississippi, which makes Camille the second most intense hurricane of record to hit the United States. The actual maximum sustained winds will never be known, as the hurricane destroyed all the wind-recording instruments in the landfall area. The estimates at the coast are near 200 mph. Columbia, Mississippi, located 75 miles inland, reported 120 mph sustained winds. A storm tide of 24.6 ft occurred at Pass Christian, Mississippi." (*http://www.nhc.noaa.gov/HAW2/english/history.shtml#camille*)

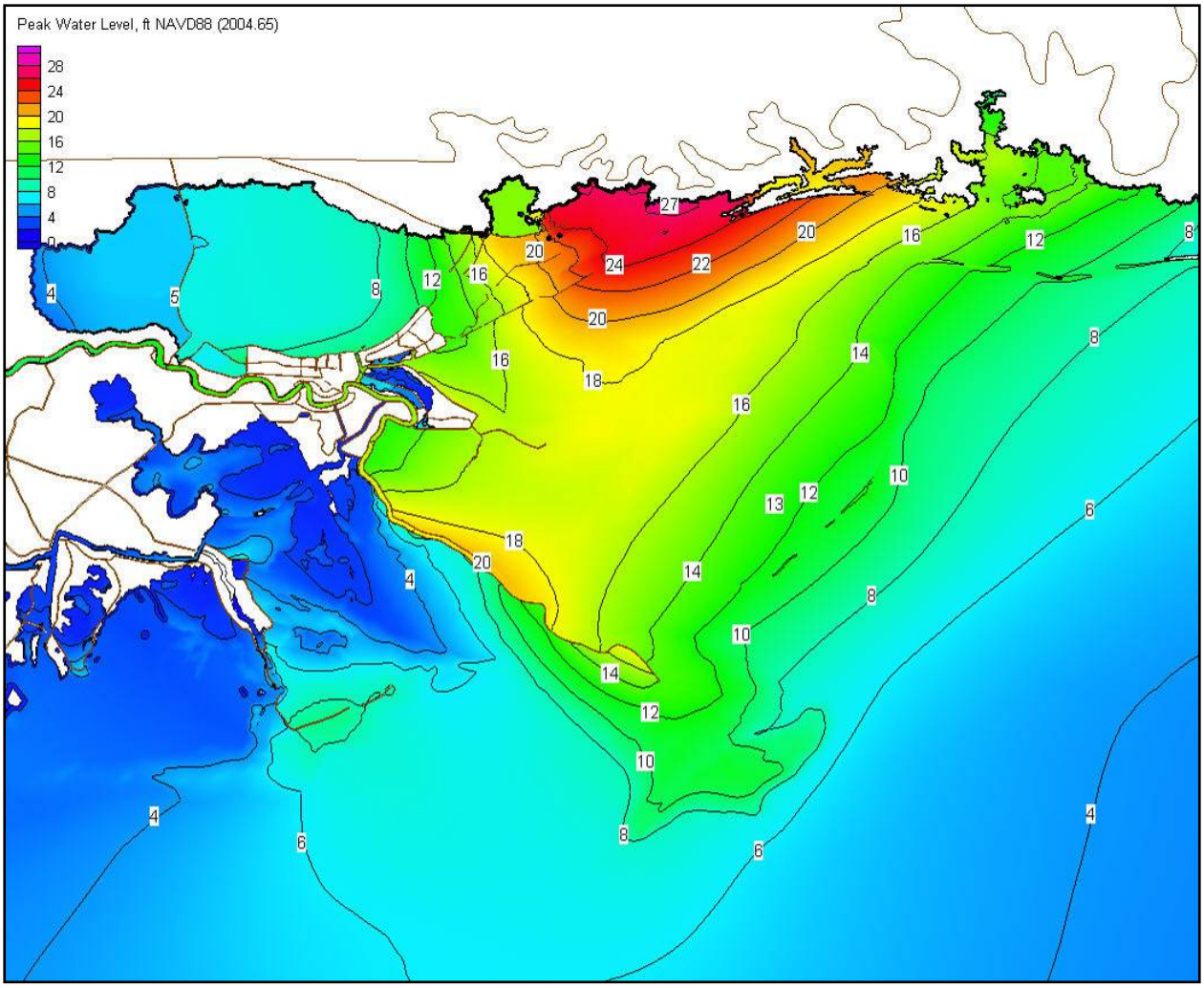

Figure 74. Maximum computed storm water level using the ADCIRC model, Mississippi to Louisiana region (water levels in feet NAVD88).

"Hurricane Camille began as a tropical wave off of the African coast on August 5, 1969. The storm developed circulation near Grand Cayman on August 14 and quickly strengthened to a major hurricane by August 15 before hitting Cuba. The warm waters of the Gulf of Mexico created perfect conditions for the storm as it gathered with estimated peak winds of 210 mph. Camille made landfall near Bay St. Louis, Mississippi, on the night of August 17, 1969. Camille dropped localized rainfall amounts of up to thirty-one inches all the way into Virginia. It recorded the highest storm surge (more than twenty-four feet) in the United States before Katrina in 2005. Camille killed 143 people along the Gulf coast and was responsible for extensive flooding, which claimed an additional 113 lives. Nearly 9,000 people were injured and 5,662 homes were destroyed. The total damage estimate was $1.42 billion." (*http://www.hq.usace.army.mil/history/Hurricane_files/Hurricane.htm*)

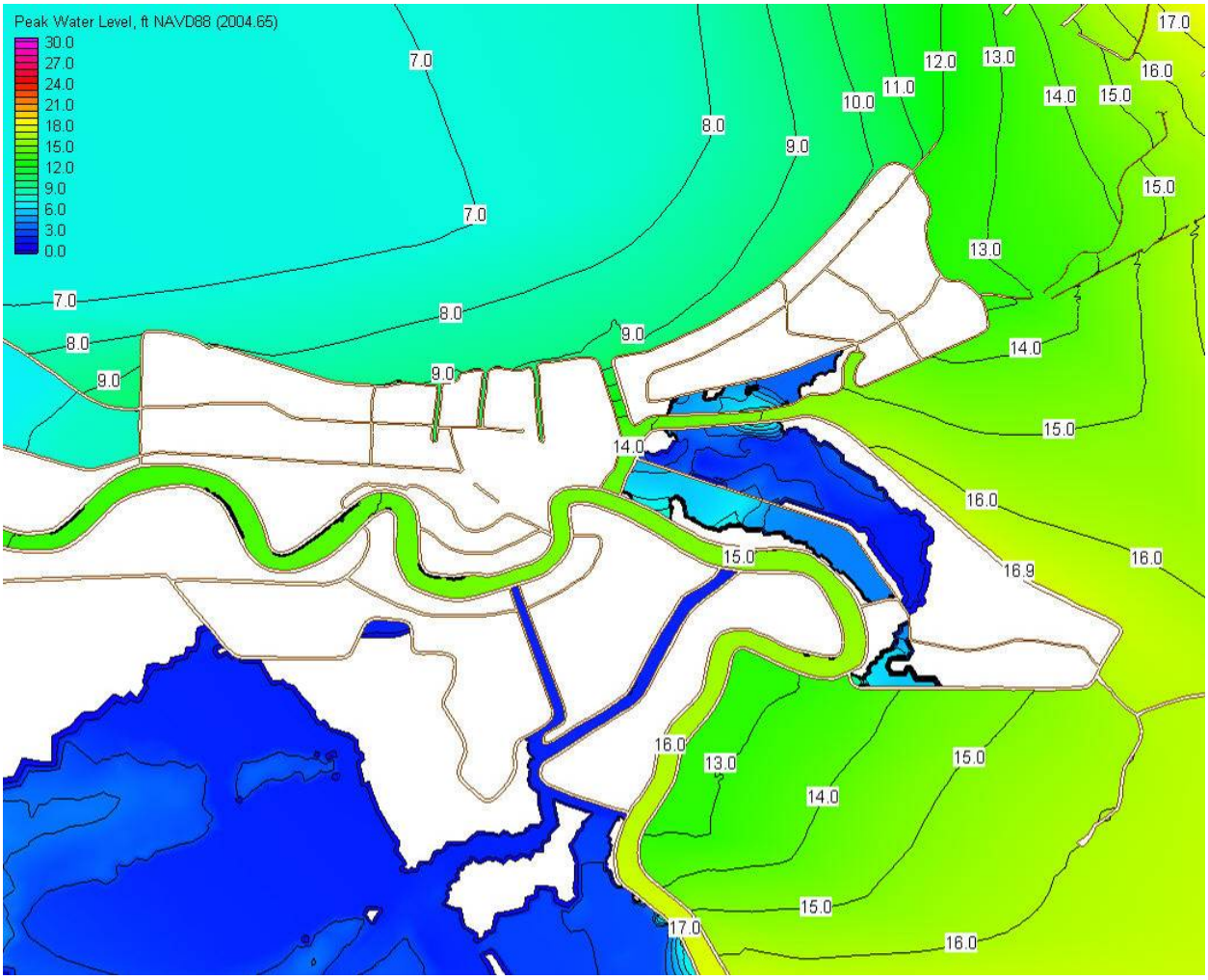

Figure 75. Maximum computed storm water level using the ADCIRC model, metropolitan New Orleans vicinity (water levels in feet NAVD88).

It is interesting to note that the two highest recorded storm surges along the U.S. coast, those for Hurricanes Camille and Katrina, occurred in close proximity to one other. As is seen for Katrina, the strong topographic control exerted by the Mississippi River delta and levees appears to be a contributor to development of high storm surge in this region. This was likely a contributing factor to the high surges that were experienced for both storms.

Computed Temporal Variation of Storm Water Level at Key Locations

Figures 76 through 79 show computed time series of water surface elevation at 16 locations throughout the hurricane protection system. Figure 76 shows locations along the south shore of Lake Pontchartrain. The computed time of arrival of the peak surge is between 1345 UTC and 1410 UTC on 29 August, 2005 (or approximately 9:00 a.m. local time, CDT). The simulated time of arrival for the peak surge appears to be slightly ahead of the observed time of arrival, which is estimated to have occurred sometime between 9:00 a.m. and 10:00 a.m. CDT. Peak water levels computed with the ADCIRC model are lower than the observed HWMs, by

approximately 2 ft. This difference is attributed to wave setup that is generated by wave breaking at the hurricane protection levees and the low terrace, which is located seaward of the levees and becomes inundated during the storm (Lakeshore Drive is on this terrace, or bench in front of the levees). Even the fine resolution adopted for the ADCIRC modeling along the south shore of the lake (300 ft) is not sufficient for accurately computing this local contribution to wave setup. High resolution hydrodynamics work done as part of the IPET investigation shows this local setup contribution to be approximately 1.5 to 2 ft. Of note in the Lake Pontchartrain hydrographs is the rapid rate of rise of water level associated with arrival of the storm, and the very slow drawdown in the lake following its passage. Katrina filled the lake in addition to tilting the water surface under the action of local wind. When the winds diminish following passage of the storm, the water surface in the lake levels out and the draining process occurs albeit at a slow rate.

Figure 77 shows the same information for four locations adjacent to Lake Borgne, three along the St. Bernard Parish Levee adjacent to the MRGO and one along the back levee of Orleans Parish adjacent to the GIWW. ADCIRC results along these levees are probably low because of the local wave setup at the levees that is not being accounted for in the regional-scale modeling. The high resolution hydrodynamic work suggests the local setup contribution along these levees is 1 to 2 ft. High water is predicted to occur between 1230 UTC and 1310 UTC (7:30 and 8:10 a.m. CDT). Peak water levels vary from 14.4 ft along the GIWW, to 15.4 ft at Bayou Bienvenue floodgate, to 16.6 ft at Bayou Dupre floodgate, to 16.7 ft at the southeastern tip of the levee adjacent to the MRGO. These largest values are about 2 ft lower than the highest observed HWM acquired at Shell Beach which is located further to the southeast along the MRGO. At the north end, the value of 15.4 ft is similar to the HWMs from Paris Road bridge, which were 15.5 ft.

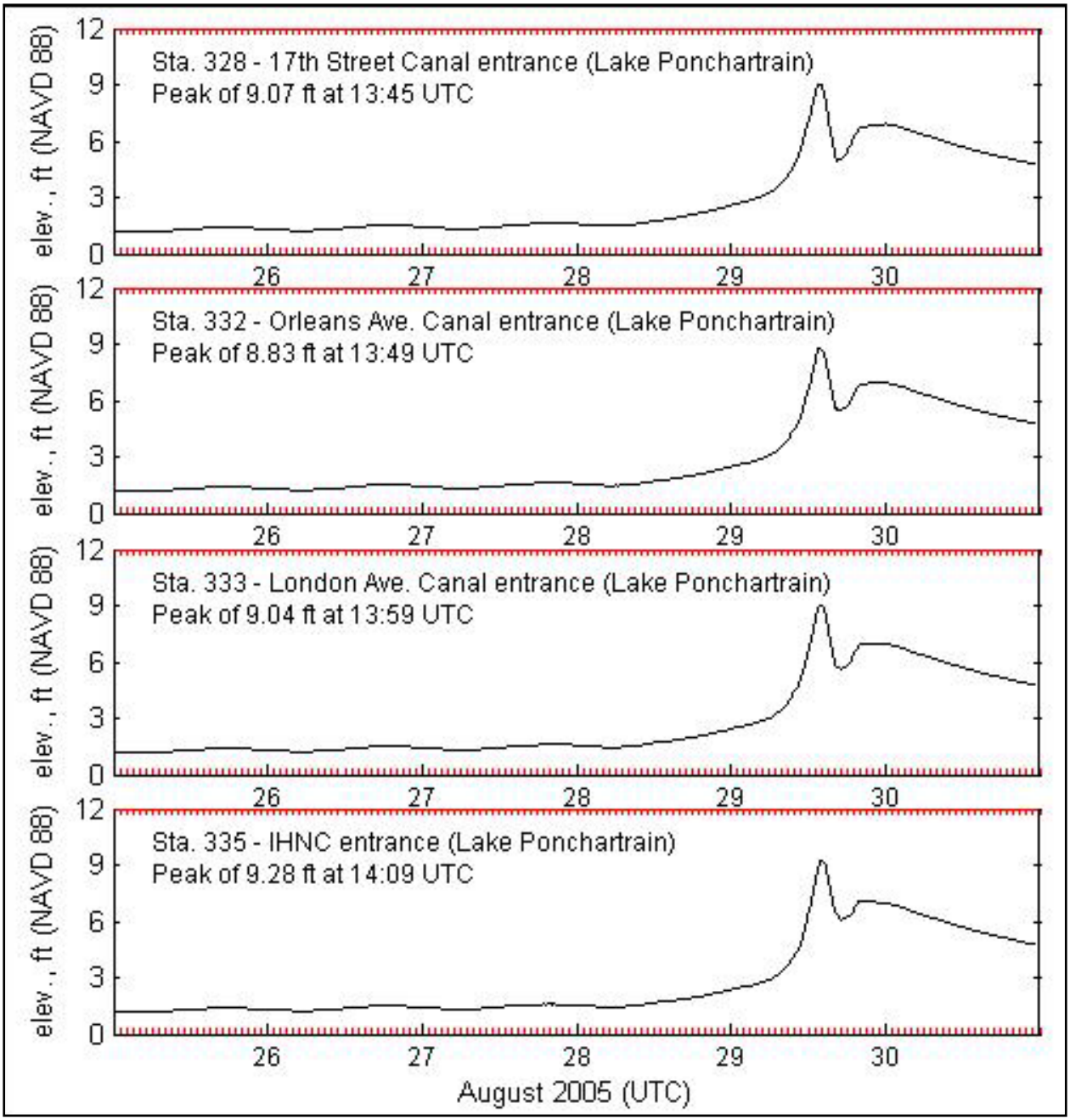

Figure 76. Change in water surface elevation, with time, for locations along the south shore of Lake Pontchartrain.

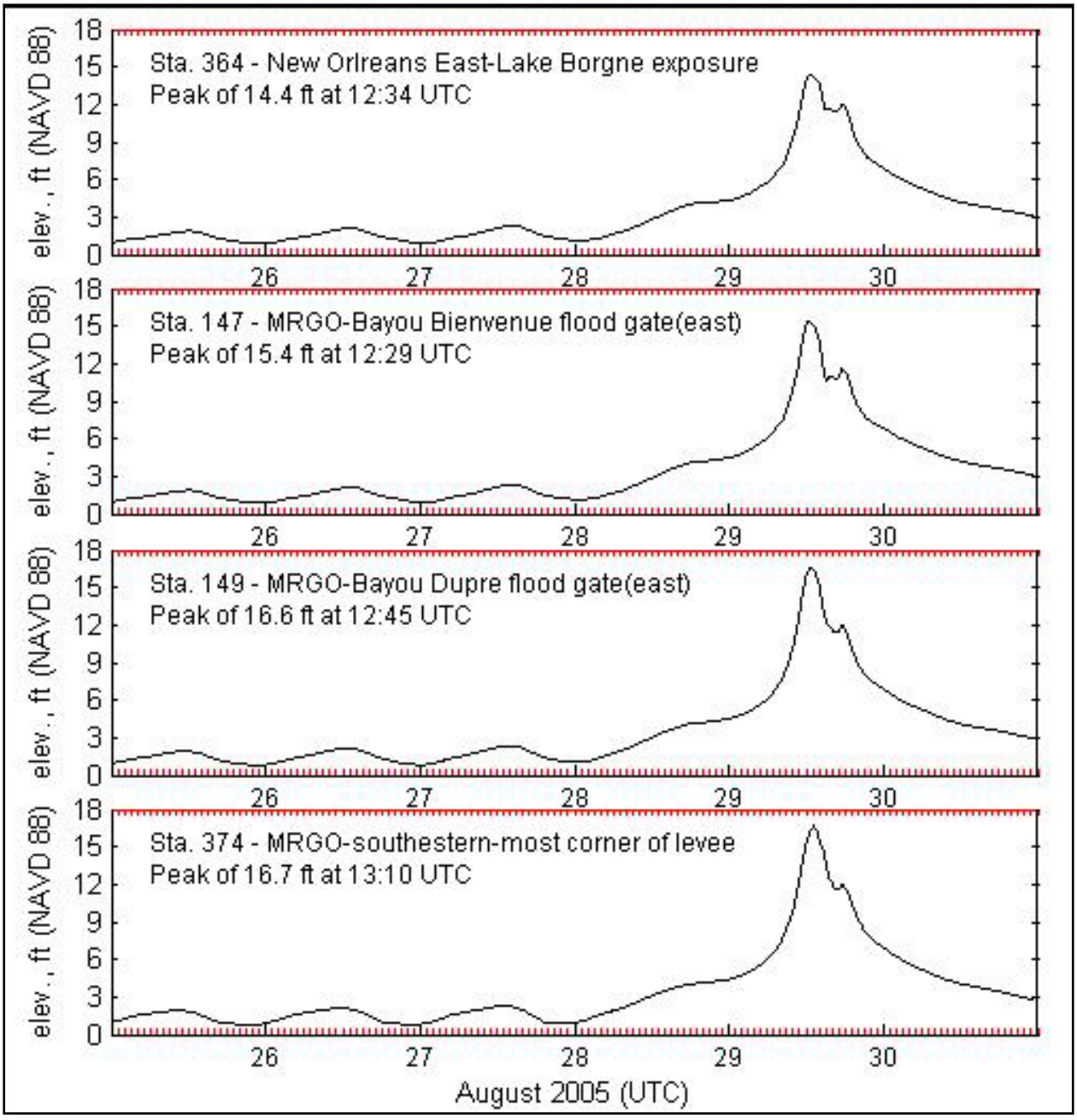

Figure 77. Change in water surface elevation, with time, for hurricane protection levee locations in the GIWW and MRGO with exposure to Lake Borgne.

Figure 78 shows results for three locations along the IHNC and one along the GIWW/MRGO (at Paris Road bridge). The computed time of peak water level is 1245 UTC (7:45 a.m. CDT), at the IHNC Lock. The observed hydrograph at the lock shows arrival of the peak surge at about 1400 UTC (9:00 a.m. CDT), or slightly later. The computed peak at Paris Road bridge is 15.2 ft; reliable HWMs show 15.5 ft. At the I-10 crossing over the IHNC, the computed peak is 12.7 ft, which is less than reliable HWMs at this same location (about 14 ft). At the confluence of the IHNC and GIWW/MRGO, the HWM data indicate a maximum of 15.2 to 15.4 ft, about 1.5 ft higher than the computed peak water level of 13.9 ft. At the IHNC Lock, computed peak water

level is 14.4 ft, and the observed peak water level is 14.3 ft. Not fully accounting for wave setup along the exposed levee systems and the level of detail reflected in the grid mesh may have some effect on the accuracy of water level computations in these canals.

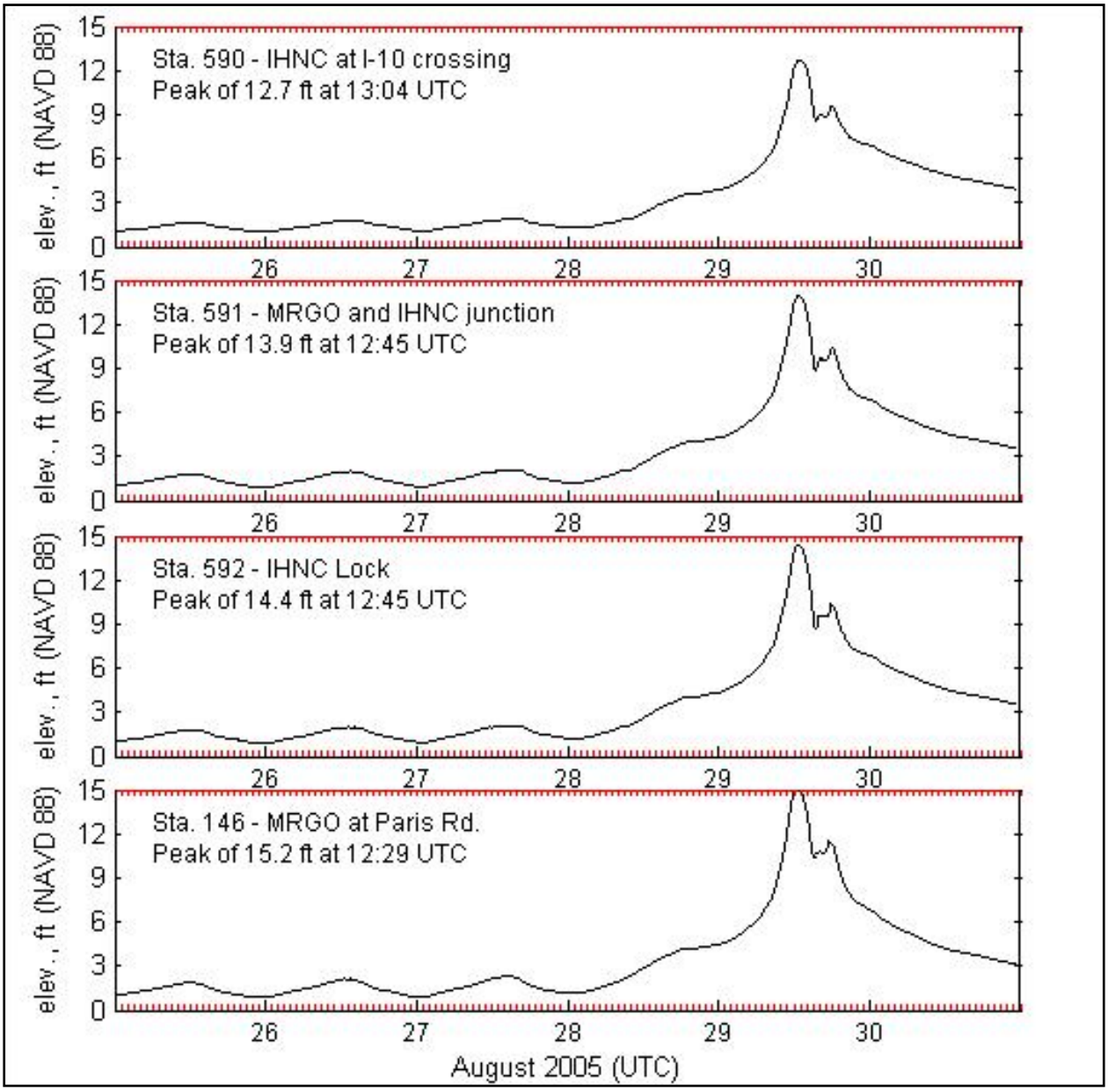

Figure 78. Change in water surface elevation, with time, for locations along the GIWW/MRGO and IHNC.

Figure 79 shows results for four locations along the hurricane protection system in south Plaquemines Parish. Arrival time of the peak water level is computed to be 1045 to 1145 UTC (5:45 to 6:45 a.m. CDT) depending on location, earlier than the time of peaks in the metropolitan New Orleans vicinity which is expected. Peak water levels range from 16.6 to 19.5 ft. The computed hydrographs show wetting and drying of the low-lying terrain under low surge

conditions (tidal effects are evident), followed by complete inundation during the peak of the storm surge wave.

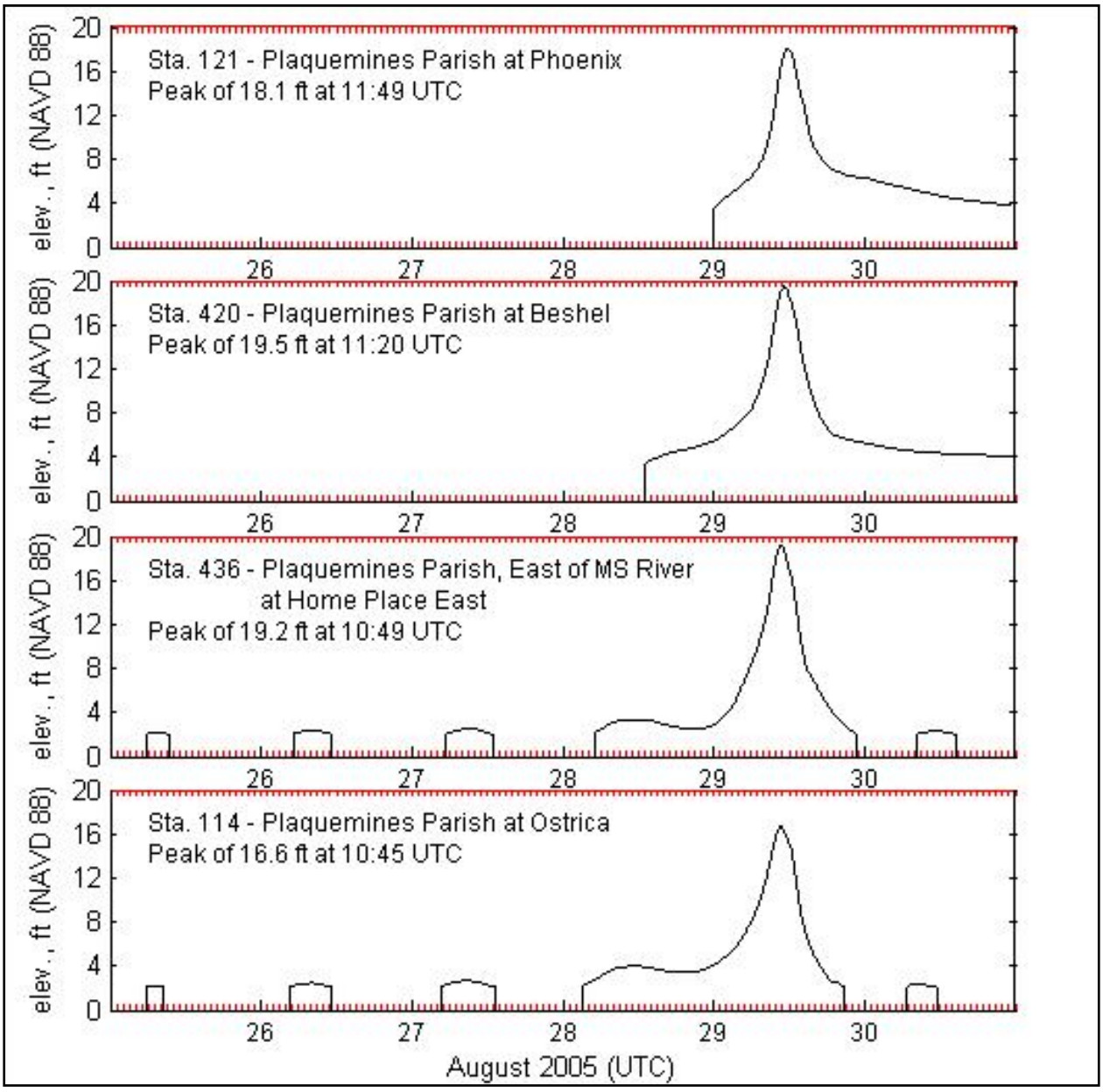

Figure 79. Change in water surface elevation, with time, for locations along the east-facing levees of south Plaquemines Parish.

Comparison: Model Results to High-Water Marks

HWMs marks were assigned reliability ratings, in terms of how well they represented the still-water level in unprotected areas. For this comparison, only marks rated "good" or "excellent" were compared to model results. The comparison was done separately for the Louisiana and Mississippi coastal regions. The data sets were separated in order to quantify

model accuracy in the area of greatest interest to the IPET investigation. Accuracy of the surge model predictions in Mississippi was also of great interest because the highest surges were observed there. The geographic region influenced by Katrina's storm surge was quite large, from the Mississippi River delta to Mobile Bay. The intent was to model the regional storm surge field as well as possible, and practicable, within the time constraints of the study. It is also important to point out that the storm surge created along the Mississippi coast greatly influences what happens in the Southeast Louisiana vicinity and in particular the surge conditions in Lake Pontchartrain.

Physical representation of geography of the Mississippi coast was done at a level of detail thought to be the minimum necessary for accurate regional storm surge simulation. Detail was added to the grid mesh in Mississippi and Alabama, including areas that would potentially become inundated, and a fourth nearshore wave model was set up for the Mississippi coast and applied to properly represent the nearshore wave radiation stress field in the region. Even though the ADCIRC grid mesh was extended into Mississippi and Alabama, the representation of elevated roadways and other features that will influence the movement of water during elevated storm surge levels was not defined in as much detail as it was in the Louisiana portion of the mesh.

Figure 80 shows differences between the computed peak water level and both good and excellent HWMs, for critical regions of the study area. The figures show the computed water level field as color shaded contours, and the symbols indicate the difference between the computed high-water level and the measured value. A positive difference indicates an overprediction by the model; negative differences indicate an underprediction. Both the difference symbols and the computed water level field are color coded using the same elevation scale. If the computed values equal the observed values, the colors will be the same. All water level differences are in feet.

Figures 81 and 82 shown comparisons between measured and predicted high water elevations for all the locations where good and excellent HWMs were acquired. Results for Louisiana are shown in Figure 81, and results for Mississippi are shown in Figure 82.

The correlation coefficient for the Louisiana comparison is 0.82, which is quite good for storm surge predictions. Overall predictive skill of the model improved noticeably with the inclusion of the final H*Wind/IOKA wind product, which underscored the value of having highly accurate wind fields. The average error is -0.6 ft; this indicates a tendency to slightly underpredict the storm water level. Some of this low bias is due to the fact that even at the very fine resolution at which STWAVE/ADCIRC modeling was done, the local setup contribution at the structures was not fully represented. The groups of points with predicted peak water levels of around 9 ft are those along the south shore of Lake Pontchartrain. The overall average absolute error is 1.3 ft.

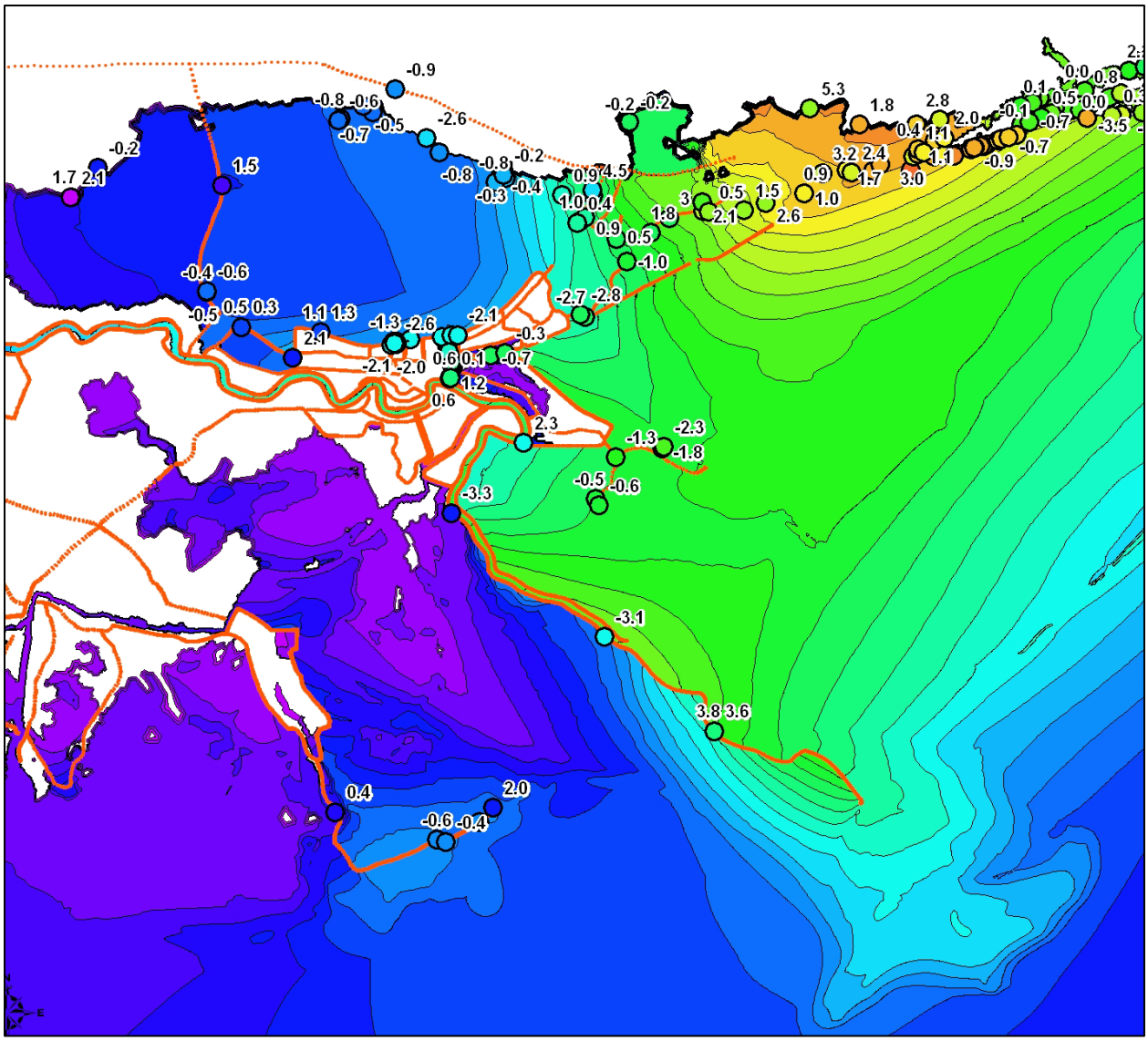

Figure 80. Regional comparison of computed and observed peak water levels.

For the Mississippi comparison, a slightly higher correlation coefficient is achieved, 0.83. This was not expected. The average error is much less, -0.25 ft, and the absolute error is the same as for the Louisiana comparison, 1.3 ft. Both sets of results are considered to be excellent for predicting a complex process like storm surge for such a complex physical system. The overall predictive skill level for the storm surge modeling is comparable to that achieved for the offshore wave modeling.

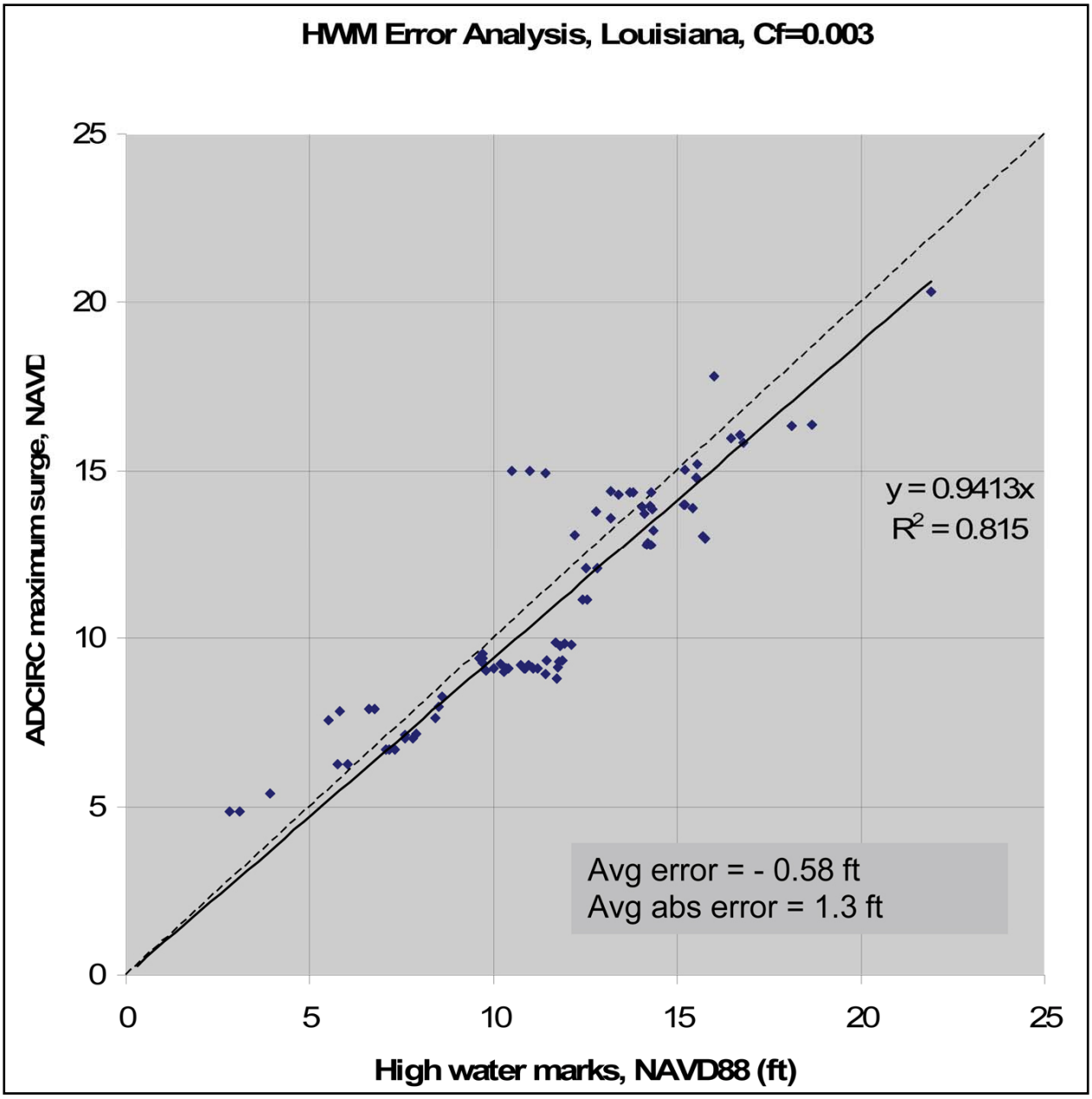

Figure 81. Comparison of computed and observed peak water levels for Louisiana.

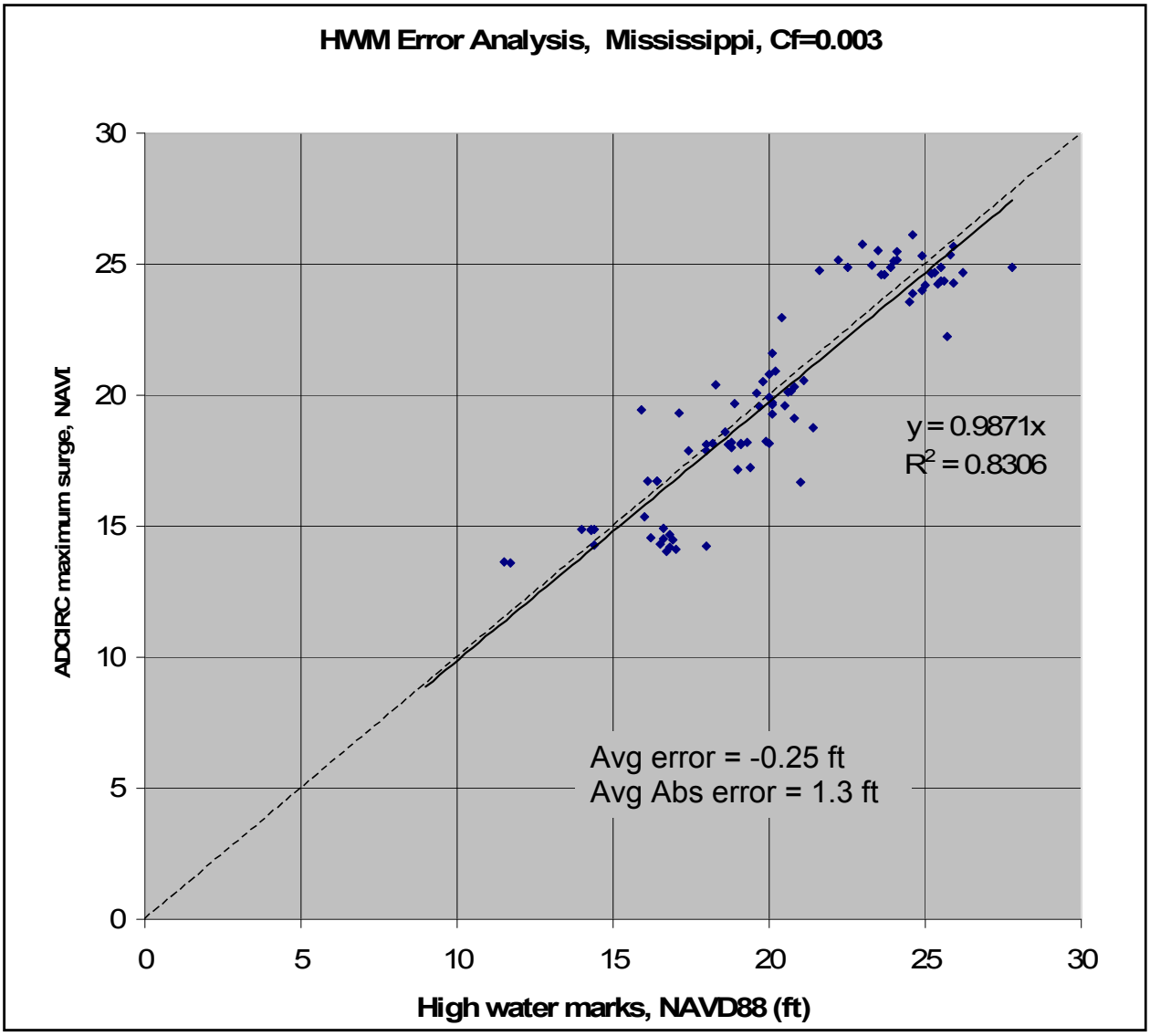

Figure 82. Comparison of computed and observed peak water levels for Mississippi.

Much more detailed documentation describing the storm surge modeling, a more detailed description of the storm surge wave propagation through the region, additional results, and the full set of model-to-measurement comparisons including hydrograph comparisons are provided in Appendix 5.

Data Products from Regional Wave and Storm Surge Simulations

A number of regional wave and water level information products were generated for use by the other components of the IPET investigation and for general information and communication purposes. The key information products were time series of wave and water level conditions, maps showing maximum wave parameters and water levels throughout the region, and animations that show how the water level and wave conditions throughout the region evolved as

the storm approached, made landfall, and passed through the region and into Mississippi. All information products are available on the IPET public web site (*https://ipet.wes.army.mil/*) along with supporting metadata. Prior sections of this volume describe the work that led to those data products.

Time series of waves were saved at approximately 600 points spaced at regular intervals around the entire periphery of the hurricane protection system (both east and west banks of the Mississippi River). These data span a period of several days. The data reflect changes in significant wave height, peak spectral wave period, and mean spectral wave direction as a function of time during the building stage of the storm, at the peak, and following passage of the storm out of the region. Water level time series (hydrographs) were saved at these same points as well as at a number of other points located outside the region but still in the ADCIRC model domain. Time series plots are also available for wave and water level conditions at all saved points along the hurricane protection system. Examples of time series data and plots have been shown in the preceding sections. The public web site contains details on the exact locations were wave and water level conditions were saved from the regional modeling, and each location is tagged with geographic coordinates. Figure 83 illustrates the density of save points in one small region of the hurricane protection system. Save points were generally defined to be a short distance away from the hurricane protection structures but far enough away to enable high-resolution modeling to pick up the details right near the structures which the regional-scale modeling was not able to resolve properly.

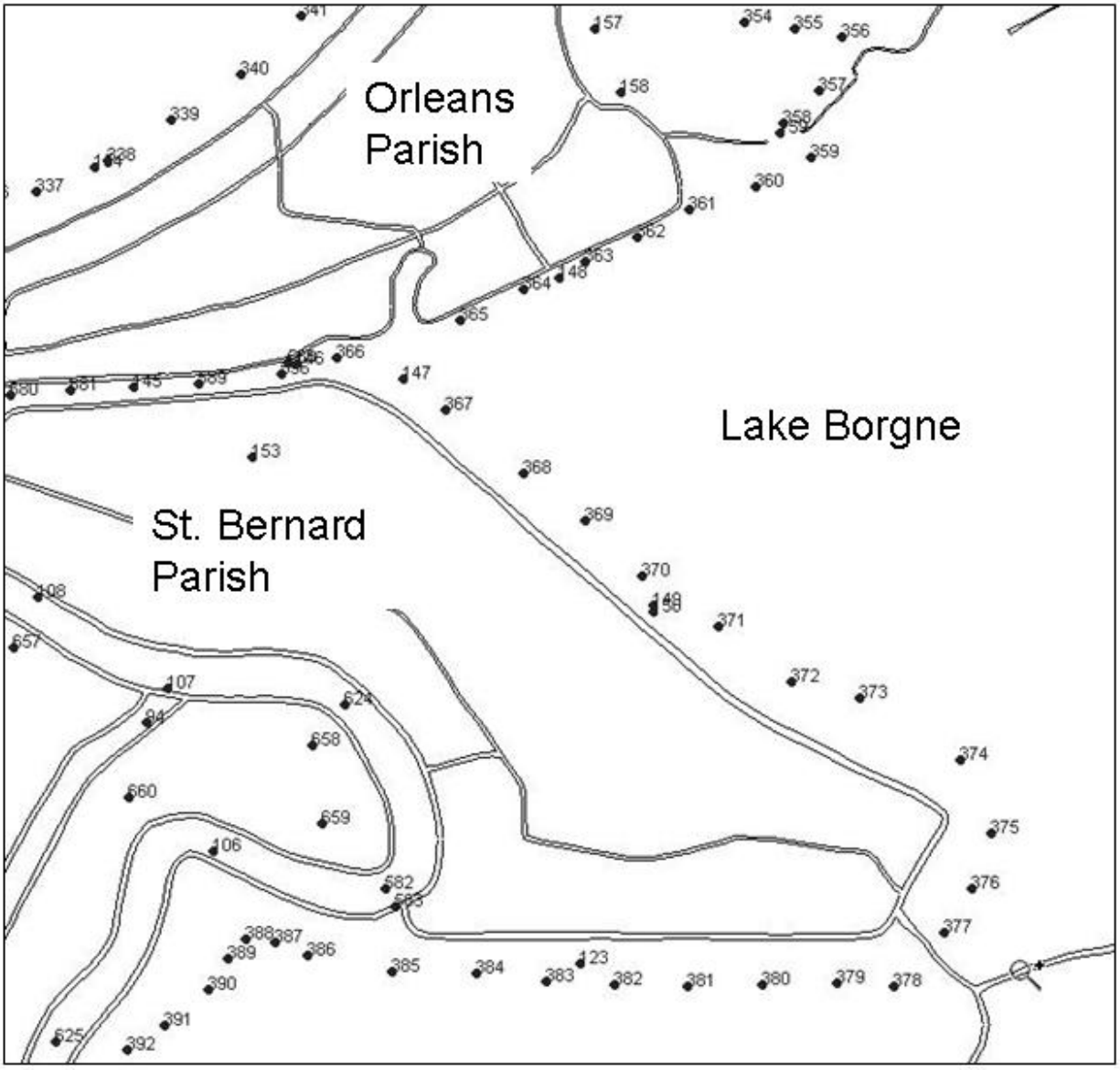

Figure 83. Time series save points along the hurricane protection system in eastern Orleans and St. Bernard Parishes.

A number of the peak wave height, wave period, and/or peak water level maps were shown in the preceding sections. In addition to the maps, animations were produced to show the temporal variation of the storm surge and wave fields. Animations are produced for several of the computational domains and subsets of those domains. They are also available on the IPET public web site.

Comparison of Katrina Wave and Water Level Maxima with Design Values

Approach and Datum Conversion

Peak wave and water level conditions experienced during Hurricane Katrina are compared to values used in design of the hurricane protection system. In the series of figures that follow, design values are shown in yellow boxes with the label "D"; computed, model-derived values are shown in blue with the label "C"; and where observations are available, measured values are shown in green boxes with the label "M". Design values were taken from design documents. Design water levels are cited in this section, not design crest elevations of the hurricane protection system levees and floodwalls.

For wave conditions, design documents cited significant wave height and period; however, they do not specify whether a peak or a mean period was used. At the time the projects were designed, the distinction between different measures of wave period was probably not made. Computed wave maxima were based on regional STWAVE model results (significant wave height and peak wave period). Measured nearshore wave conditions were only available at the entrance to the 17th Street Canal (data from two buoys in close proximity to each other); however, the measurements are of questionable accuracy at the peak of the storm. The maximum measured wave height and period values reported here are those recorded just prior to the point in time when the data appear to become suspect (data from both buoys are reported). There were no other shallow wave measurements made along the entire periphery of the hurricane protection system.

The design documents cite water levels relative to a number of different vertical datums, such as mean sea level, MSL, National Geodetic Vertical Datum, NGVD (without reference to any specific epoch), and still-water level, SWL. The earliest design documents cited SWL and MSL; later design documents tended to cite NGVD. However, it appears that the intent of the designers has always been to relate design water levels to mean sea level, and this intent has been confirmed with New Orleans District staff. That assumption is made here. All design water levels are converted to the common datum NAVD88 (2004.65) for the purposes of this comparison using datum conversions presented in Volume II. In all areas of the hurricane protection system considered here, local mean sea level (LMSL) datum is above the NAVD88 (2004.65) datum. The local mean sea level term is used, rather than simply mean sea level, to indicate that the correction does vary depending on location. To make the datum conversion from the design MSL to NAVD88 (2004.65), 0.5 ft is added to the design water level values along the south shore of Lake Pontchartrain and in the IHNC; 0.4 ft is added to values in the vicinity of GIWW and MRGO canals; and for southern Plaquemines Parish, 0.2 ft is added to design values. For measured water level conditions, at sites where hydrographs captured the peak water level, that value is presented. Where HWMs rated "excellent" are available, those values are shown. If no excellent marks are available in an area of interest, then marks rated "good" or "fair/poor" were used. Where HWMs having fair/poor reliability are shown in the figures, they are indicated with a question mark (?) following the listed elevation. Computed water level maxima were based on regional ADCIRC model results; all computed maximum water surface elevations are relative to NAVD88 (2004.65).

Wave Maxima

Figure 84 shows wave maxima for the south shore of Lake Pontchartrain in Jefferson and Orleans Parishes. Significant wave heights measured for Katrina exceeded design wave heights by 0.6 to 1.6 ft. Computed wave heights are about 0.5 ft greater than design heights. Peak wave periods during Katrina were about equal to the design values, perhaps slightly less. In general, Katrina wave conditions are similar to design values along the south shoreline of Lake Pontchartrain.

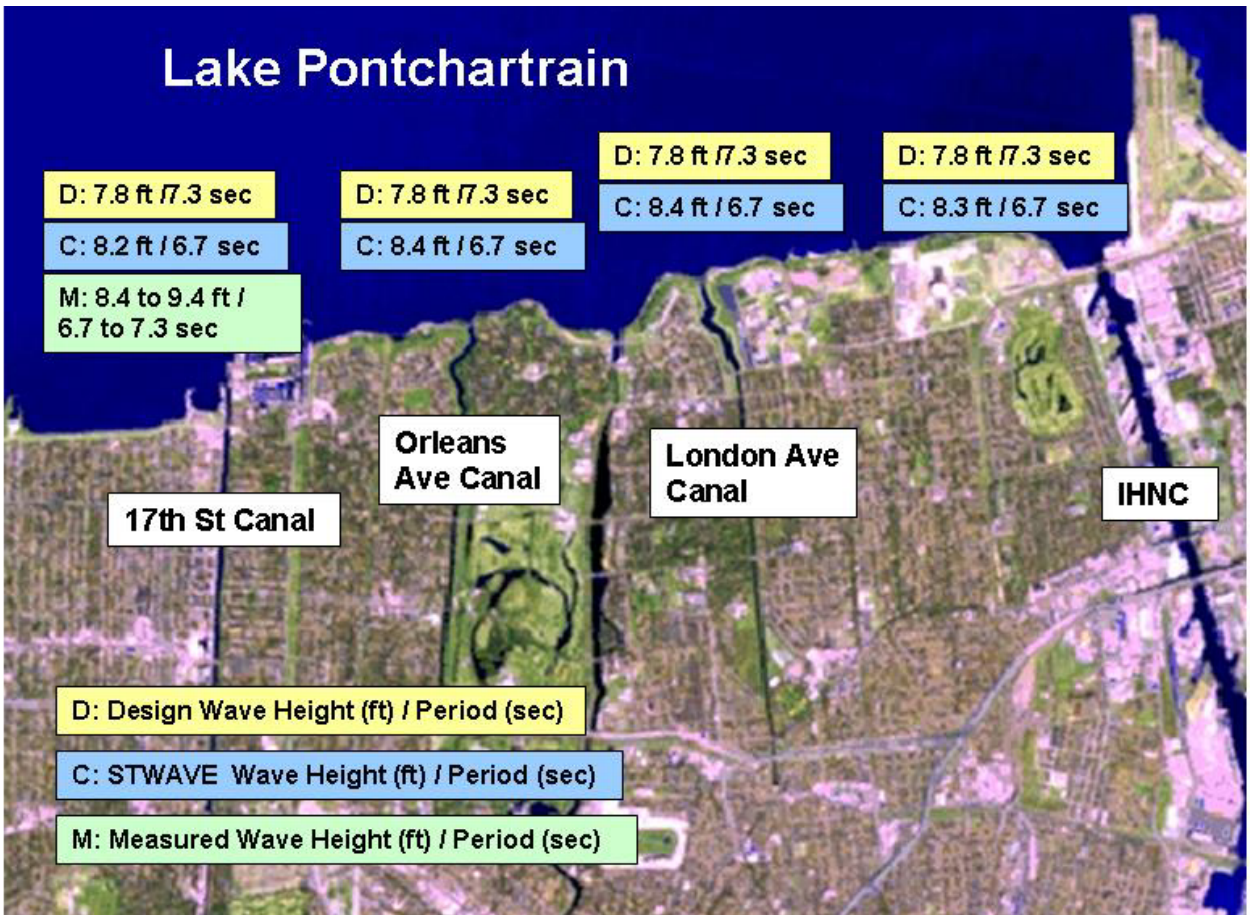

Figure 84. Wave maxima along the south shore of Lake Pontchartrain Hurricane Protection System.

Figure 85 shows wave maxima for the eastern portion of Orleans Parish. On Lake Pontchartrain, significant wave heights computed for Katrina exceeded design wave heights by 0.6 to 1.6 ft; peak wave periods were about equal to or slightly less that the design values. On the east-facing side of the parish, significant wave heights computed for Katrina exceeded the design value by 1 ft; and wave period was about equal to the design value. In general, for these two reaches of the project, Katrina wave conditions were similar to design values.

On the back levee of Orleans Parish, along the GIWW with exposure to Lake Borgne, maximum significant wave heights computed for Katrina were less than design values, but the

peak wave periods exceed the design values by about a factor of 3. This is a significant difference. The design wave periods are more typical of those for more locally-generated wind seas, or conditions with a restricted fetch. Wave model simulations show that during Katrina, the eastern-facing levees were subjected to longer-period energy propagating in from the Gulf of Mexico, past and over the barrier islands, and over the inundated marshes. Reexamination of the design wave conditions along the eastern-facing levees is recommended in light of the large differences between design periods and the wave periods generated by Hurricane Katrina. Both wave heights and wave periods define the potential for wave runup and overtopping.

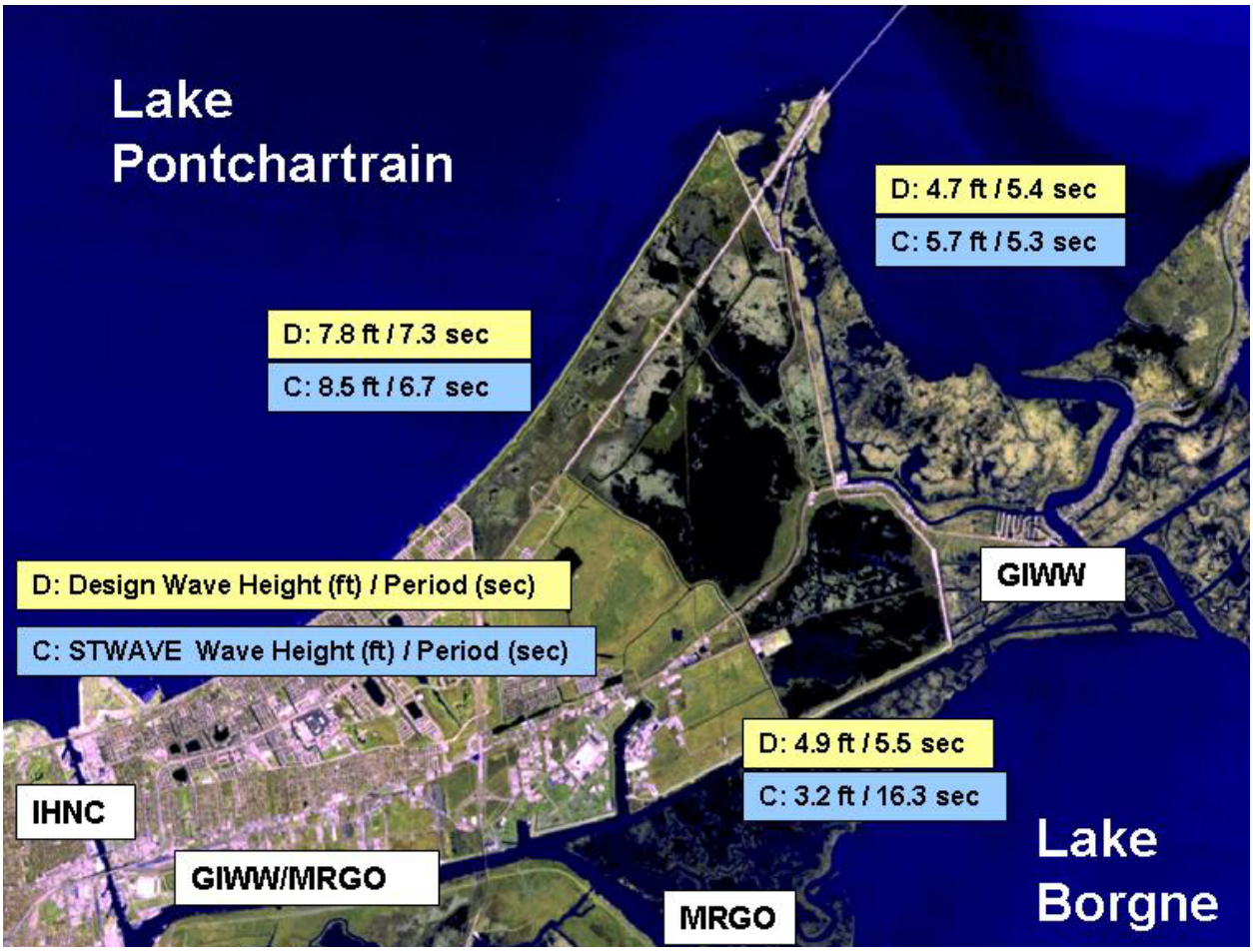

Figure 85. Wave maxima along eastern Orleans Parish Hurricane Protection System

Figure 86 shows wave maxima for the easternmost portion of St. Bernard Parish. Along the MRGO, significant wave heights computed for Katrina were less than the design wave heights by about 1.5 ft. However, peak wave periods computed for Katrina were 2.5 times greater than the design values. On the south-facing portion of the hurricane protection levee, significant wave heights computed for Katrina were less than design values by about 2.5 ft; but again, wave periods exceed design values by a factor of about 3. Design wave conditions at these locations should be reexamined as well. Lower wave heights will reduce runup; higher wave periods will increase wave runup.

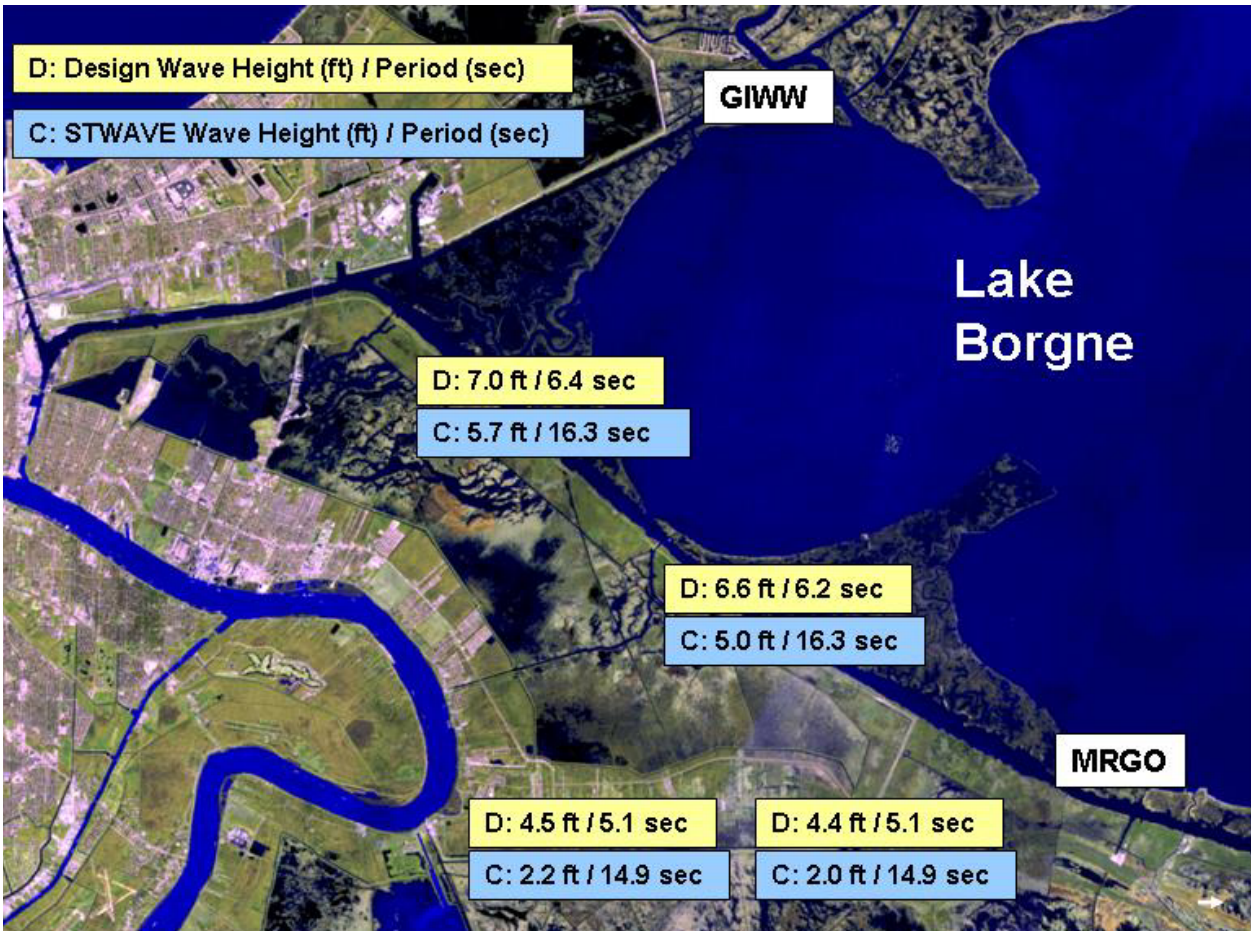

Figure 86. Wave maxima along the St. Bernard Parish Hurricane Protection System.

Figure 87 shows wave maxima for areas of south Plaquemines Parish. Along the levees east of the Mississippi River with exposure to waves approaching from the east, significant wave heights computed for Katrina exceeded design wave heights by amounts ranging from 1 to 4.5 ft. This is a significant difference, but expected in light of the fact that Hurricane Katrina had much greater wave generation potential than the SPH storms that were considered in designing the project. Peak wave periods computed for Katrina were much greater than the design periods, approximately 3 times greater.

On the west-facing levees on the west side of the Mississippi River, in some locations, computed significant wave heights computed for Katrina exceeded the design values by as much as 3 ft, and in some locations wave heights were less than design values. In all cases, the computed wave periods exceeded the design wave periods by a factor of 2.5. Hurricanes with tracks similar to Katrina, but displaced further to the west, would be expected to produce wave conditions that might significantly exceed the design values, in light of the degree of possible exposure to high wave energy from the gulf during inundated wetland conditions. Design wave conditions should be reexamined along the west-facing levees.

Figure 87. Wave maxima along hurricane protection levees in Plaquemines Parish

Water Level Maxima

Figure 88 shows water level maxima for the south shore of Lake Pontchartrain in Jefferson and Orleans Parishes. The design water level is 12.0 ft NAVD88 (2004.65) throughout this region. Observed peak water levels during Katrina at the entrances to 17th Street (10.8 ft), Orleans Avenue (11.1 ft), and London Avenue Canals (11.4 ft) ranged from 0.6 to 1.2 ft below design values. The peak values were all based on reliable HWMs and the trend in HWM data along the south shore of the lake. The HWMs at the entrances to the canals likely reflect some or all of the local contribution of wave setup caused by breaking at the hurricane protection levees. Based on results from the examination of high-resolution hydrodynamics, this local wave setup effect at the structures is on the order of 1.5 to 2 ft. Computed peak water levels, which do not reflect the local setup contribution, are approximately 3 ft lower than design values and approximately 2 ft lower than observed values.

Figure 89 shows water level maxima for eastern Orleans Parish. On the Lake Pontchartrain side, the design water level is 12.0 ft NAVD88 (2004.65), and the measured peak water level at the entrance to the IHNC was 11.8 ft. At this location, the peak water levels were at design levels. Both HWMs near Lakefront Airport and trends evident in surge model results suggest

that peak storm water levels increase to the east of Lakefront Airport, which implies that peak water levels were at or above design levels all along the lakefront of eastern Orleans Parish. Along the east-facing levees adjacent to Chef Menteur Pass, design water levels increased from 12.0 ft at South Point, to 12.6 ft at Highway 90, to 13.4 ft at the GIWW. HWMs acquired along this section of levee and near the GIWW at Chef Menteur suggest that design water levels were exceeded along this stretch of the hurricane protection system by amounts greater than 2 ft at the southern end of this reach.

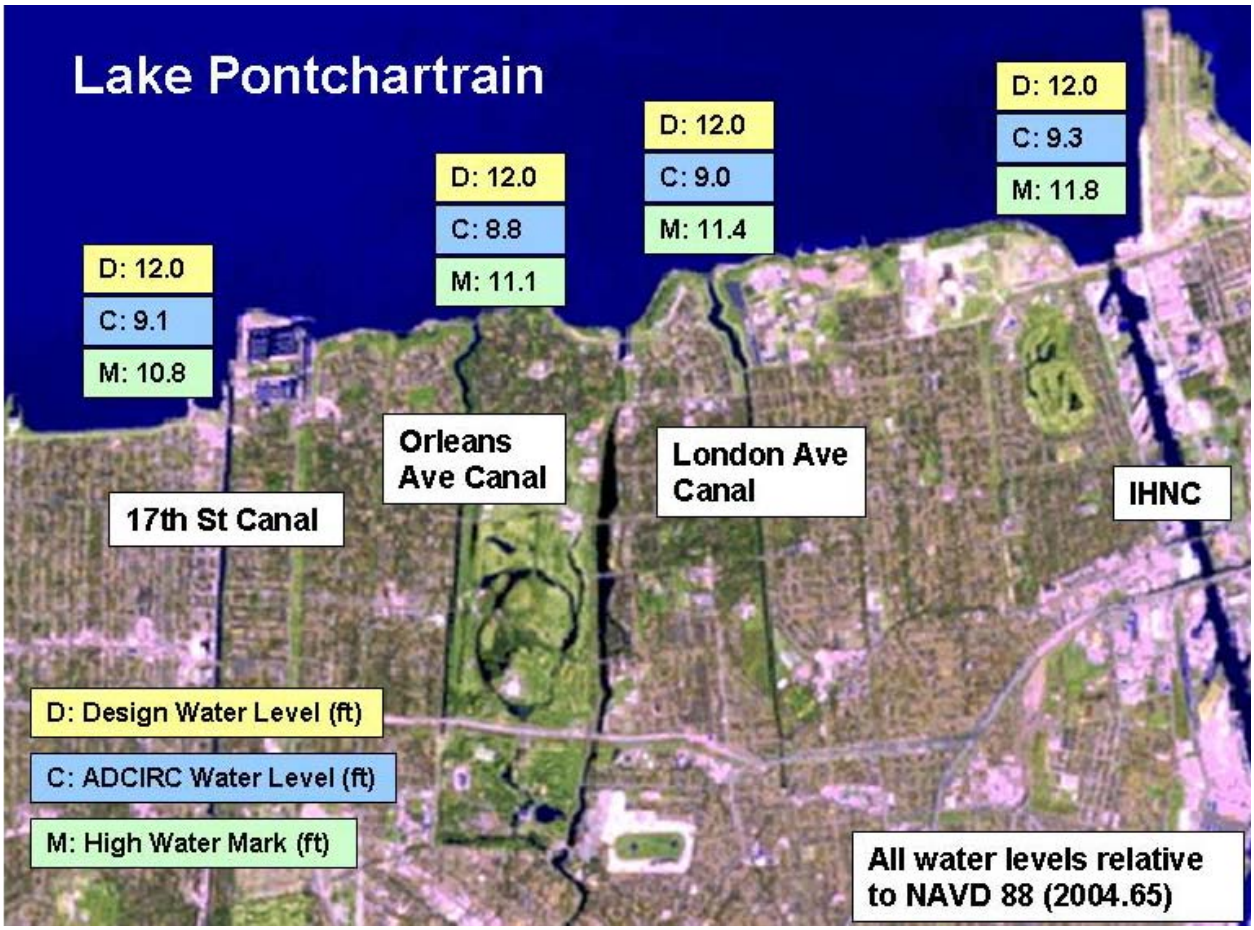

Figure 88. Water level maxima along the south shore of Lake Pontchartrain Hurricane Protection System.

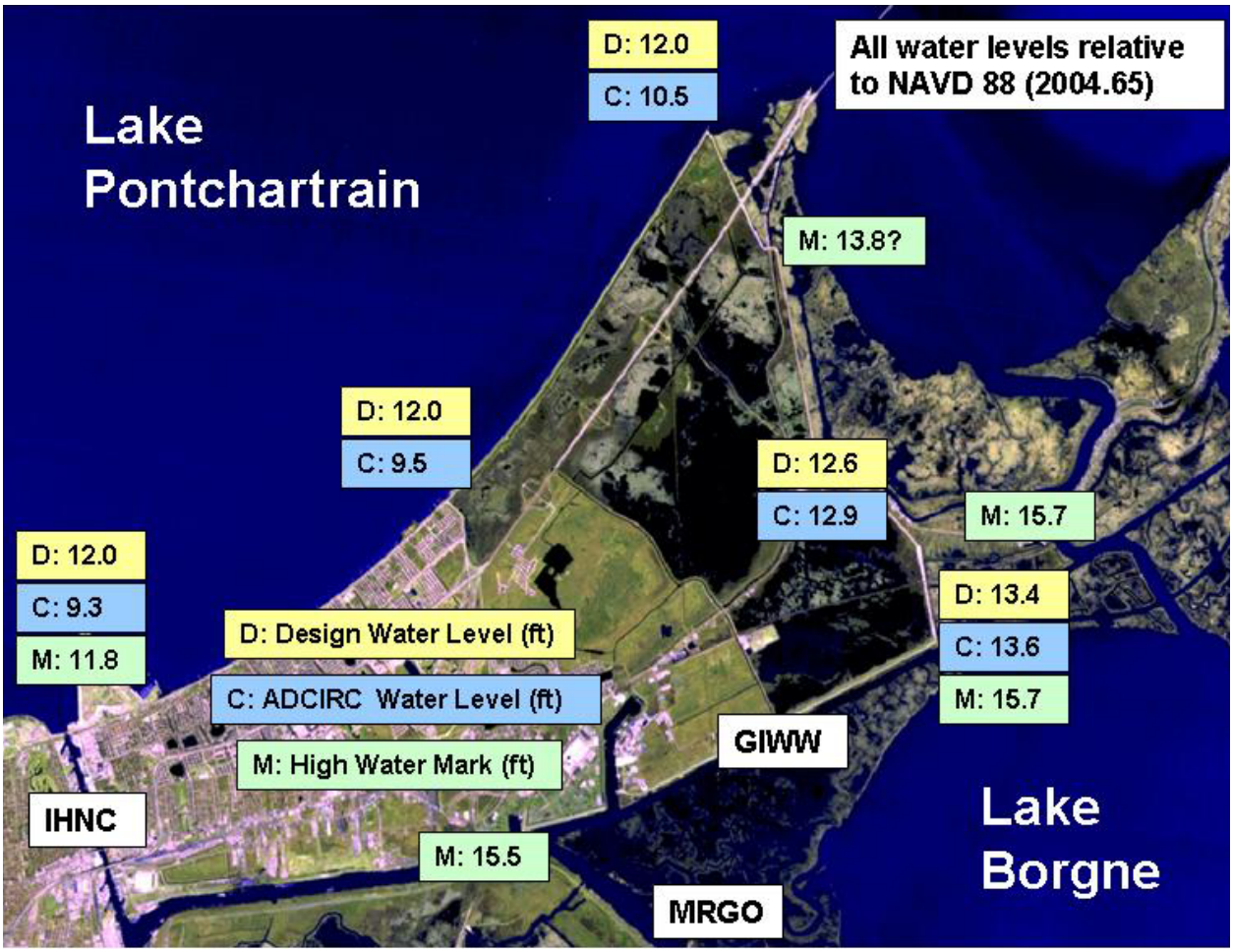

Figure 89. Water level maxima for eastern Orleans Parish Hurricane Protection System.

Figure 90 shows water level maxima for eastern St. Bernard Parish and the back levee of Orleans Parish. On the back levee, adjacent to the GIWW, with exposure to Lake Borgne, the design water level is 13.4 ft NAVD88 (2004.65). Reliable HWM data suggest that the design water levels were exceeded along this project reach by at least 2 ft. Along the MRGO adjacent to the hurricane protection levee, design water levels ranged from 12.9 to 13.4 ft. Computed maximum water levels range from 15.4 to 16.8 ft. Reliable HWMs near Shell Beach, which is further to the southeast and not fronting the hurricane protection levee, ranged from 17.1 to 18.7 ft. Reliable marks from Paris Road bridge, further to the northwest but in the GIWW/MRGO channel, were 15.5 ft. Considered together, model and measured data sources suggest that Katrina peak water levels exceeded design levels by amounts ranging from 2 to 5 ft along this section of the hurricane protection system.

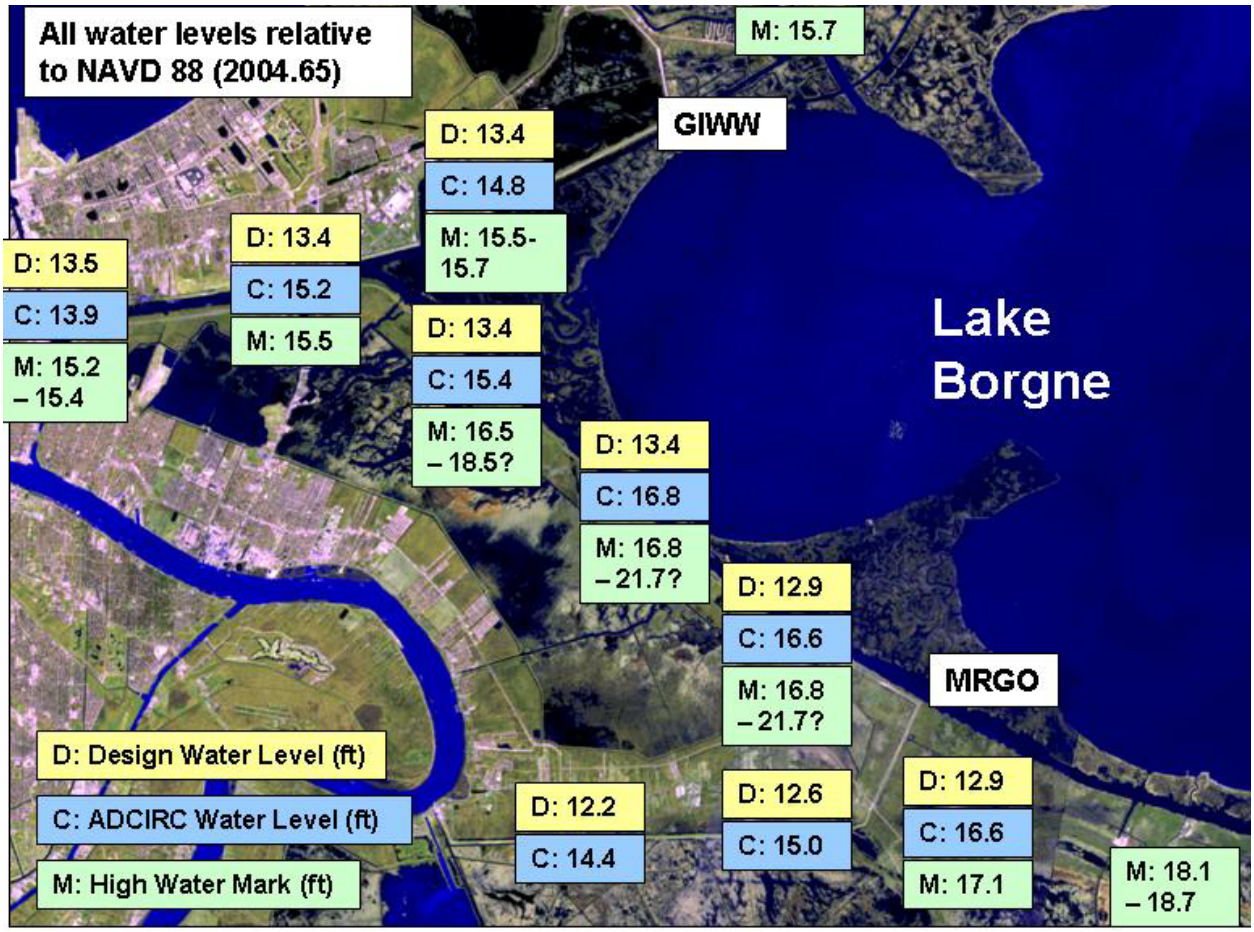

Figure 90. Water level maxima for eastern St. Bernard Parish and back levee of Orleans Parish Hurricane Protection Systems.

Figure 91 shows water level maxima along the IHNC. Between Seabrook at the north and the railroad bridge just south of the I-10 bridge, which is north of the intersection of IHNC with GIWW/MRGO, design water levels range from 11.9 to 13.4 ft NAVD88 (2004.65). HWMs suggest that water levels in this section of channel were at design levels or slightly below along the northern portion of the IHNC, and at or slightly above design levels near the bridge and confluence with the GIWW/MRGO. The design water levels reflect a gradient in peak water level within this reach of channel. Such a gradient was observed for Katrina, in the north half of the IHNC. The gradient is created by a higher surge in Lake Borgne and a lower surge in Lake Pontchartrain, and the connectivity between the two water bodies via the GIWW/MRGO channel and the IHNC channel.

In the IHNC, south of its junction with the GIWW/MRGO, design water levels are 13.5 ft. A number of reliable HWMs indicated peak water levels of 15.2 to 15.4 ft at the confluence with GIWW/MRGO. The hydrograph from the IHNC Lock indicates the peak reached 14.3 ft NAVD88 (2004.65), and numerous other reliable marks indicate peaks of 14.2 to 14.3 ft. High water values throughout this region indicate that peak water levels during Katrina exceeded design values by as much as 2 ft.

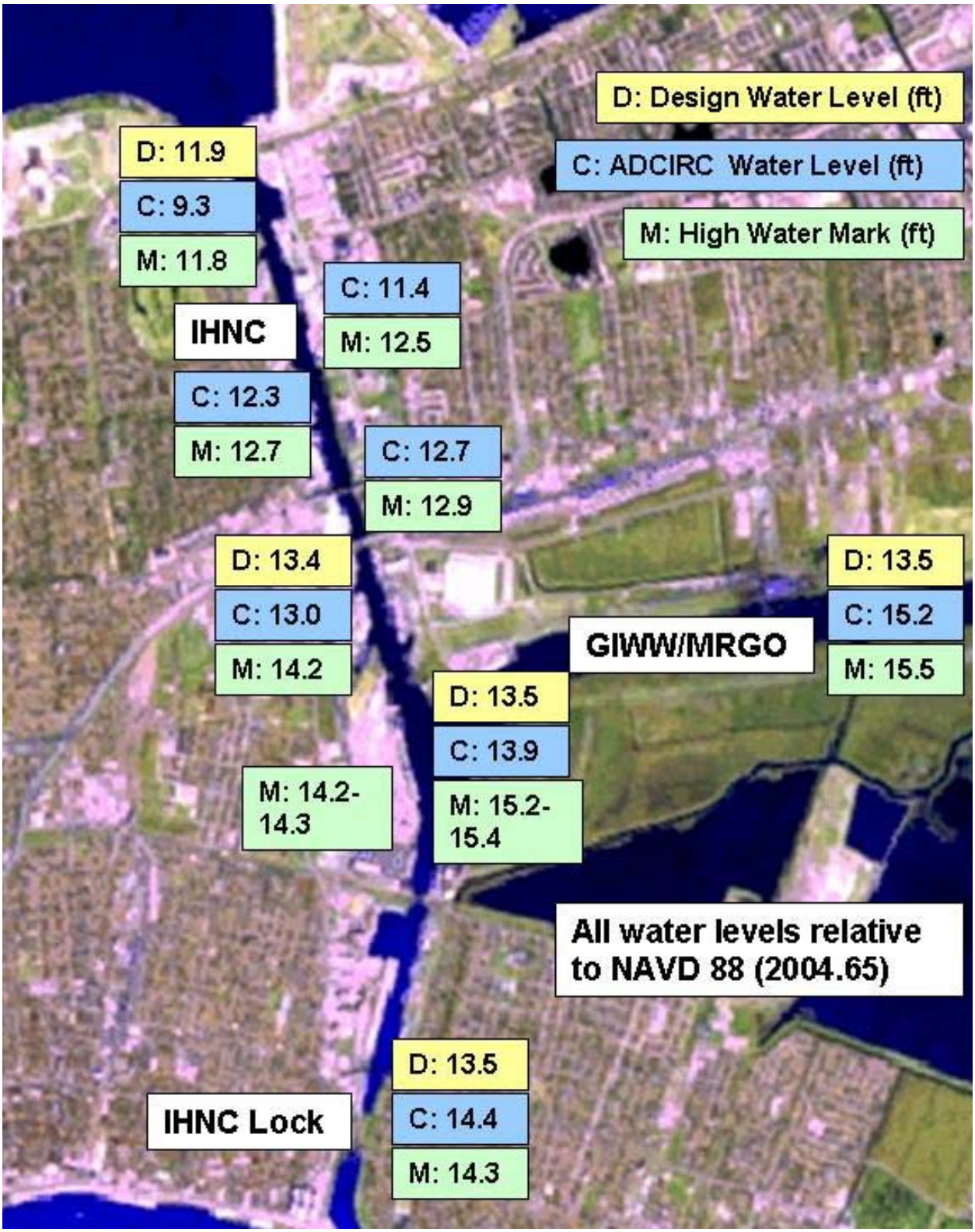

Figure 91. Water level maxima for the IHNC region of the hurricane protection system.

Figure 92 shows water level maxima for southern Plaquemines Parish. For the east-facing levees and flood walls, design water levels ranged from 12.8 to 14.2 ft NAVD88 (2004.65). Few reliable HWM data are available for this region; but model results and the few HWMs suggest that peak water levels during Katrina exceeded the design values south of Phoenix by amounts up to 5.5 ft. On the levees facing west on the west side of the Mississippi River, design water levels ranged from 9.1 to 12.2 ft NAVD88 (2004.65). Model results suggest that peak water levels during Katrina exceeded the design values along the west-facing levees by amounts ranging from 2 to 6 ft.

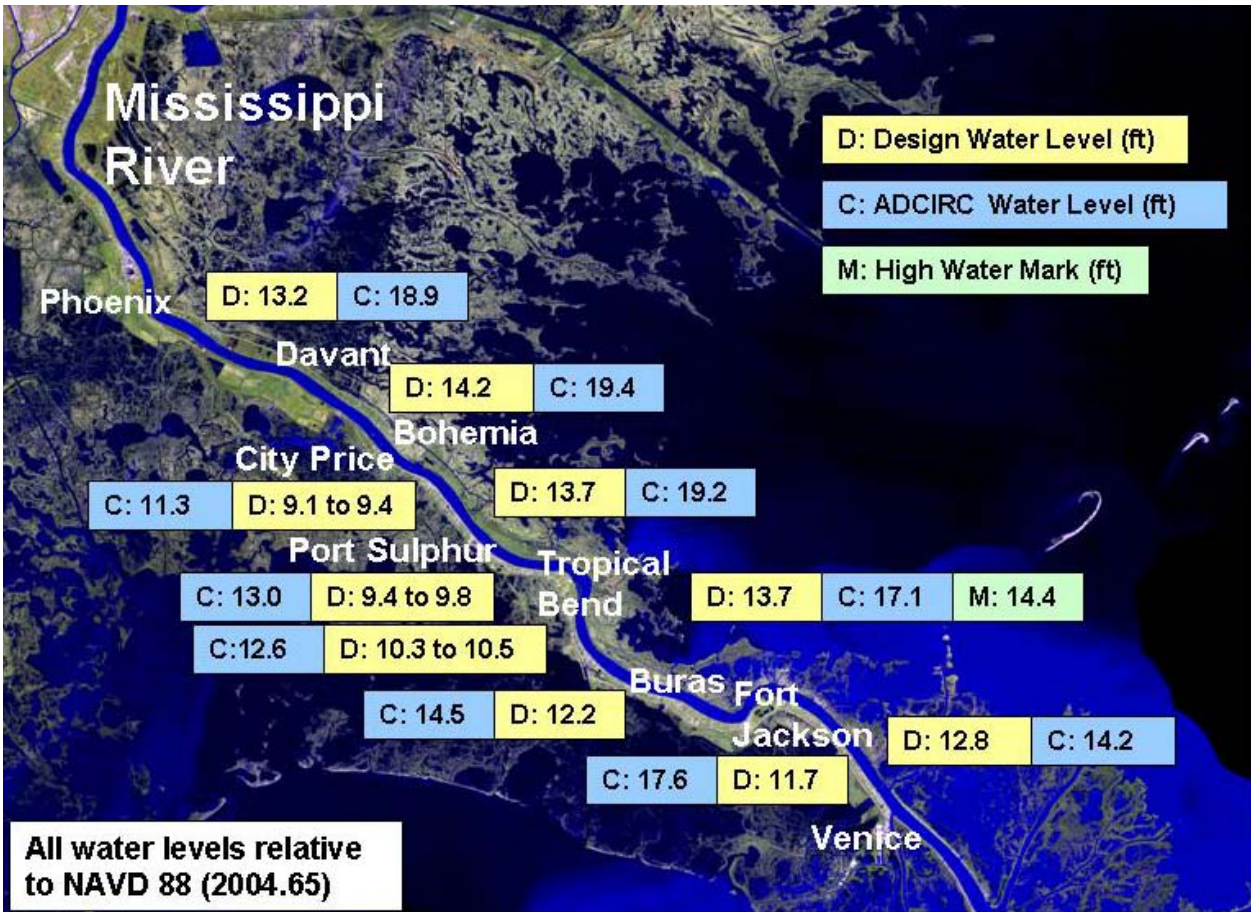

Figure 92. Water level maxima for Plaquemines Parish Hurricane Protection System.

Influence of the MRGO on Storm Surge in New Orleans Vicinity

The Mississippi River Gulf Outlet (MRGO) role in propagation of low amplitude astronomical tide and influx of higher saline water into Lake Pontchartrain has been established. Concerns have been raised regarding the role of the MRGO on storm surge propagation into the metropolitan New Orleans vicinity.

From the perspective of long wave propagation, of which the tide and storm surge are examples, the critical section of the MRGO is Reach 1, the section of waterway where the

GIWW and MRGO occupy the same channel (see Figure 93). It is through this channel that Lake Pontchartrain and Lake Borgne are hydraulically connected to one another via the IHNC. The two lakes are also connected to each other via The Rigolets and Chef Menteur Passes; the IHNC is the smallest of the three connections. Reach 1 existed as the GIWW prior to the construction of the MRGO, although the maintained depth was less. As a result of this hydraulic connection, the storm surge experienced within the IHNC and Reach 1 (GIWW/MRGO) is a function of storm surge in both lakes; a water level gradient is established within the IHNC and Reach 1 that is dictated by the surge levels in both lakes. This is true for both low and high amplitude storm surge conditions.

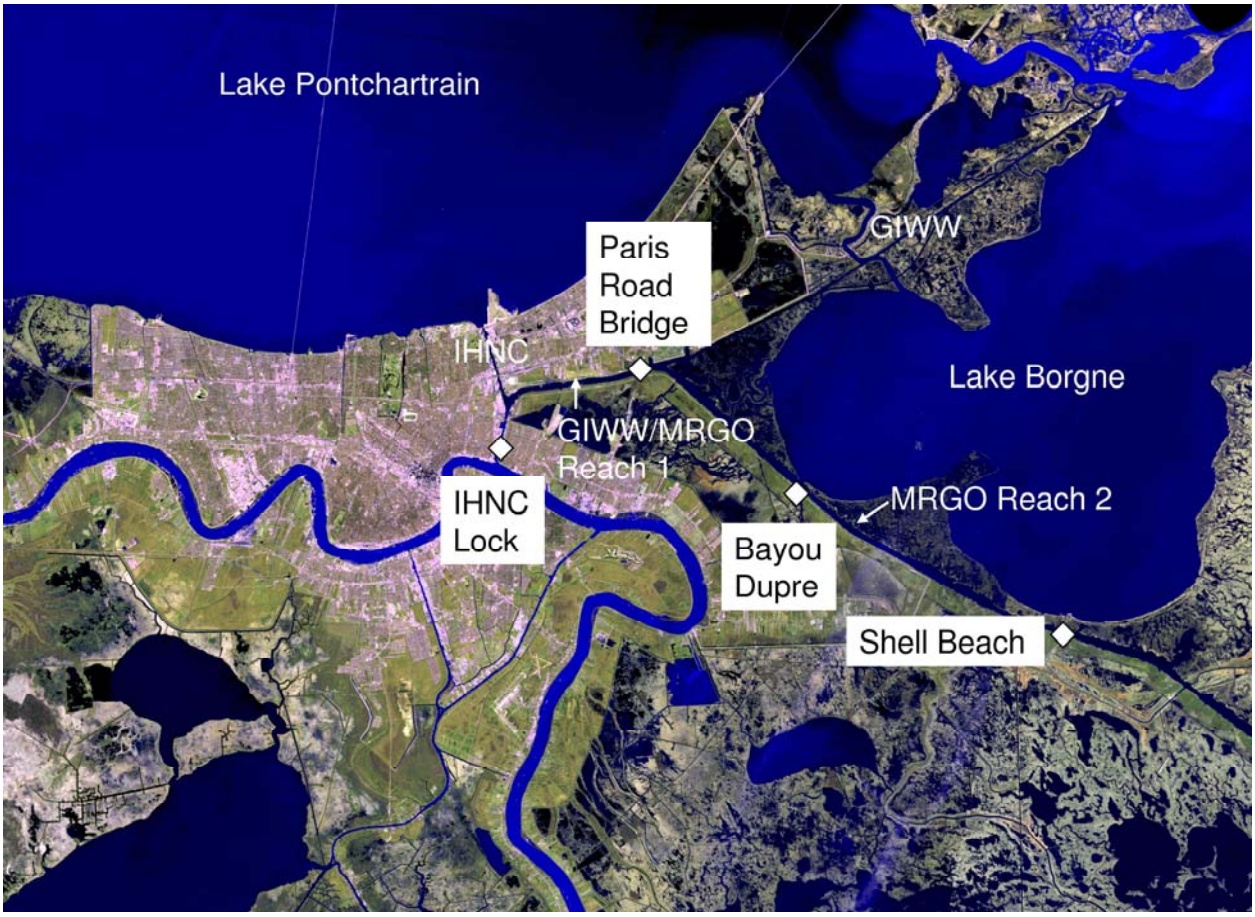

Figure 93. Location of the MRGO (Reaches 1 and 2).

To prevent storm surge in Lake Borgne from influencing water levels experienced in the IHNC or GIWW/MRGO sections of waterway, flow through the Reach 1 channel must be dramatically reduced or eliminated, either by a permanent closure or some type of structure that temporarily serves to eliminate this hydraulic connectivity. The presence of an open channel is the key factor. The hydraulic connectivity existed prior to construction of the MRGO, due to the presence of the GIWW channel. If the hydraulic connectivity between Lake Pontchartrain and Lake Borgne is eliminated at a point within Reach 1, tide or surge to the west of this point will become primarily influenced by conditions at the IHNC entrance to Lake Pontchartrain; and tide

or storm surge to the east of this point will become primarily influenced by conditions in Lake Borgne.

Most concern seems to be focused on MRGO/Reach 2 that runs from the GIWW/MRGO confluence, just east of the Paris Road bridge, to the southeast (see Figure 93). Three previous studies have been performed to examine the influence of MRGO/Reach 2 on storm surge in New Orleans and vicinity (two initiated by the U.S. Army Corps of Engineers and one commissioned by the Louisiana Department of Natural Resources), in addition to work performed to examine this issue as part of the IPET study. All studies have reached the same conclusion. The change in storm surge induced by MRGO/Reach 2 (computed as a percentage of the peak surge magnitude) is greatest when the amplitude of the storm surge is low, on the order of 4 ft or less. In these situations, changes induced by the MRGO in the metropolitan New Orleans area are rather small in terms of absolute water surface elevation changes, 0.6 ft or less in all cases and less than 0.3 ft in most cases, but this amount can be as much as 25 percent of the peak surge amplitude when the amplitude is low. When the long wave amplitude is very low, the surge is more limited to propagation via the channels, and the MRGO has its greatest influence. Once the surge amplitude increases to the point where the wetlands become inundated, this section of the MRGO plays a diminishing role in influencing the amplitude of storm surge that reaches the IHNC. For storm surges of a magnitude produced by Hurricanes Betsy and Katrina which overwhelmed the wetland system, the influence of MRGO/Reach 2 on storm surge propagation is quite small. For Katrina the influence was only a few tenths of a foot at most in the IHNC and GIWW/MRGO in terms of absolute water surface elevation changes. These small changes represent only a few percent of the surge amplitude. When the expansive wetland is inundated, the storm surge propagates primarily through the water column over this much larger flooded area, and the channels become a much smaller contributor to water conveyance. For large surge-producing storm events, construction of the MRGO channel has little influence on water levels in the metropolitan New Orleans vicinity, and in the IHNC.

The hurricane protection levees along the south side of Orleans Parish and the eastern side of St. Bernard Parish along the MRGO, which together are referred to as a funnel, can locally collect and focus storm surge in this vicinity depending on wind speed and direction. This localized focusing effect can lead to a small local increase in surge amplitude. Strong winds from the east tend to maximize the local funneling effect.

Additional detail concerning the work to examine the influence of the MRGO on storm surge, and a more detailed explanation of why the effect is so small at high storm surge levels, is included in Appendix 6, “Note on the Influence of the Mississippi River Gulf Outlet on Hurricane Induced Storm Surge in New Orleans and Vicinity.”

Wave and Surge Modeling Sensitivity Tests

Introduction

A number of tests were performed using the WAM, STWAVE, and ADCIRC models to examine sensitivity of wave and water level computations to uncertainties in primary model

input (wind and representation of several uncertain aspects of the physical system) and to examine the relative contributions of the tide and waves (through radiation stress gradients) to storm water levels. Sensitivity to treatment of surface and bottom shear stress was also examined. The different sensitivity tests are outlined below:

- Wind input
- Surface wind drag parameterization
- Deflation of the Chandeleur Islands
- Wetland roughness changes and bottom friction formulation
- Role of tide and wave forcing

Results from the sensitivity tests are summarized here. Additional results and discussion can be found in Appendices 3, 4, and 5.

Sensitivity to Wind Input

Accurate wind input is crucial to accurate modeling. The method applied in this investigation to develop surface winds was very comprehensive, the most rigorous analysis ever done by HRD for the core wind fields in a hurricane. However, the developed wind fields still have inaccuracies and therefore have uncertainty inherent in them, certainly on the order of 5 percent and perhaps more in some situations. There is also uncertainty in the gust factor used to convert 1-min average winds to 30-min or 10-min average winds. HRD and OWI recommend use of slightly different conversion factors which vary on the order of 5 percent. Sensitivity of wave and surge computations to ±5 percent change in wind speed input was assessed. Wind fields for the base case, the final H*Wind/IOKA winds, were subjected to a ±5-percent change in magnitude over the entire domain and over the entire duration of the simulation. In general, accuracy and uncertainty in wind estimates is expected to be more randomly varying in space and time; therefore, this sensitivity test is somewhat conservative. However, the ramifications of a systematic overprediction or underprediction in the surface wind fields provide valuable insight to sensitivity of results to wind field uncertainty. The wind fields were multiplied by 1.05 for the plus 5 percent case and multiplied by 0.95 for the minus 5 percent case. This approach of a simple multiplication factor produces the largest change in the wind forcing function in the core of the hurricane, and less of a change in the far field.

Offshore Wave Sensitivity

Wave model results generated using the altered wind input were then evaluated over the full grid, and at specific points in the domain where measurements were available. Model results for the altered-wind cases were compared to the base case results and compared to wave measurements. Results of these tests were input to the nearshore wave model in the form of two-dimensional wave spectra to force the sensitivity runs in the nearshore domains.

For the plus 5 percent case the magnitude of the increase in maximum significant wave height in the basin domain is from 54.7 to 57.0 ft, 2.3 ft, and its location is moved slightly north (from 26.7 deg to 27.0 deg) compared to the base case. On the regional domain, for the plus 5 percent case, increasing the wind magnitude increases the maximum value by a similar

amount, from 53.6 to 56.1 ft, or about 2.5 ft. Figure 94 shows a plot of wave height differences between the plus 5 percent case and the base case for the regional wave model domain. Red contours denote areas of wave height increase; blue denotes areas of wave height decrease. The largest increase, 6.3 ft (denoted by the black dot in the figure), was computed west of the Mississippi River delta. Generally, wave heights are increased as expected. However, as seen in Figure 94, wave heights decrease in some places. Longer period energy exists, and the increase in wind speed can increase the wave period. Longer period waves are more susceptible to depth effects, refraction, shoaling and, therefore, the pattern of wave breaking is more strongly influenced. In shallow water, there are local decreases in wave height, due to shallow water effects, such as in the vicinity of the Chandeleur Islands.

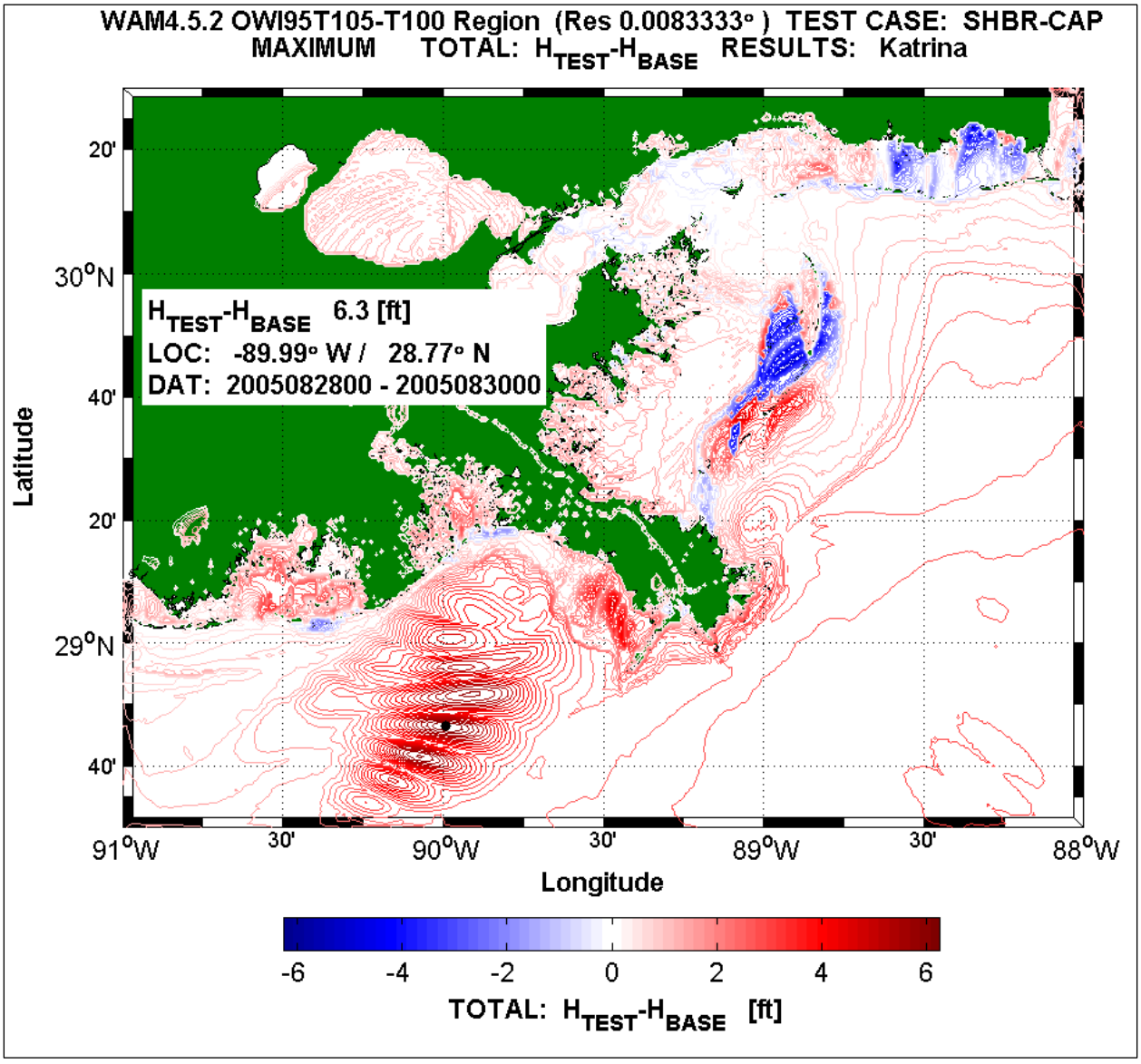

Figure 94. Color contour of the difference between Test Case 1 (plus 5 percent winds - base case) maximum wave height conditions in the region domain.

For the minus 5 percent case, results mirror those for the 5 percent wind speed increase case. Wave heights generally decrease. The magnitude of the decrease in maximum significant wave height in the basin domain is 2.4 ft, from 54.7 to 52.3 ft. For the regional domain, the maximum significant wave height decreases to 50.8 ft compared to the base case result of 53.6 ft, a net reduction of 2.8 ft. There are areas of wave height increase, despite a decrease in wind speed, as was seen for the wind-increase case.

Figure 95 shows the variation of computed significant wave height at the location of NDBC Buoy 42040, which is located in deep water east of the Mississippi River delta, for the base case, plus 5 percent and minus 5 percent cases. Recall the WAM results were found to underestimate peak wave heights at this location by 14 ft during the peak conditions of Katrina. Increases and decreases to the wind speed, by ±5 percent, change the wave heights by about 3 ft at most at this location. The wind speed changes do not explain the differences in observed and computed wave heights. The downshifting in peak wave period for the increased wind speed results occurs about an hour earlier, but not to the degree that is required to match the measurements (occurring about 7 hr earlier). The mean period results show similar trends as the wave heights, a near uniform offset between the plus and minus 5 percent simulations, remaining biased low compared to the buoy data. The model vector mean wave direction shows little change between the simulations.

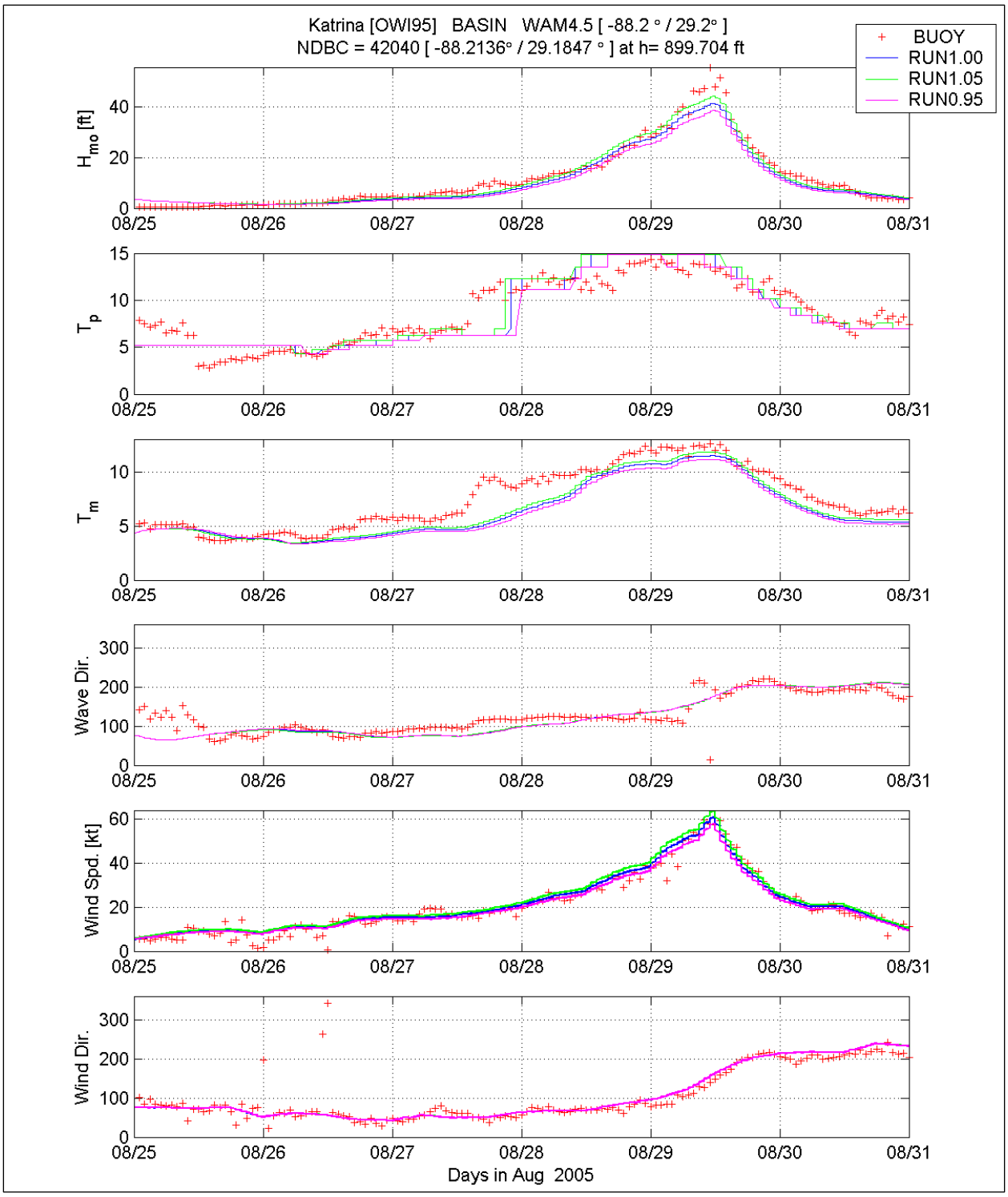

Figure 95. Comparison of WAM Cycle 4.5 basin-scale (blue line), sensitivity tests for plus 5 percent winds (green line) and minus 5 percent winds (magenta line) to the measurements at NDBC 42040. [Time is referenced to UTC].

Storm Surge Sensitivity

Increasing the wind speed by 5 percent increases peak surge by 1 to 3 ft throughout the Hurricane Katrina impacted area, with the greatest increases in water level along the Mississippi coast (see Figure 96). The maximum surge for the Mississippi coast near Hurricane Katrina landfall is approximately 2.5 to 3.4 ft greater than maximum surge for the base condition. Peak surge along the southern shoreline of Lake Pontchartrain is increased by approximately 0.6 to 1.0 ft with the increased wind speed. Along Lake Borgne, surge is increased by approximately 1 to 1.5 ft. Increases along south Plaquemines Parish, for both east- and west-facing levees, range from 1 to 2 ft. Decreasing the wind speed by 5 percent has the opposite effect, decreasing water levels by nearly the same amounts along the hurricane protection system (see Figure 97). The greatest decreases in water level are along the Mississippi coast.

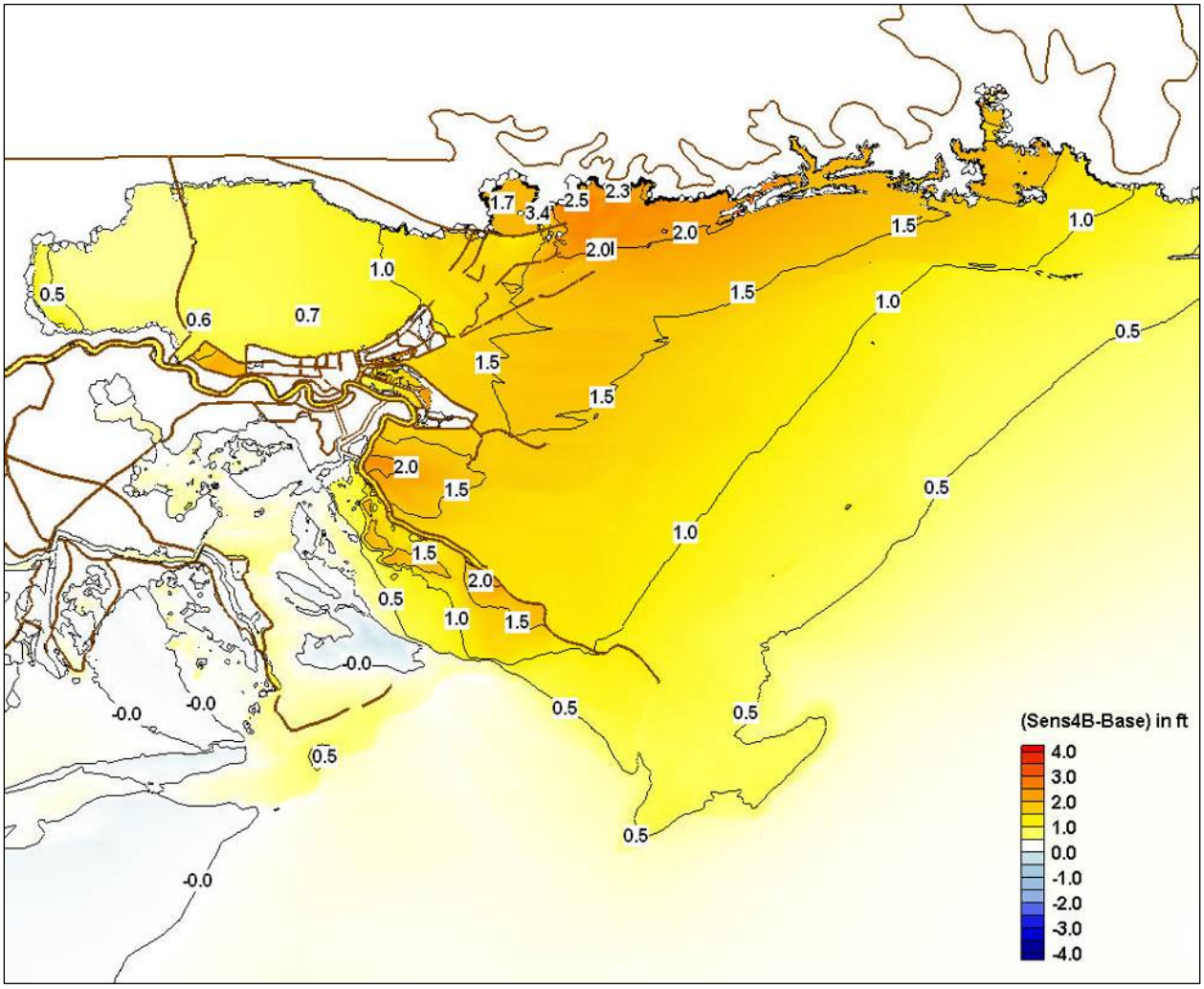

Figure 96. Difference in peak surge between sensitivity simulation with 5 percent increase in wind speed and the base simulation.

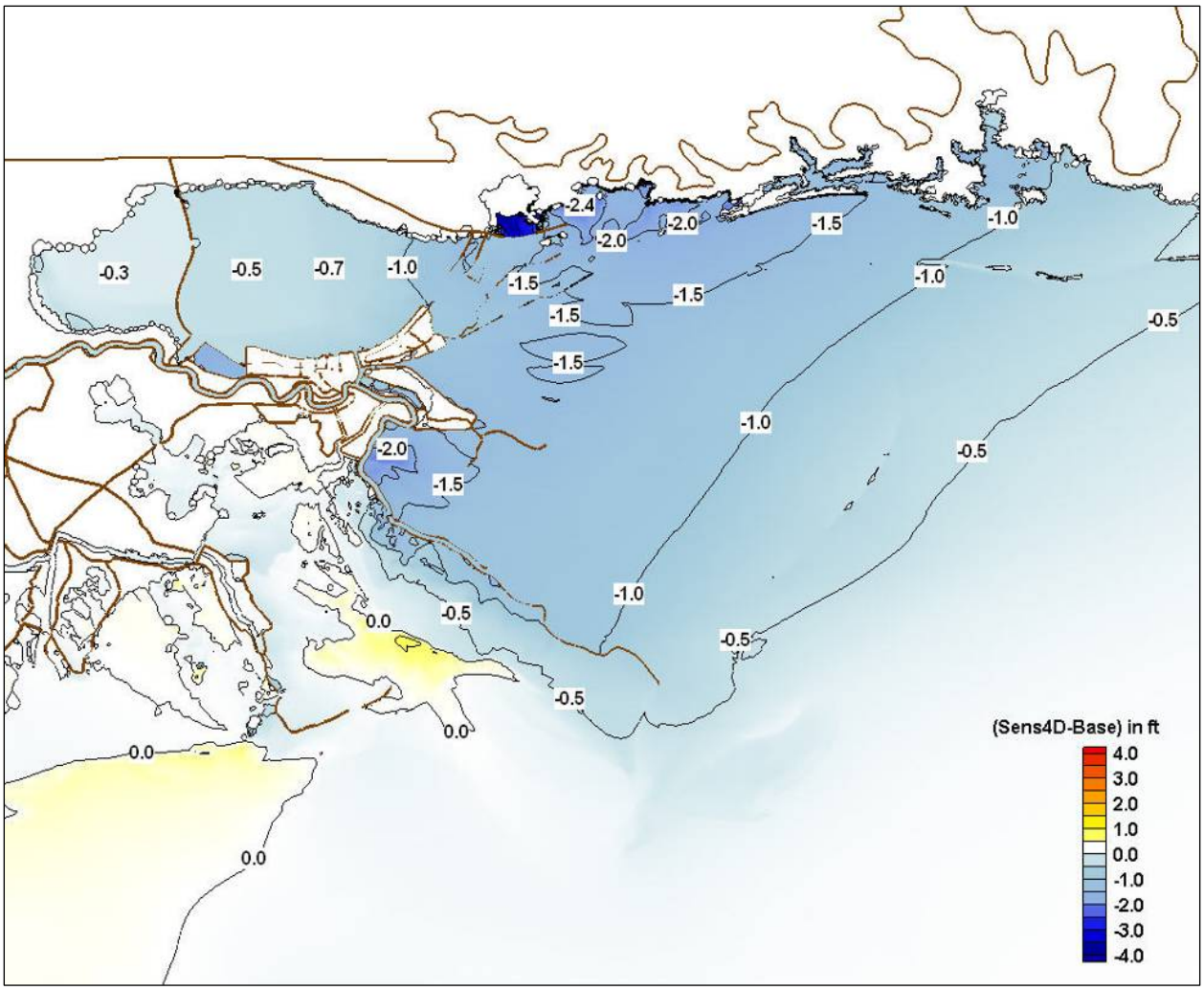

Figure 97. Difference in peak surge between sensitivity simulation with 5 percent decrease in wind speed and the base simulation.

Nearshore Wave Sensitivity

Wind input enters into STWAVE in three ways: through the offshore waves input at the boundary, through the surge, and through the local wave generation within the STWAVE grids. The importance of each component varies with location in the grid (offshore areas are influenced more by the offshore input and nearshore, protected areas by the local winds and surge). As was done for the offshore waves, two wind sensitivity simulations were performed; one increased the wind speed by 5 percent and one decreased the wind speed by 5 percent. Wind errors are likely to be random and partially cancel out through the integration of modeling, but a simplistic approach was selected to put realistic bounds on the solution. STWAVE was run for all four grids with the plus and minus 5 percent winds (and the offshore wave and surge generated from the same plus and minus 5 percent wind fields).

In Lake Pontchartrain, the maximum increase in wave height due to the plus 5 percent winds is approximately 0.8 ft on the southeast shore of the lake (Figure 98), and the maximum decrease

due to the minus 5 percent winds is approximately 0.4 ft (Figure 99). For both cases there are some larger differences on the periphery of the lake, particularly the northeast shore, where the surge is a large percentage of the water depth. The differences in wave height increase across the lake (northwest to southeast), then decrease where the waves are locally depth limited, and then increase again very near the shore due to the increase in local water depth due to the differences in surge in very shallow water.

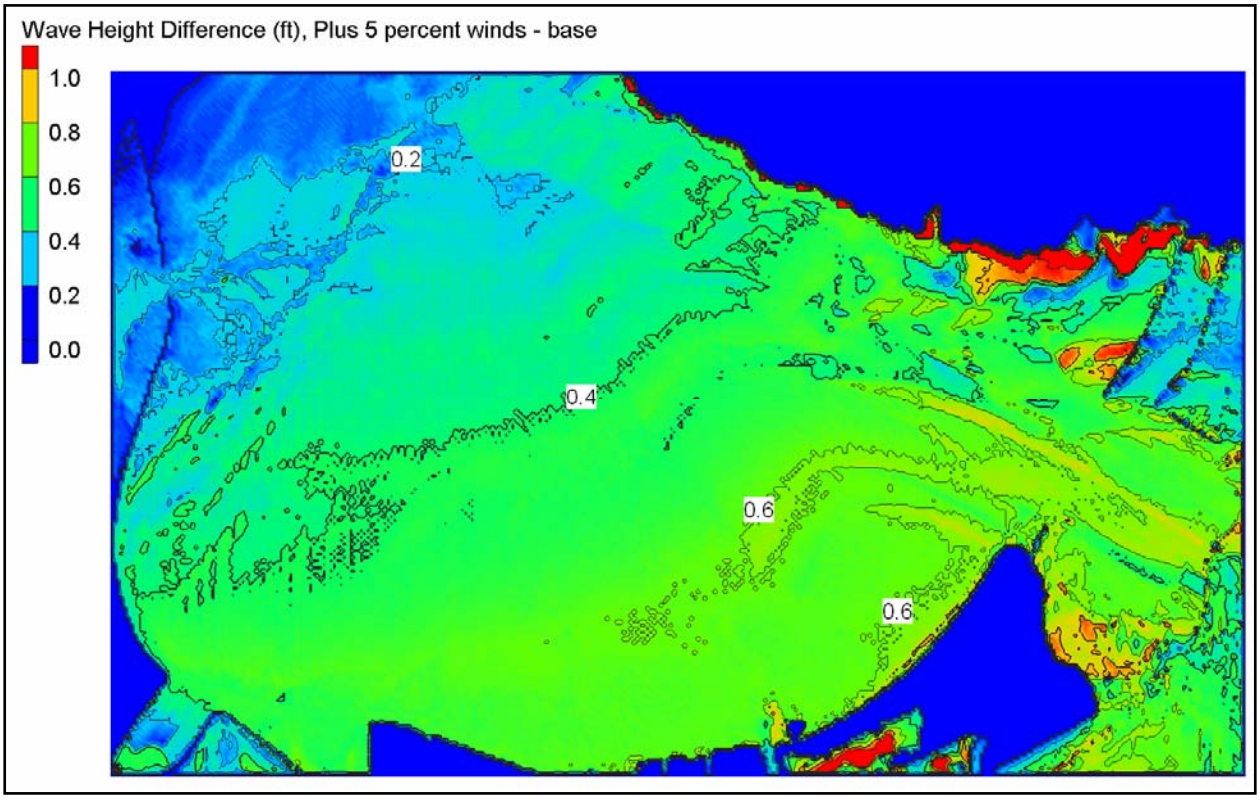

Figure 98. Differences in maximum significant wave height for sensitivity run with 5 percent increase in wind speed for Lake Pontchartrain (plus 5 percent – base).

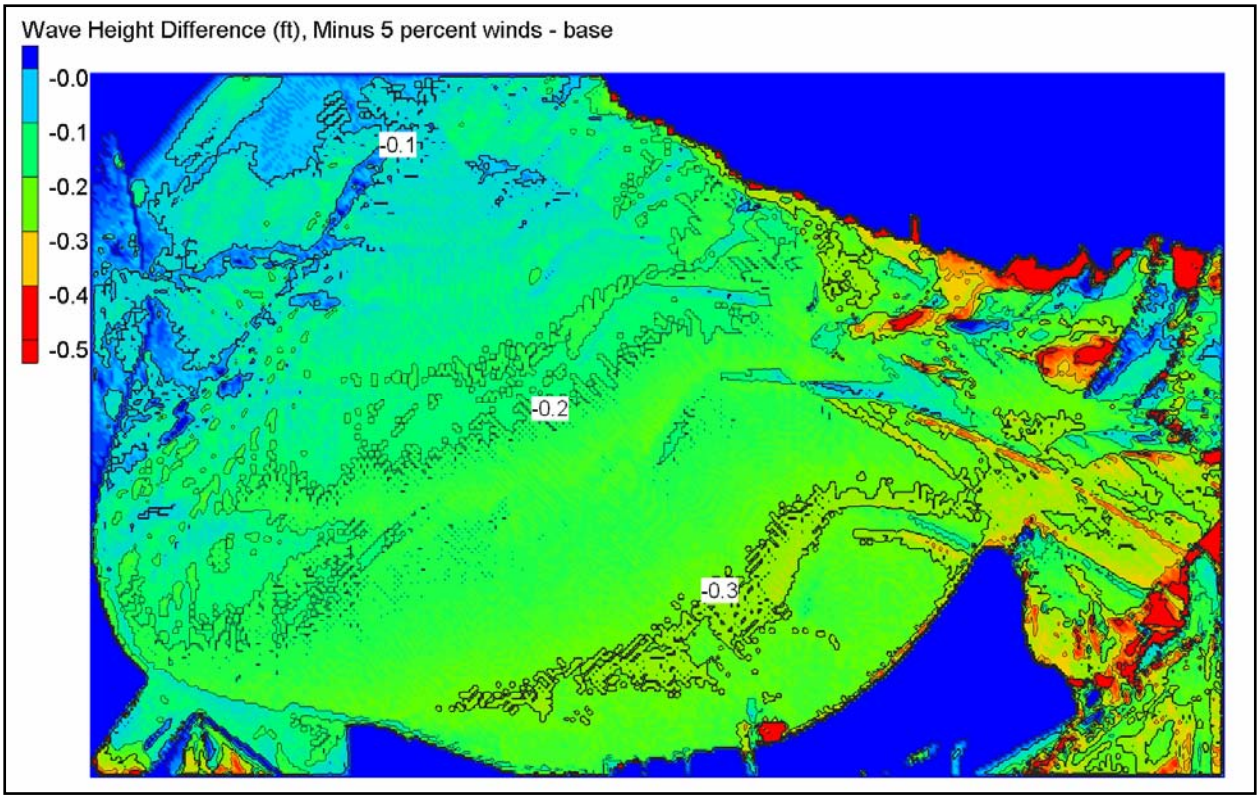

Figure 99. Differences in maximum significant wave height for sensitivity run with 5 percent decrease in wind speed for Lake Pontchartrain (minus 5 percent – base).

For the southeast grid, the maximum increase in wave height due to the plus 5 percent winds is approximately 0.5 to 1 ft along the levees (Figure 100), and the maximum decrease due to the minus 5 percent winds is approximately 0.5 to 1 ft. There are larger differences outside the Chandeleur Islands (increase of 2 to 3 ft for the plus 5 percent winds and 1.5 to 2.5 ft decrease for the minus 5 percent winds). For the south grid, the maximum increase along the barrier islands was approximately 2 ft due to the plus 5 percent winds and the maximum decrease along the barrier islands was approximately 2 ft for the minus 5 percent winds. Along the Mississippi River Levees, waves increased approximately 0.5 ft for the plus 5 percent winds and decreased 0.5 to 1 ft for the minus 5 percent winds. In the wetland areas behind the barrier islands there was a decrease in wave height of 0.5 to 1 ft for both the plus and minus 5 percent winds, most likely because winds were blowing offshore locally (reducing surge for the plus 5 percent winds). At the grid boundary, the wave heights increased 1.5 to 3.5 ft for the plus 5 percent winds and decreased 1.5 to 3 ft for the minus 5 percent winds. For the Mississippi/Alabama grid, the maximum increase in wave height due to the plus 5 percent winds is 1 to 2 ft at the barrier islands (locally up to 2.6 ft offshore of Horn Island) and 0 to 1 ft at the interior shorelines (average of approximately 0.5 ft). The maximum decrease in wave height due to the minus 5 percent winds is 1 to 2 ft at the barrier islands and 0 to 1 ft at the shoreline. The differences in peak wave period over all grids were generally 1 sec or less (increase in peak period for the plus 5 percent winds and decrease in peak period for minus 5 percent winds).

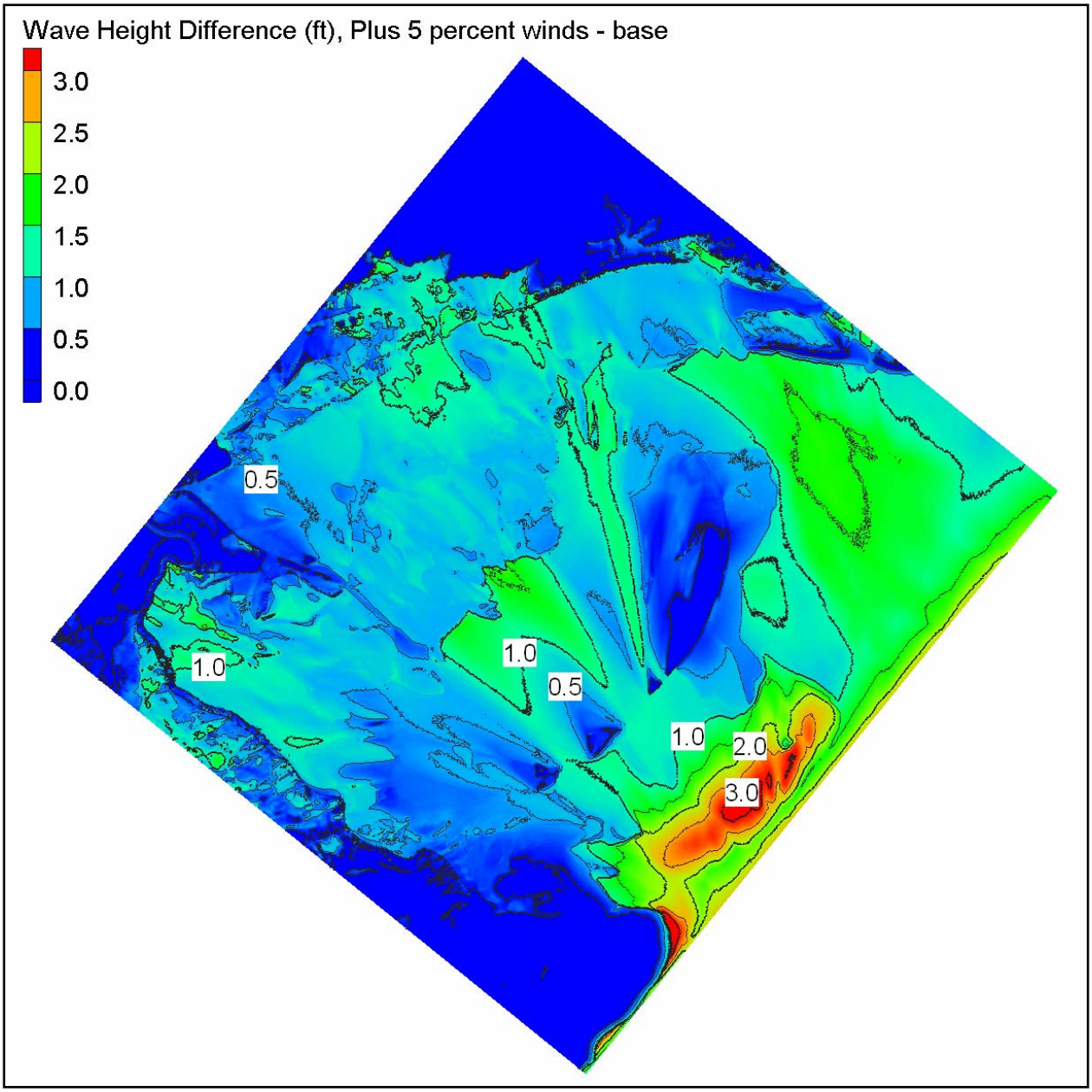

Figure 100. Differences in maximum significant wave height for sensitivity run with 5 percent increase in wind speed for Southeast Louisiana (plus 5 percent – base).

Although wind is the critical parameter for predicting waves and surge, the 5 percent increase and decrease in winds for the coupled simulations generally produced nearshore waves at the shoreline of ±1 ft (or less) of the base simulations. The differences were larger, ±1 to 3 ft, offshore of the barrier islands.

Sensitivity to Surface Wind Drag Parameterization

Work to examine the sensitivity of surge model results to a cap on the surface drag coefficient was also done. Many researchers and practitioners in the wind and offshore wave modeling communities have embraced the concept of capping the surface wind drag for high wind speeds (a cap was applied in the base case offshore wave modeling done as part of this study). The concept has not been as widely accepted in the storm surge modeling community (a cap was not imposed for the base case storm surge simulations done in this study). Additional research is needed on this topic. Sensitivity of surface wind drag formulation was only examined in the context of storm surge modeling.

The standard method for applying surface wind stress within storm surge models is the quadratic stress law via a surface drag coefficient, Cw, as is the case in ADCIRC. This coefficient is based on regression fits of field measurements, under conditions of moderate to strong wind speed, and has been found to be directly related to wind speed, wave state and atmospheric stability (Garratt 1977, Large and Pond 1981 and Trenberth et. al. 1989). The base case ADCIRC results used the wind stress formulation of Garratt in which the wind drag coefficient increases with increasing wind speed. Recent research (Powell 2003) has found that under extreme winds, the linear extrapolation of the drag coefficient provides a clear overestimate of Cw and that the enforcement of a drag coefficient limit may be appropriate. Sensitivity simulations were done to examine the influence of applying an upper limit, or cap, to the drag coefficient. Two tests were done, one using the Garratt formulation but with a limit to the drag coefficient of 0.0025, and a second using the Amorocho and DeVries (1980) wind stress formulation which has slightly more drag at lower wind speeds than the Garratt formulation, but has a cap on the wind drag coefficient of about the same value.

Figures 101 and 102 show results for the Garratt-with-limit and the Amorocho and DeVries wind drag coefficient formulations, respectively. Applying a wind drag cutoff decreases peak surge by amounts up to 4 ft, with the greatest decreases evident along the Mississippi coast (Figure 101) compared to the base case. The decrease in peak surge near St. Bernard Parish is 1 to 2 ft and the decrease near Plaquemines Parish is approximately 2 ft. Decreases in Lake Pontchartrain are approximately 0.5 to 1 ft. Applying the Amorocho and DeVries wind stress formulation results in a slightly smaller reduction in peak surge than the wind drag cutoff reduction applied to the Garratt formulation (see Figure 102), but the overall pattern is quite similar. All changes in the wind forcing cause the greatest change in peak surge along the Mississippi coast, and similar patterns of change in Plaquemines Parish, St. Bernard Parish, and Lake Pontchartrain.

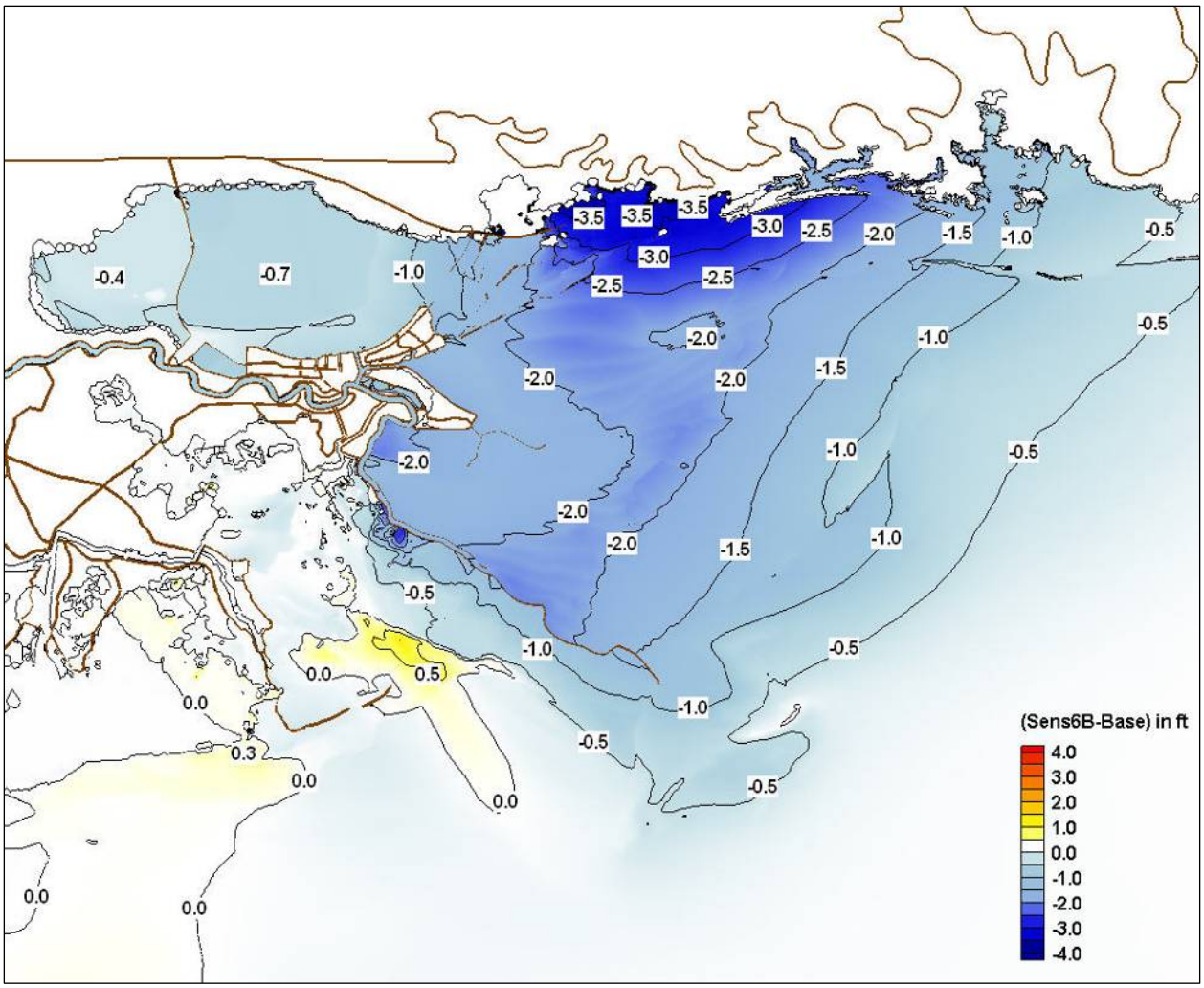

Figure 101. Difference in peak surge between sensitivity simulation with wind drag cutoff (applied to Garratt wind stress formulation) and the base simulation.

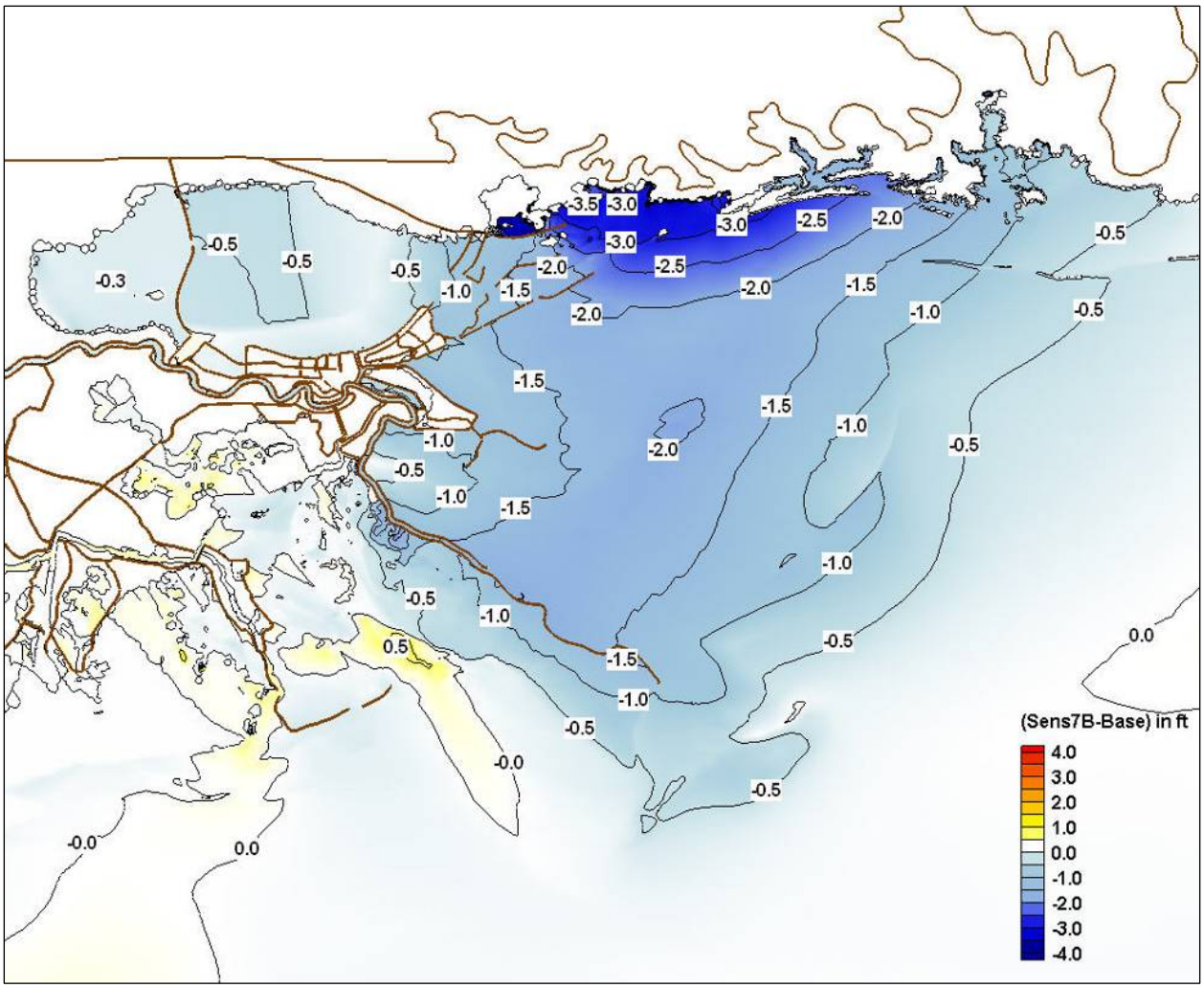

Figure 102. Difference in peak surge between sensitivity simulation with Amorocho and DeVries wind stress formulation and the base simulation.

Sensitivity to Chandeleur Island Deflation

Hurricane Katrina changed the configuration of the Chandeleur Islands, degrading their condition in terms of elevation and areal extent. Deflation of this barrier island chain has been well documented by the USGS (see *http://coastal.er.usgs.gov/hurricanes/katrina/photo-comparisons/chandeleur.html*). The majority of the loss of emergent areas was from the southern end of the main island. A LIDAR survey of the barrier islands collected after Hurricane Katrina showed that approximately half of the barrier islands that had been emergent prior to the storm were submerged after the storm. These changes occurred sometime during the storm, but exactly when during the storm and the rate at which the changes took place are unknown. Therefore, sensitivity tests were done to examination changes to nearshore wave and storm surge results attributable to these topographic changes. All base case wave and surge modeling was done assuming a pre-Katrina condition, i.e. no barrier island degradation. Model simulations were

done using post-Katrina barrier island conditions, and results were compared to the pre-Katrina base-case results.

There is also great interest in how a deflated barrier island may lead to increased erosion of wetlands and other coastal regions in the lee of these islands. Deflation of the protective barrier islands along the Mississippi and Louisiana coast may leave these regions more vulnerable to exposure and inundation associated with future hurricane storm surge and waves. This series of sensitivity tests provides some insight into this issue.

Storm Surge Sensitivity

A SHOALS LIDAR survey of the barrier island was collected after Hurricane Katrina (Fall 2005) and it shows that approximately half of the barrier island that was previously emergent had become submerged after Hurricane Katrina (Figure 103). The majority of the loss of emergent area was from the southern end of the island. The post-Katrina configuration of Chandeleur Island was incorporated into the ADCIRC mesh for the sensitivity simulation and the model was rerun. The results shown in Figure 104 indicate that deflation of Chandeleur Island provided a means for a greater volume of water to pass over the island and increase water levels landward of the island. In general, peak water levels along the east-facing levees increase 0.2 to 0.4 ft for the post-storm configuration of the islands. Peak water levels in Lake Pontchartrain increase by amounts ranging from 0.1 to 0.3 ft. The largest increase, 0.5 ft, occurs immediately in the shadow of the islands.

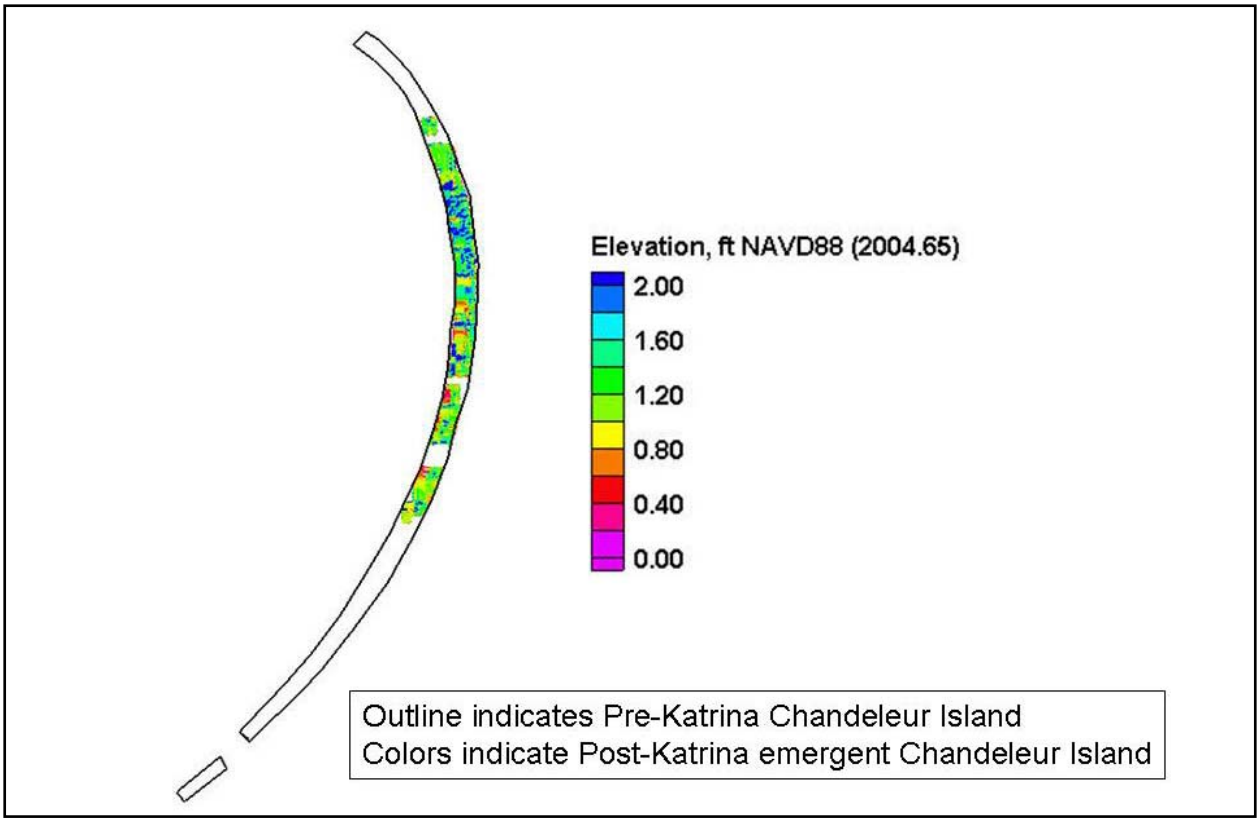

Figure 103. Pre-Katrina and post-Katrina configuration of the Chandeleur Islands.

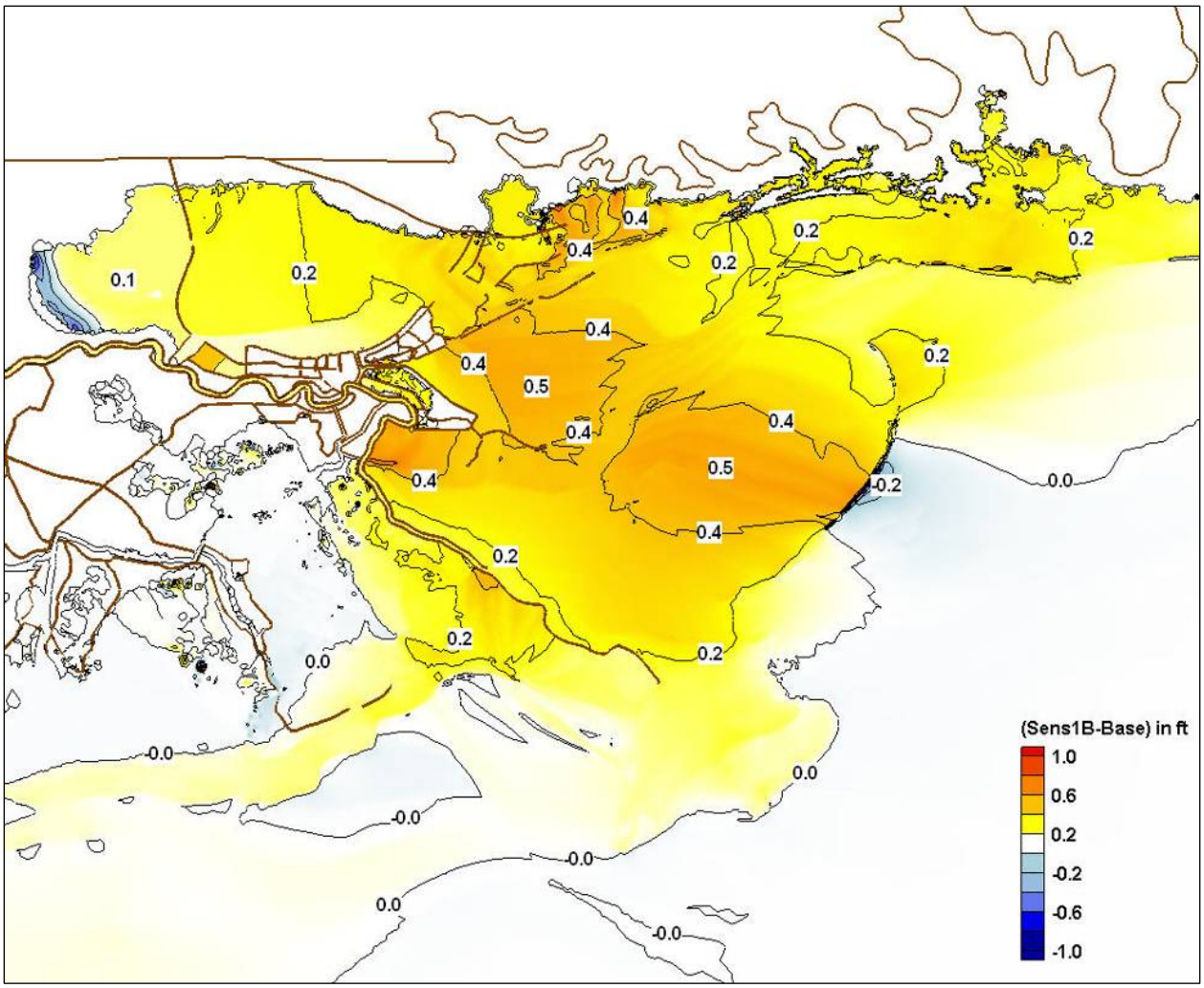

Figure 104. Difference in peak surge between sensitivity simulation with post-Katrina configuration of Chandeleur Island and the base simulation.

Nearshore Wave Sensitivity

Bathymetry interacts with wave processes through shoaling (which generally increases wave heights in shallower depths), refraction (which turns waves to be more shore-normal in shallower depths), and depth-limited breaking (which reduces wave height when the breaking threshold is reached). In general, small errors in water depth result in small errors in wave parameters (shoaling is a function of depth to exponent ¼ and breaking is approximately linearly related to depth) and the impact is typically local. A possible exception to this is wave attenuation across the barrier islands, which protect the areas in their shadow.

To investigate the impact of Chandleuer Island degradation on the nearshore waves and surge, STWAVE was run with the Chandeleurs in the same degraded state outlined above. The Chandeleurs are on the Southeast STWAVE grid, so only that grid was run. Surge values from ADCIRC with the degraded Chandeleurs were used as input together with offshore waves and winds from the base runs. Figure 105 shows the differences in maximum significant wave height

for the degraded Chandeleur run minus the base run. The maximum increase in wave height is approximately 6 ft directly in the lee of the island. Close to the shoreline, the differences are reduced to near zero. There are (very) small differences in other parts of the grid resulting from small differences in the surge. The barrier islands do significantly reduce the wave height in the nearshore area, even in a degraded state. The degraded islands allow more wave energy to pass over them and propagate into the sound. For the Chandeleurs, the impact on waves at the shoreline of the degraded islands was relatively small (because the wave height is depth limited in the shallow wetland areas between Chandeleur Sound and Lake Borgne), but increased wave energy in Chandeleur Sound would likely cause further degradation of these wetlands. The protection afforded by barrier islands for the shoreline and wetlands in their shadow is dependent on the elevation of the islands, degree of submergence of the islands during the storm, distance to the islands from the shore, and characteristics of the storm.

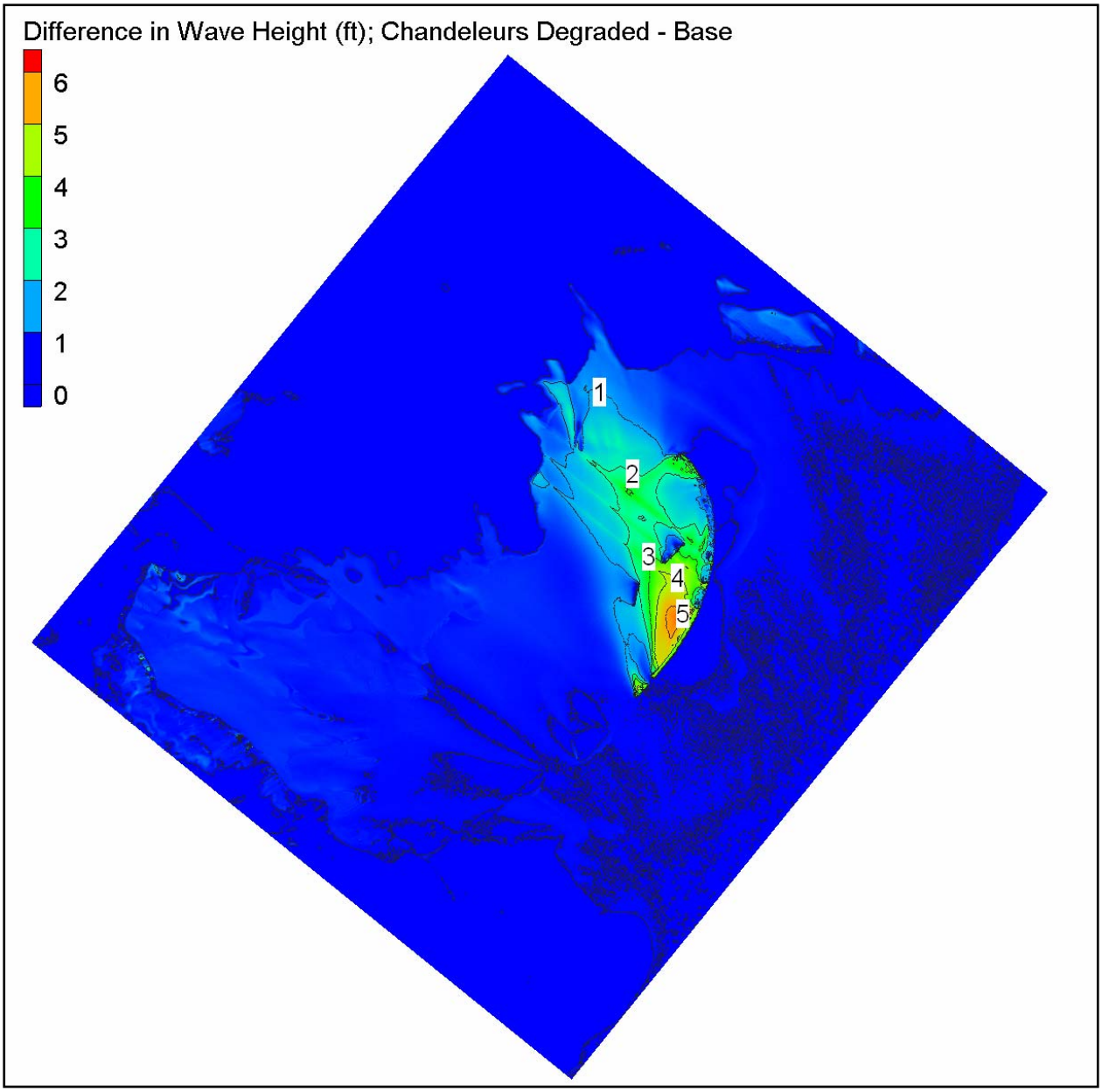

Figure 105. Differences in maximum significant wave height for sensitivity run with Chandeleur Islands degraded for Southeast Louisiana (degraded bathymetry – base).

Sensitivity to Wetland Roughness Changes and Bottom Friction Formulation

The storm altered portions of the Southeast Louisiana landscape, stripping away vegetation cover in some areas. These changes occurred sometime during the storm, but exactly when during the storm and the rate at which the changes took place are unknown. All base case wave and surge modeling was done assuming a pre-Katrina condition. Therefore, sensitivity tests were done to examine changes to wave and storm surge associated with these wetland roughness changes.

It is unclear whether or not the vegetation will recover, and if so, over what time period. The full impact of the storm on the wetlands (not only on vegetation but also on topographic relief) is unclear. There is great interest in wetland restoration of Southeast Louisiana as a means for reducing the wave and storm surge impacts of hurricanes. These sensitivity tests provide useful insights on this issue.

Storm Surge Sensitivity to Bottom Friction Formulation

Bottom friction parameterization in the base ADCIRC simulation applies a constant value of C_f. Sensitivity of model predicted peak surge to this parameter was examined by performing two variable-friction sensitivity simulations. In the first, the pre-Katrina friction formulation was changed from a single value of C_f to a spatially-varying Manning's n friction field to represent pre-Katrina vegetation. The purpose of this simulation is to examine differences between a broad (constant value) description of bottom friction versus a detailed representation of bottom friction. In the sensitivity simulation, a spatially-varying friction field was applied to represent different pre-Katrina vegetation types including herbaceous wetland, woody wetland, swamp, scrubland, orchard, grassland, pasture, crops, recreational grass, fallow, sand, gravel, Cypress forest, deciduous forest, evergreen forest, mixed forest, as well as city conditions including low residential, high residential, and commercial areas. In the second sensitivity simulation, the spatially-varying friction field was adjusted to represent post-Katrina conditions and was compared to the base condition and the pre-Katrina spatially-varying friction field simulation.

Figure 106 shows changes due to different parameterizations of the bottom friction (constant versus variable Manning's n formulations). Some areas along the Mississippi coast are increased by as much as 2.5 ft, relative to the base case. Along the east-facing levees of Southeast Louisiana, there are both increases and decreases. Decreases of up to 2 ft are evident near the area of English Turn in north Plaquemines Parish. Elsewhere along the east-facing levees, peak water levels were increased by amounts of up to 1 ft. Negligible changes occur along the south shore of Lake Pontchartrain. In general, changing the pre-Katrina friction formulation from a single value to a spatially-varying field that represented pre-Katrina vegetation results in an increase in peak water level in deeper water and a decrease in water level in the overland areas (Figure 106).

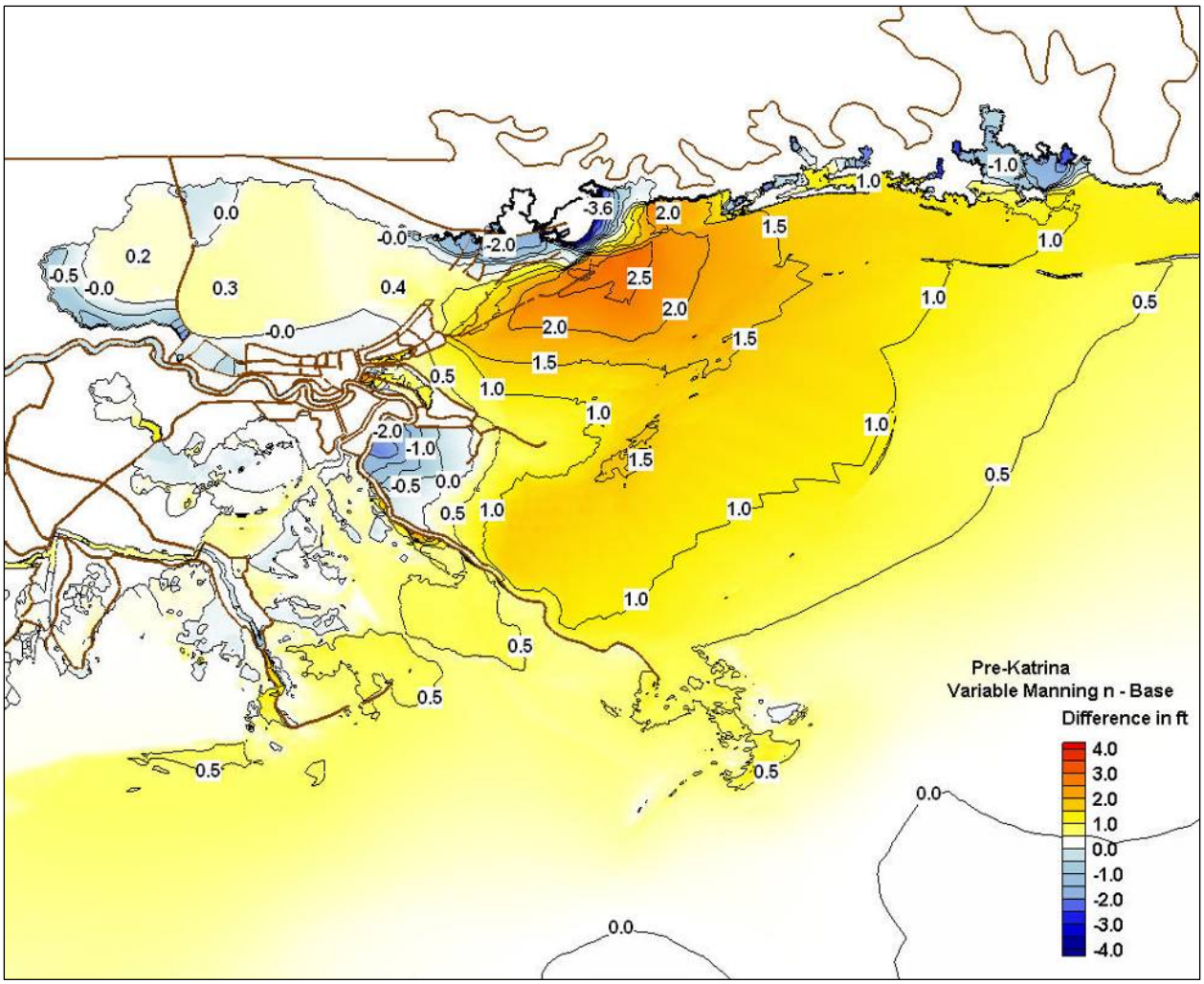

Figure 106. Difference in peak surge between sensitivity simulation with pre-Katrina variable friction and the base simulation.

Storm Surge Sensitivity to Vegetation Cover Changes

Vegetation cover changed considerably during Hurricane Katrina. A significant number of acres of wetland were lost. In the second bottom friction sensitivity simulation, changes to the spatial extent of vegetative marshes are simulated to determine the significance of marsh loss to peak surge levels. USGS maps of pre-Katrina and post-Katrina vegetation cover (Figures 107 and 108) show that there was a decrease in marsh area (increase in open water), particularly in St. Bernard and Plaquemines Parishes. Many of the wetland areas appear less solid and more web-like due to the increase in open water. In this sensitivity simulation, the spatially-varying friction field was adjusted to represent post-Katrina conditions. Frictional resistance at grid nodes that were defined to be in open water following the storm was set to open-water values.

Figure 109 shows the differences in storm surge for the spatially variable friction formulation, for pre- and post-Katrina wetland vegetation cover conditions. The comparison shows that the reduction in vegetation (increase in amount of open water) results in an increased

peak surge of 0.5 to 1.5 ft throughout a broad region. In the vicinity of English Turn, the increases are greatest, approximately 1.5 ft.

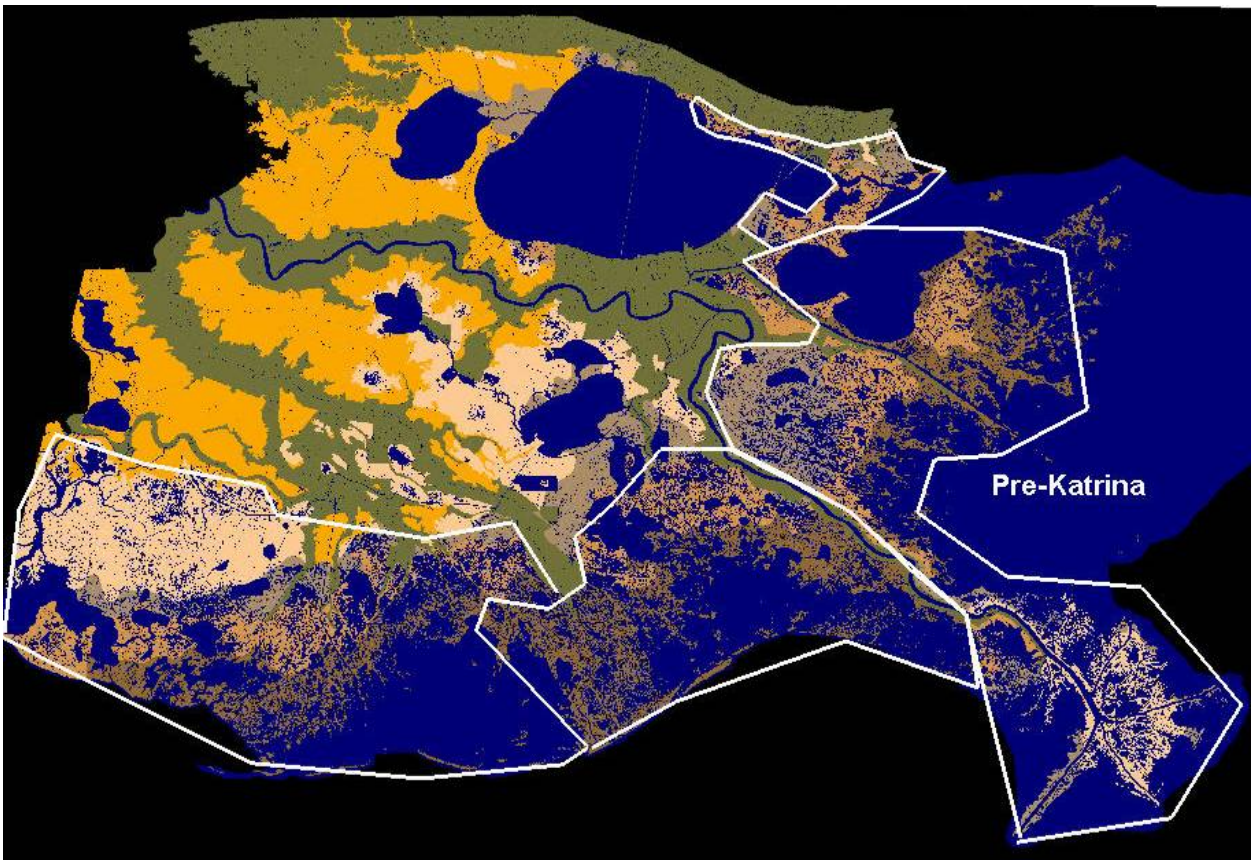

Figure 107. Pre-Katrina vegetation coverage (from the USGS).

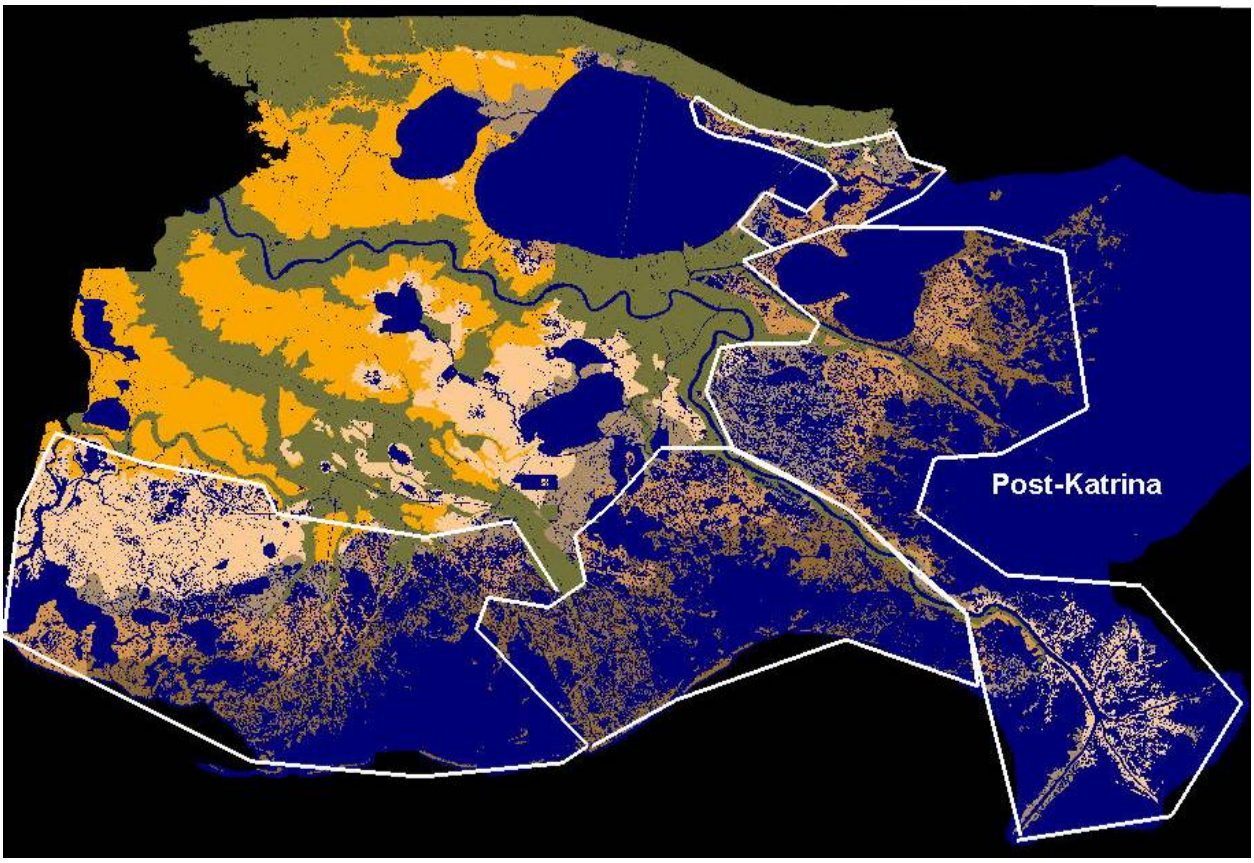

Figure 108. Post-Katrina vegetation coverage (from the USGS).

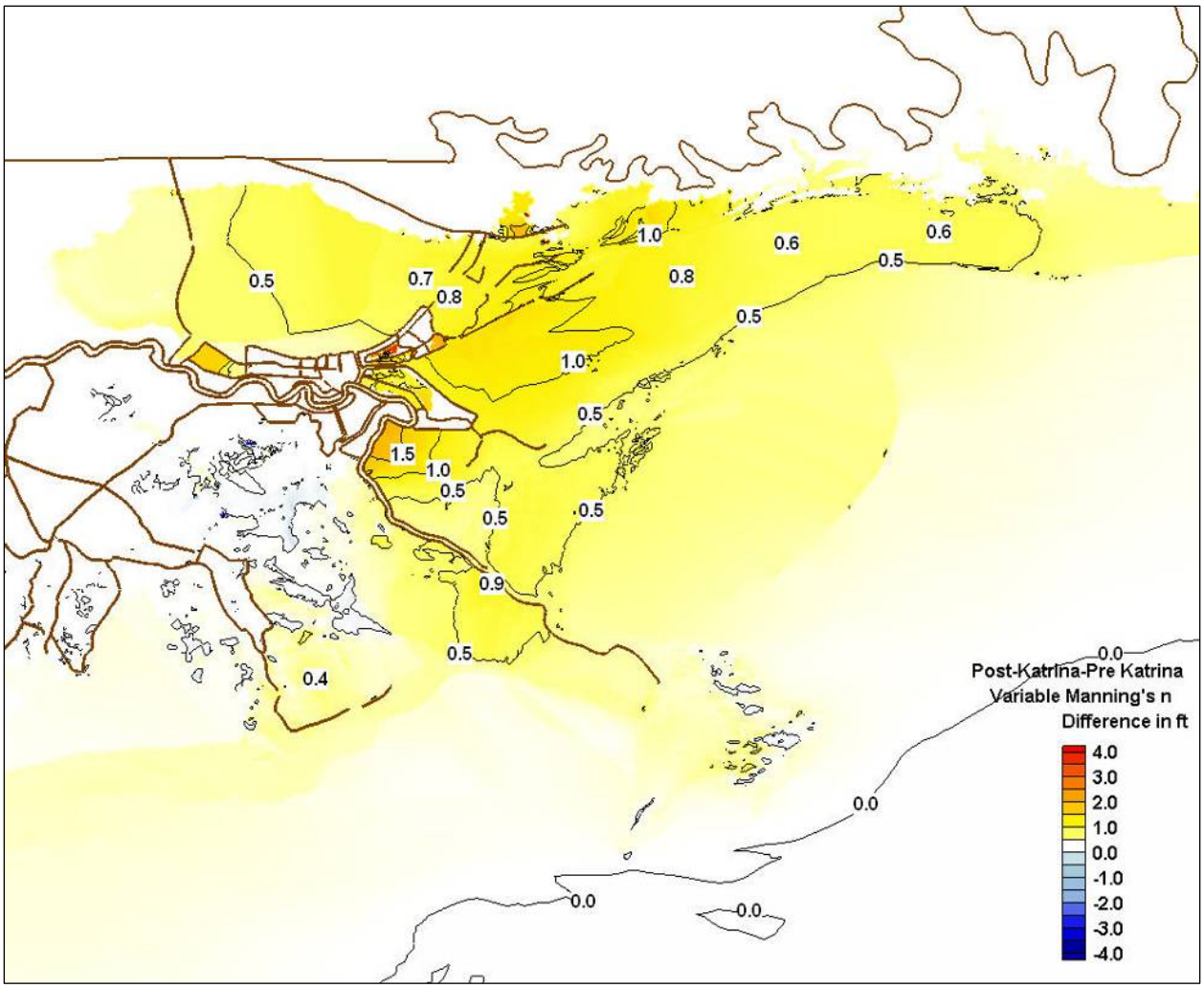

Figure 109. Difference in peak surge between sensitivity simulation with post-Katrina variable friction and pre-Katrina variable friction.

Nearshore Wave Sensitivity

All STWAVE base simulations neglected wave energy dissipation due to bottom friction. Generally, dissipation due to bottom friction in the nearshore is relatively small because the propagation distances are small, so frictional dissipation is neglected. Within the southeast grid, the propagation distances are significant, the water depths are relatively shallow, and vegetation in flooded areas may be highly dissipative, thus bottom friction may be significant. The bottom friction coefficient in STWAVE was specified as

$$C_f = g\frac{n^2}{d^{1/3}}$$

where g is acceleration of gravity, n is the Manning roughness coefficient, and d is total water depth (including surge). To investigate the impacts of bottom dissipation, STWAVE was run for

two cases with bottom friction. These cases represent spatially-varying bottom roughness for the pre-Katrina vegetation cover and the post-Katrina cover (background, open-water, Manning's *n* value of 0.02).

During Katrina, vegetation was stripped from some wetland areas, so the post-Katrina roughness values are reduced in some areas. ADCIRC was run with the same Manning's *n* values and those surge fields were used as input to STWAVE. For the base case, ADCIRC was run with a constant friction coefficient and STWAVE neglected bottom friction.

Figures 110 and 111 show the differences in maximum significant wave height for the simulation with the pre-Katrina frictional loss minus the base case and post-Katrina frictional loss minus the base case, respectively. The patterns for the two simulations are very similar, with increases in wave height in Chandeleur Sound and Lake Borgne and decreases in wave height along Plaquemines and St. Bernard Parishes and in the flooded areas between Bay St. Louis and Slidell. The maximum reductions in wave height were 3.7 ft near the Louisiana/Mississippi border and 3.5 ft near Dalcour in upper Plaquemines Parish. The maximum increases in wave height in Chandeleur Sound are 1.8 ft. It is counterintuitive that adding bottom friction would increase wave heights over large areas. The increase in wave height results from increased surge of 1 to 2.5 ft in these shallow areas. The waves in these areas are depth limited, so increasing the water depth decreases the wave dissipation due to depth-limited breaking and increases the wave height. The largest differences in wave heights between the post- and pre-Katrina bottom friction runs were reductions in wave heights of up to 1.6 ft on the Mississippi River delta, 0.7 ft across the Chandeleurs, and 0.4 ft in Chandeleur Sound and Lake Borgne. Wave heights increased in very limited areas (St. Bernard-Plaquemines border and directly in the lee of the Chandeleur and Ship Islands) by 0.3 to 0.5 ft.

The inclusion of spatially variable bottom friction tied to the vegetation type reduced wave height in very limited areas by up to 3.7 ft. Somewhat surprisingly, though, the simulations show increased wave height over broad areas in Chandeleur Sound and Lake Borgne on the order of 1 to 1.8 ft, which occurs because the surge increased in these areas and dissipation due to depth-limited breaking was reduced. The change in wave heights between the post-Katrina Manning's *n* values and the pre-Katrina values were relatively small (maximum decrease of 1.6 ft and maximum increase of 0.5 ft) and limited to small areas. The complex interaction of waves and surge in wetlands will be an important topic for continued study.

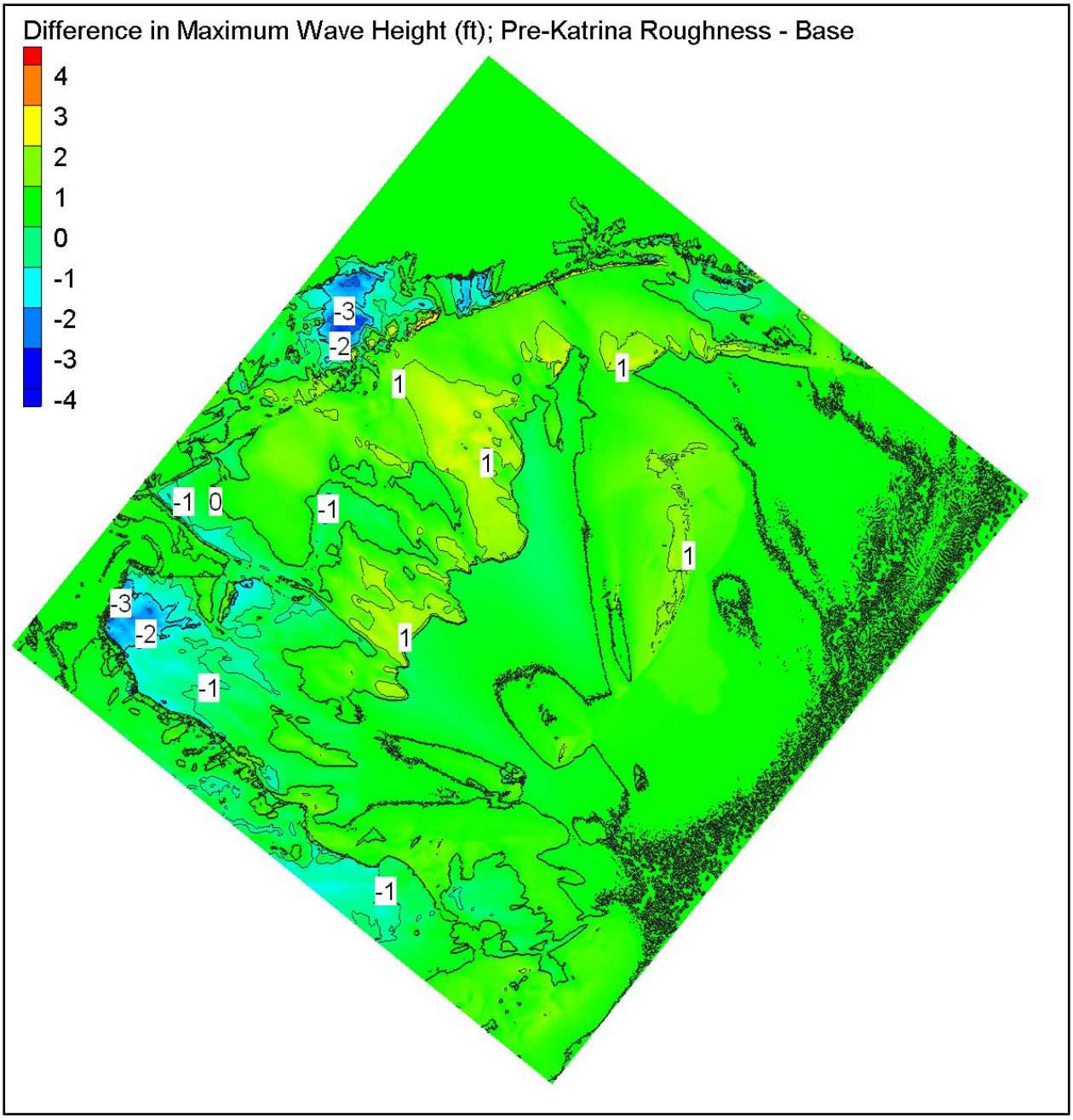

Figure 110. Differences in maximum significant wave height for sensitivity run with pre-Katrina bottom friction for Southeast Louisiana (with bottom friction – base).

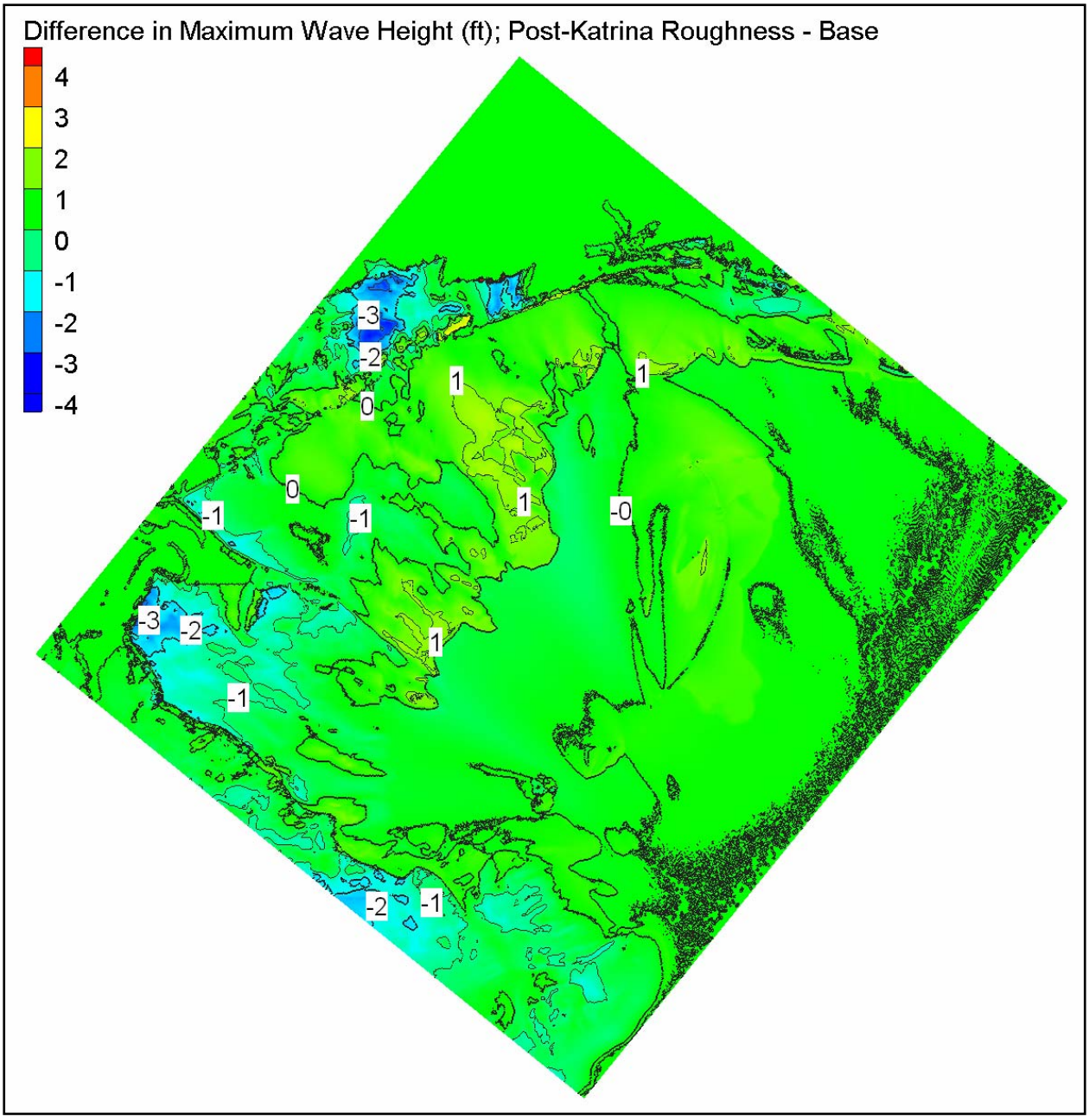

Figure 111. Differences in maximum significant wave height for sensitivity run with post-Katrina bottom friction for Southeast Louisiana (with bottom friction – base).

Contribution of Tide and Wave Setup to Storm Water Level

The primary base simulation forcing conditions are tide, storm winds and atmospheric pressures, and waves. Evaluating the relative contribution of these forcing conditions is accomplished by repeating the base condition without one forcing condition and comparing the resulting peak water level to the base condition peak water level. Two sensitivity runs were made

with one forcing condition eliminated for each simulation. Differences in the resulting peak water level maps indicate the contribution from the missing forcing condition.

Figure 112 shows that the wave setup contribution to peak water level due to wave breaking is most significant along the birdfoot delta, near Grand Isle, and shoreward of the Mississippi barrier islands and is approximately 0.5 to 2.5 ft. Along the east-facing levees of Southeast Louisiana, the contribution is 0.5 to 1 ft. Along the south shore of Lake Pontchartrain the contribution is approximately 0.3 ft. This is the regional component of wave setup that is attributed to wave breaking which occurs away from the hurricane protection levees throughout the region. Additional set up of as much as 2 ft was generated at the levees, based on the high resolution hydrodynamics work.

Figure 113 shows that the astronomical tidal contribution to peak water level is approximately 1 ft throughout the open water region, 0.2 ft in Lake Pontchartrain, and 0.5 ft in the Plaquemines and St. Bernard Parish regions.

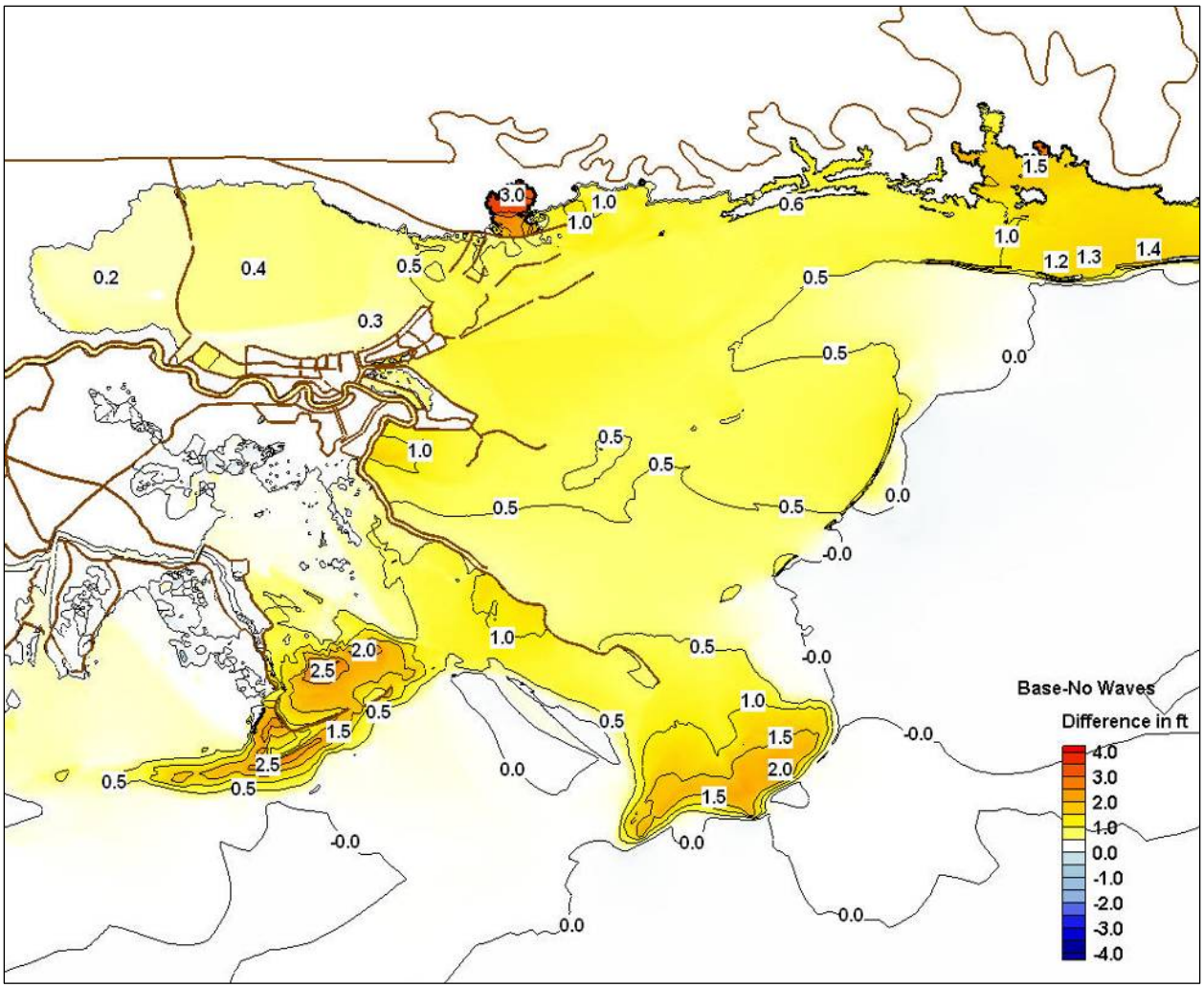

Figure 112. Difference in peak surge between the base simulation and the sensitivity simulation without wave forcing.

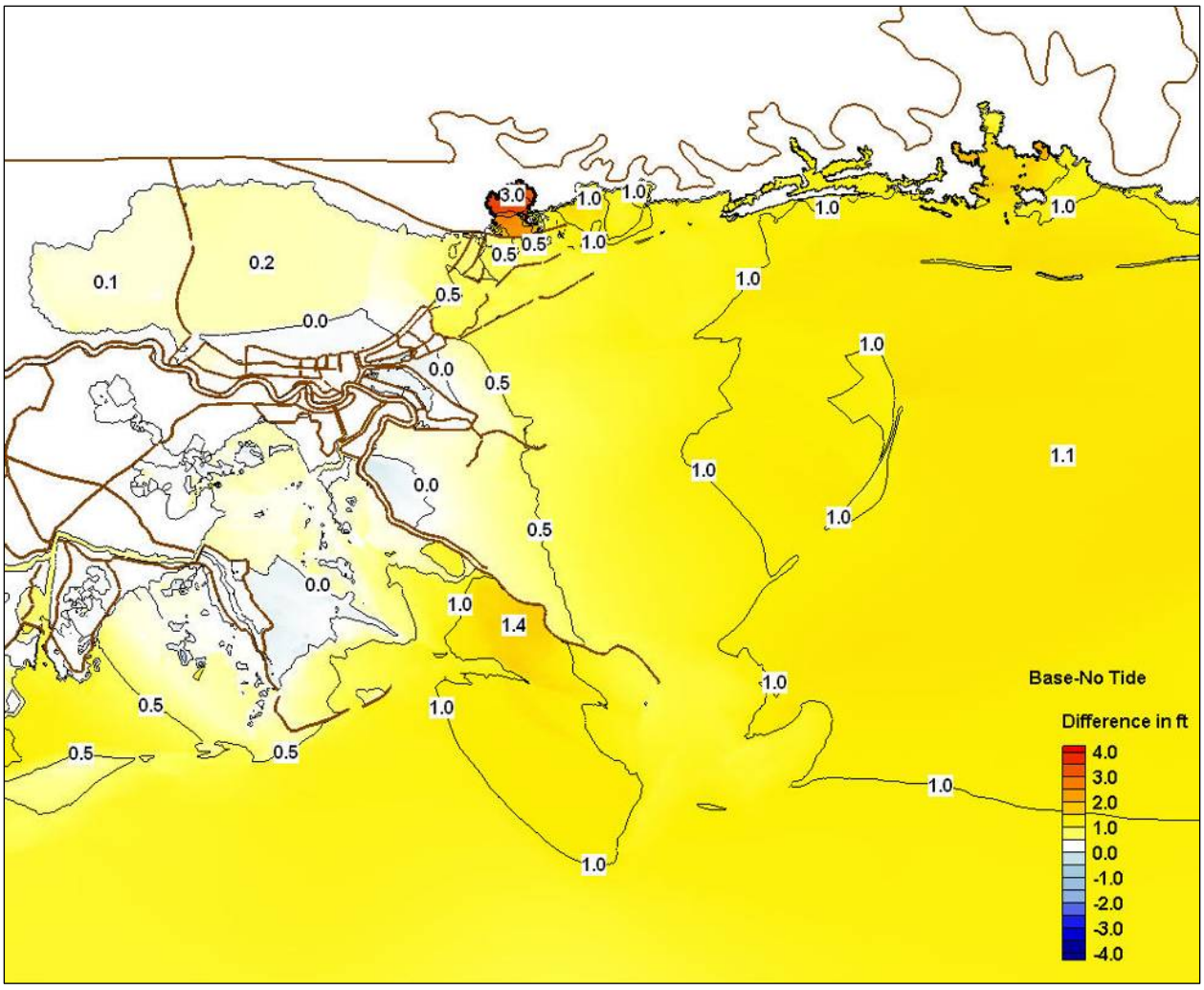

Figure 113. Difference in peak surge between the base simulation and the sensitivity simulation without tidal forcing.

Timeline for Breaching and Overtopping of the Levee and Floodwall System

Purpose and Approach

The following is a summary of the findings of the water level and eyewitness accounts studies. The primary purpose of these efforts is to aid in the development of a timeline for the overtopping and breaching of the levee and floodwall system. A secondary purpose is to provide input for calibration and validation of interior drainage investigations by defining hydraulic connectivity and collecting stage hydrographs within this extremely complex urban system. HWMs and stage hydrographs, both in protected and unprotected areas, are used herein to develop the timeline. A complete description of the hydrographs in unprotected areas and HWM data in both protected and unprotected areas is presented in Appendix 1. Additional hydrographs in protected areas are presented herein. With respect to the eyewitness accounts, over 600 people

were contacted and over 200 interviews (usually face-to-face and at the location of the eyewitness account) were conducted with people who observed flooding induced by Hurricane Katrina. Other means of establishing the timing of events included documentation of stopped-clocks in houses, and the collection of videos and still photos. Attempts were made to get data from security cameras, but these efforts produced limited results. A news release requesting eyewitness accounts was published on 16 February 2006 and a toll free number, web page, and email address were established to collect eyewitness accounts. This was a nationwide news release with a focus on the gulf south region. In addition to the development of the interviews, considerable effort has been expended in establishing the hydrologic connectivity of this extremely complex system. Appendix 7 includes a summary of all eyewitness interviews.

For this summary, eight sub-areas have been identified. The general locations of these areas are shown in Figures 114 and 115. These include: (1) 17th Street; (2) London West; (3) London East; (4) Inner Harbor Navigation Canal (IHNC) West; (5) Bartholomew Golf Course; (6) New Orleans East; (7) Lower Ninth Ward and St. Bernard Parish; and (8) New Orleans Downtown.

As is expected in a study such as this, there are often discrepancies in the data that must be addressed. The most reliable data came from time-stamped digital photographs and videos where the flooding (locations, elevations, directions of flows, etc) are clearly evident and documented. The next level of reliability is a log where an individual recorded events and times during the storm. Unfortunately these data were not available at all locations. Consequently, this study relies heavily on actual eyewitness accounts and stopped-clock data to establish the timeline of events. However, it is not uncommon for eyewitness accounts in the same area to differ considerably with respect to the timing and magnitude of events. Some eyewitnesses have very fuzzy recollections of events, particularly with respect to times, while others were much more clear and aware of times. Stopped-clock data often provided critical insight into the timing of events, but there was also uncertainty in these data. The following protocol was developed for the collection of stopped-clock data: (1) clock must be battery operated; (2) batteries must be in the clock; (3) evidence of inundation must exist; and (4) clock must be in its original location. Both eyewitnesses and clocks are types of evidence that gain strength in numbers. The final timeline conclusions presented herein were not based on any single data point, but rather resulted from careful consideration and weighing of all data.

Unless otherwise noted, in this Timeline section of the report, all elevations are referenced to NAVD88 (2004.65) and times are referenced to both UTC and CDT. Eyewitness accounts were reported in CDT. References to times in UTC are added to enable references to other information presented throughout the report.

Figure 114. Location of timeline study areas west of IHNC.

Figure 115. Location of timeline study areas east of IHNC.

17th Street

The location of the 17th Street study area is shown in Figure 116. Also shown in Figure 116 are the approximate locations of eyewitness accounts for which times of flooding were available. Although this area has been covered extensively, the number of people identified as having remained in the area during Hurricane Katrina is fairly small. However, there is a good degree of confidence in the results in this area, owing to the consistency of the eyewitness accounts and supporting time-stamped data. The general consensus is that the initial breach occurred early on the morning of Monday, 29 August.

Stage hydrograph information in the flooded area affected by the 17th Street breach was very limited. However, a gauge was maintained on the suction side of Pump Station (OP) 10 (Figure 116), which allowed the development of a stage hydrograph for that area shown (see Figure 117). The stage data in Figure 117 are referenced to NAVD88 (2004.65). The variability in stage from 1000 to about 1400 UTC (5:00 a.m. CDT until about 9:00 a.m. CDT) reflects the pumping operations at this site. However, after about 1400 UTC (9:00 a.m. CDT), the pumps were no longer able to keep up with the rising water and pumping ceased. Another stage hydrograph was developed in this area at site 12 (Figure 116) based on an eyewitness account. The homeowner at this site called a friend and left messages on her cell phone concerning water levels. Each message was time tagged, beginning at 1149 UTC (6:49 a.m. CDT) on Monday and ending at 8:30 p.m. CDT Monday. A survey of these points produced the stage hydrograph which is shown along with the OP 10 data in Figure 117. As shown in Figure 117, the Site 12 stages are significantly higher in the early morning period than at OP 10. This likely reflects the effects of pumping at OP 10. However, by about 1900 UTC (2:00 p.m. CDT), the two are in close agreement. The OP 10 data indicate that by midnight on Monday, the water elevations had begun to level off with stage of about 3.2 ft, which matches closely with the HWMs in this area. It should be noted that both these hydrographs represent the water levels about 2 miles south of the breach, and therefore, do not illustrate the rapid water level increases experienced near the breach.

A hydrograph of canal water levels was developed from the gauge data at OP 6 located at the south end of the 17th Street Canal. However, after a detailed analysis of the data, it was determined that the data were unreliable and were not considered in this study. A detailed description of the analysis of this gauge data is contained in Appendix 1.

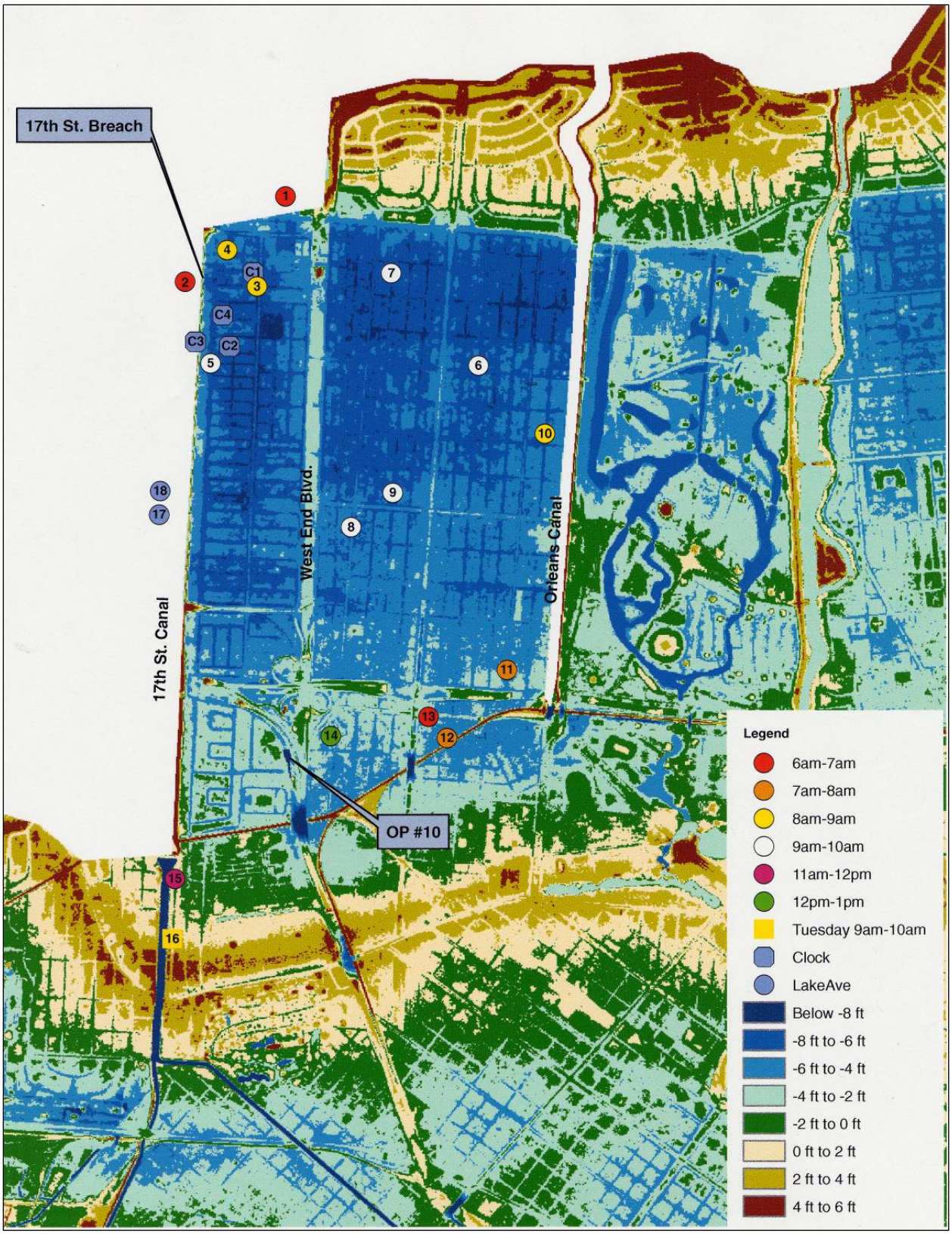

Figure 116. 17th Street area with approximate locations of eyewitness accounts and stopped clocks. [Times are referenced to CDT].

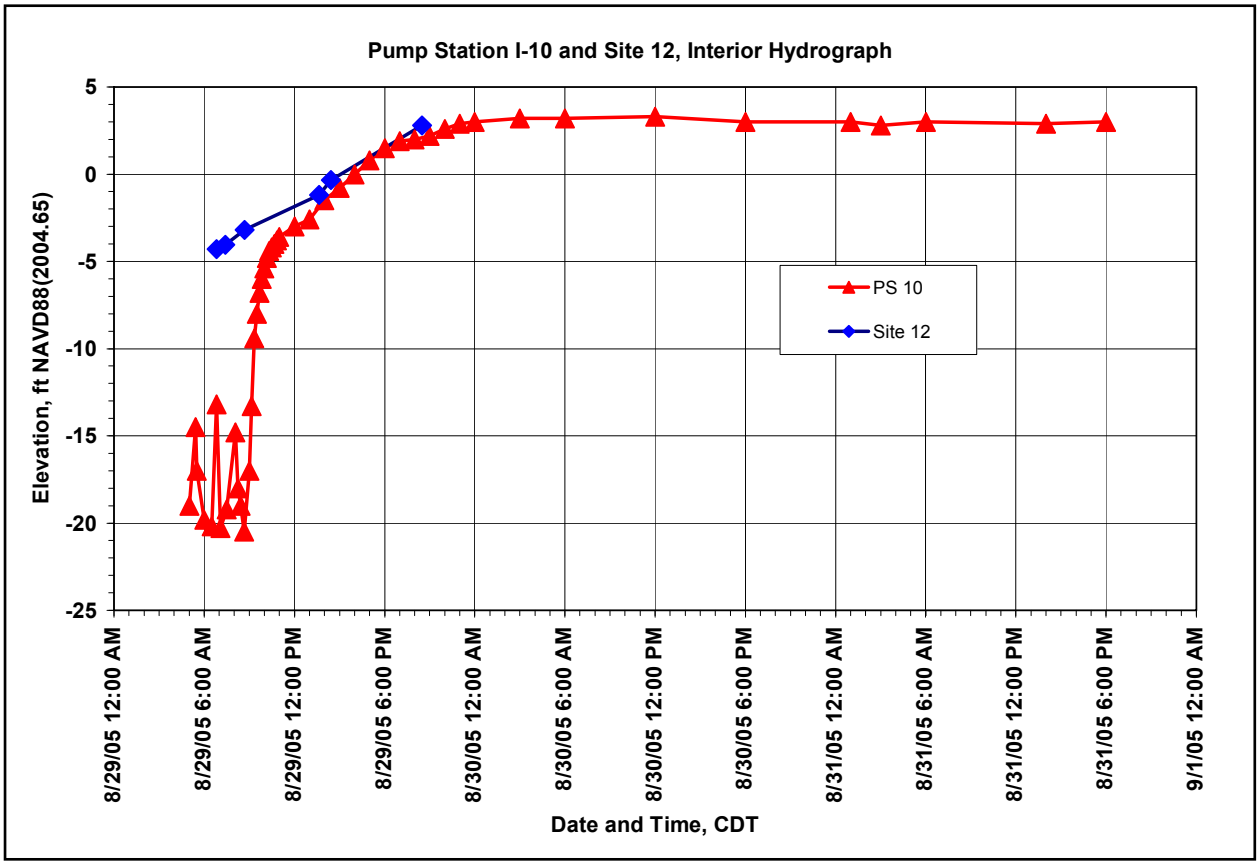

Figure 117. Stage hydrograph at Pump Station OP 10 and at Site 12. [Times are referenced to CDT]

While there is the expected range of eyewitness times throughout this area, two reliable accounts state that the initial breach was first observed around daybreak about 1130 UTC (6:30 a.m. CDT) on Monday. One account is from a man in the Lake Marina Tower high-rise building just north of the breach (Site 1 in Figure 116) who had a telescope trained on the floodwall area. He reported that just as dawn broke, he saw one section of the wall was breached (leaning over). Sometime later when he looked the breach had fully developed. He also reported that there was a large amount of debris piled up against the north side of Hammond Highway bridge (Figure 118). Another eyewitness, who lived on the west side of the canal in Jefferson Parish, used a pallet as a ladder and looked over the west floodwall directly across from the breach area (Site 2). He observed a single section (probably a panel) leaning over at about daybreak. He also reported that the water was moving very fast in the canal with no significant waves, and that the water was about 1 ft below the top of the wall at that time (approximately 1130 UTC (6:30 a.m. CDT)). He also reported that the water was going over the top of wall where the wall was leaned over. He left and came back about 2 to 3 hr later and observed that there were a number of sections all the way down or gone, suggesting full development of the breach. Based on these two accounts, it appears that there was a small breach that had occurred early in the morning by about daybreak (about 1130 UTC (6:30 a.m. CDT)). According to eyewitness accounts in the immediate vicinity of the breach there was no significant flooding in the area in the early morning prior to about 1400 UTC (9:00 a.m. CDT) suggesting that the flow through the breach during this period was not large. However, according to eyewitness accounts

closest to the breach (Sites 3 to 5 in Figure 116), the situation changed dramatically about 1400 UTC (9:00 a.m. CDT), with a rush of water being reported. One account is from an eyewitness whose house was within 100 yards of the breach (Site 3 in Figure 116).

Figure 118. This image shows debris accumulated on north side of Hammond Highway bridge over the 17th Street Canal shortly before 2000 UTC (3:00 p.m. CDT) on Monday, 29 August 2005. The bridge railing is visible in lower left corner.

He reported that about 1330 UTC (8:30 a.m. CDT) he observed clear water in the streets near the top of the curb, and was not concerned. However, at 1400 UTC (9:00 a.m. CDT) he heard loud noises and observed black water (filled with garbage) pouring into his house. He was certain of the time because he had just heard the radio announcer announce the time as 1355 UTC (8:55 a.m. CDT). He noted that the water was flowing from the west with tremendous force (knocking over oak trees in his yard) and that within 10 min his first floor was filled with water. He estimated the water depth in his house to be about 6 to 7 ft based on his floating sofa hitting the 8-ft ceilings. The other eyewitness accounts (Sites 4 and 5 in Figure 116) reported similar occurrences with times of the initial wave of water ranging from 1345 to 1415 UTC (8:45 to 9:15 a.m. CDT), and a rapid filling of their homes. Video taken from the Lake Marina Tower (Site 1) just north of the breach area shows initial flooding of the Lake Mariana parking

lot between 1400 and 1415 UTC (9:00 and 9:15 a.m. CDT). Shortly after 1600 UTC (11:00 a.m. CDT), the video clearly shows the fully developed breach in the 17th Street Canal (Figure 119).

Figure 119. This video frame shows the breach in the 17th Street Canal floodwall and flooding in Lakeview about 1620 UTC (11:20 a.m. CDT) on Monday, 29 August 2005. The portion of the breach shown in this image is near the intersection of Bellaire Drive and Stafford Place. (Video provided by National Geographic Television).

There were a number of stopped clocks recorded in the vicinity of the breach with the elevation of four being surveyed (Sites C1 to C4 in Figure 116). The times on these clocks range from 8:00 to 8:45, which might suggest the breaches occurred earlier than the eyewitness accounts. However, it is not clear at this time whether these readings represent a.m. or p.m. While it is possible that the water reached levels high enough to stop the clocks in the morning, it is also possible that these times could reflect the flooding later in the evening. The surveyed elevations of the clocks were generally between 2.3 and 2.8 ft, with one clock at 3.1 ft. These elevations are all slightly less than the observed high water in this area of 3.4 ft. According to the stage hydrograph (Figure 117) at OP 10, which is about 2 miles south of the breach (Figure 116), the stages between 8:00 and 9:00 p.m. CDT range from about 2.2 ft to 2.6 ft, which is in the same range as the clock data. Therefore, it is difficult at this time to state with certainty whether the clocks represent a.m. or p.m. Eyewitness accounts appear to be more reliable for the initial flooding times.

East of the slightly elevated West End Boulevard, the eyewitness accounts generally suggest (with one unexplained outlier at Site 10) a slight time lag, with the first signs of flooding

occurring between 1430 and 1500 UTC (9:30 and 10:00 a.m. CDT) (Sites 6 to 9 in Figure 116). One eyewitness (Site 6) remembers looking at his watch, and places the onset of flooding at precisely 1432 UTC (9:32 a.m. CDT). Thus, it appears that within 30 min to 1 hr following the major breach, the floodwaters had moved into the area between West End Boulevard and Orleans Canal. Further south near I-10 between Canal Street and Orleans Canal, there are three early accounts (Sites 11 to 13) that report the onset of flooding between 1200 and 1300 UTC (7:00 and 8:00 a.m. CDT). At this time, these early flooding times are unexplained. At Sites 11 and 12 (Figure 116), it is possible that the initial reports of water may have simply been rain water piling up in the streets, while the major flooding may have occurred sometime later. At Site 13 (Figure 116), water is definitely reported in the home, which is on a slab foundation, at 1200 UTC (7:00 a.m. CDT), but it is possible that the timing may be off. It is equally possible that these accounts are accurate, resulting from some, as yet determined, source of water. A possible explanation of this water source could be the backflow from the Orleans Canal, but this has not been conclusively documented.

An eyewitness account at Site 14 (Figure 116) just south of the I-610 Loop, states that the first signs of flooding were not observed until about 1730 UTC (12:30 p.m CDT) on Monday. Based on the ground elevation at this site (about -2 to -3 ft), this appears to be compatible with the OP 10 hydrograph. At Site 15 (Figure 116), the homeowner reported water flowing under her house into the canal on the suction side of OP 6 about 11:30 p.m CDT on Monday. The ground elevation at this site is about 1 to 2 ft. At Site 16 (Figure 116), which is on the high ground of Gentilly Ridge, water was not observed until about 1500 UTC (10:00 a.m. CDT) on Tuesday. This homeowner also reported that the water level in the canal equalized with the water level in the street about 0700 UTC (2:00 a.m. CDT) on Wednesday. An eyewitness who returned on Tuesday to assist with rescue efforts reported strong north-to-south currents in the vicinity of the I-10/I-610 interchange on Tuesday morning. The eyewitness at Site 12 reported strong north-to-south currents at the Canal Street railroad underpass on Monday about 9:00 p.m. CDT.

Based on the above data, it appears that the initial failure of the floodwall (single panel) occurred early on the morning of the 29th at least by about 1130 UTC (6:30 a.m. CDT), and was probably fully developed (probably catastrophically) by about 1400 UTC (9:00 a.m. CDT). If the initial breach occurred around 1130 UTC (6:30 a.m. CDT) , then according to the constructed Lake Pontchartrain stage hydrograph based on digital pictures and eyewitness accounts (Figure 120), the stage in the canal would only have been at about elevation 7.3 ft, which would be well below the top of the wall. According to post-Katrina surveys, the top of the 17th Street floodwall is about 12.4 ft at the breach. However, there are some eyewitness accounts that might suggest higher water elevations in the canal during this early time period. As noted above the eyewitness who observed the initial breach from the west side of the canal reported that the water was about a foot below the top of the wall at this time (1130 UTC (6:30 a.m. CDT)). The other eyewitness who observed the initial failure with the telescope reported that there were no significant waves in the canal, and that the water level was only about 1.5 ft below the top of the floodwall. He also reported a large amount of debris piled up against the north side of the Hammond Highway bridge, but no significant amount of debris south of the bridge in the canal. Another eyewitness who lives in Jefferson Parish immediately behind the west side of the wall reported waves overtopping the wall at about 1300 UTC (8:00 a.m. CDT) (Site 17 in Figure 116). He also took a picture, which shows the wave splash (wave splash is partially

hidden by tree limbs). He also noted that while there was wave overtopping, there were no significant amounts of water building up in this area.

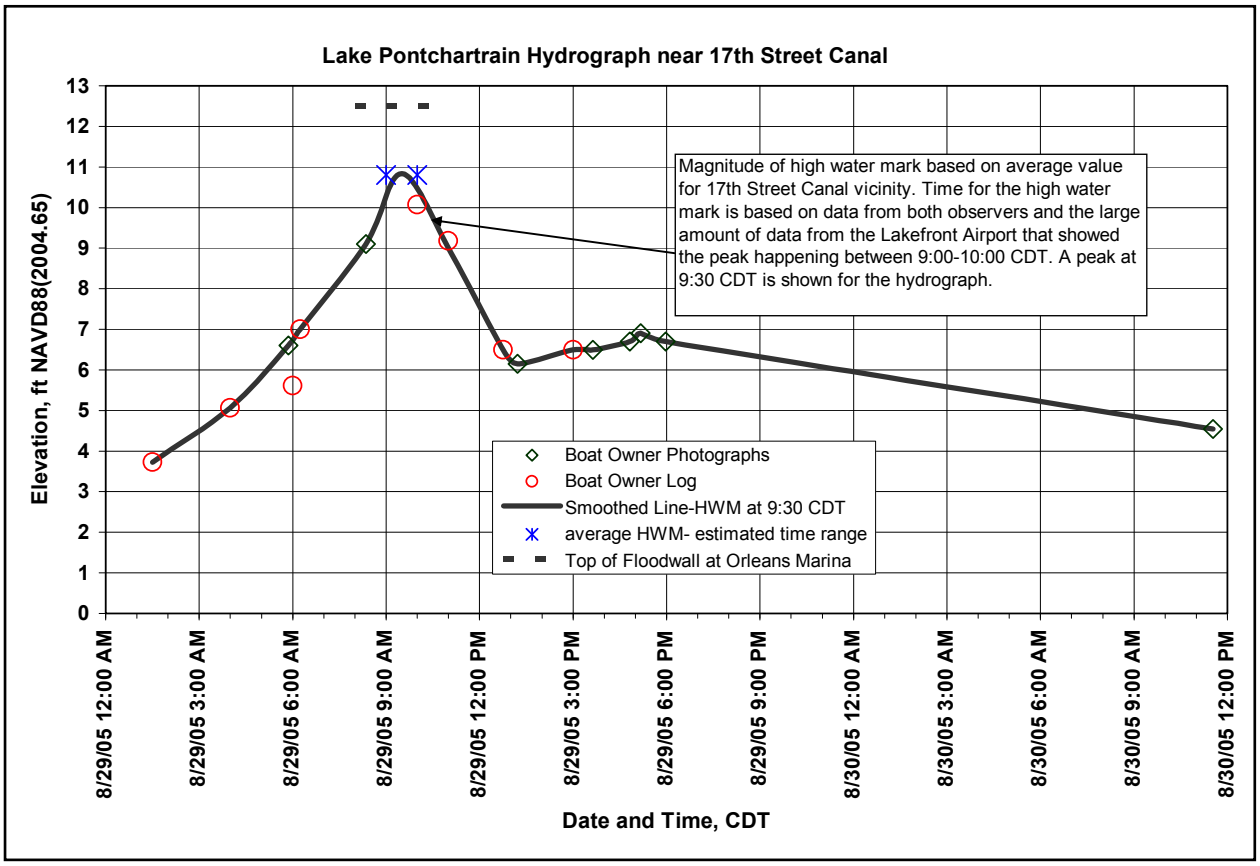

Figure 120. Stage hydrograph for 17th Street Canal entrance and vicinity based on digital photographs and eyewitness account.

At about 1500 UTC (10:00 a.m. CDT), he looked over the floodwall and reported that the water level was about 2 ft below the wall, which is consistent with the lake hydrograph. Another eyewitness at Site 18 (Figure 116) reported water and wood debris coming over the wall with the waves. He was not sure of the time, but said that it was between 1000 and 1100 UTC (5:00 and 7:00 a.m. CDT). After about 1400 UTC (9:00 a.m. CDT) he no longer saw the waves. This observation is consistent with a catastrophic breach at 1400 UTC (9:00 a.m. CDT) that would likely lower canal water levels. At present, it is difficult to reconcile these eyewitness accounts of higher water levels with the stage hydrograph in Figure 120.

London West

The location of the London West study area is shown in Figure 121. Unfortunately there were no eyewitnesses found in the immediate vicinity of the breach. However, there were a number of stopped clocks recorded within about a ten-block area near the breach. Figure 122 is a stage hydrograph developed from the stopped-clock data.

As shown in Figure 122, the earliest stopped-clock time is about 1100 UTC (6:00 a.m. CDT) However, since there are no other data supporting a breach at this early time, this time is not considered to be reliable. The next earliest time in Figure 122 is at 1230 UTC (7:30 a.m. CDT), which is also shown as Site C1 in Figure 121. At Site C2, another stopped clock was located adjacent to the breach and was found to indicate a time of 1210 UTC (7:10 a.m. CDT). This clock was not surveyed and therefore is not included in Figure 122, however, it was at a relatively low elevation in the house, and would have been inundated early. This was also a wind-up clock, but was considered to be reliable because the homeowner was sure that he had wound it the night before the hurricane. Eyewitness accounts at Sites 1 and 2 (Figure 121) reported major flooding at 1200 UTC (7:00 a.m. CDT) while the eyewitness at Site 3 experienced flooding at 1220 UTC (7:20 a.m. CDT). Other eyewitnesses who live on the east side of the canal crossed the bridge at Fillmore in the 1300 to 1330 UTC (8:00 to 8:30 a.m. CDT) timeframe heading towards Paris Street, and observed water flowing on the west side of the canal from north to south. Therefore, based on these data, it appears that the breach in the London West floodwall occurred in the 1200 to 1230 UTC (7:00 to 7:30 a.m. CDT) timeframe. Sites 4-6 indicate flooding times between 1445 and 1500 UTC (9:45 and 10:00 a.m. CDT). These later times probably reflect distance from the breach and/or higher ground elevations at these locations. Sites 7 and 8 are located on higher ground, and show times of 2300 and 1700 UTC (6:00 p.m. and noon CDT), respectively.

South of Mirabeau Avenue (Figure 121), there is a wide variation in times, but it appears that flooding in this area generally occurred in the late morning to mid afternoon. Thus, it appears that the flood waters from the breach had to fill the low-lying areas to the north of Mirabeau Avenue before the higher areas south of Mirabeau Avenue were affected. Further south near the high ground of Gentilly Ridge, there are two reports at Sites 19 and 20 of flooding at about 1800 UTC (1:00 p.m. CDT) on Monday. Two eyewitnesses at Sites 17 and 18 near Gentilly Ridge did not report flooding until Tuesday morning. However, the reports at Sites 17 and 18 are not consistent with the other reported times in this area. This discrepancy probably reflects uncertainty with respect to the timing at Sites 17 and 18. Another eyewitness reported that between 1500 and 1600 UTC (10:00 and 11:00 a.m. CDT), water was flowing over Gentilly Ridge from south to north towards the Humanity Street area near the end of the London Avenue Canal.

In summary, it appears that the breach on London West occurred in the 1200 to 1230 UTC (7:00 to 7:30 a.m. CDT) timeframe. According to eyewitness accounts and the hydrograph in Figure 122, water levels continued on a slow rise reaching an elevation of about 0 ft by about 2100 UTC (4:00 p.m. CDT) on Monday, and peaking at about 2.8 ft on Tuesday about 0600 UTC (1:00 a.m. CDT). The 2.8 ft elevation is equal to the HWM elevations in this area. If it is assumed that the breach occurred at 1230 UTC (7:30 a.m. CDT), then the corresponding stage in the canal according to the hydrograph in Figure 120 would be about 8.9 ft which would be about 4 ft below the top of the wall based on a floodwall height of 12.9 ft. According to the two eyewitnesses that ran across the Fillmore Bridge towards Paris Street, the water level in the canal was only about a foot below the top of the wall in the 1300 to 1330 UTC (8:00 to 8:30 a.m. CDT) timeframe. Although these appear to be credible eyewitnesses, uncertainty exists with respect to the exact times these observations were made.

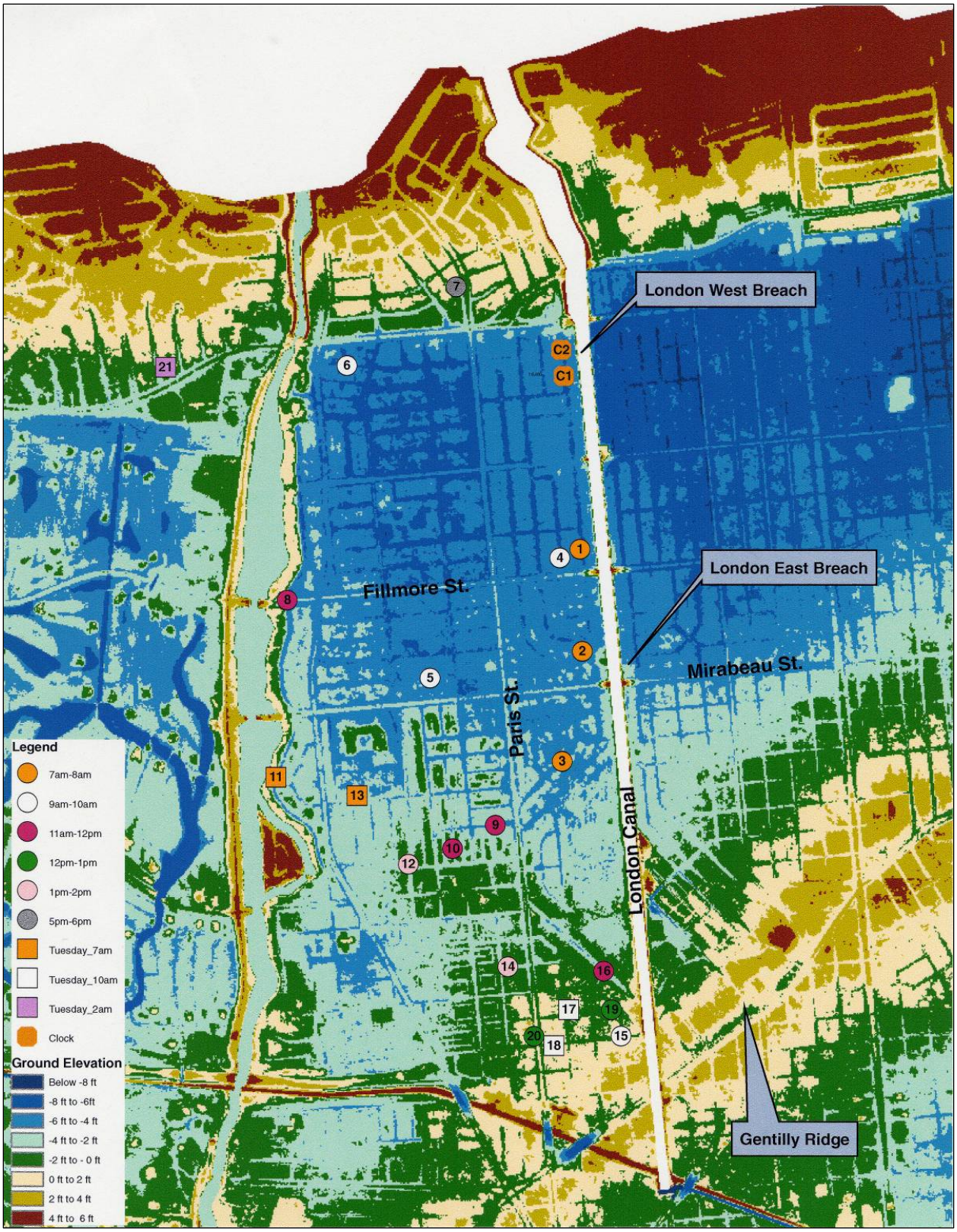

Figure 121. London West area with approximate locations of eyewitness accounts and stopped clocks. [Times are referenced to CDT].

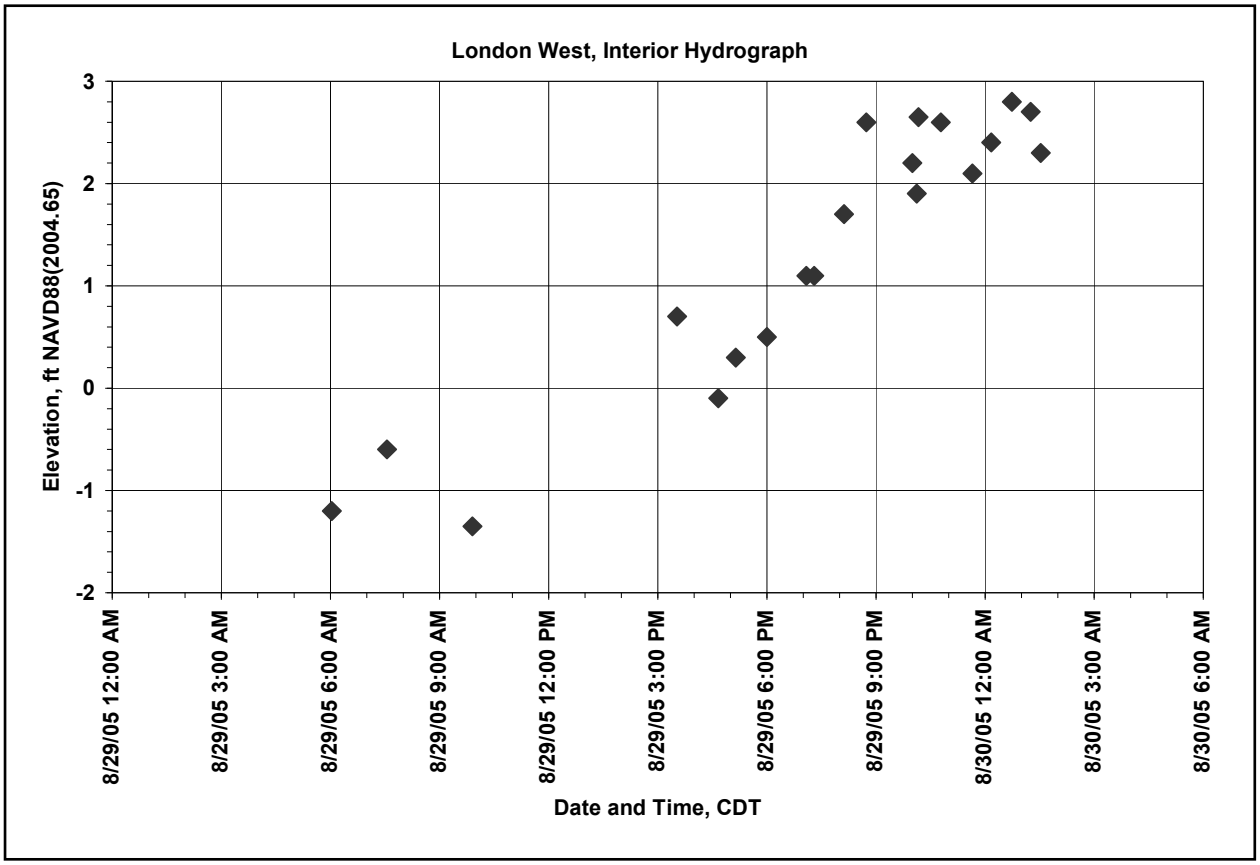

Figure 122. Stage hydrograph for London West based on stopped-clock data. [Times are referenced to CDT].

London East

The location of the London East study area is shown in Figure 123. As shown in Figure 123, there were a large number of people who remained in their homes during the hurricane. The earliest reported account of flooding was between 1200 and 1300 UTC (7:00 and 8:00 a.m. CDT) on Monday by an individual that lives right at the breach (Site 1 in Figure 123). Another individual at Site 2 reported that the water came up really fast from the west at about 1300 UTC (8:00 a.m. CDT). Another report of an early time was at Site 3. This individual reported that at 1230 UTC (7:30 a.m. CDT) there was not much water in the street, so he decided to go back to sleep. However, before he could get to sleep, he heard a gurgling sound and when he got out of bed there was water in his house. He said that the water was up to the window ledges and coming into his house. He and a friend got the neighbor from next door and went up on the floodwall berm and headed south. At one point they lifted one of them up to look over the wall and said that the water was about one foot below the top of the wall. As they got to the location of the breach they heard a loud cracking sound and at the same instant, the wall burst open in front of them and water gushed out “like twenty fire hydrants.” They immediately reversed direction and ran back to Fillmore Street and crossed over at the bridge towards Paris Street. They reported seeing water moving in this area from north to south, and had to swim to reach the Beacon Light Church, where they stayed for several days. The interview with the neighbor

revealed a similar account. He reported that he was asleep between about 1130 and 1200 UTC (6:30 and 7:00 a.m. CDT) when a friend woke him up and he found water coming into his house. He said that by the time he got dressed, the water was about knee deep in the house and was flowing up through the toilets and sinks. He and his friends went west up onto the levee and headed towards Mirabeau Avenue.

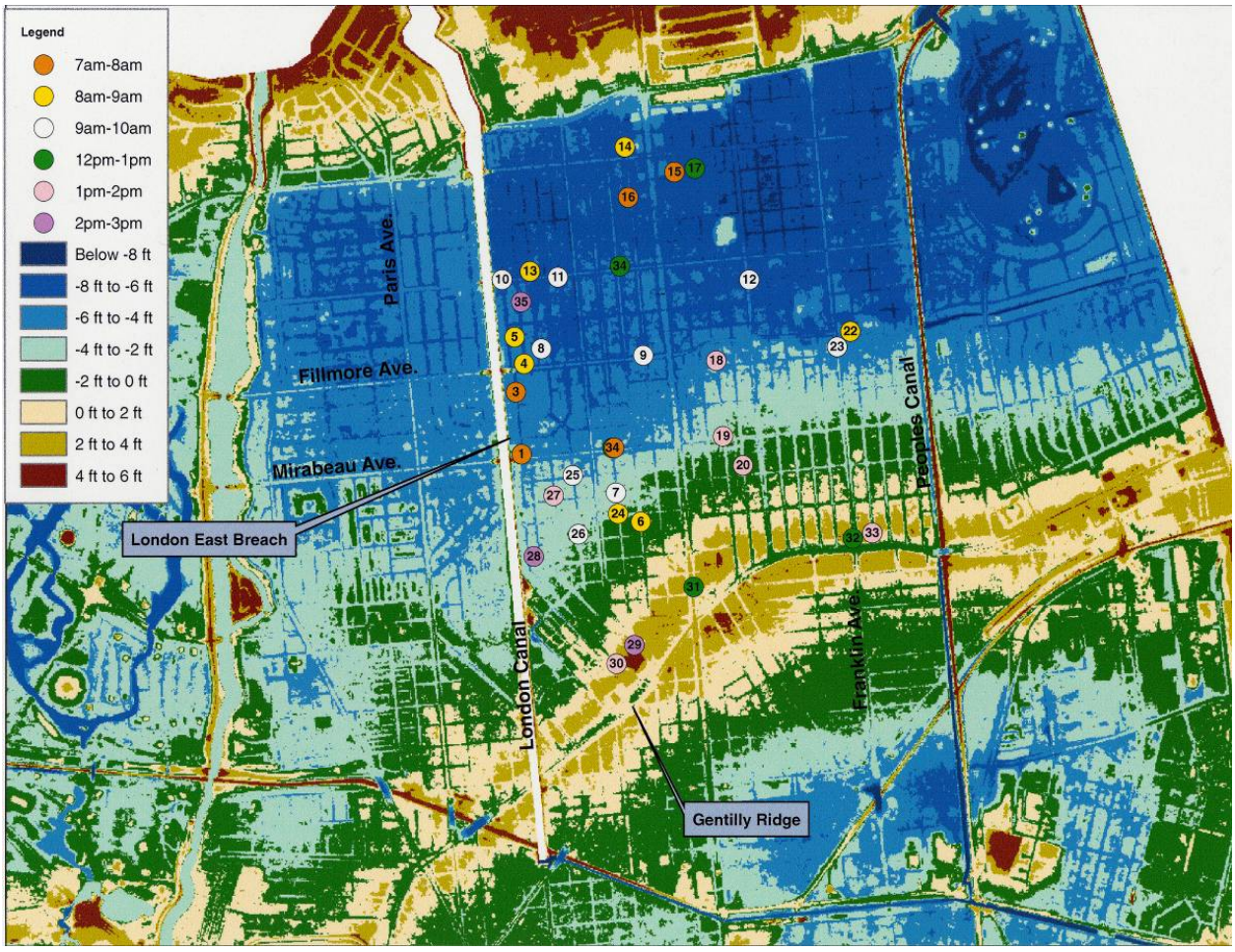

Figure 123. London East area with approximate locations of eyewitness accounts. [Times are referenced to CDT].

When they got to the breach location, he said that water was pouring through the breach like a river. He estimated that the time between waking up and getting to the breach site was about 30 min, which would be in the 1200 to 1230 UTC (7:00 to 7:30 a.m. CDT) timeframe. He said that he is 5 ft 9 in., and that the water coming through the breach was over his head while he was standing on the levee. He also stated that he felt that the breach had occurred sometime before they got there due to the large amount of water in the streets and houses in the area. He said that they walked north to Fillmore Street where they crossed over going west towards Paris Street. At the Fillmore bridge, he climbed up on a ladder and looked across the canal. He reported that the water level was about 1 ft below the top of the floodwall, and that the water was moving very fast towards the south. After crossing the canal, they encountered water and eventually had to swim to get to Paris Street. When they finally got to the Beacon Light Church, he noticed a clock

on the wall that read 1348 UTC (8:48 a.m. CDT). He thought the clock was operational, but could not say for certain. He also said that the time between seeing the breach at Mirabeau Avenue and getting to the church was about an hour. If it is assumed that the clock at the church was correct, then he would have been at the breach around 1245 UTC (7:45 a.m. CDT). Based on all these accounts, it appears that the London East breach occurred in the 1200 to 1300 UTC (7:00 to 8:00 a.m. CDT) timeframe.

At Site 4 (Figure 123), the eyewitness reported that by 1400 UTC (9:00 a.m. CDT) there was 2 ft of water in the street moving with a strong current from south to north. By 1700 UTC (noon CDT), they reported that the water was about 6 ft high in the street. Another eyewitness at Site 6 (Figure 123) reported flooding between 1330 and 1400 UTC (8:30 and 9:00 a.m. CDT).

North and east of the breach there are several reports (Sites 8 to 12) of flooding occurring around 1500 UTC (10:00 a.m. CDT), which probably reflect the time required to fill up the low-lying areas north of Mirabeau Avenue. However, there are several early times of flooding reported in the northern part of the area (Sites 13 to 16) that can not be explained at this time. Just east of Elysian Fields, there are three accounts (Sites 18 to 20 in Figure 123) that place the flooding times between 1900 and 2030 UTC (2:00 and 3:30 p.m. CDT). These later times seem to be reasonable given the higher ground elevations in this area. However, just east of these sites are two accounts (Sites 22 and 23 in Figure 123) that place the flooding much earlier, between 1345 and 1445 UTC (8:45 and 9:45 a.m. CDT). Both eyewitnesses at Sites 22 and 23 reported that the water was flowing south to north from the Gentilly Ridge area, suggesting that water was flowing over Gentilly Ridge from the IHNC West area. Just south of here at Site 32 (Figure 123), an eyewitness had video footage showing water flowing down Franklin Street from Gentilly Ridge to the north at about 1730 UTC (12:30 p.m. CDT) (Figure 124). As noted in the London West section of this report, an eyewitness reported flow going over Gentilly Ridge near the south end of the London Avenue Canal between 1500 and 1600 UTC (10:00 and 11:00 a.m. CDT). Thus, it seems possible that the flow from the IHNC West area could have been supplying water to the London East and West areas by mid-morning. However, these early times for flow going over Gentilly Ridge must be reconciled with the later observed flooding times along the ridge itself. For instance, at Sites 29-33 near Gentilly Ridge, the reported times of flooding range from 1730 to 2000 UTC (12:30 to 3:00 p.m. CDT). However, it is possible that the water could have been flowing over some selected low areas in the streets through Gentilly Ridge into the northern areas in the mid morning time frame, and that it was only later in the day before the higher areas along the ridge itself were actually flooded. In particular, Franklin Avenue provides a flow path with an invert elevation of about 0 ft while the surrounding ground elevations range from about 2 to 4 ft. The potential for water crossing the Gentilly Ridge in morning is also supported by the IHNC West data discussed in the next section.

For this area, a stage hydrograph was developed from an eyewitness video located at Site 34 in Figure 123 during the storm. The hydrograph is shown in Figure 125. The video starts about 1625 UTC (11:25 a.m. CDT) on Monday and extends through Wednesday at 1800 UTC (1:00 p.m. CDT). There were also three surveyed stopped-clock data points (also shown in Figure 125) that matched well with the hydrograph. This set of stopped-clock data was collected for the specific purpose of evaluating the reliability of stopped-clock data as source of data for construction of stage hydrographs. As shown in Figure 125, the stopped-clock data match well

with the hydrograph from the observed points from the video. According to the hydrograph in Figure 125, the water level rose at a little less than about 1 ft/hr from about noon to 9:00 p.m. CDT. After that it rose very slowly, peaking at about 2.8 ft on Tuesday at 1:00 a.m. CDT, an elevation consistent with surveyed HWMs in this area.

In summary it appears that the London East Breach occurred between about 1200 and 1300 UTC (7:00 and 8:00 a.m. CDT) on Monday. Assuming the breach occurred at 1300 UTC (8:00 a.m. CDT), the corresponding elevation in the canal would have been about 9.5 ft, according to the stage hydrograph for London Avenue Canal (see Appendix 1). The elevation of the floodwall in this vicinity is about 12.9 ft.

Figure 124. This image shows a south to north flow on Franklin Avenue at the Gentilly Road intersection about 1730 UTC (12:30 p.m. CDT) on Monday, 29 August 2005.

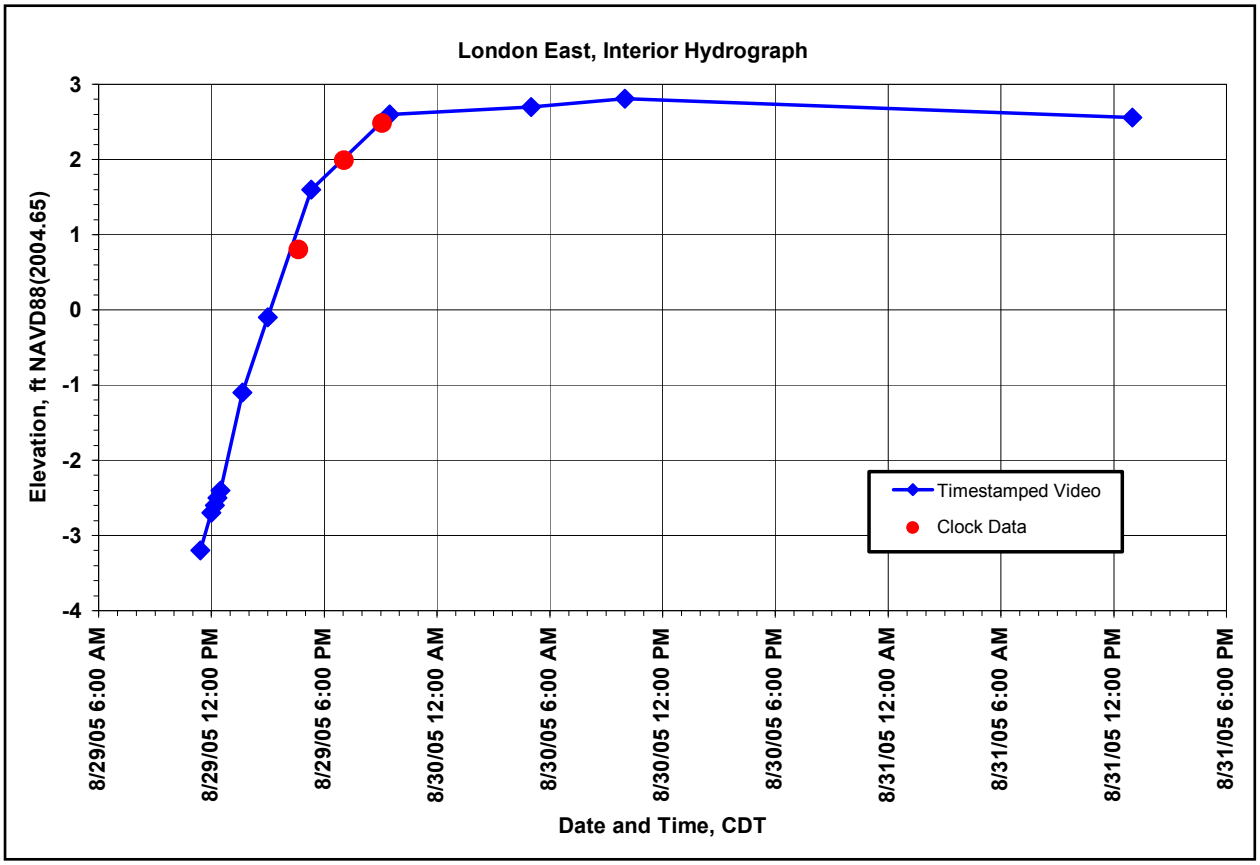

Figure 125. Stage hydrograph for London East based on video at Site 34 and stopped clocks. [Times are referenced to CDT].

Inner Harbor Navigation Canal (IHNC) West

The location of the IHNC West study area is shown in Figure 126. There are three breach locations on the west side of the canal. These include the breach near I-10 through the railroad line, and the breach in the floodwall and earth levee near OP 19. The elevation of the floodwall along the west side of the canal is about 13 ft, while the earth levee elevation is about 11 ft. Also providing early flooding to this area is the USACE floodwall that is south of the east end of the earth levee. This floodwall extends down to France Road and ranges in elevation from 11.8 to 12.6 ft. Figure 127 is an overhead view of this area on 31 August showing the floodwall and earth levee breaches.

There are numerous eyewitness accounts in this area that are remarkably consistent. Many recall seeing the first signs of rushing water between 1100 and 1200 UTC (6:00 and 7:00 a.m. CDT) on the 29th. Flow over the floodwalls and from the breach or breaches would quickly enter the east-west Florida Canal, thereby providing a possible explanation of the early flooding times in the eastern portion of the study area. The north-south Peoples Canal also provides a direct conduit of water to the northern areas, both north and south of Gentilly Ridge.

HWMs vary through this area, generally reflecting the passage of the flood wave coming from the IHNC. Immediately west of the IHNC to about Peoples Canal, the HWMs range from about 4.2 to 5.3 ft with an average value of 4.6 ft. East of Peoples Canal to the vicinity of Elysian Fields, the HWMs range from about 3.4 to 3.6 ft with an average of 3.5 ft. Further to the south, the HWMs are only about 2.6 ft. These higher water elevations just west of the IHNC appear to reflect the initial wave of water from the IHNC, while the lower elevations further west reflect the spilling of water into larger areas. As mentioned above, it appears that water entered this area from the IHNC very early on Monday morning. One of the earliest credible accounts is from an eyewitness at Site 1 (Figure 126) who reported rapidly rising waters between 1030 and 1100 UTC (5:30 and 6:00 a.m. CDT). He climbed into his attic and was able to use the ladder to estimate the water depths in his house. His daughter called at 1100 UTC (6:00 a.m. CDT) while he was in the attic, and he told her that the water was 2 ft in the house at that time. By about 1230 UTC (7:30 a.m. CDT), he estimated the water to be about 6 ft high in the house. A battery-operated clock about 5.5 ft up the wall had stopped at 1302 UTC (8:02 a.m. CDT). Other eyewitness accounts in this area between IHNC and Peoples Canal (Sites 2, 3, 4, 5, 6, 7, and 8) reported a massive rush of water and rapid filling in the 1130 to 1200 UTC (6:30 to 7:00 a.m. CDT) timeframe. A stopped clock at Site C1 (Figure 126) shows a time of 1245 UTC (7:45 a.m. CDT) at an elevation of about 2.3 ft. At Site 9, just west of the Peoples Canal, there is an eyewitness account of water entering the house at 1105 UTC (6:05 a.m. CDT) on Monday. This was a very time-conscious individual who reported that at that time water began to gush into his house, spewing out of the floor furnaces. He noted that the water was coming directly from the Peoples Canal and flowing very fast. By 1145 UTC (6:45 a.m. CDT), he noted that the water was about 2 to 3 ft high in his house. Thus it appears that the Florida and Peoples Canals provided a direct conduit for the water from the IHNC. A stopped clock (Site C3) near Site 9 showed a time of 1245 UTC (7:45 a.m. CDT) at an elevation of 3.39 ft which was about 4.8 ft above the floor. This elevation is close to the observed HWMs in this area. Another eyewitness at Site 10 did not report the rush of water in this area until about 1445 UTC (9:45 a.m. CDT). However, it is felt that the earlier reported times at Sites 9 and C3 are more reliable.

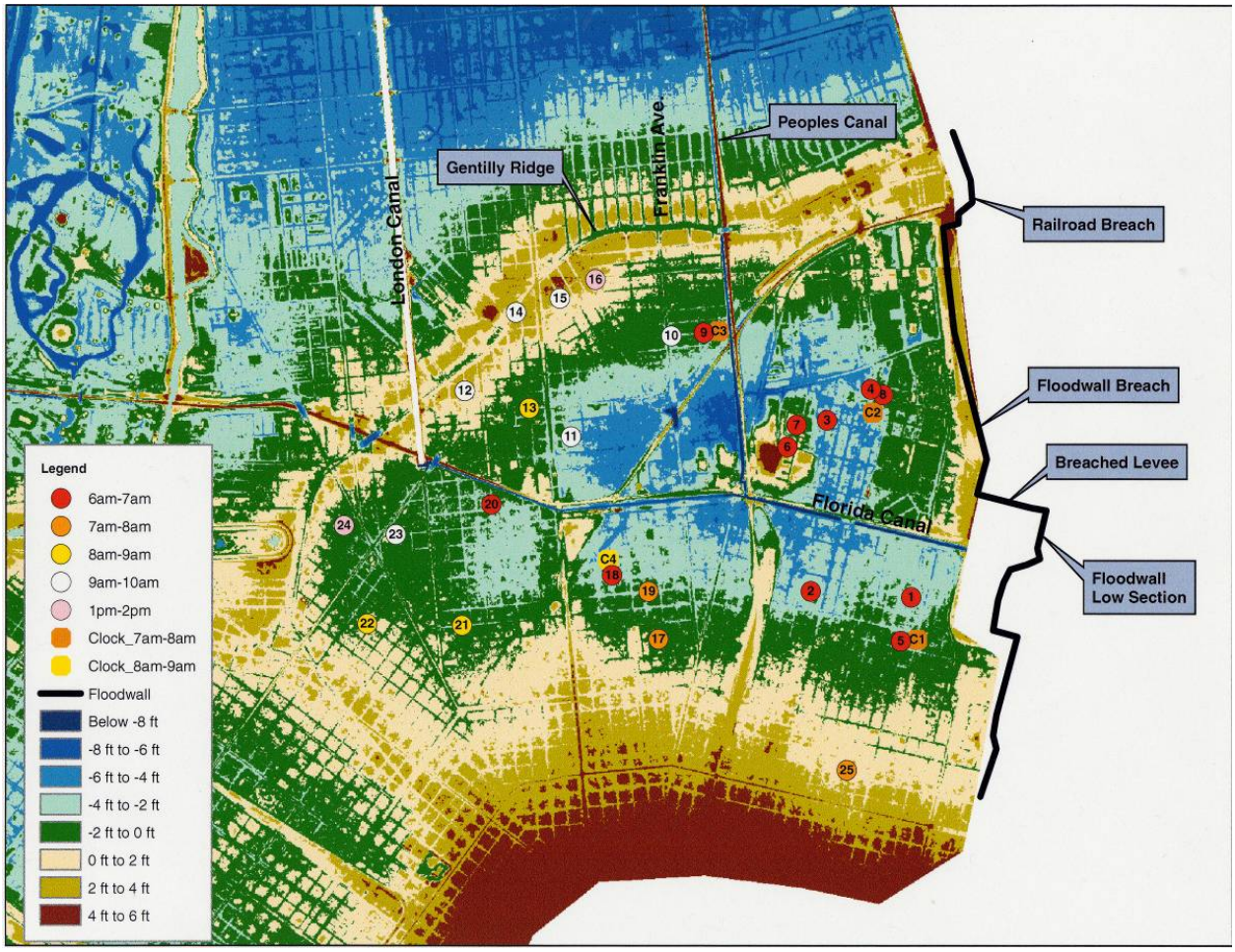

Figure 126. IHNC West area with approximate locations of eyewitness accounts and stopped clocks. [Times are referenced to CDT].

At Sites 11 to 15 (Figure 126), the eyewitnesses reported that the flooding began between 1400 and 1530 UTC (9:00 and 10:30 a.m. CDT). This somewhat later time probably reflects the higher ground elevation and the time required to fill the low-lying areas to the east. Based on a ground elevation at these sites of about 1 to -1 ft, it is possible that water would have begun to flow across low areas in the Gentilly Ridge in this timeframe. For instance, the controlling elevation along Franklin Avenue through Gentilly Ridge is only about 0 to 1 ft. Therefore, water could begin to flow across the ridge at this location, thereby providing an explanation of the flooding times and direction of flow at Sites 22 and 23 (Figure 123) in the London East area. At Site 16 (Figure 126), which is close to the high ground at Gentilly Ridge, the reported time of flooding was about 1830 UTC (1:30 p.m. CDT).

Figure 127. Floodwall and earth levee breaches on west side of the Inner Harbor Navigation Channel.

In the area just south of the Florida Canal and west of the Peoples Canal, the eyewitness accounts at Sites 17, 18, and 19 indicate that the water entered this area between 1200 and 1300 UTC (7:00 and 8:00 a.m. CDT). A stopped clock at Site C4 (Figure 126) indicated a time of 1322 UTC (8:22 a.m. CDT) at an elevation of 3.45 ft, which is near the observed high-water elevations in this area. The rates of water level rise reported by these eyewitnesses appear to be somewhat less than those closer to the IHNC. This may reflect the spreading of the floodwaters over larger areas before reaching these sites. These sites also appear to be on somewhat higher ground. Further to the west at Site 20, there is an eyewitness account of a rapid rush of water entering her house around daybreak (about 1130 UTC (6:30 a.m. CDT)). This account may be reasonable since her house is close to the Florida Canal. To the south and west of this location at

Sites 21, 22, and 23, flooding did not occur until between 1400 and 1500 UTC (9:00 and 10:00 a.m. CDT). At Site 24 which is on the higher ground near Gentilly Ridge, it was early afternoon on Monday before flooding was observed.

Figure 128 shows a hydrograph of water elevation in feet versus time for the area west of the IHNC and south of Gentilly Ridge. This hydrograph was developed from eyewitness accounts (Sites 1, 2, 3, 4, 9, 17, and 18) of times and elevations in their houses and surveyed stopped-clock data (Sites C1-C4). While there is scatter in the data in Figure 128, it does capture the general shape of the hydrograph for this area. This hydrograph is represented by the "eyeball" regression plotted in Figure 128. Based on the eyewitness accounts, stopped clocks, and the hydrograph in Figure 128, it appears that water began to enter the area by about 1100 UTC (6:00 a.m. CDT), rising rapidly at a rate of about 3 to 6 ft/hr in the low-lying areas immediately west of the IHNC.

Gauge records on the IHNC at I-10 (Figure 129) were examined to determine if additional insight could be gained with respect to overtopping and/or breaching along the IHNC West floodwall system. According to the USGS gauge at I-10, there is a dramatic drop in stage of about 5 ft at about 0930 UTC (4:30 a.m. CDT), while the Orleans Levee District Gauge flattens out during this same period. Following this period, the stages at both gauges continue to rise. While these data should not be viewed as absolute (particularly the 5-ft drop in stage) these gauge records suggest that something may have occurred to impact the gauges in the 0900 to 1000 UTC (4:00 to 5:00 a.m. CDT) timeframe. These gauge changes could be the result of breaches along the east and/or west sides of the IHNC, or mechanical problems, including debris accumulation, with the gauges themselves. Therefore, there is insufficient data to conclude that the gauge changes reflect overtopping or breaching at this time.

A staff gauge at the IHNC Lock (Figure 129) read by the lock operator also provides insight into the timing of overtopping of the floodwalls and levee along the IHNC. The elevation of the east-west earth levee (Figure 126) is about 11 ft. According to the hydrograph at the lock (Figure 129), that has the same high-water elevation (14.3 ft) as HWMs in the area near the earth levee, this earth levee would have overtopped at about 1045 UTC (5:45 a.m. CDT) on Monday. The floodwall near the breach is at about 13 ft, and according to Figure 129 would not have overtopped until about 1230 UTC (7:30 a.m. CDT). There is also a low section of floodwall that runs south from the earth levee along the IHNC where the elevation averages about 12 ft for a distance of about 450 ft, and 12.6 ft or less over a distance of 1,400 ft down to the Florida Avenue bridge. The high-water elevation at this floodwall is about 15.3 ft. If the IHNC Lock hydrograph is adjusted to reflect the actual peak water level at this location, this floodwall would begin overtopping at about 1130 UTC (6:30 a.m. CDT) over the low area at 12 ft and over the entire length by about 1145 UTC (6:45 a.m. CDT). Therefore, the only known sources of water (assuming no breach in the floodwall or earth levee) in the 1100 to 1200 UTC (6:00 to 7:00 a.m. CDT) timeframe when the IHNC West area was experiencing rapidly rising water would be from the 1,500-ft earth levee, the low sections (approximately 1,800 ft) of floodwall, and possibly the 35-ft breach at the I-10 railroad gate. It should be noted that these hydrographs capture the mean water levels and do not reflect wave activity that could have been present. Wave effects would be greatest on the floodwall south of the earth levee that is exposed to both the GIWW and the IHNC. Wave effects on the earth levee were likely significant but less than on the south

floodwall. Therefore, it is possible that waves could have been putting significant amounts of water over the floodwall and levee much earlier than is indicated by the hydrographs. These earlier times are more consistent with the early eyewitness accounts in the IHNC West area.

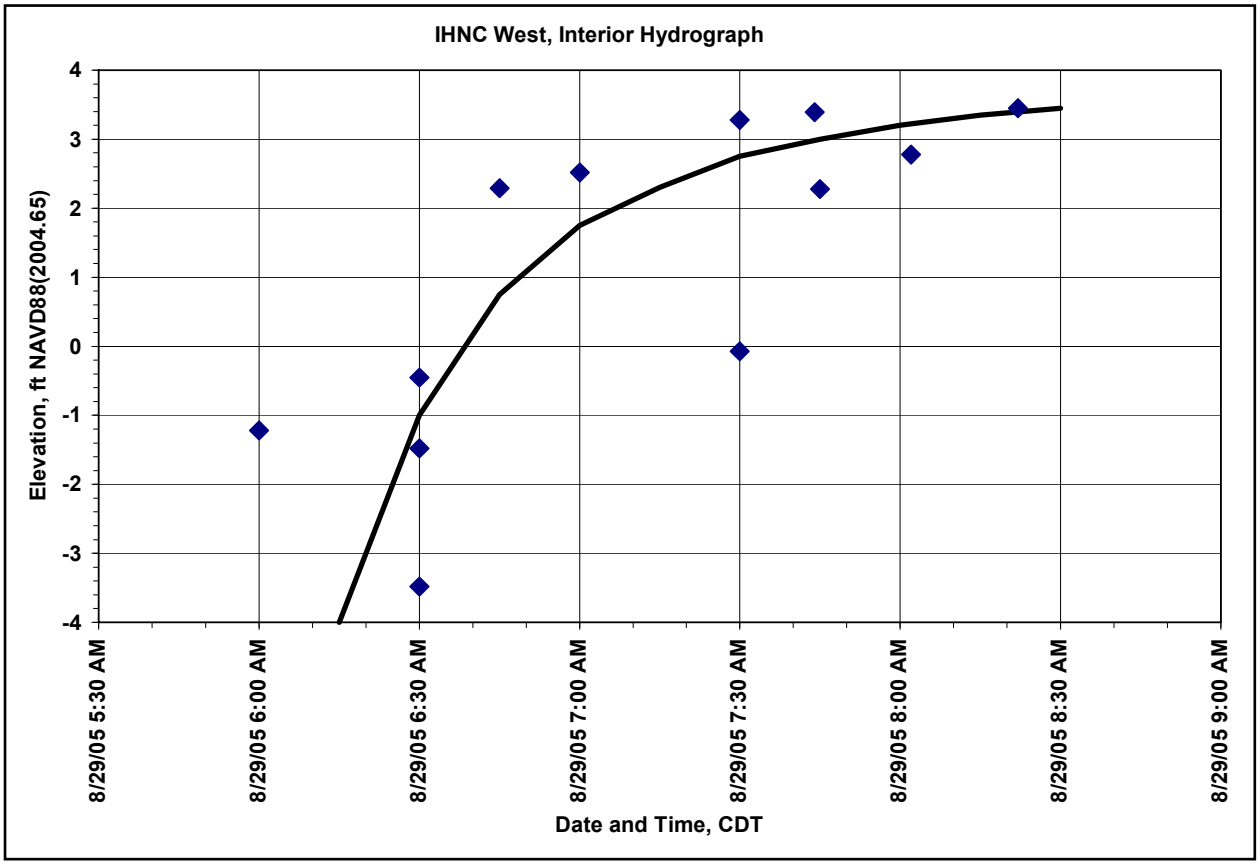

Figure 128. IHNC West hydrograph based on eyewitness accounts and stopped clocks. [Time is referenced to CDT].

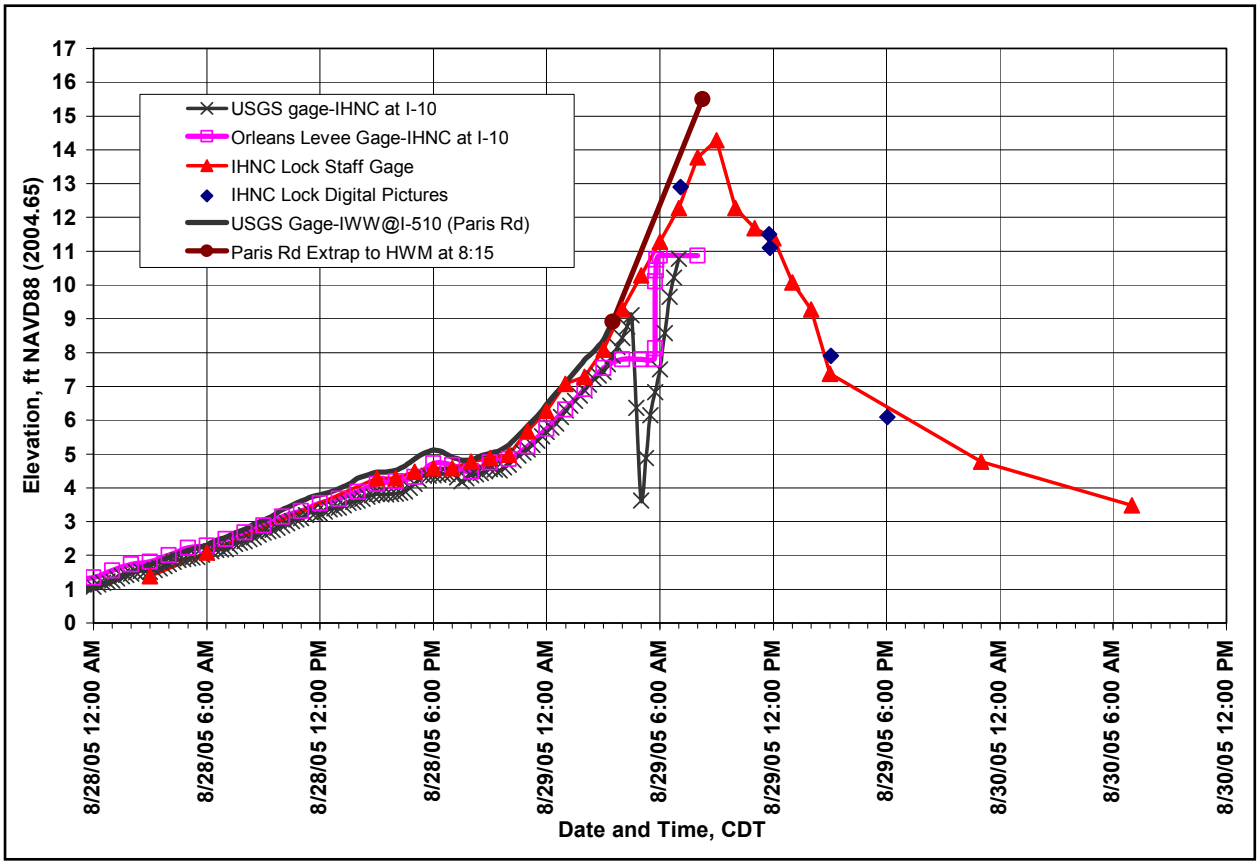

Figure 129. IHNC hydrographs. [Times are referenced to CDT]

In summary, it appears that floodwaters from the IHNC began to enter the low lying areas immediately to the west of the canal by at least 1045 UTC (5:45 a.m. CDT), or probably even earlier due to wave overtopping effects or possibly breaching of the earth levee, the floodwall, or the railroad opening. Although it is clear that water entered the IHNC West area very early on Monday morning, the data are insufficient to provide the timing of the breaches at the earth levee, the floodwall, and the railroad sand bag closure. In the low-lying areas immediately to the west of the IHNC, the water rose rapidly in the range of about 3 to 6 ft/hr, peaking early with observed HWMs ranging from about 4.2 to 5.3 ft. After filling these low-lying areas, the floodwaters began to fill the surrounding higher elevation areas in the 1400 to 1530 UTC (9:00 to 10:30 a.m. CDT) timeframe. The rate of rise in these areas was also slower. By midmorning the water levels had risen to the point where flow would have begun to cross Gentilly Ridge into the areas north of the ridge.

Bartholomew Golf Course

The location of the Bartholomew Golf Course area is shown in Figure 130. This area is bounded on the north by Lake Pontchartrain, on the east by the IHNC floodwall, on the south by Gentilly Ridge, and on the west by the railroad grade and Peoples Canal. There are four ways for water to enter this area: (1) overtopping of the hurricane protection levee along

Lake Pontchartrain; (2) overtopping of the IHNC floodwall; (3) flow over Gentilly Ridge from the south; and (4) from Peoples Canal through the railroad grade.

As shown in Figure 130, there is considerable variation in the reported times of flooding in this area, ranging from early morning to late afternoon. This variability may reflect the fact that this area received water from several sources.

At Sites 1 and 2 in Figure 130, two eyewitnesses observed the floodwall overtopping early in the morning on 29 August. At Site 1, the eyewitness reported this overtopping to have occurred at about 1330 UTC (8:30 a.m. CDT), which is consistent with the time of peak water from the IHNC Lock hydrograph. The eyewitness at Site 2 could only say that it was in the early morning timeframe. Both these eyewitnesses noted that this was more wave splashing rather than complete overtopping. They also noted that while this did put water in the street and up to the back of their houses that it ran off quickly, and that the major flooding did not occur until later in the day. The early times reported at Sites 3 and 4 (1130 and 1230 UTC (6:30 and 7:30 a.m. CDT), respectively) may reflect runoff from wave overtopping. Another source of water to this area was through the railroad grade from Peoples Canal. There are several subsurface drains connecting Peoples Canal with this area, as well as an open 6-ft culvert near Site 7 in Figure 130 where a large scour hole on the east (golf course) side of the railroad grade provided evidence of flow from the Peoples Canal (Figure 131). These openings provide a direct conduit of water to this area and, therefore, could provide water from the IHNC and London East areas. Therefore, floodwaters from the IHNC could have traveled along the Peoples Canal to this area in the early to midmorning timeframe.

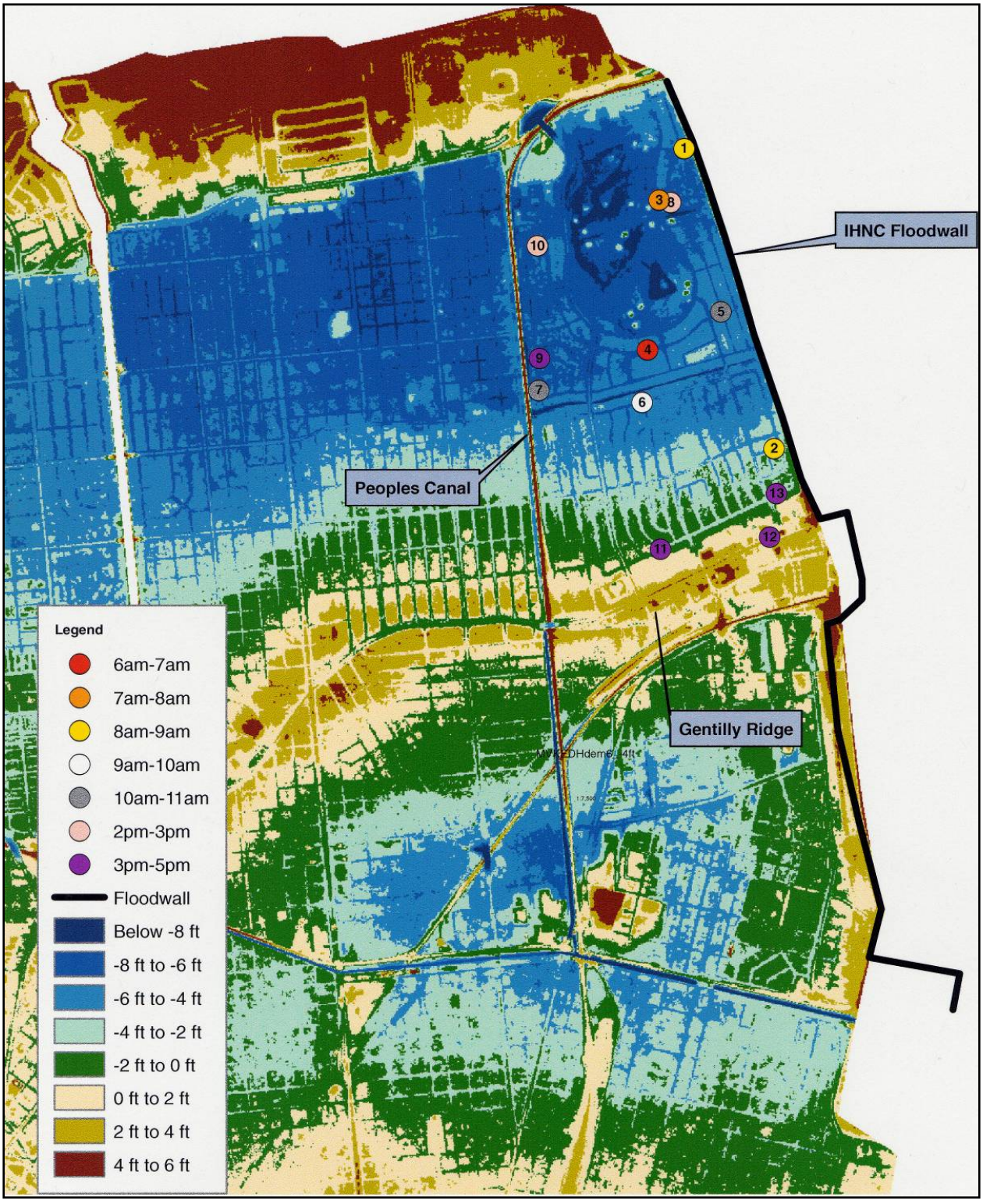

Figure 130. Bartholomew Golf Course area with approximate locations of eyewitness accounts. [Times are referenced to CDT].

Numerous eyewitnesses reported water spewing up through the storm drains consistent with backflow from Peoples Canal. Figure 132 shows water backing up through the storm drains from Peoples Canal on the campus of the Baptist Theological Seminary on Monday afternoon. At Sites 5 to 7, floodwaters are reported in the 1500 to 1600 UTC (10:00 to 11:00 a.m. CDT) timeframe. The eyewitness at Site 1 also reported that after the initial waters from the overtopping had run off, he began to see significant flooding beginning about 1600 UTC (11:00 a.m. CDT). Therefore, the majority of eyewitnesses in this area observed flooding in the midmorning timeframe. However, at Sites 8 to 10, flooding is not observed until midafternoon. There were also accounts of water coming under the Chef Menteur (Gentilly) overpass into the area from the south. The first signs of flooding on Gentilly Ridge were not reported until the 2000 to 2100 UTC (3:00 to 4:00 p.m. CDT) timeframe (Sites 11 to 13). These later times probably reflect the higher elevation of the ridge in this area compared to those which are further west.

Figure 131. Scour hole east of railroad grade indicating flow from Peoples Canal into the Bartholomew Golf Course area.

Figure 132. Water backing up through storm drain on the campus of the Baptist Theological Seminary on Monday afternoon.

In summary, the major sources of water to the Bartholomew Golf Course area are flow from the Peoples Canal, and from the IHNC west area crossing over Gentilly Ridge. Early flooding of a fairly short duration was also reported along the IHNC floodwall from wave overtopping. Although there is some variability in eyewitness accounts, it appears that major flooding began in the midmorning timeframe in the low lying areas. Flooding along the higher ground at Gentilly Ridge did not occur until later in the afternoon.

New Orleans East

The location of the New Orleans East study area is shown in Figure 133. The New Orleans East area is bounded on the south by the GIWW, on the west by the IHNC, and on the north and east by Lake Pontchartrain and marshlands. Significant levee overtopping and breaches occurred all along the GIWW. There were also a few breaches along the floodwall on the IHNC near I-10, as well as overtopping of the floodwall near the Lakefront Airport. Overtopping also occurred along the levee at Lake Pontchartrain, but to a much lesser degree than on the GIWW. Therefore, the New Orleans East area received floodwaters from all directions.

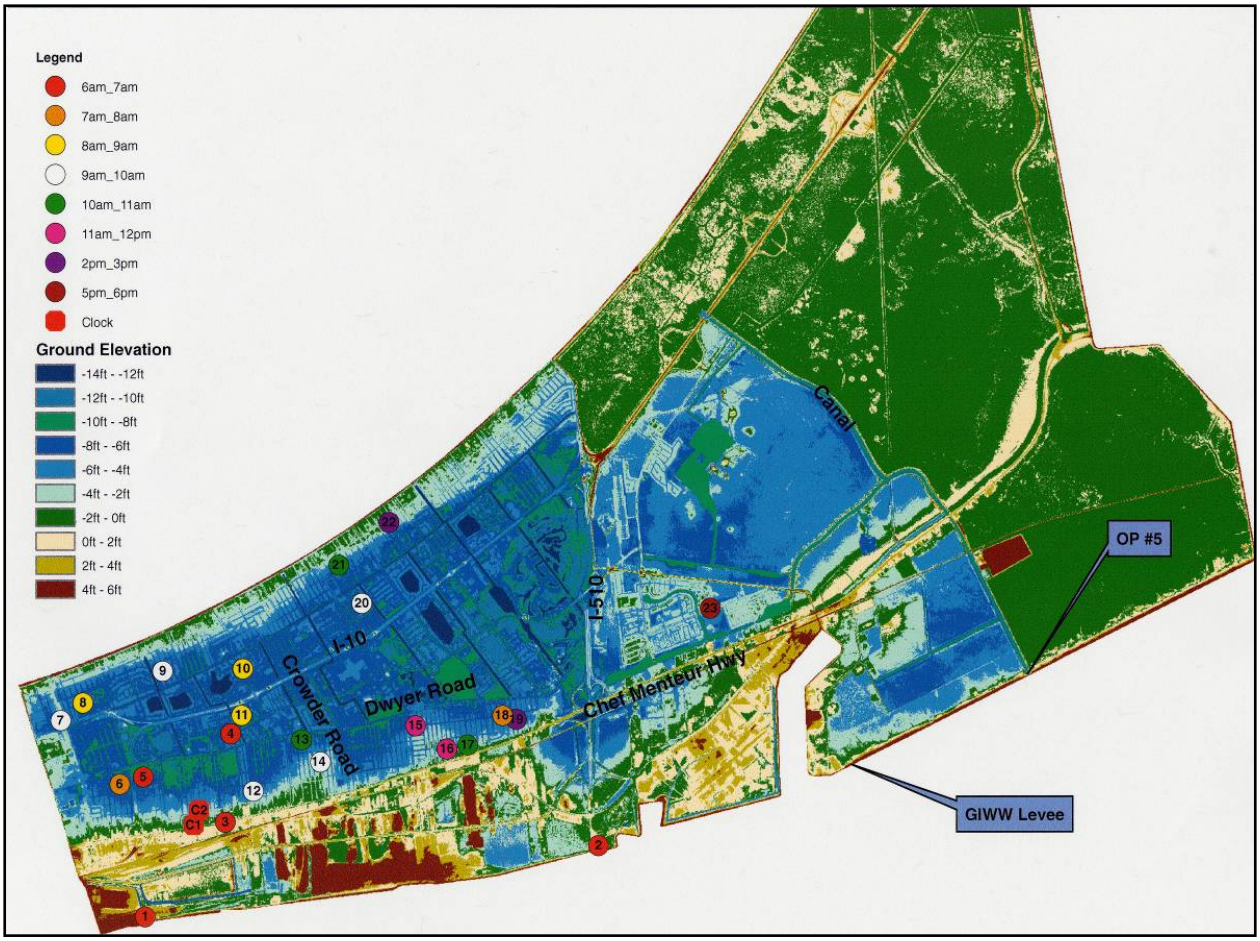

Figure 133. New Orleans East area with locations of eyewitness accounts and stopped clocks. [Time is referenced to CDT].

Approximately 25 eyewitness interviews have been conducted in the New Orleans East area. Stopped-clock data have also been gathered in this area, as well as video footage of the levee overtopping at the Michoud power plant. At Site 1 (Figure 133) an operator at OP 20 pump station stated that as soon as it became light enough to see (about 1120 UTC (6:20 a.m. CDT)), he observed water flowing over the levee for as far as he could see. The elevation of the levee near this location is about 13 ft but drops to as low as 12.5 ft (based on pre-storm LIDAR data adjusted to NAVD88 (2004.65) about 2 miles east of OP 20. He indicated that the water was overtopping the levee by at least 2 ft until about 1600 UTC (11:00 a.m. CDT). He also reported that he could see across the GIWW to the south at this time, and that water was also going over the levee into the sub-basin north of the Lower Ninth Ward and St. Bernard Parish area. The elevation of this levee just south of the GIWW ranges from 11.1 to 15 ft (based on pre-storm LIDAR data adjusted to NAVD88 (2004.65). Further to the east at the Michoud power plant (Site 2) water was observed flowing over the levee about 1115 UTC (6:15 a.m. CDT), continuing to about 1500 UTC (10:20 a.m. CDT). It should be noted that when the observers were first able to see (shortly after 1100 UTC (6:00 a.m. CDT)), the levees were already overtopping. Therefore, the initiation of overtopping must have begun sometime prior to about 1115 UTC (6:15 a.m. CDT). Based on extrapolating the Paris Road USGS gauge up to a peak

water level of 15.5 ft at 1315 UTC (8:15 a.m. CDT, the low spot in the levee would have began overtopping at about 1100 UTC (6:00 a.m. CDT) and likely earlier because of wave activity (Figure 129). Also, according to the extrapolated Paris Road USGS gauge, the overtopping of the 13-ft levee would have began about 1130 UTC (6:30 a.m. CDT). Once again, this would likely have been earlier because of wave activity.

At Site 3 just north of the Chef Menteur Highway, an eyewitness reported that the water was flowing over the east-west railroad line from south to north between 1130 and 1200 UTC (6:30 and 7:00 a.m. CDT). A survey of a HWM in this area indicates that the water was almost 5 ft over the railroad line at this location. Two stopped clocks that were surveyed in this area (Sites C1 and C2) indicated times of 1145 and 1125 UTC (6:45 and 6:25 a.m. CDT), thereby supporting the observed early flooding times. Another eyewitness at Site 4 reported that the water began to pour into his house about 1100 UTC (6:00 a.m. CDT), and that within about 15 min it was chest high. At Site 5, the eyewitness thought it was some time between 1130 and 1230 UTC (6:30 and 7:30 a.m. CDT) when the water started to rise rapidly. Just to the east, at Site 6, the eyewitness stated that it was between 1230 and 1300 UTC (7:30 and 8:00 a.m. CDT) when the flooding began. North of Dwyer Road, the flooding times are a little later, in the 1300 to 1500 UTC (8:00 to 10:00 a.m. CDT) timeframe (Sites 7 to 11). Several eyewitness accounts just south of the Lake Pontchartrain Levee reported floodwaters arriving in the 1300 to 1400 UTC (8:00 to 9:00 a.m. CDT) timeframe from the south. A hydrograph was developed at Sites 6 and 9 based on surveyed elevations of eyewitness accounts (Figure 134). These data document the rapid rise in water elevation of about 3 to 4 ft/hr in this area in the early morning hours. The drop in water level shown at Site 6 was reported by several eyewitnesses and appears to represent leveling off of water levels as the floodwaters move eastward.

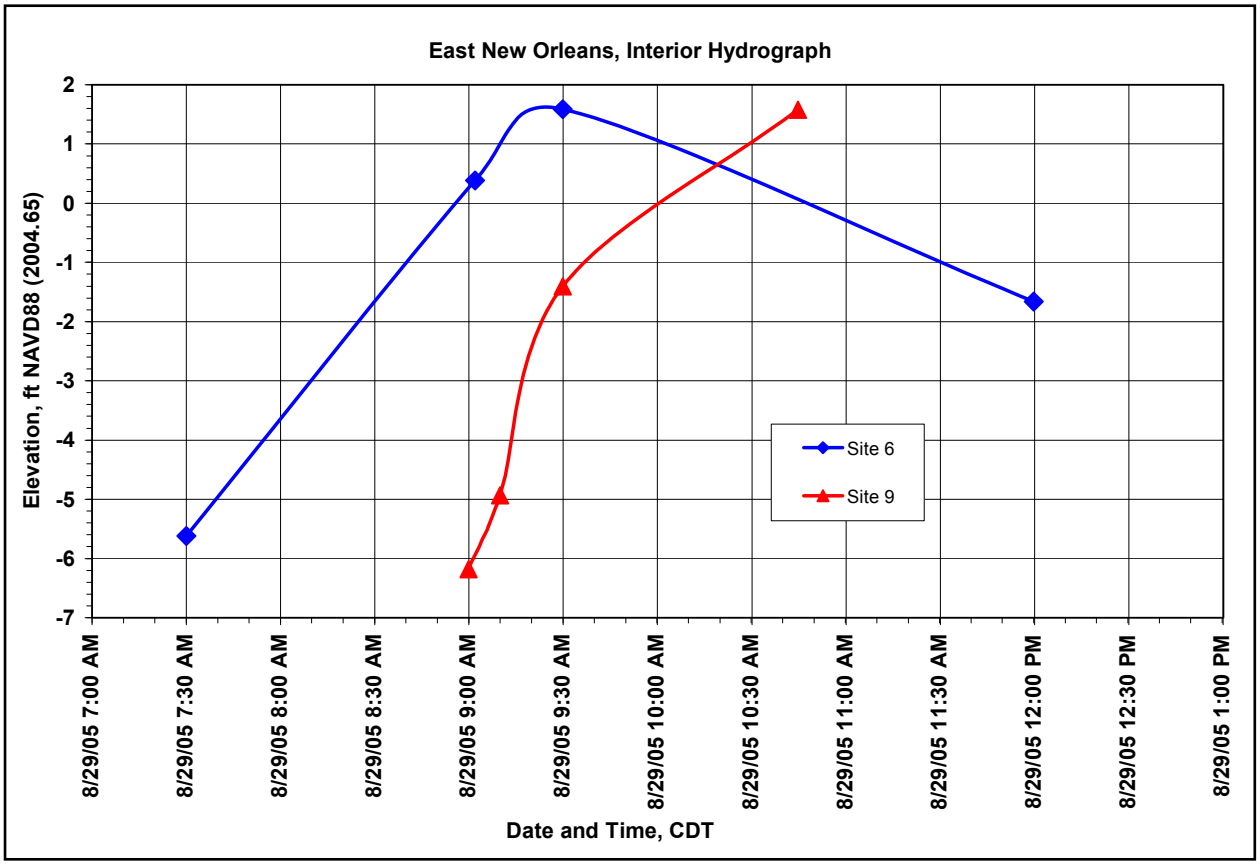

Figure 134. New Orleans East hydrographs based on surveyed elevations of eyewitness accounts at Sites 6 and 9. [Times are referenced to CDT].

Farther east between Crowder Road and I-510, the flooding times are generally in the late morning to early afternoon (Figure 133, Sites 13 to 23). The overtopping of the GIWW east of I-510 was also extensive with floodwaters moving both to the north and west. Vegetative evidence indicates that the floodwaters flowed east to west across the canal that connects to the OP 15 pump station. At some point the floodwaters would have merged with the flow coming from the west; however, the location and timing of this is not known.

In summary, it appears that floodwaters entered the East New Orleans area from several locations. West of I-510, the dominant source of water appears to be from the overtopping and breaching of the levee system along the GIWW between the IHNC and the confluence with the MRGO. It appears that this overtopping occurred early on Monday morning by about 1100 UTC (6:00 a.m. CDT) or possibly earlier. These floodwaters moved both north and east, eventually merging with the floodwaters coming from the overtopping and breaching of the GIWW Levees to the east of the MRGO confluence.

Lower Ninth Ward and St. Bernard Parish

The location of the Lower Ninth Ward and St. Bernard Parish study area is shown in Figure 135. This area is bounded on the south by the Mississippi River, on the west by the

IHNC, and on the north and east by the GIWW and MRGO. A local levee separates the Lower Ninth Ward and St. Bernard Parish into a northeastern section that is primarily marsh and a southwestern section that is primarily populated. The primary sources of flooding for this area are the overtopping and two breaches along the IHNC, and the overtopping and numerous breaches along the GIWW and MRGO. Data in this area include eyewitness accounts, stopped clocks, and video footage.

There have only been a limited number of interviews collected in the Lower Ninth Ward, primarily due to the fact people have only recently been allowed back in to this area. One eyewitness at Site 3 (Figure 135) reported that shortly after about 0930 UTC (4:30 a.m. CDT) on Monday he observed water flowing into his home, and that by about 1000 UTC (5:00 a.m. CDT) the water was at the top of his first floor. He stated that the flow was coming down Galvez Street from the west. Another eyewitness at Site 4 reported seeing flood waters at about 1030 UTC (5:30 a.m. CDT). He and his wife took refuge in a neighbor's two-story house, and he noted that within a short time, the water was about 3 to 4 ft above the second story floor. At OP 5 (Site 9), there is an entry in the log book which states that at 1030 UTC (5:30 a.m. CDT) the power was turned off to the pump station for safety due to high water levels. One of the operators at OP 5 stated that he first observed flooding at about 0930 UTC (4:30 a.m. CDT) on Monday, and that by 1030 UTC (5:30 a.m. CDT), the water was entering the station. Thus, the eyewitness accounts indicate that water was entering the northern region of the Lower Ninth Ward early on Monday morning, possibly as early as 0930 UTC (4:30 a.m. CDT).

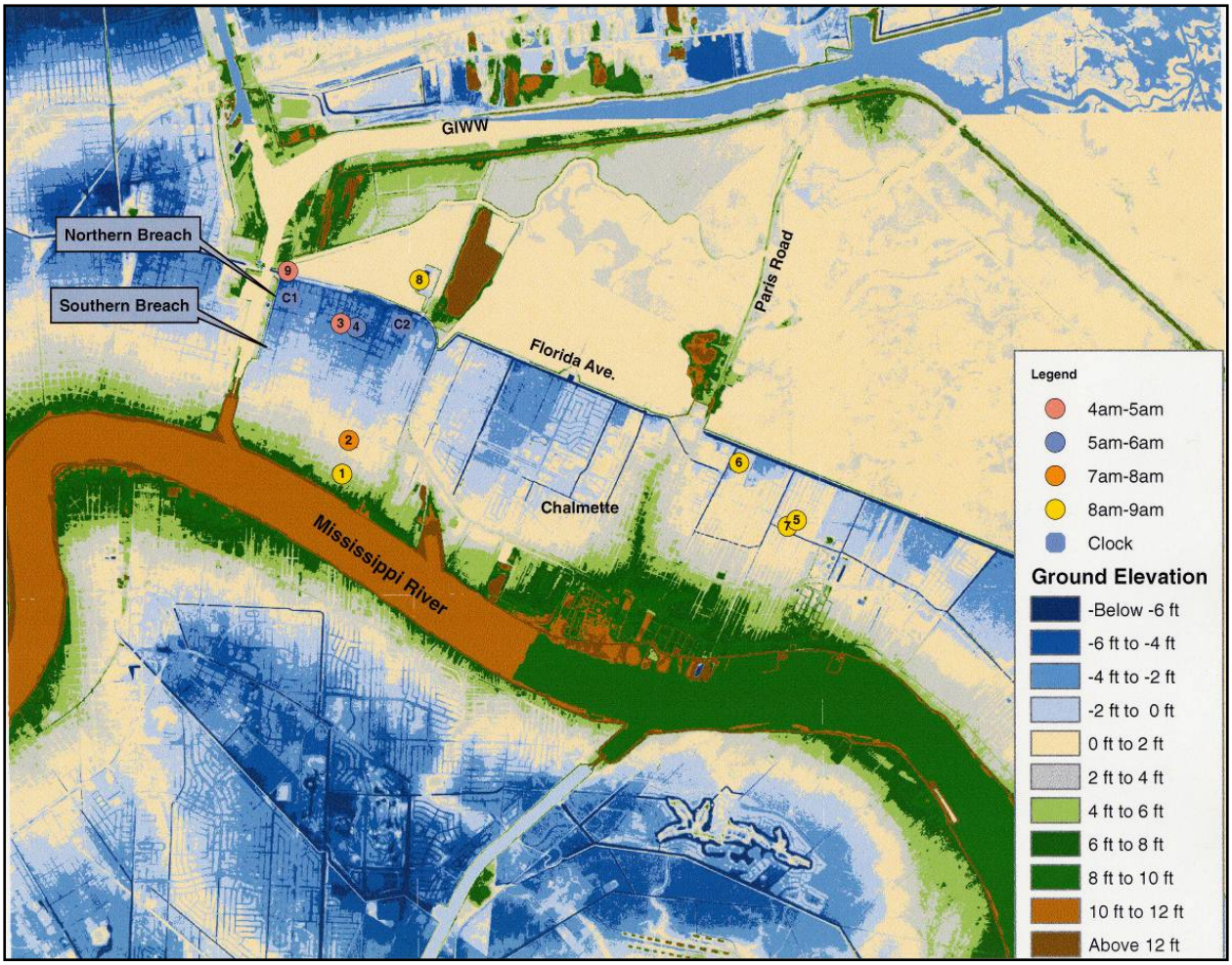

Figure 135. Lower Ninth Ward and St. Bernard Parish study area with locations of eyewitness accounts and stopped clocks. [Time is referenced to CDT].

Two sets of stopped-clock data were also obtained in this area to provide more insight into the time of flooding. In the area around Site C1, which is immediately east of the northern breach on the IHNC, data from nine stopped clocks were obtained (Figure 135). Further east around Site C2, data from eight additional clocks were obtained. The elevation of these clocks was surveyed relative to observed HWMs, which for this area were about 10.5 ft. A stage hydrograph was developed from these data and is shown in Figure 136. This hydrograph reveals the rapid water level rise that occurred early on Monday morning. At Site C1, two of the clocks indicate a time of about 1015 UTC (5:15 a.m. CDT), while two other clocks at the same elevation indicate a time of about 1130 UTC (6:30 a.m. CDT). Four other clocks at higher elevations at Site C1 also indicate a time of about 1130 UTC (6:30 a.m. CDT). Also plotted in Figure 136, is the floor elevation of station OP 5 which was shut down at 1030 UTC (5:30 a.m. CDT). This point agrees with the two 1015 UTC (5:15 a.m. CDT) clock readings, which further supports the earlier flood times. The ground elevation in this area is about -6 ft, which would indicate that at +2 ft, the water level had to have risen about 8 ft, before the clocks became inundated. Therefore, the actual breach time would have had to have been sometime prior to the recorded times on the clocks, which would be in agreement with the eyewitness accounts of about 0930 UTC

(4:30 a.m. CDT). At Site C2, which is on slightly higher ground and further to the east, the hydrograph in Figure 136 indicates that significant flooding began by about 1230 UTC (7:30 a.m. CDT). This hydrograph seems to be compatible with the hydrograph developed at the Jackson Barracks (Site 1 in Figure 135), which is also shown in Figure 136. A time-stamped photograph taken at Site 1 reveals that at 1246 UTC (7:46 a.m. CDT), the floodwaters had not yet reached this location. However, by about 1300 UTC (8:00 a.m. CDT), the floodwaters were reported to be coming down the street from the north in front of the HQ building, and at 1313 UTC (8:13 a.m. CDT) the water was already up to the wheels on a truck cab (Figure 137). Using the time-stamped photographs at the Jackson Barracks, the hydrograph in Figure 136 was developed by surveying the observed water levels. This hydrograph shows that the water rose rapidly starting about 1300 UTC (8:00 a.m. CDT), and peaked at elevation 10.5 ft at about 1945 UTC (2:45 p.m. CDT). Ground elevation in this area is about +4 ft. Another eyewitness at Site 2, reported water shooting up through her floor furnace at about 1230 UTC (7:30 a.m. CDT) on Monday, and that within about 15 min the water was about 9 ft deep in her house. Site 2 is slightly east of Site 1 and appears to be at a lower elevation.

Based on the eyewitness accounts and stopped-clock data, it appear that waters began entering the Lower Ninth Ward prior to 1030 UTC (5:30 a.m. CDT), and possibly as early as 0930 UTC (4:30 a.m. CDT). Potential sources of water include overtopping of the IHNC floodwall, the two breaches in the IHNC floodwall, and flow from the overtopping of the GIWW Levee. As indicated in the New Orleans East section, an eyewitness reported flow overtopping the GIWW Levee shortly after about 1100 UTC (6:00 a.m. CDT). This water would have to fill the area between the GIWW Levee and the local levee at Florida Avenue before spilling over into the populated region of the Lower Ninth Ward.

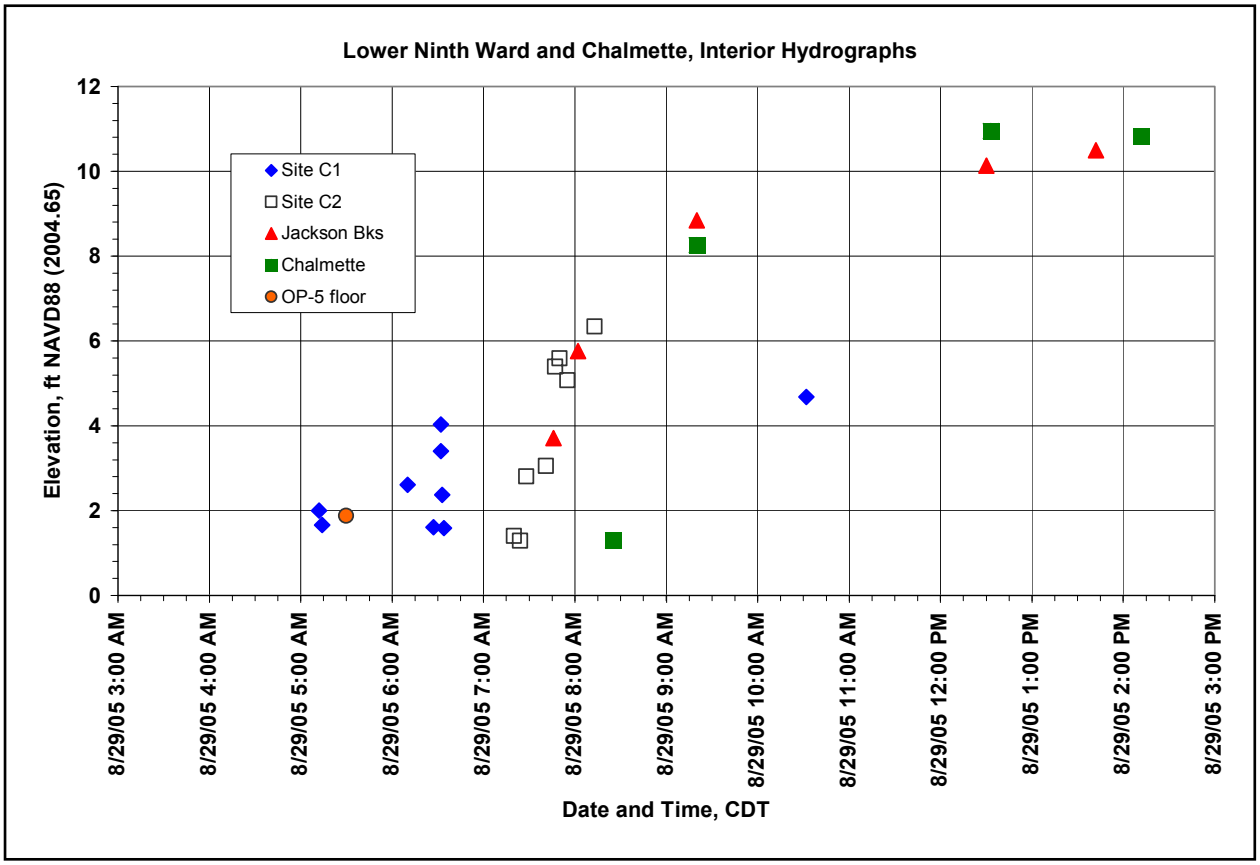

Figure 136. Chalmette and Lower Ninth Ward hydrographs. [Time is referenced to CDT].

Figure 137. Photograph of the water rising on Delery Street just west of Jackson Barracks. The photo was taken at about 1300 UTC (8:00 a.m. CDT), Monday, 29 August 2005.

Based on levee profiles and extrapolation of the Paris Road gauge up to the peak water level at 1315 UTC (8:15 a.m. CDT), the low area in the levee on the south side of the GIWW at 11.1 ft would have overtopped at about 1000 UTC (5:00 a.m. CDT). However, several eyewitness accounts at the water treatment facility (Site 8), located just north of the local sheet-pile levee at Florida Avenue reported that their local facility levee which is about elevation 11 ft did not overtop until about 1400 UTC (9:00 a.m. CDT). Preliminary information indicates that the local sheet pile levee at Florida Avenue is slightly higher than the water treatment facility levee. Therefore, it does not appear that the waters from the GIWW would have entered the area south of Florida Avenue in the early morning timeframe. Another source of water would be the overtopping of the IHNC floodwall. According to the lock hydrograph in Figure 129, the IHNC floodwall, at elevation 12.5 to 13 ft, would have overtopped at about 1230 UTC (7:30 a.m. CDT). While this time would be in agreement with the observed flooding at the Jackson Barracks (Site1), and at Site 2, it is much too late to account for the earlier times at Sites 3, 4, 9, and C1. Another alternative is that the early flooding was caused by one or both breaches on the IHNC. If it is assumed that the breaches occurred early, say at 1000 UTC (5:00 a.m. CDT), then the corresponding stage in the IHNC would have been about 10.3 ft. according to the lock hydrograph. Based on the above information, it appears that one or both of the breaches along the IHNC occurred early on Monday morning prior to 1030 UTC (5:30 a.m. CDT), and possibly as early as 0930 UTC (4:30 a.m. CDT). Although breaching may have occurred early at one or both locations, the storm surge was of sufficient magnitude to continue to raise the levels in the IHNC, eventually overtopping the floodwall in the 1230 UTC

(7:30 a.m. CDT) timeframe. A more detailed hydrologic analysis may provide insight into the sequencing of the two breaches.

Further east in St. Bernard Parish, eyewitness accounts, stopped-clock data, and video footage indicate that the floodwaters first entered the areas east of Paris Road (Chalmette) from the northeast. Video footage in the Corinne Estates Subdivision in Chalmette (Site 5 in Figure 135) provides good documentation of this flooding. The video also shows large clumps of marsh grass moving in a northeast to southwest direction, clearly indicating flows from the marsh lands surrounding Lake Borgne and the MRGO. Presence of marsh grass was a common feature on houses and other structures through this entire area, but it was rarely, if ever seen west of about Paris Road. Figure 138 shows the marsh grass and typical inundation level for the homes in this area. Statements and video acquired to date indicate a time of about 1320 UTC (8:20 a.m. CDT) as the arrival time of waves of black water that quickly filled the streets and houses in the Chalmette area. This is verified by video footage from a security camera at the Channel 8 TV tower near the intersection of Magistrate Street and Marietta Drive (Site 6). The camera footage shows water entering the area to the northeast of the tower at about 1320 UTC (8:20 a.m. CDT) and rising very quickly. The two eyewitnesses in the Corinne Subdivision (Sites 5 and 7) also stated very similar times for the water entering their location which is about 0.5 mile away from the TV tower. By approximately 1400 to 1430 UTC (9:00 to 9:30 a.m. CDT), the houses in the vicinity of Corinne Estates Subdivision were inundated to at least 8 to 10 ft deep. A hydrograph was developed at Site 5 based on the video footage, and is shown in Figure 136. As shown in this hydrograph, water levels peaked in this area at about 10.8 ft. As the floodwaters continued to move west, they eventually merged with the water from the IHNC. The exact time and location of this is uncertain but appears to be in the vicinity of Paris Road in the midmorning timeframe.

Figure 138. Marsh grass and typical inundation level for the homes in Chalmette area.

In summary for the Lower Ninth Ward, it appears that flooding began early on Monday morning. Eyewitness accounts and stopped-clock data indicate that floodwaters began entering the Lower Ninth Ward prior to 1030 UTC (5:30 a.m. CDT) and possibly as early as 0930 UTC (4:30 a.m. CDT). These early times suggest that the water entered through one or both of the breaches in the IHNC Floodwall. The floodwall was overtopped later at about 1230 UTC (7:30 a.m. CDT). Time-stamped photographs confirm that flooding had occurred by about 1300 UTC (8:00 a.m. CDT) near the Jackson Barracks along the southern end of this area near the St. Bernard Parish line. The floodwaters from the IHNC moved east, eventually merging with the waters from the Chalmette area near Paris Road in the midmorning timeframe. Flooding in the Chalmette area came from the northeast, entering this area about 1320 UTC (8:20 a.m. CDT). Water levels for the Lower Ninth Ward and St. Bernard Parish peaked at about 10.5 to 11 ft.

New Orleans Downtown

The location of the New Orleans Downtown area is shown in Figure 114. As indicated in the previous sections, the breaching and overtopping of the floodwalls and levees generally occurred early (between about 1130 and 1300 UTC (6:30 and 8:00 a.m. CDT)) on Monday. These floodwaters filled the areas in the immediate vicinity of the breaches first and then began to spread out to the New Orleans Downtown area. Interviews with eyewitnesses in the downtown area revealed times ranging from about noon on Monday to Wednesday, depending on location

and topography. Gauge data are available at the Palmetto Canal which drains much of the New Orleans Downtown area. Figure 139 shows the hydrographs developed at three gauge locations along Palmetto Canal. Also shown in Figure 139 is the OP 10 hydrograph for comparison. As indicated in Figure 139, there is a significant time lag between the OP 10 and Palmetto hydrographs. According to the OP 10 hydrograph, the water levels rose rapidly on Monday, peaking on Tuesday morning, and then beginning a slow fall.

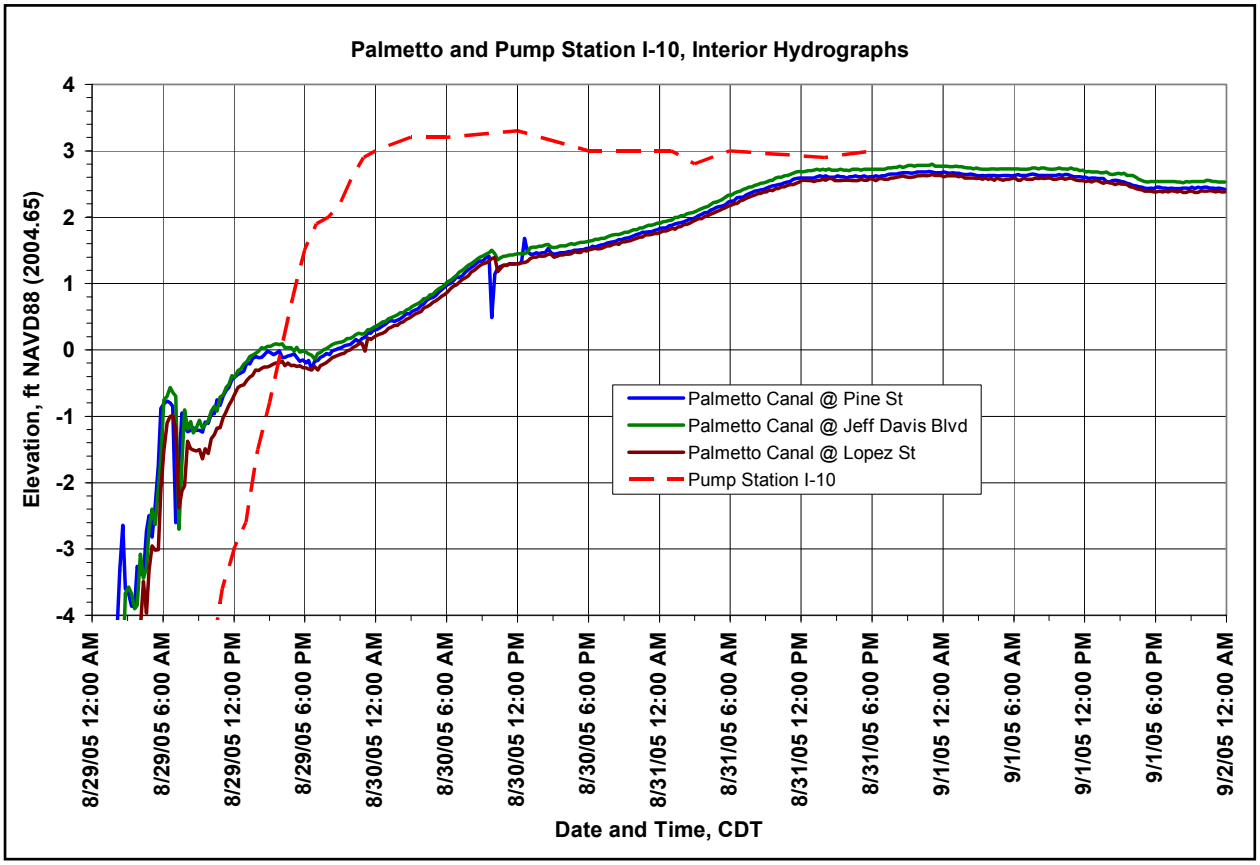

Figure 139. Stage hydrographs at Pump Station OP 10 and Palmetto Canal at Pine Street, Lopez Street, and Jeff Davis Street. [Times are referenced to CDT].

The Palmetto hydrograph indicates that stages gradually rose for several days, peaking about noon on Wednesday at an elevation of about 2.6 ft.

High-Resolution Hydrodynamics: Detailed Waves, Water Levels, Overtopping, and Forces on Structures

Overview

This portion of the report focuses on providing high resolution time histories of water levels, waves, overtopping, and related forces on levees and floodwalls in the New Orleans area; and, in particular, provides estimates of conditions at the locations of levee and floodwall failures at the time of failure. The approach taken here is to blend detailed-resolution models with observations

and measurements to obtain best estimates of conditions within the New Orleans area during Hurricane Katrina. Outputs from the regional modeling effort described previously in this Volume are combined with observations to form boundary conditions appropriate for driving the various models used here. The outputs from these models are compared wherever possible to information available on conditions during the storm, and this information is assimilated into the final estimates of overtopping rates and forces on structures, sometimes by direct minor modification of the values and sometimes via model calibration. All elevations in the high-resolution hydrodynamics section are referenced to NAVD88 (2004.65). Times in this section are referenced to UTC in general; but in places, the corresponding times in CDT are also noted.

Figure 140 shows the geographic areas covered by the detailed-hydrodynamic modeling performed here. In areas exposed to the open gulf in St. Bernard and Plaquemines Parishes, and New Orleans East, massive quantities of water were driven against many miles of coastal levees. Since appropriate levee heights were modeled in the regional-scale ADCIRC and STWAVE runs, the effects of levee overtopping are implicitly included in the boundary conditions provided for the high-resolution calculations from these runs. The incorporation of HWMs into boundary conditions in these areas should account for additional effects due to breaching where they are significant. Figure 141 shows the approach used in obtaining estimates of setup, runup and overtopping of the large flood protection levees, along with potential forces related to these phenomena. As shown here, COULWAVE was considered capable of accurately simulating these processes on the large earthen levees and was, in conjunction with water levels from the ADCIRC regional model runs, modified to reflect information from HWMs. In areas with waves propagating across vertical walls, a complete Navier-Stokes model was used to simulate the wave processes in place of the Boussinesq approximation.

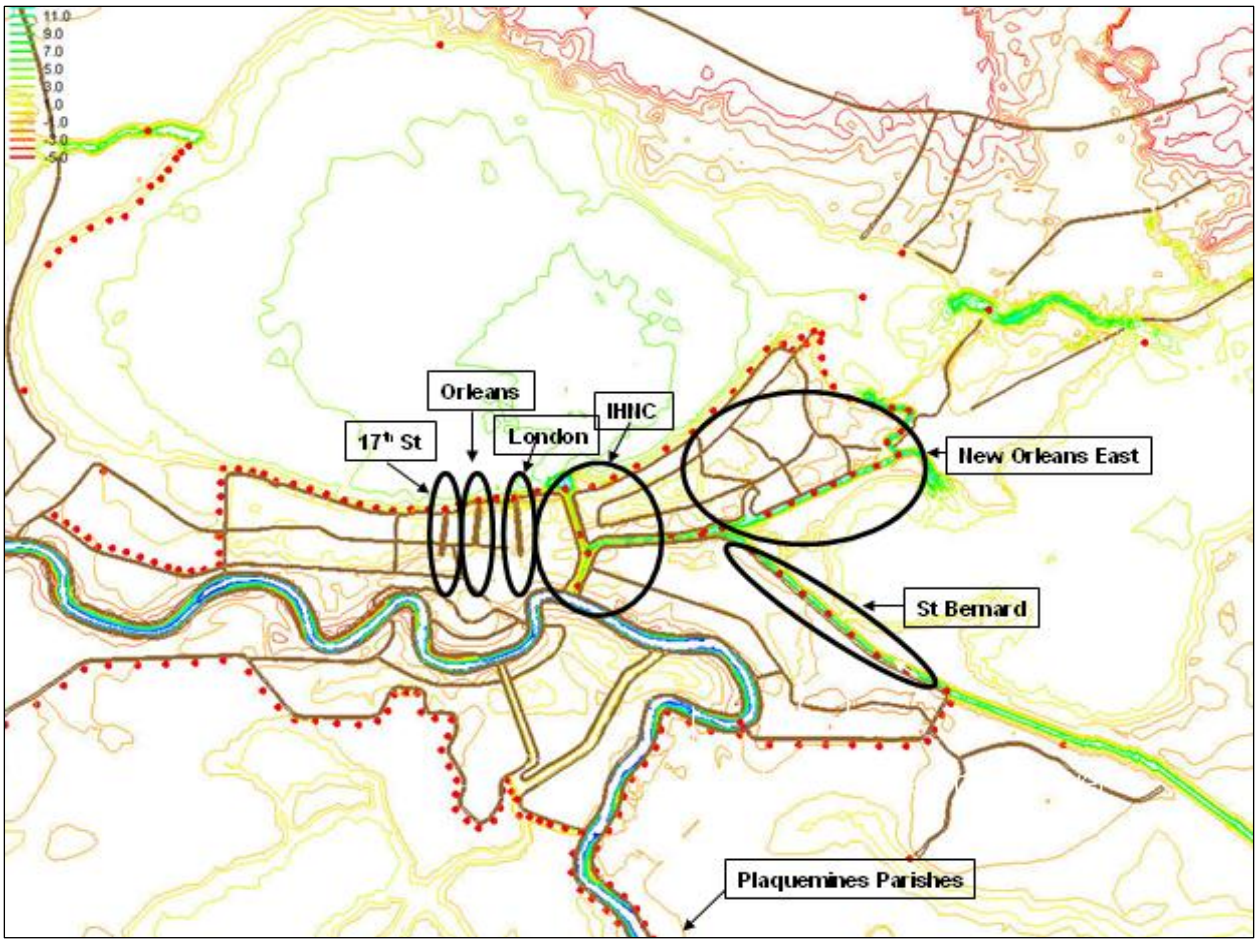

Figure 140. Geographic areas analyzed within the scope of the detailed hydrodynamics portion of the report.

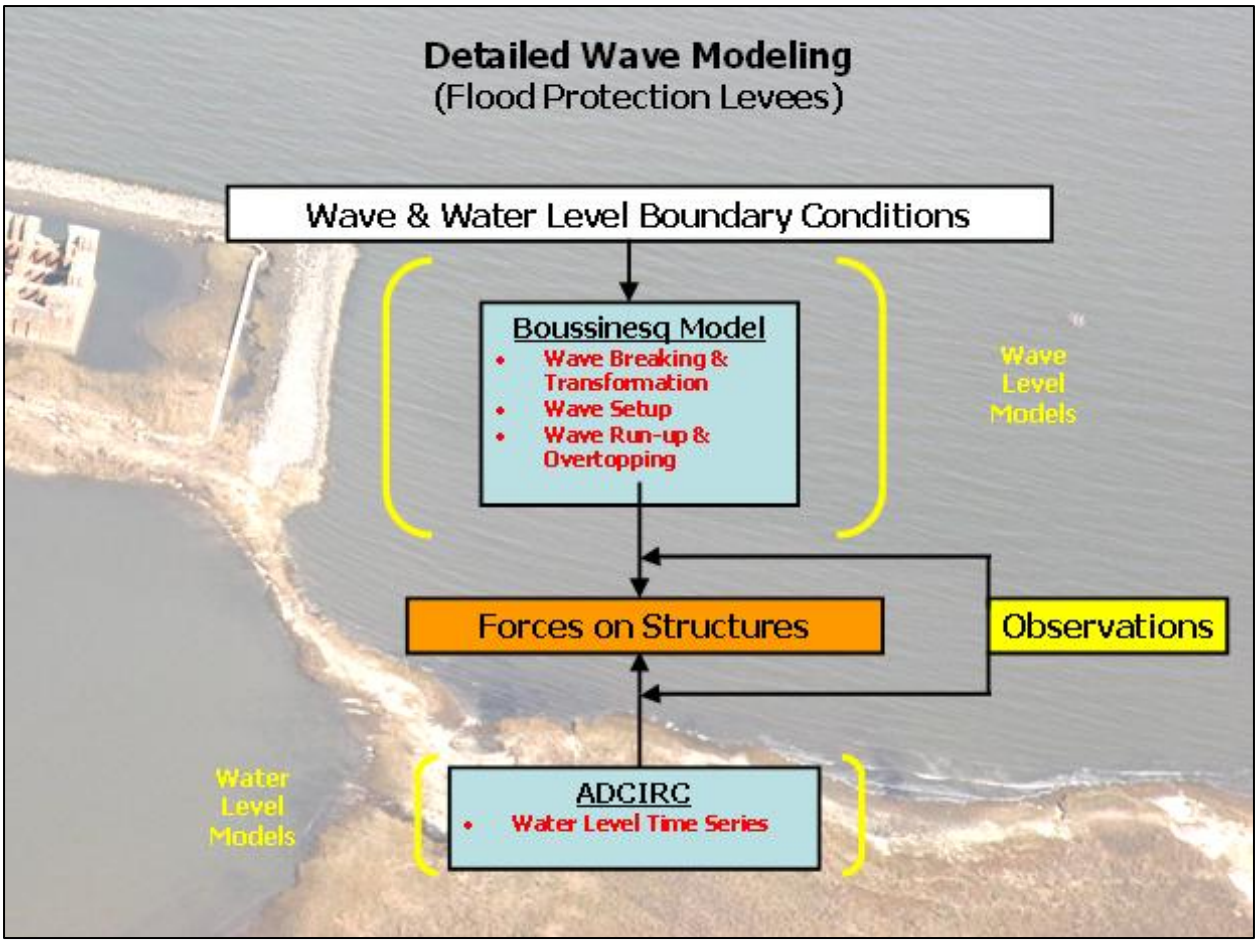

Figure 141. Conceptual diagram of modeling processes and data assimilation used for estimating conditions in the vicinity of large flood protection levees.

In contrast to the situation along the open gulf, water levels within outfall and navigation canals can depend strongly on the time of breaching and size of the breaches relative to canal cross sections. For these canals, as will be discussed in more detail subsequently, observations were used as the primary basis for water level boundary conditions. Waves were not measured within the canals; however, evidence gleaned from video images was used to provide at least a qualitative check on estimated wave heights and periods within the canals.

As a baseline study, a series of ADCIRC model tests were performed to examine the variation of water surface elevation (WSE) and current speeds within the 17th Street Canal for the case of no breaching. In idealized tests with no wind forcing within the canal (Appendix 13), the WSE time series throughout the canal varied little (less than 0.1 ft) from the input forcing hydrograph at the Lake Pontchartrain boundary for simulated boundary conditions equivalent to those during Katrina. This shows that water levels within un-breached outfall canals will tend to remain approximately equal to the level at the boundary, plus the effect of wind setup along the canal. During these tests, steady currents were quite small (less than 0.3 ft/sec) with some seiching (possibly due to numerical effects) producing velocities on the order of 1.1 ft/sec.

Figure 142 shows the set of models applied to the problem of estimating water levels, waves, and resulting forces within the outfall and navigation canals. A combination of parametric and numerical (ADCIRC) models were used to estimate water levels and a combination of three wave models [a physical model, a Boussinesq model (COULWAVE), and a phase-averaged spectral model (STWAVE)] were used to estimate wave conditions within the canals. The physical model provided an objective estimate of 1) wave transformation and decay in the entrance to the 17th Street Canal and 2) wave decay during propagation under the "hurricane proof" bridge near the entrance of this canal. Results from the physical model were also used to "tune" the "bridge decay" within COULWAVE and STWAVE. COULWAVE model provided estimates of 1) potential long-period wave energy resonating within the canal, 2) wave transformation due to combined refraction, diffraction, and reflection, and 3) distributions of forces on floodwalls. Since neither the physical model nor the Boussinesq model addresses local wave generation, STWAVE was used to estimate local wave generation within the canals. No single model was capable of handling all of these important aspects of wave generation, propagation, and decay within the canal areas. A modified version of STWAVE was also used to estimate wave conditions within the IHNC in the vicinity of the floodwalls that breached in the Lower Ninth Ward area.

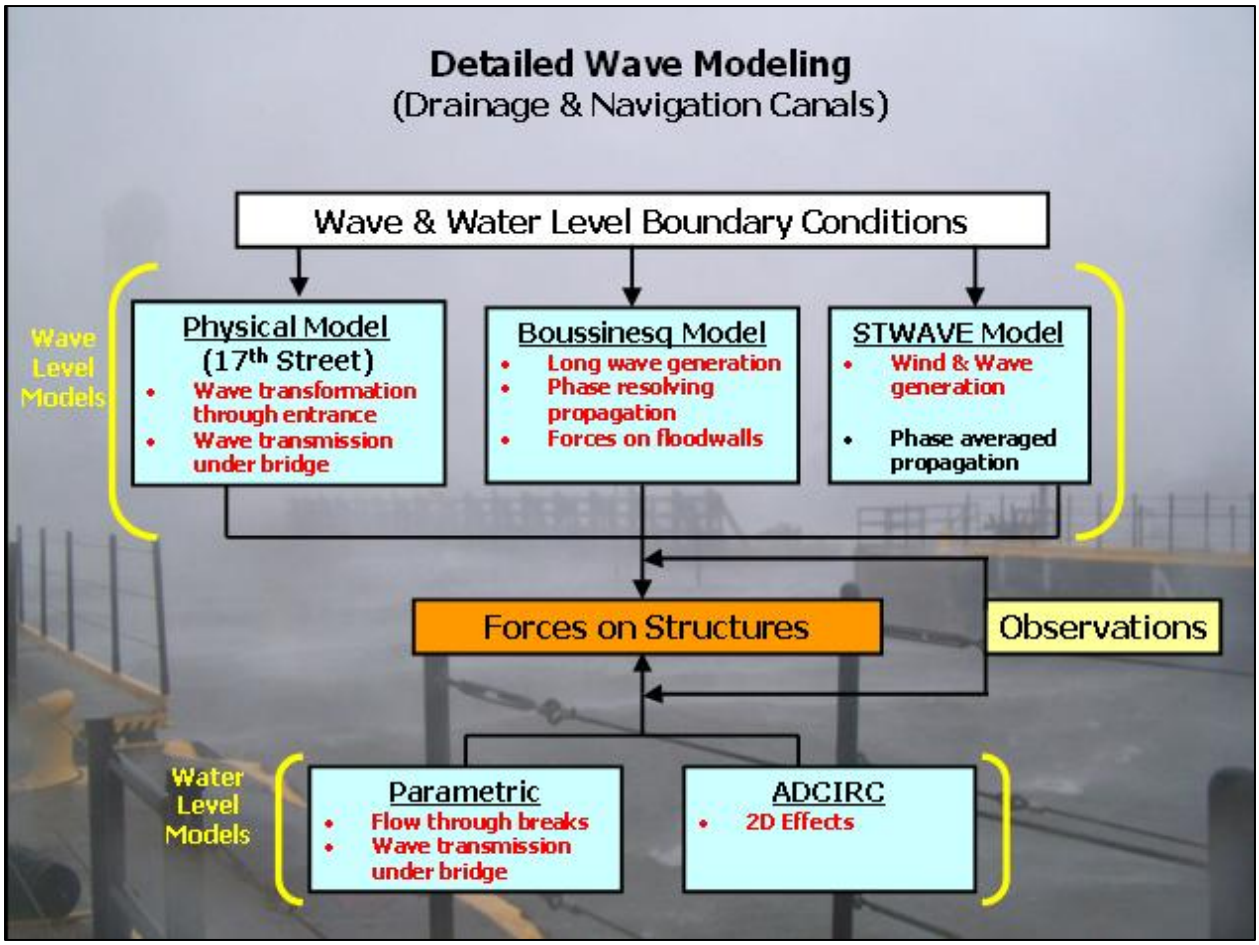

Figure 142. Conceptual diagram of modeling processes and data assimilation used for estimating conditions inside the three outfall canals and navigation canal.

Detailed Time History of Water Levels, Waves, and Related Forces

This section of Volume IV is organized geographically, with the brief descriptions of modeling applications, data assimilation methods and results. Technical details may be found in the referenced Appendices.

17th Street Canal

Introduction. The analysis of the hydrodynamic conditions in the 17th Street Canal have benefited by unusually good documentation although uncertainties remain regarding some of the failure details including the breach evolution and the hydraulic effects of flow blockage. The following sections describe the available information regarding the failure sequence and hydrodynamic and meteorological inputs into the system. This is followed by a description of the wave and hydraulic (both physical and hydrodynamic) models that have been applied to investigate the time histories of water levels in the canal and the wave propagation from Lake Pontchartrain into the canal. Where uncertainties exist, various scenarios have been explored in the computations.

Description of Flood Wall and Levee Failure and Associated Timing

Figure 143 presents an oblique photograph showing the 17th Street Canal failure which is located on the east side of the canal approximately 1,000 ft south of the Hammond Highway bridge. At the time of this photograph, considerable debris has accumulated on the north side of the bridge.

Figure 143. 17th Street Canal on 29 August 2005. Looking south showing breach and debris accumulated against lake side of Hammond Highway bridge.

Although there are several valuable eyewitness accounts and some photographic accounts of flood wall and levee failure, considerable uncertainty of the timing remains. Part of this is due to variances in the eyewitness accounts and between eyewitness accounts and limited quality photographic evidence.

An eyewitness living on the west side of the canal reported that one panel on the east side was leaning sometime between 1100 and 1130 UTC (6:00 and 6:30 a.m. CDT) on the morning of 29 August 2005. He revisited the area sometime between 1400 and 1430 UTC (9:00 and 9:30 a.m. CDT) and reported that the breach width had increased to its full width, approximately 450 ft. A second eyewitness who lived on the west side of the canal reported waves propagating down the canal and overtopping the west floodwall adjacent to his patio at approximately

1400 UTC (9:00 a.m. CDT). Scaling images from a video taken from a high vantage point at approximately 1600 UTC (11:00 a.m. CDT) indicates that the water levels in the vicinity of the canal breach were at an elevation of approximately 4 to 5 ft.

Water Levels in Lake Pontchartrain and in the 17th Street Canal

Water levels in Lake Pontchartrain are available based on HWMs, surveyed elevations of stopped clocks, time-stamped photographs, and results from numerical model simulations. The reconstructed water level time history in Lake Pontchartrain based on all available information will be used for purposes here. Specifically, the water level history as shown by the solid line in Figure 144 is the basis for further application in this study.

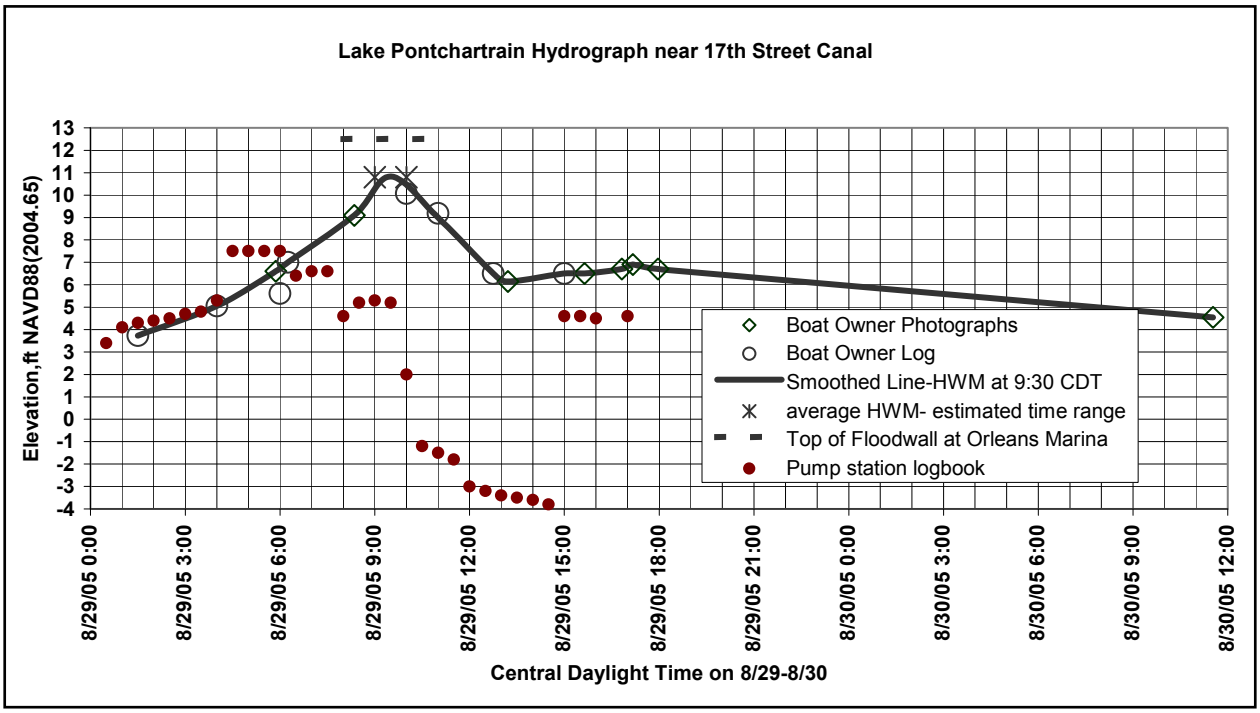

Figure 144. Estimated water levels in Lake Pontchartrain near north end of 17th Street Canal. The solid line is used for analysis purposes here. [Times are referenced to CDT]

Other Data Considered and Used in Analyses

There are two additional sources of data that were considered. Initially, the water level data from the pump station at the south end of the 17th Street Canal were considered to be valid. These data are based on a bubbler-type gauge that depends on 60-cycle power and are shown as the solid dots in Figure 144. Interruption of the 60-cycle power supply appears to have occurred sometime between 0900 and 1000 UTC (4:00 and 5:00 a.m. CDT) and it caused a loss of pressure to the bubbler gauge and an associated degradation of the recorded pressure. Subsequent tests of the effect of loss of power to this gauge convincingly demonstrated that the gauge was unreliable after it lost power, particularly after approximately 7:30 a.m. CDT.

The second type of data that proved extremely useful was based on surveys across the canal breach. These surveys documented that the maximum elevation of the topography across the breach was reasonably uniform with an elevation ranging from – 1.0 to 0 ft. This information would refute the very low water levels (as low as -4 ft) at the canal south end as reported by the bubbler gauge as discussed above and as shown in Figure 144.

The 17th Street Physical Model

An undistorted physical model with scale 1:50 was constructed at ERDC in Vicksburg. The primary purpose of this model was to investigate the reduction of wave heights as they propagate down the canal. A secondary purpose was to investigate the hydraulic effects of clogging by debris at the Hammond Highway bridge. Figure 145 shows the configuration of the model. The full length of the canal was not represented geometrically in the model. Rather the geometry represented was the northern portion of the canal extending south well beyond the breach limits. The remaining surface area of the model was represented in the form of a large rectangular basin.

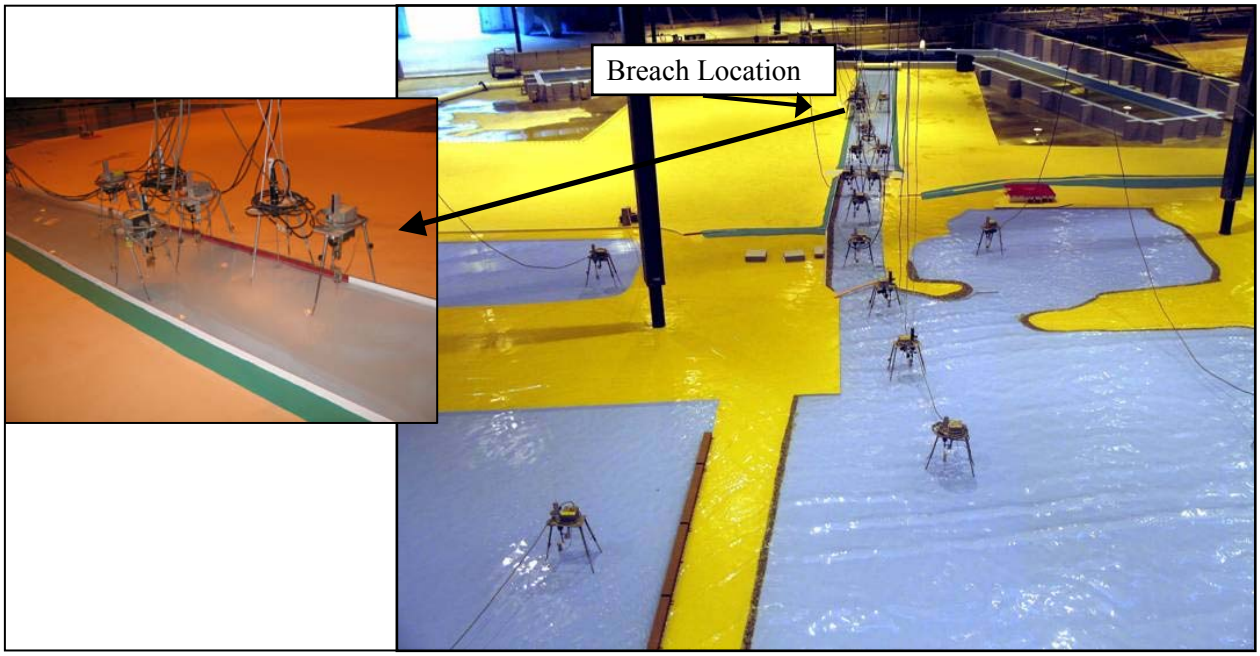

Figure 145. Views of 17th Street Canal model.

Figure 146 presents the surge and wave conditions represented at the -14-ft contour, lakeward of the 17th St. Canal used as boundary inputs for water level and wind waves in the physical model. In Figure 146, in addition to storm water level, wave height, peak period and the mean direction from which the waves are propagating are presented. A wave direction value of zero indicates waves coming from true north. The wave conditions were based on both wave measurements and modeling using STWAVE forced by high accuracy reconstructed winds. Both unidirectional and directional waves were simulated in the physical model tests. Figure 147 presents two of the directional spectra tested. It was found, as shown in Figure 148, that the wave heights decayed quite rapidly as the waves entered the canal. The decay was especially rapid as the waves passed under the Hammond Highway bridge.

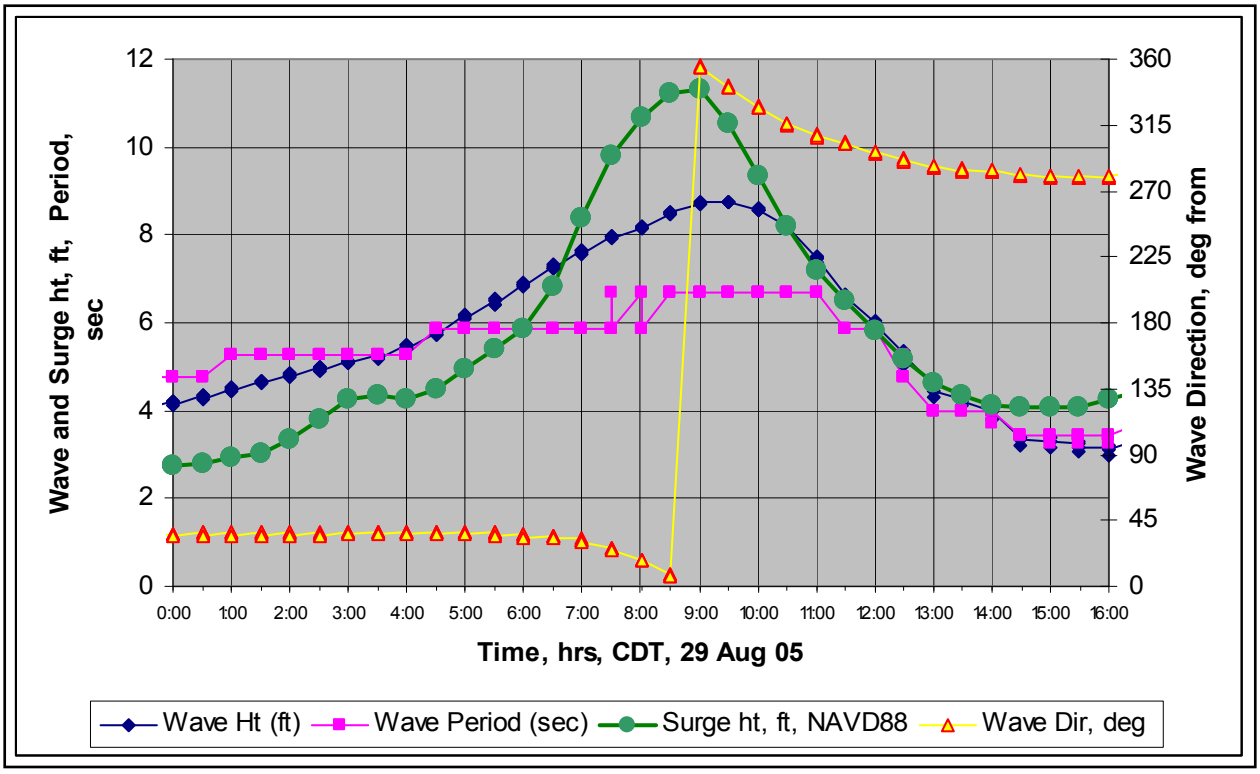

Figure 146. Wave and water level characteristics tested in the model.

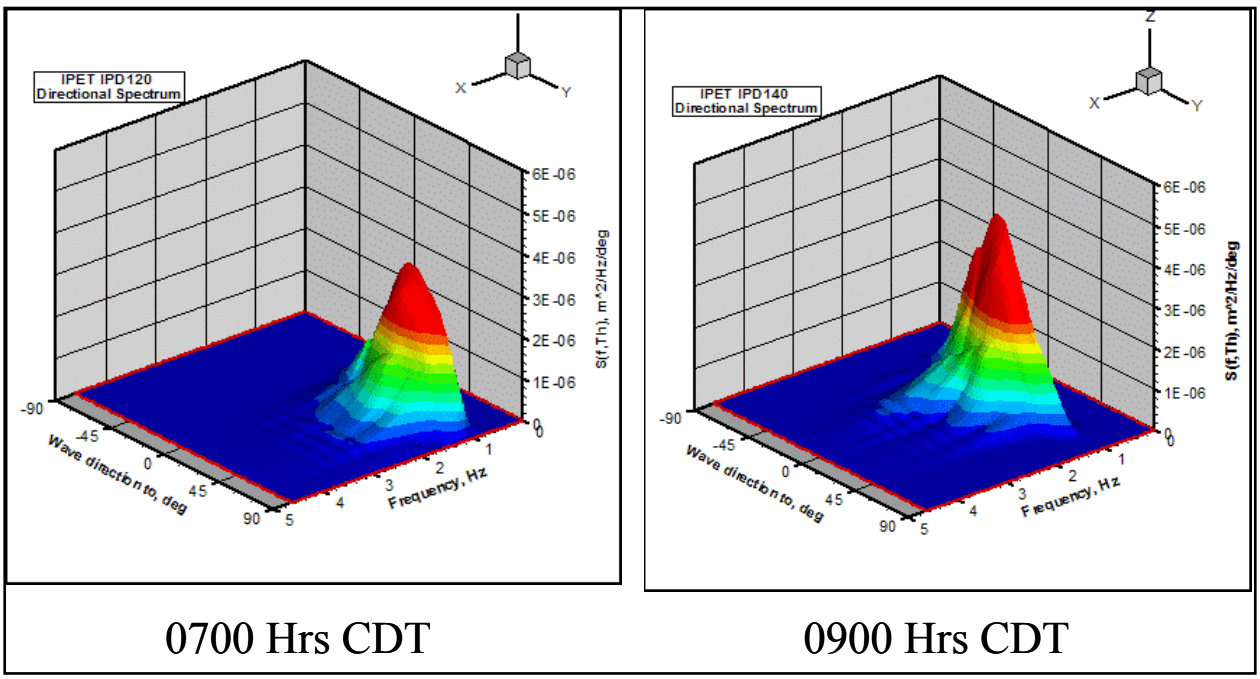

Figure 147. Examples of two directional spectra tested in the model (note, spectrum is in unscaled physical model units that were programmed to operate the directional spectral wave generator; to convert to prototype frequency, divide by 7.07 time-scale factor). [Times are referenced to CDT].

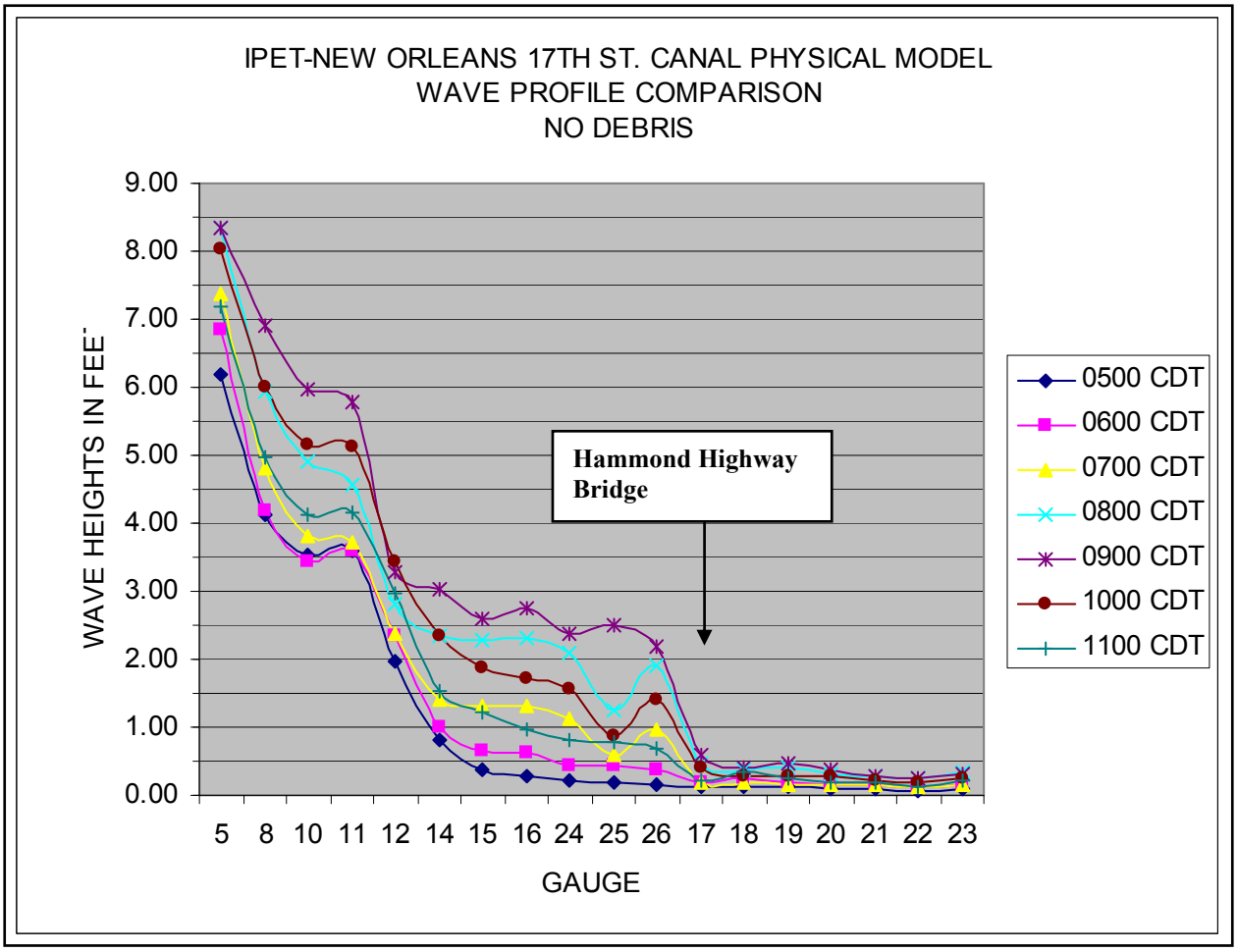

Figure 148. Decay of significant wave height at various times as the waves approach and enter the 17th Street Canal.

Wave Calculations in 17th Street Canal

Wave calculations in the canal were also carried out using the STWAVE and Boussinesq models for comparison with the physical model and to determine forces and moments on the floodwall at the time of failure. The STWAVE calculations account for energy input by wind, a process that is not possible in the physical model and predicted slightly higher waves in the canal. It was determined that the maximum wave heights in the canal ranged between 1 and 1.5 ft. Figure 149 presents an example of wave simulations by the Boussinesq model.

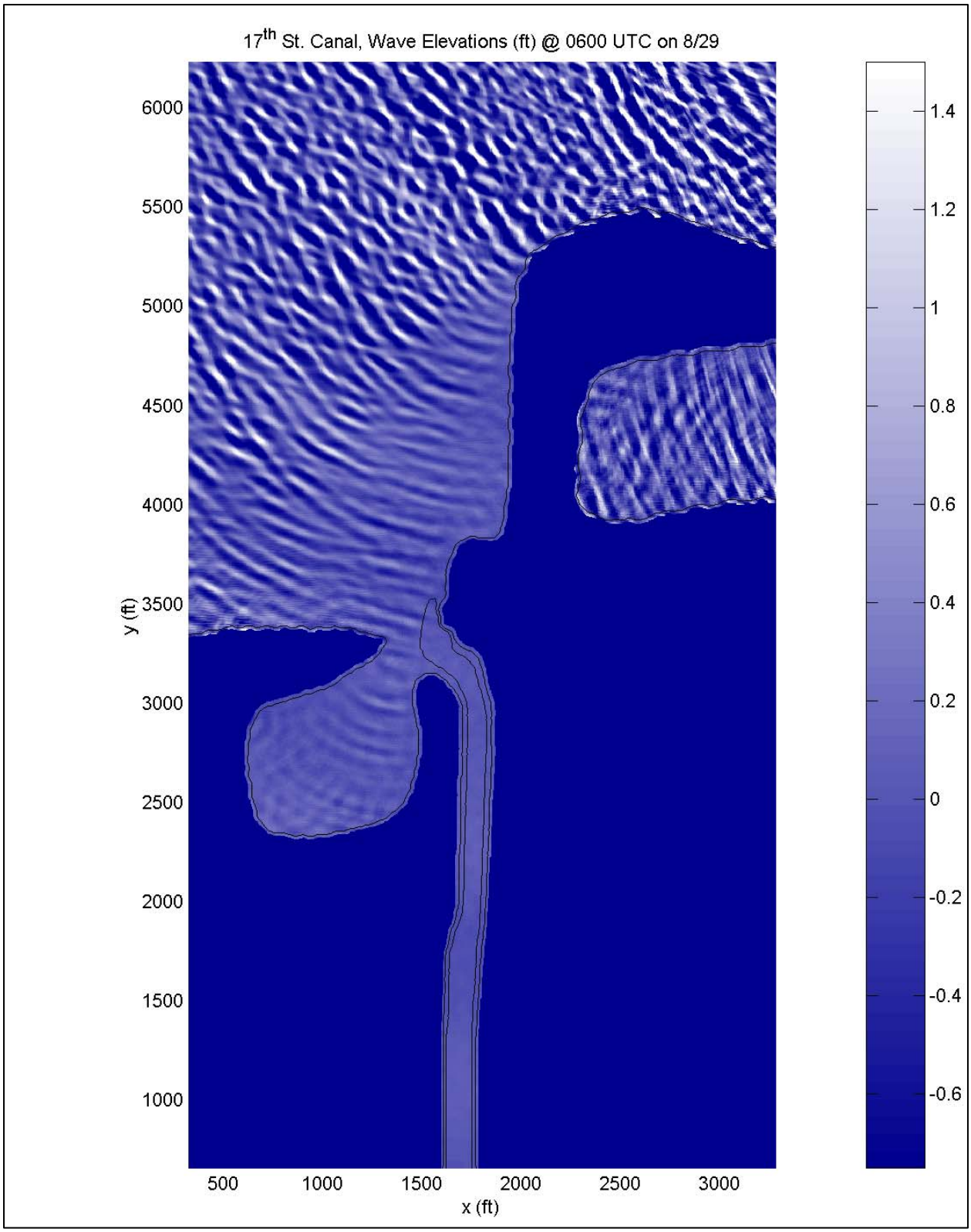

Figure 149. Snapshot of wave simulation at the 17th Street Canal entrance using the Boussinesq model. [Time is referenced to UTC.]

Hydraulic Calculations in the 17th Street Canal

Steady state hydraulic calculations were carried out for the canal considering four scenarios. These scenario characteristics are presented in Table 7. Only a sampling of results will be presented here. Appendix 10 contains the full 17th Street Canal results.

Table 7
Characteristics of Scenarios Considered

Scenario	Description	Plots Presented in Appendix
1	Base Conditions: Breach Width = 200 ft, 6:00 through 9:00 a.m. CDT, and 450 ft for > 9:00 a.m. CDT	Breach Discharge, Water Surface Profiles Along Canal
2	Sensitivity to Friction Factors of ± 50% Variation	Breach Discharge for Various Friction Factors
3	Sensitivity to Debris Blockage of Flow by Reductions of 25% and 50%	Breach Discharge, Water Surface Profiles Along Canal
4	Reduced Initial Breach Width	Water Surface Profiles at Lake and Breach

Figure 150 presents the calculated water levels along the canal for the base case. The Hammond Highway bridge exerts a substantial effect of the hydraulics of the canal especially when the water level rises sufficiently high to cause closed rather than open channel flow under the bridge.

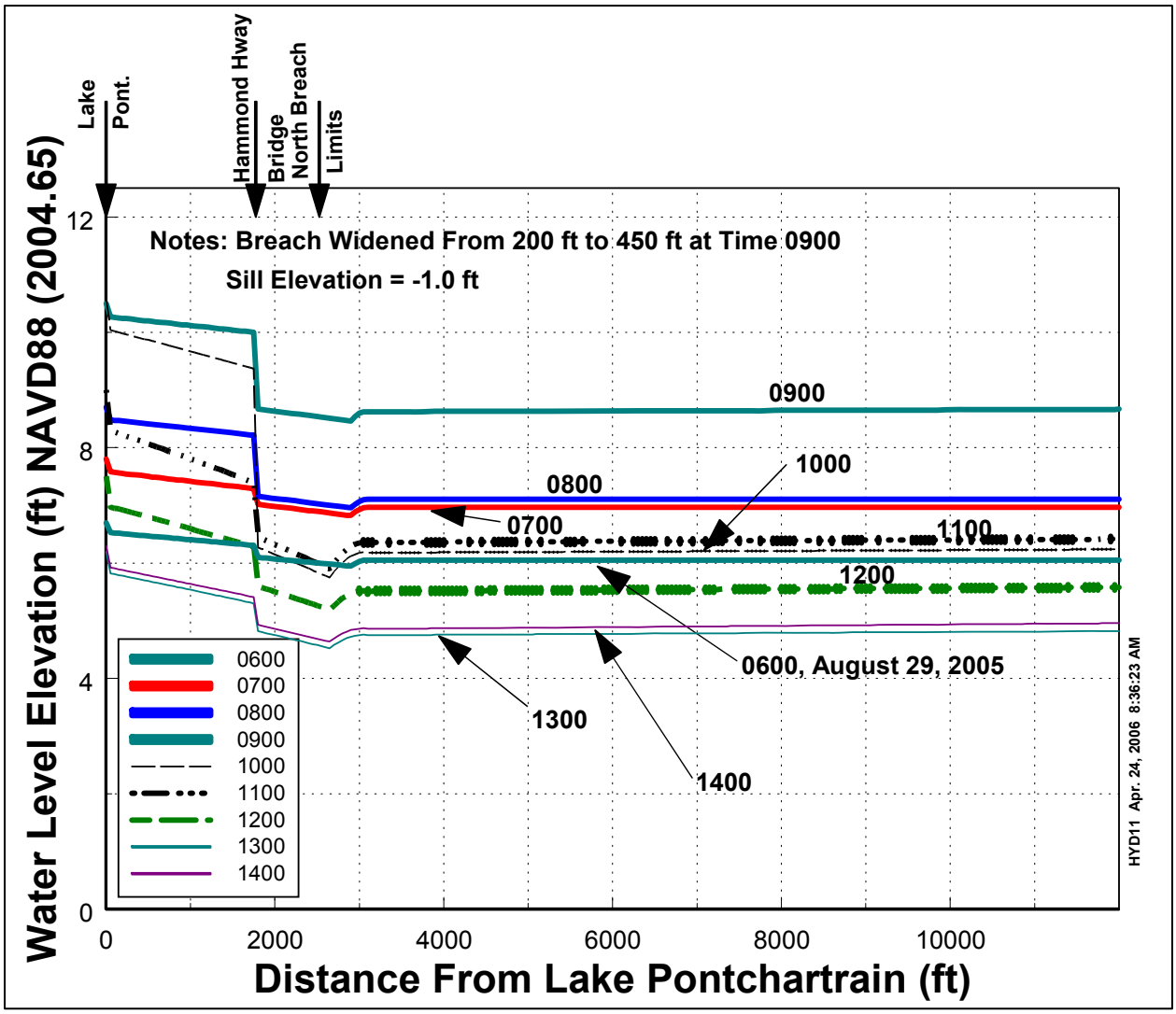

Figure 150. Water levels along 17th Street Canal. Scenario 1. [Times are referenced to CDT].

The discharges relevant to the canal including the pump discharge, the breach discharge, and the discharge from the lake are presented in Figure 151. It is seen that the maximum discharges are approximately 28,000 ft^3/s.

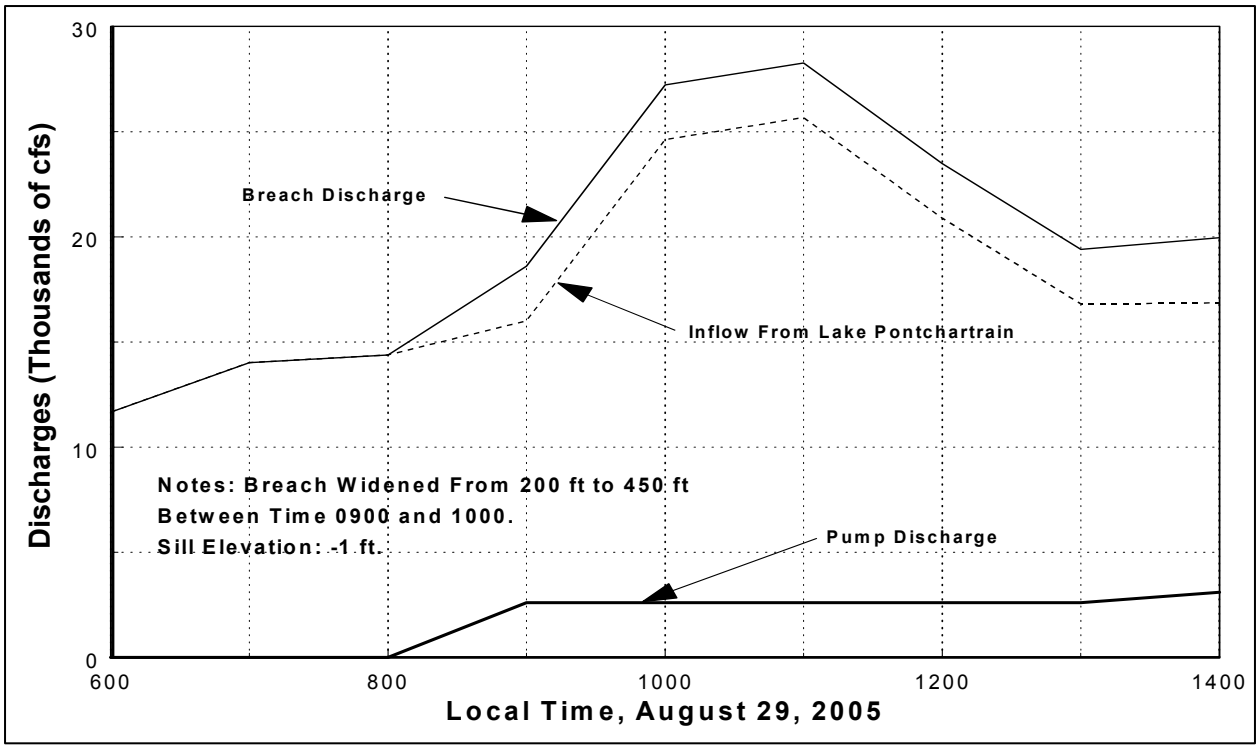

Figure 151. Time histories of breach and other discharges. Scenario 1. [Times are referenced to CDT].

Scenario 2 examined the sensitivity of breach discharges to changes in the value of the base Weisbach-Darcy friction coefficient from its reference value, $f = 0.08$ by ± 50 percent. It was found that the associated changes in peak breach discharge ranged between -8 percent and +4 percent. Thus, the breach discharges are very insensitive to the values of the Weisbach-Darcy friction coefficient.

Scenario 3 simulated water level and breach discharges due to debris blockage at the Hammond Highway bridge of 25 percent and 50 percent. The peak discharges were reduced by 18 percent and 36 percent, respectively. For the greater blockage of 50 percent, the water level in the canal near the breach was in essential agreement with the video taken at approximately 1600 UTC (11:00 a.m. CDT) (water level of 4 ft ±).

Finally, Scenario 4 was conducted to evaluate the effect of an early failure of only one panel of the east floodwall. This scenario simulated a breach width of only 30 ft from 1100 through 1400 UTC (6:00 a.m. through 9:00 a.m. CDT). It was found that this narrow breach resulted in water levels at the breach that were only slightly less (< 0.2 ft) than the lake levels.

Wave Forces and Moments on Floodwall at Time of Initial Crack Formation

Wave forces and wave moments can be significant relative to the corresponding static values. At the time of initial crack formation, the water level was approximately 7.0 ft, and considering the base of the floodwall to be 2 ft and a wave height of 1.5 ft, the maximum dynamic forces and moments are 32 percent and 52 percent greater than their corresponding static values.

Orleans Canal

Introduction. There were no breaches or flood wall failures in the Orleans Canal. A broad weir at approximately 8.3 to 9.8 ft elevation is located at the south end of the canal resulting in water levels that sloped approximately uniformly from Lake Pontchartrain to the weir for lake levels that exceeded the weir elevation. For lake levels lower than the weir elevation, the water level was nearly horizontal.

Lake Water Levels. As for the 17th Street Canal, lake water levels have been established by numerical modeling, eyewitness accounts, HWMs, and photographic documentation. Based on all available information and data, the reconstructed lake water level is shown in Figure 152.

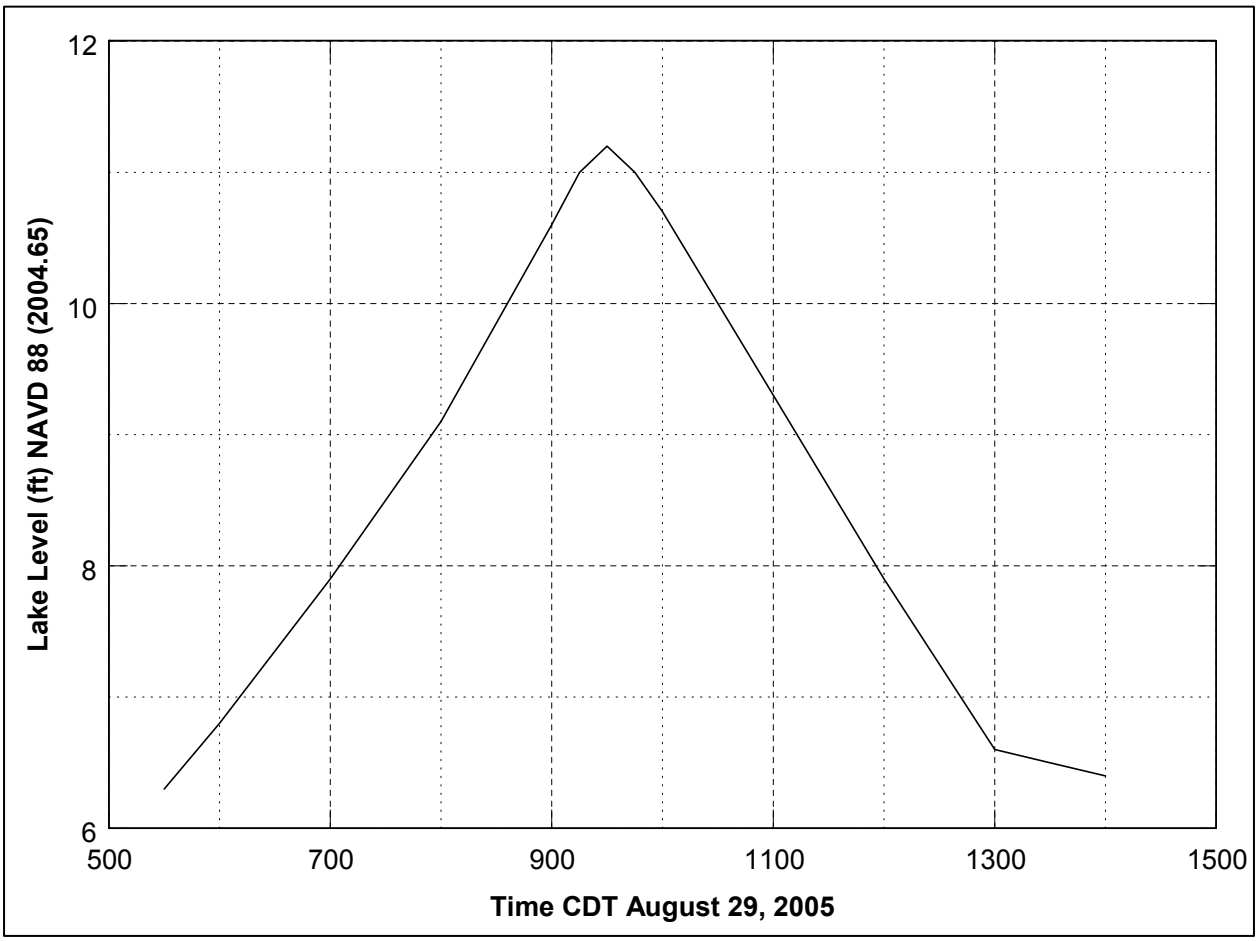

Figure 152. Reconstructed water levels in Lake Pontchartrain near north end of Orleans Canal. [Times are referenced to CDT].

Wave Conditions. The significant wave height, peak period, and direction in Lake Pontchartrain near the north end of Orleans Canal are presented in Figure 153.

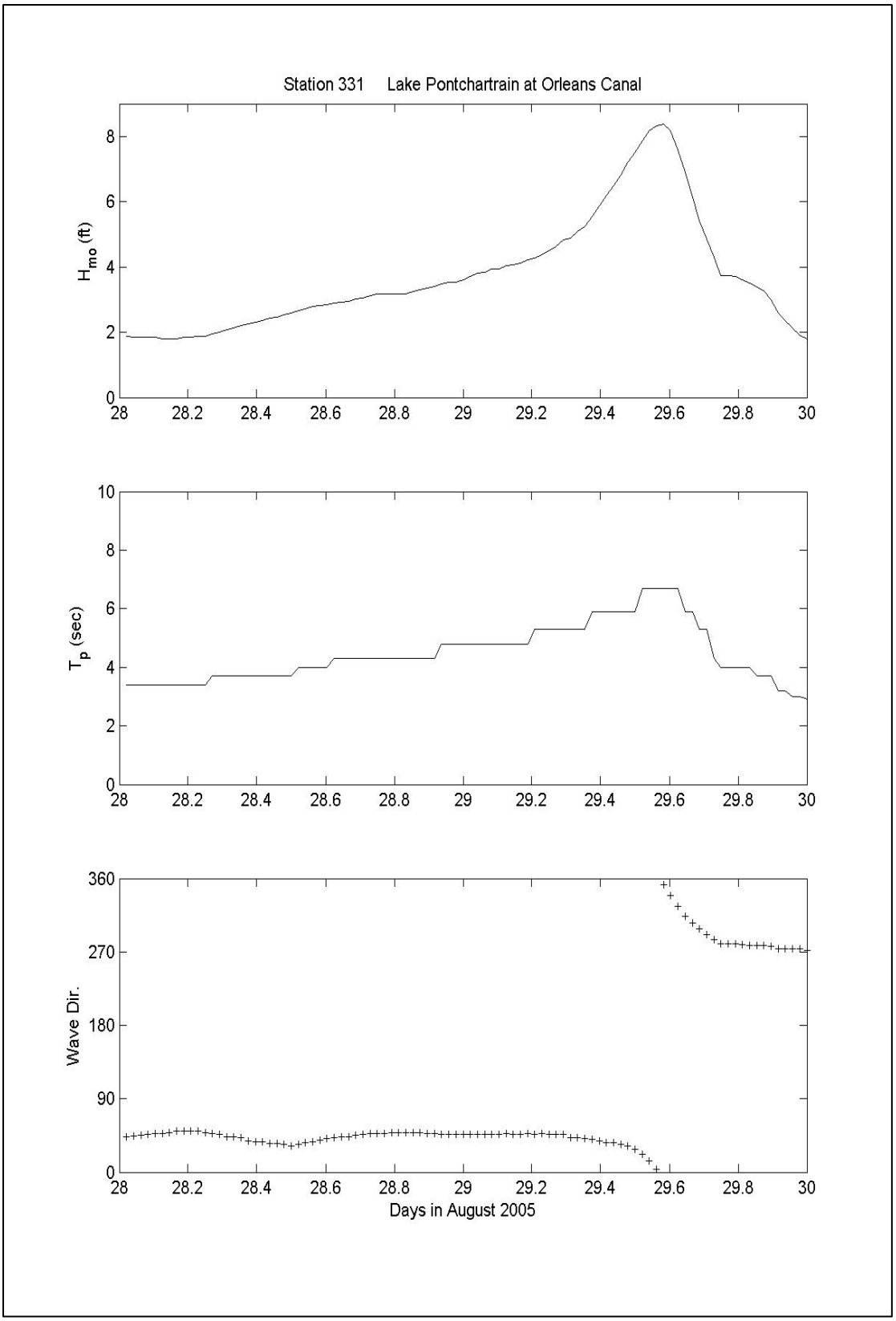

Figure 153. Significant wave height, peak wave period, and mean wave direction in Lake Pontchartrain near north end of Orleans Canal. [Times are referenced to UTC].

Because no failures occurred in this canal, no further analyses have been carried out; however, it should be noted that floodwall heights above the interior levee sills along the Orleans Avenue Canal were up to almost 10 ft. Consequently, forces on these walls were probably considerably higher than forces on the walls in both the 17th Street and London Canals.

London Avenue Canal

Introduction. The characteristics of the two breaches in the London Avenue Canal are not as well established as for the 17th Street Canal. Although there is good documentation for the final widths, the sill elevations and the breach evolutions are known only qualitatively, thus limiting the confidence associated with the analysis results.

Timing and Characteristics of Breach Failures. Figure 154 presents photographs of the two failures. The northern breach just south of Robert E. Lee Boulevard occurred on the west side of the canal and is the wider and shallower of the two breaches. The southern breach on the east side of the canal and just north of Mirabeau Avenue is the narrower and deeper breach. The widths of the northern and southern breaches are approximately 300 and 80 ft, respectively. The best timing of the northern breach has been established to have occurred between 1200 and 1230 UTC (7:00 and 7:30 a.m. CDT) and that at the southern breach between 1200 and 1300 UTC (7:00 and 8:00 a.m. CDT).

(a) North breach near Robert E. Lee bridge (b) South breach near Mirabeau Avenue

Figure 154. London Avenue Canal breaches.

Lake Water Levels. As for the 17th Street Canal, lake water levels have been established by numerical modeling, eyewitness accounts, HWMs and photographic documentation. Based on comparison of the representations with high quality HWMs, the reconstructed lake water level shown in Figure 155 was used as the basis for analysis purposes here.

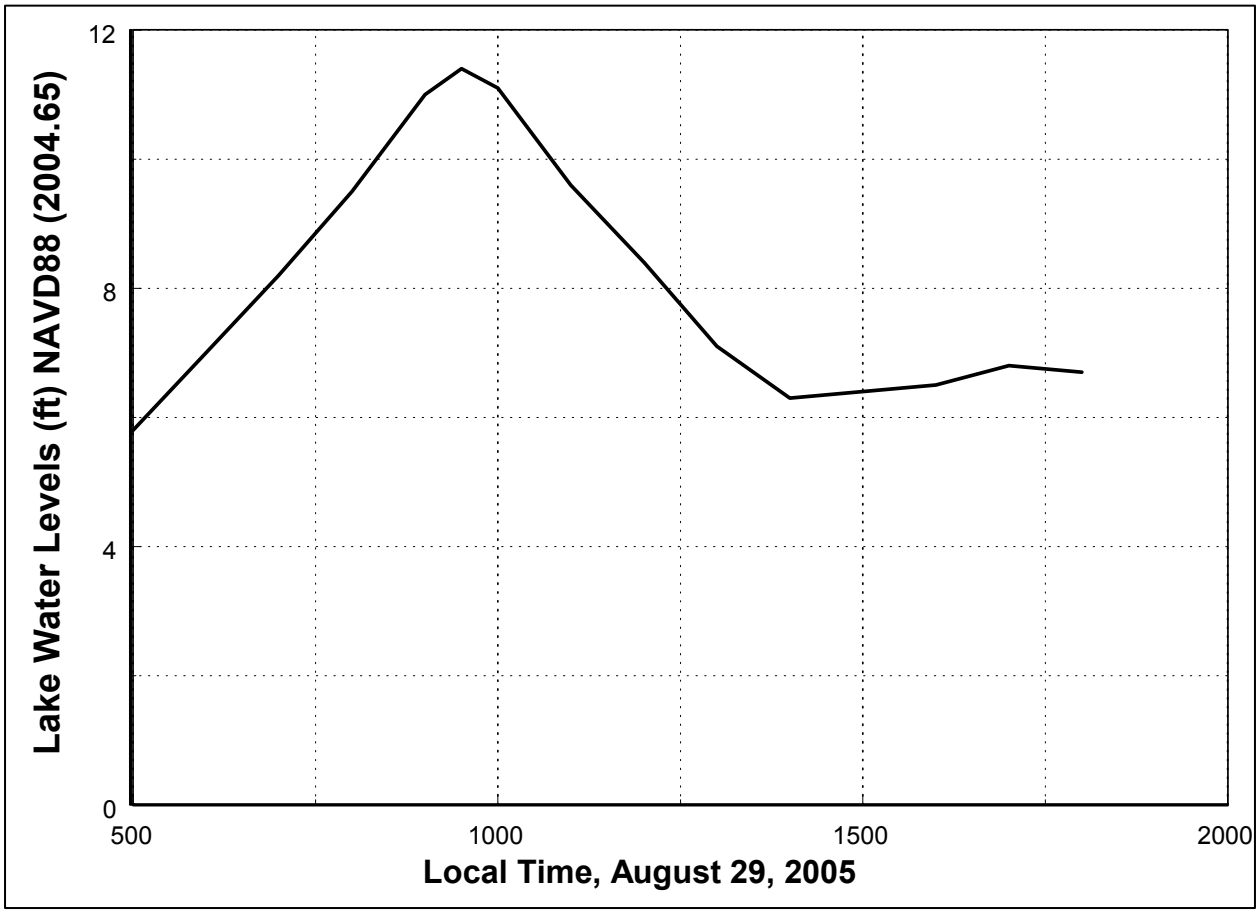

Figure 155. Estimated water levels in Lake Pontchartrain near north end of London Avenue Canal. [Times are referenced to CDT].

Hydraulic Analysis. The same general procedure was followed for the London Street Canal as for the 17th Street Canal. Results will be presented for breach discharges and water levels in the canal. The full analysis for this canal is presented in Appendix 11.

Figure 156 shows the breach, pump and lake discharges. It is seen that the maximum total peak breach discharge is approximately 22,000 ft^3/s. The peak discharges through the north and south breaches are (coincidentally) approximately the same. Recall that the north breach was wider than the south breach; however, the sill elevation was higher at the north breach. Initially before breaching occurs, at calculation times of 1100 and 1200 UTC (6:00 and 7:00 a.m. CDT), the flow is out of the canal into Lake Pontchartrain in accord with the pump flows into the canal at the south end.

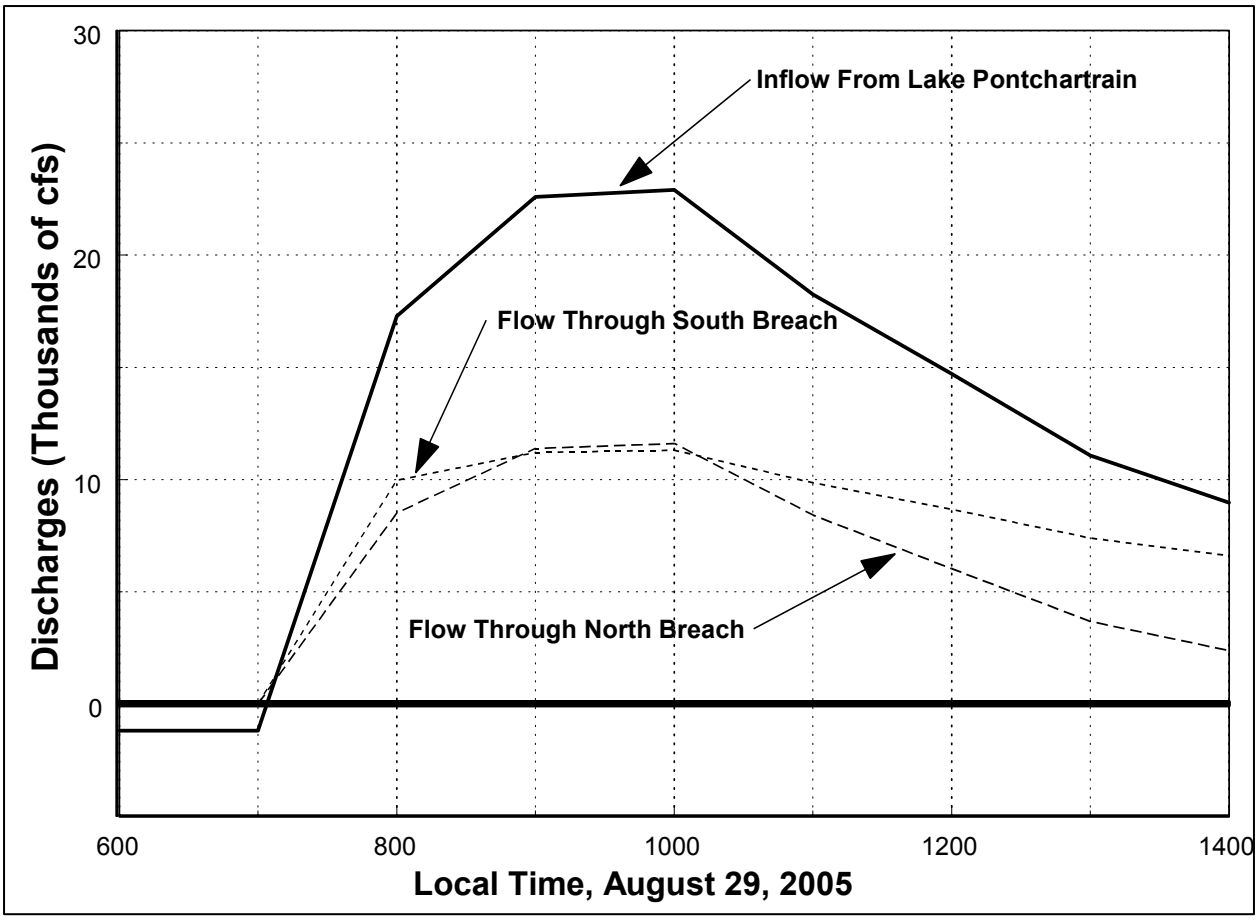

Figure 156. Time history of breach and lake discharges. [Times are referenced to CDT].

Figure 157 presents the distribution of water levels along the London Avenue Canal for times from 1100 to 1900 UTC (6:00 a.m. to 2:00 p.m. CDT) on 29 August 2005. The water levels at 1100 and 1200 UTC (6:00 and 7:00 a.m. CDT) prior to breach occurrence are nearly horizontal with the water surface sloping downward very slightly toward the lake to accommodate the pump flow.

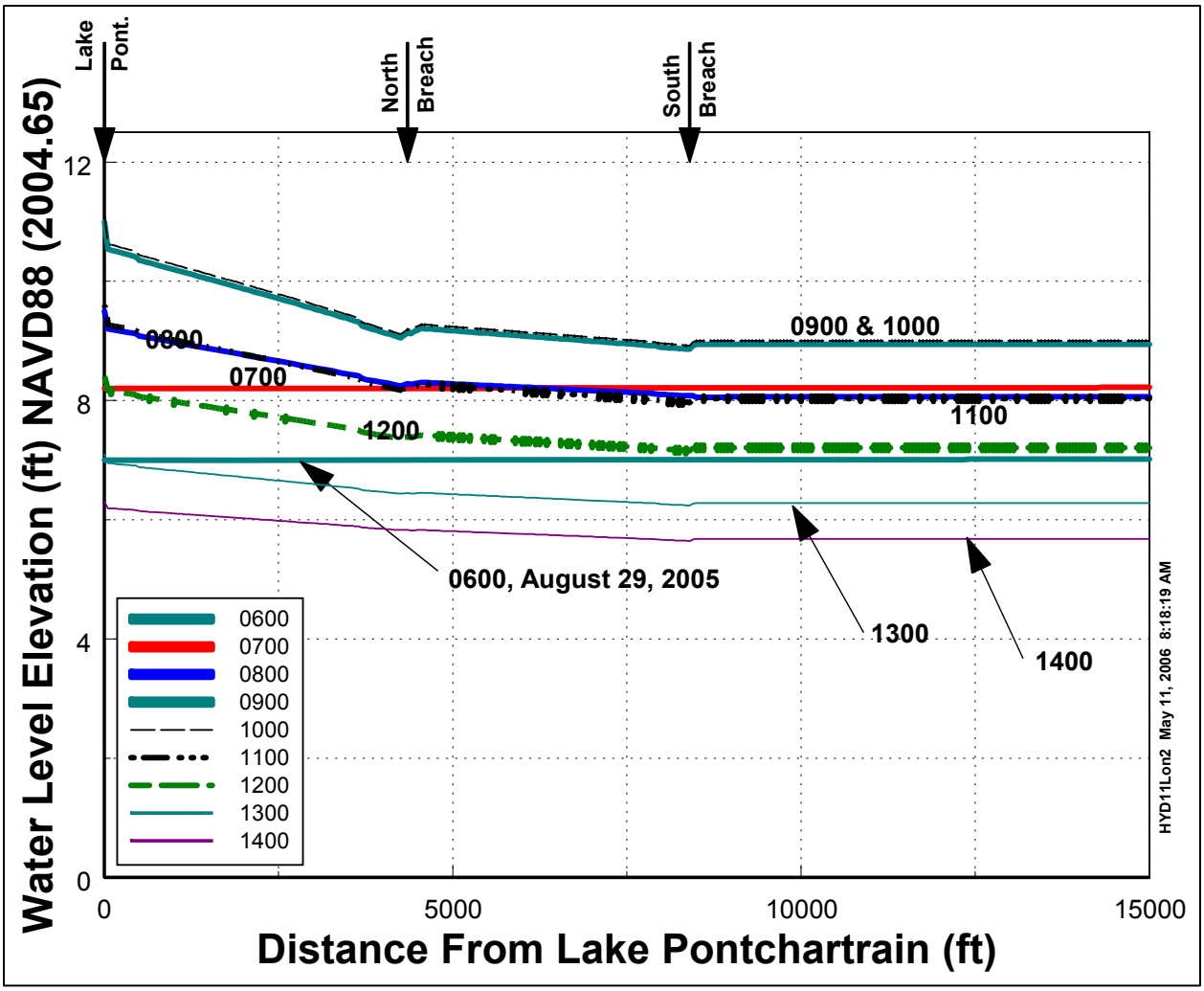

Figure 157. Water levels along London Avenue Canal for various times. [Times are referenced to CDT].

As can be seen in Figure 158, the time series of wave heights, periods, and directions estimated at the entrance of the London Avenue Canal were very similar to conditions at the 17th Street Canal. STWAVE and Boussinesq simulations indicate that the significant wave heights within the canal remained less than 1.5 ft during Hurricane Katrina.

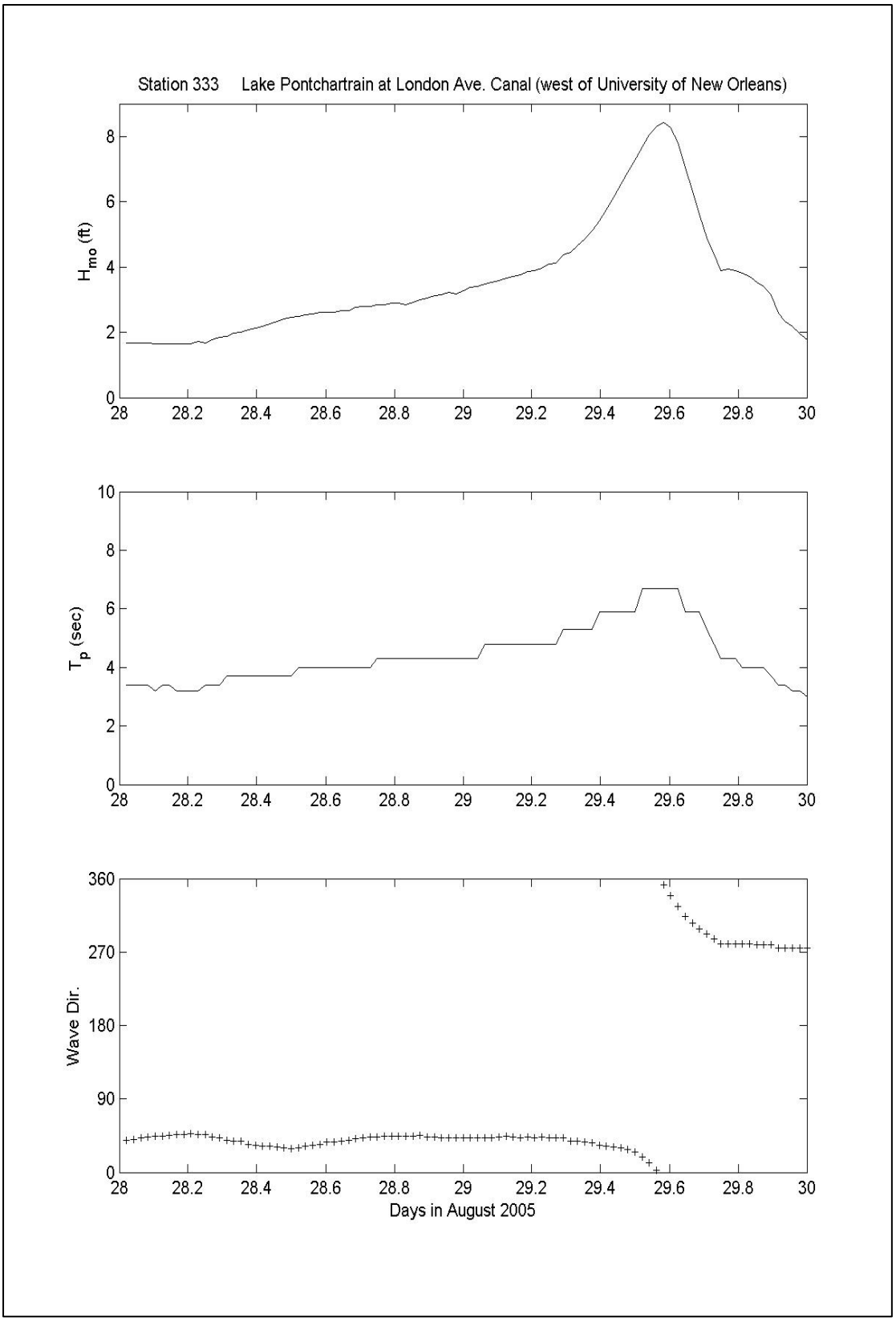

Figure 158. Time series of wave heights, periods, and directions at the entrance to London Avenue Canal. [Time is referenced to UTC].

Inner Harbor Navigation Canal (IHNC)

As discussed in the Timeline section of this report, it appears that areas in the vicinity of the IHNC began to flood at times ranging from about 0930 to 1300 UTC (4:30 to 8:00 a.m. CDT). Figure 159 reproduces the hydrograph shown in the Timeline section with the earliest time of flooding designated by a vertical line. The water level at this time is approximately 10 to 10.5 ft at the Lower Ninth Ward floodwall. Although flooding in most areas is consistent with local overtopping, as confirmed in many instances by eyewitness accounts, the IHNC floodwall in the northern section of the Lower Ninth Ward maintains an elevation of 12.5 to 13.0 ft; consequently, the early time of flooding suggests that possibly one or both of the breaches into the Lower Ninth Ward occurred before they were overtopped.

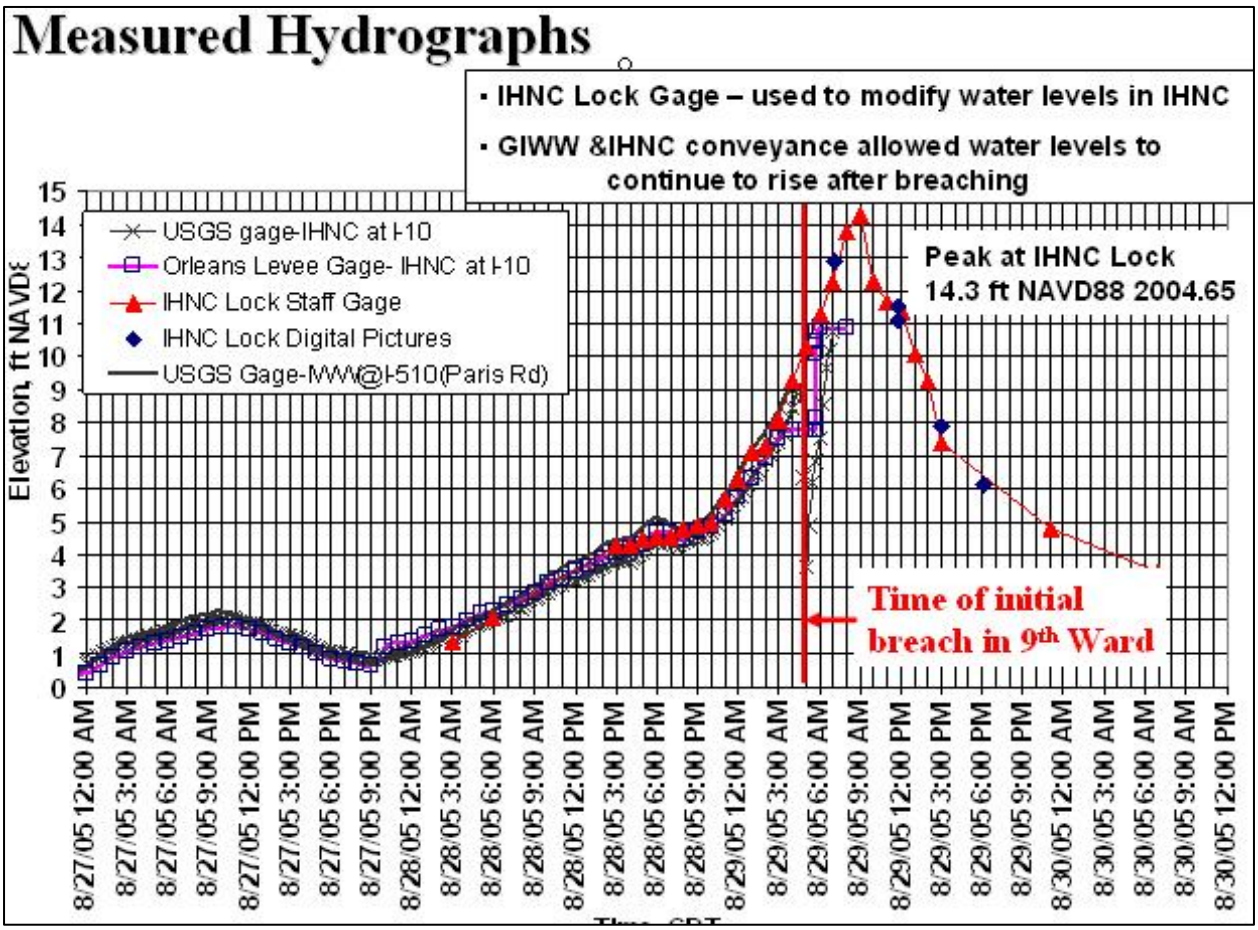

Figure 159. Hydrograph of water levels measured at gauges within the IHNC. Vertical line designates approximate time of initial flooding in Lower Ninth Ward. [Times are referenced to CDT].

Water levels within the IHNC were taken from the regional-scale ADCIRC runs with no adjustment, since the agreement between model results and observations was in general quite good. This provided time histories throughout the storm for all sites of interest, without the need for additional detailed sub-scale modeling. Maximum water levels used for detailed analyses were chosen to be consistent with the levels shown in Figure 160.

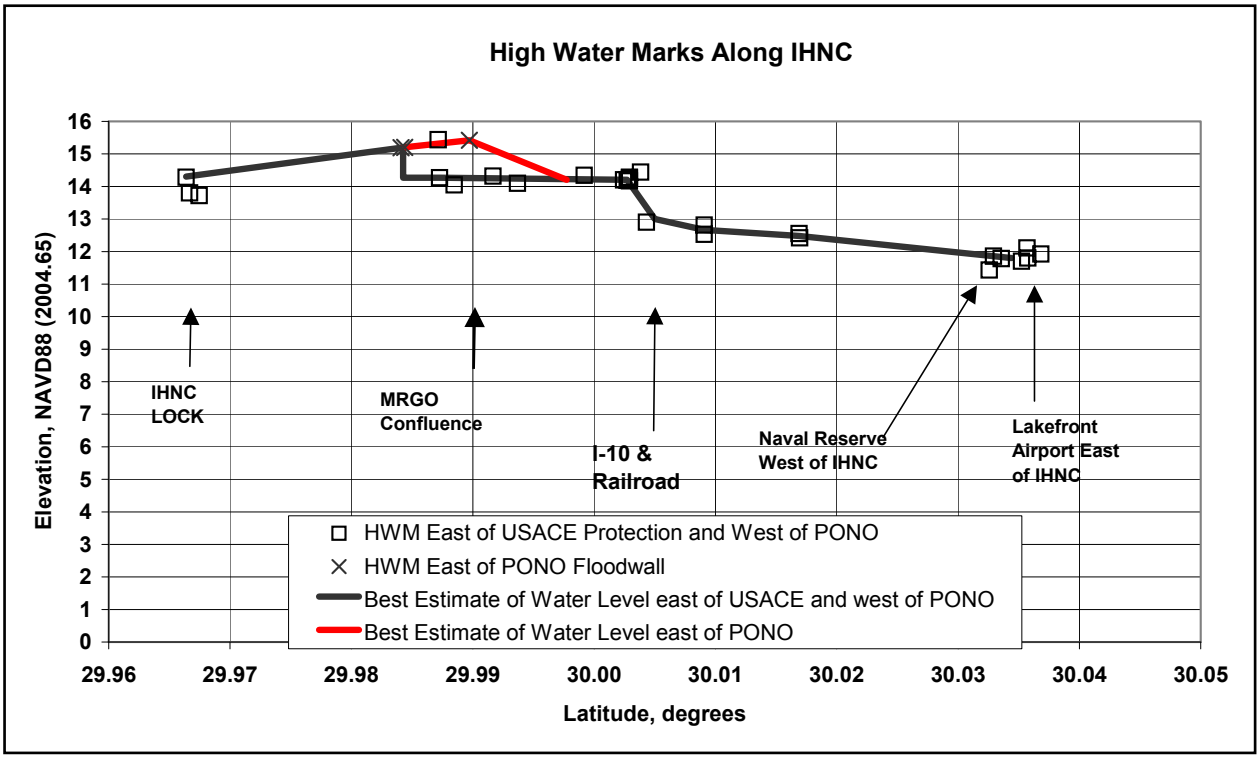

Figure 160. Estimated distribution of maximum water levels along the IHNC.

Both the Boussinesq model and a slightly modified version of the STWAVE model were utilized to estimate waves propagating into the IHNC from the MRGO/GIWW and from Lake Pontchartrain, The effects of local wave generation were also included within STWAVE, but as mentioned previously could not be included within the Boussinesq runs. Figures 161 and 162 from the STWAVE runs show the distribution of maximum conditions along the canal for waves entering the IHNC from the east (through the MRGO/GIWW) and from the north (from Lake Pontchartrain), respectively. Details of modifications to STWAVE and the model applications are given in Appendix 14. A grid spacing of 65.62 ft was used for these simulations.

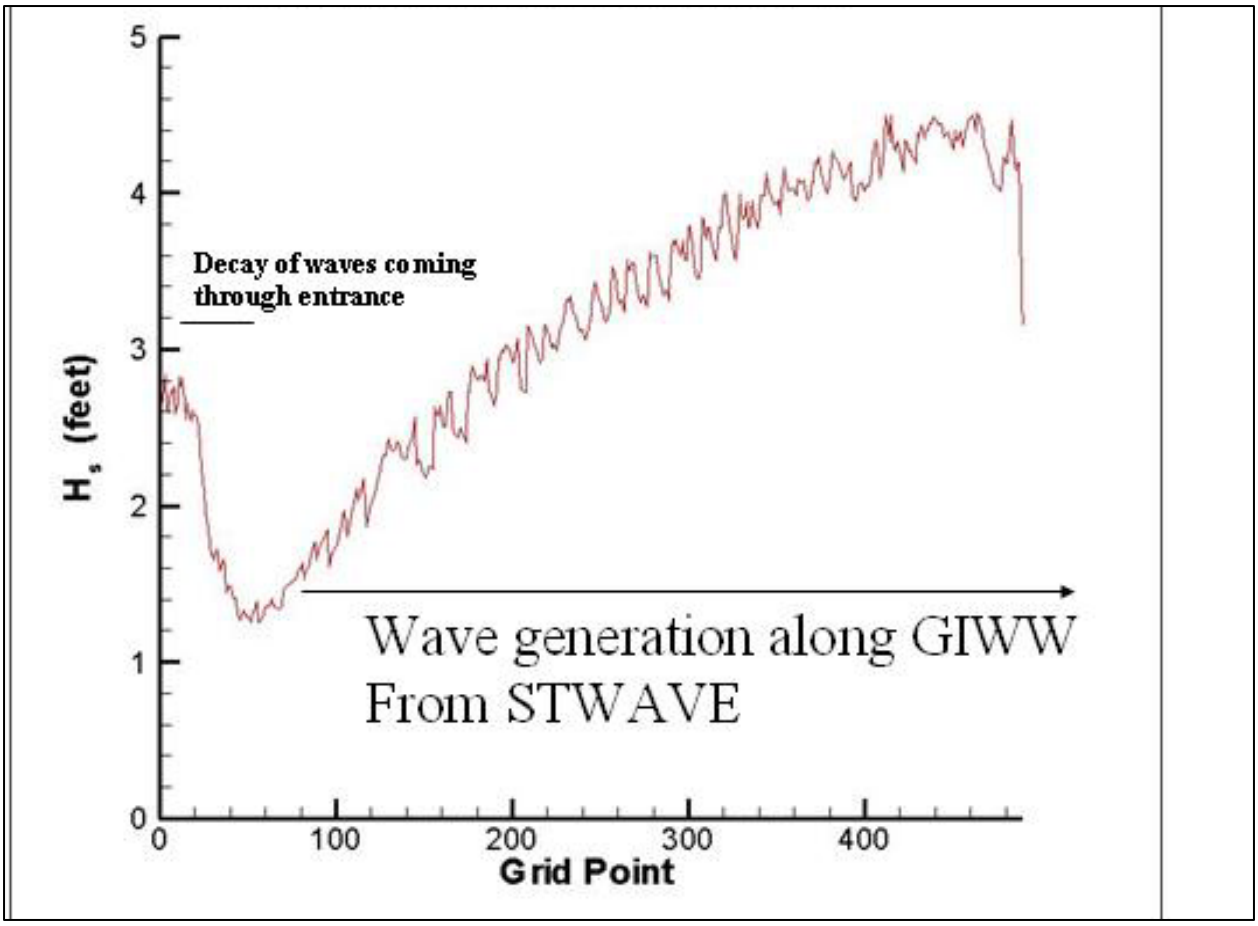

Figure 161. Line of maximum wave heights within the MRGO/GIWW entrance to the IHNC showing decay of waves coming in through the entrance and local generation of waves within the canal. Grid spacing is 65.62 ft.

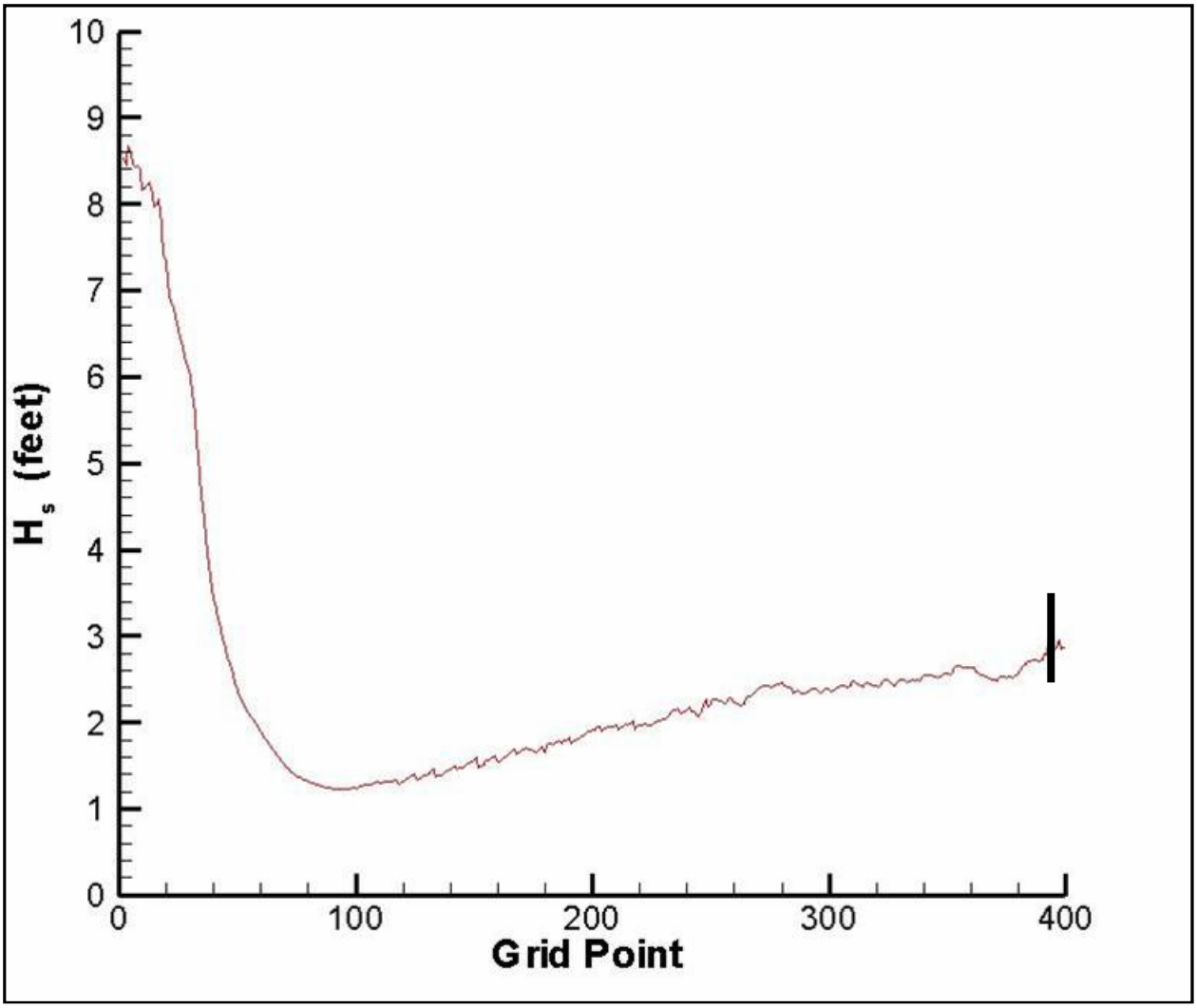

Figure 162. Line of maximum wave heights along the IHNC for waves entering from Lake Pontchartrain. This shows the decay of waves coming in through the entrance and local generation of waves within the canal. Grid spacing is 20 meters (66 ft). Vertical bar around grid point 400 represents range of estimates of wave height near this point made from photographs.

As can be seen in Figure 161, waves entering the MRGO/GIWW from relatively open waters decay rapidly from almost 3 ft to about 1.2 ft within about one-half mile. However, the winds for the entire 0600-to-1100 UTC (1:00-to-6:00 a.m. CDT) timeframe on the 29th are relatively well-aligned with the axis of the MRGO/GIWW; consequently, local wave generation is quite important here, with wave heights of over 4 ft produced in the vicinity of the GIWW/MRGO – IHNC intersection during peak wind conditions at 1030 UTC (5:30 a.m. CDT) of about 80 knots out of the east. These waves are quite short with peak periods in the range of 3.5 to 4.0 sec. The Boussinesq model was utilized to approximate waves within the IHNC, based on boundary conditions derived from the STWAVE. A modified version of STWAVE was also run in this same area, due to the large spatial extent of the region being modeled. Results from the STWAVE runs showed that the primary source of wave energy incident upon the floodwalls along the Lower Ninth Ward came from waves reflected back to the east side of the canal from the west side. Due to all the irregularities along the west side of the IHNC and the range of types

of slopes and materials, it is difficult to estimate the reflection coefficient for this area with much certainty. Sensitivity tests show that for coefficients of energy reflection in the 50 percent to 80 percent range, wave heights of approximately 2 to 3 ft would be incident on the Lower Ninth Ward floodwalls.

The largest waves entering the IHNC from Lake Pontchartrain boundary lag the large waves entering from the MRGO/GIWW by about 4 hr, with peak conditions occurring around 1430 UTC (9:30 a.m CDT). Similar to waves entering the MRGO/GIWW, these waves decay rapidly and within less than a mile have been reduced to about 1.2 ft. As was the case in the MRGO/GIWW, local wave generation contributes significantly to the evolution of the wave field propagating down the canal from the north. In this case the maximum winds for generation down this portion of the canal occur at about 1430 UTC (9:30 a.m. CDT) on the 29th and are about 61 knots out of the north. As seen in Figure 162, the lower wind speeds and possibly some of the bridges along the canal result in significant wave heights that are slightly smaller than those generated down the MRGO/GIWW – about 2.8 ft compared to over 4 ft. The wave periods are also slightly lower than the peak conditions along the MRGO/GIWW, falling in the range of 3.0 to 3.5 sec. As can be seen in Figure 162, the estimated wave height and period from STWAVE appear consistent with photographic evidence at the extreme southern end of the IHNC, near the Mississippi River Lock.

As shown in Appendix 14, waves at the confluence of the IHNC and MRGO/GIWW entering from the north and east can be treated independently for a number of reasons. First, about a 4-hr phase difference exists in the peak of the wave time histories at the two boundaries. Second, due to the rapid decay of waves entering from the boundaries, waves from the boundaries are less than 0.5 ft at the MRGO/GIWW – IHNC confluence for all time modeled. Third, the local winds align with the MRGO/GIWW axis about 4 hr earlier than with the northern IHNC axis.

The Boussinesq model was used to investigate wave conditions in the vicinity of the breaches in the Lower Ninth Ward, using wave spectra from STWAVE at the MRGO/GIWW – IHNC confluence (Figure 163). The Boussinesq model was not used to provide estimates of wave force on the IHNC walls near the failure because the Boussinesq model is not capable of simulating overtopping of vertical structures such as canal walls. The Navier-Stokes hydrodynamic model was employed at this location. The model used is called COBRAS, developed principally by Prof. Phil Liu at Cornell University. This numerical model is able to accurately simulate wave overtopping, 2D(V) turbulence and vorticity, and importantly, overtopping of vertical structures.

Motivated by the barge that floated through the IHNC, the mechanics of a freely floating barge under the action of wind were examined analytically and the results are presented in Appendix 17. The governing nonlinear equation of motion was developed and solved for the transient barge motion. Under the example wind speed considered (100 mph (87 knots)) the barge approached its steady state (terminal) speed in a relatively short distance, a finding that simplified later analysis. Examples for a lightly loaded and a fully loaded barge were evaluated. For a barge at rest against a floodwall, the steady state forces and moments were small relative to their hydrostatic counterparts. This considers the barge contact with the floodwall to be uniform; a concentrated loading contact could result in considerably larger local forces and moments. For

a barge moving at terminal speed, the forces and moments are greater relative to their hydrostatic components and depend on both the interaction deformation and contact characteristics. The effects of barge draft are somewhat tempered as the more fully loaded barges with greater mass have smaller terminal speeds. The examples were not intended to replicate Katrina conditions but rather to illustrate the kinematics and dynamics associated with a floating barge for possible later use and to corroborate the expectation that barge impacts are capable of inflicting consequential damage to floodwalls.

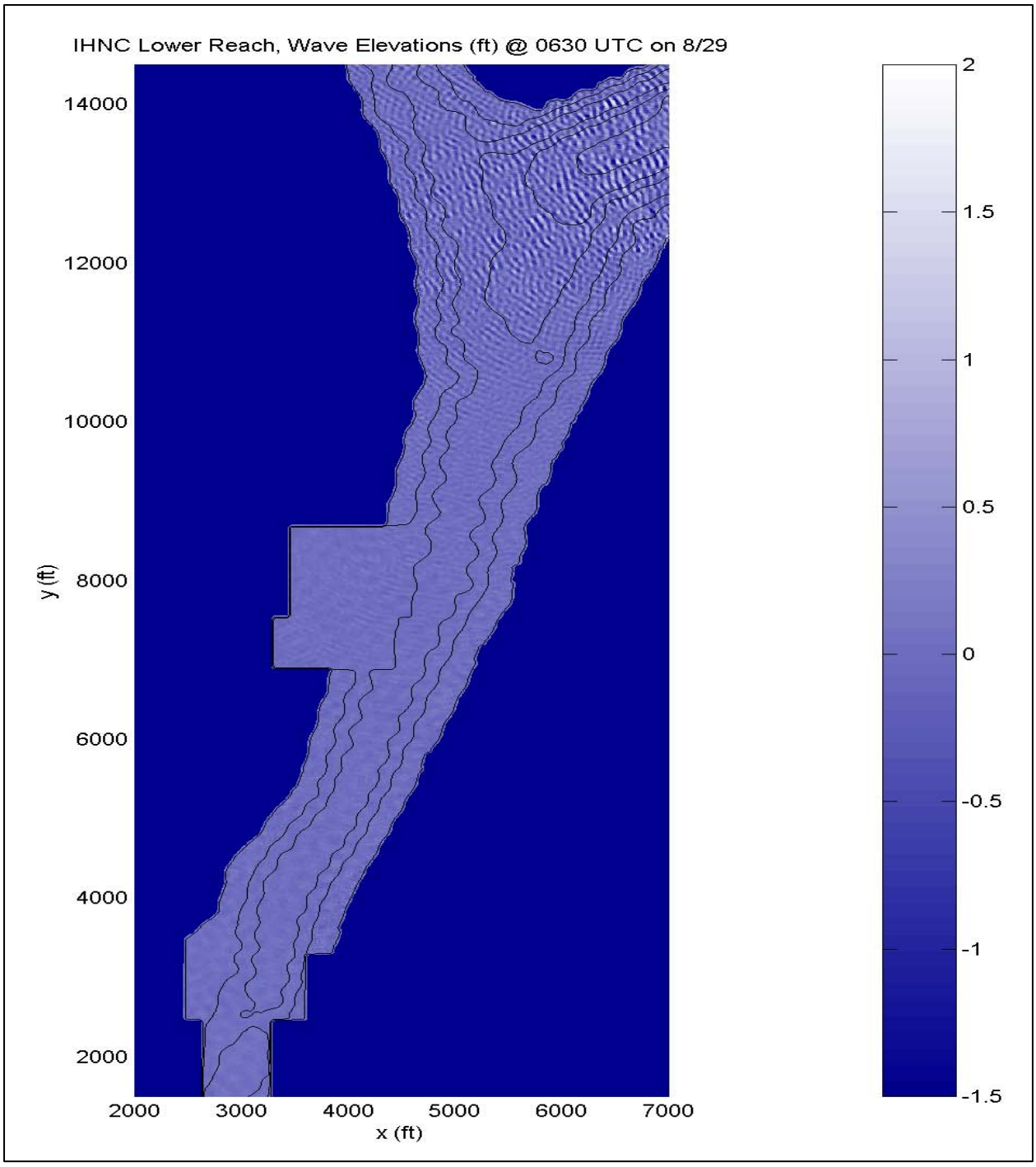

Figure 163. Region of IHNC modeled in Boussinesq simulations. [Time is referenced to UTC].

Flood Protection Levees along St. Bernard. The northeast-facing flood protection levees in St Bernard Parish along the MRGO were exposed to very high surge and waves during Katrina; and as seen in the post-Katrina assessment, much of this section of the hurricane protection system was damaged by the storm. The timeline report indicates that overtopping and breaching of the major flood protection levees along the MRGO/GIWW began early on the morning of the

29th. While some of the water entering the Chalmette area was observed to enter from the northwest (i.e. from breaches and overtopping of floodwalls and levees along the IHNC), as noted in the Timeline section of this volume, overtopping and breaching of the flood protection levees and subsequent overtopping of the back levee is likely responsible for much of the flooding and high velocities occurring in much of the Chalmette area.

Four locations along the northeast-facing hurricane protection system levees were chosen for detailed analysis here (Locations 1 to 4 shown in Figure 164) using COULWAVE. Details of the model and its application are provided in Appendix 15. Calculated time histories of water levels at these four points, relative to the tops of the levees, are given in Figure 165, along with the 2 percent probability-of-exceedance wave runup elevations. Wave runup is computed as the upward vertical distance from the still-water level. The probability of exceedance of wave runup is computed based on the percent of waves producing a runup higher than the given statistic. In other words, the exceedance is calculated based on the number of waves rather than the number of runups. These estimated mean water levels include all tidal, atmospheric pressure, wind, and wave contributions adjusted to agree with available HWM information. The 2 percent exceedance runup values were chosen as an indicator of when significant wave overtopping would have begun at these sites. As can be seen in Figure 165, levee heights vary along this section of the hurricane protection system, with the elevations at either end being 2 to 3 ft higher than levee elevations in the middle of the section.

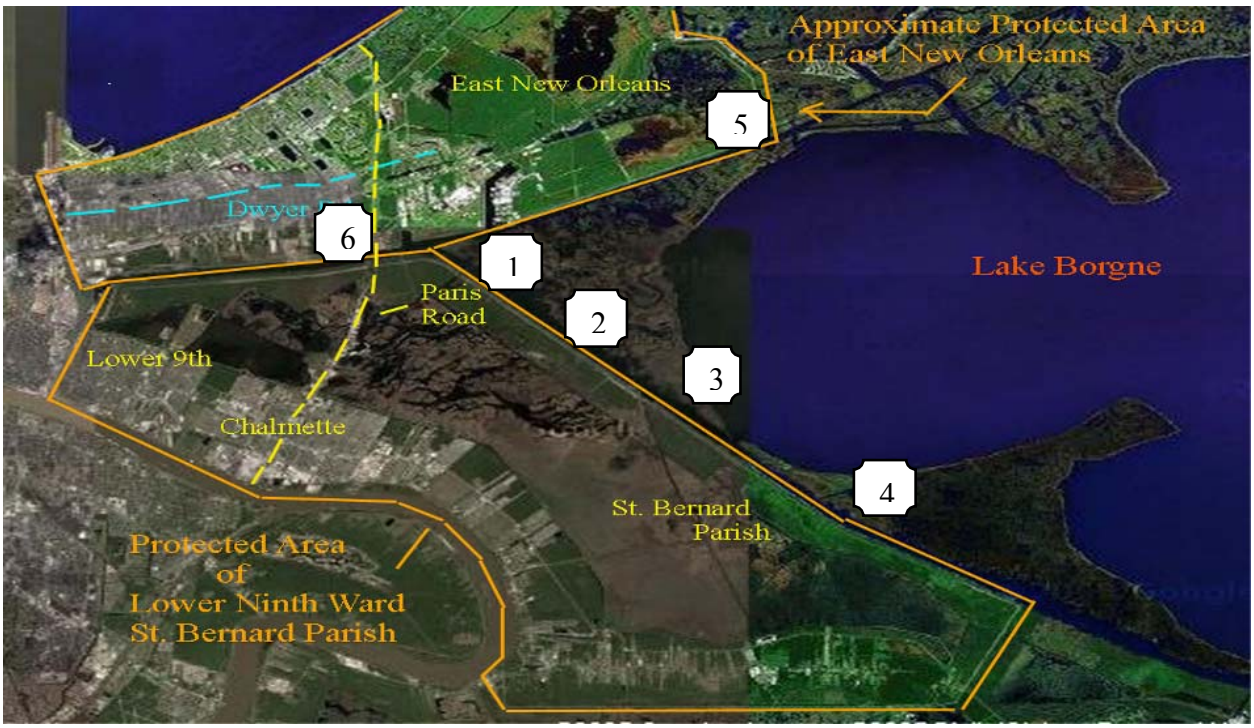

Figure 164. Detailed study locations in St. Bernard Parish and East New Orleans.

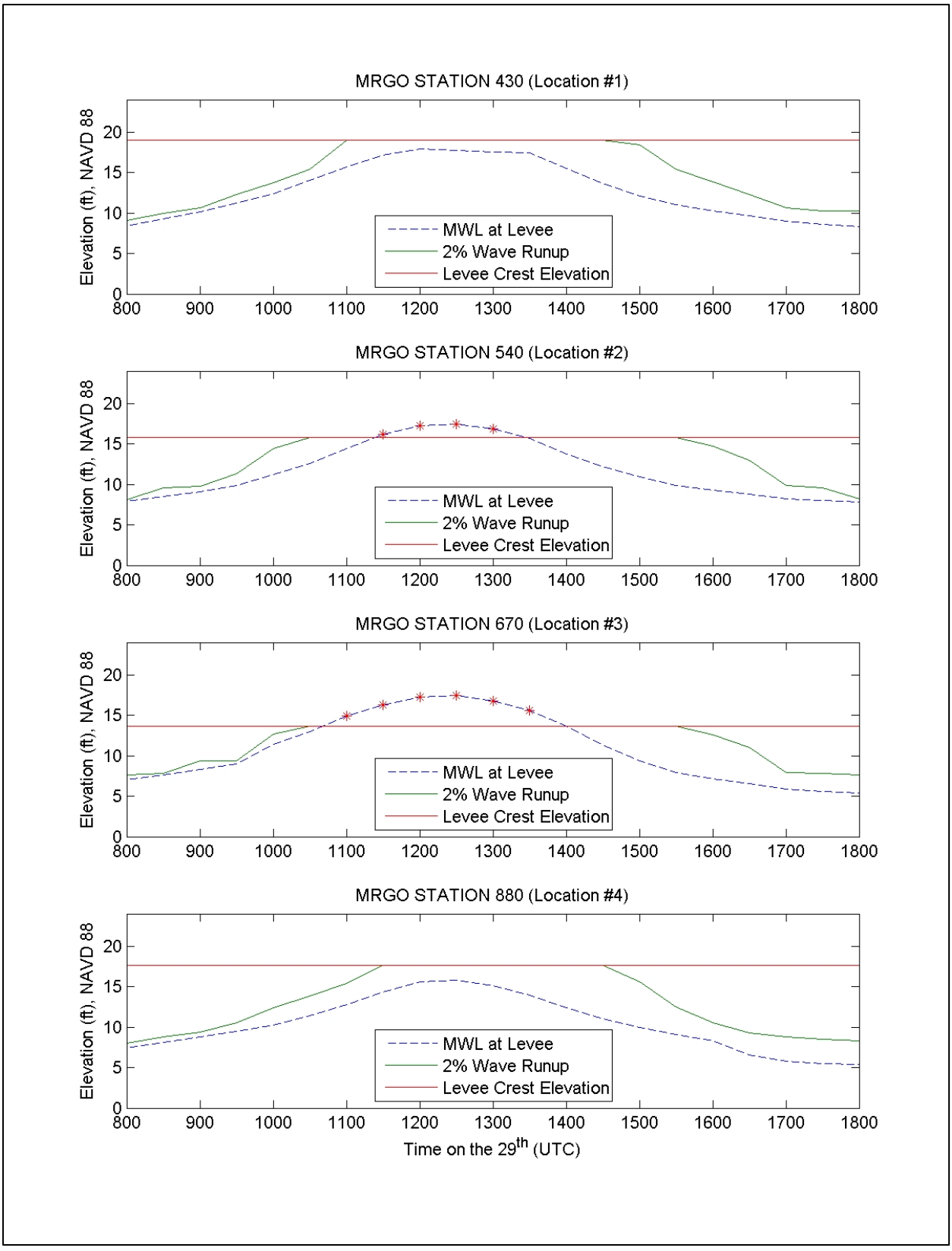

Figure 165. Hydrographs of water levels and 2 percent exceedance runup elevations, along with levee crest elevations at the four locations shown in Figure 164. [Times are referenced to UTC].

Figures 166 and 167 show the time series of incident significant wave heights and peak spectral periods, respectively, at all four locations. Peak wave heights are in the 5- to 6-ft range; and a comparison of Figures 165 and 166 shows that these peak wave conditions lag the peak surge by about 2 to 3 hr; however, incident waves are still quite large at the time of peak surge, with significant wave heights in the range of 4 to 5 ft. Directions of wave approach are essentially all out of the east-southeast during the time of large waves.

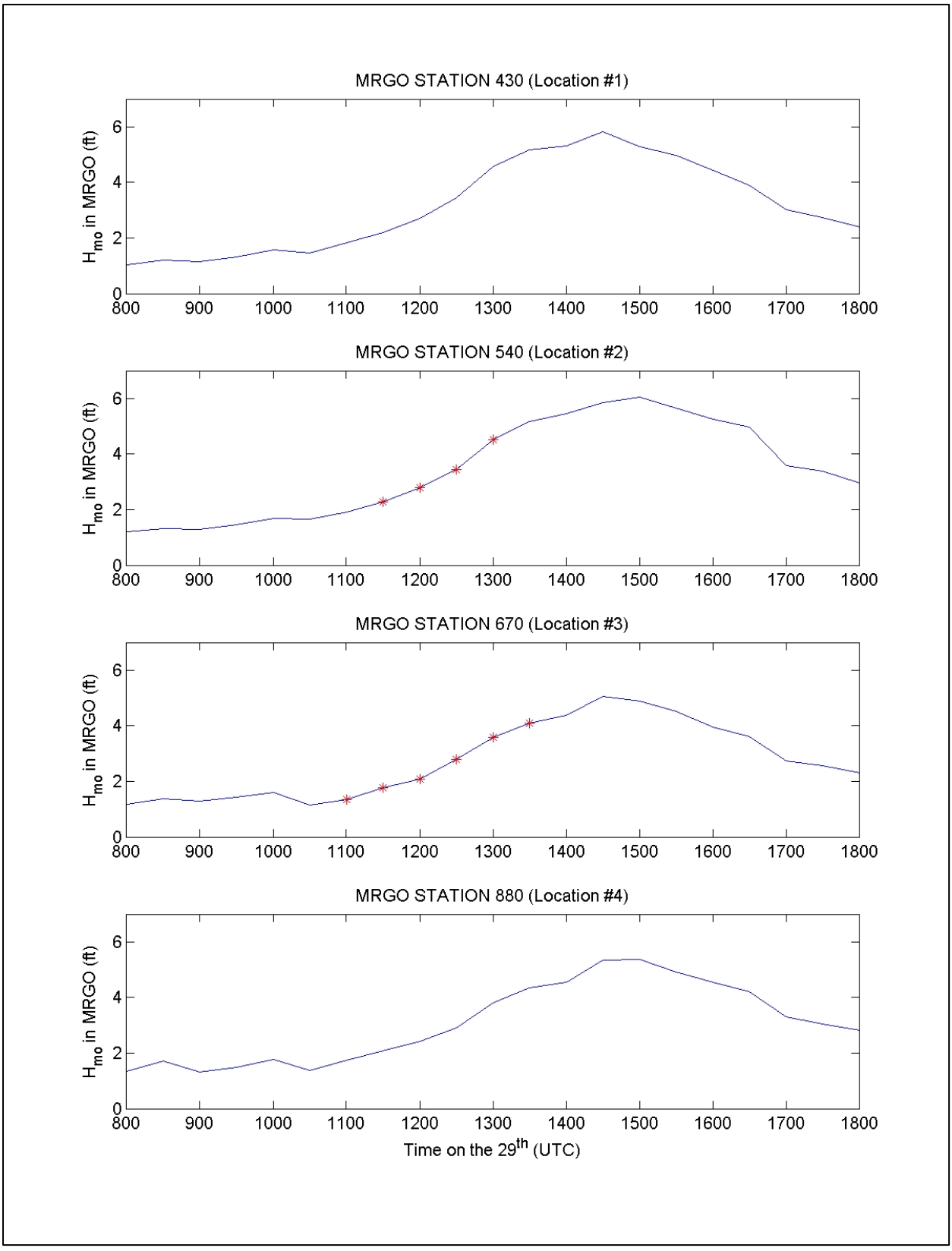

Figure 166. Time series of significant wave heights at the four locations shown in Figure 164. [Times are referenced to UTC}.

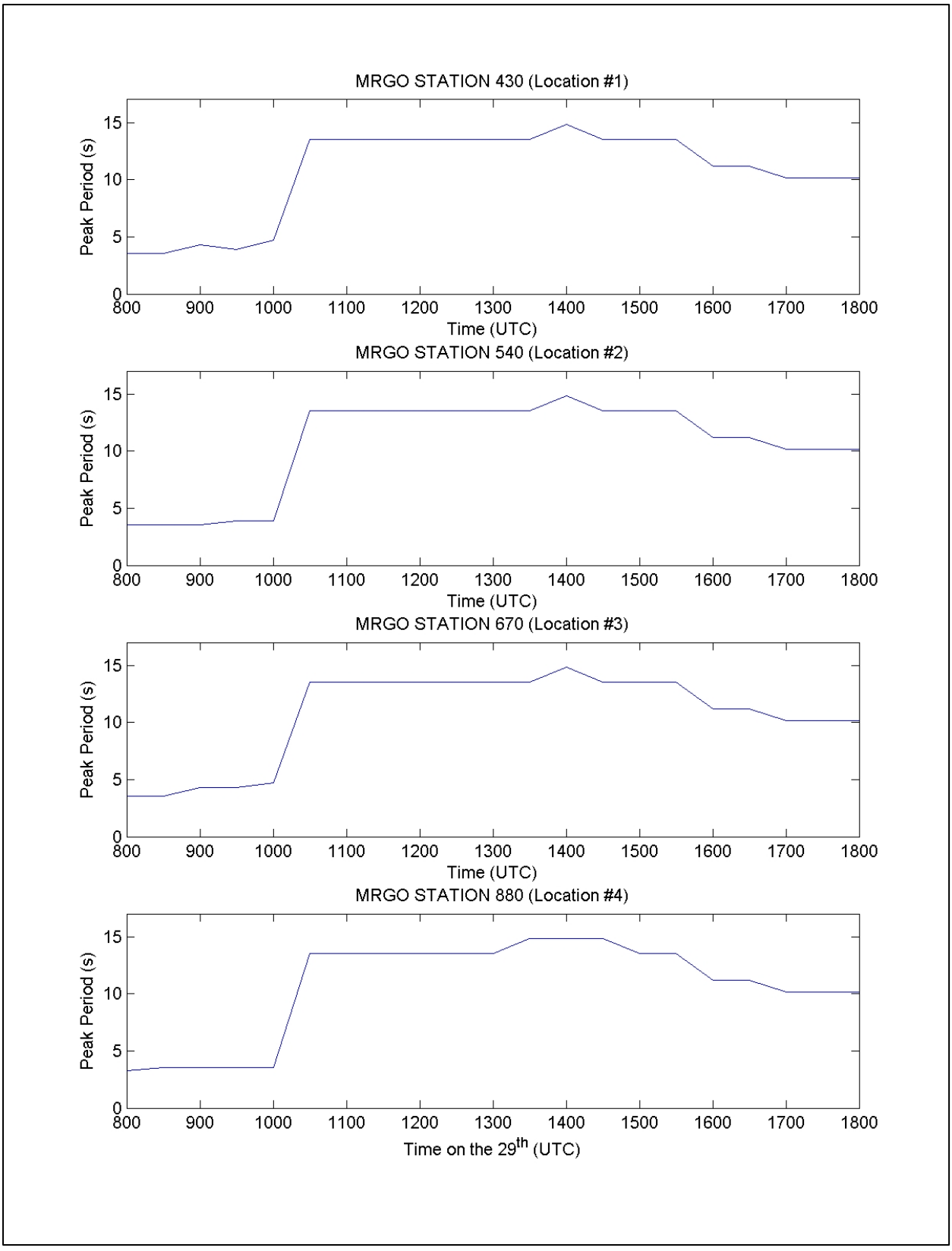

Figure 167. Time series of peak spectral periods at the four locations shown in Figure 164. [Times are referenced to UTC].

Figure 168 shows the estimated velocities over the crest of the levee at these four locations; Figure 169 shows the velocities along the front face of the levees; Figure 170 shows the velocities along the back face of the levees; and Figure 171 shows the overtopping rates for these same locations. In most places along the St. Bernard Parish Levees along the MRGO, wave runup and overtopping will be of primary concern, rather than direct forces on vertical walls; consequently, the focus of this section will be on velocities (related to erosion/breaching potential) and to overtopping rates (related to flooding behind the levees).

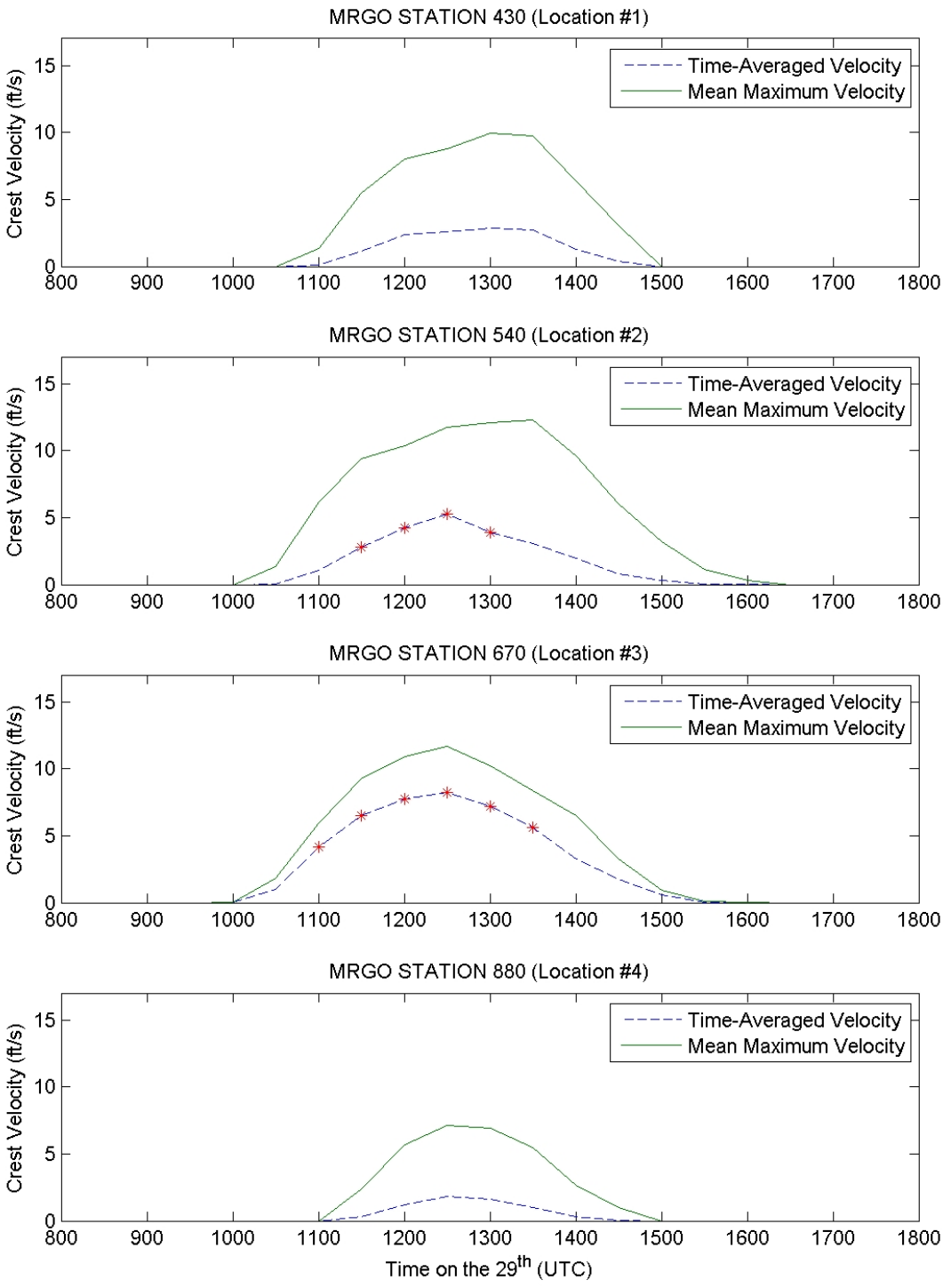

Figure 168. Estimated velocities over levee crest for the four locations shown in Figure 164. [Times are referenced to UTC].

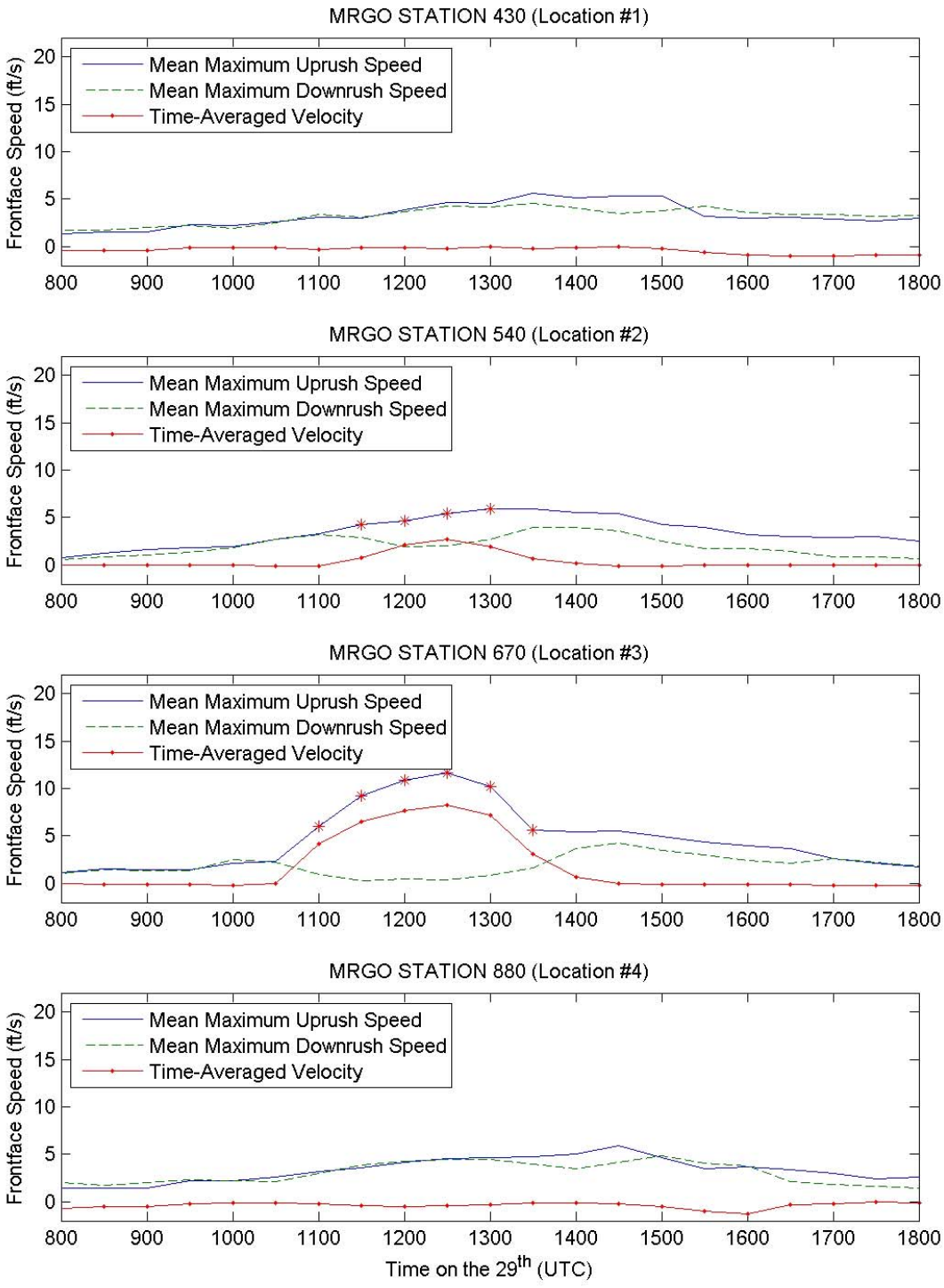

Figure 169. Velocities along the front face of the levees at the four locations shown in Figure 164. [Times are referenced to UTC].

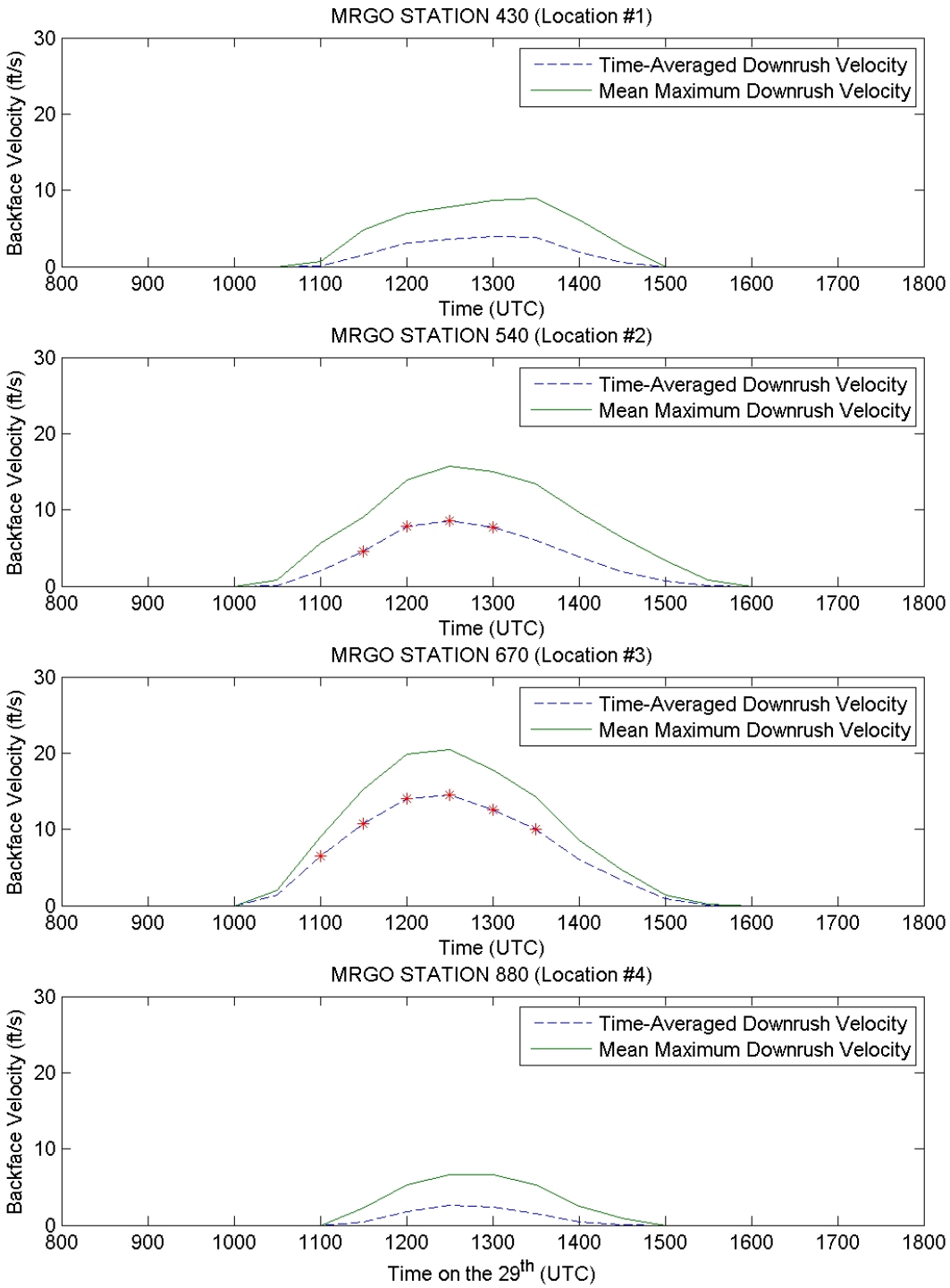

Figure 170. Velocities along the back face of the levees at the four locations shown in Figure 164. [Times are referenced to UTC].

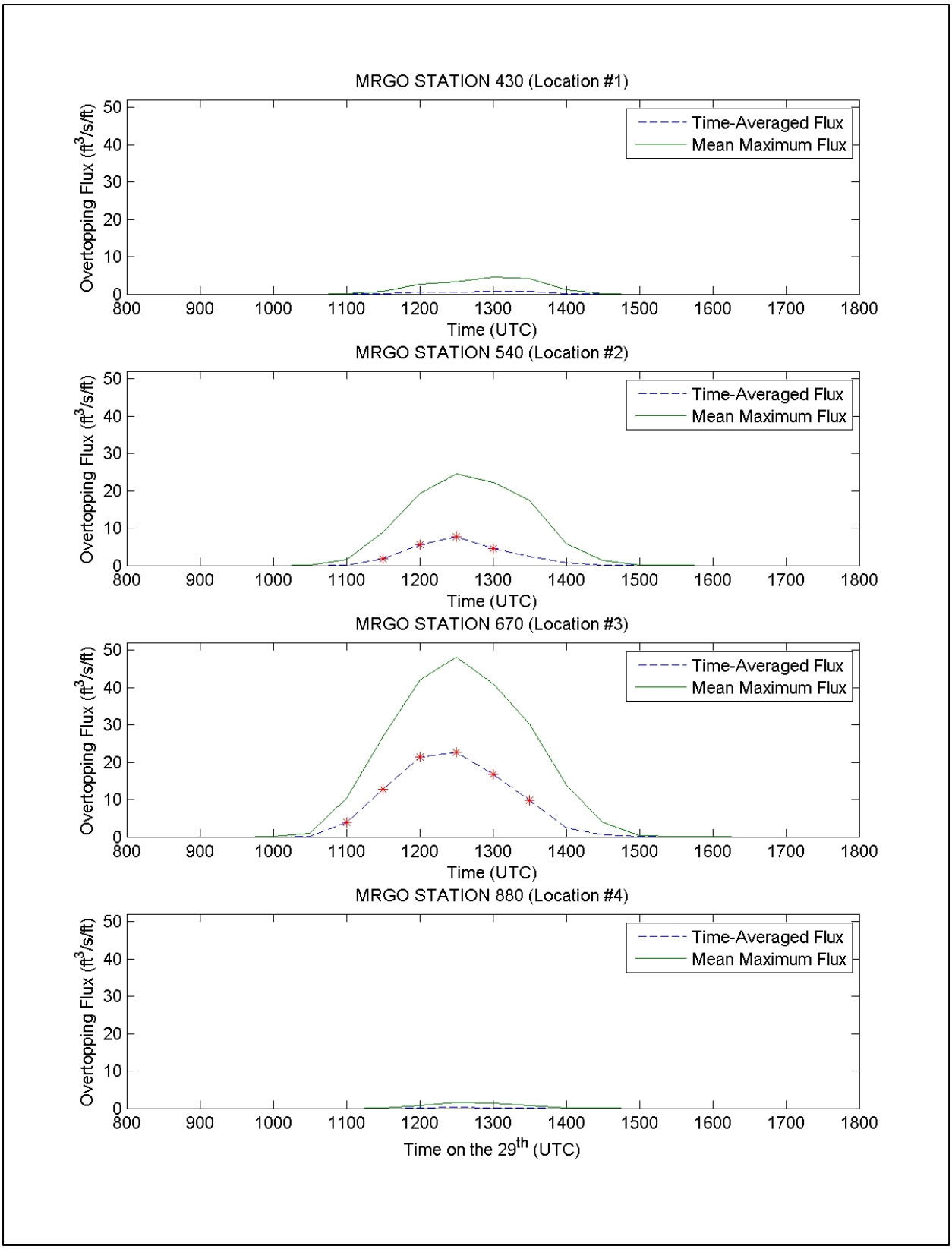

Figure 171. Overtopping rates for all four locations shown in Figure 164. [Times are referenced to UTC].

During Katrina, estimated mean water levels never rose above the top of the levee at Location 1; however, substantial wave overtopping is estimated to have begun around 1100 UTC (6:00 a.m. CDT) and persisted for 4 hr until about 1500 UTC (10:00 a.m. CDT). Overtopping rates for this site are shown in Panel 1 of Figure 171, for the hypothetical case of no change in levee erosion/breaching during the storm. The estimated mean flux rate (the time-averaged flux shown in Figure 171) is equal to the volume rate of water coming into the region behind the levee per foot along the levee. The largest value of this parameter is around 0.8 $ft^3/s/ft$ along the levee crest. To put this into context, if an overtopping rate of 0.8 $ft^3/s/ft$ occurred over a one-mile stretch, a pumping rate of about 4,000 ft^3/s would be required to keep up with the total volume of water entering the area behind the levee.

Analyses of topographic information from pre- and post-Katrina LIDAR surveys are contained in Appendix 16. Figure 172 shows one section from this appendix. As can been seen in the appendix, considerable erosion/breaching occurs along these levees over much of this area. In the vicinity of Location 1, it is likely that wave overtopping was the initial mechanism creating the incipient erosion along these levees. Given the wave periods incident on the levee in this area, this area would have been exposed to several hundred waves per hour overtopping the levee crests around the time of the peak surge. Once wave-induced erosion lowered the levee crests to a point where the mean water levels exceeded the crest elevation, the erosion/breaching process would be exacerbated by the combination of mean flow over/through the levee and wave velocities.

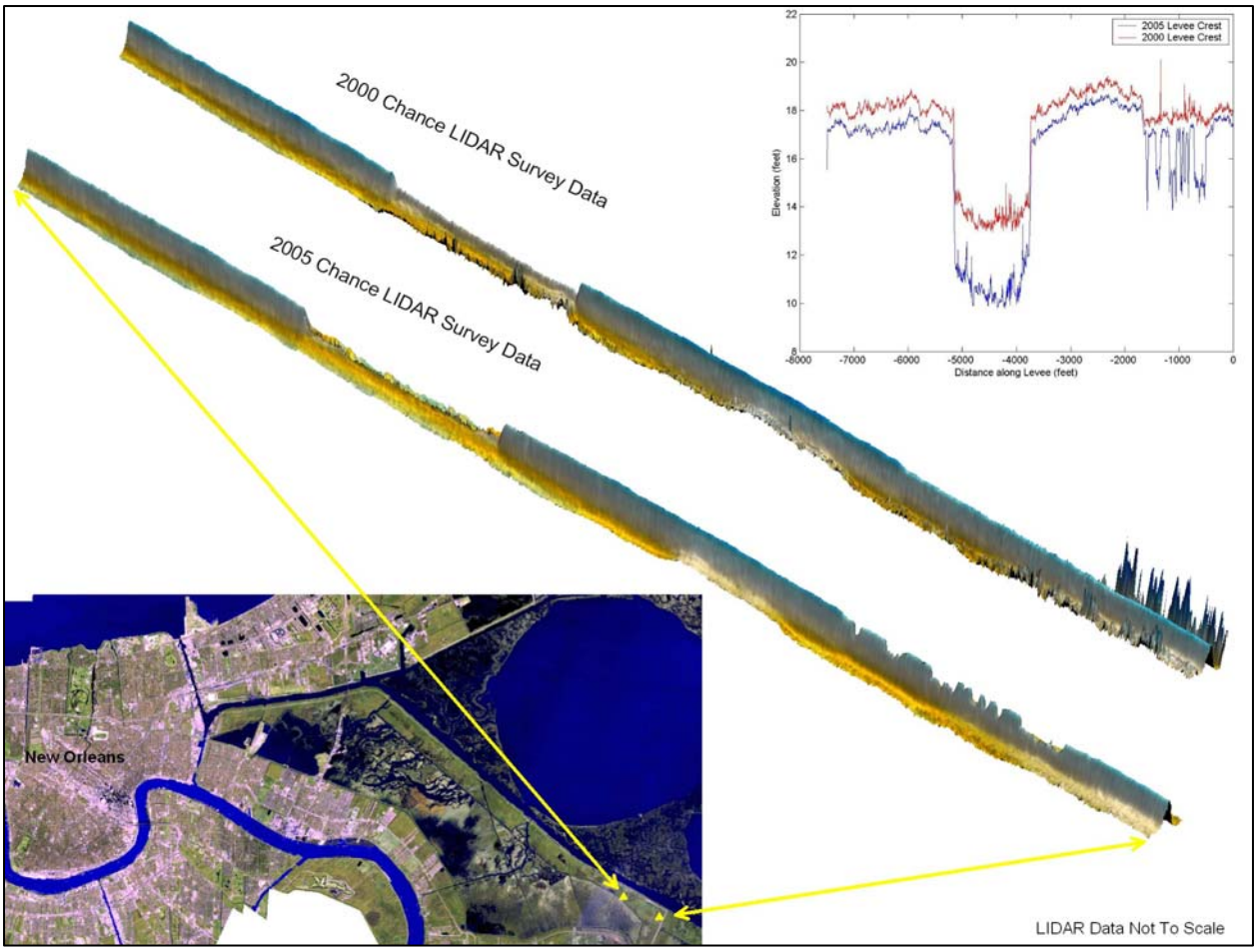

Figure 172. Topographic information from pre- and post-Katrina LIDAR surveys

At Location 2, waves began to substantially overtop the levee at around 1030 UTC (5:30 a.m. CDT) and at 1130 UTC (6:30 a.m. CDT) the mean water level began to overtop the levee crest. At the peak surge condition, the mean water level was about 1.5 ft above the levee crest at this location. If levees had not eroded and breached, mean flow overtopping would have persisted for about 2 hr until 1330 UTC (8:30 a.m. CDT) and substantial wave overtopping would have persisted for about 5 hr, until about 1530 UTC (10:30 a.m. CDT). Panel 2 of Figure 171 gives the overtopping rates, assuming no levee erosion/breaching. Whereas the estimated maximum overtopping rate at Location 1 at the peak of the storm was only 0.8 $ft^3/s/ft$, the estimated overtopping rates at Location 2 are around 8 $ft^3/s/ft$, an order of magnitude increase in overtopping rates. Overtopping in this area, even without erosion/breaching would have poured over 40,000 ft^3/s per mile of levee over the tops of these levees into the area behind the St. Bernard Parish hurricane protection levees. As was the case at Location 1, considerable erosion/breaching occurred at Location 2 (as can be seen in the pre- and post-Katrina LIDAR surveys shown in Appendix 16). Given that wave overtopping appears to be capable of producing significant levee erosion on the levees in this area once the mean water level comes within a foot or two of the levee crest elevation (as seen at Location 1), erosion of these levees probably began around 1030 UTC (5:30 a.m. CDT). Consequently, actual overtopping rates

during the storm would probably have been considerably higher than this at the peak of the storm.

Location 3 is the location with the lowest levee crest elevation. At this site, it is estimated that substantial wave overtopping began at about 1030 UTC (5:30 a.m. CDT) and the mean water level began overtopping at about 1100 UTC (6:00 a.m. CDT). At the time of peak surge, the water level is almost 3 ft above the crest of the levee. Given no erosion/breaching of the levees, mean water level overtopping would have persisted for about 3 hr until 1400 UTC (9:00 a.m. CDT) and substantial wave overtopping would have persisted for about 5 hr until about 1530 UTC (10:30 a.m. CDT). Panel 3 of Figure 171 gives the estimated overtopping rates for the case of no levee erosion/breaching. Similar to the situation at Location 2, overtopping rates would have been extremely large, even without erosion/breaching of the levees. In this case at the peak of the storm, even for the hypothetical case of no erosion/breaching, about 20 $ft^3/s/ft$ (100,000 ft^3/s for a one-mile length of levee) would have been coming over the top of this levee.

At Location 4, it is estimated that there is no overtopping by the mean water level, but substantial wave overtopping occurred for about 3 hr from around 1130 to 1430 UTC (6:30 to 9:30 a.m. CDT). Panel 4 of Figure 171 gives the estimated overtopping rates for this site. Here, peak overtopping rates are only about 0.2 $ft^3/s/ft$, which would have produced only about 1,000 ft^3/s per mile of levee.

Flow Rates over MRGO Levee

In this section, flow rates into St. Bernard Parish from overtopping of the MRGO Levee are estimated. Output from the Boussinesq model was used to compute the overtopping rates because this is presently the only tool available for computing combined wave and steady flow overtopping. Analysis of the Boussinesq results yielded a relationship between surge elevation over the crest and overtopping. The Boussinesq results fit the broad crested weir relationship $q = 0.54\sqrt{g}(h_s - h_c)^{1.5}$ for surge elevations above the levee crest where g is the acceleration of gravity, h_s is the surge elevation, and h_c is the crest elevation of the levee. For surge elevations below the levee crest, a wave overtopping equation would be appropriate as discussed in Appendix 9. However, herein a simpler approximate equation is utilized of similar accuracy to the overall effort. The final relation that best fit the results of the Boussinesq modeling is

$$\begin{aligned} q &\approx 0 \qquad for\ (h_s - h_c) < -1.76' \\ q &= 1.42(h_s - h_c) + 2.5 \qquad for\ -1.76' < (h_s - h_c) \le 0 \\ q &= 2.8(h_s - h_c)^{1.5} + 2.5 \quad for\ (h_s - h_c) > 0 \end{aligned} \tag{1}$$

where q is in units of cubic feet per second per foot of levee crest length and h_s and h_c are in feet. Equation 1 is dimensionally inconsistent. Therefore, the coefficients in the relation are not dimensionless. The fit of the model described by Equation 1 is shown in Figure 173.

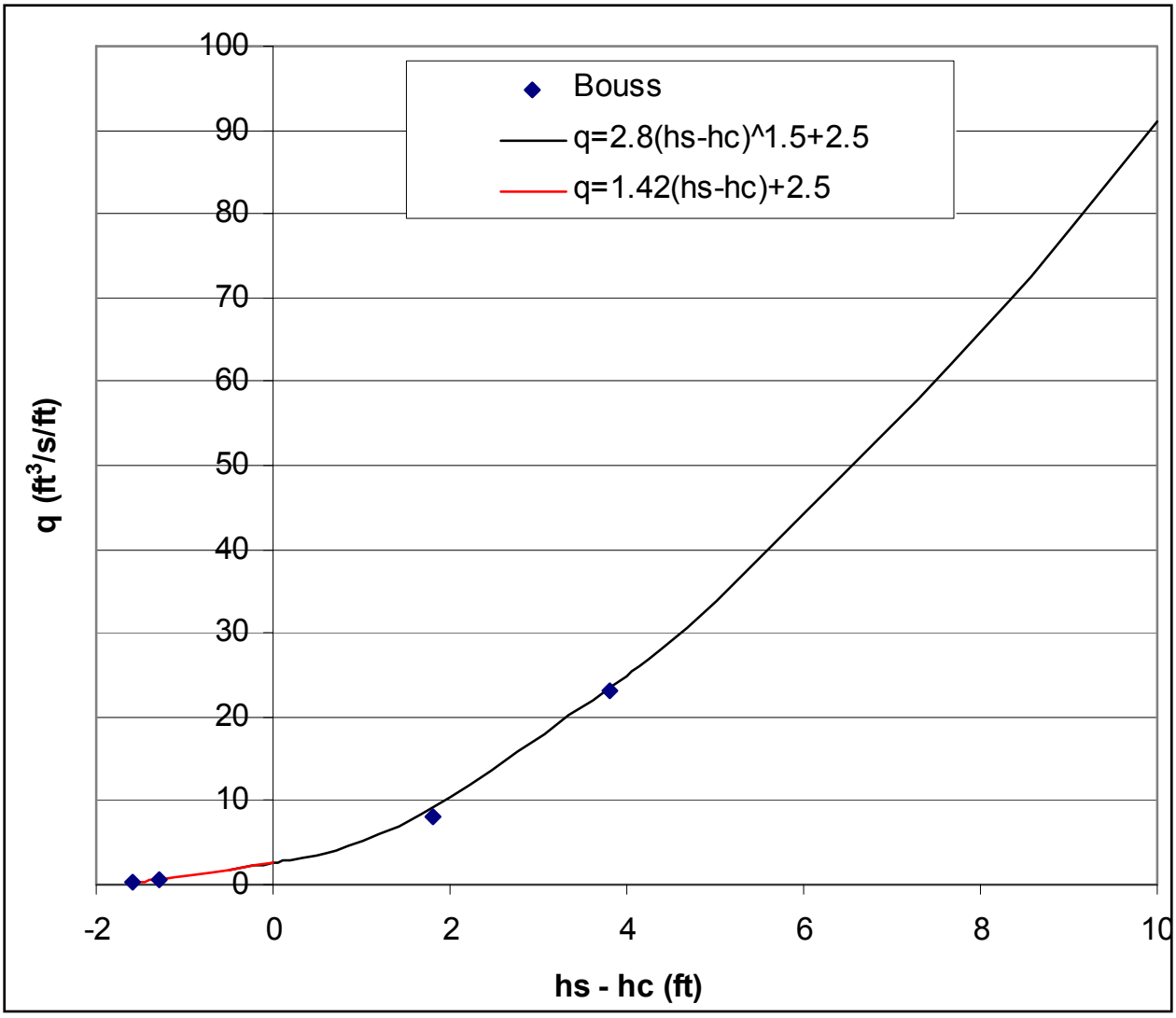

Figure 173. Boussinesq and Equation 1 overtopping flow rate as a function flood thickness over levee crest.

Equation 1 was applied over the entire levee crest to determine flow rates at the time of maximum surge, roughly 1230 UTC (7:30 a.m. CDT) on the 29th. For this analysis, the pre-Katrina and post-Katrina levee crest center-line elevations were used along with ADCIRC results adjusted to match HWMs as discussed in Appendix 15. The results are shown in Figure 174. In this figure, the horizontal axis is the distance along the levee beginning at a location just north of Bayou Bienvenue at the southern end of the radius of the bend as the MRGO Levee turns into the GIWW Levee. Very high overtopping rates, which exceed the range of Boussinesq results, are noted in specific locations where the levee crest eroded heavily.

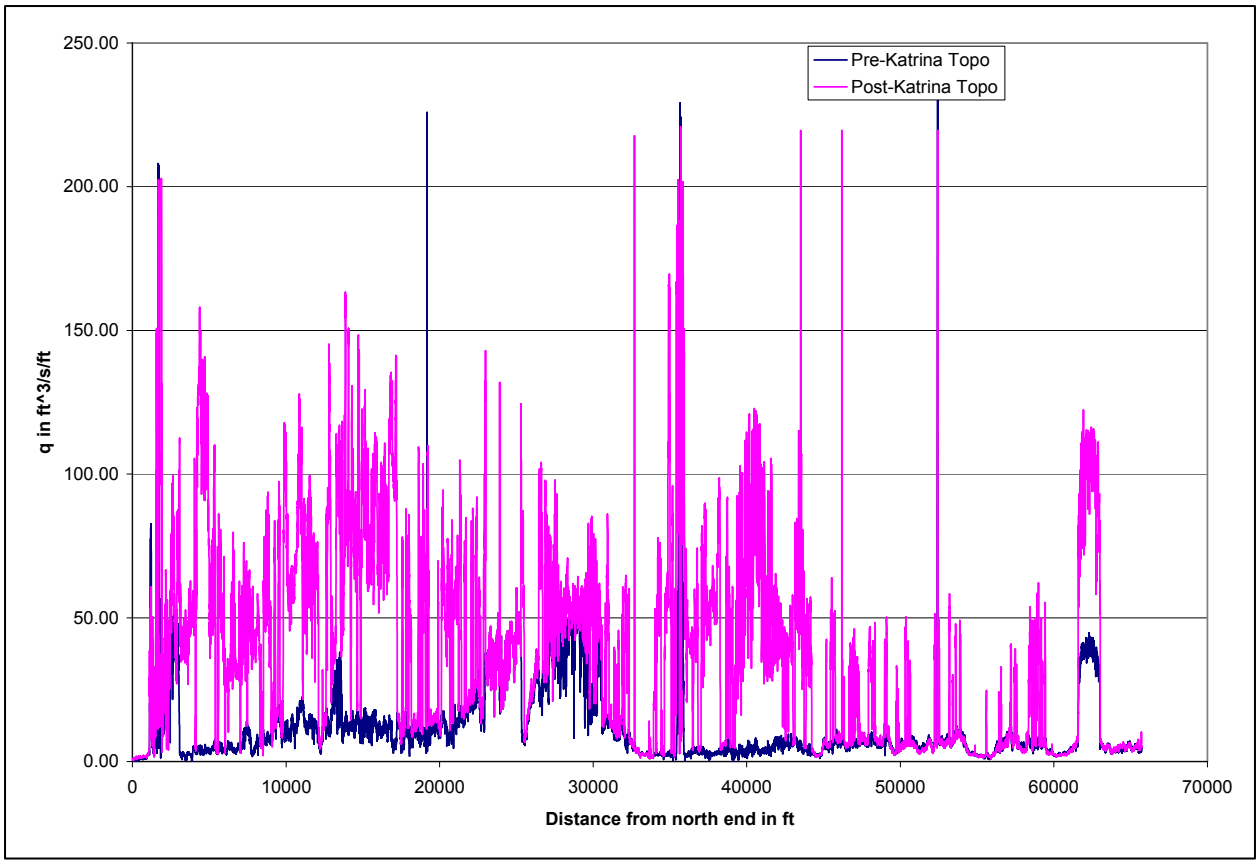

Figure 174. Overtopping rates for pre-Katrina and post-Katrina LIDAR survey crest heights along center line of MRGO levee corresponding to maximum surge elevation at approximately 1230 UTC (7:30 a.m. CDT) on 29 August.

Equation 1 is used to extend those results to include overtopping for the post-Katrina levee elevation. Equation 1 results will differ somewhat from the Boussinesq results because the Boussinesq analysis implicitly includes coupled wave runup and overtopping, wave setup and steady overtopping, which vary in time and space. Figure 175 shows overtopping and crest elevation as a function of time for Station 430 (corresponds to Location 1 in Figure 164) for both the pre-Katrina and post-Katrina levee elevations. The maximum pre-Katrina overtopping rate is $q = 0.7$ ft^3/s/ft, which is the same as found using the Boussinesq model. The levee crest as a function of time was approximated as a smooth function between the pre-Katrina elevation and the post-Katrina elevation at Station 430. For this station, the maximum overtopping using the post-Katrina levee elevation is 46 ft^3/s/ft. These values can be compared to existing guidance in the Corps' Coastal Engineering Manual for threshold dike erosion of 0.01 to 0.1 ft^3/s/ft. Results for Station 540 (corresponds to Location 2 in Figure 164) are shown in Figure 176. In this case, Equation 1 predicted a maximum pre-Katrina $q = 9$ ft^3/s/ft, which is roughly the same as the Boussinesq model. For this station, the maximum overtopping using the post-Katrina levee elevation is 34 ft^3/s/ft. Results for Station 670 (corresponds to Location 3 in Figure 164) are shown in Figure 177. Equation 1 predicted a maximum pre-Katrina $q = 25$ ft^3/s/ft, which is also roughly the same as the Boussinesq model. For this station, the maximum overtopping using the post-Katrina levee elevation is 45 ft^3/s/ft. Results for Station 880 (corresponds to Location 4 in Figure 164) are shown in Figure 178. In this case, Equation 1 predicted a maximum pre-Katrina

q = 2.8 $ft^3/s/ft$, which is also roughly the same as the Boussinesq model. For this station, the maximum overtopping using the post-Katrina levee elevation is 8 $ft^3/s/ft$.

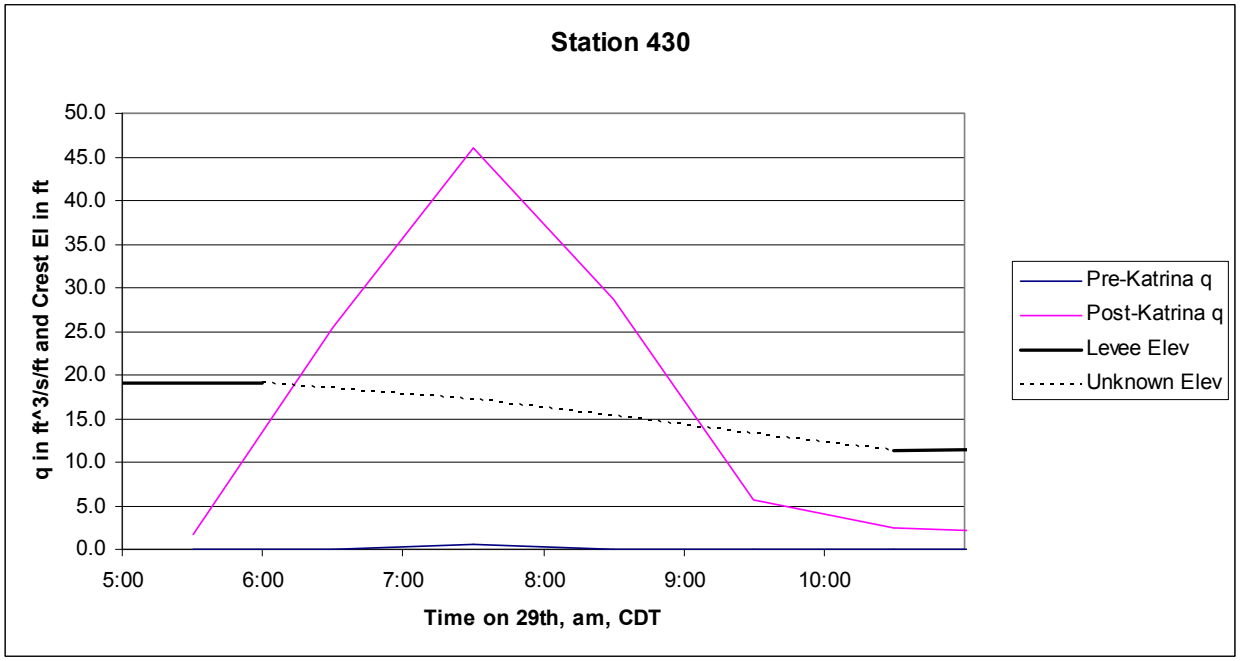

Figure 175. Approximate overtopping rate and levee crest height during storm as a function of time for Station 430 (Location 1 in Figure 164) using Equation 1.

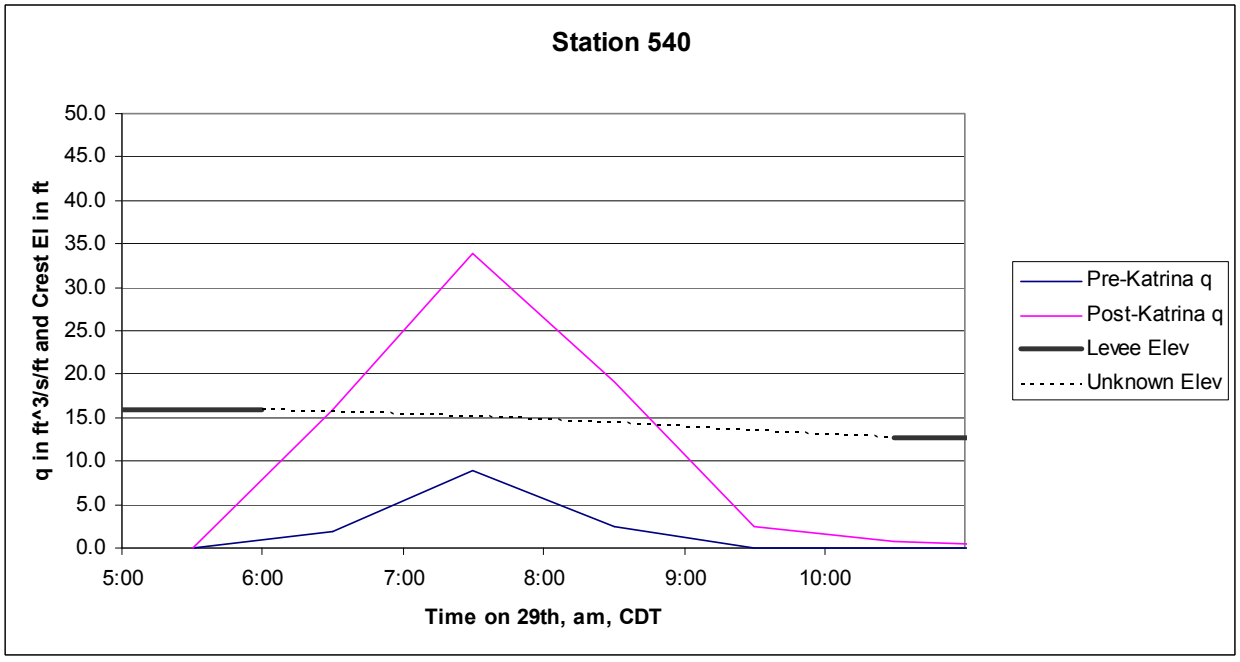

Figure 176. Approximate overtopping rate and levee crest height during storm as a function of time for Station 540 (Location 2 in Figure 164) using Equation 1.

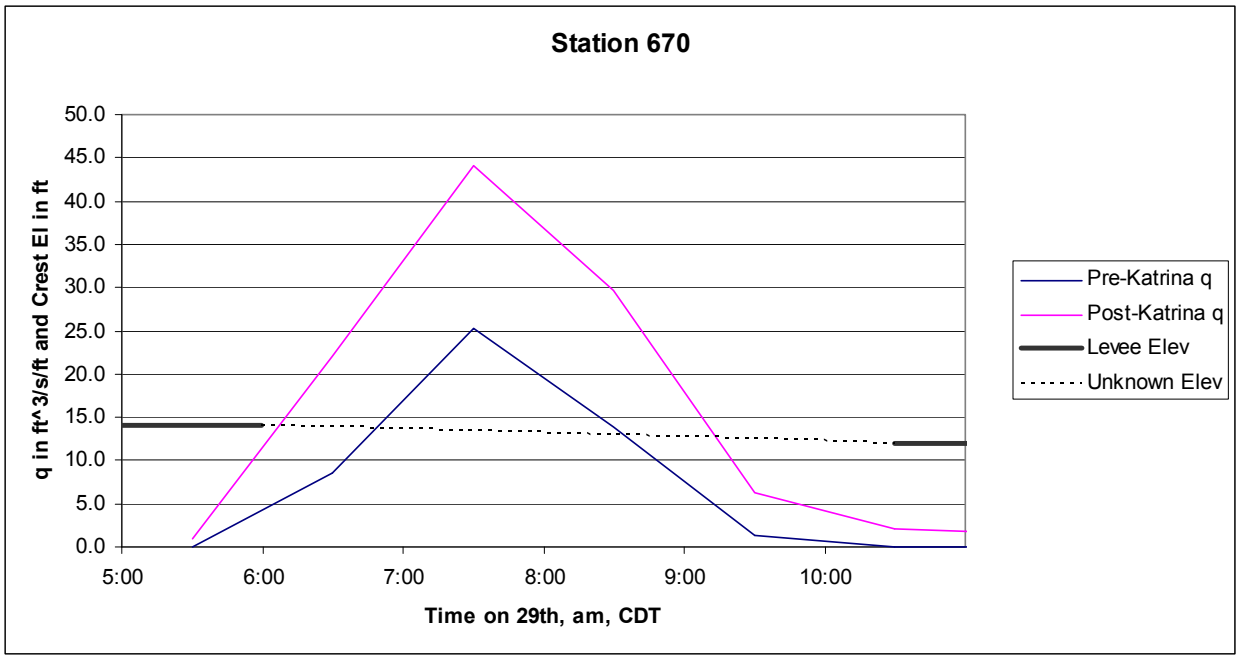

Figure 177. Approximate overtopping rate and levee crest height during storm as a function of time for Station 670 (Location 3 in Figure 164) using Equation 1.

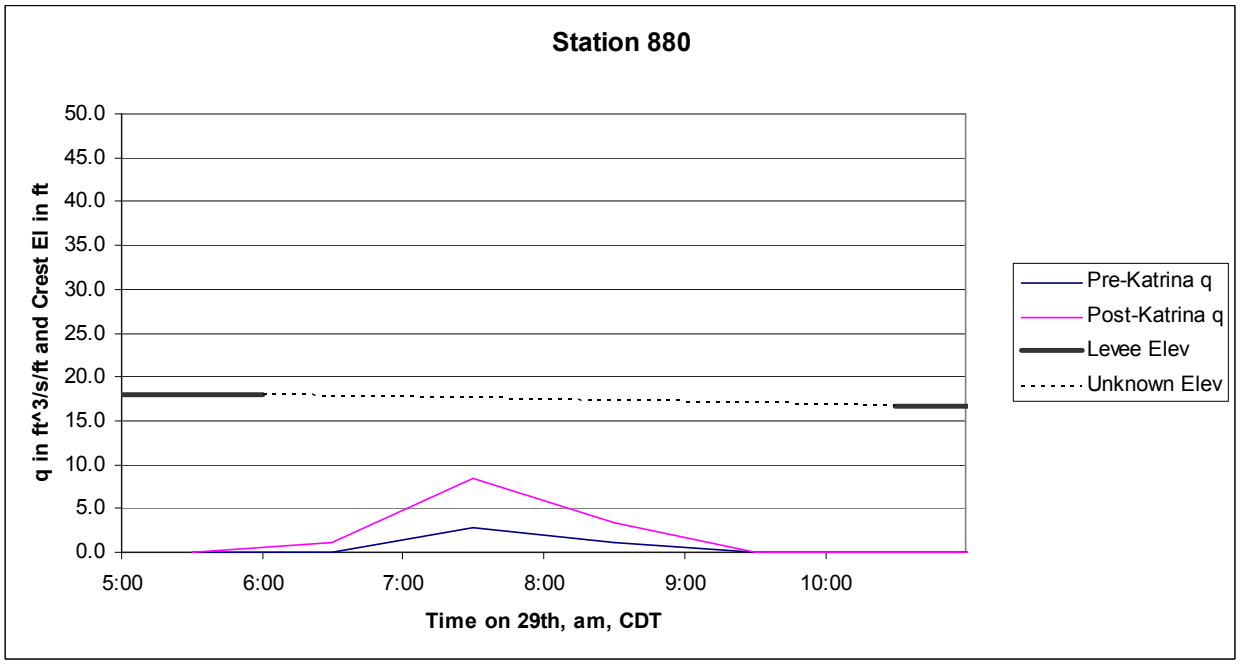

Figure 178. Approximate overtopping rate and levee crest height during storm as a function of time for Station 880 (Location 4 in Figure 164) using Equation 1.

For flood modeling, an estimate of the total flood volumes is necessary. The level of this analysis is very crude because the calibration of Equation 1 to the uncalibrated Boussinesq model provides only a rough approximation and the elevation of the levee is roughly quantified

from the LIDAR data. However, there are no other tools or data available at this time to make this approximation.

In order to approximate flooding volumes, the levee crest was averaged over reaches of roughly constant elevation. The final averaged pre-Katrina levee crest elevation along with surge heights for the period prior to, and including, the peak surge are shown in Figure 179. Also shown in Figure 179, as vertical lines, are the four locations used in the Boussinesq model effort to quantify overtopping. A similar plot with post-Katrina averaged levee crest elevation and post-peak surge levels is shown in Figure 180.

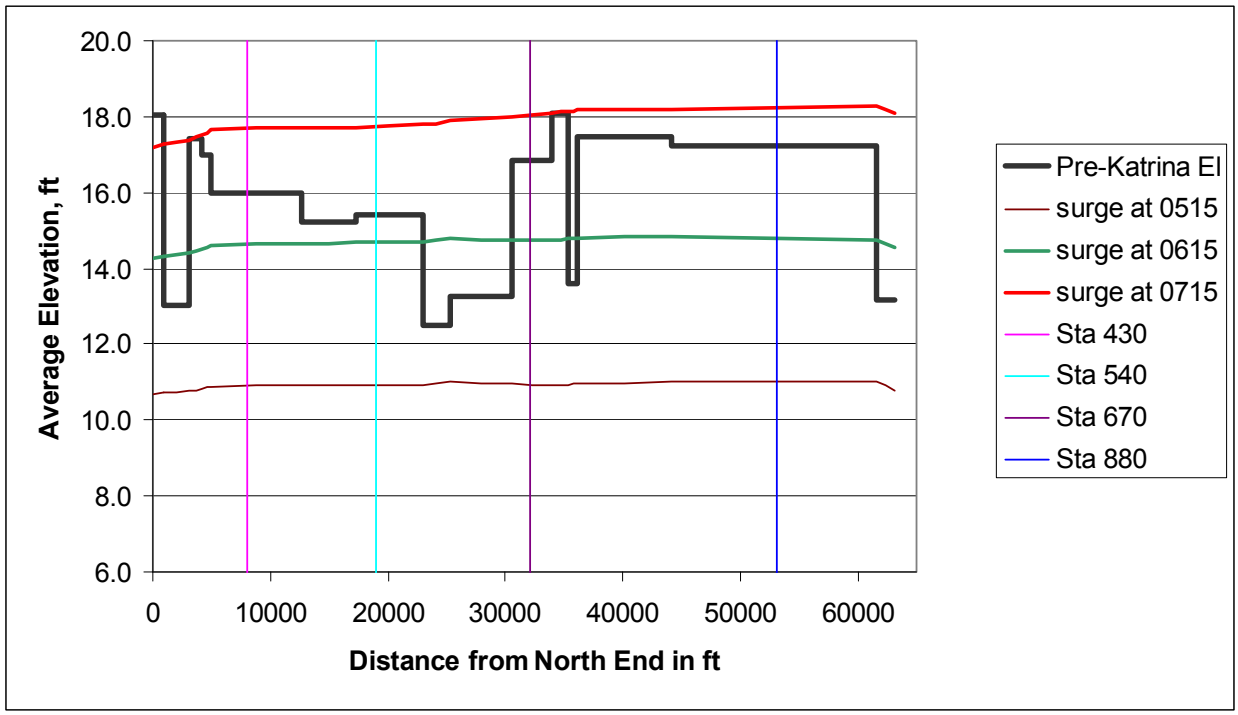

Figure 179. Pre-Katrina average levee crest elevation, pre-peak surge levels, maximum surge level and Boussinesq analysis stations. [Times are referenced to CDT].

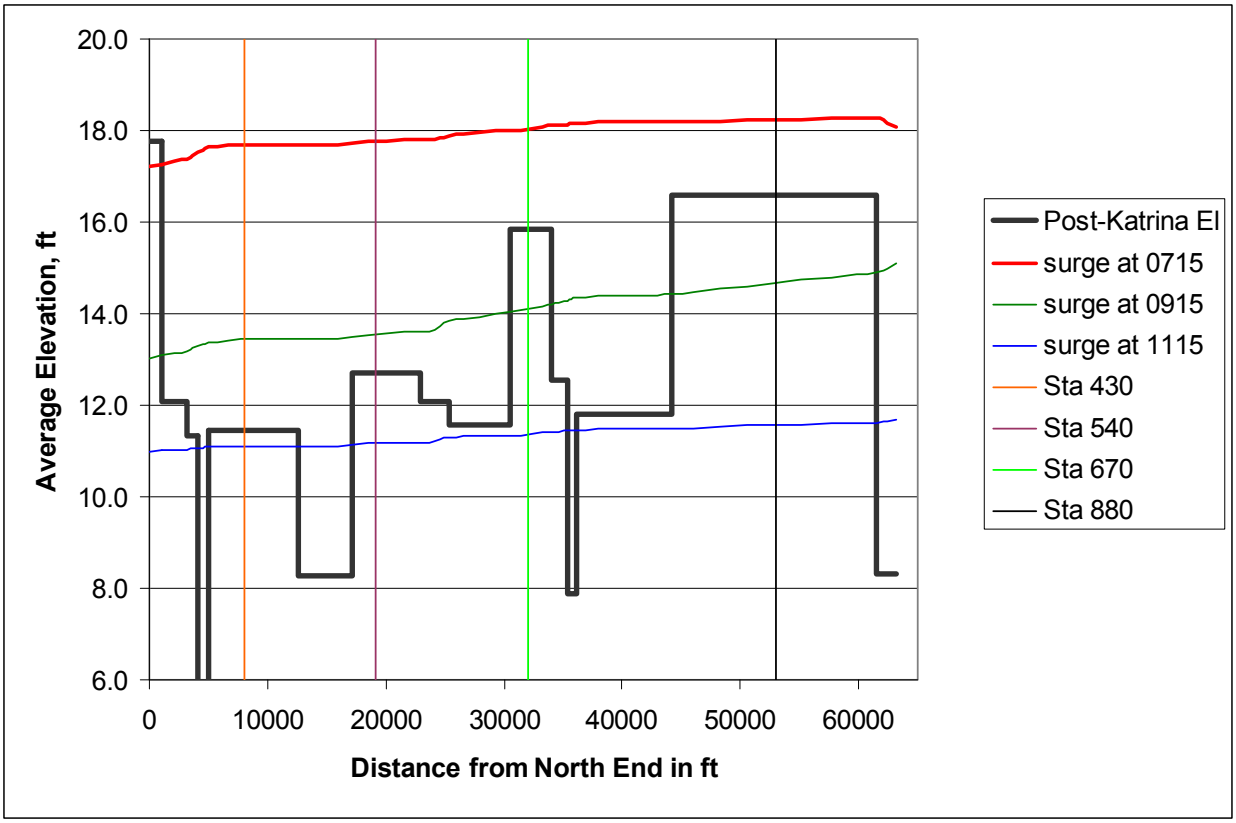

Figure180. Post-Katrina average levee crest elevation, maximum surge level, post-peak surge levels, and Boussinesq analysis stations. [Times are referenced to CDT].

These locally averaged levee crest levels and locally averaged surge levels were used to determine average total overtopping into the lee of the MRGO Levee using Equation 1. The final calculation is a summation of overtopping along the entire levee crest. The total volumetric overtopping rate as a function of time is shown in Figure 181. In this case, the wave-only contribution for relatively low surge levels is assumed to be negligible, as shown in Equation 1. It should be noted that the contribution from overtopping along the southern levee that runs east-west along St. Bernard Parish was not included in this analysis due to time constraints. However, it is expected that this contribution would likely be significant.

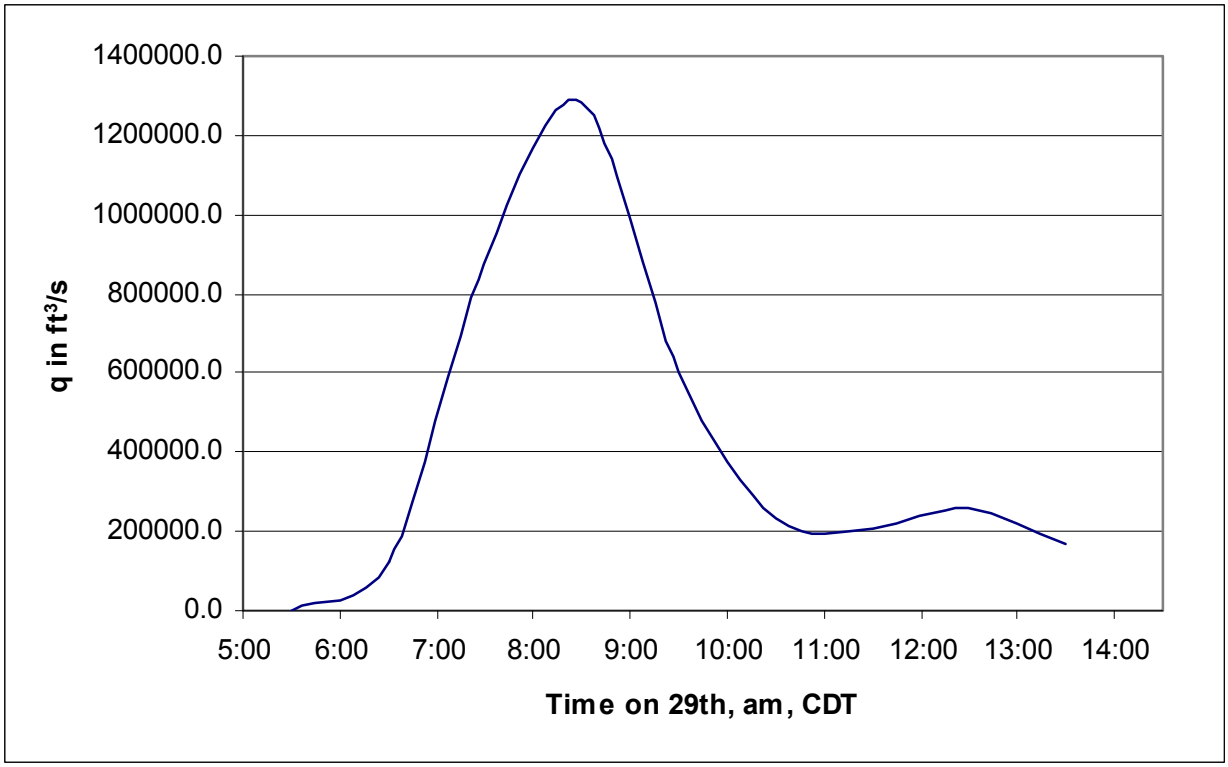

Figure 181. Integrated volumetric overtopping as a function of time for the MRGO Levee for lower surge level. [Times are referenced to CDT].

The uncertainty in surge levels indicates that the maximum surges could have been about 1 ft higher. Using these values, the total flow over the MRGO Levee is computed and summarized in Figure 182.

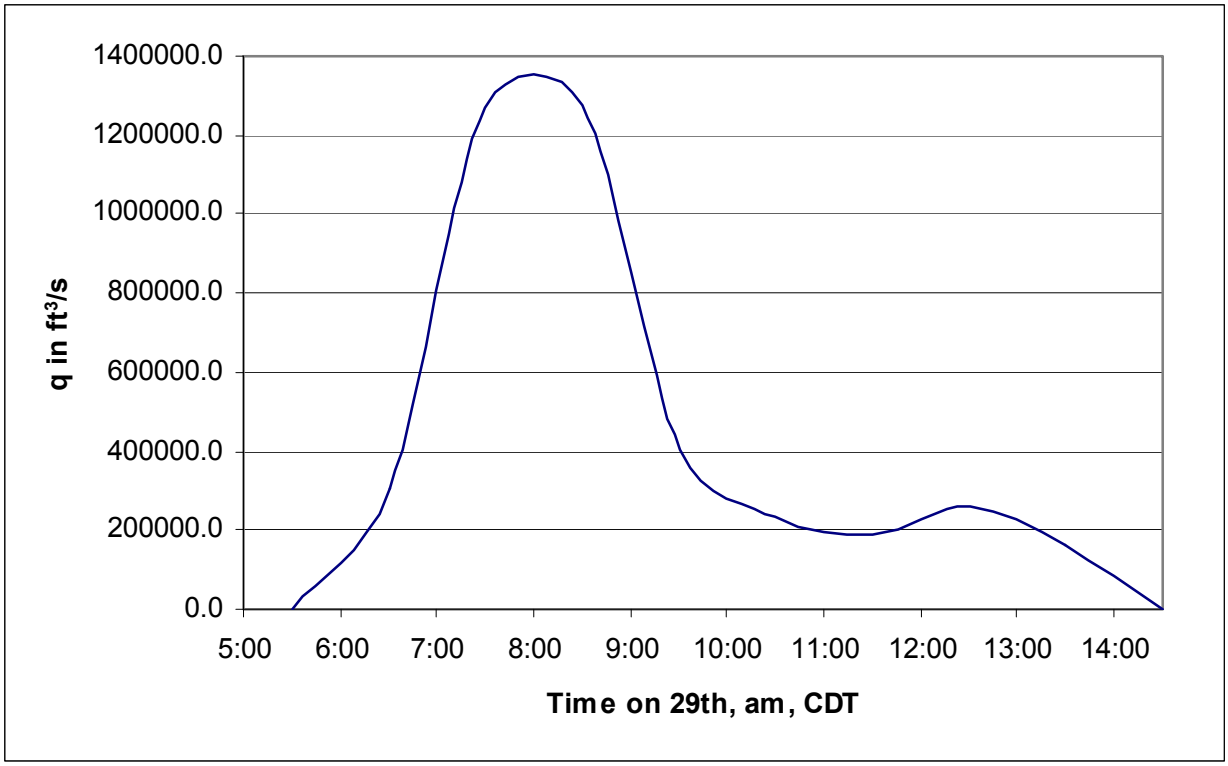

Figure 182. Integrated volumetric overtopping as a function of time for the MRGO Levee for higher surge level. [Times are referenced to CDT].

Figure 183 shows a typical "snapshot" of maximum velocities under a wave passing over a levee in this area, as described in Appendix 15. A very notable feature of these velocities is their asymmetry with respect to the levee crest, with the velocities on the front side of the levee (the part of the levee exposed to direct wave approach) being consistently lower than velocities on the back side of the levee.

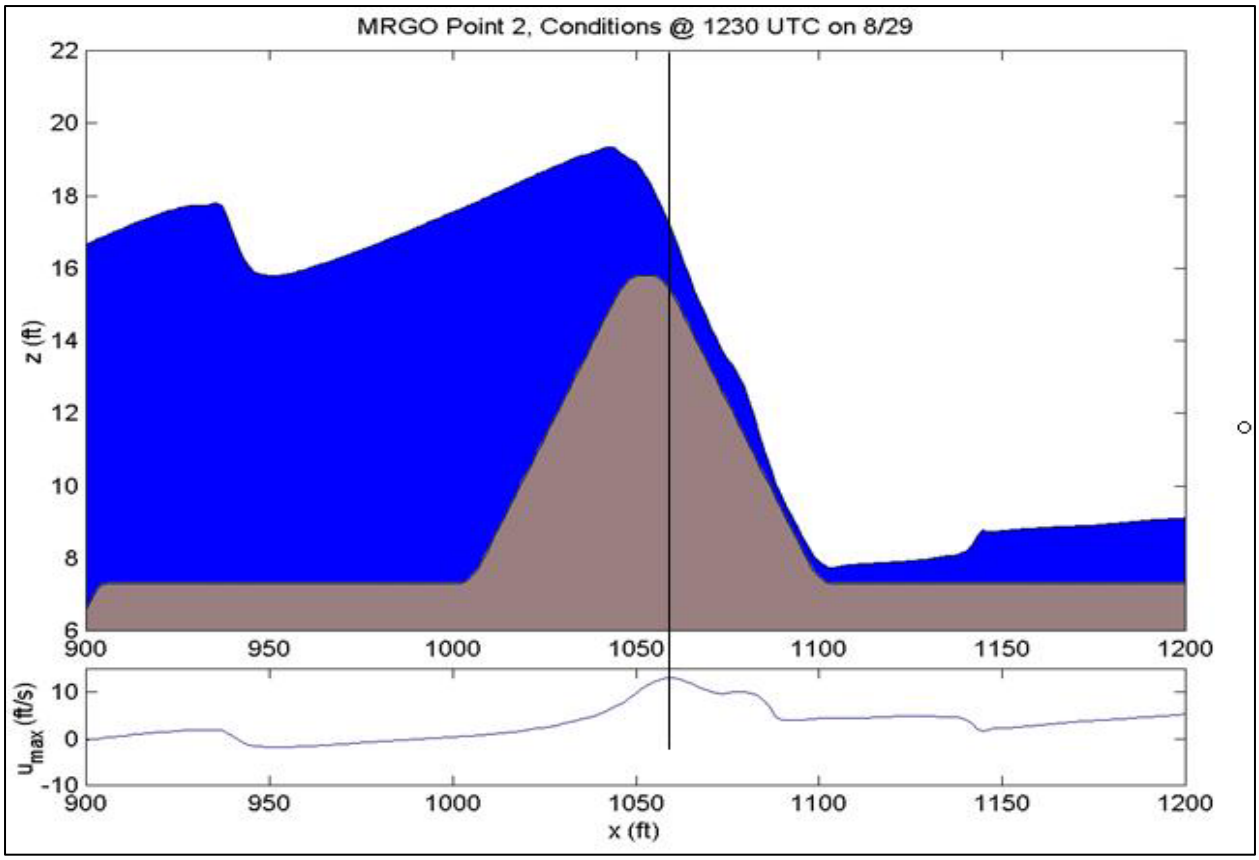

Figure 183. Snapshot of near-bottom velocities for a wave passing over levee from Boussinesq simulations.

Typical maximum velocities on the crest, front face, and back face of the levees have been shown in Figures 168, 169, and 170, respectively. For the case of the front face, two lines are shown since wave velocities are associated with both the uprush and downrush of the waves on the levee. As can be seen in Figures 168 to 170, average maximum velocities on the back face of the levees are consistently higher than velocities on the front face and are slightly higher than velocities on the crest of the levee, with average maximum values on the back face around 11 ft/sec, average maximum velocities at the crest around 10 ft/sec, and average maximum uprush velocities on the front face around 6 ft/sec. On a horizontal bottom, erosion potential tends to be related to the velocity cubed. Hence, our results suggest that erosive forces are more concentrated on the backs of levees rather than the fronts in situations with substantial wave overtopping and when both mean water level and wave overtopping are combined.

Flood Protection Levees along New Orleans East

The New Orleans East Levees were subjected to a combination of high surges and direct wave attack, from the southeast tip of the levee system to the area where the MRGO/GIWW begins to be sheltered by the St. Bernard Levee system As shown in Figure 164, two points along the New Orleans East Levees (Locations 5 and 6) were selected to examine the differences in conditions at the exposed and sheltered levee sections in this area. Along the exposed levees

characterized by conditions at Location 5, considerable erosion and breaching occurred. Here, at the time of peak surge, the significant wave height is about 4.2 ft with a peak period of about 14 sec and a propagation direction that is almost normal to the exposed levee.

Figure 184 shows a photograph taken near Location 6 on the morning of Hurricane Katrina. Conditions shown in the picture led many to speculate that this levee section would have been severely damaged during the storm; however, post-Katrina surveys showed that only minimal erosion occurred along the back side of this levee. At the sheltered site (Location 6), the waves are almost as large (significant wave height equal to 4.0 ft with a period of 13.5 sec) but are directed almost parallel to the levee crest. Figure 185 shows a snapshot from the Boussinesq simulation using COULWAVE. Substantial differences in predicted velocities are seen between water flowing over the levees under these two conditions. For the case of normally incident waves, peak water velocities associated with the passage of a wave crest are around 12.5 ft/sec. While for the case of the parallel waves, peak water velocities are only in the 5 to 6 ft/sec range. It is likely that the difference between the back face velocities along the exposed and sheltered levee sections, related to differences in wave directions relative to the levee crest, are responsible for the different levels of erosion/breaching observed in these locations.

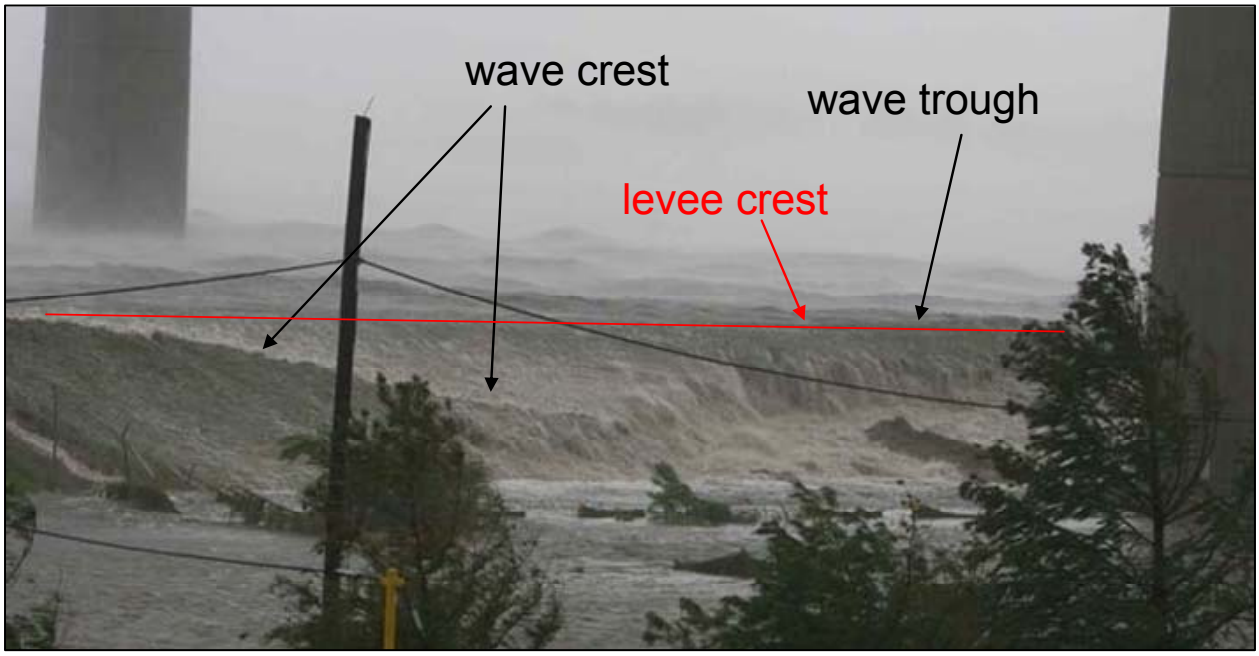

Figure 184. Photograph of conditions in the vicinity of Paris Road along the GIWW/MRGO on the morning of Hurricane Katrina. Photograph shows overtopping of levee. The time of the photo is not known with certainty. View is from the north side of the levee, looking towards the southwest. Waves are traveling from the east (left side of photo) towards the IHNC.

Figure 185. Side angle view of numerical waves overtopping the levee near the Paris Road Bridge. The levee is shown as the submerged black shape. View is looking towards the southwest; waves are from the east (left side of image).

Waves and Surges in Plaquemines Parish. Waves and surges in Plaquemines Parish substantially exceeded the tops of the levees. As was noted for the case of floodwalls along the IHNC, the Boussinesq model approximation does not provide a suitable solution in the vicinity of vertical walls. Consequently, the Navier-Stokes model was used to simulate conditions at the flood protection levees which are topped by a floodwall along the Mississippi River in the vicinity of Davant. Figure 186 shows the location of the point for this simulation and Figure 187 shows a snapshot of a simulated wave overtopping the floodwall at this location.

Figure 186. Location of point in Plaquemines Parish simulated with Navier-Stokes model.

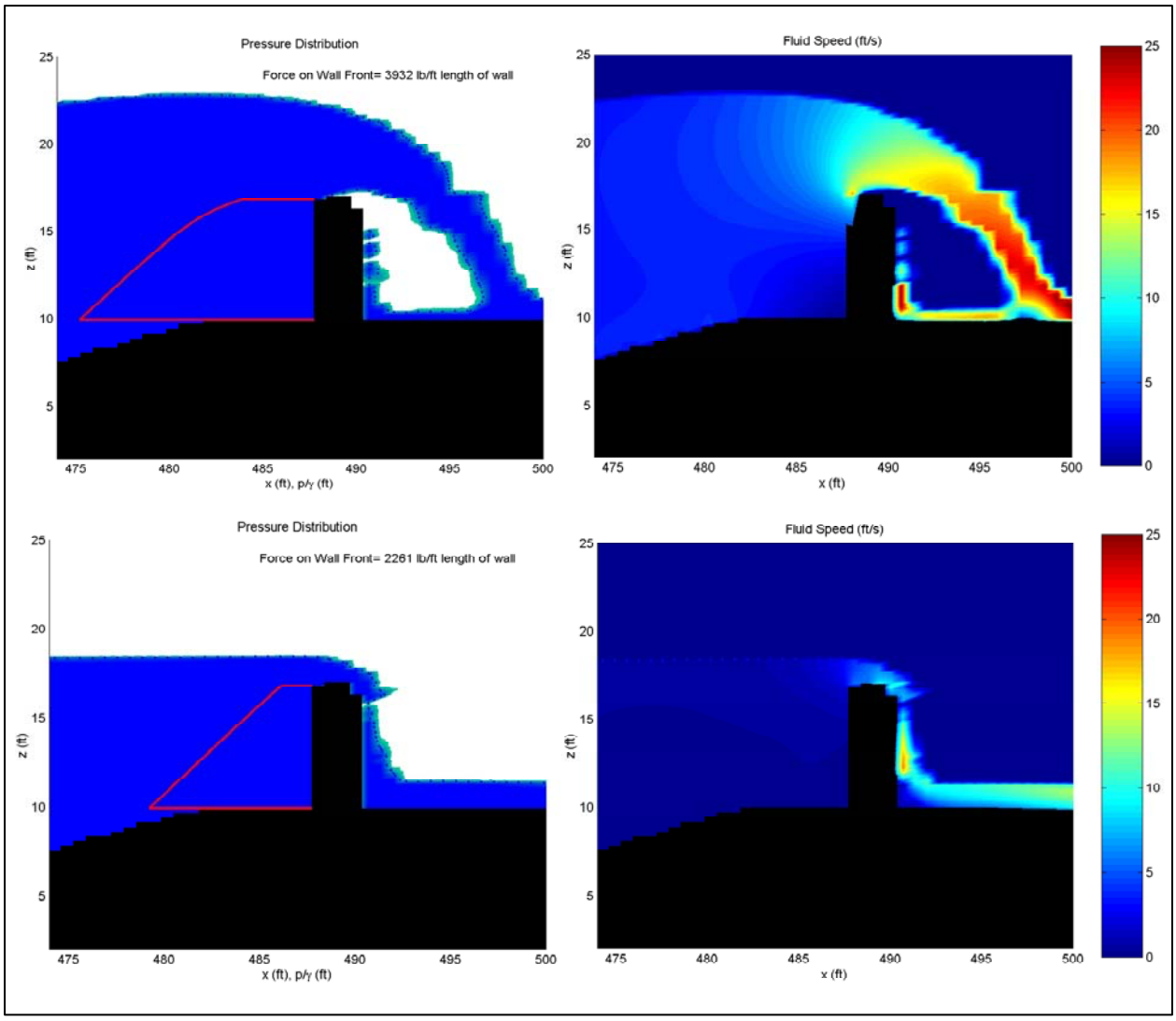

Figure 187. Pressure distribution (left) and fluid speed field (right) under the wave crest (top) and wave trough (bottom) for wave overtopping the levee wall.

In this simulation, the wave crest water passes over the top of the floodwall with a velocity of about 25 ft/sec, creating a jet of water that lands 5 to 10 ft behind the wall. As noted in Appendix 15, forces of over 3,900 lb/ft were estimated as representative of the mean wave force on the front face of the wall. For larger waves, forces of over 6,000 lb/ft would be expected. This is consistent with the post-Katrina observations that many of the walls in this area of Plaquemines Parish were severely damaged with extensive overtopping trenches behind them.

Examination of Basic Engineering Analyses for Design. Appendix 9 examines a number of basic engineering approaches to the estimation of detailed hydrodynamics for Hurricane Katrina. This is included here to provide an indication of how well such approaches fare in situations of the type studied here. Since such methods are often used as a first estimate of conditions before detailed numerical models are exercised, this information should be very useful information for future design and planning efforts of the type needed for the New Orleans area.

Findings and Lessons Learned

During the course of work to characterize regional and local hydrodynamic conditions created by Hurricane Katrina, as well as the forces and loadings on levees and floodwalls, a number of findings were established. From these findings valuable lessons were learned. Key findings and lessons learned are summarized here.

Katrina generated a storm surge and wave environment unparalleled in the history of New Orleans. Hurricane Katrina was a very large Category 3 storm when it passed the New Orleans area on the morning of 29 August. Twenty-four hours earlier this storm had been the largest Category 5 and most intense (in terms of central pressure) storm on record within the northern Gulf of Mexico. During Katrina, at a location due east of the Mississippi River delta and just offshore in deep water, NOAA Buoy 42040 recorded the highest significant wave height (55 ft) ever measured in the Gulf of Mexico. That observation matched the largest significant wave height ever recorded by a sensor within NOAA's buoy network, in any ocean. The large size of Katrina throughout its history, combined with the extreme waves generated during its most intense phase, enabled this storm to produce the largest storm surges that have ever been observed within the Gulf of Mexico, as determined from analyses of historical records. Reliable HWMs in Mississippi measured as much as 28 ft. As another example of Katrina's strength, the previous highest HWM was from Hurricane Camille, 24.6 ft, the only Category 5 storm to make landfall in the Gulf of Mexico over the interval that records have been kept (approximately 150 years). The maximum storm surge created by Katrina along the Southeast Louisiana coast was approximately 20 ft, which surpassed all previous observed high-water levels for the area.

Accurate simulation of surge and waves requires high-resolution definition of geographic features and highly accurate wind information. Representation of the physical system and accurate model input are the two most important factors that define accuracy of wave and storm surge modeling. Geography of Southeast Louisiana is very complex: many circuitous channels (some very deep), large expanses of irregularly-shaped wetland, a vast network of levees and elevated roadways, and complicated inundation/drainage pathways dictate water movement throughout the region. Accurate regional-scale surge modeling requires that all these important geographic features to be resolved with sufficient detail. The unstructured spatial discretization features of the ADCIRC model allow accurate representation of such a complex physical system in an optimal manner. Accurate wave modeling and wave-surge model coupling require high resolution of shallow water areas and areas with large depth gradients; this enables sufficient resolution of the breaking wave zone. Model results produced in this study demonstrated a very high degree of skill for this type of complex-phenomenon modeling. Correlation coefficients (r-squared values) between 0.8 and 0.9 were achieved for both wave and surge predictions, compared to measurements. Modeling success also was attributed in large part to the very high quality of wind input, the key driver of wave and storm surge generation.

The more sophisticated modeling available today provides significantly more detailed insight on variations in surge and wave environments with time and location. The wave and storm surge modeling (using the Corps' WAM, STWAVE, and ADCIRC standard prediction models) provided considerable insight into how water surrounding such a complex physical system responds to an equally complex hurricane wind system. The hurricane protection system

in Southeast Louisiana is very long and expansive, having a highly irregular layout. These factors coupled with a translating counterclockwise rotating wind field about the center of a hurricane produced a complicated pattern of wave and storm surge development and evolution. Propagation of an evolving storm surge wave influences the water depth, which in turn exerts strong influence on the local wave field. The wave field is not only a function of what is locally generated by the wind. It is also heavily influenced by wave conditions generated by the hurricane while it was still well off the coast. Those waves propagated into the region well ahead of the storm's arrival. As a consequence of all these factors, there is considerable spatial variation in the peaks and temporal variability in wave conditions and storm surge as a hurricane passes through the region. Where data were available that captured the temporal variation of wave and water level conditions, it was evident that the models reproduced the dominant features of this complex evolutionary process. For example, storm surge development in Lake Pontchartrain occurs through a filling process, which is driven by the water surface gradient between it and Lake Borgne, and local wind which acts to tilt the water surface of the lake toward the downwind direction. Another obvious behavior of the system was the dramatic difference between surge and wave climate generated by Katrina along the east-facing levees of the east bank of the Mississippi River, versus wave and water level conditions experienced along the northern parts of the west bank. The levee systems along the Mississippi River exert considerable control on the movement of water and development of the storm surge and wave conditions. In general, conditions on the east side of the Mississippi River Levee systems were much more severe than those along most of the west bank. This suggests that there might be some opportunity to exploit this pronounced difference in system-wide behavior in preparations for future approaching hurricanes that track similar to, or east of, the track taken by Hurricane Katrina.

While the Katrina generated surge in Lake Pontchartrain was comparable to the hurricane protection system design criteria, for the remainder of the system, Katrina surge was significantly greater than design assumptions. Peak water levels along the south shore of Lake Pontchartrain, at lakefront entrances to the three drainage canals and the IHNC, ranged from 10.8 to 11.8 ft NAVD88 (2004.65). These values were slightly below or at the design water levels. The same is true for the northernmost section of the IHNC, north of the I-10 bridge over the canal, and for some distance to the east of Lakefront Airport along the Lake Pontchartrain shoreline of east Orleans Parish. Everywhere else along the east bank portion of the protection system, the maximum water levels produced by Katrina (14 to 20 ft) exceeded design values. Along the east-facing levees of St. Bernard and Plaquemines Parishes, the storm piled water up against the levee system to levels that exceeded design values by as much as 5.5 ft.

With the exception of Plaquemines Parish, Katrina-generated wave heights were similar to hurricane protection system design assumptions. Wave periods along the GIWW, MRGO and Plaquemines protection levees were approximately three times those considered in the SPH design, dramatically increasing wave runup and overtopping. Along the south shore of Lake Pontchartrain, significant wave heights produced by Katrina were between 8 and 9 ft, slightly exceeding design values. Wave periods were consistent with design values, about 7 sec. Wave heights and periods were consistent with design values along the east-facing levees of eastern Orleans Parish. Levees adjacent to Lake Borgne, and the east-facing levees to the south in Plaquemines Parish, were subjected to long-period storm wave energy

from the Gulf of Mexico that propagated between and over the inundated barrier islands and inundated wetlands. Wave periods along these east-facing levees were 15 to 16 sec, approximately three times greater than design values. Wave heights along the east-facing St. Bernard Parish protection levees (heights as great as 6 ft) were less than or consistent with design values. Along the east-facing levees of Plaquemines Parish, wave heights reached 10 ft, and they significantly exceeded design values in places. In light of the exposure of levees in St. Bernard and Plaquemines Parishes to long-period hurricane wave energy from the gulf, design wave values should be reassessed for these levee systems. Wave height and period are both important in dictating runup and overtopping of levees and floodwalls.

For significant storm events, the southeast trending MRGO channel has little influence on the water levels inside the IHNC. The channel into IHNC from the GIWW has a very large influence on storm water levels. From the perspective of storm surge propagation into the IHNC and New Orleans Metropolitan area, the critical section of channel is the one where the GIWW and MRGO occupy the same channel. It is through this connection that Lakes Pontchartrain and Borgne are hydraulically connected to one another via the IHNC. A water level gradient is established within the IHNC and the GIWW/MRGO; the gradient is determined by the storm surge levels in both lakes. The presence of an open channel is the key factor. The hydraulic connectivity existed prior to construction of the MRGO, due to the presence of the GIWW channel. Three previous studies have been performed to examine the influence of the southeast-trending section of the MRGO on storm surge propagation into the New Orleans vicinity. This issue was also examined as part of this study. All studies have reached the same conclusion. For storm surges of a magnitude produced by Hurricane Katrina, which overwhelmed the wetland system, the influence of the southeast-trending MRGO channel on storm water levels is quite small. For Katrina the influence was only a few tenths of a foot at most in the IHNC and GIWW/MRGO channel sections. These small changes represent only a few percent of the surge amplitude. When the expansive wetland is inundated, the storm surge propagates primarily through the water column over this much larger flooded area, and the channels become a much smaller contributor, as a percentage, to total water movement.

Meteorological designations alone, such as the Saffir-Simpson scale, are misleading with regard to the criteria for design or performance of effective hurricane protection systems. Katrina, a Category 3 storm at landfall, generated surges of 24 to 26 ft at Biloxi, MS. In the vicinity of Biloxi, the surge produced by Camille was 15.8 ft, the highest surge that had ever been recorded at that location prior to Katrina. In other words, Katrina (a Category 3 storm at landfall) generated substantially higher surges than Camille (a Category 5 storm at landfall) in the area where they both made a direct hit. Maximum sustained wind speed is the hurricane parameter used to define hurricane strength, or category, in the Saffir-Simpson intensity scale. Through time, storm surge values have been tagged to different categories of intensity. Although maximum sustained wind speed is a very important parameter, storm surge levels are dictated by many more factors. Radius-to-maximum-winds and the rate at which wind speed decreases away from the maximum wind zone both determine the extent of the storm's wind fields which are of primary importance in storm surge and wave generation. Geographic, or topographic, controls that limit the movement of water pushed by the wind in shallow water are crucial in storm surge generation for Southeast Louisiana and Mississippi. The Mississippi River delta and levee systems along the river act to catch water that is blown into the region along the Mississippi and

Alabama continental shelves. Forward speed of the hurricane is also important, as is phasing of peak storm surge with the astronomical tide. Whereas the Saffir-Simpson scale is a good predictor of wind damage from hurricanes, it is not a particularly good predictor of the surge and wave generation potential for these storms.

Current models have uncertain accuracy in treating the effects of wetland and marsh environments on storm surge and waves. Sensitivity tests showed that wave and surge model computations are somewhat sensitive to the methods used to characterize frictional resistance of wetlands and to the values of frictional resistance assigned to different types of wetland landscape. Results showed that storm surge is reduced in some areas, whereas it is increased in others. Likewise, wave height is reduced in some areas and increased in others. Wave height increases are primarily due to the fact that increased water depths associated with increases in storm surge enable larger local wave heights to be sustained. The interactive coupling between waves and storm surge, and the effects of frictional resistance on both phenomena is a complicated physical process. This is certainly a technical area where more research and development is needed, as are data sets that that can be used to definitively characterize the role of wetland vegetation in altering wave and storm surge conditions in Southeast Louisiana, for varying states of inundation. The effect of marsh environments on storm surge and waves is expected to vary with the degree of inundation.

Measurements of temporal variation in wave and water level conditions, and wind, through the peak of the storm were extremely scarce. Of the few sensors deployed in the high impact zone, nearly all were damaged or malfunctioned. None of the self-recording instruments that were in place to record water levels successfully captured water level changes through the peak of the storm in the high impact zone. All malfunctioned prior to the peak. A lock operator reading a staff gauge during the storm was able to capture a reliable hydrograph in the IHNC. Two other hydrographs that captured the peak along the south shore of Lake Pontchartrain, one a partial hydrograph, were able to be reconstructed after the storm from a series of digital photographs of water surface relative to a physically identifiable object. These reconstructed hydrographs proved to be very valuable. Use of carefully shot digital imagery provides an alternate means for acquiring such crucial data sets. A series of three very small wave buoys were deployed in Lake Pontchartrain just prior to the storm. Two of three buoys were recovered, but data quality at the peak of the storm for both gauges that survived is considered suspect. Most anemometers for measuring surface winds also failed prior to the storm peak. There is a great need for hardened, self-powered instrumentation that can reliably capture temporal changes in waves and water levels, and wind, throughout the storm. Such information is essential for evaluating design assumptions and approaches. Hurricanes are the design events, and there is a paucity of data for characterizing waves and water levels during hurricanes along the periphery of the hurricane protection system, particularly those portions of the system that are most exposed to high wave and surge conditions coming in from the east and southeast.

About 10 to 15 percent of HWMs were considered to be reliable measures of peak storm water level. Of the many hundreds of HWMs collected in Louisiana and Mississippi, a relatively small percentage of HWMs were rated to be reliable measures of storm surge (the peak still-water level that was experienced during the storm). The most reliable marks were those measured in the interior of structures on walls, in places where oscillatory wave motions were

minimized. Exterior debris lines and marks, wrack lines, debris that had settled into position on a horizontal surface, or debris that had lodged in a fence were deemed to be less reliable indicators of peak storm water level. This judgment was made in light of other processes that might be reflected in those types of marks. HWM collection that is intended to capture peak storm surge (i.e., still water) should focus on the interior of structures, which are not so completely sealed that water could not easily enter but where influences of local wave and wind action are minimized. Multiple marks should be sought and acquired if possible within the same structure to reduce uncertainty in high-water estimation at that location. Debris lines and wrack lines on levees might be reliable indicators of wave runup, if that measure of water surface elevation is sought. Likewise, exterior marks which include the influence of water surface fluctuations associated with passage of wave crests may also be of value if that measure of water surface is sought. Digital photographs or imagery that show the water surface in relation to some physically identifiable, and surveyable, object can provide highly reliable estimates of storm water levels.

Resolution of wave setup is a critical element in the estimation of design levels of levees in this area. Hurricane Katrina produced extremely energetic wave conditions along the entire coast of Louisiana. Significant offshore wave heights along the Southeast Louisiana coast ranged from 55 ft due east from the tip of the Mississippi River delta to 20 to 25 ft just north of the Chandeleur Island chain, with peak wave periods of approximately 15 to 16 sec. Considerable wave breaking took place seaward of the Chandeleur Islands. In Lake Pontchartrain, wave heights reached 8 to 9 ft with periods of about 7 sec. High resolution (as fine as 300 ft) was added to the ADCIRC grid mesh to resolve areas of intense wave breaking along the barrier islands, the periphery of the coastal wetlands fronting Southeast Louisiana, and along the periphery of Lake Pontchartrain. The STWAVE model was run at fine resolution. The high resolution adopted and use of coupled wave and surge models was able to capture the contribution of wave setup to storm surge away from coastal structures, a contribution of up to 2.5 ft depending on location. But even though the ADCIRC model contained contributions of both direct forcing and wave-related radiation stresses in its estimates of storm surge heights, local wave setup not resolved by the ADCIRC grid contributed 1.5 to 2 ft of additional setup along exposed levees in St. Bernard Parish, Plaquemines Parish, and New Orleans East, as well as along the south shore of Lake Pontchartrain. This additional setup contribution was estimated using Boussinesq wave modeling applied with much higher resolution.

Wave and surge overtopping created very high water velocities on the top and land side of exposed levees along MRGO and in Plaquemines Parish. Maximum velocities from combined waves and storm surge overtopping, which appear capable of eroding unarmored earthen levees, occurred along the back sides of levee crests. These velocities were related to the passage of waves over top of levees in situations where the water levels were near or above the elevation of the levee crest.

Small differences in water levels make a substantial difference in overtopping rates. Analyses of overtopping along the MRGO in St. Bernard Parish showed that estimated overtopping rate was only about 1 $ft^3/s/ft$ along the levee when the water level was approximately equal to the elevation of the levee; while, for the situation with the water level about 4 ft above the elevation of the levee, the overtopping rate was over 20 $ft^3/s/ft$ along the

levee. Consequently, it is critical to ensure maximum accuracy in all water level estimates used for planning and design in this area.

Velocities along overtopped levees are significantly affected by variations in wave direction. In studies of velocities along the New Orleans East Levee, wave propagation direction relative to the crest of a levee made a substantial difference in the velocities along the crest and back side of levees, with normally incident waves creating about 50 percent higher velocities than the same waves propagating parallel to the crest. This means that estimates of wave-generated currents along levees for design must consider wave direction in their formulation.

Local wave generation can contribute significantly to wave conditions within outfall and navigation canals in the New Orleans area. Local wave generation in the outfall canals during Katrina generated higher wave conditions over much of the length of the canal than were associated with the waves entering the canals from primary generation areas (either Lake Pontchartrain or the Gulf of Mexico). In the most extreme case examined here, wave heights of over 4 ft were generated within the GIWW/MRGO canal entering the IHNC from the east. This occurred early on 29 August when wind speeds of 80 knots were aligned almost directly parallel to the axis of the GIWW/MRGO.

Barge impacts in high-wind/high-wave situations have the potential to inflict consequential damage to floodwalls. During high wind events, as might be expected intuitively, barges floating in the vicinity of floodwalls can be rapidly accelerated to velocities capable of exerting impact forces on floodwalls that are comparable or larger than hydrostatic forces typically used for design.

References

Amorocho, J. and J.J. DeVries. 1980. A new evaluation of the wind stress coefficient over water surfaces. *J. Geophys. Res*. 85(C1): 433-442.

Booij, N., IJ. G. Haagsma, L.H. Holthuijsen, A.T.M.M. Kieftenburg, R. C. Ris, A. J. van der Westhuysen, and M. Zijlema. 2004. *SWAN Cycle III Version 40.41 Users Manual*. Delft University of Technology, Delft, The Netherlands, 118 p. http://fluidmechanics.tudelft.nl/swan/index.htm

Booij, N., R. C. Ris, and L.H. Holthuijsen. 1999. A third-generation wave model for coastal regions, part I: model description and validation," *J. Geophys. Res*. 104(C4): 7649-7666.

Blain, C. A., J .J. Westerink, and R. A. Luettich. 1994. The influence of domain size on the response characteristics of a hurricane storm surge model. *J. Geophys. Res. - Oceans* 99(C9): 18467-18479.

Blain, C. A., J. J. Westerink, and R. A. Luettich. 1998. Grid convergence studies for the prediction of hurricane storm surge. *Int. J. Num. Meth. Fluids* 26: 369-401.

Cardone, V.J., A.T. Cox, J.A. Greenwood, and E.F. Thompson, 1994. Upgrade of the tropical cyclone surface wind field model. *Miscellaneous Paper CERC-94-14*, U.S. Army Corps of Engineers.

Cox, A. T., and V. J. Cardone. 2000. Operational system for the prediction of tropical cyclone generated winds and waves. *6th International Workshop on Wave Hindcasting and Forecasting*, November 6-10, 2000, Monterey, CA.

Cox, A. T., J. A. Greenwood, V. J. Cardone, and V. R. Swail. 1995. An interactive objective kinematic analysis system. Preprints, *Fourth International Workshop on Wave Hindcasting and Forecasting*, Banff, Alberta, Canada, Atmospheric Environment Service, 109-118.

Feyen, J. C., J. J. Westerink, J. H. Atkinson, R. A. Luettich, C. Dawson, M. D. Powell, J. P. Dunion, H. J. Roberts, E. J. Kubatko, and H. Pourtaheri. 2005. A basin to channel scale unstructured grid hurricane storm surge model for southern louisiana. *Monthly Weather Review*, In Preparation.

Garratt, J.R. 1977. Review of drag coefficients over oceans and continents. *Mon. Wea. Rev.* 105: 915-929.

Holland, G. L. 1980. An analytical model of the wind and pressure profiles in hurricanes. *Mon. Wea. Rev.* 108: 1212-1218.

Jelesnianski, C. P., and A. D. Taylor. 1973. A preliminary view of storm surges before and after storm modifications. *NOAA Technical Memorandum ERL WMPO-3.*

Jensen, R. E. and V. J. Cardone. 2005. Modeling in the Core of Hurricanes: Perspectives from the 2004 Hurricane Season. Waves in Shallow Water Environments Presentation.

Kalany, E., M. Kanamitsu, R. Kistler, W. Collins, D. Deaven, L. Gandin, M. Iredell, S. Saha, G. White, J. Woollen, Y, Zhu, M. Chelliah, W. Ebisuzaki, W. Higgins, J. Janowiak, K.C. Mo, C. Ropelewski, J. Wang, A. Leetmaa, R. Reynolds, R. Jenne, and D. Joseph, 1996. The NCEP/NCAR 40-year reanalysis project. *Bull. American Met. Society.* **77**(3): 437-471.

Knabb, R. D., J. R. Rhome, and D. P. Brown, 2005. *Tropical storm report Hurricane Katrina 23-30 August 2005*. National Hurricane Center, Dec 2005.

Komen, G. J., L. Cavaleri, M. Donelan, K. Hasselmann, S. Hasselmann, and P.A.E.M. Janssen. 1994. Dynamics and modelling of ocean waves. Cambridge, UK: Cambridge University Press, 560 pages.

Large, W.G. and S. Pond. 1981. Open ocean momentum flux measurements in moderate to strong winds. *J. Phys. Oceanogr.* 11: 324-336.

Powell, M. D., S. H. Houston, L. R. Amat, and N. Morisseau-Leroy. 1998. The HRD real-time hurricane wind analysis system. *J. Wind Engineer. Ind. Aerody*. (77&78): 53-64.

Powell, M., P. Vickery and T. Reinhold, 2003. Reduced drag coefficient for high wind speeds in tropical cyclones. *Nature*, 422: 279-283.

Smith, J. M., A. R. Sherlock, and D. T. Resio. 2001. *STWAVE: Steady-state spectral wave model user's manual for STWAVE, Version 3.0*. ERDC/CHL SR-01-1. U.S. Army Engineer Research and Development Center.

Thompson, E. F., and V. J. Cardone. 1996. Practical modeling of hurricane surface wind fields. *ASCE J. of Waterway, Port, Coastal and Ocean Engineering,* 122**(**4): 195-205.

Tolman, H. L. 1998. A new global wave forecast system at NCEP. In *Ocean wave measurements and analysis vol. 2*, ed. B. L. Edge and J. M. Helmsley, ASCE, 777-786.

Tolman, H. L. 1999. User manual and system documentation of WAVEWATCH-III version 1.18. Technical Note, 110 pp.

Trenberth, K.E., W.G. Large, J.G. Olsson. 1989. The effective drag coefficient for evaluating wind stress over the oceans, *J. Climate*, 2: 1507-1516

Westerink, J. J., J. C. Feyen, J. H. Atkinson, R. A. Luettich, C. N. Dawson, M. D. Powell, J. P. Dunion, H. J. Roberts, E. J. Kubatko, and H. Pourtaheri. 2005. A new generation hurricane storm surge model for Southern Louisiana, *Bulletin of the American Meteorological Society*, In Review, 2005.